



THE UNIVERSITY OF  
**SYDNEY**

## **COPYRIGHT AND USE OF THIS THESIS**

This thesis must be used in accordance with the provisions of the Copyright Act 1968.

Reproduction of material protected by copyright may be an infringement of copyright and copyright owners may be entitled to take legal action against persons who infringe their copyright.

Section 51 (2) of the Copyright Act permits an authorized officer of a university library or archives to provide a copy (by communication or otherwise) of an unpublished thesis kept in the library or archives, to a person who satisfies the authorized officer that he or she requires the reproduction for the purposes of research or study.

The Copyright Act grants the creator of a work a number of moral rights, specifically the right of attribution, the right against false attribution and the right of integrity.

You may infringe the author's moral rights if you:

- fail to acknowledge the author of this thesis if you quote sections from the work
- attribute this thesis to another author
- subject this thesis to derogatory treatment which may prejudice the author's reputation

For further information contact the University's Director of Copyright Services

**[sydney.edu.au/copyright](http://sydney.edu.au/copyright)**

Sydney College of the Arts  
The University of Sydney

DOCTOR OF PHILOSOPHY  
2013

THESIS

GREEN ware:  
Low-temperature ceramics incorporating recycled  
waste

by

Brett Smout

July 2013

This volume is presented as a record of the work undertaken for the degree of  
Doctor of Philosophy at Sydney College of the Arts, University of Sydney.

## **Acknowledgments**

I thank and acknowledge my supervisor Jan Guy, who consistently supported the introduction of new ideas, provided critiques and commentary, offered links to other artists' work and rigorously reviewed the text. I also thank my associate supervisor Chris Ling, who gave valuable instruction in X-ray diffraction and also rigorously reviewed the text, and facilitated support from the Chemistry Department at the University of Sydney. Thanks to Denis Whitfield, whose masters and PhD theses provided starting points for this research. I acknowledge the facilities, facilitation and technical assistance of staff at the Sydney College of the Arts, University of Sydney. I also acknowledge the facilities and scientific and technical assistance of staff in the Australian Microscopy and Microanalysis Research Facility at the Electron Microscope Unit, University of Sydney, and the assistance of Associate Professor Stuart Reid and his students in the Department of Civil Engineering at the University of Sydney. Thanks also to Ms. Vivilia Widjaja, who assisted in obtaining equipment from Indonesia, and to my family for their patience and support.

“Waste not, want not” said Miss Copsey.

## Table of Contents

<b>Acknowledgments</b> .....	<b>iii</b>
<b>Table of Contents</b> .....	<b>iv</b>
<b>List of Illustrations</b> .....	<b>x</b>
<b>List of Tables</b> .....	<b>xxviii</b>
<b>List of Abbreviations</b> .....	<b>xxxi</b>
<b>Abstract</b> .....	<b>xxxii</b>
<b>Introduction</b> .....	<b>1</b>
<b>Chapter 1: Personal Motivations: Climate science, socio-political influences and ceramic practice</b> .....	<b>9</b>
Formative influences .....	9
Twenty-first century socio-political attitudes to global warming .....	11
Formalism and consideration of the impact of ceramic process on form .....	12
Increasing atmospheric CO <sub>2</sub> and global warming.....	15
Effects of warming and elevated CO <sub>2</sub> on the ocean and sea creatures.....	16
Firing ceramics—energy required .....	24
Fuels commonly used in Western ceramics .....	24
Firing temperatures of clays in common use .....	27
<b>Chapter 2: Environmental Art</b> .....	<b>30</b>
A brief survey of environmental art.....	30
Use of waste in the creation of artworks.....	37
Transformations: clay and our environment .....	40
Ceramic artists' writing about environmental concerns .....	47
<b>Chapter 3: Sustainability, Green Chemistry and Engineering</b> .....	<b>49</b>
<b>Chapter 4: Classification of Clays</b> .....	<b>52</b>
Clays for low-temperature bodies.....	54
Ball clay .....	54
Illite .....	55
Montmorillonite .....	55
<b>Chapter 5: Desirable Characteristics of Glass/Ceramic Body to be Developed</b> .....	<b>58</b>
Desirable characteristics of a body when raw .....	58
Plasticity .....	58
Dry strength .....	59
Wet to dry shrinkage.....	63
Desirable characteristics of fired ceramics .....	63
Colour .....	63
Translucency .....	64
Acoustic resonance .....	65
Hardness .....	65
Fired strength, porosity and permeability .....	65
Permeability .....	66
Porosity.....	66

Test for fired strength.....	67
<b>Chapter 6: Sintering and Vitrification.....</b>	<b>68</b>
Methods of lowering sintering temperature.....	70
Physiochemical approaches .....	70
Physiomechanical approaches .....	72
Thermophysical approaches.....	73
Considerations when firing ceramics.....	73
<b>Chapter 7: Inclusion of Industrial, Municipal or Agricultural Waste in Clay             and Glaze .....</b>	<b>74</b>
Glass .....	74
Paper.....	76
Paper sludge ash .....	77
Fly ash.....	77
Wood ash .....	78
Incinerated sewage sludge ash.....	78
Sugar cane bagasse ash.....	78
Rice husk ash.....	79
Corn cob ash .....	86
Rock .....	86
Tannery sludge.....	87
Mixed wastes.....	87
Silica fume (micro silica).....	88
Review of Whitfield's sources of industrial or agricultural waste in New South Wales.....	88
<b>Chapter 8: Materials Selection, Sourcing and Preparation .....</b>	<b>93</b>
Sugar cane bagasse ash.....	93
Rice husk ash.....	109
Corn cob ash .....	116
Corn seeper sludge .....	124
Paper sludge ash .....	130
Cullet .....	131
Unimin cullet .....	131
Visy cullet conveyor belt debris.....	133
Cleaned glass waste held back from domestic kerb-side recycling .....	136
Prego marble-cutting dust .....	138
Perlite fines.....	139
Perlite: Unexpanded ore.....	142
Dunmore latite .....	143
Quarry tailings .....	145
Bungendore sand mine tailings.....	145
Marulan quarry tailings .....	151
<b>Chapter 9: Comparative Observations of Absorption Rates and             Suspension in Water: quarry tailings, ball clay and bentonite</b>	<b>156</b>
Absorption .....	156
Comparative absorption of water by English bentonite and Arumpo bentonite .....	158
Swelling of English bentonite and Arumpo bentonite after saturation.....	158
Suspension.....	160
<b>Chapter 10: Initial Treatment and Handling Experiments with Quarry             Tailings .....</b>	<b>164</b>

Preparation.....	164
Extrusions.....	165
Bowls thrown with quarry tailings .....	166
<b>Chapter 11: Triaxial Blend Methodology .....</b>	<b>171</b>
Triaxial blend method .....	171
Method of forming body-test samples from triaxial blends .....	174
Slab rolling and cutting .....	174
Extrusion.....	175
Marking wet samples for shrinkage calculations.....	175
Observations and ratings used to describe qualities of samples.....	175
Nomenclature for triaxial blends .....	177
<b>Chapter 12: Three Triaxial Blends: Workability, drying and shrinkage of samples.....</b>	<b>179</b>
Triaxial blend: Arumpo Cullet Cold House Fines Latite (ACCL) .....	179
Triaxial ACCL: Handling and drying properties.....	182
Triaxial ACCL: Wet to dry shrinkage.....	187
Triaxial flux mix 1/Bungendore/Marulan (BM1).....	191
Triaxial BM1: Handling and drying properties .....	192
Triaxial BM1: Wet to dry shrinkage.....	197
Triaxial flux mix 2/Bungendore/Marulan (BM2).....	199
Triaxial BM2: Handling and drying properties .....	201
Triaxial BM2: Wet to dry shrinkage.....	204
<b>Chapter 13: Three Triaxial Blends: Fired shrinkage and appearance after firing to 800°C.....</b>	<b>207</b>
Firing procedures .....	207
Triaxial ACCL: 800°C .....	208
Triaxial ACCL: Shrinkage from dry after firing to 800°C.....	208
Triaxial ACCL: Shrinkage from wet after firing to 800°C .....	211
Floating ceramic body (ACCL11; 800°C.) .....	214
Triaxial BM1: Shrinkage from wet, after firing to 800°C.....	215
Triaxial BM1: Shrinkage from dry, after firing to 800°C.....	216
Slumping.....	219
Triaxial BM1: Fired to 800, 850, 900 and 950°C.....	219
Triaxial BM2: 800°C.....	222
Triaxial BM2: Shrinkage from dry to 800°C .....	224
BM2 Shrinkage from wet to 800°C .....	228
BM2.7 – BM2.10 after firing to 800, 850, 900 and 950 °C .....	230
<b>Chapter 14: Use of Energy from Rice Husks and Corn Cobs .....</b>	<b>233</b>
Obtaining domestic gasifiers .....	233
Biomass kiln construction .....	234
Firing with rice husks and a gasifier .....	235
Burning domestic corn cob waste in a gasifier .....	237
Producing sodium silicate from rice husk ash: Trial 1.....	239
<b>Chapter 15: Material Characterisation by X-ray Diffraction .....</b>	<b>241</b>
<b>Chapter 16: Typical Percentage Analysis of Recovered Materials.....</b>	<b>261</b>
<b>Chapter 17: Surface Effects: Glaze, slip and engobe tests.....</b>	<b>263</b>
Triaxials BM1 and BM2: Engobe and glaze tests.....	264
Cone 010 vitreous engobe.....	265
Glaze tests at 900°C.....	267

Reformulating engobes using waste materials .....	272
Vitreous engobes .....	273
<b>Chapter 18: Bodies with Self-glazing Properties .....</b>	<b>276</b>
<b>Chapter 19: Bodies Using Only Recycled Materials .....</b>	<b>278</b>
Cullet and perlite additions to Bungendore tailings.....	278
Cullet addition to an optimal blend of Bungendore and Marulan quarry tailings .....	280
Discussion .....	282
Quarry tailings terracotta body: 1080–1100°C .....	282
Low-firing terracotta body: 1050–1090°C (BM1.14C) .....	283
<b>Chapter 20: Reformulation to Reduce Flux, Extend Vitrification Range         and Decrease Porosity .....</b>	<b>284</b>
Flux material properties .....	284
Flux solubility, salt migration and deflocculation .....	289
<b>Chapter 21: Toxicity Considerations.....</b>	<b>291</b>
Rating and labelling systems .....	291
Australian Poison Standards.....	292
Storage requirements classification .....	292
CAS number .....	292
Four hazard categories of health, flammability, reactivity, and contact....	292
Eliminated materials .....	296
Materials requiring additional attention to avoid acute injury during glazing, firing or clean-up procedures .....	296
Materials requiring caution to avoid dangers associated with chronic exposure .....	297
<b>Chapter 22: Craze Control and Reduction of Porosity .....</b>	<b>298</b>
Bodies with magnesia content .....	299
<b>Chapter 23: Triaxial BM11 .....</b>	<b>302</b>
Triaxial BM11: Composition.....	302
Scaled up triaxial blending for greater sample size .....	304
Triaxial BM11: Handling properties .....	309
Triaxial BM11: Efflorescence.....	312
Triaxial BM11: Shrinkage wet to dry.....	315
Triaxial BM11: Fired to 850, 900, 950 and 1000°C.....	316
Triaxial BM11: Fired to 850°C .....	317
Triaxial BM11: Fired to 900°C .....	319
Triaxial BM11: Fired to 950°C .....	321
Triaxial BM11: Fired to 1000°C .....	323
Absorption and porosity.....	325
Triaxial BM11: Absorption and porosity after firing to 850°C.....	327
Triaxial BM11: Absorption and porosity after firing to 900°C.....	329
Triaxial BM11: Absorption and porosity after firing to 950°C.....	332
Triaxial BM11: Absorption and porosity after firing to 1000°C.....	333
Triaxial BM11: Observations and data across increasing temperatures.....	337
<b>Chapter 24: Further Tests Exploring Properties of Interesting Bodies....</b>	<b>353</b>
Preparation of larger batches of bodies from triaxial BM11 .....	354
Bodies fired above 1000°C.....	354
BM11.6 .....	354
Low-fire self-glazing tile body: 980–1040°C (BM11.6).....	356



BM11.9 .....	356
BM11.10 .....	356
Low-fire self-glazing body: 980–1100°C (BM11.10) (wt%) .....	358
<b>Chapter 25: Body Additions to Reduce Thixotropy and Efflorescence ...</b>	<b>359</b>
<b>Chapter 26: Tests of Fired Strength .....</b>	<b>366</b>
Strength testing procedure .....	367
<b>Chapter 27: Attempts at Producing Casting Slips .....</b>	<b>371</b>
<b>Chapter 28: Investigations into Glazes using Recycled Materials .....</b>	<b>373</b>
Glazes developed from triaxial recycle 1 .....	373
Cone 9 quarry dust tenmoku glaze (R14) .....	377
Cone 9 quarry dust black glaze (R10) .....	378
Cone 9 sugarcane ash grey glaze (R4) .....	378
Cone 5–6 pale khaki gloss (R1) .....	381
Cone 5–6 mid-khaki gloss (R3) .....	382
Cone 5–6 khaki gloss (R6) .....	383
Cone 5–6 brown gloss (R10) .....	384
Cone 5–6 deep chocolate gloss (R15) .....	385
Cone 03 cream matte (R1) .....	387
Cone 03 mud satin matte (R3) .....	388
Cone 03 olive satin matte (R6) .....	389
Cone 03 brown dry glaze (R13) .....	390
Cone 06 pale yellow matte glaze (R1) .....	392
Cone 06 dry brown/wet olive lichen transition glaze (R4) .....	393
Cone 06 dry brown glaze (R8) .....	394
Ionic potential .....	395
Low-fire glazes .....	396
Low-fire triaxial 1 .....	398
950–1000°C (cone 08–06) lithium crystal glaze (L1.15) .....	400
950–1000°C (cone 08–06) corn ash glaze (L1.5) .....	404
950–1000°C (cone 08–06) corn ash lithium sparkle glaze (L1.14) .....	405
950–1000°C (cone 08–06) transparent gloss (L1.6) .....	406
950–1000°C (cone 08–06) transparent gloss (L1.3) .....	407
950–1000°C (cone 08–06) crystalline matte (L1.10) .....	408
950–1000°C (cone 08–06) corn ash matte (L1.8) .....	409
950–1000°C (cone 08–06) corn ash camouflage matte (L1.13) .....	410
Low-fire triaxial 2 .....	411
Sugarcane ash glaze (L2.1) .....	411
950°C (cone 08) matte & 1000–1100°C (cone 06–03) gloss .....	411
Rice husk ash glaze (L2.15) .....	412
950–1000°C (cone 08–06) matte .....	412
1050–1100°C (cone 05–03) satin to gloss .....	412
950–1000°C (cone 08–06) RHA transparent gloss (L2.14) .....	415
950–1000°C (cone 08–06) rice husk/sugarcane ash glaze (L2.6) .....	416
Low-fire triaxial 3 .....	417
950–1000°C (cone 08–06) corn/sugarcane ash sandy matte (L3.1) .....	417
1050–1100°C (cone 05–03) rock dust gloss (L3.11) .....	418
Low-fire triaxial 4 .....	419
950–1050°C (cone 08–05) Bungendore mine tailings glaze (L4.1) .....	421
950°C–1050°C (cone 08–05) Marulan quarry tailings glaze (L4.15) .....	422
<b>Chapter 29: Glaze, Engobe and Body Interactions .....</b>	<b>423</b>

Colourant additions to selected glazes .....	434
<b>Chapter 30: Slump Tests for Selected Bodies.....</b>	<b>445</b>
<b>Chapter 31: Studio Tests using Bodies and Glazes Developed .....</b>	<b>447</b>
BM11.6A.....	447
Glazing and firing .....	451
Scaled up production of BM1.14C and BM11.6B .....	459
Ware produced using BM11.6B.....	459
Cone 08 glaze (Glaze 18).....	462
Cone 08 glaze (Glaze 19).....	463
Blends with a proprietary body .....	465
<b>Conclusion .....</b>	<b>468</b>
<b>List of Plates.....</b>	<b>473</b>
<b>References.....</b>	<b>474</b>
<b>Appendices.....</b>	<b>506</b>
Appendix 1: Orton standard cones: temperature equivalents & Seger cone formulae.....	506
Appendix 2: Norkse Skog paper sludge analysis .....	507
Appendix 3: Cullet technical data .....	508
Appendix 4: Rice husk gasifier stove operating instructions.....	509
Appendix 5: ASTM standard C-373.....	511
Appendix 6: Cold Over Boiled Porosity—COVB.....	513
Appendix 7: Data from strength tests .....	515
Appendix 8: Report on clay body BM11.6B—Geoff Crispin .....	516
Appendix 9: WMF technical data.....	518
<b>Appendix 10. Conceptual Artworks Developed from the Research .....</b>	<b>519</b>
<i>Screaming Cans</i> .....	521
<i>Switch</i> .....	523
<i>Human</i> .....	525
<i>Carbon Fix</i> .....	527
<i>Thin Air</i> .....	529
<i>Crack</i> .....	538
<i>Certain Doubts</i> .....	543
<i>Solar Panel</i> .....	545
<i>Cooling Tower 1</i> .....	547
<i>Shocked!</i> .....	560

## List of Illustrations<sup>1</sup>

Figure 1: House-truck interior (Bennetts, 2012) .....	10
Figure 2: Raku fired clay pendant sold at the New Zealand Nambassa festival in 1979 .....	10
Figure 3: Greenpeace climate change activism (Greenpeace/Alcock).....	12
Figure 4: Powershift conference delegates in Sydney .....	12
Figure 5: <i>Bankivia fasciata</i> (Beechey, 2012).....	13
Figure 6: Scanning electron micrographs of diatoms:.....	13
(A) <i>Biddulphia reticulata</i> (B) <i>Diploneis</i> sp. (C) <i>Eupodiscus radiates</i> (D) <i>Melosira varians</i> (Tiffany).....	13
Figure 7: Brett Smout Seashell Vases 2008 (38cm x 18cm & 25cm x 14cm).....	14
Figure 8: Time series of atmospheric carbon dioxide levels recorded at Cape Grim, Tasmania since 1984 (Commonwealth Scientific and Industrial Research Organisation; NOAA).....	16
Figure 9: <i>Clio pyramidata</i> (Hopcroft, 2006).....	17
Figure 10: Clownfish ( <i>Amphiprion percula</i> ) (Newbert, 2009) .....	18
Figure 11: Comparison of energy input per serve with various cup types (Hocking, 1994).....	19
Figure 12: Environmental impact categories.....	19
Figure 13: Benelux advertising (Stichting Disposables Benelux, 2007) ....	20
Figure 14: Environmental impact of varying cleaning systems for re-usable cups versus disposable cups.....	21
Figure 15: Environmental impact of cold-cleaned earthenware mug versus disposable cups .....	22
Figure 16: Australian appliance energy-rating label (Commonwealth of Australia Department of Climate Change and Energy Efficiency, 2009).....	23
Figure 17: Factory electric kiln (Royal Stafford Tableware Ltd, 2012) .....	24
Figure 18: Controlled application and firing: Hürten handled centrepiece (Spode, n.d.) .....	25
Figure 19: Salting a suburban coal-fired kiln, Dunedin, New Zealand, 1980	25
Figure 20: Brett Smout Salt-glazed coal-fired beakers 1980.....	26
Figure 21: Joseph Beuys, 7000 Oaks, 1982 (uncredited) .....	31
Figure 22: Buster Simpson Hudson River Purge, 1983 (Simpson, 1983–1991).....	31

---

<sup>1</sup> Uncredited figures were created or adapted by the thesis author

<b>Figure 23: Mel Chin Revival Field 1991 (Chin, 2001).....</b>	<b>32</b>
<b>Figure 24: Agnes Denes pictured in Wheatfield—A Confrontation 1982 (Denes, 2011).....</b>	<b>33</b>
<b>Figure 25: Anna Garforth Moss Graffiti 2008 (Garforth, 2009) .....</b>	<b>33</b>
<b>Figure 26: Anna Garforth Moss Graffiti 2008 (Garforth, 2009) .....</b>	<b>33</b>
<b>Figure 27: Michael Heizer Double Negative 1969 (Kessel).....</b>	<b>34</b>
<b>Figure 28: Mel Henderson Oil 1964 (Henderson &amp; Cohen).....</b>	<b>35</b>
<b>Figure 29: Ken &amp; Julia Yonetani Still Life—The Food Bowl 2011 (Yonetani) .....</b>	<b>35</b>
<b>Figure 30: The Glue Society Hot With Chance Of A Late Storm 2006 (Beaumont, 2006) .....</b>	<b>36</b>
<b>Figure 31: Julie Wilson-Foster Flotilla 2005 (Wilson-Foster) .....</b>	<b>37</b>
<b>Figure 32: Tanam Untuk Kehidupan Insect 2007 (Crosby).....</b>	<b>38</b>
<b>Figure 33: Adrian Kondratowicz Trash 2008 (Kondratowicz).....</b>	<b>38</b>
<b>Figure 34: John Dahlson Triptych 2005 (Dahlson).....</b>	<b>39</b>
<b>Figure 35: John Dahlson Thong Totems 2003 (Dahlson) .....</b>	<b>39</b>
<b>Figure 36: Elpida Hadzi-Vasileva Make A Wish 2011 (Gibson) .....</b>	<b>40</b>
<b>Figure 37: Andy Goldsworthy White Walls 2007 (Goldsworthy).....</b>	<b>41</b>
<b>Figure 38: Elizabeth Stanek, Andrea Thompson &amp; Valerie Ortani Fragile Ecologies 2006 (Binrock, 2006) .....</b>	<b>42</b>
<b>Figure 39: Elizabeth Stanek, Andrea Thompson &amp; Valerie Ortani Fragile Ecologies 2006 (Binrock, 2006) .....</b>	<b>42</b>
<b>Figure 40: Elizabeth Stanek, Andrea Thompson &amp; Valerie Ortani Fragile Ecologies 2006 (Binrock, 2006) .....</b>	<b>43</b>
<b>Figure 41: Ken Yonetani installing tiles (Hee) .....</b>	<b>44</b>
<b>Figure 42: Ken Yonetani Fumie Tiles 2003 (Hee) .....</b>	<b>44</b>
<b>Figure 43. Ken Yonetani Fumie Tiles 2003 (Hee).....</b>	<b>44</b>
<b>Figure 44: Steve Harrison Native Bai Tunze Bowl 2008 (Harrison) .....</b>	<b>47</b>
<b>Figure 45: Steve Harrison Native Bai Tunze Bowl 2008 (Harrison) .....</b>	<b>47</b>
<b>Figure 46: Classification of silicates on a structural basis (Bailey) .....</b>	<b>52</b>
<b>Figure 47: Diagram of the clay mineral family (Cardew, 1977).....</b>	<b>53</b>
<b>Figure 48: Open versus closed porosity (Jaouen, n.d.) .....</b>	<b>66</b>
<b>Figure 49: Effect of ashing temperature on specific surface area and average pore diameter.....</b>	<b>83</b>
<b>Figure 50: Specific surface area and specific pore volume of calcined RHA .....</b>	<b>84</b>
<b>Figure 51: Broadwater sugar mill .....</b>	<b>94</b>
<b>Figure 52: Number 1 boiler submerged ash hopper, Broadwater sugar mill.....</b>	<b>94</b>

<b>Figure 53: Number 12 boiler belt, Broadwater sugar mill.....</b>	<b>95</b>
<b>Figure 54: Number 1 boiler belt, Broadwater sugar mill.....</b>	<b>95</b>
<b>Figure 55: Below number 1 boiler belt, Broadwater sugar mill.....</b>	<b>96</b>
<b>Figure 56: Bagasse ash (number 1 boiler belt) calcined at 600°C.....</b>	<b>97</b>
<b>Figure 57: Bagasse ash (number 1 boiler belt) calcined at 700°C.....</b>	<b>97</b>
<b>Figure 58: Bagasse ash (number 1 boiler belt) calcined at 800°C.....</b>	<b>98</b>
<b>Figure 59: Bagasse ash (number 1 boiler belt) calcined at 900°C.....</b>	<b>98</b>
<b>Figure 60: Bagasse ash (number 1 boiler belt) calcined at 600°C.....</b>	<b>99</b>
<b>Figure 61: Bagasse ash (number 1 boiler belt) calcined at 700°C.....</b>	<b>100</b>
<b>Figure 62: Bagasse ash (number 1 boiler belt) calcined at 800°C.....</b>	<b>101</b>
<b>Figure 63: Bagasse ash (number 1 boiler belt) calcined at 900°C.....</b>	<b>102</b>
<b>Figure 64: Bagasse ash (number 1 boiler belt) calcined at 800°C and hand-ground.....</b>	<b>103</b>
<b>Figure 65: Bagasse ash (number 12 boiler belt) calcined at 600°C.....</b>	<b>104</b>
<b>Figure 66: Bagasse ash (number 12 boiler belt) calcined at 700°C.....</b>	<b>104</b>
<b>Figure 67: Bagasse ash (number 12 boiler belt) calcined at 800°C.....</b>	<b>105</b>
<b>Figure 68: Bagasse ash (number 12 boiler belt) calcined at 900°C.....</b>	<b>105</b>
<b>Figure 69: Bagasse ash (number 12 boiler belt) calcined at 600°C.....</b>	<b>106</b>
<b>Figure 70: Bagasse ash (number 12 boiler belt) calcined at 700°C.....</b>	<b>107</b>
<b>Figure 71: Bagasse ash (number 12 boiler belt) calcined at 900°C.....</b>	<b>108</b>
<b>Figure 72: Rice husk as received .....</b>	<b>109</b>
<b>Figure 73: RHA calcined at 600°C.....</b>	<b>110</b>
<b>Figure 74: RHA calcined at 700°C.....</b>	<b>110</b>
<b>Figure 75: RHA calcined at 800°C.....</b>	<b>111</b>
<b>Figure 76: RHA calcined at 900°C.....</b>	<b>111</b>
<b>Figure 77: RHA calcined at 600°C.....</b>	<b>112</b>
<b>Figure 78: RHA calcined at 700°C.....</b>	<b>113</b>
<b>Figure 79: RHA calcined at 800°C.....</b>	<b>114</b>
<b>Figure 80: RHA calcined at 900°C.....</b>	<b>115</b>
<b>Figure 81: RHA calcined at 800°C and hand-ground .....</b>	<b>116</b>
<b>Figure 82: Shredded husks and corn trash .....</b>	<b>117</b>
<b>Figure 83: Conveyor belt showing shelled cobs.....</b>	<b>117</b>
<b>Figure 84: Corn cob ash calcined at 600°C in open container.....</b>	<b>117</b>
<b>Figure 85: Corn cob ash charcoal from calcining at 600°C in closed container.....</b>	<b>118</b>
<b>Figure 86: Corn cob ash after calcining to 700°C .....</b>	<b>118</b>
<b>Figure 87: Corn cob ash after calcining at 800°C.....</b>	<b>119</b>

<b>Figure 88: Corn cob ash calcined at 600°C .....</b>	<b>120</b>
<b>Figure 89: Corn cob ash calcined at 700°C .....</b>	<b>121</b>
<b>Figure 90: Corn cob ash calcined at 800°C .....</b>	<b>122</b>
<b>Figure 91: Corn cob ash calcined at 900°C .....</b>	<b>123</b>
<b>Figure 92: Corn seeper sludge pipe .....</b>	<b>124</b>
<b>Figure 93: Corn seeper sludge vat .....</b>	<b>124</b>
<b>Figure 94: Corn seeper sludge as received .....</b>	<b>124</b>
<b>Figure 95: Corn seeper sludge calcined at 600°C .....</b>	<b>125</b>
<b>Figure 96: Corn seeper sludge calcined at 700°C .....</b>	<b>125</b>
<b>Figure 97: Corn seeper sludge calcined at 800°C .....</b>	<b>125</b>
<b>Figure 98: Corn seeper sludge calcined at 600°C .....</b>	<b>126</b>
<b>Figure 99: Corn seeper sludge calcined at 700°C .....</b>	<b>127</b>
<b>Figure 100: Corn seeper sludge calcined at 800°C .....</b>	<b>128</b>
<b>Figure 101: Corn seeper sludge calcined at 900°C .....</b>	<b>129</b>
<b>Figure 102: Recycled fibre bio-solids .....</b>	<b>130</b>
<b>Figure 103: Waste-water treatment plant bio-solids .....</b>	<b>130</b>
<b>Figure 104: Technical data for Unimin (Sibelco) cullet.....</b>	<b>131</b>
<b>Figure 105: Unimin cullet .....</b>	<b>132</b>
<b>Figure 106: Visy cullet conveyor belt dust as received .....</b>	<b>133</b>
<b>Figure 107: Visy cullet conveyor belt dust as received .....</b>	<b>134</b>
<b>Figure 108: Visy cullet conveyor belt dust as received .....</b>	<b>134</b>
<b>Figure 109: Visy cullet conveyor belt dust &lt;200 mesh .....</b>	<b>135</b>
<b>Figure 110: Comparison of Unimin cullet (left) and Visy conveyor belt dust &lt;200 mesh .....</b>	<b>136</b>
<b>Figure 111: Clear glass bottles crushed in the Bottlecycler crusher .....</b>	<b>137</b>
<b>Figure 112: Prego marble sawdust.....</b>	<b>138</b>
<b>Figure 113: Prego marble sawdust sweepings .....</b>	<b>138</b>
<b>Figure 114: Perlite AP10 white cold bag house fines .....</b>	<b>139</b>
<b>Figure 115: Perlite fines AP10 white .....</b>	<b>140</b>
<b>Figure 116: Perlite AP10 grey cold bag house fines .....</b>	<b>140</b>
<b>Figure 117: Perlite fines AP10 grey .....</b>	<b>141</b>
<b>Figure 118: Perlite unexpanded ore .....</b>	<b>142</b>
<b>Figure 119: Perlite: Unexpanded grey ore .....</b>	<b>142</b>
<b>Figure 120: Dunmore latite as received .....</b>	<b>143</b>
<b>Figure 121: Dunmore latite.....</b>	<b>144</b>
<b>Figure 122: Relief map showing location of Bungendore sand quarry....</b>	<b>145</b>
<b>Figure 123: Bungendore sand-mining plant .....</b>	<b>146</b>

<b>Figure 124: Flocculation of Bungendore tailings.....</b>	<b>146</b>
<b>Figure 125: Flocculated Bungendore tailings settling pond.....</b>	<b>146</b>
<b>Figure 126: Bungendore tailings silt pond .....</b>	<b>147</b>
<b>Figure 127: Bungendore sand quarry tailings as received .....</b>	<b>147</b>
<b>Figure 128: Bungendore tailings .....</b>	<b>148</b>
<b>Figure 129: Bungendore tailings hand-ground .....</b>	<b>149</b>
<b>Figure 130: Narrow field microscopy of Bungendore tailings .....</b>	<b>150</b>
<b>Figure 131: Relief map showing location of Marulan quarry .....</b>	<b>151</b>
<b>Figure 132: Marulan quarry blasting face .....</b>	<b>151</b>
<b>Figure 133: Marulan quarry crusher and washer .....</b>	<b>152</b>
<b>Figure 134: Marulan quarry wet sludge pond.....</b>	<b>152</b>
<b>Figure 135: Marulan quarry dried sludge pond.....</b>	<b>152</b>
<b>Figure 136: Marulan tailings, as received .....</b>	<b>153</b>
<b>Figure 137: Marulan tailings, as received .....</b>	<b>154</b>
<b>Figure 138: Narrow field microscopy of Marulan tailings .....</b>	<b>155</b>
<b>Figure 139: Water absorption of (left to right) English Bentonite, Arumpo Bentonite, Bungendore tailings, Marulan tailings, ball clay FX157</b>	
<b>Figure 140: English bentonite, Arumpo bentonite, Bungendore tailings, Marulan tailings, and ball clay FX, 24 hours after saturation...</b>	<b>158</b>
<b>Figure 141: Water absorption of English (left) and Arumpo bentonites ..</b>	<b>159</b>
<b>Figure 142: Stirring of five clay suspensions.....</b>	<b>160</b>
<b>Figure 143: Settling suspensions of (left to right) English bentonite, Arumpo bentonite, Bungendore tailings, Marulan tailings and Ball clay FX.....</b>	<b>162</b>
<b>Figure 144: Bungendore quarry tailings as received.....</b>	<b>164</b>
<b>Figure 145: Marulan quarry tailings as received .....</b>	<b>164</b>
<b>Figure 146: Sievings from Bungendore tailings.....</b>	<b>165</b>
<b>Figure 147: Sievings from Marulan tailings .....</b>	<b>165</b>
<b>Figure 148: Marulan extrusion.....</b>	<b>165</b>
<b>Figure 149: Bungendore extrusion.....</b>	<b>166</b>
<b>Figure 150: Bowl thrown from 100% Marulan tailings .....</b>	<b>166</b>
<b>Figure 151: Turned foot ring on bowl thrown from 100% Marulan tailings</b>	<b>167</b>
<b>Figure 152: Bowl thrown from 100% Marulan tailings and fired to 900° C</b>	<b>167</b>
<b>Figure 153: Bowl thrown from 100% Bungendore tailings.....</b>	<b>168</b>
<b>Figure 154: Bungendore bowl showing turned foot ring .....</b>	<b>168</b>
<b>Figure 155: Bowl of 50% Bungendore, 50% Marulan.....</b>	<b>169</b>
<b>Figure 156: Bowl thrown from Bungendore tailings fired to 800°C.....</b>	<b>169</b>

Figure 157: Bowl of 50% Bungendore, 50% Marulan tailings fired to 800°C .....	170
Figure 158: Bowl of 50% Bungendore, 50% Marulan tailings fired to 800°C .....	170
Figure 159: Diagram of triaxial (15 samples) .....	172
Figure 160: Triaxial blend preparation (15 sample) .....	172
Figure 161: BM1 triaxial for glaze/engobe tests .....	173
Figure 162: BM2 triaxial for glaze/engobe tests .....	173
Figure 163: Triaxial sample slips drying before kneading and bagging ..	173
Figure 164 (clockwise from top left): Template, 50 mm profile, extruder, needle cutter .....	174
Figure 165: Slab-cutting process .....	174
Figure 166: Extrusion process .....	175
Figure 167: 50-millimetre marking process .....	175
Figure 168: Measuring dried shrinkage .....	177
Figure 169: Nomenclature for Triaxial 'X' .....	177
Figure 170: Triaxial ACCL for glaze/engobe test .....	180
Figure 171: ACCL Triaxial samples bagged .....	181
Figure 172: ACCL 1 before kneading .....	182
Figure 173: ACCL 1 after kneading .....	182
Figure 174: ACCL 1 extrusions and template-cut slabs .....	183
Figure 175: ACCL 2 extrusions and template-cut slabs .....	183
Figure 176: ACCL 3 extrusions and template-cut slabs .....	183
Figure 177: ACCL 4 extrusions and template-cut slabs .....	184
Figure 178: ACCL 5 extrusions .....	184
Figure 179: ACCL 6 extrusions and template-cut slabs .....	184
Figure 180: ACCL 7 extrusions and template-cut slabs .....	184
Figure 181: ACCL 8 extrusions and template-cut slabs .....	185
Figure 182: ACCL 9 extrusions and template-cut slabs .....	185
Figure 183: ACCL 10 extrusions and template-cut slabs .....	185
Figure 184: ACCL 11 .....	185
Figure 185: ACCL 11 hand rolled samples .....	186
Figure 186: ACCL 12 hand rolled samples, extrusions and template-cut slab .....	186
Figure 187: ACCL 13 hand rolled samples, extrusions and template-cut slabs .....	186
Figure 188: ACCL 14 hand rolled samples, extrusions and template-cut slabs .....	187



Figure 189: ACCL 15 before Tylose addition.....	187
Figure 190: ACCL 15 hand-formed samples, extrusions and slab .....	187
Figure 191: Triaxial ACCL: Extrusion length after drying from 50mm .....	188
Figure 192: Triaxial ACCL: Wet to dry shrinkage (%), trimetric view .....	189
Figure 193: Triaxial ACCL: Wet to dry shrinkage (%), trimetric view, framing samples 1–3–6–10–15.....	189
Figure 194. Triaxial ACCL: Wet to dry percentage shrinkage, Trimetric view. Framing samples 1-2-4-7-11. ....	190
Figure 195. Triaxial ACCL: Wet to dry percentage shrinkage, Trimetric view. Framing samples 11-15.....	190
Figure 196: BM1.2 extrusions and template-cut slabs .....	193
Figure 197: BM1.3 extrusions and template-cut slabs .....	193
Figure 198: BM1.4 extrusions .....	193
Figure 199: BM1.5 extrusions and template-cut slabs .....	194
Figure 200: BM1.6 extrusions and template-cut slabs .....	194
Figure 201: BM1.7 extrusions and template-cut slabs .....	194
Figure 202: BM1.8 extrusions and template-cut slab .....	195
Figure 203: BM1.9 extrusions and template-cut slabs .....	195
Figure 204: BM1.10 extrusions and template-cut slabs .....	195
Figure 205: BM1.11 extrusions and template-cut slabs .....	195
Figure 206: BM1.12 extrusions and template-cut slab .....	196
Figure 207: BM1.13 extrusions and template-cut slabs .....	196
Figure 208: BM1.14 extrusions and template-cut slabs .....	196
Figure 209: BM1.15 extrusions and template-cut slabs .....	197
Figure 210: Triaxial BM1: Wet to dry shrinkage (%), dynamic view .....	198
Figure 211: Triaxial BM1: Wet to dry shrinkage (%), trimetric view (framing samples 1–3–6–10–15) .....	198
Figure 212: Triaxial BM1: Wet to dry shrinkage (%), trimetric view (framing samples 1–2–4–7–11) .....	198
Figure 213: Triaxial BM1: Wet to dry shrinkage (%), trimetric view (framing samples 11–15) .....	198
Figure 214: BM2.2 one day after microwaving to remove moisture .....	201
Figure 215: BM2.2 three days after microwaving, showing liquid run-off	201
Figure 216: BM2.3 extrusions and template-cut slabs .....	202
Figure 217: BM2.4 extrusions and template-cut slabs .....	202
Figure 218: BM2.5 extrusions and template-cut slabs .....	202
Figure 219: BM2.6 extrusions and template-cut slabs .....	202
Figure 220: BM2.7 extrusions and template-cut slabs .....	203

Figure 221: BM2.8 extrusions and template-cut slabs .....	203
Figure 222: BM 2.9 extrusions and template-cut slabs .....	203
Figure 223: BM2.10 extrusions and template-cut slabs .....	203
Figure 224: Triaxial BM2: Wet to dry shrinkage (%), trimetric view.....	206
Figure 225: Triaxial BM2: Wet to dry shrinkage (%), trimetric view, framing samples 4–7–11.....	206
Figure 226: Triaxial BM2: Wet to dry shrinkage (%), trimetric view, framing samples 3–6–10–15.....	206
Figure 227: Triaxial BM2: Wet to dry shrinkage (%), trimetric view, framing samples 11–15.....	206
Figure 228: Triaxial BM2: Wet to dry shrinkage (%), trimetric view, framing samples 7–10.....	206
Figure 229: Standard firing schedule.....	207
Figure 230: Kiln shelf with labelled samples .....	208
Figure 231: Slump test set-up.....	208
Figure 232: Triaxial ACCL. Extrusions fired to 800°C.....	208
Figure 233: Triaxial ACCL. Dry to 800°C shrinkage (%), trimetric view....	210
Figure 234: Triaxial ACCL. Dry to 800°C shrinkage (%), trimetric view. Framing samples 1–3–6–10–15.....	210
Figure 235: Triaxial ACCL. Dry to 800°C shrinkage (%), trimetric view. Framing samples 1–2–4–7–11.....	210
Figure 236: Triaxial ACCL. Dry to 800°C shrinkage (%), trimetric view. Framing samples 11–15.....	210
Figure 237: Triaxial ACCL. Dry to 800°C shrinkage (%), trimetric view. Framing samples 3-5-8-12 .....	210
Figure 238: Triaxial ACCL. Dry to 800°C shrinkage (%), dynamic view. Framing samples 1(at left)–15(at right) .....	210
Figure 239: ACCL. Curvilinear shrinkage trend: samples 11–15.....	211
Figure 240: Triaxial ACCL. Wet to 800°C shrinkage (%), trimetric view...	212
Figure 241: Triaxial ACCL. Wet to 800°C shrinkage (%), trimetric view. Framing samples 1–3–6–10–15 .....	212
Figure 242: Triaxial ACCL. Wet to 800°C shrinkage (%), trimetric view. Framing samples 1–2–4–7–11 .....	212
Figure 243: Triaxial ACCL. Wet to 800°C shrinkage (%), trimetric view. Framing samples 11–15.....	212
Figure 244: Triaxial ACCL. Wet to 800°C shrinkage (%), trimetric view. Framing samples 2–5–9–14 .....	212
Figure 245: Triaxial ACCL. Fired to 800°C .....	213
Figure 246: ACCL Triaxial slump tests after firing to 800°C .....	213
Figure 247: ACCL11 floating ceramic sample .....	214

Figure 248: Triaxial BM1. Wet to 800°C shrinkage (%), trimetric view .....	216
Figure 249: Triaxial BM1. Wet to 800°C shrinkage (%), trimetric view. Framing samples 3–6–10–15 .....	216
Figure 250: Triaxial BM1. Wet to 800°C shrinkage (%), trimetric view. Framing samples 2–4–7–11 .....	216
Figure 251: Triaxial BM1. Wet to 800°C shrinkage (%), trimetric view. Framing samples 11–15.....	216
Figure 252: Triaxial BM1. Dry to 800°C shrinkage (%), trimetric view showing expansion samples 14 & 15 .....	218
Figure 253: Triaxial BM1. Dry to 800°C shrinkage (%), trimetric view. Framing samples 3–6–10–15 .....	218
Figure 254: Triaxial BM1. Dry to 800°C shrinkage (%), trimetric view. Framing samples 2–4–7–11 .....	218
Figure 255: Triaxial BM1. Dry to 800°C shrinkage (%), trimetric view. Framing samples 11–15.....	218
Figure 256: Triaxial BM1. Fired to 800°C. Samples 2–15.....	218
Figure 257: Triaxial BM1 slump tests after firing to 800°C: Samples BM1.2- BM1.15.....	219
Figure 258: Triaxial BM1: Samples BM1.2–BM1.15 after firing to (from top to bottom) 800, 850, 900 and 950°C .....	220
Figure 259: Triaxial BM1 samples BM1.2 and BM1.3 fired to 800 (top) and 850°C .....	221
Figure 260: Samples BM1.7–BM1.10 after firing (from top to bottom) to 800, 850, 900 and 950°C.....	222
Figure 261: Samples BM1.7–BM1.10 after firing (from top to bottom) to 800, 850, 900 and 950°C .....	222
Figure 262: Triaxial BM2 fired to 800°C. Samples 3–15.....	223
Figure 263: Triaxial BM2 fired to 800°C. Samples 3–15.....	223
Figure 264: Triaxial BM2. Slump tests fired to 800°C: samples BM2.3–BM2.10 .....	224
Figure 265: Triaxial BM2. Dry to 800°C shrinkage (%), trimetric view. Framing expanded samples.....	225
Figure 266: Triaxial BM2. Dry to 800°C shrinkage (%), trimetric view. Framing samples 11–15.....	225
Figure 267: Triaxial BM2. Dry to 800°C shrinkage (%), trimetric view. Framing samples 6–10–15 .....	225
Figure 268: Triaxial BM2. Dry to 800°C shrinkage (%), trimetric view. Framing samples 5–9–14 .....	225
Figure 269: Triaxial BM2. Wet to 800°C shrinkage (%), trimetric view. ....	229
Figure 270: Triaxial BM2. Wet to 800°C shrinkage (%), trimetric view. Framing samples 4–7–11 .....	229

Figure 271: Triaxial BM2. Wet to 800°C shrinkage (%), trimetric view. Framing samples 11–15.....	229
Figure 272: Triaxial BM2. Wet to 800°C shrinkage (%), trimetric view. Framing samples 6–10–15 .....	229
Figure 273: Triaxial BM2. Wet to 800°C shrinkage (%), trimetric view. Framing samples 7–10 .....	229
Figure 274: Samples BM2.4–BM2.6 after firing to 800°C .....	230
Figure 275: Samples BM2.7–BM2.10 after firing (top to bottom) to 800, 850, 900 and 950°C.....	230
Fig 276: Domestic use of rice husk stove.....	233
Figure 277: Burnt rice husk in biomass gasifier .....	234
Figure 278: Metal rubbish bin .....	235
Figure 279: Re-used kiln lid .....	235
Figure 280: Rubbish bin with spy-hole .....	235
Figure 281: Secured fibre blanket .....	235
Figure 282: Rubbish bin kiln in position.....	236
Figure 283: Rice husk stove in position .....	236
Figure 284: Charcoal stove in position .....	236
Figure 285: Rice husk and charcoal firing chart .....	237
Figure 285: Corn cobs drying on kiln.....	238
Figure 287: Dried and charred cobs.....	238
Figure 288: Charcoal stove with dried cobs .....	238
Figure 289: Cobs burning without primary air .....	238
Figure 290: Cobs burning with primary air .....	238
Figure 291: Cobs nearing complete combustion .....	238
Figure 292: Corn cob and charcoal firing chart .....	239
Figure 293: Equipment and materials for experimental production of sodium silicate .....	240
Figure 294: Mix 1: 30g RHA, 100ml Drain Clear, 50ml Water.....	240
Figure 295: Mix 2: 30g RHA, 60ml Drain Clear, 90ml Water.....	240
Figure 296: Mix 3: 30g RHA, 60ml Drain Clear, 140ml Water.....	240
Figure 297: Three mixes ready for firing.....	240
Figure 298: Split kiln shelf, spilt mixes .....	240
Figure 299: Filling sample holders .....	242
Figure 300: Prepared sample holders .....	242
Figure 301: Loading samples into rack.....	242
Figure 302: PANanalytical Xpert diffractometer.....	242
Figure 303: XRD chart: Marulan tailings .....	247

Figure 304: XRD chart: Marulan tailings (re-test).....	248
Figure 305: XRD chart: Bungendore tailings.....	249
Figure 306: XRD chart: Bungendore tailings (re-test) .....	250
Figure 307: XRD chart: Dunmore latite .....	251
Figure 308: XRD chart: Perlite CBHF AP10 (white).....	252
Figure 309: XRD chart: #12 boiler belt ash (1 hour at 800°C).....	253
Figure 310: XRD chart: #1 boiler belt ash (1 hour at 800°C).....	254
Figure 311: XRD chart: RHA (1 hour at 800°C) .....	255
Figure 312: XRD chart: Corn seeper sludge ash (1 hour at 800°C) .....	256
Figure 313: XRD chart: Arumpo bentonite.....	257
Figure 314: Mineralogical and chemical properties of two samples of Arumpo bentonite .....	257
Figure 315: XRD chart: English bentonite .....	258
Figure 316: XRD chart: Australian bentonite.....	259
Figure 317: XRD chart: Corn cob ash (1 hour at 800°C) .....	260
Figure 318: WEW engobe applied to BM1.13 bisque and fired to 950°C (unglazed) .....	264
Figure 319: CB1 slip applied to BM1.13 bisque and fired to 950°C (unglazed) .....	264
Figure 320: BM1 Triaxial fired to 900°C.....	265
Figure 321: BM2 Triaxial fired to 900°C.....	266
Figure 322: Glaze BM2.2 applied to raw and bisque BM1.13, and over engobe, fired to 900°C .....	268
Figure 323: Glaze BM2.2 applied to bisque BM1.13, and over raw and bisque engobe, fired to 900°C.....	269
Figure 324: Glaze BM2.2B applied to raw and bisque BM1.13, and over engobe, fired to 900°C .....	270
Figure 325: Glaze BM2.2B applied to high bisque BM1.13 with engobe, and to Walker's white raku body, and fired to 900°C .....	271
Figure 326: BM2.2 glaze on 800°C bisque BM1.13 bowl, seeping after being fired to 900°C, filled with water, and left to stand overnight.....	272
Figure 327: Towers thrown from BM2.7 (left) and BM2.9 .....	276
Figure 328: Melted towers at 950°C: BM2.7 (left) and BM2.9 .....	277
Figure 329: B1 extrusions and template-cut slabs .....	279
Figure 330: Towers made from BM1.11 (left) and B1, fired to 950°C.....	279
Figure 331: BM1.14 (top) and BM1.14C fired to 1050°C.....	281
Figure 332: BM1.14 (top) and BM1.14C fired to 1100°C.....	282
Figure 333: Common flux ranges .....	285

<b>Figure 334: Eutectic points .....</b>	<b>286</b>
<b>Figure 335: Scaled up triaxial blending .....</b>	<b>305</b>
<b>Figure 336: Extrusions .....</b>	<b>305</b>
<b>Figure 337: Slabs cut with needle tool.....</b>	<b>305</b>
<b>Figure 338: Bars marked for shrinkage .....</b>	<b>306</b>
<b>Figure 339: Efflorescence test disc.....</b>	<b>307</b>
<b>Figure 340: Test tiles .....</b>	<b>307</b>
<b>Figure 341: Triaxial sample range .....</b>	<b>307</b>
<b>Figure 342: Dried test pieces .....</b>	<b>308</b>
<b>Figure 343: BM11.3 efflorescence test.....</b>	<b>312</b>
<b>Figure 344: Efflorescence tests: Unfired discs of BM11 triaxial samples 1–10 .....</b>	<b>313</b>
<b>Figure 345: BM11 sample discs fired to 900°C: Extent of efflorescence and self-glazing on samples 1–6 .....</b>	<b>314</b>
<b>Figure 346: All BM11 sample discs fired to 900°C: Extent of efflorescence and self-glazing.....</b>	<b>315</b>
<b>Figure 347: Triaxial BM11. Wet to dry shrinkage (%), trimetric view.....</b>	<b>317</b>
<b>Figure 348: Triaxial BM11. Wet to dry shrinkage (%), trimetric view. Framing samples 1–2–4–7–11 .....</b>	<b>317</b>
<b>Figure 349: Triaxial BM11. Wet to dry shrinkage (%), trimetric view. Framing samples 1–3–6–10–15 .....</b>	<b>317</b>
<b>Figure 350: Triaxial BM11. Wet to dry shrinkage (%), trimetric view. Framing samples 11–15.....</b>	<b>317</b>
<b>Figure 351: BM11 triaxial fired to 850°C.....</b>	<b>317</b>
<b>Figure 352: Triaxial BM11. Dry to 850°C shrinkage (%), trimetric view ....</b>	<b>319</b>
<b>Figure 353: Triaxial BM11. Dry to 850°C shrinkage (%), trimetric view. Framing samples 1–2–4–7–11 .....</b>	<b>319</b>
<b>Figure 354: Triaxial BM11. Dry to 850°C shrinkage (%), trimetric view. Framing samples 1–3–6–10–15 .....</b>	<b>319</b>
<b>Figure 355: Triaxial BM11. Dry to 850°C shrinkage (%), trimetric view. Framing samples 11–15.....</b>	<b>319</b>
<b>Figure 356: BM11 triaxial fired to 900°C.....</b>	<b>319</b>
<b>Figure 357: Triaxial BM11. Dry to 900°C shrinkage (%), trimetric view ....</b>	<b>321</b>
<b>Figure 358: Triaxial BM11. Dry to 900°C shrinkage (%), trimetric view. Framing samples 1–2–4–7–11.....</b>	<b>321</b>
<b>Figure 359: Triaxial BM11. Dry to 900°C shrinkage (%), trimetric view. Framing samples 1–3–6–10–15.....</b>	<b>321</b>
<b>Figure 360: Triaxial BM11. Dry to 900°C shrinkage (%), trimetric view. Framing samples 11–15.....</b>	<b>321</b>
<b>Figure 361: BM11 triaxial fired to 950°C.....</b>	<b>321</b>

Figure 362: Triaxial BM11. Dry to 950°C shrinkage (%), trimetric view ....	323
Figure 363: Triaxial BM11. Dry to 950°C shrinkage (%), trimetric view. Framing samples 2-4-7-11 .....	323
Figure 364: Triaxial BM11. Dry to 950°C shrinkage (%), trimetric view. Framing samples 6-10-15 .....	323
Figure 365: Triaxial BM11. Dry to 950°C shrinkage (%), trimetric view. Framing samples 11-15.....	323
Figure 366: BM11 triaxial fired to 1000°C.....	323
Figure 367: Triaxial BM11. Dry to 1000°C shrinkage (%), trimetric view ..	325
Figure 368: Triaxial BM11. Dry to 1000°C shrinkage (%), trimetric view. Framing samples 2-4-7-11 .....	325
Figure 369: Triaxial BM11. Dry to 1000°C shrinkage (%), trimetric view. Framing samples 6-10-15 .....	325
Figure 370: Triaxial BM11. Dry to 1000°C shrinkage (%), trimetric view. Framing samples 11-15.....	325
Figure 371: Dried and fired test bars separated with spacers prior to addition of distilled water .....	326
Figure 372: Dried and fired test bars soaking in distilled water .....	326
Figure 373: Apparatus for determining volume of fired bars using Archimedes' principle.....	326
Figure 374: Triaxial BM11. Absorption at 850°C, top view .....	328
Figure 375: Triaxial BM11. Absorption at 850°C, trimetric view .....	329
Figure 376: Triaxial BM11. Absorption at 850°C, trimetric view. Samples 1-2-4-7-11.....	329
Figure 377: Triaxial BM11. Absorption at 850°C, trimetric view. Samples 1-3-6-10-15.....	329
Figure 378: Triaxial BM11. Absorption at 850°C, trimetric view. Samples 11-15.....	329
Figure 379: BM11 triaxial. Absorption at 900°C, top view .....	331
Figure 380: BM11 triaxial. Absorption at 900°C, trimetric view. Samples 1-2-4-7-11.....	331
Figure 381: BM11 triaxial. Absorption at 900°C, trimetric view. Samples 1-3-6-10-15.....	331
Figure 382: BM11 triaxial. Absorption at 900°C, trimetric view. Samples 11-15.....	331
Figure 383: BM11 triaxial. Absorption at 950°C, trimetric view .....	333
Figure 384: BM11 triaxial. Absorption at 950°C, trimetric view. Samples 2-4-7-11 .....	333
Figure 385: BM11 triaxial. Absorption at 950°C, trimetric view. Samples 6-10-15.....	333

Figure 386: BM11 triaxial. Absorption at 950°C, trimetric view. Samples 11-15 .....	333
Figure 387: BM11 triaxial. Absorption at 1000°C.....	335
Figure 388: BM11 triaxial. Absorption at 1000°C.....	335
Figure 389: BM11 triaxial. Absorption at 1000°C, trimetric view. Samples 2-4-7-11.....	335
Figure 390: BM11 triaxial. Absorption at 1000°C, trimetric view. Samples 11-15.....	335
Figure 391: BM11 triaxial. Absorption at 1000°C, trimetric view. Samples 6-10-15.....	335
Figure 392: BM11 triaxial. Absorption at 1000°C, trimetric view. Samples 7-10.....	335
Figure 393: BM11.1: 850°C (top) and 900°C.....	337
Figure 394: BM11.1 porosity and shrinkage.....	337
Figure 395: BM11.2: 850 (top), 900, 950 and 1000°C.....	338
Figure 396: BM11.2 porosity and shrinkage.....	338
Figure 397: BM11.3: 850 (top) and 900°C.....	339
Figure 398: BM11.3 porosity and shrinkage.....	339
Figure 399: BM11.4: 850 (top), 900, 950 and 1000°C.....	340
Figure 400: BM11.4 porosity and shrinkage.....	340
Figure 401: BM11.5: 850 (top), 900, 950 and 1000°C.....	341
Figure 402: BM11.5 porosity and shrinkage.....	341
Figure 400: BM11.6: 850 (top), 900, 950 and 1000°C.....	342
Figure 404: BM11.6 porosity and shrinkage.....	342
Figure 405: BM11.7: 850 (top), 900, 950 and 1000°C.....	343
Figure 406: BM11.7 porosity and shrinkage.....	343
Figure 407: BM11.8: 850 (top), 900, 950 and 1000°C.....	344
Figure 408: BM11.8 porosity and shrinkage.....	344
Figure 409: BM11.9: 850 (top), 900, 950 and 1000°C.....	345
Figure 410: BM11.9 porosity and shrinkage.....	345
Figure 411: BM11.10: 850 (top), 900, 950 and 1000°C.....	346
Figure 412: BM11.10 porosity and shrinkage.....	346
Figure 413: BM11.11: 850 (top), 900, 950 and 1000°C.....	347
Figure 414: BM11.11 porosity and shrinkage.....	347
Figure 415: BM11.12: 850 (top), 900, 950 and 1000°C.....	348
Figure 416: BM11.12 porosity and shrinkage.....	348
Figure 417: BM11.13: 850 (top), 900, 950 and 1000°C.....	349
Figure 418: BM11.13 porosity and shrinkage.....	349



Figure 419: BM11.14: 850 (top), 900, 950 and 1000°C .....	350
Figure 420: BM11.14 porosity and shrinkage .....	350
Figure 421: BM11.15: 850 (top), 900, 950 and 1000°C .....	351
Figure 422: BM11.15 porosity and shrinkage .....	351
Figure 423: BM11.6 self-glazed exposed side (top) and unglazed protected side after firing to 1050°C.....	355
Figure 424: Bm11.9 fired to 1100°C .....	356
Figure 425: BM11.10 after firing to 1050°C: Exposed (top) and protected surfaces .....	357
Figure 426: BM11.10 fired to 1100°C: Exposed surface .....	357
Figure 427: BM11.10 fired to 1100°C: Protected surface.....	358
Figure 428: Effloresced exposed sides (left) and unaffected protected sides (right) of BM11.2 (top), BM11.4, BM11.5, and BM11.6 (bottom) after firing to 1000°C .....	360
Figure 429: Efflorescence comparison of BM11.6 (top) and BM11.6A treated with barium carbonate to reduce efflorescence.....	363
Figure 430: Efflorescence comparison of BM11.6 (top) and BM11.6A fired to 1000°C.....	363
Figure 431: BM11.6 self-glazed exposed side (top) and unglazed protected side after firing to 1050°C.....	364
Figure 432: BM11.6A unglazed exposed side (top) and unglazed protected side after firing to 1050°C.....	364
Figure 433: Test disc of BM11.2 fired to 950°C .....	366
Figure 434: Apparatus for stress tests .....	367
Figure 435: Four-point stress test used for bars .....	367
Figure 436: Ring stress test used for discs.....	368
Figure 437: Triaxial BM11: Glaze/engobe tests at (l to r) 1000, 1100, 1200 and 1280°C.....	375
Figure 438: Triaxial recycle 1: Gas fired to 1280°C (light reduction).....	376
Figure 439: Triaxial recycle 1 fired to 1200°C.....	379
Figure 440: Triaxial recycle1 fired to 1100°C.....	386
Figure 441: Triaxial R1 fired to 1000°C.....	391
Figure 442: Triaxial recycle 1 .....	395
Figure 443: Low-fire corn ash 1 at (l to r) 950, 1000, 1050 and 1100°C.....	399
Figure 444: Lithium 60 low COE at 950°C (left), and 1000°C (centre & right).....	400
Figure 445: Glaze triaxial low-fire 1, 1000°C .....	402
Figure 446: Reflectivity of glazes in triaxial low-fire 1 after firing to 1000°C .....	403

Figure 447: Magnified angle view of L1.14 fired to 1000°C showing floating wrinkled flakes reflecting light.....	405
Figure 448: Low-fire sugarcane ash at (l to r) 950, 1000, 1050 and 1100°C	411
Figure 449: Low-fire RHA glaze at (l to r) 950, 1000, 1050 and 1100°C.....	412
Figure 450: Low-fire 2 triaxial after firing to 950°C .....	413
Figure 451: Low-fire 2 triaxial after firing to 1000°C .....	414
Figure 452: Low-fire 2 triaxial after firing to 1000°C showing reflectivity	414
Figure 453: Low-fire corn/sugarcane ash at (l to r) 950, 1000, 1050 and 1100°C.....	417
Figure 454: Low-fire rock at (l to r) 950, 1000, 1050 and 1100°C.....	418
Table 87: Glaze triaxial low-fire 4: Corner recipes .....	419
Figure 455: Low-fire 4 triaxial at 950°C .....	419
Figure 456: Low-fire 4 triaxial at 1000°C .....	420
Figure 457: Low-fire 4 triaxial at 1050°C .....	420
Figure 458: Low-fire 4 corner glazes A,B,C (l-r) at 1100 °C .....	421
Figure 459: Low-fire Bungendore at (l to r) 950, 1000, 1050 and 1100°C .	421
Figure 460: Low-fire Marulan at (l to r) 950, 1000, 1050 and 1100°C.....	422
Figure 461: Glaze 1 and 2 on different combinations of body and slip, fired to 850°C.....	423
Figure 462: Glaze 3 and 4 on different combinations of body and engobe, fired to 850°C.....	424
Figure 463: Glaze 3 and 4 on four different bodies, 900°C.....	425
Figure 464: Glaze 5 and 6 on four different bodies, 900°C.....	426
Figure 465: Glazes 7–11 on selected bodies and engobes, 950°C .....	427
Figure 466: Glazes 12–15 on selected bodies and engobes, 950°C .....	428
Figure 467: Glazes 7–10 on selected bodies and engobes, 980°C .....	429
Figure 468: Glazes 11–14 on selected bodies and engobes, 980°C .....	430
Figure 469: Glaze 15 on selected bodies and engobes, 980°C .....	431
Figure 470: Glazes 7–10 on selected bodies and engobes, 1000°C .....	432
Figure 471: Glazes 11–14 on selected bodies and engobes, 1000°C .....	433
Figure 472: Glaze 15 on selected bodies and engobes, 1000°C .....	434
Figure 473: Colourant additions to glazes applied to raw Marulan cone 08 high expansion engobe, over raw BM11.3, 850°C.....	435
Figure 474: Colourant additions to glazes applied to raw Marulan cone 08 high expansion engobe (E6), over raw BM11.3A, 900°C.....	438
Figure 475: Colourant additions to glazes 7–10 applied to raw BM11.2, 950°C.....	439
Figure 476: Colourant additions to glazes 11–15 applied to raw BM11.2, 950°C.....	440

Figure 477: Colourant additions to glazes 7–10 applied to raw BM11.6B, 950°C .....	441
Figure 478: Colourant additions to glazes 11–15 applied to raw BM11.6B, 950°C .....	442
Figure 479: Colourant additions to glazes 7–11 applied to raw BM11.6A, 1000°C .....	443
Figure 480: Colourant additions to glazes 12–15 applied to raw BM11.6A, 1000°C .....	444
Figure 481: Bowl thrown from BM11.6A, bisque fired to 700°C .....	448
Figure 482: Bowl: BM11.6A, bisque fired to 700°C, showing turned foot ring .....	448
Figure 483: Bowl thrown from BM11.6A, bisque fired to 700°C .....	449
Figure 484: Bowl: BM11.6A, bisque fired to 700°C, showing turned foot ring .....	449
Figure 485: Bowl thrown from BM11.6A, bisque fired to 700°C .....	450
Figure 486: Bowl: BM11.6A, bisque fired to 700°C, showing turned foot ring .....	450
Figure 487: Cone 08 after reading 940°C .....	452
Figure 488: Cone 08 after reading 950°C .....	452
Figure 489: Bowl 1 thrown from BM11.6A, fired to 940°C, Glaze 17.4.....	453
Figure 490: Bowl 1 thrown from BM11.6A, fired to 940°C, Glaze 17.4.....	453
Figure 491: Bowl 2 thrown from BM11.6A, fired to 950°C, Glaze 17.4.....	454
Figure 492: Bowl 2 thrown from BM11.6A, fired to 950°C, Glaze 17.4.....	454
Figure 493: Bowl 2: BM11.6A, fired to 950°C, Self-glazed exterior, unglazed foot ring .....	455
Figure 494: Bowl 3: BM11.6A fired to 940°C. Glazes 17.2 (interior) and 17.4 (rim) .....	455
Figure 495: Bowl 3: BM11.6A fired to 940°C. Glazes 17.2 (interior) and 17.4 (rim) .....	456
Figure 496: Bowl 3: BM11.6A, 940°C. Self-glazed exterior, unglazed foot ring. Glaze 17.4 (rim).....	456
Figure 497: Bowl 4: BM11.6A fired to 950°C. Glazes 17.2 (interior) and 17.4 (rim) .....	457
Figure 498: Bowl 4: BM11.6A fired to 950°C. Glazes 17.2 (interior) and 17.4 (rim) .....	457
Figure 499: Bowl 4: BM11.6A, 950°C. Glaze 13.4 (rim). Self-glazed exterior, unglazed foot ring .....	458
Figure 500: Bagged and labelled pugs of experimental clays .....	459
Figure 501: Bowl thrown by Geoff Crispin from BM11.6B, bisque fired to 800°C .....	459
Figure 502: Vase by Geoff Crispin from BM11.6B, bisque fired to 800°C	460

Figure 503: Bowl by Geoff Crispin. BM11.6B, glazed with 13.1 and fired to 975°C .....	461
Figure 504: Bowl by Geoff Crispin. BM11.6B, glazed with 7.4 and fired to 975°C .....	461
Figure 505: Bowl 5: BM11.6B, 950°C. Glaze 18.4.....	462
Figure 506: Bowl 6: BM11.6B, 950°C. Glaze 19 without colourant addition	464
Figure 507: Bowl 7: BM11.6B, 950°C. Glaze 19 with 4% copper carbonate	464
Figure 508. BM11.6B 50: 50 WMF blend fired to 900°C. 15x20cm.....	467
Plate 1. Brett Smout Thin Air Bottling. 2010. South Coast, NSW, Australia. (Rigg, W.) .....	532
Plate 2. Brett Smout Thin Air Bottling (2). 2010. South Coast, NSW, Australia.....	533
Plate 3. Thin Air 'marketing shots' .....	535
Plate 4. Thin Air 'marketing shots' 2.....	536
Plate 5. Brett Smout Crack Wrap 2010 .....	539
Plate 6. Destruction of Tinsley Cooling Towers [Siandara (2008)] .....	548
Plate 7. Wallerawang, NSW cooling tower .....	551
Plate 8. Pylon at Wallerawang, NSW. ....	552
Plate 9. Pylon at Sherbrook, NSW. ....	552
Plate 10. Pylon at Auckland, NZ.....	552
Plate 11. Pylon at Sherbrook, NSW. ....	552
Plate 12. Shukhov Oka Towers 1988. ( Kazus, I.) .....	555
Plate 13. Shukhov Oka Tower 2006 (Tomilov, V.).....	556
Plate 14. Shukhov tower destroyed (Mihadzr, 2005c).....	557
Figure 508: BM11.6B 50: 50 WMF blend fired to 900oC. 15x20cm.....	497

## List of Tables

Table 1: Tichane's (1990) earthenware body recipes .....	27
Table 2: Shrinkage, firing range and vitrification point of some commercially available Australian clays.....	28
Table 3: Typical energy content of fossil and biomass fuels .....	79
Table 4: RHA analyses (wt%) .....	82
Table 5: Content of carbon, hydrogen and nitrogen: rice husk and RHA at 500°C .....	83
Table 6: Need of crushing and extent of sintering of selected wastes (Whitfield, 1993).....	89
Table 7: Analyses of selected wastes (adapted from Whitfield, 2003) .....	90
Table 8: Analyses of selected crushed wastes (Whitfield, 1993) .....	91
Table 9: Selected elements from Norske Skog analysis .....	130
Table 10: Fractions obtained from Visy conveyor belt cullet dust .....	135
Table 11: Elapsed time for absorption of 50 mg in 300 ml water: five clays....	156
Table 12: Triaxial ACCL: Corner recipes .....	179
Table 13: Triaxial ACCL: Blend recipes (wt%) .....	180
Table 14: Triaxial ACCL: Dry length at 50 mm wet .....	188
Table 15: Triaxial ACCL: Wet to dry percentage shrinkage .....	188
Table 16: Triaxial ACCL: Wet to dry percentage shrinkage .....	189
Table 17: Triaxial BM1: Batch corner recipes .....	191
Table 18: Triaxial BM1: Blend recipes (wt%) .....	192
Table 19: Triaxial BM1: Wet to dry shrinkage .....	197
Table 20: Triaxial BM1: Wet to dry shrinkage .....	198
Table 21: Triaxial BM2: Corner recipes.....	200
Table 22: Triaxial BM2: Sample recipes (wt%) .....	200
Table 23: Triaxial BM2: Wet to dry shrinkage .....	204
Table 24: Triaxial BM2: Wet to dry shrinkage .....	204
Table 25: ACCL blend samples: Dry to 800°C shrinkage .....	209
Table 26: ACCL triaxial: Dry to 800°C shrinkage .....	209
Table 27: ACCL: Wet to 800°C shrinkage.....	211
Table 28: Triaxial BM1: Shrinkage from wet to 800°C .....	215
Table 29: Triaxial BM1: Wet to 800°C shrinkage .....	215
Table 30: Triaxial BM1: Dry to 800°C shrinkage/expansion.....	216
Table 31: Triaxial BM1: Dry to 800°C shrinkage .....	217
Table 32: Triaxial BM1 slump test result .....	221

Table 33: Triaxial BM2: Dry to 800°C shrinkage .....	224
Table 34: Triaxial BM2: Dry to 800°C shrinkage .....	225
Table 35: Triaxial BM2: Wet to 800°C shrinkage .....	228
Table 36: Triaxial BM2: Wet to 800°C shrinkage .....	228
Table 37: Triaxial BM2 slump test results .....	231
Table 38: Percentage analysis of English bentonite .....	258
Table 39: Typical chemical composition of Australian bentonite.....	259
Table 40: Percentage analyses of recovered materials .....	262
Table 41: Batch recipes for glazes BM2.2 and BM2.2B.....	267
Table 42: White engobe batch recipe conversions .....	273
Table 43: Coefficients of expansion (COE) and estimated melting temperatures of engobe fluxes.....	274
Table 44: Coefficients of expansion (COE) of experimental engobes.....	275
Table 45: Batch recipes: BM1.14 and BM1.14C .....	281
Table 46: Flux material properties.....	287
Table 47: J. T. Baker SAF-T-DATA labelling system: Storage colour codes ..	292
Table 48: Collated hazard information (part one).....	294
Table 49: Collated hazard information (part two) .....	295
Table 50: Advantages and disadvantages of cone 06 talc body .....	301
Table 51: BM11 triaxial blend recipes .....	304
Table 52: BM11 triaxial: Handling properties .....	310
Table 53: BM11 triaxial: Handling properties (continued) .....	311
Table 54: BM11 triaxial: Handling properties (continued) .....	312
Table 55: BM11 triaxial blend: Wet to dry shrinkage.....	315
Table 56: BM11 triaxial blend: Wet to dry shrinkage.....	316
Table 57: BM11 Triaxial blend: Dry to 850°C shrinkage .....	318
Table 58: BM11 triaxial blend: Dry to 850°C shrinkage.....	318
Table 59: BM11 triaxial blend: Dry to 900°C shrinkage.....	320
Table 60: BM11 triaxial blend: Dry to 900°C shrinkage.....	320
Table 61: BM11 triaxial blend: Dry to 950°C shrinkage.....	322
Table 62: BM11 triaxial blend: Dry to 950°C shrinkage.....	322
Table 63: BM11 triaxial blend: Dry to 1000°C shrinkage.....	324
Table 64: BM11 triaxial blend: Dry to 1000°C shrinkage.....	324
Table 65: BM11: Absorption and porosity measurements after firing to 850°C	327
Table 66: Triaxial BM11: Absorption after firing to 850°C .....	328
Table 67: Triaxial BM11: Absorption and porosity after firing to 900°C .....	330
Table 68: BM11 triaxial: Absorption after firing to 900°C .....	330

Table 69: BM11 triaxial: 950°C absorption and porosity .....	<b>332</b>
Table 70: BM11 triaxial: Absorption after firing to 950 °C .....	<b>332</b>
Table 71: BM11 triaxial: Absorption and porosity after firing to 1000°C .....	<b>334</b>
Table 72: BM11 triaxial: Absorption after firing to 1000°C .....	<b>334</b>
Table 73: Bodies selected for further experiment.....	<b>353</b>
Table 74: Batch recipes of BM11.6 and BM11.6A .....	<b>362</b>
Table 75: Equivalent 60 second stress test: weighted average of bars and disks.....	<b>369</b>
Table 76: Triaxial R1: Corner recipes .....	<b>373</b>
Table 77: Triaxial recycle 1: Blend recipes .....	<b>374</b>
Table 78: Triaxial recycle 1: Blend formulae .....	<b>374</b>
Table 79: Triaxial recycle 1: Ionic potentials .....	<b>395</b>
Table 80: Expansion coefficients and estimated melting temperatures of analysed raw materials .....	<b>396</b>
Table 81: Expansion coefficients and estimated firing temperatures of selected fluxes and frits.....	<b>397</b>
Table 82: Expansion coefficients and estimated firing temperatures of low-fire glaze recipes.....	<b>398</b>
Table 83: Glaze triaxial low-fire 1: Corner recipes .....	<b>398</b>
Table 84: Glaze triaxial low-fire 1: Blend recipes .....	<b>401</b>
Table 85: Glaze triaxial low-fire 2: Corner recipes .....	<b>411</b>
Table 86: Glaze triaxial low-fire 3: Corner recipes .....	<b>417</b>
Table 87: Glaze triaxial low-fire 4: Corner recipes .....	<b>419</b>
Table 89: Batch recipes BM11.3A and BM11.6B.....	<b>436</b>
Table 90: Slump tests for selected bodies .....	<b>446</b>
Table 91: Experimental and proprietary blends. Malleability 6 weeks after blending and bagging.....	<b>466</b>
Table 92: Wet to fired shrinkage BM11.6B & BM1.14C blended with WMF....	<b>466</b>
Table 93: Average apparent porosity. BM11.6B & BM1.14C blended with WMF	<b>467</b>

## List of Abbreviations

ACCL	Arumpo Cullet Coldbag House Fines Latite
ALS	Australian Laboratory Services
ASTM	American Society for Testing and Materials
CAS	Chemical Abstracts Service
CAD	Computer-Aided Design
COE	Coefficient of Expansion
CSA	Canadian Standards Association
CSIRO	Commonwealth Scientific and Industrial Research Organisation
CT	Cristobalite & Tridymite
IPCC	Intergovernmental Panel on Climate Change
LOC	Loss on Combustion
LPG	Liquified Petroleum Gas
MSDS	Material Safety Data Sheet
NCECA	National Council for Education in Ceramic Art
NOAA	National Oceanic and Atmospheric Administration
NSW	New South Wales
PSA	Paper Sludge Ash
RHA	Rice Husk Ash
SCBA	Sugar Cane Bagasse Ash
SEM	Scanning Electron Microscope
SHAB	Shrinkage Absorption
UTS	University of Technology, Sydney
WEW	Walker's Earthenware White
WMF	Walker's Middle Fire
XRD	X-ray Diffraction



## **Abstract**

This project investigates the possibility of producing vitrified studio ceramics below 1000°C, incorporating industrial and agricultural wastes from New South Wales (NSW), Australia. The thesis describes the research context, summarises some related research, documents the experiments conducted, and presents the results obtained, as well as documenting mixed-media studio works.

Ceramic firing practices and the energy inputs required are placed within the socio-political context of the climate change debate. A brief survey of environmental art includes a discussion of material and process choices, and leads to definition of sustainability and brief explanations of green chemistry and green engineering.

There is reference to classification of clays, and to desirable characteristics of clay bodies including workability, low shrinkage during drying, dry strength, fired strength, resistance to abrasion and lack of permeability. Approaches for lowering the temperature of sintering and vitrification are reviewed, and a survey of literature on the inclusion in clay and glaze of industrial, municipal and agricultural waste includes previously researched materials from within NSW.

The selection and collection of waste materials for tests is documented, microscopy provides information about their morphology, and quarry tailings are compared with other proprietary materials known to have a fine particle size. Further characterisation of the waste materials is achieved by X-ray diffraction and percentage analysis.

The process of triaxial blending is adapted to apply to clay bodies, with flux materials chosen to extend the temperature range within which a sample would not slump, achieve an acceptable level of vitrification and low porosity, influence the expansion of body and glaze to counteract crazing, introduce control over salt migration, and reduce hazard profiles. Preparation of test pieces is in accordance with international standards, as is test methodology. Fired strength

is tested, and a novel method of displaying shrinkage and absorption trends is presented and utilised.

A range of engobes and low-fire bodies is developed, including bodies containing only recycled materials, and bodies that self-glaze at 950°C. Coloured glazes are shown to interact dramatically with bodies below 1000°C. Low-fire ceramic articles are made from the clays and glazes developed. Additives and procedural changes successfully counteract thixotropy and efflorescence resulting from flux inclusion, and proprietary clay is blended with low-fire clays to achieve a compromise between workability and extent of vitrification.

The use of domestic biomass gasifiers to produce ash is documented, as is the construction and use of a kiln to harvest the energy released, and the creation of a number of conceptual artworks exploring themes of the environment, energy, consumption and waste.

#### Creative work

A supplementary body of work was exhibited at the Sydney College of the Arts Mid-Year Postgraduate Degree Show from Wednesday 26 June to Friday 5 July 2013. This work included video, sculpture, digital images on fabric, and conceptual and functional ceramics made from experimental low-fire clays.

## Introduction

This research investigates the possibility of developing low firing temperature clay and glazes for use in studio ceramics, incorporating selected industrial and agricultural wastes produced in New South Wales (NSW), Australia. The thesis describes the research context, summarises some related research, documents the experiments conducted, and presents the results obtained, as well as documenting mixed-media studio works.

To convey the extent of the challenge involved in undertaking this project, it is necessary first to define what is meant by *low temperature* within the field of studio ceramics, and to define a number of terms associated with heating clay (the process referred to as firing).

The amount of time a clay is exposed to heat affects the product (Norton & Hodgdon, 1931). The combined effect of time and temperature is referred to as *heat work*. The extent of heat work applied is observed through the placement in the kiln of pyrometric *cones*. These cones are proprietary formulations of raw materials fashioned into elongated trigonal pyramids designed to soften and bend from an upright position when a certain amount of heat work has been completed (Walker, 2010).

Studio ceramics can be heated to temperatures across a continuum, and there are loosely defined categories referred to as *firing ranges* (Peterson, 2012). At the low temperature extreme is *Egyptian paste*, a self-glazing clay of poor workability usually fired within a range of 900–1000°C (cone 010 to cone 06) (Ceramics Today, n.d.). Industrial ceramics may be fired as high as 1400°C (Guy, 2009). Peterson (2012) provides cone numbers and temperatures for the following common studio ceramic firing ranges:

- low-fire: cone 06–cone 3 (999–1100°C)
- mid-range: cone 4–cone 7 (1186–1240°C)
- high-fire: cone 8–cone 10 (1260–1300°C).

Therefore, low-fired clays (those fired between 1000°C and 1100°C) are not unknown. However, as Peterson points out, 'they are softer which means that they are less durable and will absorb liquids' (Peterson, 2012). A clay that is soft

and absorbent has not *vitrified* during firing. *Vitrification* is the process whereby a clay forms a glassy ceramic that is not absorbent (American Ceramic Society, 2005). Vitrification follows and overlaps with a process of *sintering*, in which a porous mass densifies and strengthens (Green, Guillon & Rodel, 2008). Densification is accompanied by a decrease in *porosity*, ‘the volume fraction of voids contained in a solid, often expressed as a percent’ (American Society for Testing and Materials (ASTM) International, 2006). The extent to which these processes occur within a given firing range depends to a large extent on the mix of materials that form a clay *body*. This term *body* usually refers to clay that has been intentionally formulated or batched. The aim of this research was to produce a clay body that vitrified below 1000°C, to obtain the qualities of durability and non-absorption usually associated with bodies fired to much higher temperatures. It was intended that by reducing the firing temperature of a newly prepared body, the required energy input, emissions and expense of firing could all be reduced.

In the prevailing physical, social, economic and political environment at the time this project commenced, a personal motivating concern was that production of ceramics would become more expensive, more regulated and less popular with schools and communities. This would result in a decreased appreciation for the enriched experience of living that can result from the use of handcrafted domestic ware, with its satisfying heft, its sense of intimacy conveyed by makers’ marks, and its fascinating historical allusions (Guy, 2009):

*The object is made with the hand, the lived body, and therefore, always has an intimate relationship with it and with other bodies. When I hold the handmade object whether it is ancient or contemporary, I enter a relationship, not only with the maker, but the history of the world. (Guy, 2009, p.216)*

This project was commenced in the middle of 2008. Two years previously, in America, Al Gore had popularised the climate change debate via the movie *An Inconvenient Truth* (Guggenheim, 2006). In Australia, Prime Minister Kevin Rudd had been elected after describing climate change as the great moral challenge of our generation (Rudd, 2007). The motivation for embarking on this project arose from identification with these very publicly expressed concerns for the environment. Accepting personal responsibility for the possible effect on the

environment of my then current practice of firing relatively high-temperature ceramics led to the consideration of methods of clay formulation that would assist in reducing energy use and carbon emissions associated with studio ceramics.

Chapter 1 provides further explanation of how this project arose from reflection on my ceramic practice within the socio-political context of the climate change debate, and briefly covers findings related to increasing atmospheric carbon dioxide (CO<sub>2</sub>) levels, the scientific explanation for global warming, ocean surface warming and acidification, and some of the consequences for affected sea life. These explanations are followed by a description of selected public responses from individuals and groups, and a brief discussion of Australian government legislation and regulation. The focus then shifts to a brief description of the energy inputs required for ceramics, and some of the firing methods in common use.

Chapter 2 begins by providing a brief survey of environmental art, and refers to a number of twentieth and twenty-first century artists who have incorporated waste in their creations. Consideration is also given to artworks made of clay; the first of the artworks generated by the research process appears here—a piece of published writing that draws connections between three exhibitions and three possible positions on anthropogenic climate change. The chapter continues with a discussion of some environmental concerns expressed by ceramicists, and commentary on the material and process choices of ceramicists.

This discussion of material and process choices is followed, in Chapter 3, by a definition of sustainability and brief explanations of green chemistry and green engineering. The implication is that in addition to lowering firing temperature, the project requires some consideration of factors related to the material composition and processing of a clay body.

Chapter 4 uses the classification of clays provided in the ceramics literature to focus on naturally occurring constituent clays that could be expected to be of some utility in formulating a low-temperature body.

Chapter 5 focuses on some sought after characteristics of clay bodies. In the *raw* or unfired state, when forming processes are applied to malleable clay that stiffens as it dries, these include workability, the extent of shrinkage during drying and the dry strength obtained. Once the ceramic has been fired, desired characteristics can include fired strength, resistance to abrasion and lack of permeability. As these characteristics depend considerably on the amount of sintering and vitrification achieved, three basic approaches for lowering the temperature of sintering and vitrification are reviewed in Chapter 6. Each approach is accompanied by examples from the literature. Chapter 6 concludes by noting some points to be remembered when firing bodies containing waste carbonaceous materials.

Chapter 7 provides a survey of literature on the inclusion of industrial, municipal and agricultural waste in clay and glaze. Particular attention is paid to Whitfield's (1985) work on clay from sand quarry tailings, and on his later work on selected industrial wastes from NSW in Australia (Whitfield, 1993). This matches the aim of using as many recycled constituent materials as possible, and the desirability of obtaining those materials from within NSW. The chapter assesses properties of materials with respect to the current project and narrows the range of waste materials for further consideration.

Chapter 8 documents the collection of selected waste materials, provides images of the materials as collected or received, and includes microscopy to provide information about their *morphology* (shape, size and structure).

Chapter 9 explores further the quarry tailings, using time-lapse photography to document the rates at which the tailings absorbed water and the length of time that particles were visibly in suspension. The experiments compare quarry tailings with other proprietary materials known to have a fine particle size.

Chapter 10 documents the first attempts to assess the workability of the quarry tailings, showing how the clay was prepared, describing the performance of some simple tests, and picturing bowls successfully formed from quarry tailings using standard studio techniques and fired to 800°C.

Chapter 11 begins the iterative process of *triaxial blending*, in which three batches of materials are blended in various proportions to produce a systematic variation in constituents (Currie, 2000). Normally, this process is applied to glazes. In this case, it was adapted to apply to clay bodies. The process of preparing the bodies and forming samples to test for desired characteristics is covered and a rating scale is introduced, as is nomenclature for referring to the results, which are supplied in Chapter 12.

The results in Chapter 12 include handling and drying properties, and percentage shrinkage from wet to dry. Shrinkage data is presented in triaxial format, making trends easy to see at a glance.

Chapter 13 describes and records the appearance and shrinkage results of the same triaxials when fired to 800°C, and to a range of higher temperatures up to 950°C. These results, which were promising due to the melting of some samples, also indicated that *slumping* (collapse of form) could occur within a narrow temperature range, so further triaxials would be required.

At this point in the research, there was a diversion from clay and glaze formulation as a result of a process consideration. Two of the agricultural wastes obtained (dry rice husks and freshly shelled corn cobs) had required a process of firing in a kiln to produce ash for use in clay or glaze. There was considerable smoke released during the process and the use of electricity to produce the ash seemed to contradict the broad aims of the project. Chapter 14 documents the procurement of simple domestic biomass gasifiers, and the construction and use of a kiln to harvest the energy from gasifying the husks and cobs, while simultaneously producing the ash required.

Chapter 15 documents the characterisation of the waste materials by X-ray diffraction (XRD). The process of triaxial blending does not require intimate

knowledge of the character of the materials being blended, but characterisation can assist in making choices about materials to blend.

Chapter 16 provides a percentage analysis of materials sent to Australian Laboratory Services (ALS) in Brisbane, Australia for analysis.

Chapter 17 provides more results of the same triaxial blends previously used to develop sample clay bodies. Here, the samples are applied by brush to triangles of fired clay. The potential for use of some samples for surface treatment is discussed. *Engobes* (opaque surface coverings with high clay content) and glazes are applied—alone and in combination—to samples and a bowl formed from a mix of quarry tailings. Faults including *crazing* (cracking of the glaze surface) and leaking (due to lack of vitrification) are depicted.

Chapter 18 documents the use of two of the samples that formed self-glazing bodies at 950°C. The slumping that is displayed confirmed the need for further triaxial blending, because bodies that were adjacent on the triaxial blend were shown to have advanced to greatly differing extents of sintering and vitrification.

Chapter 19 investigates the formulation of bodies containing only recycled materials, and describes experiments conducted to determine the effect of additions of fine cullet to a blend of tailings chosen to produce the best combination of handling and sintering properties. As a result, additional bodies vitrifying below 1100°C are identified for further use.

The following three chapters (Chapters 20, 21, & 22) provide the background research and rationale for the choice of materials for the next triaxial blend and next glazes. The requirements to be balanced were: i) extending the temperature range within which a sample would not slump, but would produce an acceptable level of vitrification and low porosity; ii) retaining a range of fluxes; iii) influencing the expansion of body and glaze to counteract crazing; iv) introducing some control over salt migration and self-glazing; and v) eliminating materials with significant hazard profiles.

In Chapter 23, the findings of the preceding three chapters are used to form the three batches to be blended as a new triaxial. Alteration of the recipes to be



blended is described, and a method of scaling the blending process to produce large numbers of samples is presented. Preparation of test pieces in accordance with international standards is described, the test methods are presented, and handling properties, salt migration, shrinkage to dry, fired shrinkage, absorption and porosity results are provided for a range of temperatures up to 1000°C. A novel method of displaying absorption trends is presented and utilised.

Chapter 24 details properties observed when further experimentation was conducted using selected bodies from earlier tests. The properties under investigation included handling requirements, appearance, absorption, shrinkage and fired strength. Some bodies that had not vitrified in earlier tests were fired to higher temperatures; one promising terracotta body received a 20% (by dry weight) addition of cullet, and one body received additives intended to reduce thixotropy and efflorescence. An interesting low-fire self-glazing body is pictured. Bodies vitrifying below 1100°C are identified for further use.

Chapter 25 documents the success of additions of two materials intended to counteract some of the undesirable effects of flux inclusion, namely *thixotropy*, where a body softens upon agitation, and *efflorescence*, the visible accumulation of migrated salts upon the surface of the ware.

Chapter 26 contains descriptions of the preparation of test pieces for tests of fired strength, according to the specifications of the University of Sydney Department of Civil Engineering (Reid, 2011a), and the method and results of testing conducted in collaboration with students supervised by Professor Reid.

Chapter 27 documents short-lived attempts at making casting slips. These attempts were unsuccessful due to the alkalinity of the flux materials and the associated thixotropy of the blends in use.

Chapter 28 demonstrates the development of some glazes containing recycled materials, with tests completed across a range of firing temperatures, before concentrating on glazes below 1000°C. This is followed, in Chapter 29, by a description and images of dramatic interactions between low-fire glazes and the

bodies to which they were applied, and, in Chapter 30, slump tests of selected bodies.

Chapter 31 displays some low-fire ceramic articles made from the clays and glazes developed, and reports on additional experiments blending proprietary clay with low-fire clays to achieve a compromise between workability and extent of vitrification.

The conclusion summarises the achievements of the research, acknowledges limitations and suggests potential avenues for further investigation.

While the focus of the thesis is in part resolutely technical, it was also conducted with the intention of developing artistic practice, and potentially influencing processes chosen by ceramicists with environmental concerns. It was conducted within the Department of Contemporary Arts at Sydney College of the Arts. Therefore, the thesis is cross-disciplinary in nature, requiring a scientific approach within a visual arts frame.

It was initially intended that the artworks to emerge from this project would do so as a result of the qualities discovered in the ceramic bodies developed. While this technological determinism has certainly occurred to some degree, there have also been many unintended and welcome consequences of undertaking the research within a school of art that values and teaches about conceptual art. The development of a number of conceptual artworks is described. These works explore the themes of the environment, energy, consumption and waste. Some of these artworks were formed from the clay and glazes developed and described within this research, but others were made from diverse materials. Often they emerged as a by-product, from a recycling of the technical research.

In order to demonstrate the cross-disciplinary nature of the research, the thesis is appended with images and accounts of how these conceptual artworks emerged from the research experience, materials and motivating concerns.

## **Chapter 1: Personal Motivations: Climate science, socio-political influences and ceramic practice**

This chapter begins by providing some personal history to give some context to this project. It charts how my ceramic practice began in the 1970s, discusses some changing perceptions, and introduces some scientific observations and explanations related to climate change. Several actual and potential consequences of increasing atmospheric CO<sub>2</sub> levels are reviewed, as is media coverage of the diversity of responses. Relevant Australian government legislation and regulations relating to energy use are mentioned before attention turns to the energy inputs required for ceramics.

### **Formative influences**

I grew up in New Zealand in the hippie-influenced 1960s and 1970s. During this period, the ceramic artist or craftsperson was regarded as a symbol of resistance to the industrial juggernaut, producing domestic ware that bestowed upon its buyers a warm glow of connection to the earth.

*When a potter produces a pot which serves well a human need, this in itself and its symbolism is the acme of human perfection reflecting social conscience, a synthesis of material and spiritual values...* (Simpson, 1967, p.5)

*In contact with these objects that reflect the individual variation of their creators we appreciate values that industrialism alone cannot sustain.* (Roberts, 1966, p. 25)

*In our society the people who make pots seem to be those who are looking for warmer and more human values...* (Mason, 1967, p.33)

I began to absorb these values when at 17 years of age I enrolled in a pottery night class at a local school, where there was a 60 cubic foot diesel-fired kiln.

At the time, pottery was in fashion and pottery mugs were to be found in many kitchens. At Nambassa, 'a series of multi-faceted hippie festivals held between

1976 and 1981 on farms in country Waihi and Waikino in New Zealand—Aotearoa’ (Ward & Terry, 2011), house trucks displayed pottery on shelves (fig. 1 (Bennetts, in Mombass, 2012)).



*Figure 1: House-truck interior (Bennetts, 2012)*

I went to Nambassa in a hired truck with a bunch of friends in peasant dresses (the women) and long hair (everyone), and soaked up the music and lifestyle advice, ate healthy food, and came away happy, having purchased a suitable pottery memento (fig. 2).



*Figure 2: Raku fired clay pendant sold at the New Zealand Nambassa festival in 1979*

The following year, I undertook a certificate course in ceramics. I was soon able to sell everything I made, seconds were snapped up at the markets, and I was comfortable in my view of myself as an eco-friendly craftsman. However, when I began considering this doctoral project, I was in twenty-first-century Sydney,

and in the prevailing socio-political climate, I had become less comfortable about the ecological credentials of my craft.

### **Twenty-first century socio-political attitudes to global warming**

In Western society during the early twenty-first century there was a period of heightened public concern about global warming, and about environmental issues in general. The recycling of paper and consumables packaging had become a widely accepted global campaign promoted by all levels of government and marketed with the assistance of symbols, advertising and regulation. Human impact on the environment was at the forefront of public attention in America and Australia, and climate change was higher on the list of public concerns in both countries than is currently the case.<sup>2</sup>

In an article in *New Scientist* magazine, Nicholas Stern, who chaired the Intergovernmental Panel on Climate Change, wrote:

*Action is needed to further spread existing low-carbon technologies, such as 'green' household appliances. This can be done by creating carbon markets in which the price of emitting carbon reflects the potential impact of those emissions, and by introducing energy efficiency standards to incentivise innovation, for example. (Stern, 2009)*

The media in Sydney, Australia had reported similar concerns. Sydney newspaper headlines had government and regulatory bodies warning of the potential economic impacts of reducing greenhouse gas emissions, and of the imposition of carbon taxes and the potential for industries to generate carbon credits (Irvine, 2008). Irvine quoted the head of the Reserve Bank of Australia Glenn Stevens as saying:

*Australians must accept that emissions trading is designed to make them pay more and lower their standard of living, at least where energy use is concerned. (Irvine, 2008)*

---

<sup>2</sup> Since 2009, Americans have become relatively more concerned about the economy and less concerned about the environment and global warming (Nisbet, 2011). In particular, young adult Americans are relatively uninformed and less concerned than they were in 2009 (Miller, 2012). Australian support for action on climate change has decreased since 2009, but young adult Australians are more likely than older Australians to support action and to believe in anthropogenic climate change (Connor & Stefanova, 2012).

In May 2009, *Greenpeace* activists beamed energy conservation messages onto the Loy Yang A Power Station in Australia (fig. 3).



**Figure 3: Greenpeace climate change activism (Greenpeace/Alcock)**

Image reproduced from <http://www.greenpeace.org.au/climate/>

The Australian population was also mobilising. Over 2,000,000 Sydneysiders switched off their lights for Earth Hour in March 2009. In July that year, Sydney's youth joined in a three-day *Powershift* conference, wearing green hard hats to symbolise their intent to make an impact on industry (fig. 4).



**Figure 4: Powershift conference delegates in Sydney**

### **Formalism and consideration of the impact of ceramic process on form**

I had been designing ceramics and using fused deposition prototype modelling (Smut, 2005). Prototype modelling is a design process that results in the production of a three-dimensional (3D) form. This form can then be used as a

model, from which moulds can be made for use in slip casting or press-moulding. The pieces were designed in 3D using a computer-aided design (CAD) program and the files were supplied as stereolithography files, which determined the pattern in which a ¼ mm thick tube of hot acrylonitrile butadiene styrene was extruded in the prototype modeller.

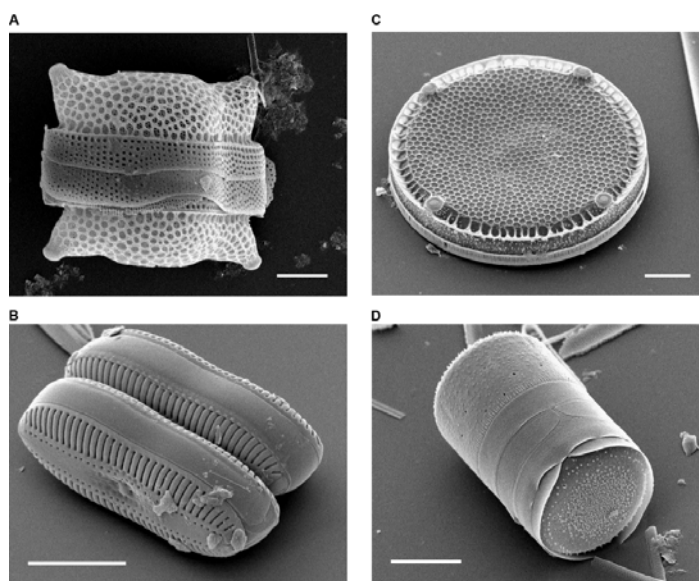
The decision to use prototype modelling was triggered by admiration for the protective calcium carbonate forms produced by *Bankivia fasciata* seashells such as those seen in Figure 5, and smaller organisms such as the diatoms seen in Figure 6.



**Figure 5: *Bankivia fasciata* (Beechey, 2012)**

Image reproduced from

[http://seashellsofnsw.org.au/Trochidae/Pages/Umboniinae/Bankivia\\_fasciata.htm](http://seashellsofnsw.org.au/Trochidae/Pages/Umboniinae/Bankivia_fasciata.htm)



**Figure 6: Scanning electron micrographs of diatoms:**

**(A) *Biddulphia reticulata* (B) *Diploneis* sp. (C) *Eupodiscus radiates* (D) *Melosira varians* (Tiffany)**

Images reproduced from <http://www.plosbiology.org/article/info:doi/10.1371/journal.pbio.0020306>

The manner in which the onscreen design could be ‘grown’ using coordinates and mathematical formulae, and the manner in which the plastic model was formed by the laying down of material, were chosen as processes analogous to the growth of shells. The choice of this mimetic process was the result of a bias towards formalism, an approach in which the form of a piece takes precedence over conceptual considerations.



*Figure 7: Brett Smout Seashell Vases 2008 (38cm x 18cm & 25cm x 14cm)*

This approach was subverted, in effect, by the knowledge that the process of high-temperature firing of the porcelain shell series (e.g. barium glazed oxidised forms shown in fig. 7) was a process resulting in carbon emissions, and the realisation that these emissions were contributing to ocean acidification, which in turn threatened the ability of marine organisms to form the shells that had inspired the work. The connection between carbon emissions and a threat to shell formation is explained in more detail below.



## **Increasing atmospheric CO<sub>2</sub> and global warming**

The scientific consensus is that increasing CO<sub>2</sub> levels are at least partly the result of human activity, with anthropogenic changes predominantly driven by advanced economies since the Industrial Revolution (Jones, 2011). The relationship between changes in CO<sub>2</sub> levels and atmospheric temperature was first calculated accurately in 1896, when the term 'greenhouse effect' was coined (Jones, 2011). CO<sub>2</sub> is a 'greenhouse gas' that traps heat in the atmosphere, so the more of it that there is, the more heat is trapped. Although CO<sub>2</sub> levels have been higher in the distant past, they were stable at around 280 parts per million for 10,000 years before the Industrial Revolution, but have since climbed to 391 parts per million (Jones, 2011).

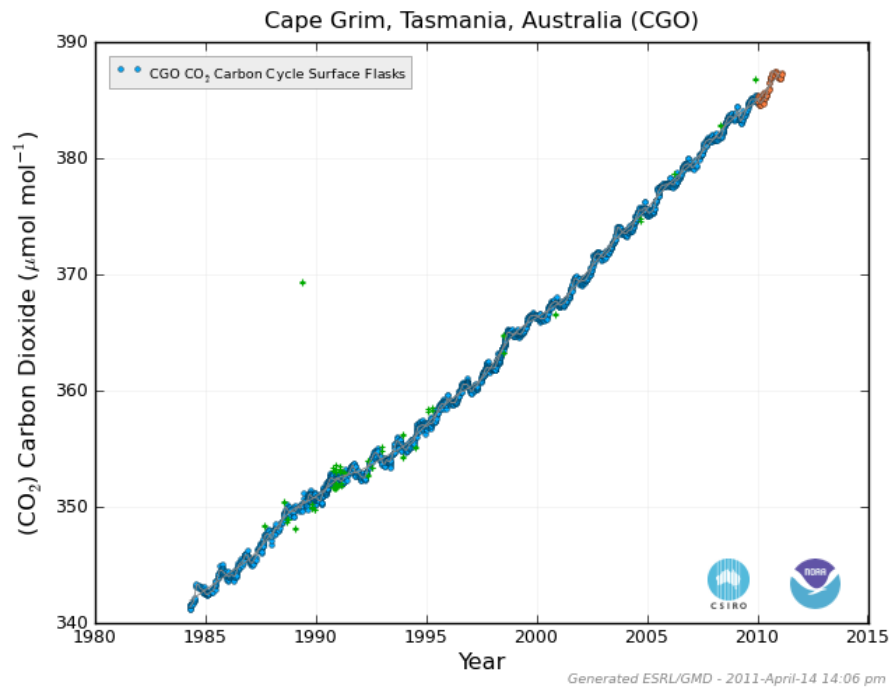
In Australia, carbon dioxide levels are measured at the Australian Bureau of Meteorology's Cape Grim Observatory in Tasmania (Commonwealth Scientific and Industrial Research Organisation, 2008). The Cape Grim Observatory contributes data to the National Oceanic & Atmospheric Administration (NOAA) Global Monitoring Division Earth System Research Laboratory at Moana Loa in Hawaii, which has been keeping records of carbon dioxide levels since 1958 (NOAA, 2011a):

*Data are reported as a dry air mole fraction defined as the number of molecules of carbon dioxide divided by the number of all molecules in air, including CO<sub>2</sub> itself, after water vapor has been removed. The mole fraction is expressed as parts per million (ppm). (NOAA, 2011a)*

Although it is not the only factor, the rate of global warming is influenced by the amount of CO<sub>2</sub> in the atmosphere:

*We know that CO<sub>2</sub> is a greenhouse gas because it absorbs and emits certain frequencies of infrared radiation. Basic physics tells us that gases with this property trap heat radiating from the earth, that the planet would be a lot colder if this effect was not real and that adding more CO<sub>2</sub> to the atmosphere will trap even more heat. (Brahic & Le Page, 2007, p. 1)*

Carbon dioxide levels have been recorded at Cape Grim, in Tasmania, Australia, since 1984 (fig. 8).



**Figure 8: Time series of atmospheric carbon dioxide levels recorded at Cape Grim, Tasmania since 1984 (Commonwealth Scientific and Industrial Research Organisation; NOAA)**  
Image reproduced from NOAA website (NOAA, 2012)

*The concentration of CO<sub>2</sub> in the atmosphere in 2011 was 390 parts per million—higher than at any time for the past 800,000 years. (Australian Government Bureau of Meteorology & CSIRO, 2012, p. 3)*

In the United States (US), the National Aeronautics and Space Administration (NASA) reports that the first decade of the twenty-first century had the warmest average global temperatures on record (Voiland, 2010). Atmospheric temperature and atmospheric CO<sub>2</sub> also increase the temperature and reduce the pH of the oceans, as explained below.

### **Effects of warming and elevated CO<sub>2</sub> on the ocean and sea creatures**

Increasing carbon dioxide concentration in the air has direct implications for the amount of carbon dioxide absorbed by the ocean. When the ocean becomes carbonated, it becomes more acidic, because the carbon forms carbonic acid. Some of the effects of this were described in a report from a workshop sponsored by the US National Science Foundation, the US National Oceanic and Atmospheric Administration, and the US Geological Survey titled *Impacts of*

*Ocean Acidification on Coral Reefs and other Marine Calcifiers: a guide for future research* (Kleypas et al., 2006):

*Since 1980 ocean uptake of the excess CO<sub>2</sub> released by anthropogenic activities is significant; about a third has been stored in the oceans. The rate of atmospheric CO<sub>2</sub> increase, however, far exceeds the rate at which natural feedbacks can restore the system to normal conditions. Oceanic uptake of CO<sub>2</sub> drives the carbonate system to lower pH and lower saturation states of the carbonate minerals calcite, aragonite, and high-magnesium calcite, the materials used to form supporting skeletal structures in many major groups of marine organisms. (Kleypas et al., 2006, p. 1)*

Not only is shell formation slowed; increasing the level of carbon dioxide in seawater increases the level of carbonic acid, which results in the calcium carbonate shells dissolving (Henderson, 2006). This was first made evident to one of the authors of the above report, Victoria Fabry, when she was researching small swimming snails called *Clio pyramidata* (fig. 9) (Barry, 2006). She had stored some of these live molluscs in sealed jars, and she noticed that their shells were dissolving while they were still alive. Because the jars were sealed, the molluscs' respiration had increased the CO<sub>2</sub> content and the level of carbonic acid was sufficient to dissolve their shells (Henderson, 2006).



**Figure 9: *Clio pyramidata* (Hopcroft, 2006)**

Image by Hopcroft reproduced from <http://www.newscientist.com/article/dn9108-zooplankton-survey-plumbs-the-depths.html>

Acidification also affects other creatures, including fish. The small *Clownfish* (fig. 10) popularised by the animated movie *Finding Nemo* is one species affected by acidification. Philip Munday and colleagues at James Cook University in Townsville found that larval *Clownfish* lose the sense of smell they use to navigate and avoid predators when CO<sub>2</sub> levels reach those expected by the end of this century (Munday et al., 2009).

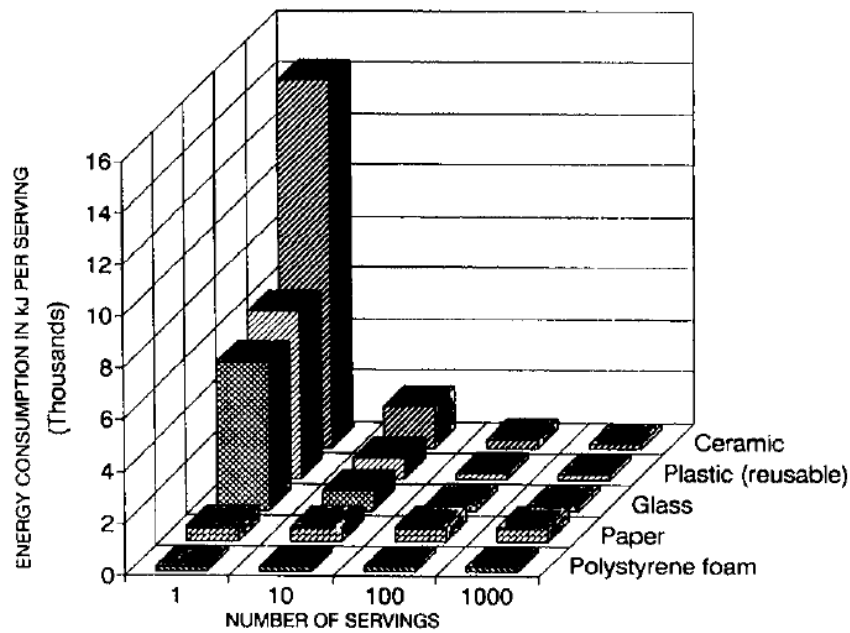


**Figure 10: Clownfish (*Amphiprion percula*) (Newbert, 2009)**

Increasing sea surface temperature has effects too, with tropical fish swimming faster in warmer water, and warmer water resulting in the East Australia current getting stronger and carrying warm water further south so that species dispersal will be affected (Booth, 2011).

In 2009, consumers were making green choices, and informing others by way of distributed media including blogs. One blogger (VanCott, 2009) referenced Hocking's (1994) research into the comparative energy consumption levels of differently fabricated cups. Hocking analysed five different types of re-usable and disposable hot drink cups with respect to their overall energy costs during fabrication, use and disposal, and graphed his findings (fig. 11).

The vertical axis is the energy consumption per serving, and the horizontal is the number of servings from single use to 1000 re-uses. There are five types of cups. The front two types are disposables. Because they are disposed of after a single use, the energy per use remains the same. The ceramic cup requires much more energy to produce, and because energy is also required to wash cups between uses, a ceramic cup must be used between 100 and 500 times to reach the point at which it breaks even with a disposable.



**Figure 11: Comparison of energy input per serve with various cup types (Hocking, 1994)**  
 Reprinted from Hocking, 1994

In a study commonly cited, ceramic cups were branded as more environmentally damaging than was commonly thought (Bamford, 2010). A study conducted for a party with a direct interest in disposable cups (Stichting Disposables Benelux) investigated the relative environmental impact of 1000 uses of a re-usable porcelain cup and saucer, a re-usable earthenware mug, a disposable paper cup and a disposable polystyrene cup (Ligthart & Ansems, 2007). In performing this analysis, the authors considered multiple aspects of life cycle and multiple environmental impacts (fig. 12).

Environmental effect category	Abbreviation
Abiotic mineral resources depletion potential	ADP
Global warming potential	GWP
Ozone depletion potential	ODP
Human toxicity potential	HTP
Fresh water aquatic eco-toxicity potential	FAETP
Marine aquatic eco-toxicity potential	MAETP
Terrestrial eco-toxicity potential	TETP
Photochemical ozone creation potential	POCP
Acidification potential	AP
Eutrophication potential	EP

**Figure 12: Environmental impact categories**  
 Adapted from Ligthart & Ansems, 2007, p.26

This led to cautious endorsement of disposable drinking systems. When the report was complete, Benelux began advertising using the slogan ‘Single use cups are the winners!’ (fig. 13).

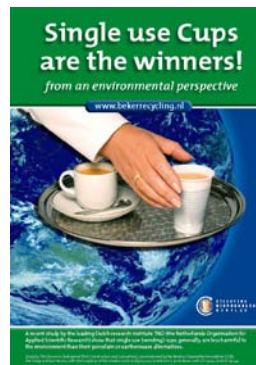


Figure 13: Benelux advertising (Stichting Disposables Benelux, 2007)

Careful inspection of the report reveals a number of interesting factors that lead to the authors’ actual conclusion that:

*The question ‘What is better for the environment, drinking coffee out of a disposable or re-usable cup?’ can therefore only be answered on the basis of the specific operating situation.*

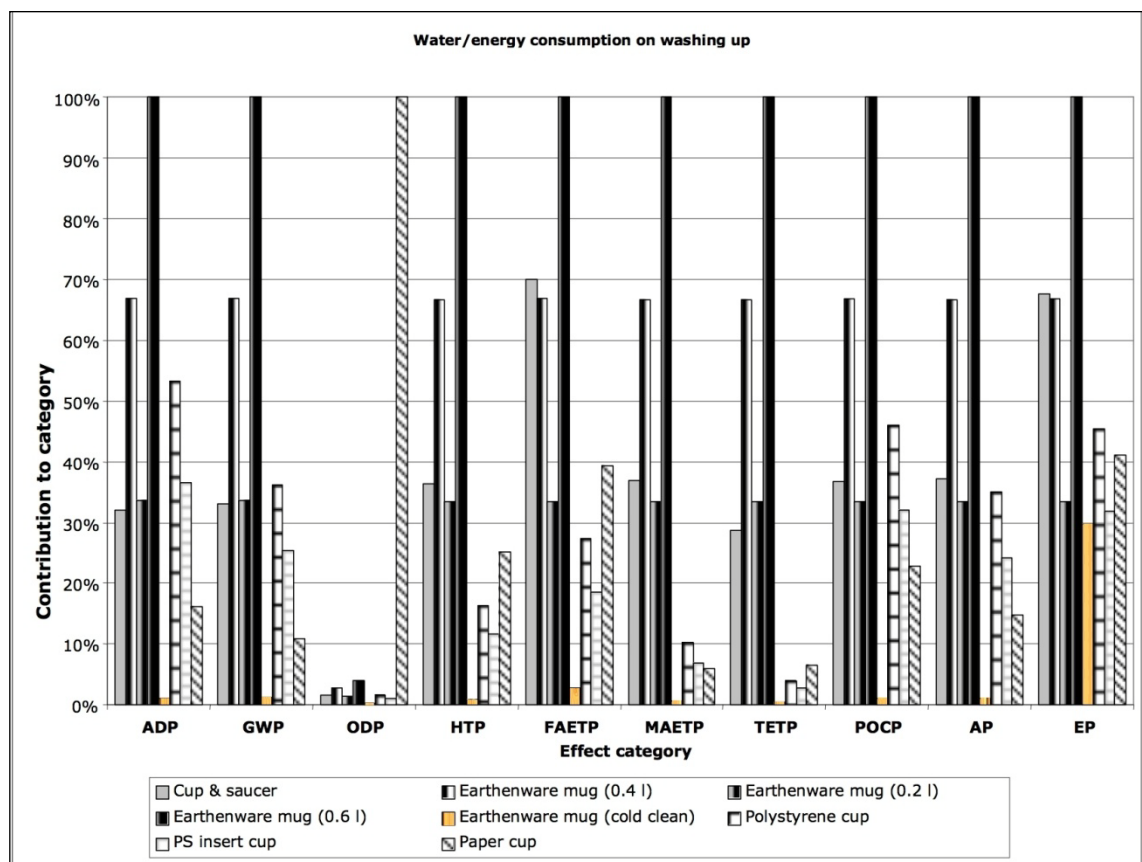
(Ligthart & Ansems, 2007, p.11)

While the environmental impact of the disposable systems was largely a result of the production of raw materials and its conversion into cups, and the mitigation of impact was dependent on recycling, the environmental impact of porcelain and earthenware re-usable cups was based primarily on the impact of washing. Re-use of any cup type by the original user before washing or discard reduces the energy cost and environmental impact per use in direct proportion to the number of such re-uses, over a large enough number of wash cycles of the re-usable cups. Ligthart and Ansems (2007) found that under a specified automated washing system, using a porcelain cup and saucer four to five times between washes removed the environmental toxicity disadvantage. As most users prefer to wash their drinking receptacles between uses:

*The frequency of cleaning and use of energy per clean are crucial here. Because the user is left plenty of freedom for this, the ultimate burden on the environment is therefore strongly user-related.*

(Ligthart & Ansems, 2007, p.11)

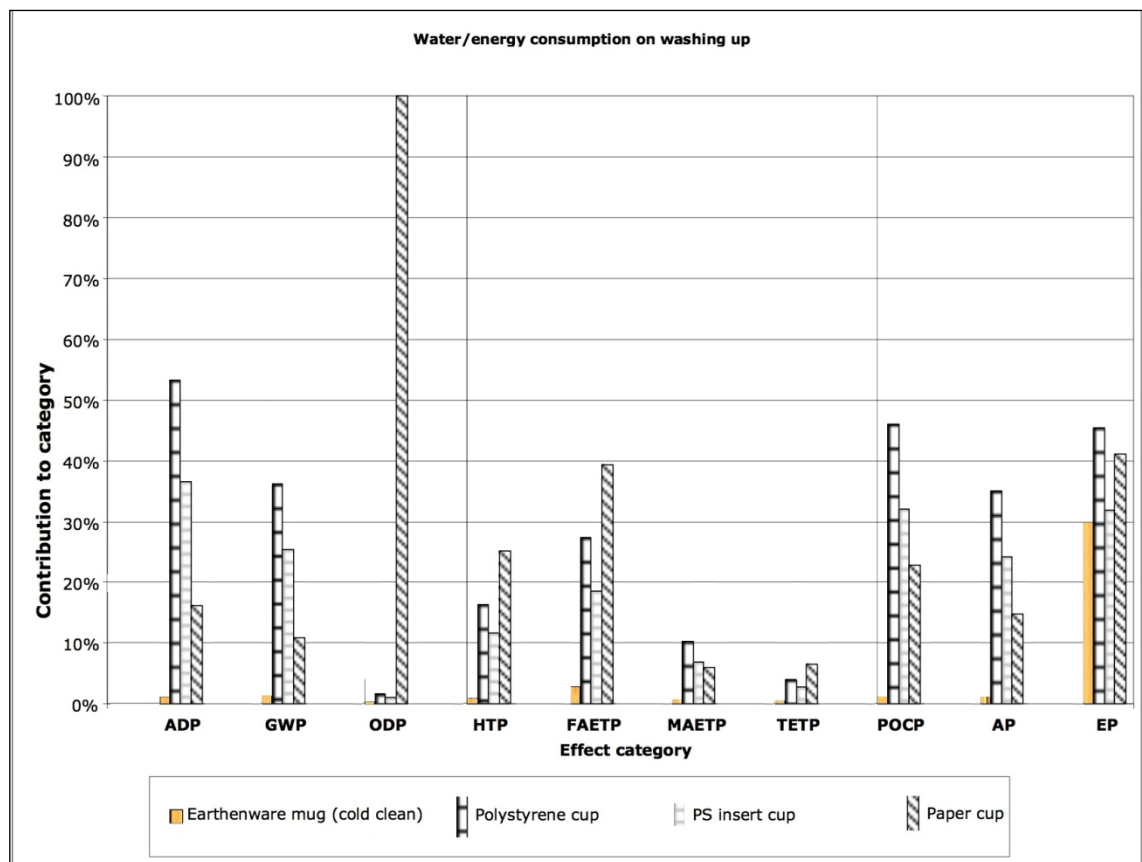
This finding was vividly apparent in Lighthart and Ansem's analysis. Using their assumed cleaning scenarios, the earthenware mug was found to have a greater environmental impact than the porcelain cup and saucer, which had a greater impact than the disposables. This was because of the assumption that, unlike the cup and saucer, the mug would be hand-washed using nearly half a litre of hot water. When the researchers changed the cleaning system to cold water, the earthenware mug performed best of all the drink receptacles in all environmental categories over 1000 uses (fig. 14).



**Figure 14: Environmental impact of varying cleaning systems for re-usable cups versus disposable cups**  
Adapted from Lighthart & Ansems, 2007, p.70

What do these findings mean? Ceramic cups can be the winners! By taking into account more environmental impact factors than Hocking, Lighthart and Ansem improved the environmental credentials of ceramics. In their brochure, Benelux admit that 'the porcelain cup or earthenware mug is ... more environmentally friendly than a single use cup if it is used more than four times in a row without being washed' (Stichting Disposables Benelux, 2007, p.3). Winning the battle

for least environmental impact depends on the number of times a mug is used, and particularly on how many times the use is repeated before washing with hot water. After the bar chart above was placed in an image manipulation program to remove the bars for hot-washed re-usables, it became obvious that if a repeatedly used earthenware mug is rinsed in cold water rather than hot, it outperforms disposables dramatically. For example, under the modelling performed, paper cups have 100 times more impact on ozone depletion, and polystyrene cups have 15–20 times more impact on global warming (fig. 15).

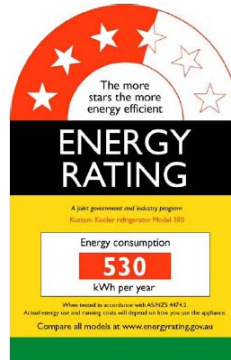


**Figure 15: Environmental impact of cold-cleaned earthenware mug versus disposable cups**  
Adapted from Ligthart & Ansems, 2007, p.70

Cold washing dramatically reduces the number of repeat uses required to lower the environmental impact of a ceramic cup below the impact of single use disposables. The report does not stipulate the number of repeat uses, but one could guess from the relatively minimal impact of the earthenware mug washed in cold water that rinsing in cold water may reduce the required number to a single-digit figure.



For reasons of hygiene, and especially if there is a period of time between consumption of a beverage and cleaning of the cup, many users may choose to wash their cup in hot water. If an automatic dishwasher is used to wash crockery in Australia, it is likely to have been supplied with an energy-rating label such as that pictured below (fig. 16).



**Figure 16: Australian appliance energy-rating label (Commonwealth of Australia Department of Climate Change and Energy Efficiency, 2009)**  
Image reproduced from <http://www.energyrating.gov.au>

The energy-rating of appliances has become a well established regime and such labels will be familiar to most. There are also voluntary standards on products including ceramic and stone tiles, and endorsement schemes on consumer goods. It is likely that in future, there will be more legislation and standards imposed by governments. In Australia, mandatory reporting of greenhouse gas emissions and energy use came into effect from July 2008 as required under the National Greenhouse and Energy Reporting Act 2007 (Australia, 2007).

Educational institutions may well consider energy and fossil-fuel use when making decisions about infrastructure. The teaching of visual arts in schools and universities is an important component of the development of the visual arts, but the provision of the facilities necessary for ceramics is constrained by space requirements, fire-safety standards and the complexity of equipment operation, and by capital, operating and materials costs. Having largely addressed concerns with effluent, educational communities are likely to count the environmental and financial cost of energy input when making decisions about studio facilities, especially as they relate to high-visibility equipment such as kilns.

At the beginning of this chapter, there was concern expressed for both the environment and the future of ceramics, which is, especially in educational settings, a highly visible consumer of energy. One alternative would be to refrain from energy-intensive studio and industrial ceramics, but many of us are committed to these practices. Another alternative is to seek mechanisms by which reductions in fossil-fuel use and carbon emissions might be achieved. The three most obvious mechanisms by which such reductions might be achieved are better insulation of kilns, use of alternative fuels and adoption of lower firing temperatures. A brief review of recent trends follows.

### **Firing ceramics—energy required**

Considerable energy inputs are required in the firing of ceramics. In the field of ceramic art, attention has been paid to reducing the cost of firing and associated effluent since the first 'oil shock' (Fresh et al., 1978; Glick, 1978). Energy use per item has decreased with advances in refractory insulating materials made available by industrial and aerospace research (Colson, 1975). These materials have been utilised in studio and industrial kilns, with accompanying decreases in energy use.

### **Fuels commonly used in Western ceramics**

The use of heat produced from electricity provides the most controllable form of firing ceramics, and electric kilns are common in industrial settings (fig. 17).



**Figure 17: Factory electric kiln (Royal Stafford Tableware Ltd, 2012)**  
Reprinted from <http://www.royalstafford.co.uk/Biscuit.htm>

Industrial ceramicists work to minimise variation in product appearance, and seek to achieve maximum control in order to achieve replicable results such as those in the Hürten handled centrepiece previously produced (circa 1870) at Spode (fig. 18).



**Figure 18: Controlled application and firing: Hürten handled centrepiece (Spode, n.d.)**  
Reprinted from <http://www.spodemuseumtrust.org/index.html>

Studio ceramicists make conscious choices as to how much variation is desirable. At one extreme is the control provided by an electric kiln with a computerised firing program, similar to that used in industry. At the other is a wood- or coal-fired kiln with clay and glazes sensitive to atmosphere and to impurities such as ash, salt, soda or borax introduced with, or in addition to, the fuel (fig. 19).



**Figure 19: Salting a suburban coal-fired kiln, Dunedin, New Zealand, 1980**

Twentieth- and twenty-first-century studio ceramicists have frequently chosen to fire with carbonaceous fuels in a deliberate relinquishment of control, anticipating serendipitous effects considered to enrich the finished product:

*...glazes are apt to vary, not only according to temperature but as a result of fortuitous differences in the kiln atmosphere, such, for example, as may be caused by the different sorts of wood fuel.*  
(Leach, 1976, p. 163)

The carbonaceous substances most commonly combined with oxygen to produce heat to fuel ceramics production have been wood, dung, coal, peat, gas and oil (Shaw, 1972). These fuels have the advantage of easily producing, via manipulation of the fuel-to-air ratio, the reducing atmosphere required by various glaze and surface effects. The variability in degree of reduction throughout a kiln employing these fuels, together with the range of impurities deposited on the ceramic surface, produce contrasting results in identically prepared pieces (fig. 20).



**Figure 20: Brett Smout Salt-glazed coal-fired beakers 1980**

Although no published evidence is available, the focus on environmental concerns has probably resulted in a change in the firing regimes in common use in suburban Australia. It is no longer acceptable to produce smoke in a suburban setting, so diesel- and wood-fired kilns are unusual in that context. Salt-firing has to some extent been replaced by soda-firing, and coal-firing is virtually unknown. Urban and suburban kilns are predominantly fired with

electricity, liquified petroleum gas (LPG) or natural gas. Electricity in Australia is predominantly produced by coal-fired power stations, so all three methods are converting fossil carbon into atmospheric carbon.

Some developing economies depend on biomass for firing ceramics. Some attention is given to the use of biomass as a fuel source later herein (Chapter 14). The immediate topic for further exploration is the temperature at which clay is fired.

### **Firing temperatures of clays in common use**

Efforts have been made to reduce the temperatures at which clays are fired. The firing temperature of some porcelains is now less than 1300°C, and there has been a trend towards greater use of prepared mid-range stoneware clay bodies and cone 6 glazes in studio ceramics, despite the higher material cost that reflects rarity and intensity of processing.

However, although the industrial ceramics/glass literature refers to the development of lower temperature earthenware bodies, these are primarily for brick and tile manufacture. To date, few references have been found in studio ceramic literature to low-temperature bodies other than to Egyptian paste bodies, high porosity bodies and talc bodies predominantly used for slip casting in hobby ceramics (Conrad, 1981). In the hobby ceramics movement, slip cast forms are sold as greenware or bisque to enthusiasts, who apply proprietary glazes, decals and surface finishes.

Tichane (1990, pp. 289–291) provides, without details of porosity or firing range, recipes for earthenware bodies. Their compositions suggest they would be un-vitrified at the suggested firing temperatures (Table 1).

*Table 1: Tichane's (1990) earthenware body recipes*

	Cone 08 (955°C) (%)	Cone 06 (999°C) (%)	Cone 05 (1046°C) (%)
Ball clay	70	60	15
Brick clay			75
Silica (300-mesh)	20		10
Talc	10	40	

The lower-firing prepared clay bodies commercially available in Australia generally have firing ranges that commence at approximately 1000°C, with vitrification occurring near or above 1200°C, as exemplified by the data supplied by Walker Ceramics (Table 2).

**Table 2: Shrinkages, firing ranges & vitrification points of some commercially available Australian clays**

Body	Method	Mesh (#)	Shrinkage (%)		Range (°C)	Vitrification point (°C)
			Wet to dry	Dried to fired (°C)		
superfine terracotta	filter-pressed	120	3.5	8.1@1060	1000–1170	1200
fine terracotta	filter-pressed	60	3.5	4.1@1060	1000–1170	1200
terracotta 14-mesh	filter-pressed	14	3.5	2.2@1060	1000–1200	1225
school terracotta	machine-mixed	N/A	4.6	2.4@1060	1000–1200	1225
hand-building terracotta	machine-mixed	N/A	2.0	2.0@1060	1000–1200	1225
white earthenware middle-fire	filter-pressed	80	2.3	1.2%@1100 6.0%@1250	1060–1250	1250
pink earthenware ironstone	filter-pressed	60	3.2	2.0@1060	1060–1120	1225
	filter-pressed	60	3.0	2.5@1135	1120–1135	1200
Auscrafit Ultra White	filter-pressed	80	3.0	1.3@1060	1000–1100	1180

Adapted from tables available at the Walker Ceramics website (<http://www.walkerceramics.com.au>)

Commercialisation and marketing of a low-temperature body and safe glazes may be possible. In Australia, in the 1980s, Russel Cowan produced a manganese-blended clay firing from 1000°C to a maximum of 1080°C (Cowan, 1989, p.10). However the clay bodies marketed to ceramic artists in Australia typically fire between 1100° and 1300°C, often with considerable porosity and presumably with a lack of strength at the lower end of this temperature range.

These undesirable characteristics are also present in lower-firing clay formulations provided for studio ceramicists who may wish to blend their own clay bodies. For example, Conrad (1981) reports that absorption percentages at cone 012 (approximately 880°C) are 15.2% for a talcware body and 7.0% for a self-glazing body.

Discouraging as this is, the availability of pyrometric cones that deform into a fused ceramic at low temperatures demonstrates that low-temperature bodies can be formulated. For example, the molecular composition of a Seger cone deforming at 900°C is provided as 0.3 Al<sub>2</sub>O<sub>3</sub>, 3.50 SiO<sub>2</sub>, 0.7 CaO, 0.3 K<sub>2</sub>O, 0.2 Fe<sub>2</sub>O<sub>3</sub> (Ryan, 1978, p. 85), and alumino-silicate cones are formulated for temperatures as low as 790°C (see Appendix 10). Of course, many of the unfired and fired properties of a body formulated to this composition may be unsuitable for producing ceramic objects, because the formulation is specifically designed to have a narrow vitrification range, and warping or slumping of forms would be expected (Ford, 1967).

The development of a vitrified lower temperature body for ceramic artists would enable energy savings and reduced carbon emissions. Any reduction in the energy used in producing ceramics will contribute to reducing the environmental impact at the point of production, and contribute to combatting claims that disposables are better for the environment. The inclusion of agricultural or industrial waste may further contribute to sustainability.

This technical project was undertaken within the Sydney College of the Arts, University of Sydney. This institution was an optimal environment for developing clay and glazes for studio ceramics. It also provided an opportunity to expand my artistic practice. The review of environmental art in the next chapter provides some context to the integration of technical and conceptual aspects of this project.

## **Chapter 2: Environmental Art**

While the focus of the thesis is in part resolutely technical, it was also conducted with the intention of developing artistic practice, and potentially influencing processes chosen by ceramicists with environmental concerns. This chapter provides a brief survey of environmental art, in order to demonstrate that a range of actions and ecological interventions are regarded as artistic practice, and to provide a context for the question of whether the current technical project bears any relationship with art.

### **A brief survey of environmental art**

Artists are social commentators, often stimulating thinking where there is complacency, promoting debate, raising awareness of issues and contributing to societal change. This has certainly been the case with rising concerns about the environment, and many artists practice a category of art known as 'eco art'. Lipton & Watts (2004) propose eco art as a term encompassing earth art, land art and environmental art. Since the 1960s, earth art has been recognised in the West as a genre in which works are made in the natural environment from natural materials, but not necessarily on the monumental scale of land art, which involves sculpting the landscape, nor with the activist or consciousness-raising intent of environmental art (Lipton & Watts, 2004). Environmental art is characterised by greater variation in scale and in media used, need not be positioned outdoors, and can include remediation of the built environment, in which case it can be considered the hybrid sub-category of land art and environmental art referred to as 'reclamation art'.

Reclamation art, as pioneered by Alan Sonfist (Bijvoet, 1997), Joseph Beuys, and contemporaries including Richard Long and Hamish Fulton (Beardsley, 1988) and Robert Morris (Strelow et al., 2004) is a process by which degraded or derelict sites are transformed and rehabilitated for public use (Strelow et al., 2004). Beuys, for example, undertook a project of planting 7000 oak trees (fig. 21).





**Figure 21: Joseph Beuys, 7000 Oaks, 1982 (uncredited)**

Image reproduced from <http://www.lightsgoingon.com/2011/09/art-and-ecology-joseph-beuys/> (Gill, 2011)

In 1983, Buster Simpson dropped a series of giant limestone antacid tablets into the Hudson River to neutralise acidity attributed to acid rain (fig. 22).



**Figure 22: Buster Simpson Hudson River Purge, 1983 (Simpson, 1983–1991)**

Image reproduced from [http://www.greenmuseum.org/content/artist\\_index/artist\\_id-21.html](http://www.greenmuseum.org/content/artist_index/artist_id-21.html)

Simpson reports on his website that:

*The process of adding limestone to acidic rivers is now standard practice with environmental agencies.*

(<http://www.bustersimpson.net/riverpurge/>)

Mel Chin adopted the idea of cleaning toxic ground with the *Datura* plant through the process of hyperaccumulation:

*Hyperaccumulation is this notion that the plants can suck up so much metal—and we're talking about heavy metals, not everything—that the plant itself was twenty to forty per cent heavy metal when you*

*ashed it, so you could sell it as an ore and pay for this process.*  
(Chin, 2001)

Chin contacted the scientist (Dr. Rufus Chaney) who was studying hyperaccumulation in the lab. The scientist suggested he needed to do a replicated field test to establish whether the process that worked in the lab also worked in the field. Chin took up the challenge (fig. 23), saying: 'art can mutate into a science project dedicated to providing the world this information' (Chin, 2001). He saw the project as sculpture analogous to carving away pollution (Chin, 2001).



**Figure 23: Mel Chin Revival Field 1991 (Chin, 2001)**  
Image reproduced from <http://melchin.org/oeuvre/revival-field>

In 1982, Agnes Denes created *Wheatfield—A Confrontation*, in which she planted a New York City landfill with wheat. The photo of Denes in the wheat field (fig. 24) was published in the book (Manacorda, 2009) accompanying an exhibition at Barbican Gallery entitled *Radical Nature*. This exhibition surveyed works that emphasised solutions to the apparent segregation between the natural environment and urban environments (Porritt, 2009).

Denes (2011) states that 'earthworks are different from ecological works in intent, form and execution', and says of 'Wheatfield':

*Planting and harvesting a field of wheat on land worth \$4.5 billion in the hub of the Great City created a powerful paradox. It was a symbol, a universal concept that represented food, energy, commerce, world trade, economics. It referred to mismanagement, waste, world hunger and ecological concerns. It called attention to our greed and misplaced priorities.* (Denes, 2011, p. 37)



**Figure 24: Agnes Denes pictured in *Wheatfield—A Confrontation* 1982 (Denes, 2011)**

Image reproduced from <http://www.worldchanging.com/archives/010132.html>

More recently, artists including Anna Garforth have been using vegetation in the form of moss to create artworks in urban environments (figs. 25 and 26).



**Figure 25: Anna Garforth *Moss Graffiti* 2008 (Garforth, 2009)**

Image reproduced from <http://www.environmentalgraffiti.com/featured/moss-grass-graffiti/2147/2>



**Figure 26: Anna Garforth *Moss Graffiti* 2008 (Garforth, 2009)**

Image reproduced from <http://www.environmentalgraffiti.com/featured/moss-grass-graffiti/2147/2>

It is proposed herein that position in the natural environment is insufficient to qualify earth art or land art as eco art if there is no reverence towards, or at least reference to, the ecology of the area into which it is incorporated. For example, the sculptor Michael Heizer initially expressed a reverence towards the Western deserts of Northern America, and claimed that his work's interaction with the materiality of its place endowed it with superiority over

gallery-situated work, which he regarded as intrusive and self-referential (Beardsley, 1998). However, his later work deliberately prevented the viewer from interacting with the landscape exterior to the work, thereby falling prey to his own criticism of gallery-situated work—namely, that it blocked space. There was also criticism that Heizer’s work (fig. 27; Kessel, 1970) marred or degraded the environment (Auping, cited in Beardsley, 1998), and that he and artists like Smithson were ‘imposing themselves on an area that has not been touched by humans’ (Alan Sonfist in an undated interview with Auping, cited in Bijvoet, 1997).



**Figure 27: Michael Heizer *Double Negative* 1969 (Kessel)**

Image reproduced from <http://worldart.sjsu.edu/VieO640?sid=2599&x=621874>

Certainly, images of some of Heizer’s and his contemporaries’ early work leads to conjecture that some artists’ apparent fascination with the natural environment was at least matched by a desire to make their mark on a large scale, and this motivated them to impose their references upon it.

Isamu Noguchi’s unrealised 1947 *Sculpture To Be Seen From Mars* was intended to call out to the universe that ‘humanity was here’ (Kastner, 1998, p. 47). Noguchi’s proposed methodology was emulated, but his concern for the consequences of human action was not. It follows that in addition to location, there must be an ecological intent and at least benign environmental consequences for earth art or land art to merit inclusion under the umbrella of eco art.

Some artworks are clearly conducted in a spirit of protest against environmental degradation. For example, in 1964, Mel Henderson and others protested against an oil spill in San Francisco Bay by using biodegradable dye to write *Oil* on the ocean surface (fig. 28; Henderson & Cohen, 1964).



**Figure 28: Mel Henderson *Oil* 1964 (Henderson & Cohen)**

Image reproduced from from: <http://worldart.sjsu.edu/VieO53299?sid=2624&x=626473>

In 2010, Ken and Julia Yonetani drew attention to the environmental cost of farming, and to salinity in the Murray Darling Basin, a location often referred to as the food bowl of Australia, by exhibiting a number of objects cast from salt from the area (fig. 29; Yonetani, 2011).



**Figure 29: Ken & Julia Yonetani *Still Life—The Food Bowl* 2011 (Yonetani)**

Image reproduced from <http://www.artabase.net/exhibition/3319>

It is also of interest that some work that would be categorised as environmental art under the above definition, by virtue of its ecological consciousness-raising intent and its position in the natural environment, may not be benign in terms of its chemistry. This has been demonstrated vividly by the sculptural work *Hot With Chance Of A Late Storm* created by the *Glue Society* group and exhibited in the Sydney (Australia) *Sculpture by the Sea* festival. In this work, a realistic life-size *Mr Whippy* mobile ice-cream van bearing the words 'Mind that child' (as these vehicles do, to promote child safety in traffic) has almost completely melted into a puddle as a result of global warming (fig. 30).



**Figure 30: The Glue Society *Hot With Chance Of A Late Storm* 2006 (Beaumont, 2006)**  
Image reproduced from [www.sculpturebythesea.com](http://www.sculpturebythesea.com)

Paradoxically, this work is constructed from polystyrene—a petroleum-based plastic. In this case, the medium is in opposition to the message, but it can be argued that because the environmental impact of the message is so potent, possibly engendering multiple environmentally beneficial actions from its audience, the detrimental effects intrinsic to the medium should be regarded as insignificant.

Perhaps this illustrates an important distinction between what is created by an artist expressing intent at a point in time, and what is lived by artists who express their values over the course of their lives. Joseph Beuys is a case in point. Beardsley (1988, p. 159) describes Beuys as 'an artist for whom the morally and socially engaged act was entirely synonymous with art; his life was his art'. This description of a morally and socially engaged act is one to which the current research project aspires.

Since this project also aims to incorporate industrial and agricultural waste into the ceramics developed, reference is briefly made to a number of artists who have used waste in the construction of art works.

### **Use of waste in the creation of artworks**

Julie Wilson-Foster collected discarded plastic shopping bags to create sculptures drawing attention to the impact of waste on the environment (fig. 31).



**Figure 31: Julie Wilson-Foster *Flotilla* 2005 (Wilson-Foster)**  
Image reproduced from [www.jwf-artist.com/](http://www.jwf-artist.com/)

In Bahasa, Indonesia, *sisa* means leftovers or remains (Crosby, 2007). The sculpture by Tanam Untuk Kehidupan (fig. 32), which was constructed from discarded objects, was part of a curated exhibition rejecting hyper-consumption and overdevelopment (Crosby, 2007).



**Figure 32: Tanam Untuk Kehidupan *Insect* 2007 (Crosby)**  
Image reproduced from <http://www.gangfestival.com/program.html>

Adrian Kondratowicz designed *Trash*, a work made from biodegradable, bright pink garbage bags for New York City, bringing attention to the issue of waste in a humorous fashion (fig. 33) (Dembosky, 2008).



**Figure 33: Adrian Kondratowicz *Trash* 2008 (Kondratowicz)**  
Image reproduced from <http://www.streeteditors.com/archives/4481#more-4481>



John Dahlson is an Australian environmental artist whose practice includes work assembled from articles washed up on beaches. Dahlson's (2001–2010) photographs of two works appear below (fig. 34 and fig. 35).

Dahlson says:

*I see the real need for the massive social transformations that are essential, to adequately deal with such crises as the depletion of fossil fuels and climate change. I hope this work can be a timely reminder to us all of the limited supply of these petroleum-based materials, which is a direct result of our current collective global mass consumerism. (Dahlsen, n.d.)*



**Figure 34: John Dahlson Triptych 2005 (Dahlson)**

Image reproduced from <http://www.johndahlsen.com/index.html>



**Figure 35: John Dahlson Thong Totems 2003 (Dahlson)**

Image reproduced from [http://www.johndahlsen.com/detail\\_totem/Thongtotems.html](http://www.johndahlsen.com/detail_totem/Thongtotems.html)

In 2011, artist Elpida Hadzi-Vasileva undertook a residency at Pied-a-terre restaurant in London, and used kitchen waste to create artworks that were subsequently displayed in the restaurant (Austen, 2011). Gibson's (2011) image below (fig. 36) shows *Make A Wish*, a series of quail sterna that she gold-plated and assembled for a wall piece:

*I am interested in the transformation of something that is disgusting when you talk about it, but when you have finished working on it, becomes a thing of beauty. (Austen, 2011, p. 62)*



**Figure 36: Elpida Hadzi-Vasileva *Make A Wish 2011* (Gibson)**  
Image reproduced from *New Scientist* No. 2831, 24 September 2011, p. 62

Reviewing these works led to the consideration of how clay has been used to make environmental statements. The following section is reproduced from a published essay about three exhibitions using clay in various forms (Smout, 2011).

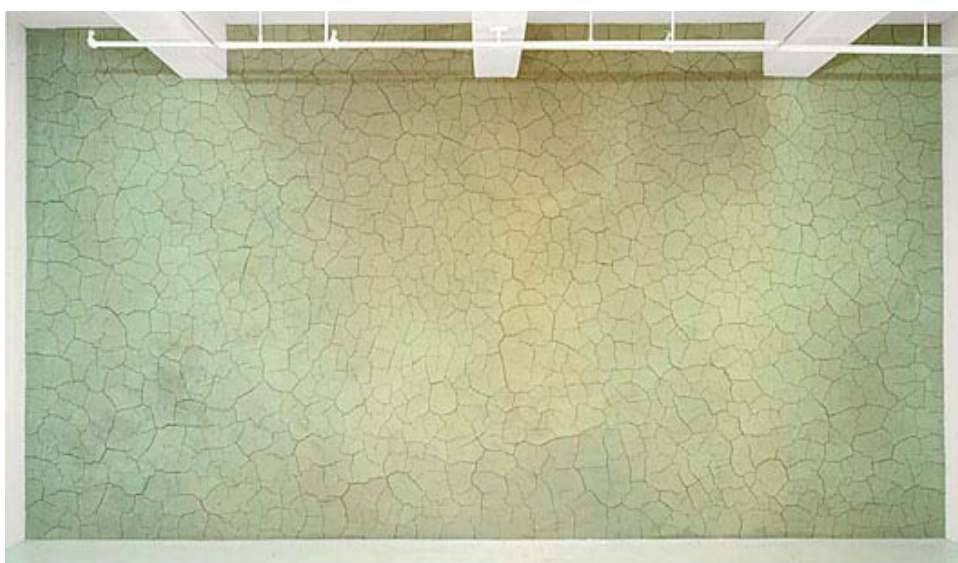
### **Transformations: clay and our environment**

There has been talk about climate change and global warming. We have been debating whether it exists; if so, what the causes might be; and finally, what we (or preferably someone else) should do about it. In the midst of all the claims and counter-claims, statistics and rhetoric, science and religion, there is, of course, the contribution of art. This article describes recent contributions of several artists working with clay, suggests that audience interaction with their work illustrates different perspectives about human impact on the environment, and reflects on their potential for prompting a range of responses from studio ceramicists.

When we visit a gallery, we enter an artificial environment designed to focus our attention and enable us to interact with the artworks. The environment is

established as installation of the work proceeds. Three recent exhibitions have taken their audiences into gallery environments where the installed clay works underwent dramatic changes during the course of the exhibition. Each of these exhibitions was fascinating in its own right. Of particular interest here is the extent to which the changes that occurred were the result of audience participation, the extent to which audience members were aware of this, and the extent to which changes in their behaviour could influence the outcomes.

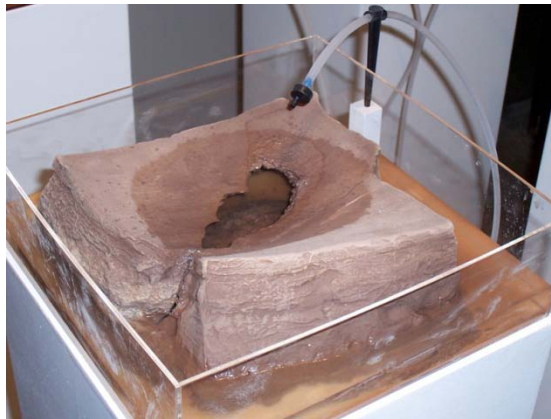
The first of the three exhibitions referred to was by Andy Goldsworthy. In May 2007, Goldsworthy installed a layer of damp white porcelain onto the walls of the otherwise empty *Galerie Lelong* in New York (fig. 37). These *White Walls* were roped off and the audience was not permitted to touch the installation. Over time, the clay dried, cracked and fell off the walls. Successive visitors arrived at points of increasing degradation, and only repeat visitors witnessed more than one stage of the transformation into a pile of debris. Gallery visitors were in the position of observers, witnesses to a process of destruction over which they had no influence. The devastation would have happened even without their presence. Perhaps the process was imperceptibly hastened by the heat emanating from their bodies, the draught from the doorway caused by their entrances and exits, and the vibrations from their footsteps, but essentially they were bystanders.



**Figure 37: Andy Goldsworthy *White Walls* 2007 (Goldsworthy)**

Image reproduced from *This Week in New York* website: [twi-ny.com/twiny.06.06.07.html](http://twi-ny.com/twiny.06.06.07.html)

In contrast, the installation *Fragile Ecologies* at the 2006 National Council for Education in Ceramic Art (NCECA) conference in Portland, USA, positioned observers as accidental participants in the transformation of an ecological system. Artists Elizabeth Stanek, Andréé Singer Thompson and Valerie Ortani installed wet clay slabs, dry blocks, miniature clay boulders and mounds of powdered clay in a number of partially enclosed environments (Jones, 2006). They positioned sensors near each exhibit, and the proximity and movement of delegates triggered a variety of impacts upon the established ecologies. Applications of water dripped from above to splash and carve channels (fig. 38) or trickled around to rise like an eroding tide (fig. 39).



**Figure 38:** Elizabeth Stanek, Andrea Thompson & Valerie Ortani *Fragile Ecologies* 2006 (Binrock, 2006)

Image © Simmons, reproduced with permission from [mike.binrock.net/tags/sculpture](http://mike.binrock.net/tags/sculpture)

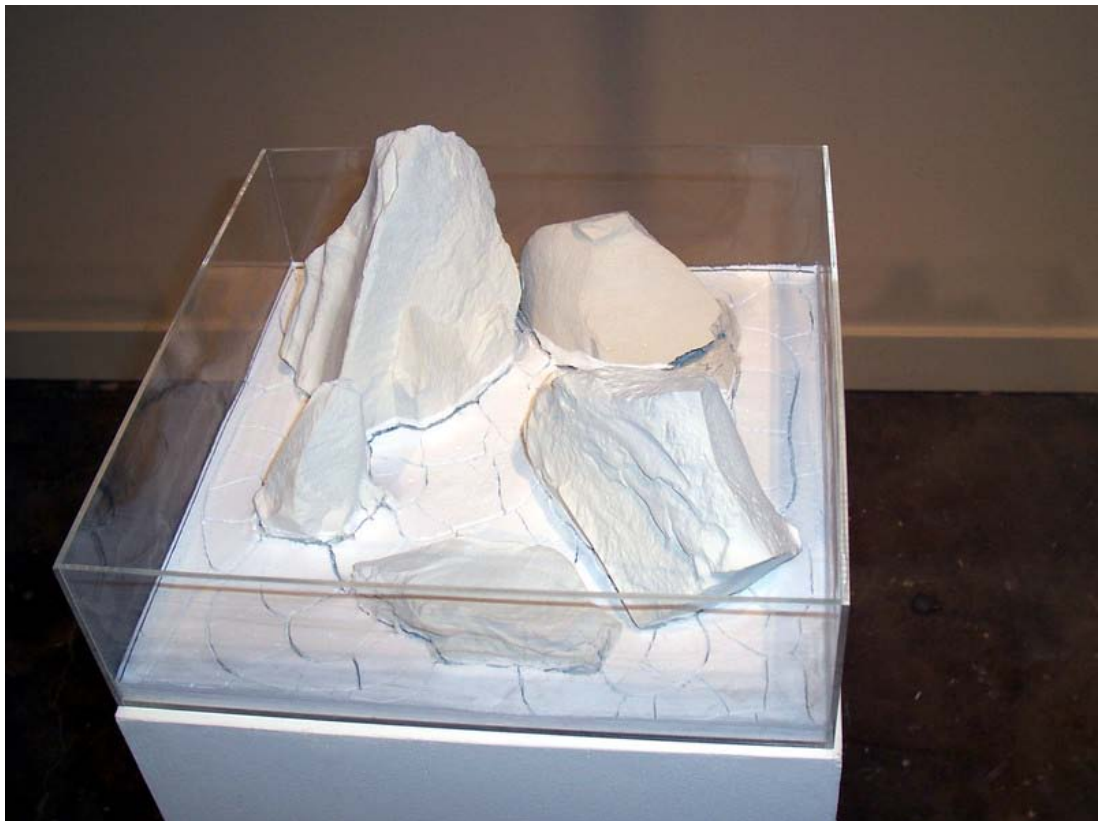


**Figure 39:** Elizabeth Stanek, Andrea Thompson & Valerie Ortani *Fragile Ecologies* 2006 (Binrock, 2006)

Image © Simmons, reproduced with permission from [mike.binrock.net/tags/sculpture](http://mike.binrock.net/tags/sculpture)

Air blown by fans or heat from heat-lamps accelerated drying processes, cracking and warping the original forms. Participants could potentially notice the unintended impact of their presence, evaluate the cumulative impact of their

own and others' actions and choose whether to repeat the actions that caused an obvious effect. The effect of their actions was indirect because it was mediated by machinery, and again they were not permitted to touch the work. The sense of responsibility was heightened, but because the results could be aesthetically pleasing and therefore regarded as desirable transformations, there was not necessarily a sense of culpability. The ecologies could easily be viewed as transformed rather than damaged (fig. 40).



**Figure 40: Elizabeth Stanek, Andrea Thompson & Valerie Ortani *Fragile Ecologies* 2006 (Binrock, 2006)**

Image © Simmons, reproduced with permission from [mike.binrock.net/tags/sculpture](http://mike.binrock.net/tags/sculpture)

The third exhibition on this continuum was at CSIRO Discovery Canberra, Australia in 2003. Australian artist Ken Yonetani deliberately and inescapably prompted audience consideration of individual and collective responsibility for environmental degradation. Over a period of months, Yonetani cast 2,200 porcelain tiles, each approximately 30 cm square and each depicting, in relief, one of ten endangered butterfly species. The fragile bisque-fired *Fumie Tiles* were installed onto the floor of the otherwise empty gallery in Canberra (fig. 41 and fig. 42).



**Figure 41: Ken Yonetani installing tiles (Hee)**  
Image reproduced from <http://www.kenyonetani.com/Kenworksfumie-tiles.html>



**Figure 42: Ken Yonetani Fumie Tiles 2003 (Hee)**  
Image reproduced from <http://www.kenyonetani.com/Kenworksfumie-tiles.html>

On the exhibition's opening night, the doors were opened and visitors entered as a group, with those at the front restricted from turning back to the entrance by the narrowness of the corridor. As a result, they were forced to walk on the tiles until the gallery widened out. The fragile tiles shattered underfoot (fig. 43).



**Figure 43. Ken Yonetani Fumie Tiles 2003 (Hee)**  
Image reproduced from <http://www.kenyonetani.com/Kenworksfumie-tiles.html>

Video footage shows the reaction of the visitors on opening night, in which the work of five months was almost completely destroyed in 45 minutes (Yonetani, 2008). Reactions included puzzlement, dismay, enjoyment of the crackling sensation underfoot, gleeful destruction, careful inspection, destructive attempts to view the range of species before they were gone, and rescue attempts. Even

those who attempted to rescue individual tiles had to accept that they had been part of the destruction. This third exhibition confronted visitors with irrevocable first-hand evidence of their culpability in a destructive process, whereby something fragile and aesthetically pleasing was reduced to rubble. There was a collective momentum to destruction, and yet individuals were innocent of all intent, at least until they became aware that taking one more step would annihilate one more butterfly. At that point, each individual had to decide what he or she would do.

These three exhibitions enable a parallel to be drawn between ourselves as visitors to a gallery environment and ourselves as part of the stream of humanity inhabiting planet Earth.

If we are in a world that parallels Goldsworthy's gallery environment, then climate transformation is a natural process that happens independently of our actions, which have negligible impact. Only a massive coordinated intervention that may be technically beyond us would prevent the transformation that is underway.

If we are in a world that parallels the fragile ecological environment of the NCECA exhibition, then our actions are the primary cause of climate transformation. The change thus far may be irreversible, but now that we have noticed, we could collectively choose to refrain from actions that may make the situation worse.

If we are in a world that parallels Yonetani's gallery environment, then we have been recklessly destructive, and our collective inability to stop ourselves will result in the extinction of many beautiful species, and severe stress on our own.

Yonetani's work may help to explain why some of us were relieved to hear that the academic integrity of the science claiming undeniable associations between industrialisation and climate change had been undermined by utilisation of unreliable or inaccurate sources in sections of the politically compromised

Intergovernmental Panel on Climate Change (IPCC) report.<sup>34</sup> Until the contributory impact of human activity is established, understood and believed on a personal level, we remain innocent of all intent—surely a more comfortable experience than consciously contributing more than our share to an ecological transformation that could harm so many.

The intrinsic characteristics of clay were fundamental to the impact of the work presented in these three exhibitions. All were of relevance to those of us who work with the elements of earth, water, air and fire to create ceramic articles of extreme longevity. We have a love for clay and what can be done with it. As we extract heat from sources including electricity, coal, wood, LPG and diesel, and perhaps share the delights of shooting flames into the night sky, the question of whether we should change our behaviour in response to reports of global warming is one for each of us. The answer to this question depends on whether global warming is real, on whether our behaviour is partly responsible, and finally on whether changing our behaviour would have any noticeable benefit. Judgements will be left to our descendants—to those who, like gallery visitors on successive days, will see the next stage of transformation.

Whatever transformation occurs, this planet, with its beautiful rocks and clays, and atmosphere that sustains and contains us, will outlast all but fragments of the ceramic objects we create. The choices we make as artists are recorded on the clay we work with, on those fragments of ceramic made durable by fire. Perhaps the individual choices we make about the ways we live and work will also accumulate and be recorded on the ecological history of the planet.

---

<sup>3</sup> Emails revealed the private efforts by the IPCC author and the former director of the East Anglia Climate Research Unit, Jones, to blunt the sceptics' scrutiny of some of his early temperature research and argue against freedom of information (FOI) requests for this data. The unvarnished comments in some of the emails from Jones have damaged the reputation of the world's leading climate research units. The IPCC was drawn into the crisis when a British science reporter picked up a howling error in one of the critical 2007 reports handed down under Pauchari. The error was not contained in the scientific findings of observed climate change or its advice to government, but in a 938-page report on the impacts of warming. That report included a reference to a claim that the Himalayan glaciers could melt by 2035. The IPCC and Pauchari compounded the error, many believe, by their slowness to issue a correction. (Wilkinson, 2009)

<sup>4</sup> Posted online: ClimateGate theory: The uncovering fo [sic] a series of emails that shows leading scientists connected to the IPCC have engaged conspiracy to defraud by manipulating data, intimidating peers who disagree, rejoicing at the death of detractors and refusing (illegally) to release raw data on which their models are based. (Cubby, 2009)



## Ceramic artists' writing about environmental concerns

Environmental artists who create impermanent works (for example Graddy, 2005; McEwan, 2007) and visual artists who comment publicly on environmental concerns (for example, Harrison, 2008) attempt to minimise the environmental impact of their processes and production. Ceramic artists have been among those making environmental commentary through their work, via publications and media and through online discussion (Harrison, 2008; Jones, 2006; McEwan, 2007). Inevitably, some of the discussion has focused on the environmental impact of producing ceramics.

Steve Harrison is one Australian potter who has been espousing and practising an ecologically considerate approach. He has exhorted others to use waste timbers to fire kilns, and to conduct shorter firings in better-insulated kilns, in order to reduce carbon emissions (Harrison, 1989). He has converted his studio to operate on solar power (Harrison, 1992), and prepares his clays and glazes from local materials (Harrison, 2009) (fig. 44 and fig. 45).



**Figure 44: Steve Harrison Native Bai Tunze Bowl 2008 (Harrison)**  
Image reproduced from <http://www.ceramicart.com.au/ct24.shtml>



**Figure 45: Steve Harrison Native Bai Tunze Bowl 2008 (Harrison)**  
Image reproduced from [http://www.craftaustralia.org.au/library/review.php?id=a\\_more\\_assured\\_maturity](http://www.craftaustralia.org.au/library/review.php?id=a_more_assured_maturity)

Of course, there is a range of opinion among ceramic artists regarding the necessity to consider environmental concerns when producing ceramic art. Following publication of Harrison's (2009) article, artist concerns about the green credentials of studio ceramics formed one of the longest running discussions of the *Ceramics in Australia* listserv in recent history. This was apparent by the varied emailed contributions to the topic of sustainability in May 2009. Some expressed concern about the ecological defensibility of wood firing (Winter, 2009), even though it is less damaging to the environment than firing with LPG or, worse, with electricity (Rye, 2009). Some provided suggestions for lowering emissions through process modifications such as stack scrubbers (Dellow, 2009) or single firing (Shatrov, 2009). Some argued that the contribution of individual ceramicists is insignificant (Vaux, 2009) or that accountability for unjustifiable emissions is unnecessary, simply because one should not be accountable to others (Howard, 2009). The debate thus moves into ideas of ethics and has also taken on a moral complexion, with reports of ceramicists being viewed as sinners with large carbon footprints (Winter, 2009). There are also those who propose taking an analytical approach by applying the concept of food miles to ceramics, so we arrive at considerations of 'clay miles' and life cycle analysis (Johnston, 2009).

This chapter has provided a brief survey of environmental art, referenced artists who have incorporated waste in their creations, reviewed some artworks made of clay, sampled ceramicists' views regarding the environmental impact of firing, and concluded with concepts emerging from the sustainability literature. This literature is discussed in the next chapter.

### Chapter 3: Sustainability, Green Chemistry and Engineering

In his 2005 essay on sustainability and sustainable development, Tapas Das from the Washington Department of Ecology notes that in order to be classified as sustainable, production must be (i) economically viable, (ii) environmentally responsible, (iii) safe for both producers and consumers and (iv) a contribution to societal good. In order to satisfy the first three requirements, Das exhorts producers to practise green chemistry and green engineering, which he defines as follows:

*Green chemistry is the process of designing of chemical products and chemical processes that reduces or eliminates the use and/or generation of hazardous substances. (Das, 2005a, p. 193)*

*Green engineering is the design, commercialisation and use of processes and products that are feasible and economical while minimising both the generation of pollution at the source and the risk to human health and the environment. (Das, 2005a, p. 197)*

Many of the 12 principles of green chemistry formulated by Anastas and Warner (1998) are applicable to ceramic processes, including: waste prevention, reduction or elimination of by-products, use and generation of least toxic substances, minimal use of solvents and additives, optimal energy efficiency, use of renewable biomass, use of catalysts to reduce energy needs, and effective monitoring of emissions. Green engineering adds to this list: conservation of resources and ecosystems, integration of local materials, minimisation of material diversity, and Life Cycle Assessment or Life Cycle Product and Process Design (Anastas & Zimmerman, 2003; Das, 2005a, 2005b).

Life Cycle Assessment involves auditing and quantifying all the environmental impacts for a product from when the raw materials are gathered, and at each stage of metamorphosis until all the raw materials are dissipated back into the environment (Das, 2005b). As such, it involves a systematic assessment of adherence to the principles identified above. Life Cycle Assessment is done in retrospect. Designing with advance consideration of the staged impact of a

process or product to make it 'benign by design' (Cote & Smolenaars, 1997) is referred to as Life Cycle Product and Process Design (Das, 2005a).

Where an existing process or product is intended to be re-designed, Life Cycle Product and Process Design includes a Life Cycle Assessment before and after redesign, with the redesign taking into account existing and potential legislation, emerging technology, and changing customer preferences, as well as reviewing chemistry and engineering to reduce environmental impact. The time, resources and expense required to conduct life cycle analyses inevitably lead to incomplete analyses due to lack of information or investment decisions regarding the ratio of cost to benefit (Das, 2005b). A thorough analysis and design may have up-front costs, but may also minimise non-productive by-products or wastes that have consumed investment and which, depending on their level of toxicity, have treatment and disposal costs requiring investment at the end of the cycle. There is therefore potential for considerable loss of investment at the end of the cycle, and in keeping with the adage 'Better late than never', there is scope for investment recovery.

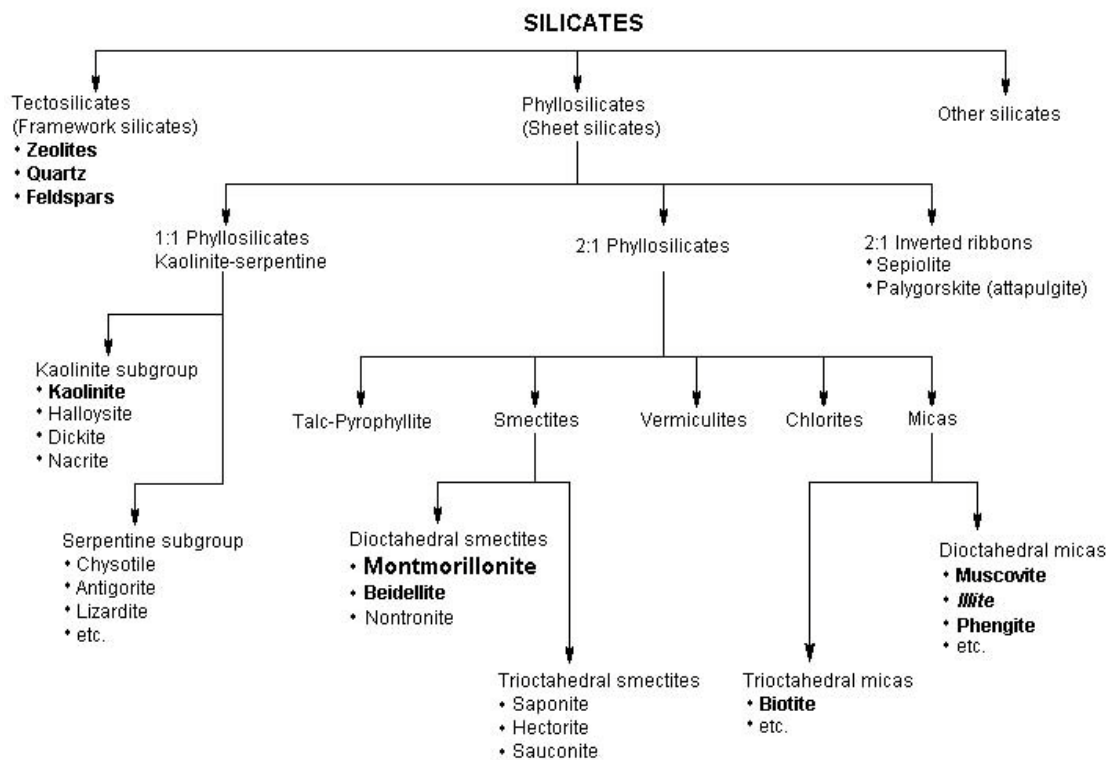
Investment recovery aims to reduce disposal and increase recycling and re-use, and can be conducted by the producer or by a specialist company occupying the 'decomposer niche' identified by Cote (2003) as the societal position equivalent to organisms that feed on waste. Despite the unbidden mental imagery, negative connotations and caste implications of this nomenclature, the terminology captures both economic opportunism and a holistic environmental perspective involved in investment recovery, and the current project to utilise waste clearly occupies this niche. Balancing the anxiety provoked by this attribution of parasitic opportunism is the reassuring thought that recycling has, at least temporarily, become a populist moral crusade that assigns noble qualities to those who practise it. Ceramic artists concerned about the environmental impact of their art may therefore take comfort from using a clay body that incorporates industrial and agricultural waste.

What might be the possible constituents of a clay body that is benign by design? The following chapter employs the classification of clays provided in the

ceramics literature to focus on naturally occurring constituent clays that could be expected to be of some utility in formulating a low-temperature body.

## Chapter 4: Classification of Clays

The American Ceramic Society defines clay as ‘a fine-grained rock which, when suitably crushed and pulverized, becomes plastic when wet, leather-hard when dried and on firing is converted to a permanent rock-like mass’ (Grimshaw, 1971, p. 29). The characteristic of becoming ‘plastic when wet’ is usually attributed to the structural nature of the silicates present in clay being phyllosilicates or sheet silicates, where the sheets slide over one another when water is adsorbed on their surfaces. Bailey’s (1980) diagram shows the classification of silicates on a structural basis (fig. 46).



**Figure 46: Classification of silicates on a structural basis (Bailey)**

Image reproduced from [www.inchem.org/documents/ehc/ehc/v231eh02.gif](http://www.inchem.org/documents/ehc/ehc/v231eh02.gif) (p. 15)

*Minerals that can be frequently found in bentonite or kaolin are in bold; the main components are in large typeface. Illite is a component of common soil and sediments and is classified as a mica. (Adamis & Williams, 2005, p. 15)*

It must be noted, however, that there is no agreed authoritative source for classification of clays, and there is disagreement between sources. Konta

(1995) includes montmorillonite, beidellite, nontronite and saponite among the smectites, as does Bailey (1980). Konta (1995, p. 277) refers to all the smectites as strongly expanding three-sheet phyllosilicates. Cardew (1977) makes no reference to smectites, and refers to all the above minerals as members of the montmorillonite group, then divides only montmorillonite into swelling and non-swelling subtypes.

Cardew's (1977, p. 24) diagram of the clay mineral family (fig. 47) also differs from Bailey's in the categorisation of illite, since Cardew does not classify illite as a mica. There is some consensus that it should be thus classified (McMeekin, 1985; Tichane, 1990).

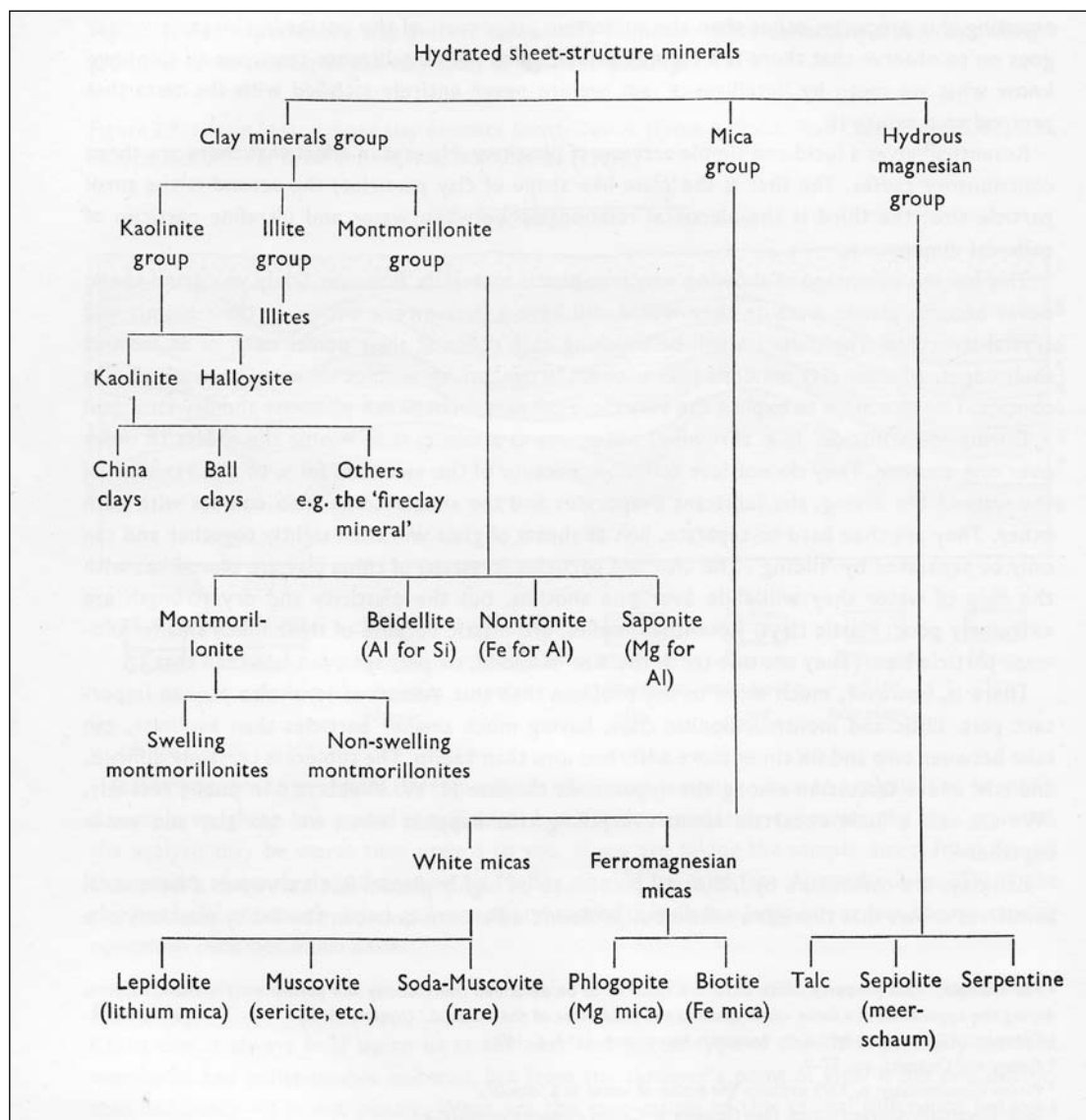


Figure 47: Diagram of the clay mineral family (Cardew, 1977)

Cardew's classification system is still useful for the studio ceramicist because it separates china clays, ball clays, and fire clays, a distinction which, as explained below, has some relevance for this research.

### **Clays for low-temperature bodies**

For the purposes of developing a low-temperature body, the expected inclusion of substantial proportions of non-plastic flux materials directs investigative attention towards clays that may compensate by contributing most to plasticity. These include only ball clays from the kaolinite group (china clays are excluded due to non-plasticity and fire clays due to refractoriness), illites and montmorillonites. Although these three clays are classified separately, they often co-occur in clay deposits (McConville & Lee, 2005), as described below. This explains some of the discrepancies between the classification diagrams reproduced above. The three types of clay expected to assist in adding plasticity to a low-fire fluxed body are presented below. Factors considered relevant to body formulation are addressed.

#### **Ball clay**

Ball clays are secondary clays, having been weathered from feldspars and carried from their primary location by glacier, wind, or, most frequently, water (Rhodes, 1973). The weathering process leaches fusible alkalis and an abrasive water-borne journey with natural levigation, and subsequent sedimentation produces greatly diminished particle size. The journey also results in additions of organic matter and other minerals including both illite and montmorillonite (Tichane, 1990). Due to the contribution to plasticity from these additives and their variability within deposits, Tichane recommends use of more than one ball clay, in order to minimise the impact of sudden changes in supplied ball clay on body properties. Ryan (1978) notes that iron and titanium impart colour to fired bodies, but the colour of the unfired ball clay is not a good guide to the extent to which this will occur. This is because dark organic matter in unfired ball clay will burn out.



## Illite

Illite is an extremely common sedimentary clay mica, or hydrous mica (McMeekin, 1985) which has less silica and more alumina than montmorillonite (Cardew, 1977). On this basis, illite could be expected to be less useful for promoting vitrification, but vitrification is promoted by the presence of potassium in illite (Cardew, 1977). Potassium is a low-temperature flux (Currie, 2000), but experimentation is required to determine the potential contribution of clays high in illite to a low-temperature body. Despite their prevalence, including in Australia (McMeekin, 1985, p. 72), illites are usually components of other clays and the present author has found no reference to any clay sold as illite, although Silver Hill clay from Montana in the US is available for research purposes and is reported to consist predominantly of illite (McConville & Lee, 2005). McMeekin (1985) refers to clays high in illite being used at Mittagong Pottery in NSW and in Sydney, Australia. Ryan (1978) reports that bricks are frequently made from illitic clays and Crispin (2008) suggests sourcing illitic clays from NSW brickworks.

## Montmorillonite

The montmorillonites are a subset of the class of clay minerals frequently referred to as smectites or bentonites (Tichane, 1990). Bentonite will be used as the umbrella term, as smectite and montmorillonite are occasionally named (along with illite) as constituents of bentonite, (for example, see Dananaj, Frankovska & Janotka, 2005) and as bentonite is the name under which this class of materials is commonly sold to ceramicists. Bentonites, which are named after a large deposit near Fort Benton in Central North America, are formed by decomposition of volcanic ash or lava (Hamer, 1975). Their composition varies considerably, including within deposits (Holmes, 1983) and they are variously sub-classified as swelling or non-swelling bentonites (Cardew, 1977), and sodium or calcium bentonites (Tichane, 1990). Although montmorillonite is regarded as a primary contributor to plasticity in ball clays (Tichane, 1990), Fuller's earth contains montmorillonite but is non-plastic (Cardew, 1977).

Bentonite's characteristic of swelling when wet, which makes it a useful agent for glaze suspension, results in problems in workability and in extremely high shrinkage, and renders it unsuitable as a stand-alone clay body (Rhodes 1973). During firing, the montmorillonite component is reported to liberate about 50% ultra-fine free silica, making glazed ware vulnerable to shattering (Cardew, 1977). The upper limit on the desirable percentage of bentonite in a clay body is frequently stated as being 2% (Hamer, 1975; Rhodes, 1973; Tichane, 1990), but McMeekin (1985) allows up to 5% and reports using 10–15% after treatment with dilute hydrochloric acid. Tichane (1990) recommends that bodies containing bentonite receive thorough dry mixing, thorough wet mixing and a week of aging in the wet state.

Bentonites generally require a number of features in order to be commercialised, for example, cation exchange capacity over 60, pH between 6 and 12, and low content of grit over 75  $\mu\text{m}$  (Holmes, 1983). Most bentonites have a proportion of iron oxide that can be expected to detract from the whiteness of any body in which bentonite is a constituent. Various additives, including chalk or blue colourants (Grimshaw, 1971), may be used to attempt a remedy.

Arumpo bentonite is mined 80 km northeast of Mildura, on the NSW side of the Victorian border, where it lies in a 5-metre thick band extending over 9 square km (Churchman et al., 2002). Characterisations of Arumpo bentonite performed by Churchman and colleagues indicated that it swells much less than Wyoming bentonite, has lower viscosity in aqueous suspensions of the same concentration, and very low permeability to water, even under pressure. Arumpo bentonite was also shown to consist of much smaller particles and to provide far greater external surface area as a consequence. It was reported to consist of 99% smectite/illite, with illite layers randomly interstratified at a ratio of one illite to ten smectites (Churchman et al., 2002). It has unusual properties for a bentonite, including a pH of approximately 4, and the mining company is meeting resistance in having it officially classified as a bentonite (Gardam, 2008).

Although Churchman and colleagues (2002) performed their analyses with environmental barrier applications in mind, their findings indicated that Arumpo bentonite has characteristics of interest in body formulation. A number of hypotheses arise regarding this clay, which may be classified as a non-swelling bentonite. The minimal swelling when immersed is predictive of lower wet to dry shrinkage, which has favourable implications for minimising warpage during the drying process. Because of the fine particle size, Arumpo bentonite may contribute to plasticity more than a bentonite of larger particle size. The low swelling and presumed low shrinkage may allow greater percentage additions than of other bentonites. Mixing may also be easier. The low permeability may necessitate a longer aging period to allow for even penetration of water throughout the body. Some of these hypotheses are tested later herein (Chapter 9).

Having considered the constituent clays that are likely to contribute to formulation of a low-temperature body, some consideration of the desirable characteristics of a clay body is necessary. These characteristics are identified and expanded upon in the next chapter.

## **Chapter 5: Desirable Characteristics of Glass/Ceramic Body to be Developed**

When embarking on the task of developing a new body, it is necessary to consider the range of characteristics that are generally considered to be desirable. This chapter reviews a range of these characteristics.

### **Desirable characteristics of a body when raw**

#### Plasticity

Plasticity is defined by Hamer as ‘the unique property held by clays which combines [sic] the strength of a solid with the fluidity of a liquid’ (1975, p. 226). He claims that plasticity involves no elasticity, whereas Grimshaw (1971) maintains elasticity is a precursor to flow as a body undergoes pressure. Tichane (1990) holds that a plastic body deforms under pressure, but retains its shape when pressure is removed. None of these attempts to define plasticity in clay take account of the ‘memory’ effect whereby deformations performed and corrected during construction reappear upon drying or firing (McMeekin, 1985) or where actions performed are partially undone (for example, when a wheel-thrown teapot spout unwinds). Unfortunately, no agreed standard measurement for plasticity has emerged. However, there is general agreement (for example, Grimshaw, 1971; Hamer, 1975; Tichane, 1990) on a number of factors on which plasticity depends, including: water content and dispersal; air content; the proportion and nature of non-clay additives; and constituent particle size, surface area and molecular bond, shape, orientation and uniformity.

There are calibrations available for many of these factors that determine plasticity. Modesto and Bernardin (2008) have found a simple indentation method to be a more reliable, fast, practical and precise estimation of plasticity than the Pfefferkorn method (which relies on determining the percentage of water required to obtain maximum plasticity for a body). Moore (1963) described a plastometer test based on compressive methods that may represent plasticity more accurately. He suggests that a sufficiently plastic body

should keep its shape when low stress is applied, but deform readily once its yield point has been exceeded.

The studio ceramic literature propounds reliance on the practised sensitivity of the potter or ceramicist for determining whether a body will meet the demands of their production techniques (for example, Cardew, 1977). This is indeed useful at the studio, but is too late when one is considering the contribution of various clays to a new body formulation, and does not provide a readily communicable means of comparison. Gonzalez-Murillo (2007) obtained and recorded a practical and useful visual comparison by photographing extruded body formulations and adding qualitative comments and numerical ratings of plasticity.

Grimshaw (1971) lists a number of methods of increasing body plasticity, including changing the proportion of water, vacuum pugging, removing non-plastic material, adding colloidal substances or flocculating agents, grinding to reduce particle size and increase hydrolysis, reversing the electrical charge, developing thixotropy, and increasing acidity through aging or via direct addition of weak acids. Grimshaw (1971, p. 506) regards the addition of oils or aqueous gums, colloids or 'ferments' to impart plasticity as resulting in 'pseudo-plasticity', although he provides no rationale for this label. Materials used to impart plasticity include 10% (by weight) polyalcoholvinyllic in water (Basegio et al., 2002).

### Dry strength

Dry strength is the strength of the body after shaping and drying, but before firing (Ryan, 1978). Before discussing a range of techniques and additives designed to increase dry strength, it is necessary to note the fundamental importance of the size of clay particle. Rhodes (1973, p. 15) states:

*the property of dry strength is directly related to particle size, and thus to plasticity; the more plastic a clay is, the more strength it will develop in the dry state.*

Cardew (1977, p. 257) agrees that 'Green strength is nearly always closely related to plasticity'. Grimshaw (1971, p. 555) reports that 'it is well established that the specific surface area of the particles in a dried mass is directly related to the strength developed', and Ryan restates the direct relationship: 'the higher the clay content of the body and the finer the particle size of the clay the greater will be the strength of the dry articles' (Ryan, 1978, p. 24).

Since plasticity is improved by reducing the particle size of body components, it could be assumed that the finer a body, the more plasticity and therefore dry strength it will exhibit (although plasticity and dry strength will not occur at the same time). It would follow that selecting body components with fine particle sizes (for example, ball clays rather than kaolins) and grinding or sieving to reduce particle size of coarser components would be standard practice. Tichane (1990) warns against adoption of grinding or sieving procedures as a matter of course, not only because of the time and cost associated with grinding and sizing, but because of the risk of producing a body of homogenous particle size. Homogeneity of particle size has a negative effect on the density with which particles pack together, with the higher proportion of pore space resulting in decreased dry strength (Tichane, 1990).

Grimshaw (1971) describes how the process of grading (mixing of particles of various sizes in established proportions) enables denser packing, but cautions that the benefits obtained must be weighed against the increased difficulty of removing water and organic material from the body during firing.

At odds with this is Worrall's (1986) report that his studies of kaolins and illites indicated no relationship between pore size and particle size distribution. Worrall (1986) speculates that the modes of packing differ because of differences in electrostatic attraction rather than purely because of particle size. Although he proposes that this speculation requires experimental confirmation, the explanation of deflocculation outlined below shows that bodies with the same particle size distribution can demonstrate marked differences in packing density and therefore dry strength.

In a plastic clay body, the platelets are not evenly dispersed but aggregate together in 'flocks' (Rhodes, 1973). The addition of a soluble deflocculent (commonly sodium carbonate and/or sodium silicate) increases the electrostatic forces of repulsion so the particles disaggregate and disperse (Hamer, 1975). The particles remain discrete until the body is almost dry, enabling tighter packing, and greater density and dry strength (Worrall, 1986).

Clays respond differently to the same deflocculent and testing is required to ascertain the most beneficial amount and combination. Deflocculents are used extensively in casting slips and rarely in plastic bodies (Worrall, 1986, p. 172).

There are also effects of particle alignment on dry strength in plastic clays, as well as in casting slips. When shapes are formed from plastic clay, the long axes of the platelets align parallel to the direction of the force applied, resulting in more surface contact and greater dry strength, increasing in proportion to the force applied (Ryan, 1978).

There are a number of variables contributing to dry strength besides particle size and distribution, electrostatic forces, and force applied during forming. These have been made evident as a result of the adoption of a mechanical test of dry strength. The testing procedure most commonly used to compare the dry strength of clay bodies is one whereby the modulus of rupture is ascertained by applying gradually increasing pressure to the centre point of a bar of dry clay supported by two blades at a fixed span (Reid, 2011). Using this procedure, Pask (1953) noted that different results were obtained from different ceramic laboratories testing the same clays for dry strength, and from the same laboratory when clay preparation varied. He investigated a range of variables, and found that (in addition to any variation resulting from the shape of the bar tested and the rate at which pressure was applied) mixing time and aging of the clay, extrusion variables and humidity all affected dry strength.

Grimshaw (1971) noted that materials consisting largely of plastic clay increase in strength and rigidity when dried slowly, and included binders in his claim that:

*The strongest unfired mass consists of a suitably graded mixture of angular grains of various sizes selected so as to produce as compact a mass as possible and provided with a sufficient amount of binding material to cover each particle of aggregate and bind them together.*  
(Grimshaw, 1971, p. 873)

Binders 'provide strength and plasticity to ceramic green bodies', but rapid pyrolysis of organic binders can cause 'spalling, cracking, blistering and voids' in the fired article (Tsai, 1991, p. 547). Plastic bodies with greater percentages of adhesive clays (for example, montmorillonites) can tolerate inclusion of non-plastic materials. The range of binders includes: organic gums (for example, gum Arabic, gum tragacanth), sodium alginate (Rhodes, 1977); ammonium alginate (Taylor & Bull, 1986); dextrin, flour, starch, molasses (Grimshaw, 1971), polyethylene glycol, polyvinyl alcohol (Baklouti, Chartier & Baumard, 1997); water soluble acrylic polymers, resin emulsions, methyl cellulose, hydroxymethyl cellulose, hydroxypropyl cellulose (Taylor & Bull, 1986); carboxymethylcellulose, Veegum (inorganic colloidal magnesium aluminium silicates refined from smectites) and Additive A, which is an industrial plasticiser based on lignosulfonates (Zamek, 1998).

Coarser cellulose fibres in the form of processed and unprocessed plant material (for example, paper, henequen and straw) have been used extensively to impart dry strength to adobe, brick (Gonzalez-Murillo, 2004) and studio ceramics (Conrad, 1981; Farrow, 1987; Fuzi, 2006; Gault, 1998; Goldate, 2003; Hay, 1996; Miller, 1994). Synthetic fibres have also been used, including nylon and fiberglass (Conrad, 1981).

Significant gains in dry strength may be possible by use of a combination of the techniques above. For example, Douda (1920) reported that wet grinding and small additions of caustic soda and dextrin resulted in increased dry strength of previously low-strength clay by over 2000%.

Because the dry strength of clay is significantly affected by how hydroscopic it is, there is not a direct relationship between the strength of a clay at the standard drying temperature of 110<sup>0</sup>C and its strength at room temperature and conditions (Saxe and Buckner, 1915). Saxe and Buckner (1915) note that the



strength of clays between 110°C and red heat is lower than their strength at room temperature. This is relevant to kiln stacking if pieces are supported by other pieces.

### Wet to dry shrinkage

The small particle size that increases plasticity and dry strength also increases shrinkage (Ryan, 1978). As described above, as water leaves a drying clay body, particles converge until touching. Considerable shrinkage occurs, with accompanying risks of cracking and warping. The water content of the body when the particles converge is referred to as the critical moisture content (Ryan, 1978).

Wet to dry shrinkage is calculated by measurement of a line of fixed length marked on clay of working consistency using the formula (Ryan, 1978, p, 29):

$$(\text{Wet length} - \text{dry length})/\text{dry length} \times 100\%$$

Higher wet to dry shrinkage is associated with greater risk of warping and cracking. In the current project, body formulation is aimed at increasing plasticity and dry strength, and lowering vitrification temperature through reduced particle size. Therefore, shrinkage requires monitoring.

## **Desirable characteristics of fired ceramics**

### Colour

A white-firing body is often sought after because it lends itself to additions of colourants and because applied coloured glazes appear brighter. The appearance of fired clay is also affected by light. Light can be transmitted, reflected, refracted or diffracted, and the colour of ceramic objects perceived by the same person will differ with the prevailing light conditions (Grimshaw, 1971).

Materials may be opaque or translucent, opalescent, fluorescent, phosphorescent, pleochroic<sup>5</sup> or lustrous (Grimshaw, 1971).

A test of whiteness and brightness can be made with a reflection spectrophotometer, which concentrates light reflected from a sample onto a photocell to measure the intensity (Grimshaw, 1971). This process can be used on dry clay samples, and body constituents can be selected based on whiteness. There are also methods available for removing colour from clay, including removal of iron by washing, magnetic separation, dissolution, flotation, addition of a complementary coloured material or bleaching (Grimshaw, 1971).

Discolouration can occur during firing as a result of fly ash or deposits from gasified fuel, volatilised material from nearby ware, and efflorescence of soluble material or staining by insoluble substances (Grimshaw, 1971). Discolouration can be influenced by temperature and firing conditions. For example, the tendency for iron content to stain a whiteware body yellow or grey increases with vitrification, but can be counteracted by an oxidised firing cycle with a brief period of reduction just below peak temperature (Heine, 1972).

### Translucency

Translucency refers to the extent to which light travels through a material. Comparisons require that the samples being compared are of the same thickness.

#### *Translucency tests*

Tests of increasing sophistication are possible depending on the resources available. Possibilities include holding two samples up to the light, constructing a light box and applying a strip of black adhesive tape to the back of the samples (Tichane, 1990), or using a photo-electric light meter (Haldy, Wright & Todd, 1947).

---

<sup>5</sup> A pleochroic material appears to change colour when the viewing angle is changed.

### Acoustic resonance

Conrad (1981) suggests that only bodies fired to cones 5–10 will emit a slight ring when struck. Tichane (1990) notes that the absence of ring may be indicative of cracking or under-firing if observed in a body that previously rang when struck. Grimshaw (1971) warns against relying exclusively upon any test of acoustic resonance to determine a lack of vitrification because of the multiple factors that may also affect this characteristic. These factors include micro-cracking instigated by glaze under tension (Stairs, 1997) or thermal shock (Bemis, Shiloh, & Ellingson, 1996), geometric complexity, size and heterogeneity from voids or layering (Erau, Vander Gucht & Cambier, 2004).

### Hardness

Hardness can be tested using Mohs scale:

*Mohs hardness, (is defined as the) rough measure of the resistance of a smooth surface to scratching or abrasion, expressed in terms of a scale devised (1812) by the German mineralogist Friedrich Mohs. The Mohs hardness of a mineral is determined by observing whether its surface is scratched by a substance of known or defined hardness. (Encyclopaedia Britannica, n.d.)*

A commonly used grouping is that any ceramic article that can be scratched by iron is soft and any that cannot be scratched by steel is hard (Grimshaw, 1971). For studio ceramics, it is useful for the fired article to be hard enough to resist abrasion and impact. These qualities are not necessarily correlated (Grimshaw, 1971) because impact rapidly tests multiple forms of strength: tensile (resistance to stretching); compressive (resistance to squashing); torsional (resistance to twisting); shear (resistance to cutting) and bending (resistance to bending).

### Fired strength, porosity and permeability

Grimshaw states that 'the strongest burned material consists of a mass of interlocking crystals formed *in situ* and united by a glassy cement' (Grimshaw, 1971, p. 873). According to Grimshaw (1971), fired strength is affected by various factors associated with the manner in which ceramics are fired,

including rate of temperature increase, temperature range at which any reduction occurs, intensity of reducing atmosphere, temperature reached, duration at top temperature, and rate of cooling—especially at critical points such as 573°C, when quartz inversion is accompanied by rapid contraction.

Ware that is to contain liquid is required to be impermeable, which usually implies it is not porous. These two related qualities of permeability and porosity are explained further below.

### Permeability

*Permeability may be defined as the readiness with which a substance permits a fluid to flow through it. (Grimshaw, 1971, p. 435)*

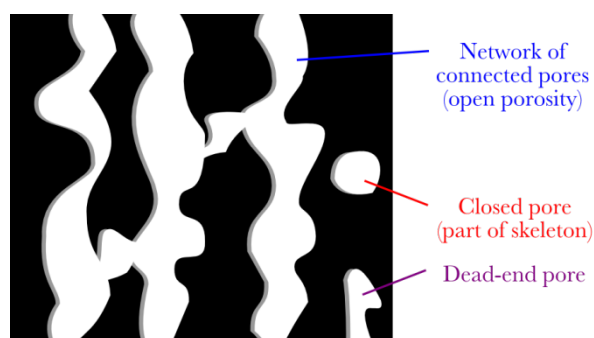
### Porosity

*The porosity of a material is defined as the total proportion of the air space contained between the solid particles of which the body is composed. Porosity should not be confused with permeability, for the latter implies interconnected voids, while the former embraces void spaces of all kinds. (Grimshaw, 1971, p. 417)*

This is further clarified by ASTM standard C242–12:

*Open porosity—the volume fraction of all pores, voids, and channels within a solid mass that are interconnected with each other and communicate with the external surface, and thus are measurable by gas or liquid penetration. (ASTM International, 2007)*

Figure 48 provides a visual representation of open and closed porosity.



**Figure 48: Open versus closed porosity (Jaouen, n.d.)**  
Reproduced from <http://apmr.matelys.com/Parameters/OpenPorosity.html>

### Test for fired strength

Because shape and glaze fit affect the strength of ceramic articles, the same shape should be used to test various bodies, and the glazed body should be tested with the knowledge that crazed glazes can instigate body cracks (Stairs, 1997). In the standard transverse test, the fired sample is supported by two blades and the force applied to the centre of the sample is gradually increased (Grimshaw, 1971). The results of multiple tests are averaged to obtain the force required to result in breakage, and the average is entered into the formula to calculate the modulus of rupture. The Digitalfire site (Hansen, 2003) provides the formula as:

$$M = 8PL/\pi 3d$$

where P = force (pounds), L = Span (inches) and d = diameter of bar at break (inches)

Grimshaw (1971, p. 861) provides the formula as:

$$T = 3Wl/2bt^2$$

where W = breaking strain (pounds), l = span (inches), b = width (inches) at break and t = depth (inches) of the test piece at break

Fired strength of shale clays has been shown to increase dramatically between 900°C and 1000°C, and again between 1000°C and 1100°C, corresponding with the development of a glassy phase (Grimshaw, 1971). The aim of the current project is to develop a body that has acceptable fired strength below 1000°C. Because of the importance of the formation of a bond through sintering and vitrification, the next chapter is devoted to definitions and descriptions of sintering and vitrification, and how these processes might be promoted at lower temperatures.

## Chapter 6: Sintering and Vitrification

Sintering and vitrification are two different but overlapping ceramic processes that result from the application of heat. Sintering involves heating a porous mass until it densifies and strengthens (Green, Guillon & Rodel, 2008). Crystal growth occurs well below the temperature of liquid formation, and as crystals interlock and merge, the void space between crystals in a sintering body shrinks (Grimshaw, 1971). This is referred to as solid-state sintering (Barsoum, 1997). Vitrification is the formation of glass in a material, and in ceramics the densification of the clay by a microscopic developing matrix of melted glass is referred to as liquid-phase sintering (American Ceramic Society, 2005). This process can advance until so much fusion has occurred that the material is described as fused (Grimshaw, 1971), and slumping of forms may result (Ryan, 1978).

From this explanation, it is apparent that glass can be part of a ceramic structure. It is also possible that a ceramic structure will contain no silicates. Although it is expected that ceramics developed through this project will be silicate-based, a brief explanation of the preceding statement will lead to consideration of some additional factors.

Barsoum defines ceramics as:

*solid compounds that are formed by the application of heat, and sometimes heat and pressure, comprising at least one metal and a non-metallic elemental solid or a non-metal, a combination of at least two non-metallic elemental solids, or a combination of at least two non-metallic elemental solids and a non-metal* (Barsoum, 1997, p. 2)

This definition encompasses both advanced and traditional ceramics. Traditional ceramics are typically silicate-based porous microstructures formed from clays and feldspars by a variety of techniques, whereas advanced ceramics may be synthetic or not silicate-based, and are generally much finer, more homogeneous and much less porous (Barsoum, 1997). The current project focuses on the formulation of a body suitable for use in traditional ceramics, but takes account of potential contributions from the field of advanced ceramics, including glass-ceramics, which are defined below:

*Glass-ceramics are polycrystalline materials of fine microstructure that are produced by the controlled crystallisation (devitrification) of a glass. (Rawlings, Wu & Boccaccini, 2006, p. 733)*

Their composition is different to the parent glass and their mechanical properties are described as superior (Rawlings et al., 2006). Glass-ceramic formation requires both (i) nucleation, where pockets of crystallisation form around a nucleating agent, and (ii) growth, where the crystal growth is fed by molecular transfer from the glass (Rawlings et al., 2006).

Barsoum (1997) devotes a chapter in his text *Fundamentals of Ceramics* to the sintering process. He describes the process from first principles and provides molecular-level illustrations and competing models for explanations of densification and coarsening (an unintended increase in grain size resulting in increased porosity). The reader is referred to this text for an in-depth scientific discussion of the sintering process. For the purposes of the current project, it will be sufficient to list factors identified as beneficial or detrimental to successful densification, so that some of these factors may be considered in preparation and firing of test bodies and in analysis of results. Except where indicated, the listed factors are distilled from detailed explanations in Barsoum's (1997) text:

- The finer the particle size, the greater the surface area, and so finer particle sizes will be beneficial for densification.
- Finer particle size will not be beneficial for densification if agglomerates form in the green body as a result of electrostatic and other surface forces.
- Deflocculation will assist in preventing agglomeration as long as the body is not dried and re-wet before shaping (Lange & Kellett, 1989).
- Narrow grain size distribution will be beneficial for densification, as the growth of abnormally large grains (and correspondent porosity) will be less likely.
- Higher density green bodies will produce higher density fired bodies than lower density green bodies of similar formulation.

- Chemically pure formulations will obtain benefits in sintering from the addition of selected impurities.
- Liquid-phase sintering will result in faster and more uniform densification than solid-state sintering.
- The penetration of grain boundaries (wetting) with the melting liquid is required for the above benefits of faster and more uniform densification to accrue.
- Densification in liquid-phase sintering will result from the wetting liquid both filling pores and rearranging solid particles.
- At least partial solubility of the solid phase in the liquid phase is required for further diffusion to follow particle rearrangement in liquid-phase sintering.
- Gases present in (or used as) the sintering atmosphere can promote or suppress densification.
- Increased temperature will enhance diffusion and sintering.

The final factor, temperature, is central to the current project, which aims to produce a sintered body below 1000°C. Accordingly, a review of methods of lowering sintering temperature follows.

### **Methods of lowering sintering temperature**

The focus of the current project is reducing the temperature at which a studio ceramic or glass-ceramic body becomes strong and non-porous. Ceramic scientists and engineers working in industry and in applied research have devoted the most attention to reducing sintering temperature. They have taken physiochemical approaches (varying the constituents), physiomechanical approaches (mechanically processing the constituents and formulations) and thermophysical approaches (controlling firing patterns) (Krupa et al., 1997).

#### Physiochemical approaches

Deliberate inclusion of auxiliary fluxes or replacement fluxes for feldspar can be traced back to the French soft porcelain, or *pate tendre*, of the eighteenth



century and subsequently to Belleek ware from Ireland (Austin & Brooks, 1941). These inclusions reduced the firing temperatures used, and the results were regarded as successful imitation porcelain.

In 1922, in an address to the Terracotta Division of the American Ceramic Society, EC Hill reported on the positive effects on absorption and fired strength of a terracotta body achieved by adding a range of fluxes (Hill, 1922). Nepheline syenite was used as the sole flux employed to lower commercial whiteware body vitrification to cone 3 (Koenig, 1942). When nepheline syenite was combined with talc (85:15), ball clay and kaolin, vitrified bodies with less than 0.3% absorption at cones 02–2 were produced (Lynch & Allen, 1950).

Russian industrial researchers found that additions of 30% montmorillonite decreased the temperature at which liquid-phase sintering occurred in kaolinitic clays used in tile manufacture (Abdrakhimov, Abdrakhimova & Abdrakhimov, 1999).

In Slovenia, alkaline germinate, which melts at around 700°C, was used as a sintering aid to reduce by 100 degrees the temperature at which potassium sodium niobate densified (Bernard et al., 2008).

Sintering temperature of an advanced ceramic was reduced from 1350°C to 875°C with the addition of barium-copper-boron ceramic powder (Kim et al., 2007). Chai et al. (2008) sintered zinc titanate ceramics at 850°C using 5% additions of borosilicate glass powder. In the field of industrial ceramics, silicate-free zinc metaborate glass binders were melted at 650°C (Barabanov et al., 2005). Guan, Chen and Luo (2007) reported sintering barium titanate at 900°C by adding 20% barium carbonate/zinc oxide/lanthanum carbonate glass as flux. Lim et al. (2007) found that when both B<sub>2</sub>O<sub>3</sub> and CuO were added, sintering of barium titanate was achieved at 900°C.

Illite is an 'aluminium-potassium mica-like non-expanding di-octahedral mineral' present in sedimentary clay and rocks (Ferrari & Gualtieri, 2006, p. 73). Illite imparts plasticity, and the inclusion of up to 35% of clays high in illite was found to increase the formation of glass and decrease the water absorption of

stoneware tile bodies, allowing lower firing temperatures (Ferrari & Gualtieri, 2006).

The temperature of liquid-phase formation in a glass batch was reduced by 100°C (to 523°C) as a result of the inclusion of 1% sodium chloride (Savard & Speyer, 1993). Sodium silicate additions reduced the heat work required to produce enamel (Manson, 1931).

Caution is suggested regarding the potential for fluxed bodies to exhibit undesirable characteristics. Some sources (Clare in Hill, 1922; Worrall, 1986) warn against using fluxes to lower the softening point of clay bodies below 1100°C because of the likelihood of slumping. Koenig (1942, p. 231) notes that 'warpage resistance depends largely on maintaining a high viscosity in the glassy phase in bodies with a high flux content ... by having a high alumina content'.

#### Physiomechanical approaches

It is noteworthy from the above that using materials with small particle size aids sintering, and processing of materials to reduce particle size is a commonly selected method of promoting sintering. This is because the densification process depends on particle-to-particle contact, and the finer the particle size, the greater the surface area available for contact, and the greater the surface energy of the powder (Ryan, 1978; Barsoum, 1997).

Tichane (1990) notes that grinding a clay body can reduce vitrification temperature by as much as 50°C.

Calcite ball-milled in ethanol to 1.5µm and pressed in a ratio of 20:80 with New Zealand kaolin was sintered into a dense anorthite ceramic at 950°C (Kobayashi & Kato, 1994). Glass batches with an average particle size of 45µm melted 35°C lower than batches with an average particle size of 250µm (Savard & Speyer, 1993)

## Thermophysical approaches

Avalova (1979) extended the vitrification range (between first sintering and deformation by bloating) of various clays, finding that slower firing resulted in increased deformation temperature. Cui and Zhou (2008) found that calcining (heating in a container) glass-ceramic composites below their sintering temperature prior to pressing (instead of melting them above their sintering temperature then grinding the insoluble glass to powder) reduced the eventual sintering temperature required.

### **Considerations when firing ceramics**

It is generally recommended that slow firing and an oxidising atmosphere should be maintained so that carbon within the body is burnt off before the surface vitrifies rather than being trapped within the body, which can be weakened and discoloured (Ryan, 1978). The implications for the current project, where incorporation of agricultural waste is intended, and vitrification is intended to be well advanced below 1000°C, are that:

- atmosphere should be strongly oxidising during the heating phase of a slow firing cycle
- cross-sections of fired bodies containing agricultural waste should be examined for internal discolouration
- tests of fired strength should be repeated if reducing atmosphere is included as a variable in the firing cycle.

## **Chapter 7: Inclusion of Industrial, Municipal or Agricultural Waste in Clay and Glaze**

As described above (Chapter 6), industry has researched methods of lowering the sintering temperature of clays and the vitrification temperature of glazes. There has also been considerable research into utilisation of waste to achieve these goals. This research, which has been motivated by concerns for cost reduction, waste minimisation and reduced energy consumption, is surveyed below.

Inclusion of silicate-based recycled industrial or agricultural waste in industrial manufacture of glassware and clay body/glaze formulation has been reported in Russia (Koval'chenko & Pavlenko, 2006), India (Rahman, 1987), the UK (Dyer & Dhir, 2001), the US (Henstock, 1976), Italy (Barbieri, Corradi Bonamartini & Lancellotti, 2000) and other Western and European countries (Dhir, Limbachiya & Dyer, 2001). Glass cullet has been included in brick and tile (Avalova, 1979), and industrial clay bodies and glazes have included rice husk ash (RHA) as a source of fine amorphous silica (Prasad, Maiti & Venugopal, 2001). Fly ash (small coal ash particles carried in flue gases) and bottom ash (larger coal ash particles that fall to the bottom of the furnace) tannery ash, sewage sludge and slag from urban waste incineration have all been utilised or trialed (Rawlings, Wu & Boccaccini, 2006). Use of other slag-type wastes reported includes copper slag, phosphorus slag and induction gasification combined cycle slag from petroleum refining, steel-fly ash (electric arc furnace dust), cement dust, fluorescent glass and waste seashell, galvanising and anodising residue, and jarosite and goethite (waste products of zinc-hydrometallurgy) (Rawlings, Wu & Boccaccini, 2006).

### **Glass**

Soda lime glass is already a vitreous silicate ... and ... vitreous silicates act as fluxes, reducing clay body maturing temperatures. (Mustafi et al., 2011, p. 169)

One of the terracotta body fluxes investigated by Hill in 1922 was powdered glass. Since that time, the addition of low-softening-temperature glass has been used frequently as an economical means of achieving reductions in sintering temperature (Guan, Chen & Luo, 2007).

The ability of soda lime cullet to form a matrix containing other ceramic materials (because of its relatively low melting point) has been exploited in the formation of industrial ceramics and building materials including tiles and cladding (Dyer & Dhir, 2001). For example, Balkyavichus et al. (2003) produced a reduction of 150°C in the sintering temperature of illitic clay tiles through additions of finely dispersed glass. Inclusions of up to 10% in building brick produced energy savings, reduced emissions and enhanced durability (Smith, 2004, p. 30).

Soda lime-silica cullet was combined with nepheline syenite to lower the firing temperature of a commercial porcelain to 1100°C (Tavornpanich, Souza & Lee, 2005). Replacement of feldspathic sand with clay and cullet up to 6% of the body formulation was successful in an Italian commercial whiteware (Rambaldi et al., 2007). Additions of 7% cullet to a Russian majolica clay body increased strength and decreased porosity in the range of 980–1000°C (Yugai, 2001). Cullet has also been used to improve the durability, appearance and mechanical strength of ceramic surfaces (Dhir & Dyer, 2001) and to lower the melting temperature of glazes and the sintering temperature of studio clay bodies. For example, the Seattle Clay Company began with recipes for various studio bodies, including a cone 06 body and a cone 06 slip, and systematically replaced one or more flux ingredients with TriVetro Corporation crushed cullet (Seattle Pottery Supply, 1999). They report minor reductions in shrinkage, and dramatic reductions in absorption. They also found that 100% cullet substitutions for 38% talc in a slowly fired (25°C/hour) cone 06 body reduced absorption from 12% to approximately 2.5%. The authors report the need for further research on improving plasticity to overcome the equally dramatic limitations on workability imposed by cullet substitutions over 20%. They also note that finer (325F grade) cullet produced better results. Their experiments adding the same cullet to cone 06 casting slip resulted in highly vitrified slips,

but also resulted in rapid degradation of moulds and rapid settling out of the glass from the slip (Seattle Pottery Supply, 1999).

Miller (1994) does not mention similar problems when using an earthenware paper-clay made from casting slip containing fine cullet, so investigation of the comparative workability of bodies made from low-fire cullet-containing slips with and without cellulose inclusion is warranted. Miller provides the following recipe, to which 30–50% pulped and drained paper was added:

FX ball clay	6 kg
BBR kaolin	5 kg
silica (300 mesh)	6 kg
fine cullet (glass)	3 kg
water	10 L
sodium silicate	70 g
Dispex (liquid)	70 g

Cullet has been combined with a binder and mixed into *pâte de verre* (glass paste) for fusing in a kiln (Kirk, 2001). An addition of 5% borosilicate glass improved the fusibility of zinc titanate ceramics at 850°C (Chai et al., 2008).

## **Paper**

Paper-reinforced clay has been used increasingly in studio ceramics since Carol Farrow published her article about developing it at art school (Farrow, 1987), and Rosette Gault popularised it with demonstrations and writings (e.g. Gault, 1998).

In Sweden, Jeoung-Ah (2006) mixed waste photocopy paper and mixed paper into an industrial porcelain body and found that it imparted superior strength and workability, and reduced weight and wet to dry shrinkage. A scanning electron microscope (SEM) revealed that tubular cellulose fibres were inundated with clay particles and water. The inclusion of kaolin, calcite and talc during paper manufacturing (Jeoung-Ah, 2006) suggests that consideration should be given to the fluxing or refractory effects of these materials.

Bennett (2008) recommends using cellulose insulation made from recycled newspaper because the boron added as a fire retardant prevents mould growth in stored clay and contributes flux to lower sintering temperature.

### **Paper sludge ash**

The production of recycled paper results in sludge, which is incinerated into paper sludge ash (PSA), much of which is deposited in landfill (Wajima et al., 2006). Wajima et al. report that the chemical analysis of PSA is similar to volcanic ash. In Australia, paper sludge is used solely for soil conditioner (Pauley, 2008).

### **Fly ash**

Spanish researchers Aineto, Acosta and Iglesias (2006) incorporated fly ash from gasification of coal and petroleum coke during electricity generation into clays of medium and high plasticity. They report that additions up to 20% produced positive effects on sintering, water absorption and mechanical strength, with negligible impact on plasticity and shrinkage. They speculate that these benefits are obtained as a result of the glass-like composition of the ash, its small particle size, and an exothermic reaction of the ash at around 750°C. Their characterisation of coal gasification fly ash revealed an absence of the quartz, lime and mullite typically found in conventional coal-fly ash. An American company has successfully pressed clay-less construction-grade bricks from coal-fly ash at room temperature (Fowler, 2011).

The addition of less than 1.5% fly ash from power stations burning natural bitumen emulsion had negative effects on the product aesthetics and production effluents in brick-making (Dondi et al., 2002).

Fly ash from municipal waste incineration usually contains so many hazardous residues (Rawlings et al., 2006) that it would not be feasible to use it in a clay body, although it has been successfully used in glass-ceramic formation. For example, fly ash from incineration of Korean municipal waste was combined

with silica, magnesium oxide and titanium dioxide, and crystallised into a glass-ceramic at 870<sup>0</sup>C (Park & Heo, 2002).

### **Wood ash**

Leach (1976) documents a long history of wood ash usage in stoneware glazes. He provides a table of analyses made of vegetable ashes in the late 1930s, and describes the customary preparation procedures used in Japan prior to incorporation of ash into glaze. The glazes referred to are all for stoneware or porcelain, and Tichane (1998, p. 83) states that the inclusion of wood ash in a low-temperature glaze is 'a contradiction in terms', but provides some suggestions to mix ash with frit or substitute ash for flux to achieve glazes around cone 04. Thurn (1945) also describes the incorporation of wood ash into a cone 04 glaze by using white lead as a flux. There is no mention of wood ash being included in a clay body.

### **Incinerated sewage sludge ash**

English researchers using 5% incinerated sewage sludge ash in brick-manufacturing trials report positive effects on linear shrinkage, green strength, sintering temperature, water absorption and fired tensile strength, but increased surface scumming as a result of soluble salt migration (Anderson, 2002).

### **Sugar cane bagasse ash**

Sugar cane grass grows 2–5 m tall and the stalks are crushed to be processed into sugar (Barroso et al., 2003). Sugar cane bagasse ash (SCBA) has been used in developing countries as a constituent in cement (Ganesan, Rajagopal & Thangavel, 2007) but relatively little reference has been made to its potential utility in ceramic bodies. This gap in the literature was recently addressed by Teixeira et al. (2008), who investigated using up to 10% SCBA from power-plant boilers as a replacement for quartz in a terracotta roofing tile. They found SCBA reduced plasticity, linear shrinkage and flexural strength below 1000<sup>0</sup>C, had



little effect on fired shrinkage, and reduced sintering temperature as a result of the flux content (Teixeira et al., 2008).

### Rice husk ash

Rice husk (also referred to as rice hull) comprises approximately 20% of a rice harvest by weight (Rama Rao, Sastry & Rohatgi, 1989). Rice husk is one of the highest energy fuels used for biomass gasification, having a calorific value around 16.7 MJ/kg (Ahmed, Ewais & Zaki, 2008). The Australian bioenergy sector rates the calorific value slightly lower at 14.4 MJ/kg—less than half the value of coal but nearly equivalent to wood (Table 3).

**Table 3: Typical energy content of fossil and biomass fuels**

<b>Solid Fuels</b>	<b>Net Heating Values (MJ/kg)</b>
<b>Biomass Fuels</b>	
Wood (wet, freshly cut)	10.9
Wood (air dry, humid zone)	15.5
Wood (air dry, dry zone)	16.6
Wood (oven dry)	20.0
Charcoal	29.0
Bagasse (wet)	8.2
Bagasse (air dry)	16.2
Coffee husks	16.0
Rice hulls (air dry)	14.4
Wheat straw	15.2
Corn (stalk)	14.7
Corn (cobs)	15.4
Cotton stalk	16.4
Coconut husks	9.8
Coconut shells	17.9
<b>Fossil fuels</b>	
Anthracite coal	31.4
Bituminous coal	29.3
Lignite	11.3
Coke	28.5

Reproduced from <http://www.aie.org.au/melb/material/resource/biofuel.htm> 8/09/2008

Inhabitants of developing countries have used rice husk as fuel in small home-built stoves (Bronzeoak, 2003). The fuel has been collected as discarded husks, and the husks, the smoke and the subsequently discarded ash have all contributed to environmental pollution in countries such as Thailand (Ueda, Kunimitsu & Shinogi, 2007). Consequently, attention has turned to

improvements in design that increase the efficiency of burning rice husk and reduce the resultant emissions (Belonio, 2005). The tendency of the husk to clog fireboxes has been overcome in large scale biomass energy production, (Ueda et al., 2007), and researchers at a Philippines university have successfully developed and marketed a rice husk stove that is clean and efficient enough for indoor use (Tandoc, 2009).

Burning rice husk produces, on average, 20% by weight RHA, with variation resulting from the ashing temperature (Rama Rao et al., 1989). Unprocessed or pelletised RHA has been used as an insulating material thrown onto molten steel to slow cooling en route to further steel processing (Bronzeoak, 2003). In a review of applications of silica made from RHA, Chandrasekhar et al. (2003) note its usefulness as a filler, abrasive and adsorbent; as a pozzolanic (reactive alumino-silicate) in cement; for soil and water treatment; and for a number of ceramic applications in addition to the possible contributions to body formulation outlined above. Several of the ceramic applications are described briefly below.

Based on early work in the former Yugoslavia, where lightweight 1700°C refractories were produced from 80% RHA and 20% fire clay, Ol'khovskii and Sartakov (1964) describe the successful experimental inclusion of ground rice husk as a superior combustible replacing sawdust in refractories. Silicon carbide has been produced from RHA (Sujirote & Leangsuwan, 2003). Other researchers developed experimental lightweight high strength refractories based on up to 80% RHA calcined at 1450°C, and noted that compositional increases in alkaline and iron oxides drastically reduced refractoriness (Adylov et al., 2005). RHA beneficiated by dilute hydrochloric acid (HCL) leaching, and calcining at 700°C successfully replaced 5% kaolinite and improved formation of pure cordierite (Kurama & Kurama, 2008).

Lithium alumina silicate glass-ceramics (prized for thermal and chemical durability) utilising RHA calcined at 1000°C were produced using the sol-gel method (Naskar & Chatterjee, 2005). RHA successfully replaced quartz in the development of ceramic pigment (Bondioli et al., 2007). Watari et al. (2006) fabricated silicon carbide from rice husk powder.

Dan, Chand and Rohatgi (1987) included up to 30% RHA and reduced the firing temperature of an Indian porcelain body, finding porosity most reduced with 10% additions. Rahman (1987) found RHA improved the fired strength of bricks fired at 1000°C. When Prasad, Maiti and Venugopal (2001) substituted 10% RHA for quartz in an Indian whiteware body fired to above 1100°C, they found it increased fired shrinkage and fired strength, and reduced thermal expansion and sintering temperature. They found that RHA inclusions up to 25% were possible, although fired strength decreased marginally. Because Sharma, Phanikumar and Varapasada Rao (2008) found that 12% addition of RHA contributed to compressive strength in swelling soils, RHA may assist green strength in studio bodies containing bentonite. However, Özel, Kurama & Ay (2002) found that when RHA was progressively substituted for 3–9% quartz in a slip casting whiteware fired at 1250°C, bulk density and fracture strength decreased, and porosity increased.

The many uses for rice husk are highlighted by the situation in Thailand, where attention has turned to proposals for apportioning rice husk supply to the competing demands for biomass fuel for rice mills and power generation, and to ash supply for soil conditioner and silicate fertiliser (Ueda et al., 2007). The price of husk was driven up accordingly and the potential for this to occur in Australia is noted. Ueda and colleagues contend that burning rice husk is carbon neutral, since the crop is grown repeatedly and the carbon emitted is the carbon absorbed during photosynthesis.

After loss on combustion (LOC) is accounted for, RHA contains 90–95% silica (Rama Rao et al., 1989) and is sometimes referred to as rice hull silica (Chang, Lin & Chen, 2001). At temperatures below 700°C, this is amorphous silica in the form of opal CT (Proctor, 1990). Variations in other chemical constituents are thought to be produced by variations in soil chemistry and fertiliser application rather than by differences between rice strains (Chandrasekhar et al., 2003). RHA analyses from various sources appear below.

Table 4: RHA analyses (wt%)

Country	USA	India (Jorhat)	India (Trivandrum)	India (Hyderabad)	Russia	Egypt	India	Turkey	Japan	China	Country
Source	Rama Rao, Sastry & Rohatgi (1989)	Rama Rao, Sastry & Rohatgi (1989)	Rama Rao, Sastry & Rohatgi (1989)	Rama Rao, Sastry & Rohatgi (1989)	Ol'khovskii & Sartakov (1964)	Ahmed, Ewais & Zaki (2008)	Prasad, Maiti & Venugopal (2001)	Özel, Kurama & Ay (2002)	Sanders (1967) <sup>6</sup>	Zhang Fukang (1986) <sup>7</sup>	Source
SiO <sub>2</sub>	94.5	94.5	91.4	89.4	90.86	66.3	88.44	88.32	96.0	94.4	SiO <sub>2</sub>
Al <sub>2</sub> O <sub>3</sub>	Trace	0.21	1.57	3.81	0.96	0.06	1.21	3.65	1.0	1.8	Al <sub>2</sub> O <sub>3</sub>
CaO	0.25	0.48	0.17	2.55	0.40	1.92	1.20	2.60	0.5	1.0	CaO
MgO	0.23	0.23	1.30	1.30	0.89		1.82	0.73	0.2		MgO
Na <sub>2</sub> O	0.78	Trace	Not examined	Not examined		0	0.50	0.10	0.3	1.3	Na <sub>2</sub> O
K <sub>2</sub> O	1.1	Trace	Not examined	Not examined		6.2	1.81		0.9	0 <sup>8</sup>	K <sub>2</sub> O
BaO											BaO
Fe <sub>2</sub> O <sub>3</sub>	Trace		0.62	1.95	0.40	0.78	0.40		0.04	0.6	Fe <sub>2</sub> O <sub>3</sub>
ZnO											ZnO
TiO <sub>2</sub>							Trace		0.2		TiO <sub>2</sub>
MnO	Trace	1.09	0.11	0.03					0.2		MnO
Cr <sub>2</sub> O <sub>3</sub>											Cr <sub>2</sub> O <sub>3</sub>
PbO											PbO
CdO											CdO
NiO											NiO
CuO											CuO
SnO <sub>2</sub>											SnO <sub>2</sub>
ZrO <sub>2</sub>											ZrO <sub>2</sub>
P <sub>2</sub> O <sub>5</sub>	0.53	Trace	Not examined	Not examined		0.07			0.02		P <sub>2</sub> O <sub>5</sub>
SO <sub>3</sub>	1.13	Trace	Not examined	Not examined	1.67						SO <sub>3</sub>
R <sub>2</sub> O					2.21						R <sub>2</sub> O
LOC					2.61	24.08	4.62	4.6			LOC

<sup>6</sup> Cited by Sutherland (2005), p. 137

<sup>7</sup> Cited by Sutherland (2005), p. 137

<sup>8</sup> K<sub>2</sub>O + Na<sub>2</sub>O = 1.3

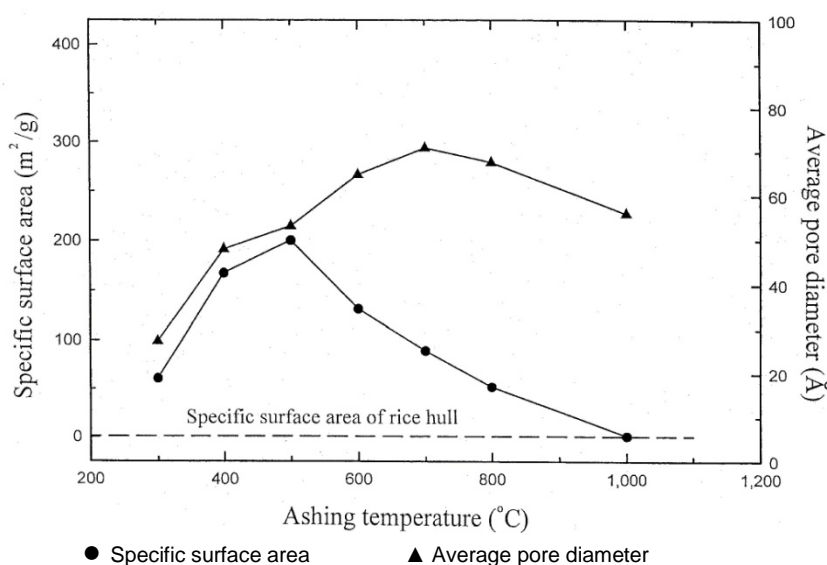
The duration for which the husk is ashed at a particular temperature affects the carbon content, with less carbon present in samples heated for longer. This was demonstrated by Chang, Lin & Chen (2001), who published results of ashing rice hull at 500°C for various durations.

**Table 5: Content of carbon, hydrogen and nitrogen: rice hull and RHA at 500°C**

	C (%)	H (%)	N (%)
rice hull	41.38	4.85	0.04
rice hull ash (6 min)	42.77	2.35	0.24
rice hull ash (12 min)	17.79	1.48	0.40
rice hull ash (18 min)	9.97	1.26	0.56
rice hull ash (30 min)	0.32	0.35	0.00
rice hull ash (60 min)	0.34	0.31	0.00
rice hull ash (120 min)	0.11	0.28	0.00
rice hull ash (180 min)	0.02	0.32	0.00

Adapted from Chang et al., 2001

Ashing temperature also affects particle size, with decreasing surface area associated with sintering above 600°C (Rama Rao et al., 1989).



**Figure 49: Effect of ashing temperature on specific surface area and average pore diameter**  
Reproduced from Chang, Lin & Chen, 2001

HCL leaching of rice husk, or RHA, has been used to purify the silica obtained up to 99% (Real, Alcalá & Criado, 1996). When acid leaching was performed before ashing, the surface area of the silica obtained was over 200 times as great as when acid leaching was performed after ashing. These researchers found that larger particle sizes resulted from the commencement of sintering due to the fluxing action of potassium. As shown below (fig. 50), a similar

increase in surface area was achieved by washing with boiling water, indicating that potassium was also removed by this alternative method.

**Table II. BET Specific Surface Area ( $S_{\text{BET}}$ ) and Specific Pore Volume of Calcined Rice Husk Samples**

Sample*	$S_{\text{BET}}$ (m <sup>2</sup> /g)	Pore specific volume (cm <sup>3</sup> /g)
A	<1	
B	<1	
C (600°C)	260	0.43
C (800°C)	211	0.36
D	209	

\*A is untreated sample, B is sample treated with HCl after combustion of the residual carbon, C is sample treated with HCl before burning the rice husks, and D is sample treated with H<sub>2</sub>O before burning the rice husks.

**Figure 50: Specific surface area and specific pore volume of calcined RHA**

Reproduced from Real et al., 1996

It was subsequently shown that acid leaching of charred RHA reduced the content of sodium and potassium by approximately 75% (Shinohara & Kohyama, 2004). Shinohara and Kohyama (2004) found less than 5% crystalline silica for unleached samples fired up to 700°C, but increasing levels of potentially harmful crystalline silica above this temperature. A further interesting result was that even washing the charred RHA with pure water of unspecified temperature prior to firing resulted in no crystalline silica being formed below 1000°C (Shinohara & Kohyama, 2004).

Implications from the above research for use of rice husk and RHA in studio ceramics are that:

- If the ash is used without washing (for example, in a glaze), more flux material will be available, but the silica will not be as fine and the raw ash should not be heated above 700°C to avoid formation of potentially harmful crystalline silica.
- If the husk is not ashed above 500°C, then washing is unnecessary because the fluxing action will not commence during ashing. Silica of fine particle size will be present, and the carbon content will be reduced to negligible levels if temperature is held at 500°C for more than 30 minutes.

- If extremely pure, small particle size silica is wanted, the rice husk should be leached in dilute HCL or washed in boiling water before ashing.
- If both flux content and pure, nano-particle size silica are wanted, the rice husk should be washed and sieved and the water retained for the flux content.
- If cristobalite is wanted, the washed husk should be heated above 1000°C, and the necessary precautions should be taken to avoid breathing dust.
- Below 1000°C, the silica from washed husk will be amorphous. This may be used to form sodium silicate, based on the research described below.

RHA has been converted into soluble sodium silicate using aqueous sodium hydroxide (NaOH) as the source of sodium (Foletto et al., 2006). Using a glass vessel, Foletto et al. combined sodium hydroxide with RHA as received from Brazilian industries. They reported 80% conversion to sodium silicate when the reaction occurred over 60 minutes at 100°C, and 92% conversion over 30 minutes at 200°C. They reported using a molar ratio of  $H_2O/SiO_2 = 22$  and  $NaOH/SiO_2 = 2$ , finding only the former ratio to be important, to reduce viscosity and enable filtering of the sodium silicate produced. The published macroscopic image of the RHA used indicates it was not burnt at sufficient temperatures to remove the carbon, which in turn would indicate that it was predominantly amorphous silica. However, their residues contained cristobalite, indicating that some of the ash received had reached temperatures above 700°C.

It is possible to produce amorphous sodium silicate using a process patented by Schimmel, Kotzian, Panter and Tapper in 1993. They used a ratio of 2:1 42% by weight NaOH in water:quartz. An aqueous solution of sodium hydroxide has been successfully and economically used to convert Brazilian RHA into sodium silicate (Foletto et al., 2006). Sodium silicate is used as a deflocculent in casting slips, and has been found to lower the heat time required to melt low-temperature enamels (Manson, 1931).

Novotny, Hoff and Schuertz patented a process for hydrothermal production of sodium silicate solutions in 1991. They stated that irrespective of the silica source, the aqueous sodium hydroxide should have a concentration range of 15

to 30%. Drain Clear™ (available in Australia) has a concentration of 16%, which indicated it would be an appropriate proprietary product with which to commence experimental production of sodium silicate from RHA.

### **Corn cob ash**

It is reported that about 25% of the biomass energy contained in corn is needed to dry it, with the balance available for other purposes (Doering, O'Hare & Peart, 1979). These purposes could include energy generation (see Chapter 14). Increasing attention is being paid to the potential for fuel production from corn cob (Christiansen, 2008), and so the availability of ash is likely to increase. There is also some promise for inclusion of corn cob ash in clay and glazes, given the finding that the alkaline components of corn cobs burnt in a fluid-bed gasifier produced problematic surface sintering of silica at 700°C (Van der Drift & Olsen, 1999).

### **Rock**

Acchar, Vieira and Segadães (2006) investigated the successful incorporation of up to 30% of the muds generated by Brazilian granite- and marble-cutting industries into a previously unusable local clay. Satisfactory control of plasticity and shrinkage resulted, and the fluxing effect contributed to sintering, with commencement of a liquid phase evident between 950°C and 1000°C.

In Portugal, Torres et al. (2009) incorporated the powdered by-product of granite cutting industries into the existing formulation of ceramic roof tiles. They found that up to 10% substitution for other non-plastics resulted in improved mechanical strength, sintered density and resistance to pyroplastic deformation above 1000°C. Below 1000°C, water absorption was decreased by 2% over the existing formulation, and at 1000°C, water absorption was decreased by 5%. At 1050°C, water absorption was markedly improved to 1%. Brazilian researchers Menezes et al. (2005) fired wall and floor tiles containing up to 35% granite sawing waste at 1200°C, but only reduced absorption once the tiles reached this temperature.



Catarino et al. (2003) investigated the use of compressed Portuguese slate powder as 100% substitute for clay and found that it formed a stronger tile at 1150°C.

Brazilian marble-cutting powder reduced the sintering temperature and improved the fired strength of a local red-clay brick, with improvements attributed to the dissociation of calcite and dolomite above 800°C, and inclusions of 15% recommended for a firing temperature of 850°C (Saboya, Xavier & Alexandre, 2007).

### **Tannery sludge**

Inclusions of up to 10% dried and powdered tannery sludge made no particular contribution to ceramic body properties, but incorporation into building materials immobilised sludge contaminants (Basegio et al., 2002). 15% Russian tannery ash was successfully incorporated as a green colourant in industrial glazes maturing at 1000°C (Levitskii & Papko, 1994).

### **Mixed wastes**

Several groups of researchers have investigated combining wastes from more than one source. Italian researchers formed glasses and glass-ceramics from a combination of cullet, bottom ash (from incinerated municipal waste) and steel-fly ash fired to 1500°C. (Barbieri, Bonamartini & Lancellotti, 2000; Lancellotti et al., 2001). Of particular interest to the current project is their finding that small additions of steel-fly ash induced earlier crystallisation in cullet, commencing at about 800°C. This was attributed to nucleation of the iron content.

Russian researchers Shil'tsina and Selinov (2000) worked with unprocessed quartz-feldspar tailings sand, mixing it with a local bentonite to which 30–50% cullet had been added. Pressing produced vitrified tiles at 1150°C. In Korea, fluorescent lamp cullet was pressed with ground seashells and sintered between 800°C and 1000°C to produce a durable glass-ceramic building

material (Yun et al., 2002). Toya et al. (2006) successfully fabricated glass-ceramic using only waste materials: waste from silica and kaolin refining (kara), and PSA.

### **Silica fume (micro silica)**

Condensed silica fumes from arc furnaces used in the ferrosilicon industry form a superfine amorphous silica powder (Bronzeoak, 2003).

### **Review of Whitfield's sources of industrial or agricultural waste in New South Wales**

Sand-washing tailings are the accumulated effluent resulting from processing sand for the concrete-manufacturing industry. Whitfield (1985) investigated the characteristics and potential for ceramic bodies to be developed from sand-washing tailings. He found that satisfactory bodies could be developed at earthenware and stoneware temperatures, but suggested that the excessive fired shrinkage and the high water content of the tailings resulted in them being more suitable as a body component than a stand-alone body.

Whitfield (1993) also obtained and examined industrial wastes from 15 Australian waste generators, and after sieving, or sieving and uni-axial pressing, heated them to cones 03 (1080°C), 5 (1180°C) and 10 (1280°C). He described the extent to which each sample was sintered. Of the industrial wastes sampled by Whitfield (1993), the most promising for incorporation into a low-temperature body are those that fused at 1080°C, followed by those that sintered at 1080°C, those that fused at 1180°C and finally those that sintered at 1180°C. Wastes that require crushing involve more energy and expense, and are therefore less preferred. Whitfield's results are presented in Table 6, showing the sample source, requirement for crushing and extent of sintering at cones 03 and 5.

**Table 6: Need of crushing and extent of sintering of selected wastes (Whitfield, 1993)**

Waste	Crushing	Sinter	
		1080°C	1180°C
Affinity Metals Ducon Hopper Dust	no	none	none
Affinity Metals Mill Bag House Dust	no	none	none
Affinity Metals Mill Cyclone Dust	no	none	none
Affinity Metals Salt Slag	yes	some	some
Ajax Foundry Slag	yes	sintered	fused
Austral Brass Foundry Waste Mould Sand	yes	slight	slight
Australian Perlite Cold Bag House Fines	no	sintered	fused
Australian Refined Alloys CuS Dross	no	fused	fused
Australian Refined Alloys Soda Based Slag	no	sintered	sintered
BHP Whyalla Ladle Slag After Nitrogen Bubbling	yes	none	none
BHP Whyalla Ladle Slag Before Nitrogen Bubbling	yes	slight	slight
BHP Whyalla Blast Furnace Slag SW Spray Cooling	no	none	none
BHP Whyalla Precipitator Flue Dust	no	slight	some
BHP Whyalla Lime Kiln Scrubber Dust	no	none	some
BHP Whyalla Pellet Plant Preheat Cyclone Dust	no	slight	some
BHP Whyalla Blast Furnace Dust Catcher Dust	no	slight	some
Boral Munmorah Primary Fly Ash	no	slight	sintered
Boral Raymond Terrace Dust	yes	slight	sintered
Boral Peats Ridge Dust	yes	slight	fused
Boral Dunmore Dust	yes	slight	fused
Boral Mugga Dust	yes	slight	sintered
Boral Picrite Dust	yes	none	sintered
Boral Port Kembla Granulated Slag	yes	slight	sintered
Cobar Mines Zinc Tailings	no	slight	sintered
Lincoln Electric Fe Scale	no	none	slight
Maxitherm Boilers Submerged Arc Welding Slag	yes	sintered	sintered
Neuchatel Vermiculite Dust	no	none	none
Pilkington Coarse Glass Dust	no	fused	fused
Pilkington Fine Glass Dust	no	fused	fused
Smorgan Electric Arc Furnace Dust	no	none	some
Tubemakers Cupola Slag	yes	sintered	sintered
Tubemakers Cupola Scrubber Sludge	no	none	fused
VDG Marble and Granite (Wet Sample)	no	slight	fused

Adapted from Whitfield (1993)

Whitfield's analysis of the seven uncrushed wastes that sintered or fused at 1080°C or 1180°C (Table 7) revealed substantial amounts of lead and manganese. Because of the toxicity of lead, and the action of manganese as a body stain and sinter retardant below 1080°C (Hamer, 1975), a decision was made to reject wastes containing lead and to minimise inclusion of manganese. It was decided to favour wastes with lower iron content in order to minimise colouration. The most promising uncrushed wastes were, in order of preference: Pilkington Fine Glass Dust, Pilkington Coarse Glass Dust, Australian Perlite Cold Bag House Fines, and VDG Marble & Granite (Wet Sample). The analyses on which this order of preference is based appear in Table 7.

Table 7: Analyses of selected wastes (adapted from Whitfield, 1993)

	Australian Perlite Cold bag House Fines	Australian Refined Alloys CuS Dross	Australian Refined Alloys Soda Based Slag	Pilkington Coarse Glass Dust	Pilkington Fine Glass Dust	Tubemakers Cupola Scrubber Sludge	VDG Marble & Granite (Wet Sample)
1080°C	sintered	fused	sintered	fused	fused	none	slightly sintered
1180°C	fused	fused	sintered	fused	fused	fused	fused
	(wt%)	(wt%)	(wt%)	(wt%)	(wt%)	(wt%)	(wt%)
SiO <sub>2</sub>	71.50	2.91	5.60	72.39	71.47	21.23	66.02
Al <sub>2</sub> O <sub>3</sub>	11.82	0.31	1.42	0.62	0.53	10.89	10.74
CaO	0.98	n.d.	n.d.	8.94	8.79	32.95	7.48
MgO	n.d.	n.d.	n.d.	3.73	3.69	1.85	1.23
Na <sub>2</sub> O	1.10	5.83	10.34	13.01	12.93	3.02	2.26
K <sub>2</sub> O	11.64	n.d.	n.d.	0.04	0.02	1.72	3.32
BaO	n.d.	n.d.	n.d.	n.d.	n.d.	n.d.	n.d.
Fe <sub>2</sub> O <sub>3</sub>	2.28	36.20	50.89	0.27	0.46	14.98	2.58
ZnO	n.d.		n.d.	n.d.	n.d.	8.33	n.d.
TiO <sub>2</sub>	0.26	0.24	0.22	0.05	0.06	n.d.	0.31
MnO	<b>0.29</b>	<b>0.22</b>	<b>0.29</b>	n.d.	n.d.	<b>2.68</b>	<b>0.04</b>
Cr <sub>2</sub> O <sub>3</sub>	n.d.	n.d.		n.d.	n.d.	n.d.	n.d.
PbO	n.d.	<b>48.37</b>	<b>24.53</b>	n.d.	n.d.	n.d.	n.d.
CdO	n.d.	n.d.	n.d.	n.d.	n.d.	n.d.	n.d.
NiO	n.d.	n.d.	n.d.	n.d.	n.d.	n.d.	n.d.
CuO	n.d.	0.43	1.49	n.d.	n.d.	n.d.	n.d.
SnO <sub>2</sub>	n.d.	n.d.	n.d.	n.d.	n.d.	n.d.	n.d.
P <sub>2</sub> O <sub>5</sub>	n.d.	n.d.	n.d.	n.d.	n.d.	n.d.	0.09
SO <sub>3</sub>	n.d.	n.d.	n.d.	0.09	0.10	1.64	n.d.
Cal		2.72	5.18	n.d.	1.20	0.68	n.d.
Sib		2.72	n.d.	n.d.		n.d.	n.d.
LOC				0.96		n.d.	6.10
	99.87	99.95	99.96	100.10	99.25	99.97	100.17

Of the crushed wastes that fused or sintered at 1180°C, the most easily crushed were Ajax Foundry Slag and Maxitherm Boilers Submerged Arc Welding Slag, but these contained 5% and 15% manganese respectively, and so they were excluded from the present study. Of the wastes crushed with more difficulty, Boral Dunmore Dust was regarded as having the most potential for inclusion in a low-fired body, based on the comparatively high silica to alumina ratio, and the higher proportion of alkaline fluxes. The presence of 8% iron oxide suggests that the amount of Boral Dunmore Dust included in a pale firing body would be minimal. Whitfield's (1993) analyses of these wastes are shown below (Table 8).

**Table 8: Analyses of selected crushed wastes (Whitfield, 1993)**

	<b>Ajax Foundry Slag</b>	<b>Boral Peats Ridge Dust</b>	<b>Boral Dunmore Dust</b>	<b>Maxitherm Boilers Submerged Arc Welding Slag</b>	<b>Tubemakers Cupola Slag</b>
1080°C	sintered	slightly sintered	slightly sintered	sintered	sintered
1180°C	fused	fused	fused	sintered	sintered
<b>Crush</b>	easy (wt%)	hard (wt%)	hard (wt%)	easy (wt%)	hard (wt%)
<b>SiO<sub>2</sub></b>	53.69	45.41	53.75	19.91	38.97
<b>Al<sub>2</sub>O<sub>3</sub></b>	12.45	14.62	16.50	24.03	20.43
<b>CaO</b>	4.03	9.79	6.63	12.65	34.11
<b>MgO</b>	2.90	9.05	3.47	19.71	1.39
<b>Na<sub>2</sub>O</b>	1.51	3.10	3.17	0.65	0.01
<b>K<sub>2</sub>O</b>	4.65	0.80	3.77	n.d.	0.06
<b>BaO</b>	n.d.	n.d.	n.d.	n.d.	n.d.
<b>Fe<sub>2</sub>O<sub>3</sub></b>	5.10	12.64	8.41	4.79	0.71
<b>ZnO</b>	n.d.	n.d.	n.d.	n.d.	n.d.
<b>TiO<sub>2</sub></b>	0.86	1.96	0.95	2.86	0.48
<b>MnO</b>	5.84	0.18	0.17	15.37	1.22
<b>Cr<sub>2</sub>O<sub>3</sub></b>	0.21	n.d.	n.d.	n.d.	n.d.
<b>PbO</b>	n.d.	n.d.	n.d.	n.d.	n.d.
<b>CdO</b>	n.d.	n.d.	n.d.	n.d.	n.d.
<b>NiO</b>	n.d.	n.d.	n.d.	n.d.	n.d.
<b>CuO</b>	n.d.	n.d.	n.d.	n.d.	n.d.
<b>SnO<sub>2</sub></b>	n.d.	n.d.	n.d.	n.d.	n.d.
<b>ZrO<sub>2</sub></b>	n.d.	n.d.	n.d.	n.d.	n.d.
<b>P<sub>2</sub>O<sub>5</sub></b>	n.d.	0.47	0.75	n.d.	n.d.
<b>SO<sub>3</sub></b>	n.d.	n.d.	n.d.	n.d.	0.37
<b>Cal</b>	8.70	n.d.	n.d.	n.d.	n.d.
<b>LOC</b>	n.d.	1.34	2.24	n.d.	1.46
	99.94	99.36	99.81	99.97	99.21

As a result of the above review of Whitfield's results, it was decided to attempt to obtain samples of Pilkington Fine Glass Dust, Pilkington Coarse Glass Dust, Australian Perlite Cold Bag House Fines, VDG Marble & Granite (Wet Sample) and Boral Dunmore Dust. Several obstacles were encountered, as explained below.

Pilkington Glass no longer operates under that name, having been replaced by Viridien, who do not sell cullet.

VDG Granite no longer exists as a company, so alternatives were investigated. The site manager from Granites of Australia Ltd estimated that granite fines from the bulk diamond saw processing of granite was perhaps 200 kg per month, but said that it was mixed with sandstone tailings and was therefore not pure, and that it was put back into the site as remediation, so was not waste. He said that there was only one company in Australia using lime sludge to hold the shot in granite cutting—Chesini in South Australia (Brown, 2008). As the presence of more than 1% calcium in a body or glaze is expected to inhibit sintering and fusion below 1100°C (Hamer, 1975), and lime sludge granite fines were assumed to be higher in calcium than diamond-cut granite fines, this waste was not considered for the current project.

Three NSW marble and granite factories using diamond saws on a small scale were approached. Two indicated that the granite dust was mixed with floor sweepings, and that unadulterated granite and marble dust was not available. A visit to Prego Marble and Granite in Sydney confirmed this, as a sample was obtained that included dust from cutting marble, granite, resin, terrazzo and other composite materials.

Three materials identified in Whitfield's (1993) research were obtained: Dunmore latite, perlite and glass cullet. These three materials, together with two quarry-tailing materials (after Whitfield, 1985) and a number of other selected materials, were obtained, prepared for use, and photographed using a standard digital camera and an electron microscope. The following chapter documents these processes.

## **Chapter 8: Materials Selection, Sourcing and Preparation**

The review of materials used internationally and in previous NSW research narrowed the field of waste materials targeted for use in this research. This chapter documents the process of selecting and obtaining materials, and preparing them for use in experimental clays and glazes.

### **Sugar cane bagasse ash**

Sugar cane is grown commercially in Australia, and the crushings (bagasse) are burnt at sugar mills to generate power, for mill operation and for supply to the national electricity grid. For example, the Sunshine Sugar Mill at Broadwater in NSW operates the mill, a 30 megawatt turbine and an 8 megawatt turbine by burning bagasse. The ash is either disposed of or returned to the cane fields as fertiliser (Farrell, 2008). Bagasse production will be augmented by the progressive decisions of Australian sugar cane growers to cease field-burning sugar cane leaf after cane harvest and using it for power generation (Courtney, 2008).

SCBA was obtained from Sunshine Sugar Mill at Broadwater in northern NSW. After the juice is extracted from the sugar cane, the plant burns the sugar cane to generate electricity to power the mill and feed the grid. The plant separates ash from the chain grates of the boilers from the remainder of the ash streams. This grate material is typically coarse and contains non-combustible material (such as stones) and some unburnt material. The remainder of the ash from dust-collection points on the furnace, gas path and the wet scrubber is sluiced to a vacuum belt where the water is removed for recycling and the dried ash is stored for transport. The management of the Sunshine Sugar Mill kindly provided access and assistance to collect ash from four different collection points.

The first collection point was the coarse ash from the number 12 boiler burner grate, just inside the mill (fig. 51).



*Figure 51: Broadwater sugar mill*

The arrow shows the point of collection of grate ash from the boiler. The ash contained partially burnt material, stones and small pieces of extraneous matter, and was not usable as received.

The second collection point was a submerged ash hopper (fig. 52).



*Figure 52: Number 1 boiler submerged ash hopper, Broadwater sugar mill*



The submerged ash from the hopper on the number 1 boiler was waterlogged and also contained some extraneous matter.

The third collection point was from the conveyor belt of the number 12 boiler. The ash was retrieved from the belt as a wet hot powder. Figure 53 shows steam rising from the collection point.



*Figure 53: Number 12 boiler belt, Broadwater sugar mill*

The fourth collection point was the conveyor belt of the number 1 boiler (fig. 54). Ash can be seen on the grate and auger in the area immediately beneath the collection point (fig. 55).



*Figure 54: Number 1 boiler belt, Broadwater sugar mill*



*Figure 55: Below number 1 boiler belt, Broadwater sugar mill*

The ash collected from the two boiler belts was of even consistency with no obvious contaminants and was damp from the sluicing operation. On this basis, the two boiler belt ashes were selected for investigation and experimentation. Ash from number 1 boiler belt was calcined in stoneware saggars in an electric kiln at 600°C, 700°C, 800°C and 900°C. The ash at 600°C was a fine and gritty grey powder, with some agglomerated lumps that crumbled when disturbed (fig.56). At higher temperatures, the consistency of the ash became less gritty, the carbon burnt out and the ash developed a terracotta colour (fig.57).



**Figure 56: Bagasse ash (number 1 boiler belt) calcined at 600°C**



**Figure 57: Bagasse ash (number 1 boiler belt) calcined at 700°C.**

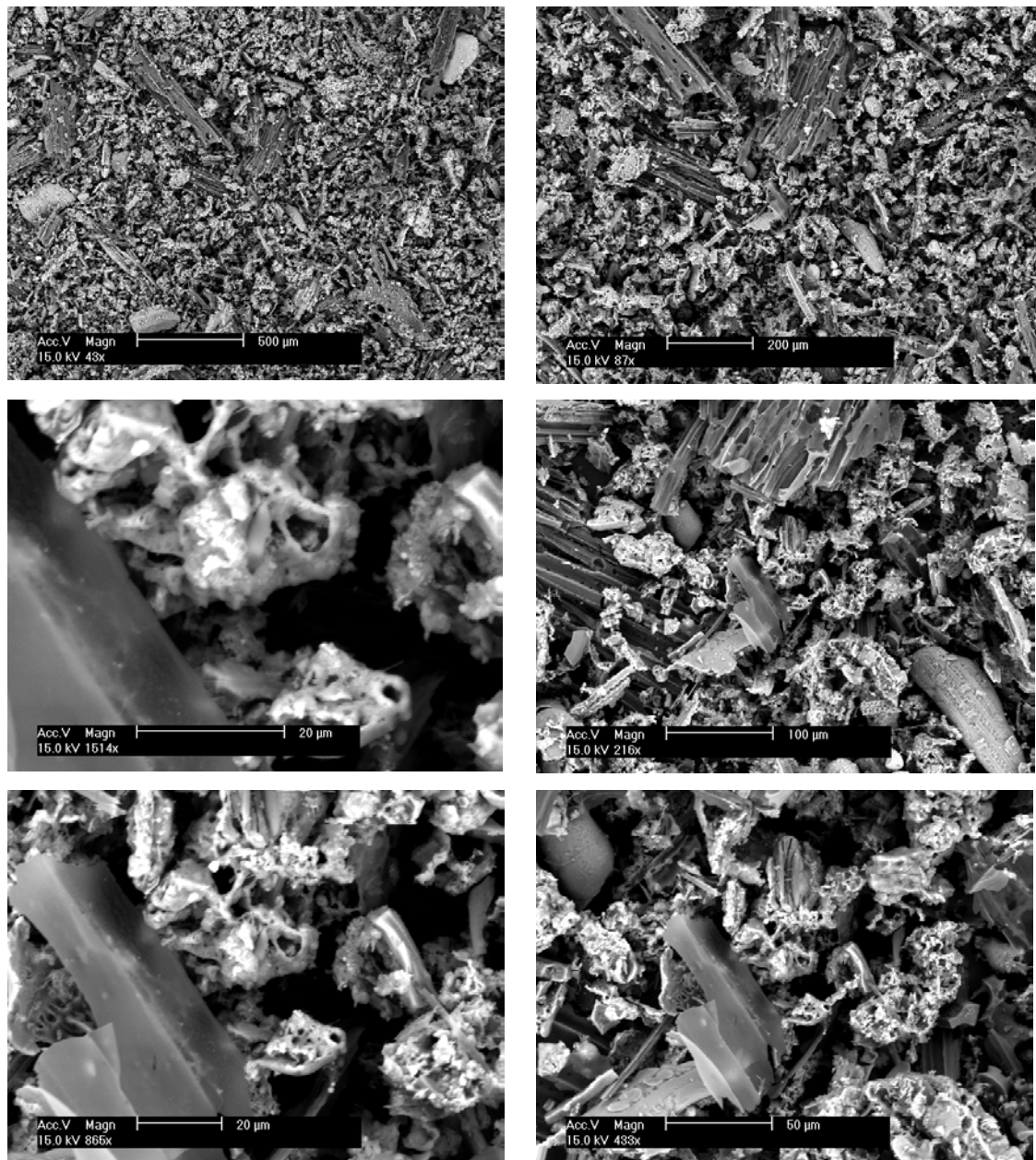


**Figure 58: Bagasse ash (number 1 boiler belt) calcined at 800°C**



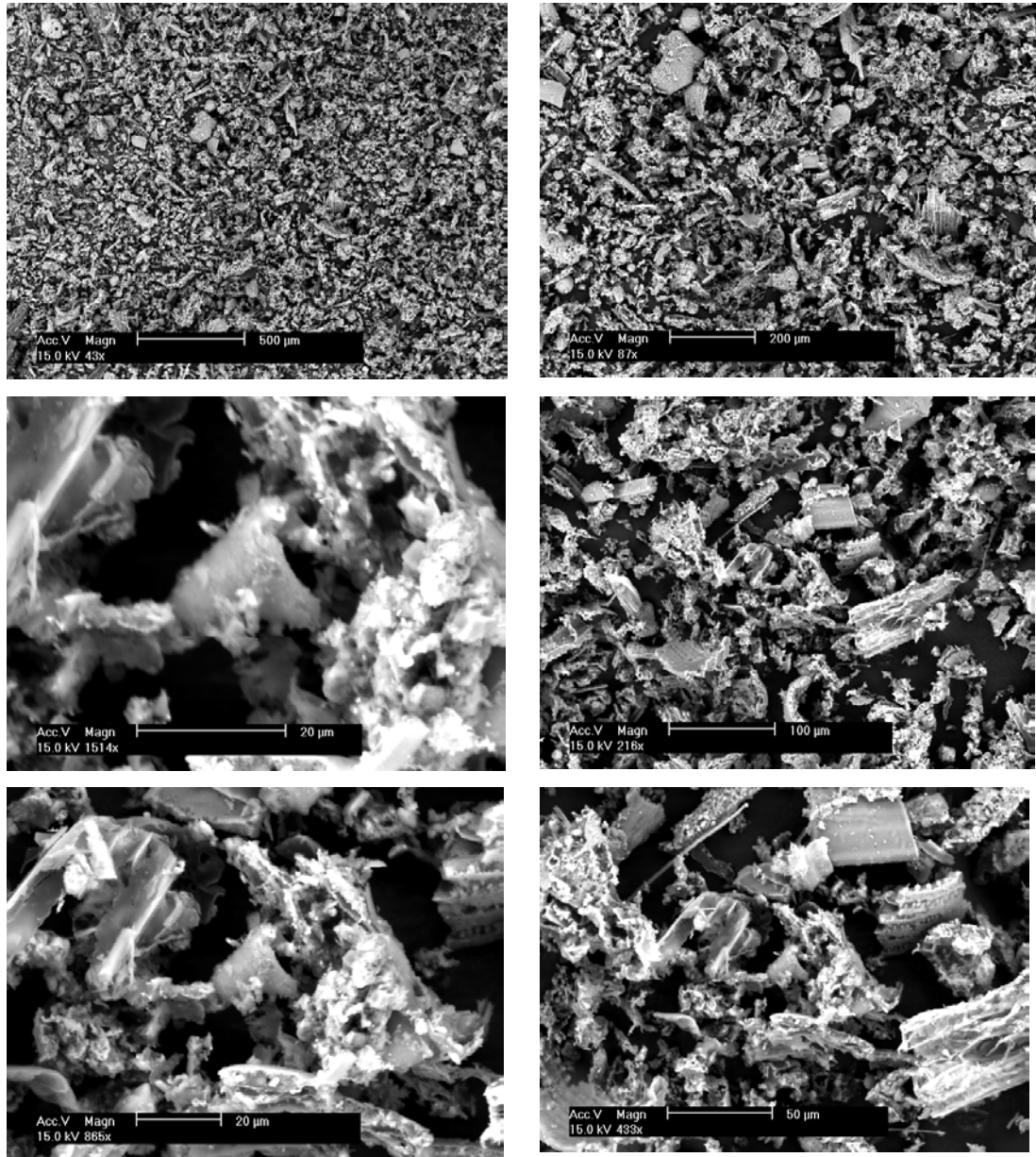
**Figure 59: Bagasse ash (number 1 boiler belt) calcined at 900°C**

EDAX microscopy revealed that the bagasse ash that had been calcined at 600°C displayed particles with contrasting morphologies. There were many fragments of opaque, translucent cellulose fibre up to half a millimetre long. These fragments had the appearance of timber that had been eaten by termites, with a cellulose structure left behind. There were also denser particles with relatively featureless curved surfaces up to 300 µ in diameter. Interspersed among these were many ragged agglomerations of material of mucous-like appearance, partially formed around voids with strands connecting clumps.



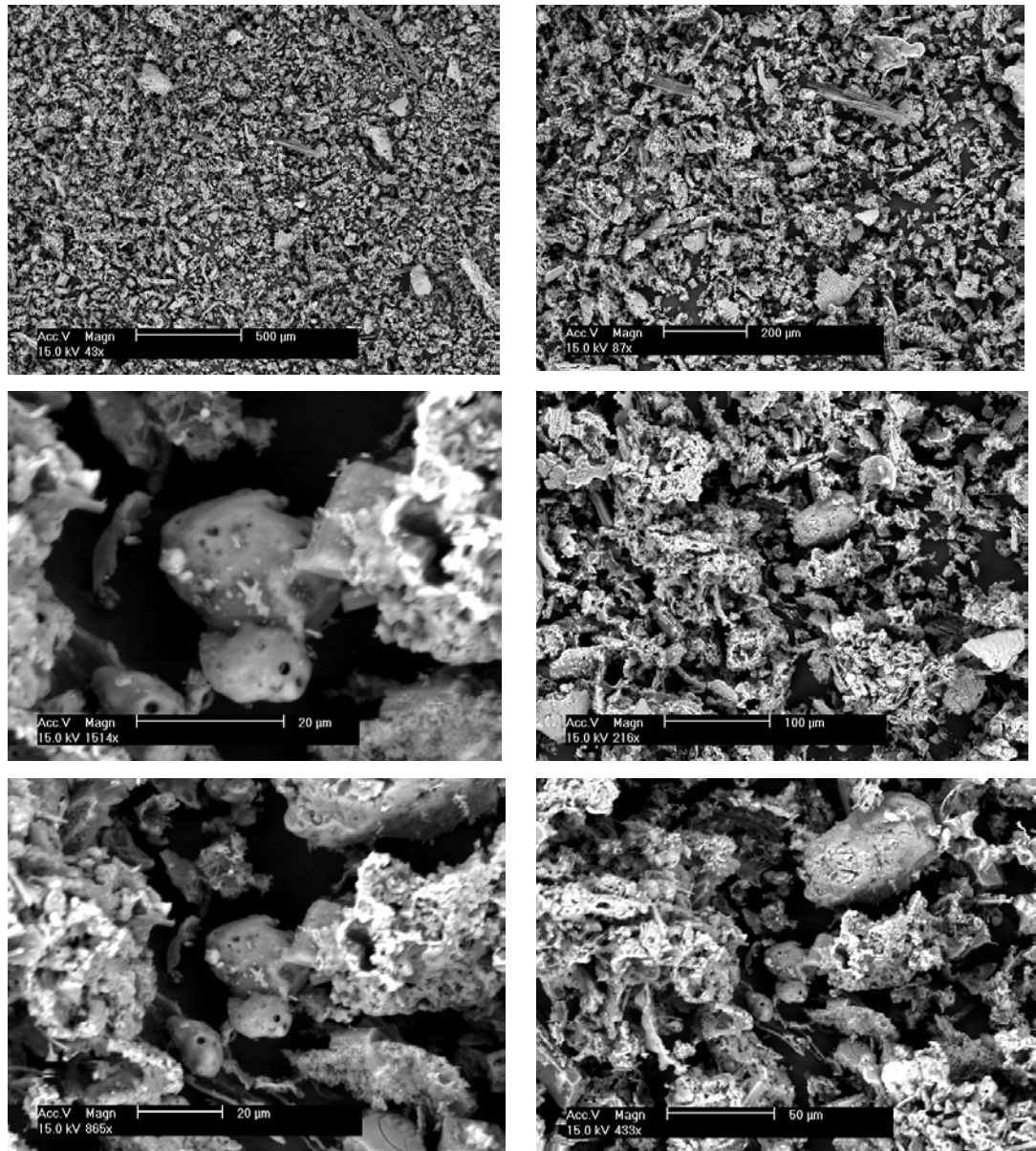
**Figure 60: Bagasse ash (number 1 boiler belt) calcined at 600°C**

At 700°C, the largest fragments of cellulose had mostly decreased in size to between 100 µm and 200 µm, and their internal morphology was more ragged and wispy.



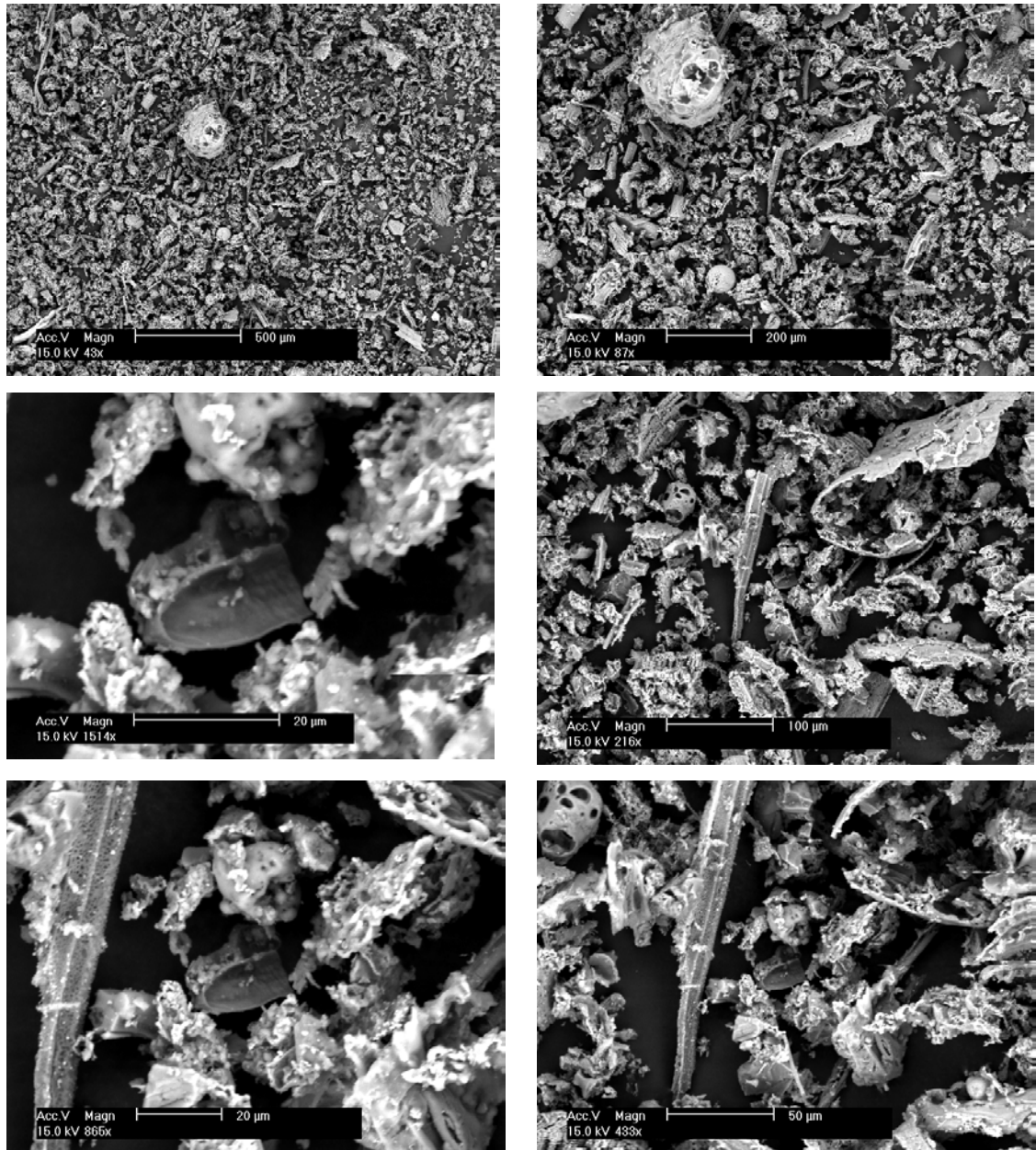
**Figure 61: Bagasse ash (number 1 boiler belt) calcined at 700°C**

At 800°C, the largest fragments of cellulose were still mostly between 100 µm and 200 µm, and they were surrounded by smaller fragments. Some particles appeared to have melted surfaces, as seen in the centre-left image in Figure 62.



**Figure 62: Bagasse ash (number 1 boiler belt) calcined at 800°C**

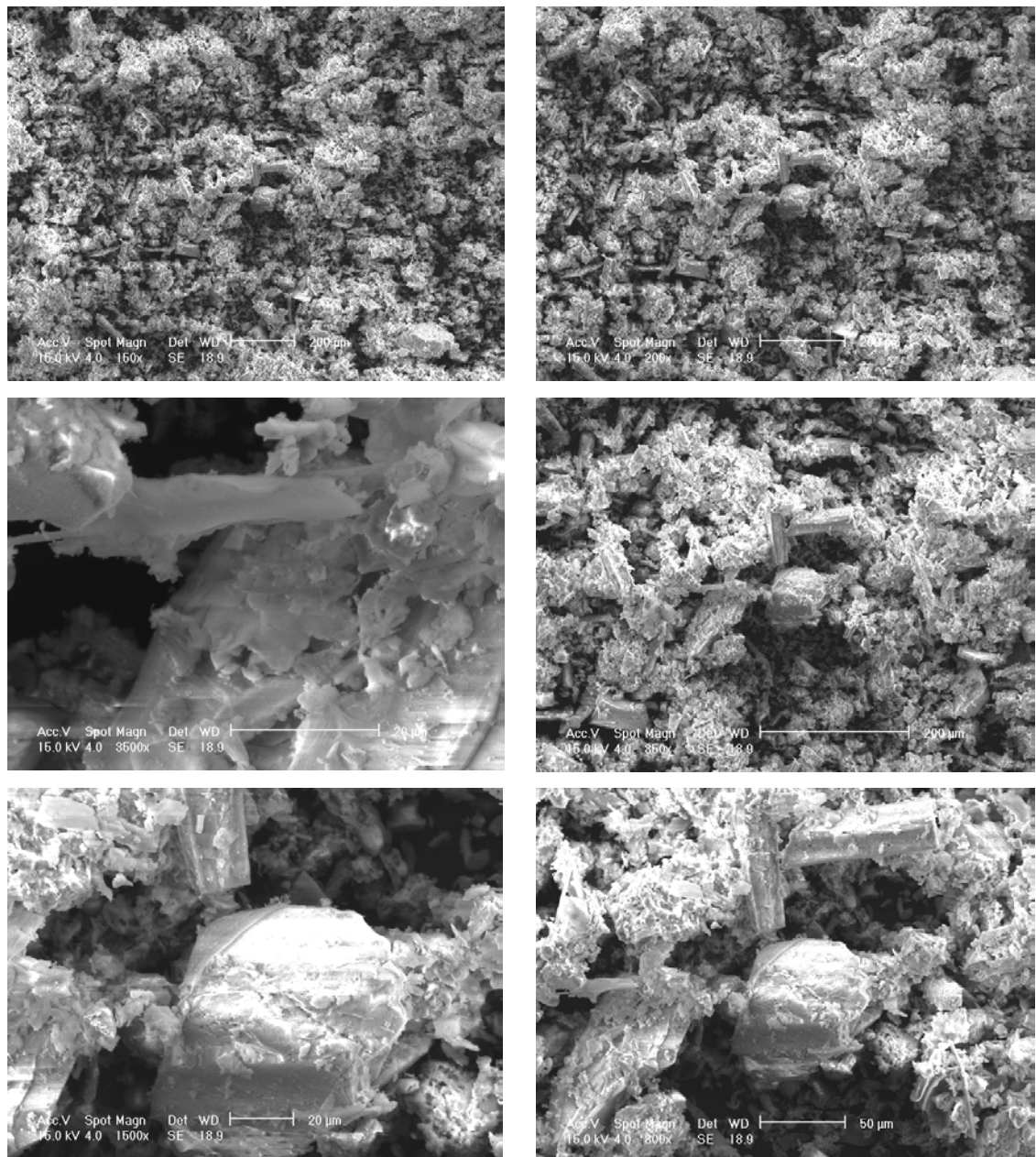
At 900°C, there was little change, as the largest fragments of cellulose were still mostly between 100 µm and 200 µm, and they were surrounded by smaller fragments. There were still some fragments with the distinct appearance of vegetable fibre, still some ragged agglomerations, and still some particles with surfaces that appeared to have melted.



**Figure 63: Bagasse ash (number 1 boiler belt) calcined at 900°C**



After hand grinding using a mortar and pestle, few of the largest particles exceeded 50  $\mu\text{m}$  in diameter. There were no well-defined cellulose fibres, since fragments with diameters as small as 1  $\mu\text{m}$  were mixed throughout the sample, and the larger fragments had surfaces impacted by the grinding process (fig. 64).



**Figure 64: Bagasse ash (number 1 boiler belt) calcined at 800°C and hand-ground**

Ash from the number 12 boiler belt was also calcined at 600°C, 700°C, 800°C and 900°C. As with ash from the other boiler belt, the ash at 600°C was a fine and gritty grey powder, with some agglomerated lumps that crumbled when

disturbed (fig. 65). At higher temperatures, the consistency of the ash again became less gritty, the carbon burnt out and the ash developed a terracotta colour (figs. 66–68).



**Figure 65: Bagasse ash (number 12 boiler belt) calcined at 600°C**



**Figure 66: Bagasse ash (number 12 boiler belt) calcined at 700°C**

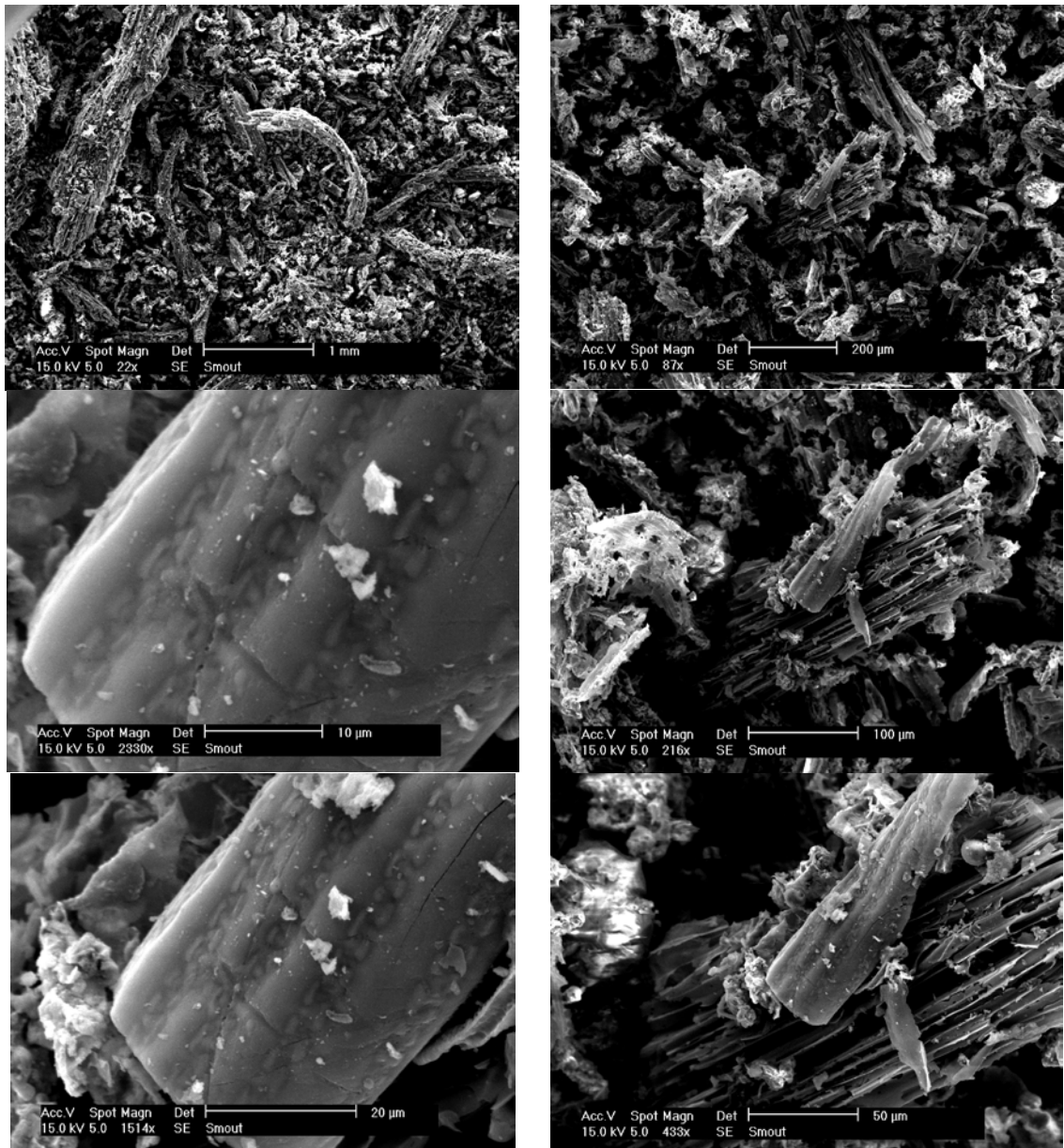


**Figure 67: Bagasse ash (number 12 boiler belt) calcined at 800°C**



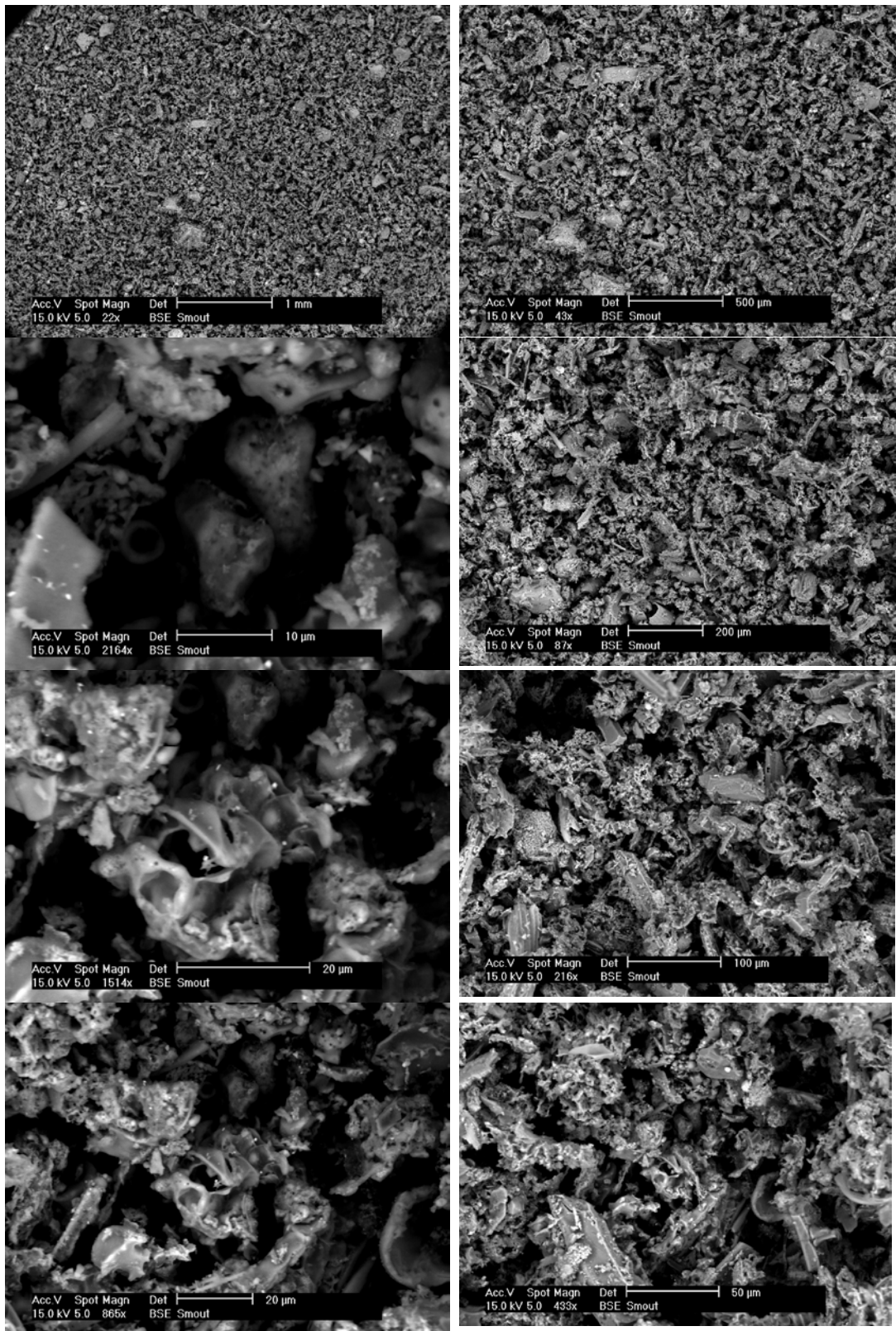
**Figure 68: Bagasse ash (number 12 boiler belt) calcined at 900°C**

Microscopy of bagasse ash from number 12 boiler belt revealed a similar trend towards decreasing size of cellulose fibres as the temperature at which the ash had been calcined increased. At 600°C, there were some fragments longer than a millimetre, and the fibrous morphology was distinct (fig. 69).



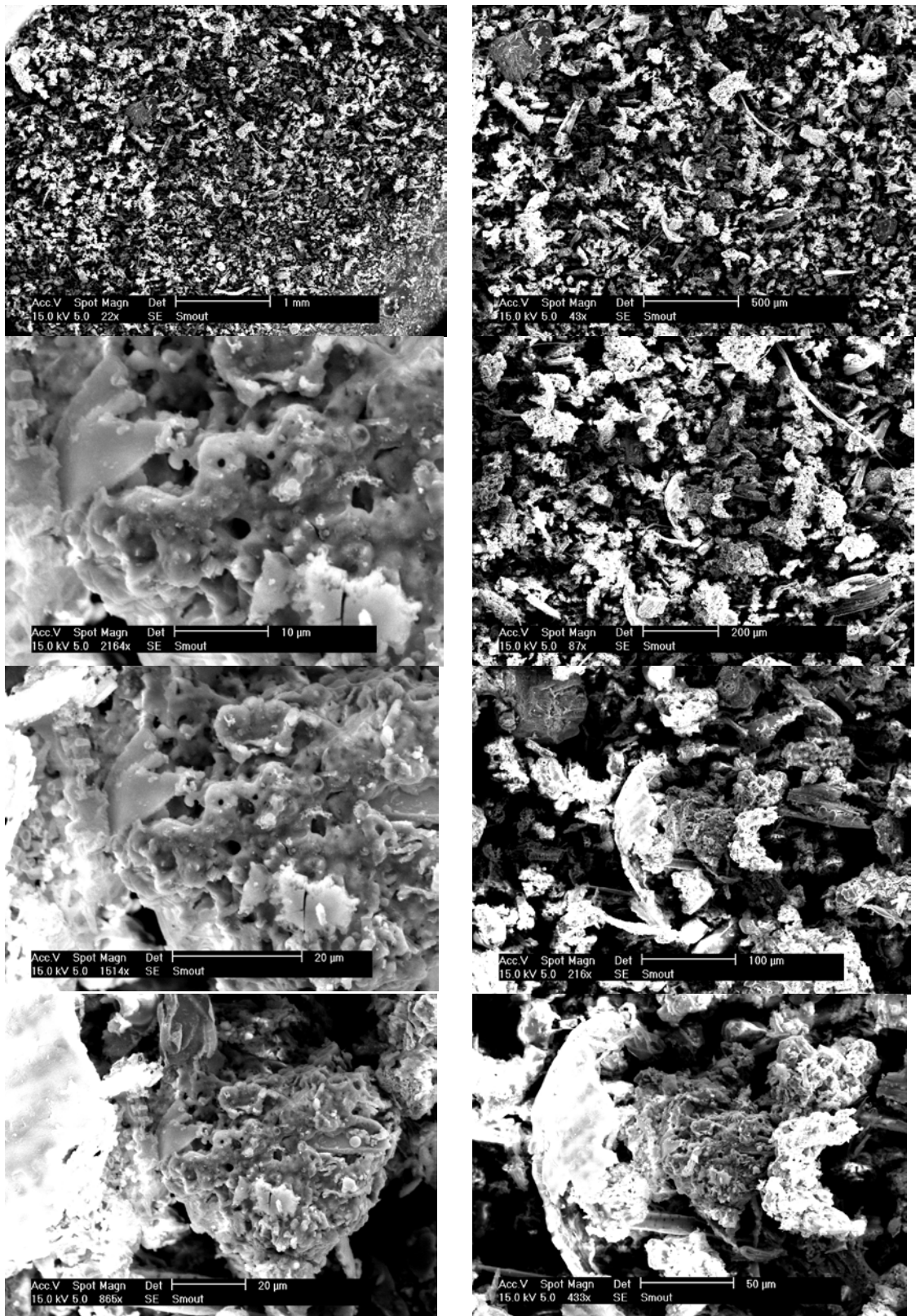
**Figure 69: Bagasse ash (number 12 boiler belt) calcined at 600°C**

The bagasse ash from the number 12 boiler belt calcined at 700°C had fewer fragments over 100 µm and there were more wrinkled fragments, with some having a melted appearance (fig. 70).



**Figure 70: Bagasse ash (number 12 boiler belt) calcined at 700°C**

The bagasse ash from the number 12 boiler belt calcined at 900°C also had few fragments over 100 µm and there were more ragged agglomerations, with some having a melted appearance (fig. 71).



**Figure 71: Bagasse ash (number 12 boiler belt) calcined at 900°C**

## Rice husk ash

Rice husk was selected as an experimental material because of its abundance and availability, potential as an energy source, and the variety of possible end uses for this highly siliceous material. Each of these factors is addressed in turn.

Australia produces approximately 1,000,000 tonnes of rice a year, falling to 15,000 tonnes in times of extreme drought (Spires, 2008). The husk is distributed in 100 kg bundles via stock-feed merchants and used as stable or cage liner, because it is lightweight and non-absorbent. Although RHA used to be produced in Australia, this ceased in 2004 (Spires, 2008).

Rice husk originating from the Coprice plant at Leeton, NSW was obtained from Papillon Stables at Centennial Park. As received, it consisted of dry light brown husks up to 1cm long (fig. 72).



*Figure 72: Rice husk as received*

The rice husk was fired to 600°C for six hours as the first stage in testing ash fired at increasing temperatures. The resultant ash was calcined again at 700 °C, 800 °C, and 900°C.

At 600°C, all husks were friable and almost all were black, with the exceptions being white or black and white (fig. 73).



*Figure 73: RHA calcined at 600°C*

At 700°C, the proportion of white husks increased (fig. 74).



*Figure 74: RHA calcined at 700°C*

The proportion of white husks further increased at 800°C (fig. 75), and at 900°C the husks were all white (fig. 76).



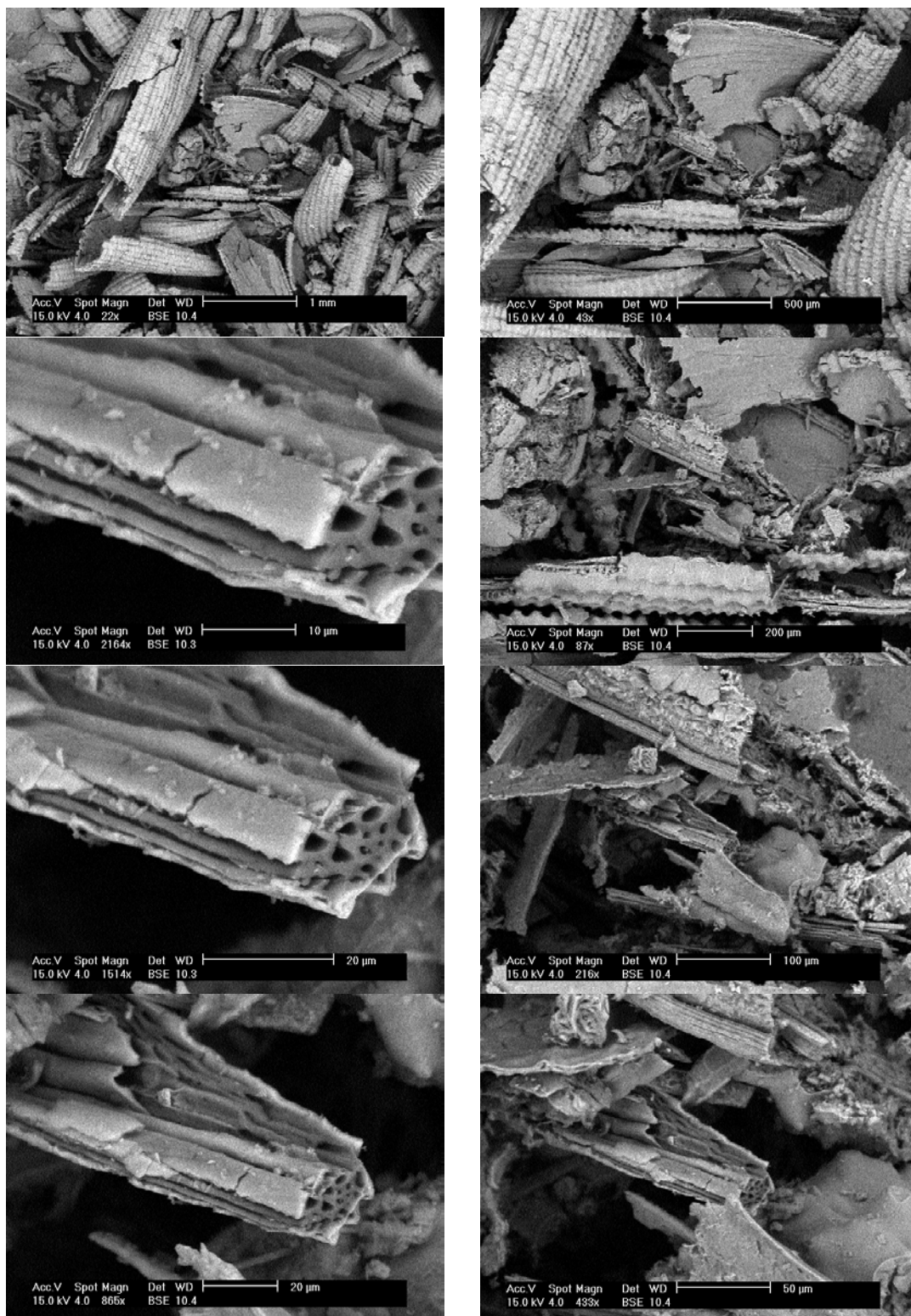


*Figure 75: RHA calcined at 800°C*



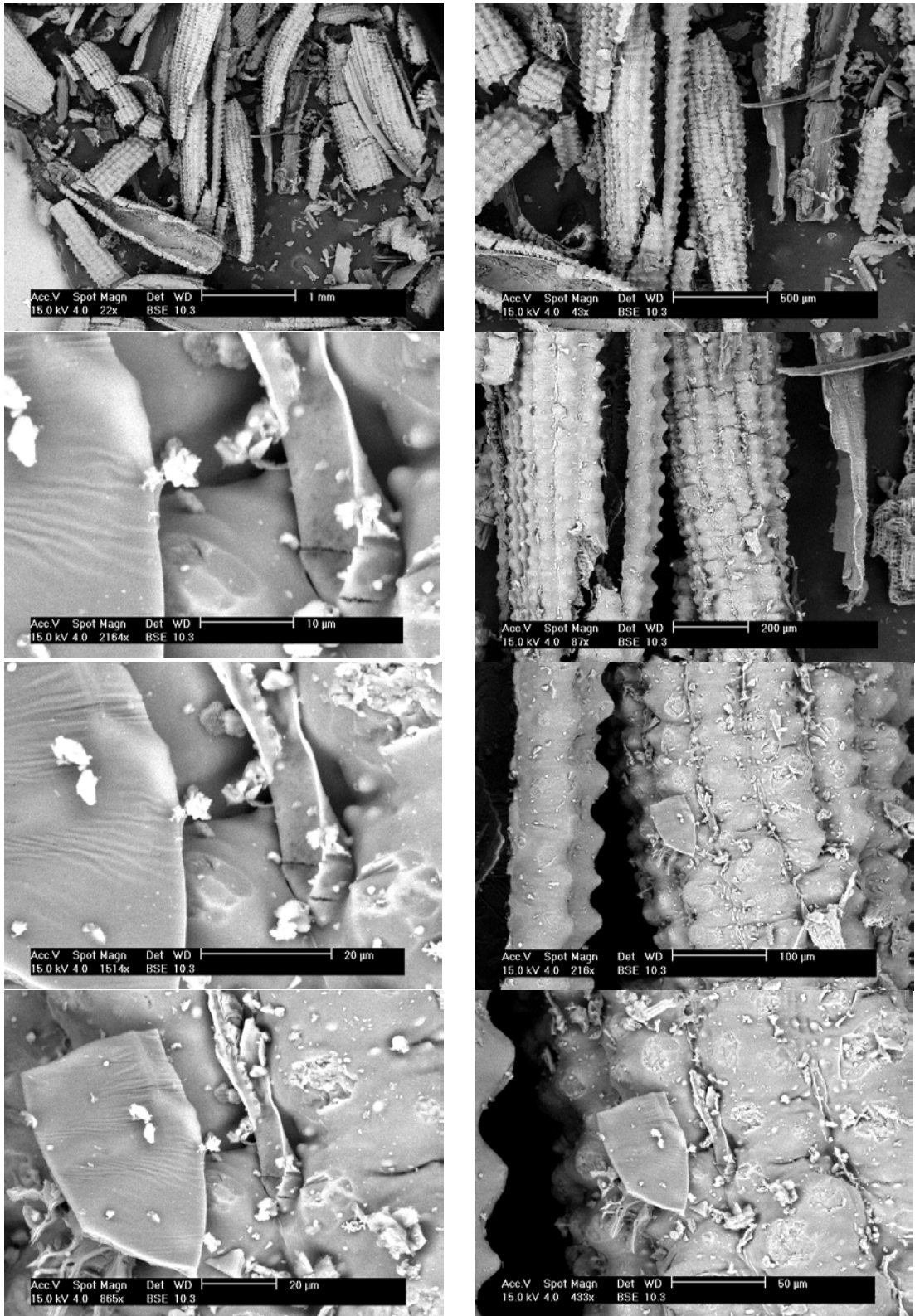
*Figure 76: RHA calcined at 900°C*

Microscopy of the ash calcined at 600°C showed that the ash consisted of individual husks that had formed a sheath over the rice. The outside of the husks had a series of nodular peaks alternating closely with depressions so that the exterior resembled a cob of corn. Although the husks had been predominantly unbroken when first calcined, transportation and handling in preparation for microscopy had resulted in fragmentation (fig. 77).

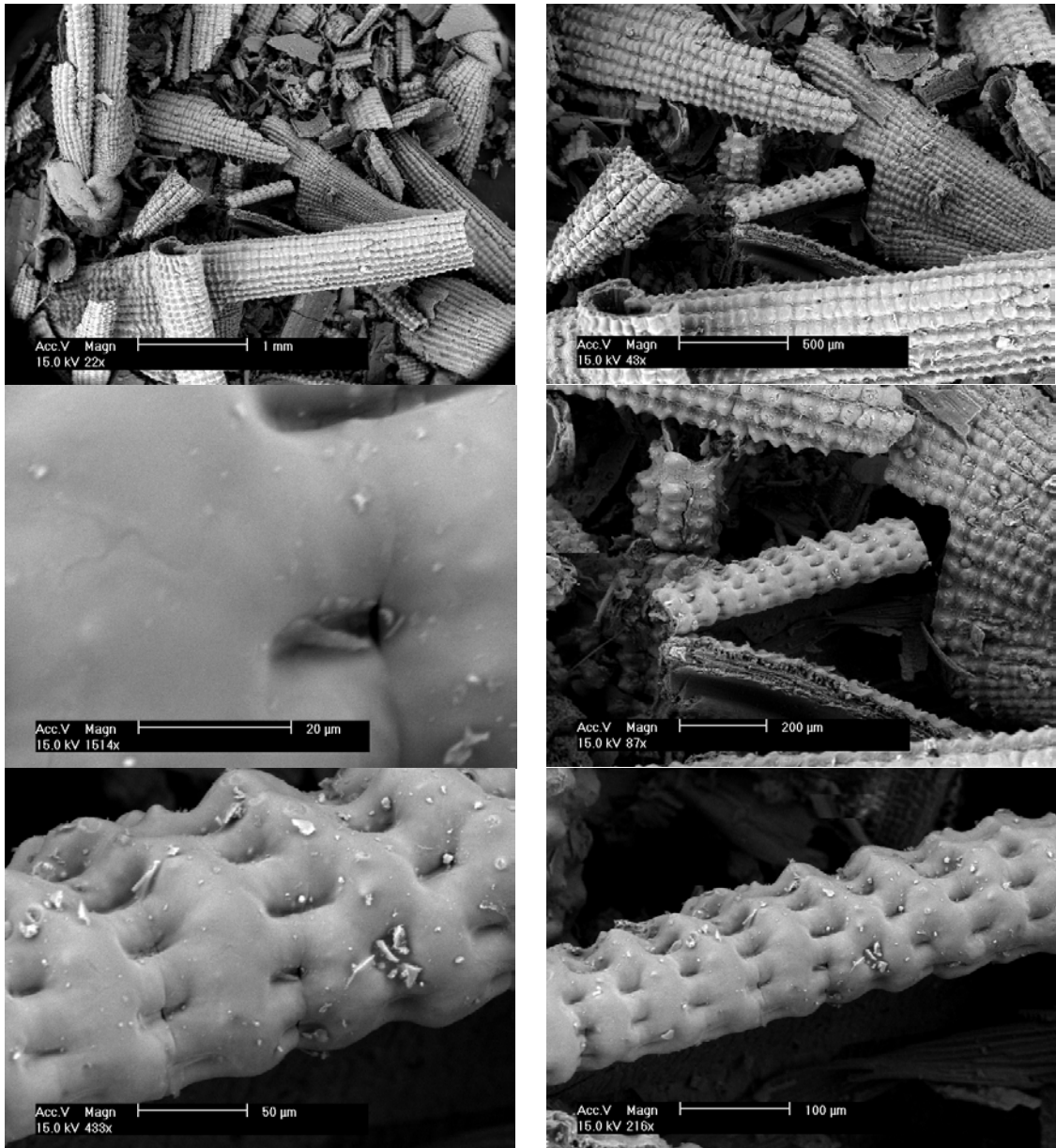


**Figure 77: RHA calcined at 600°C**

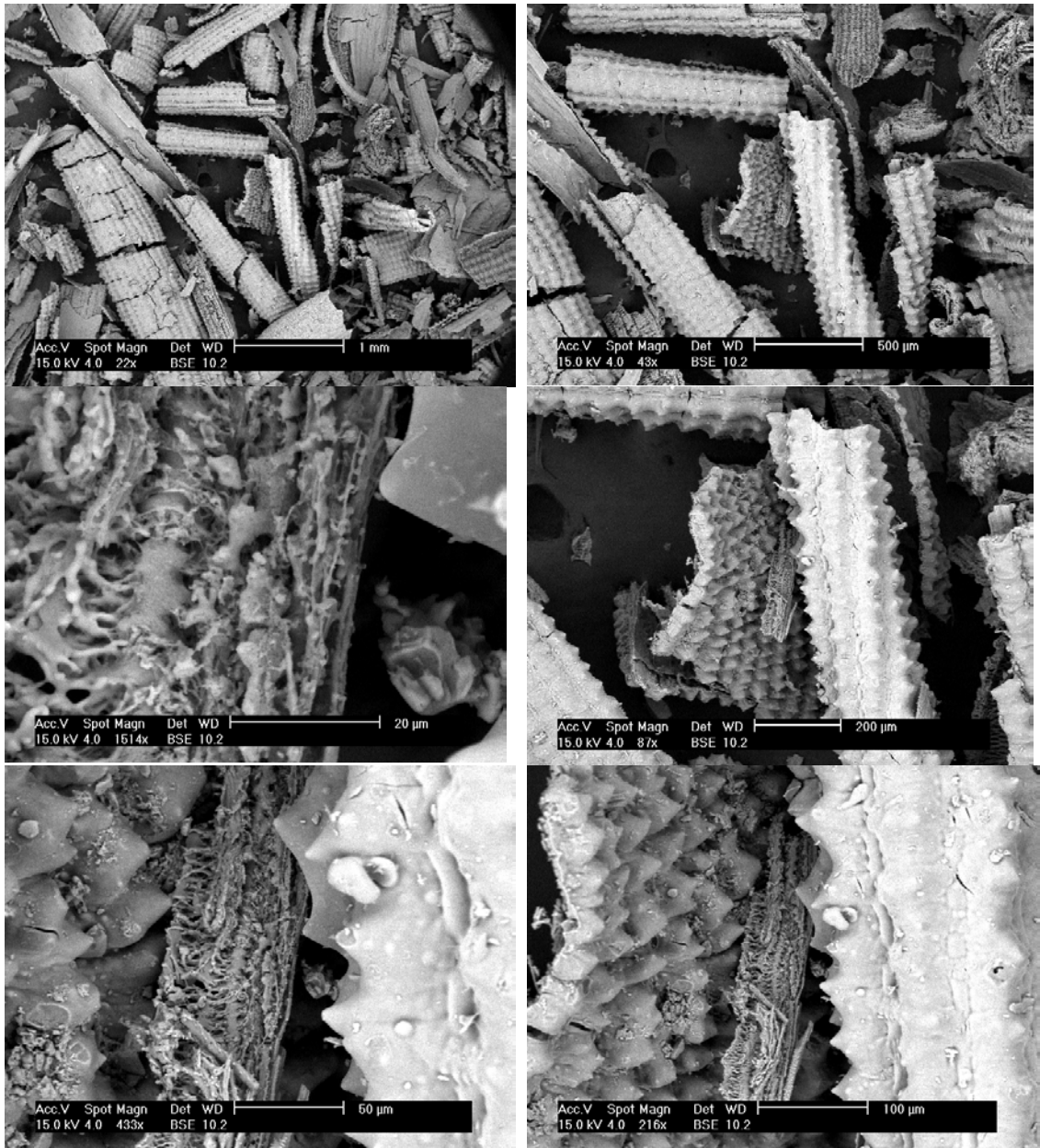
The morphology of the fragments did not significantly alter when the RHA was calcined at 700°C (fig. 78), 800°C (fig. 79) and 900°C (fig. 80).



**Figure 78: RHA calcined at 700°C**

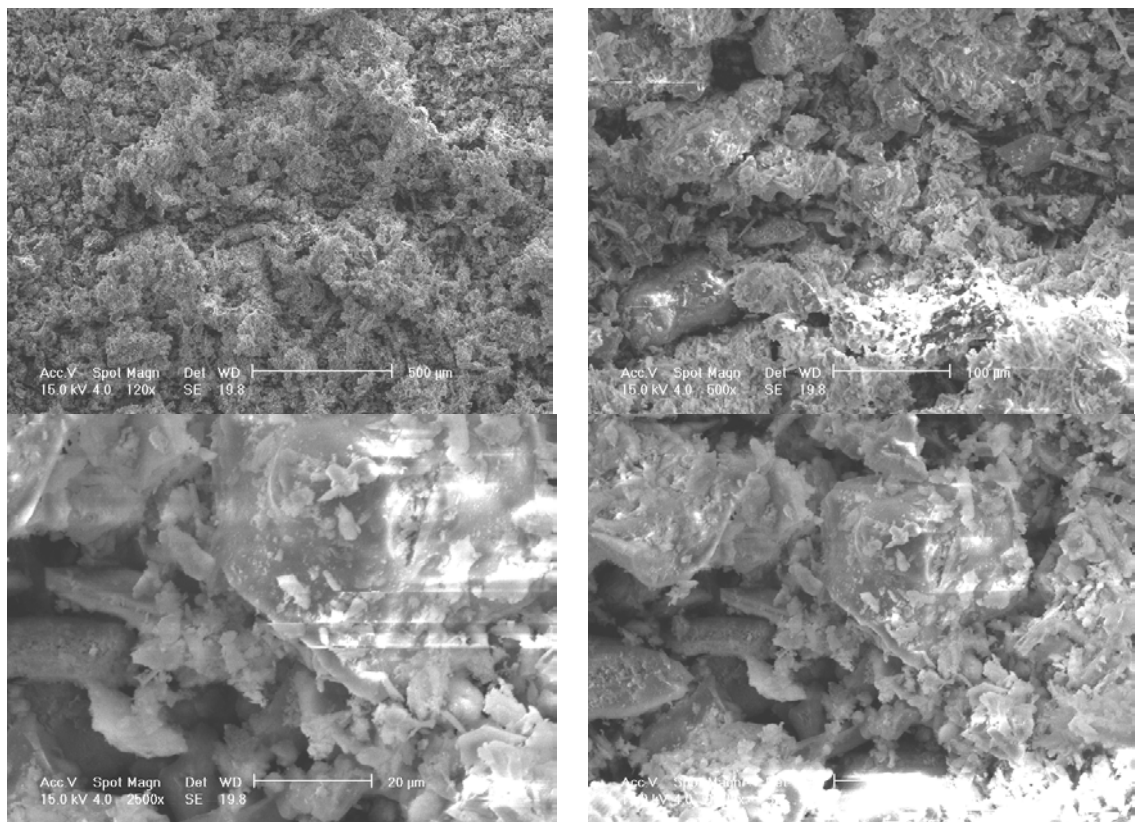


**Figure 79: RHA calcined at 800°C**



**Figure 80: RHA calcined at 900°C**

After hand grinding the RHA using a mortar and pestle, the fragments were no longer distinct and many were reduced to less than 10 µm in diameter (fig. 81).



**Figure 81: RHA calcined at 800°C and hand-ground**

### **Corn cob ash**

Corn cobs were obtained from Simplot (Australia) Ltd in Bathurst, NSW. Simplot is the major company canning sweet corn in Australia. Simplot management agreed to help with the current research by providing shelled cobs. The shelled cobs are not wasted currently, as they are trucked for dairy-cattle feed within hours of shelling (Stapley, 2008). The cannery operates on corn seasonally from December to March. Corn cobs are husked and shelled, and the husks and shelled cobs are shredded (fig. 82) and disposed of for ensilage immediately before the onset of fermentation. Several hundred shelled cobs were collected from the conveyor belt (fig. 83).



**Figure 82: Shredded husks and corn trash**



**Figure 83: Conveyor belt showing shelled cobs**

The sugar and water content of raw shelled cobs results in rapid fermentation, so they must be dried and burnt quickly (Stapley, 2008). The cobs obtained were transported to Sydney and fired that day to 600°C for six hours as the first stage in testing ash fired at increasing temperatures. Corn Cobs were calcined in open and closed containers. Corn cobs calcined in an open container formed a soft grey powdery ash with gritty pieces of cob charcoal (fig. 84).



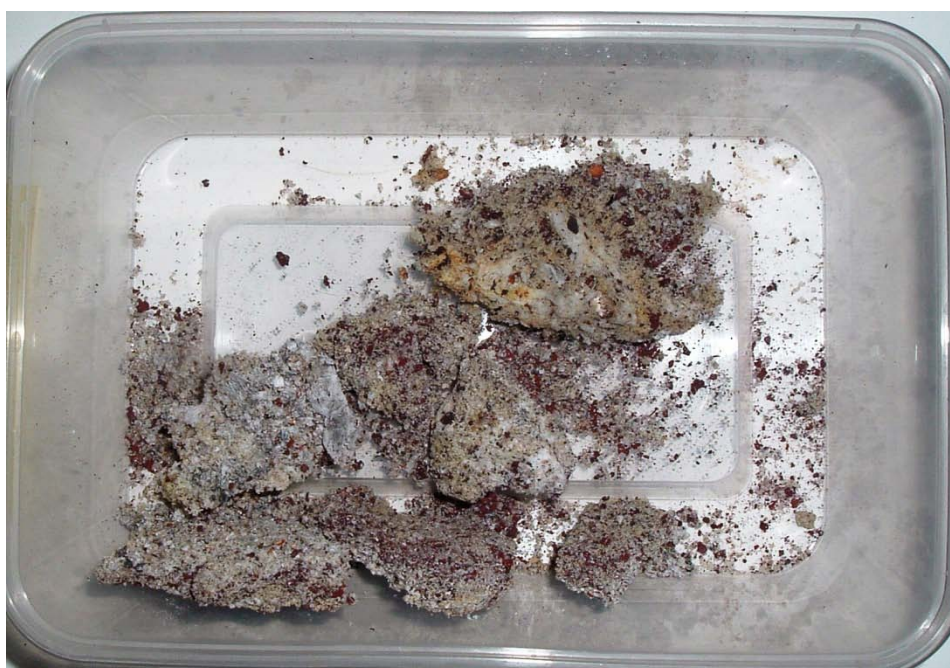
**Figure 84: Corn cob ash calcined at 600°C in open container**

Restricting air access by calcining in a closed container at 600°C resulted in the production of whole corn cobs of charcoal (fig. 85).



*Figure 85: Corn cob ash charcoal from calcining at 600°C in closed container*

The corn cob ash was calcined again at 700°C, producing a predominantly pale grey ash with pale brown staining and dark rust specks. The ash had caked together into a mass that felt rough to the touch and that broke apart when handled (fig. 86).



*Figure 86: Corn cob ash after calcining to 700°C*

After calcining at 800°C, the corn cob ash produced was composed of various shades of rust interspersed with white specks. The ash had formed a rough



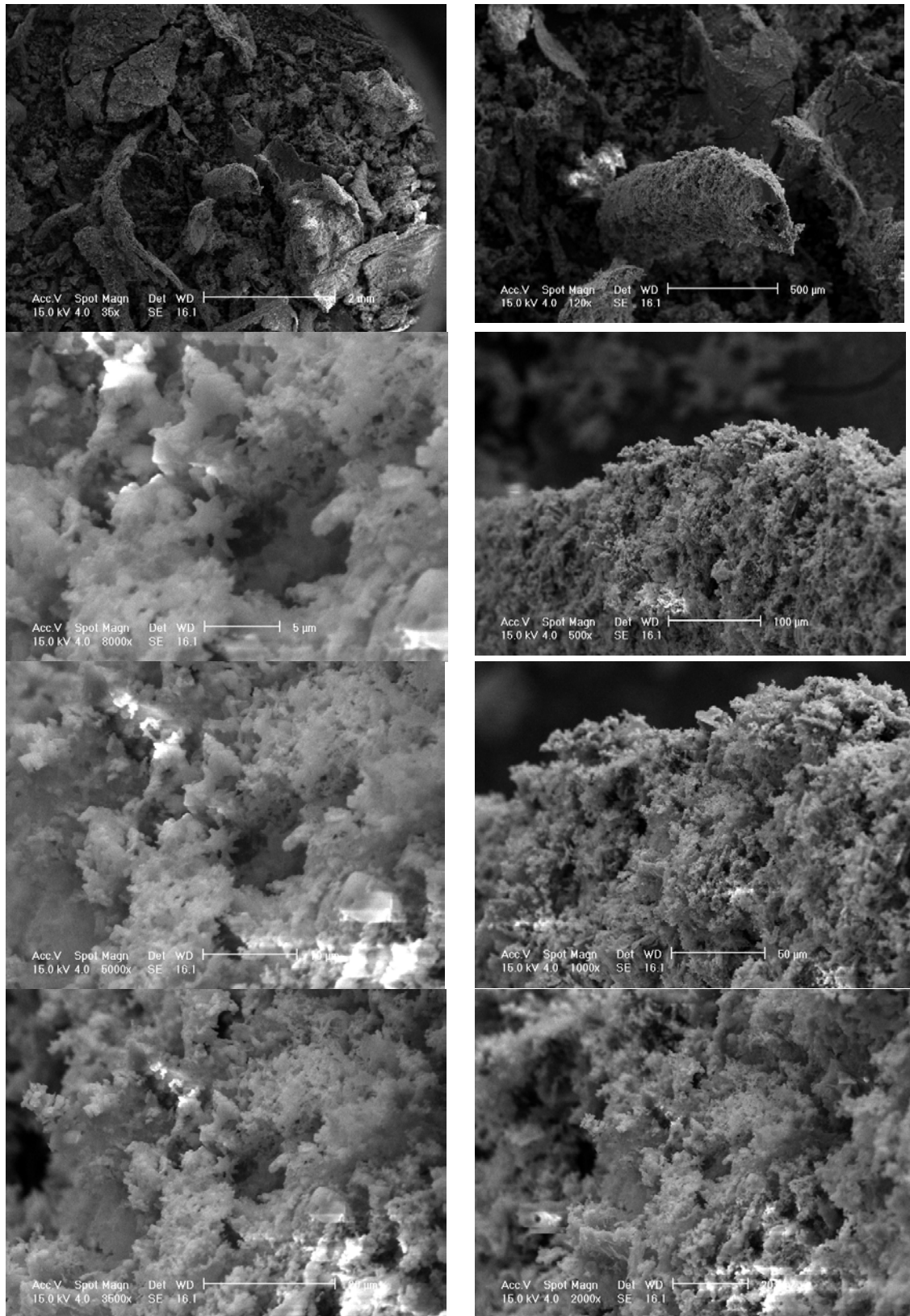
textured cake that retained its integrity when gently handled (fig. 87). Constituent particles were noticeably harder at 800°C than at 700°C, but the agglomerated cake was still easily broken into smaller pieces.



*Figure 87: Corn cob ash after calcining at 800°C*

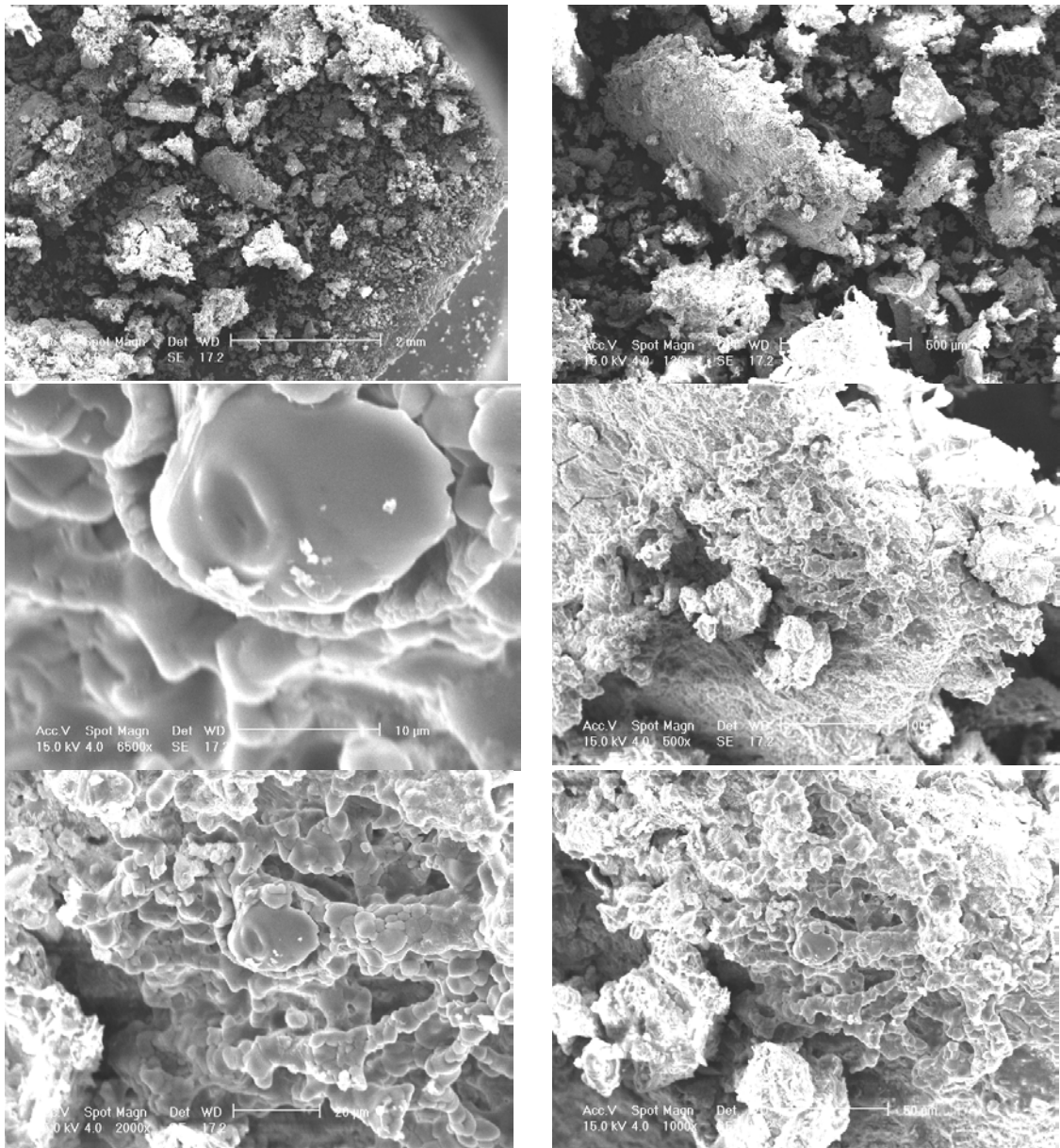
The sample selected for microscopy, from the corn cob ash calcined at 600°C, was the pale grey powdered ash without fragments of charcoal. The ash was unground.

Microscopy revealed that the sample contained pieces of ash of various shapes up to 2 mm in diameter, some of which had surfaces reminiscent of soft coral (fig. 88).



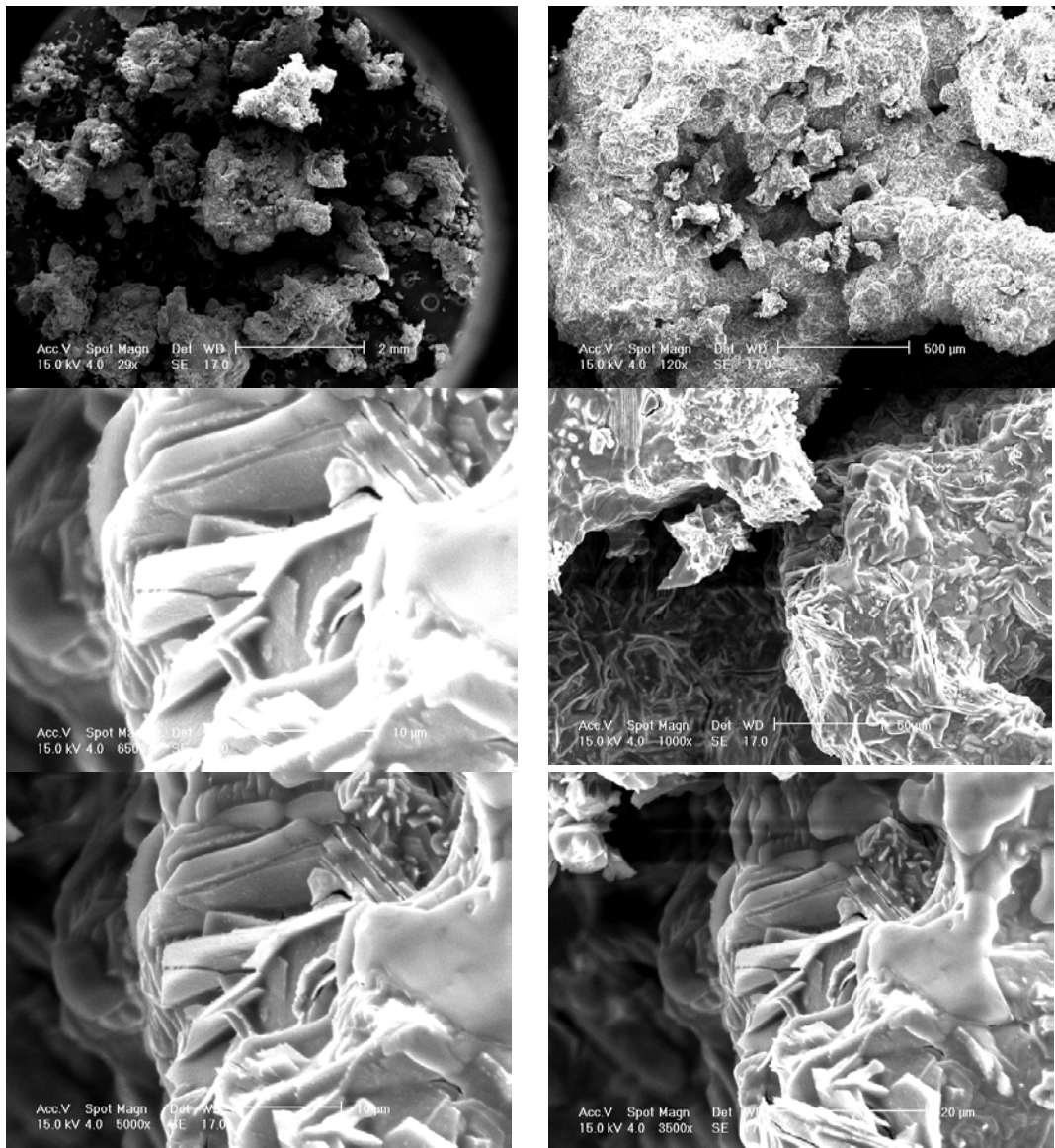
**Figure 88: Corn cob ash calcined at 600°C**

Corn cob ash calcined at 700°C displayed agglomerations up to 2 mm in diameter, surrounded by similar pieces as small as 10 µm. The surface of some pieces appeared to consist of semi-molten particles (fig. 89).



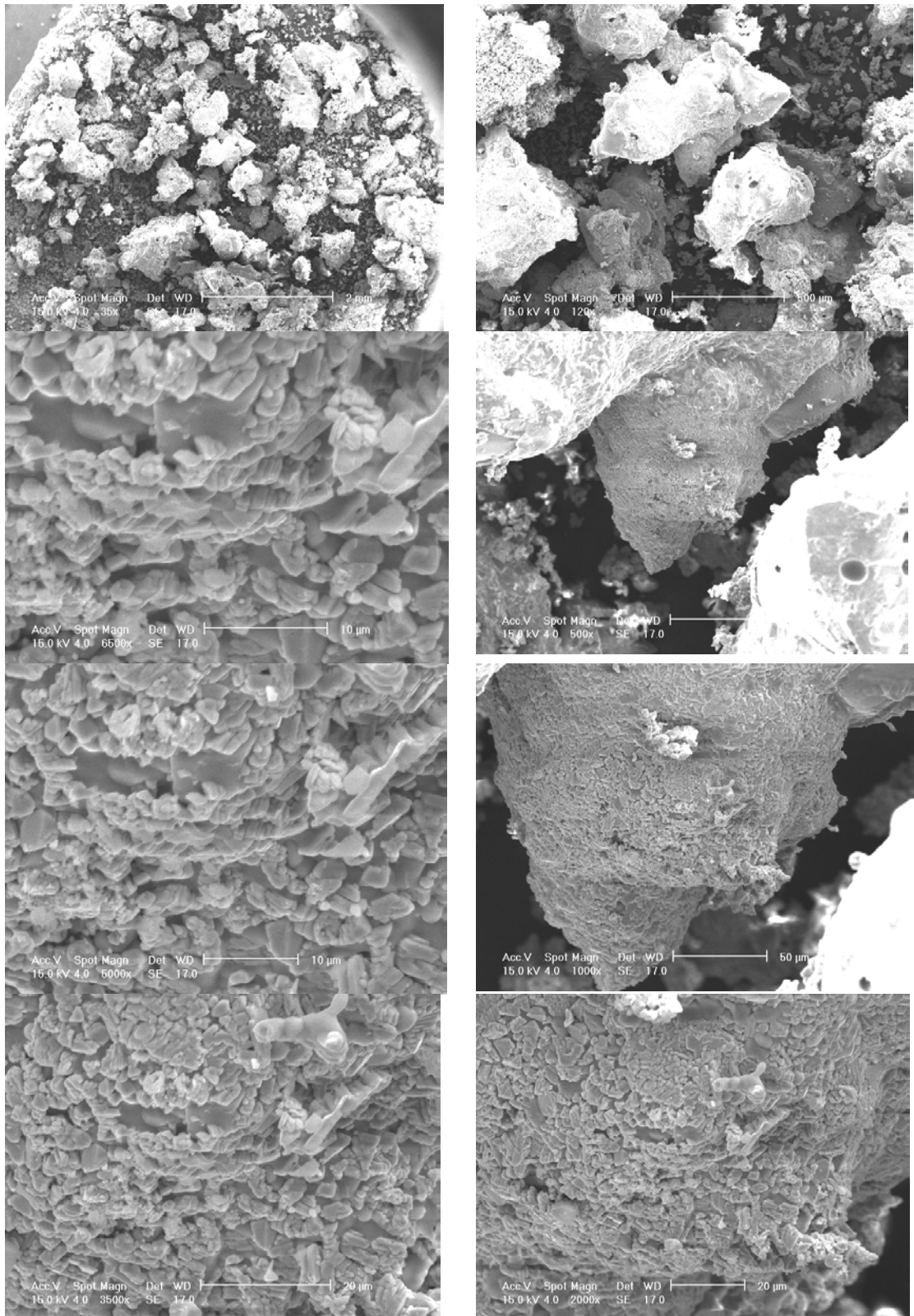
**Figure 89: Corn cob ash calcined at 700°C**

Corn cob ash calcined at 800°C also displayed agglomerations up to 2 mm in diameter, with few pieces less than 100 µm. Surfaces were wrinkled agglomerates of different soft-edged forms with appearances like melting twigs or shards, in some cases softened to the appearance of melting cheese (fig. 90).



**Figure 90: Corn cob ash calcined at 800°C**

Corn cob ash calcined at 900°C also displayed agglomerations between 10 µm and 2 mm in diameter. Surfaces appeared to have a coating of soft-edged gravel-like shapes protruding from a melted substrate (fig. 91).



**Figure 91: Corn cob ash calcined at 900°C**

As a result of these experiments, it was determined that the optimal temperature for calcining corn cob ash is 750°C, as this temperature allows minimal charcoal production and minimal sintering.

### **Corn seeper sludge**

As well as the corn trash that results from the removal of pieces of stalk and husks from the ears of corn at the Simplot plant, there is also sludge that results from the removal of the corn kernels. This is piped for collection in a vat (figs. 92 and 93). Two or three of these vats are removed as waste every day.



*Figure 92: Corn seeper sludge pipe*



*Figure 93: Corn seeper sludge vat*

A litre of seeper sludge was collected from the sludge vat. As received, corn seeper sludge was a creamy brown-coloured sludge with a consistency similar to fine porridge (fig. 94).



*Figure 94: Corn seeper sludge as received*

The sludge was calcined at increasing temperatures. Corn seeper sludge calcined at 600°C formed a black agglomeration of flakes that was broken easily into smaller lumps (fig. 95).



**Figure 95: Corn seeper sludge calcined at 600°C**

Corn seeper sludge calcined at 700°C formed a salmon-coloured agglomeration of flakes with some rust-coloured portions (fig. 96). Again, the pieces were broken easily into smaller lumps.



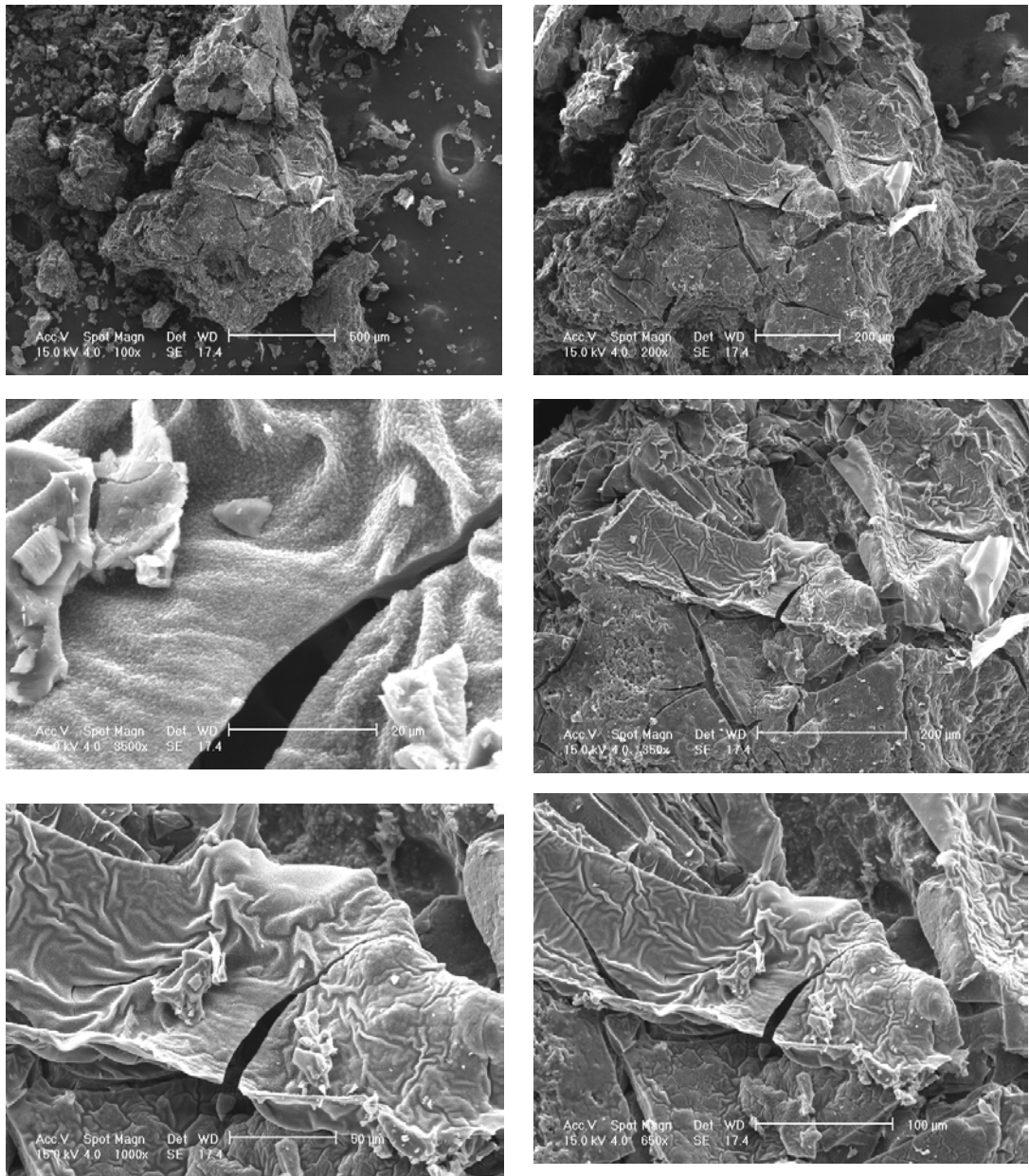
**Figure 96: Corn seeper sludge calcined at 700°C**

Corn seeper sludge calcined at 800°C formed a darker salmon-coloured agglomeration of flakes with some rust-coloured portions (fig. 97). Again, the pieces were broken easily into smaller lumps.



**Figure 97: Corn seeper sludge calcined at 800°C**

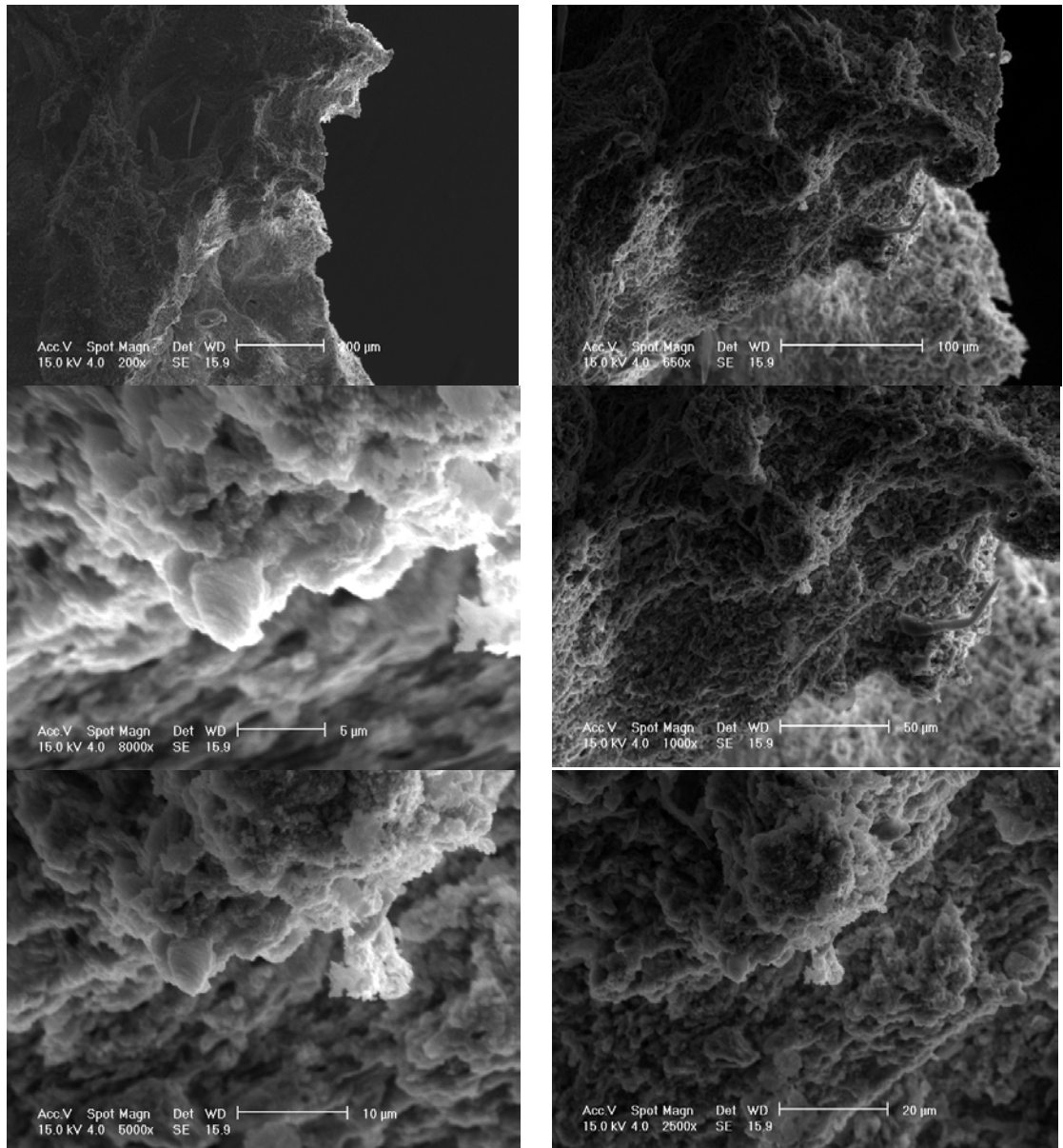
At 600°C, corn seeper sludge flakes displayed a distinctly wrinkled surface with sharp-edged cracks (fig. 98).



**Figure 98: Corn seeper sludge calcined at 600°C**

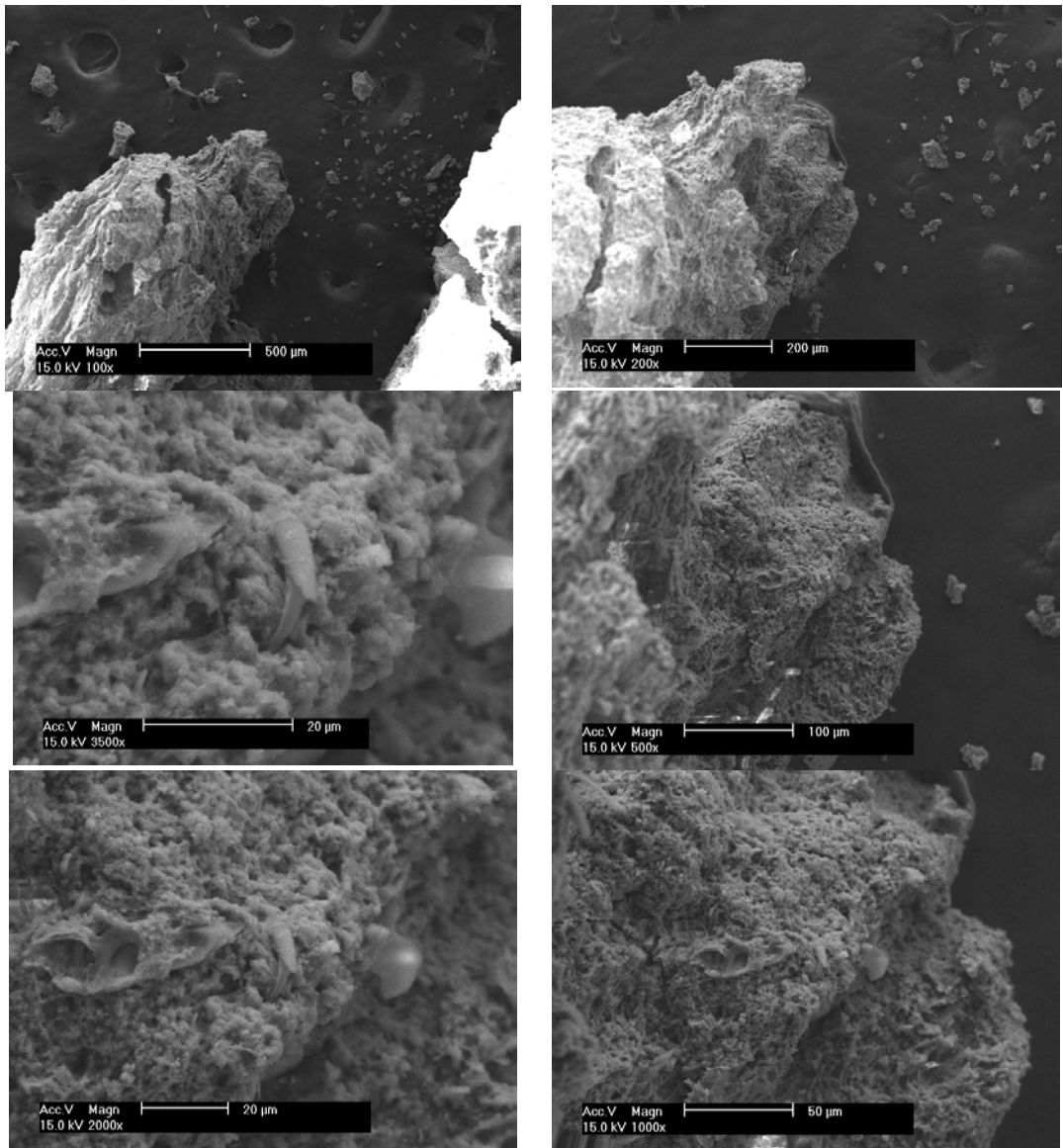


At 700°C, the surface of the corn seeper sludge flakes had a sponge-like appearance, with occasional plant-like whiskers clearly visible (fig. 99).



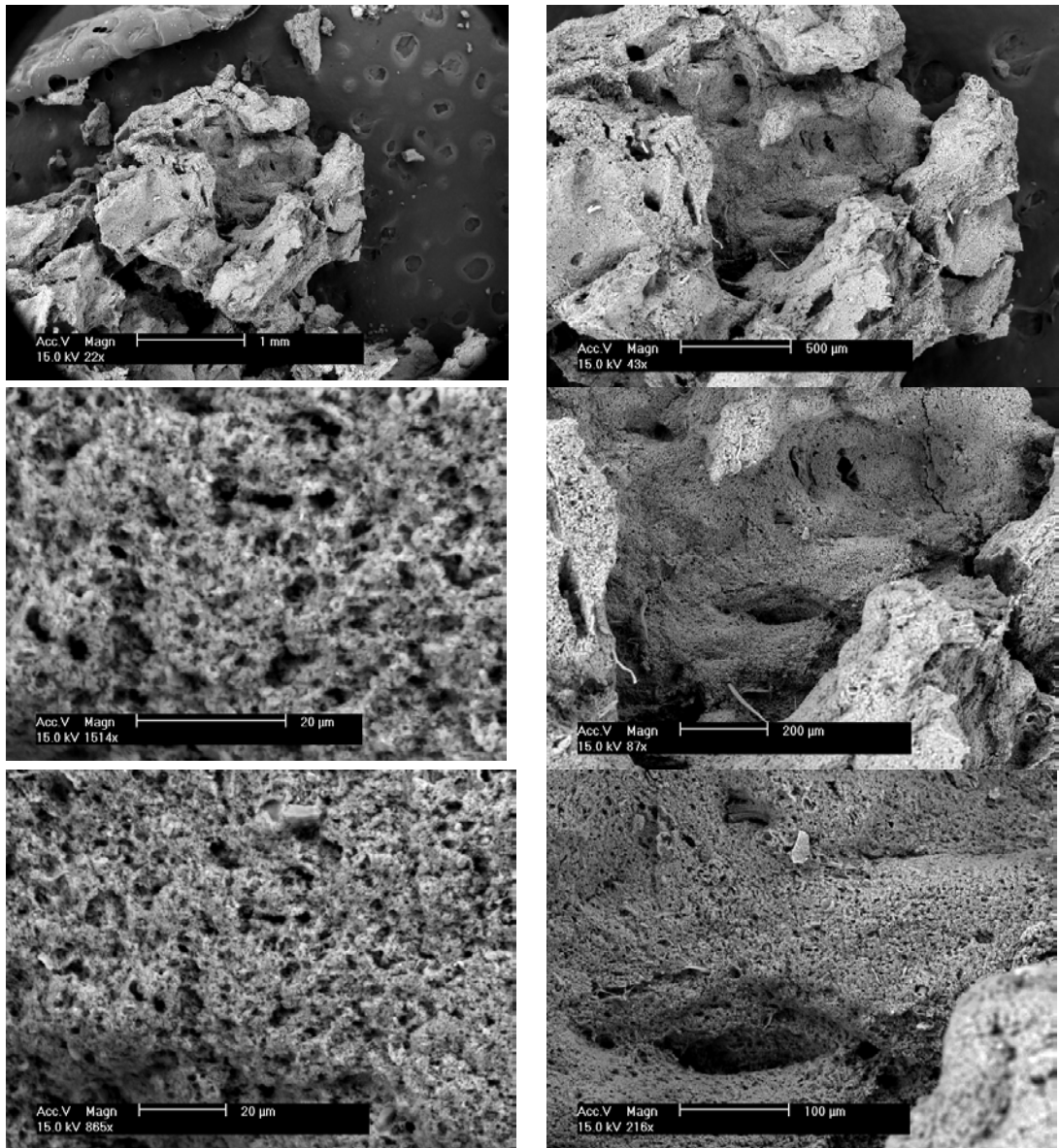
**Figure 99: Corn seeper sludge calcined at 700°C**

At 800°C, the surface of the corn seeper sludge flakes still had a sponge-like appearance with occasional plant-like whiskers clearly visible (fig. 100).



*Figure 100: Corn seeper sludge calcined at 800°C*

At 900°C, the corn seeper sludge flakes displayed a scoria-like surface and occasional plant-like whiskers were clearly visible (fig. 101).



*Figure 101: Corn seeper sludge calcined at 900°C*

## Paper sludge ash

Paper sludge was obtained from the Norske Skog paper recycling plant at Albury in NSW. The sludge as received contained approximately 40% water (figs. 102 and 103).



*Figure 102: Recycled fibre bio-solids*



*Figure 103: Waste-water treatment plant bio-solids*

Analysis supplied by Norske Skog (see Appendix 2) showed that the sludge composition differed significantly from month to month, suggesting that the potential for incorporation into a body may be limited by the variability in waste chemistry. In addition, there were concerns about the toxicity of the sludge composition. A conservative approach to the inclusion of more toxic materials suggests that the maximum levels of these materials present in the wastes should be used in considering the suitability of these materials for use. The reported maximum levels from the analyses supplied are shown in Table 9.

*Table 9: Selected elements from Norske Skog analysis*

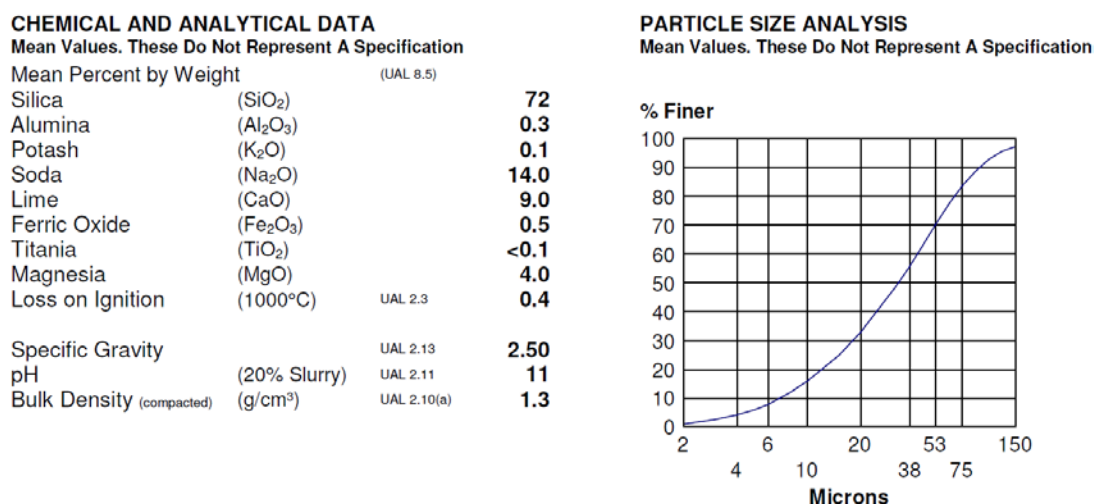
	Recycled fibre bio-solids (mg/kg)	Waste-water treatment plant bio-solids (mg/kg)
Arsenic	0.5	1.3
Cadmium	0.0	0.6
Lead	4.5	6.3
Mercury	1.0	1.8
Selenium	6.0	7.0

## Cullet

Australia recycles only a small proportion of glass intended for recycling, with the rest discarded into the environment or transported to landfill (Wilkinson & Cubby, 2008). Cullet was obtained from three sources: (1) as purchased from Unimin (Australia) Pty Ltd; (2) as received from under the Visy cullet processing plant conveyor belt at Banksmeadow, Sydney, NSW; (3) cleaned glass waste held back from domestic kerb-side recycling.

### Unimin cullet

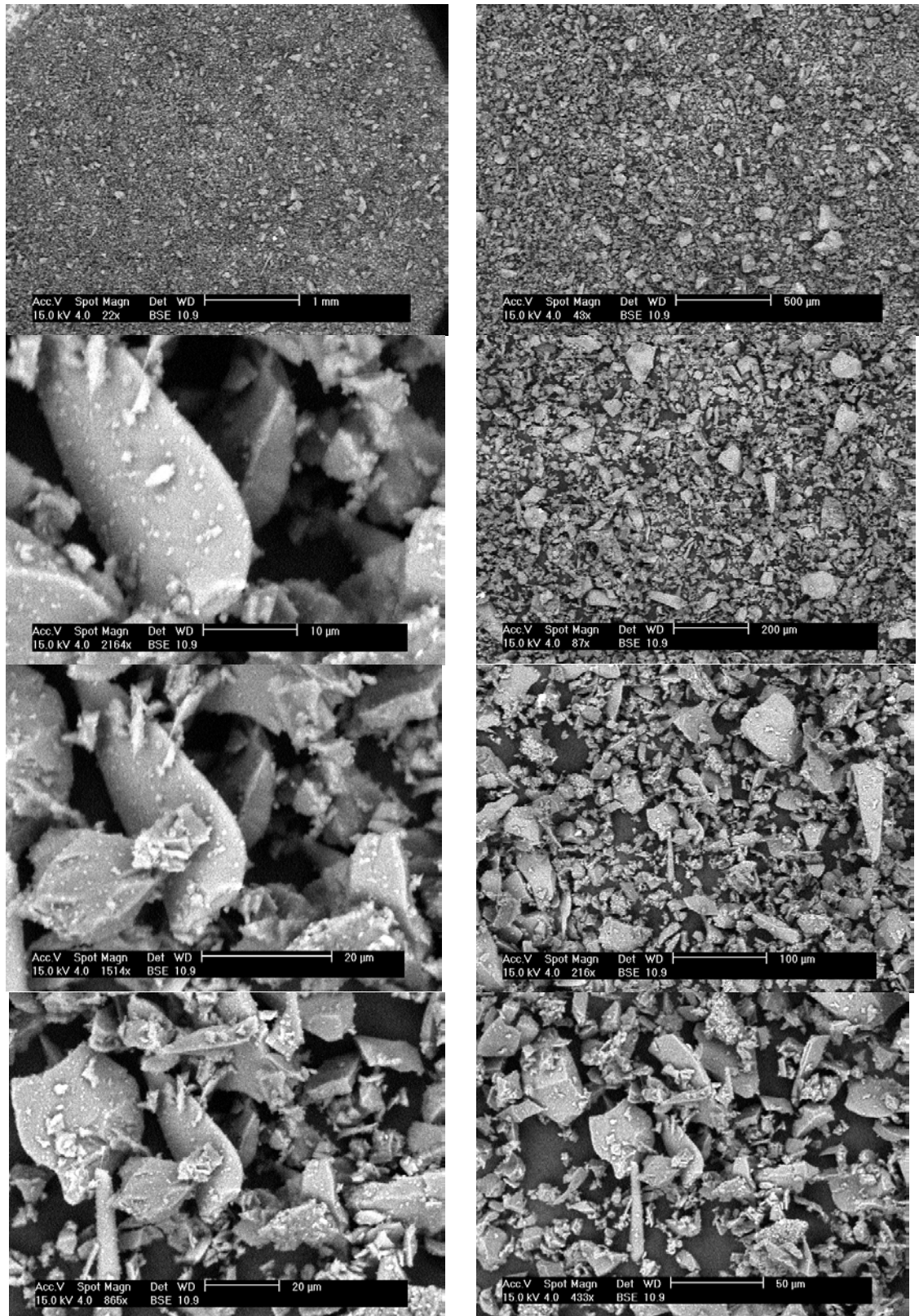
Unimin cullet can be purchased in 25 kg bags from Unimin (now Sibelco Australia). It is a fine white powder. An extract from Sibelco's technical data sheet (see Appendix 3) appears in Figure 104.



**Figure 104: Technical data for Unimin (Sibelco) cullet**

The percentage analysis is useful for calculations. It is also evident that the cullet is quite strongly alkaline, with a pH of 11. The particle size analysis was supported by microscopy results.

Microscopy of Unimin cullet showed it to be comprised of shards of glass, with most between 1  $\mu\text{m}$  and 150  $\mu\text{m}$  (fig. 105).



**Figure 105: Unimin cullet**

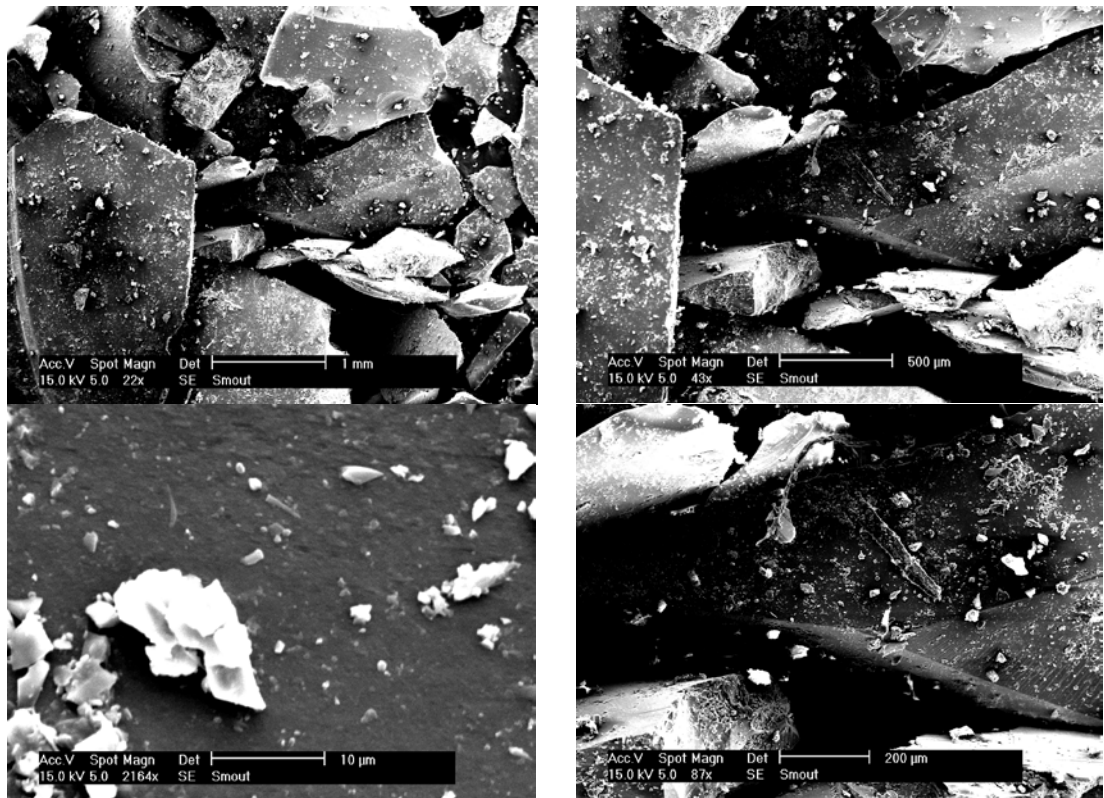
### Visy cullet conveyor belt debris

Debris was collected as it fell from the conveyor belt at the Visy cullet processing plant conveyor belt at Banksmeadow, Sydney, NSW. As received, it was a mixture of glass dust, glass sand and shards of clear, brown or green glass up to 1 centimetre in diameter (fig. 106).

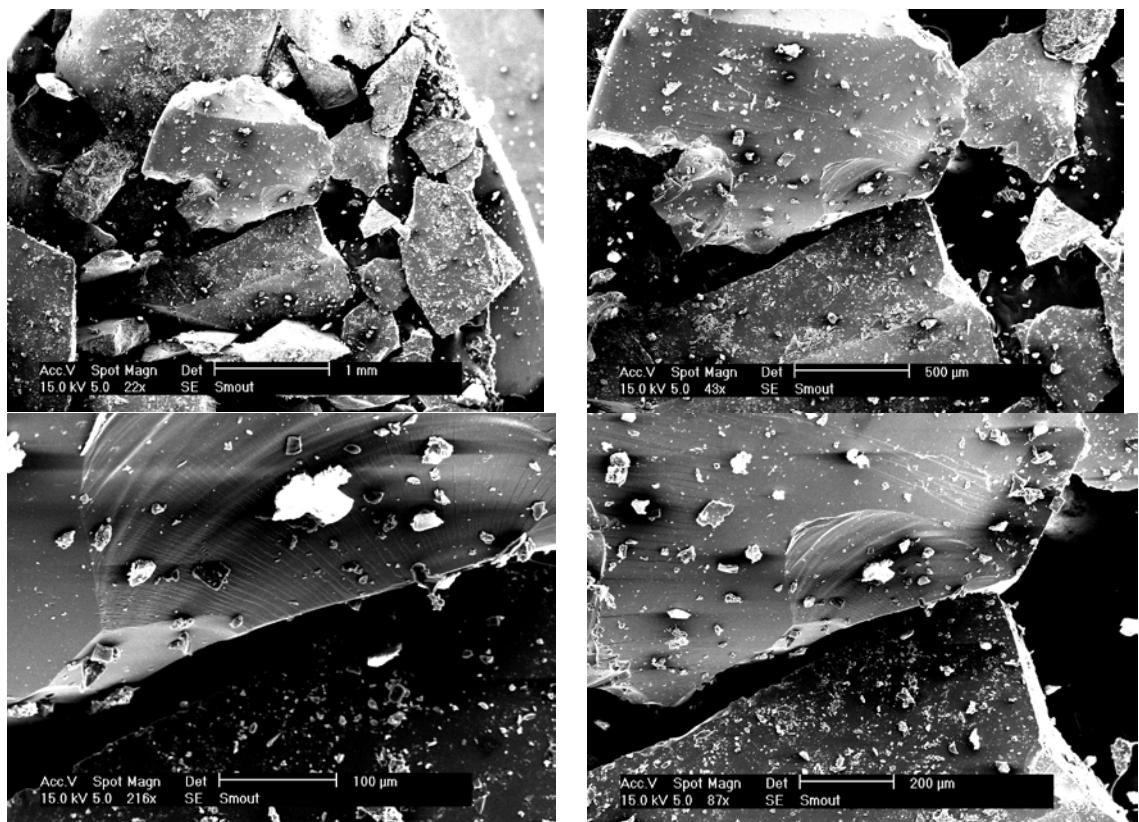


*Figure 106: Visy cullet conveyor belt dust as received*

Microscopy revealed that the bulk of the volume of the cullet dust from the Visy conveyor belt was comprised of glass sand of approximately 1 millimetre in diameter, surrounded by smaller particles of glass sand and dust, some of which had a diameter of less than 1  $\mu\text{m}$  (figs. 107 and 108).



**Figure 107: Visy cullet conveyor belt dust as received**



**Figure 108: Visy cullet conveyor belt dust as received**

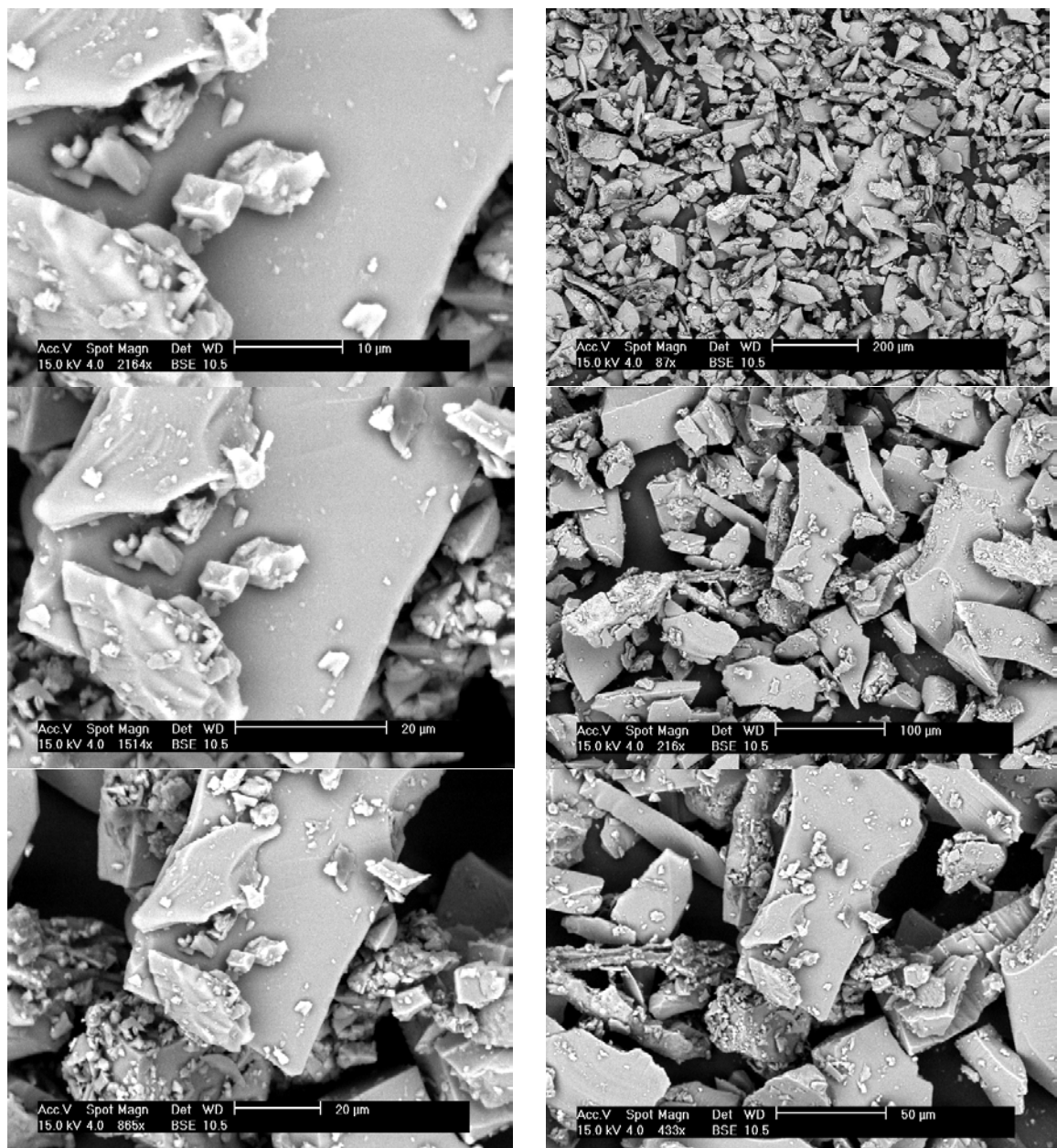
The cullet dust from the conveyor belt was fractionated by sieving through increasingly fine sieves. The fractions obtained appear below (Table 10).



**Table 10: Fractions obtained from Visy conveyor belt cullet dust**

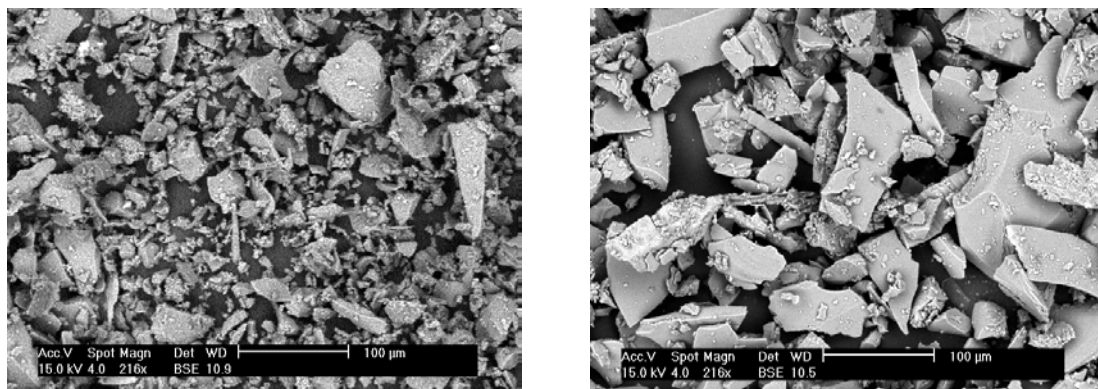
Visy conveyor cullet dust	
Fraction (wt%)	Grade
4.8	<200-mesh
6.6	>200, <100
24.8	>100, <60
22.2	>60, <40
33.2	>40, <10
8.4	>10

A sample of the dust that passed through a 200-mesh sieve was viewed under the microscope. The bulk of this sample was comprised of pieces of glass sand between 50 µm and 200 µm in diameter (fig. 109).



**Figure 109: Visy cullet conveyor belt dust <200 mesh**

Comparison of Unimin cullet and the <200 fraction of Visy conveyor dust at identical levels of magnification revealed that the Visy cullet dust had fewer smaller particles (fig. 110).



*Figure 110: Comparison of Unimin cullet (left) and Visy conveyor belt dust <200 mesh*

Small particle size is of interest to the current project because smaller cullet particles have an improved impact on sintering. It was also of interest to see whether suitably sized cullet could be produced from domestic glass waste.

#### Cleaned glass waste held back from domestic kerb-side recycling

Every household that purchases food and beverages in glass containers probably discards the bulk of those containers into waste or recycling. To find a way to re-use this material, investigations were made into methods of crushing domestic glass waste.

A company named Bottlecyclor supplies Sydney licensed premises with crushing machines into which staff feed empty bottles, thereby reducing the volume and costs for cartage to recycling facilities (Bottlecyclor, 2007). While this would appear beneficial in terms of material recovery, the end recycling facilities are not equipped to remove contaminants easily once the glass has been broken into small pieces of cullet, so material recycling facilities select only whole glass containers to send on for processing, and the broken glass goes to landfill (Horne, 2008). Quality is the main issue. As an illustration, a 3 g piece of ceramic (from a broken plate, for example) in a tonne of processed cullet will cause the glass manufacturer Australian Consolidated Industries (ACI) to reject 33 tonnes of glass (Horne, 2008).

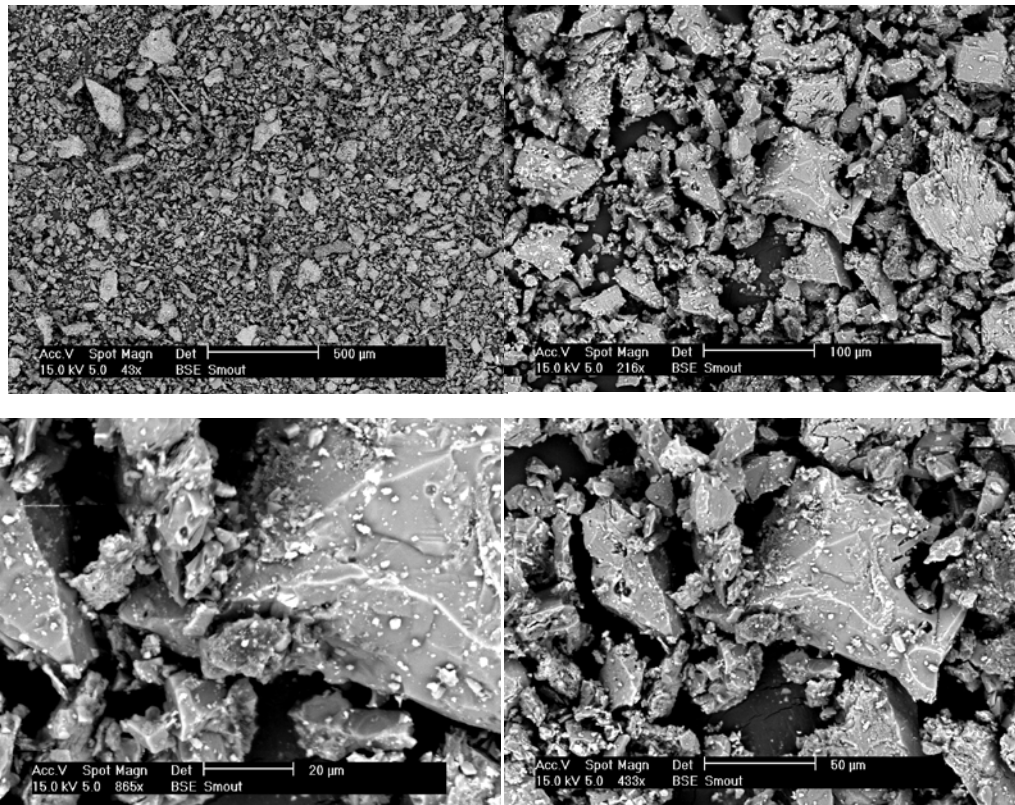
In an effort to produce uncontaminated glass frit from bottles used at home, bottles were stripped of their labels, caps and neck-rings. These bottles were crushed at the Bottlecyclor Ltd factory in St Marys, Sydney, NSW. The cullet thus obtained was too coarse for use, as most pieces were between 1 and 8 cm in diameter (fig. 111). The intention was to produce powdered glass by further processing, but to date no affordable small scale machine capable of crushing this cullet to powder has been found. As a consequence, this material has not been investigated further.



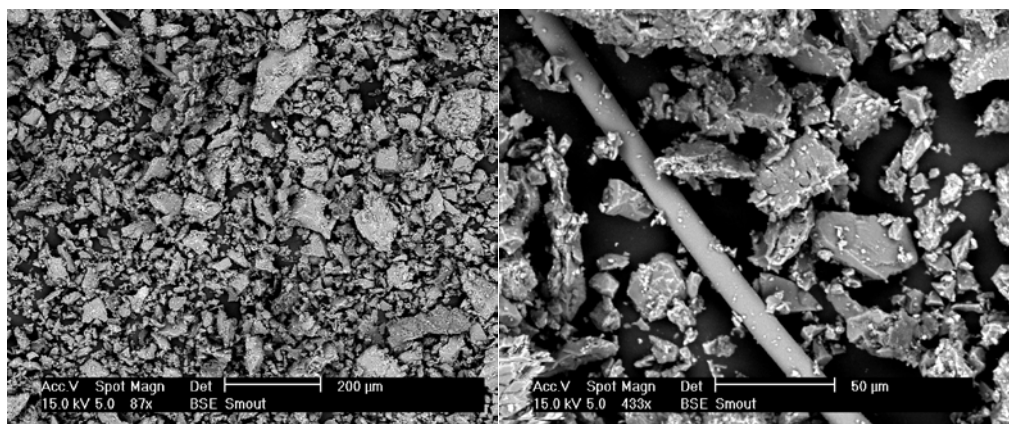
***Figure 111: Clear glass bottles crushed in the Bottlecyclor crusher***

## Prego marble-cutting dust

A visit was made to the Prego marble company in Mortdale, NSW. Sawdust was collected from beneath the saw-bench. Microscopy revealed that this sawdust was comprised of particles with a diameter as large as .25 mm, but the bulk of the dust was comprised of particles between 50  $\mu\text{m}$  and 100  $\mu\text{m}$  in diameter (figs. 112 and 113).



*Figure 112: Prego marble sawdust*



*Figure 113: Prego marble sawdust sweepings*

## Perlite fines

Perlite fines were obtained from Australian Perlite Ltd in Banksmeadow, NSW. At the time of collection, the waste from the cold bag house was being disposed of at a cost of approximately AU\$500 per week. Cold bag house fines produced as waste from both expanded Turkish white perlite and expanded grey West Australian perlite were obtained. In addition, unexpanded grey perlite ore grit was collected from the furnace surrounds. Perlite AP10 white cold bag house fines were collected as a fine white powder (fig. 114).

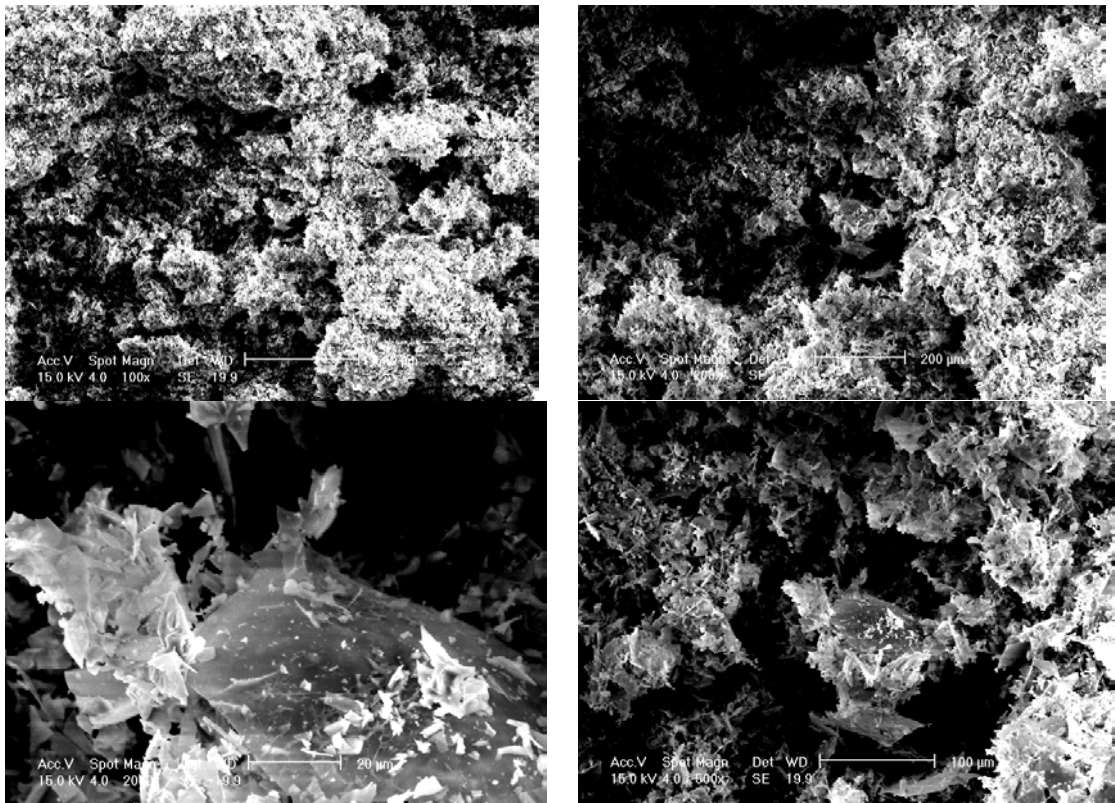


*Figure 114: Perlite AP10 white cold bag house fines*

A typical analysis of perlite was provided as 70–75% SiO<sub>2</sub>, 12–15% Al<sub>2</sub>O<sub>3</sub>, 3–4% Na<sub>2</sub>O, 3–5% K<sub>2</sub>O, 0.5–2% Fe<sub>2</sub>O<sub>3</sub>, 0.2–0.7% MgO and 0.5–1.5% CaO, with 3–5% loss on ignition (Australian Perlite Ltd, n.d.).

Microscopy of AP10 white perlite fines revealed that it consisted of fine sheets of material up to 100 µm in diameter and approximately 1 µm thick, with some sheets having flat surfaces and straight edges and others having crumpled surfaces and ragged edges. The sheets were also broken into particles, with

some having diameters less than 1  $\mu\text{m}$ . When magnified 2000 times, the fines looked something like a shredded and degrading plastic bag (fig. 115).



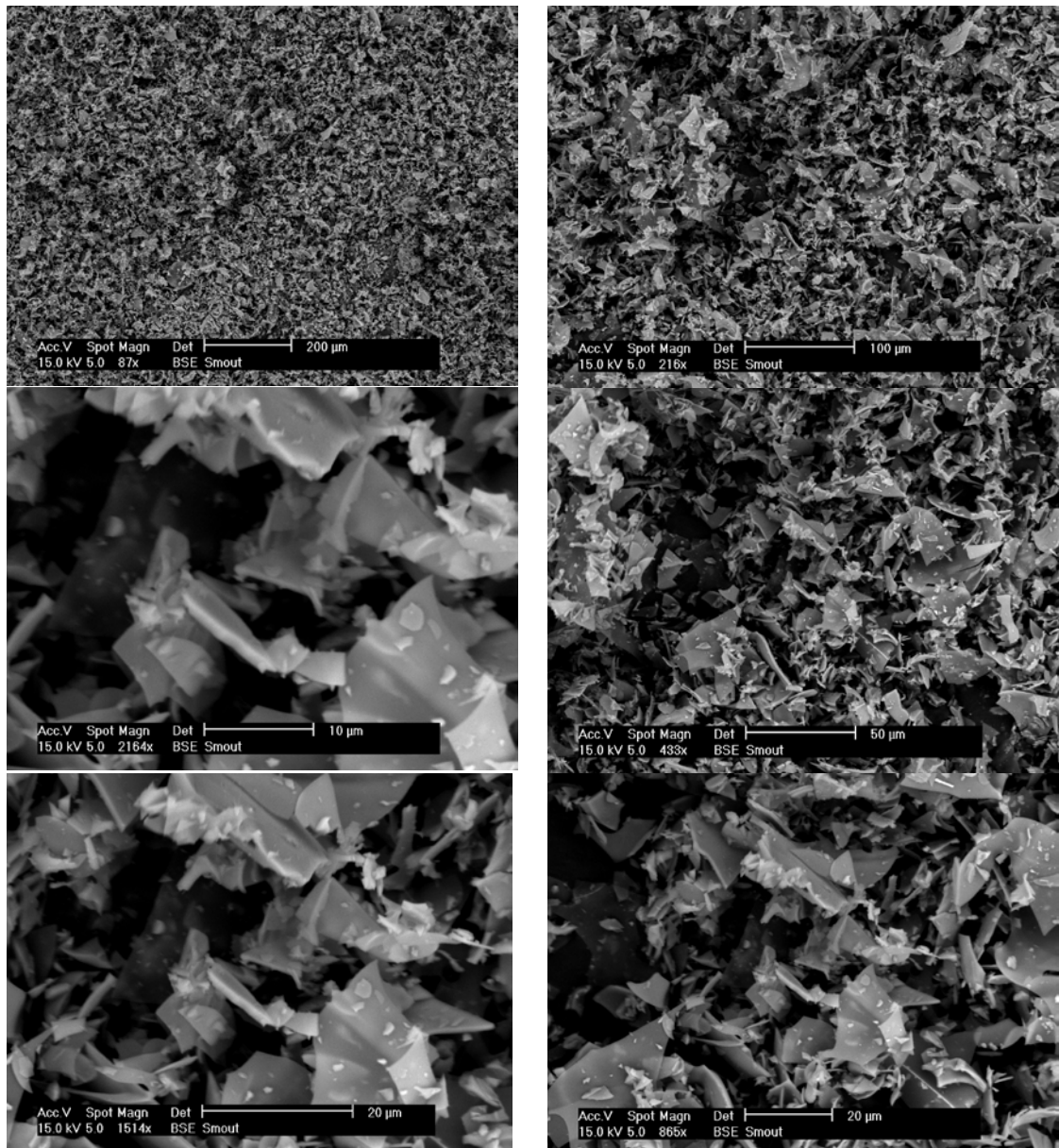
**Figure 115: Perlite fines AP10 white**

Perlite AP10 grey cold bag house fines formed a fine off-white powder (fig. 116).



**Figure 116: Perlite AP10 grey cold bag house fines**

Microscopy of AP10 grey perlite fines revealed that it consisted of fine sheets of material up to 70  $\mu\text{m}$  in diameter and approximately 2  $\mu\text{m}$  thick. Most fragments greater than 20  $\mu\text{m}$  in diameter were bent at angles close to 90°. When magnified 2000 times, the fines looked something like smashed fragments of an opaque plastic container (fig. 117).



**Figure 117: Perlite fines AP10 grey**

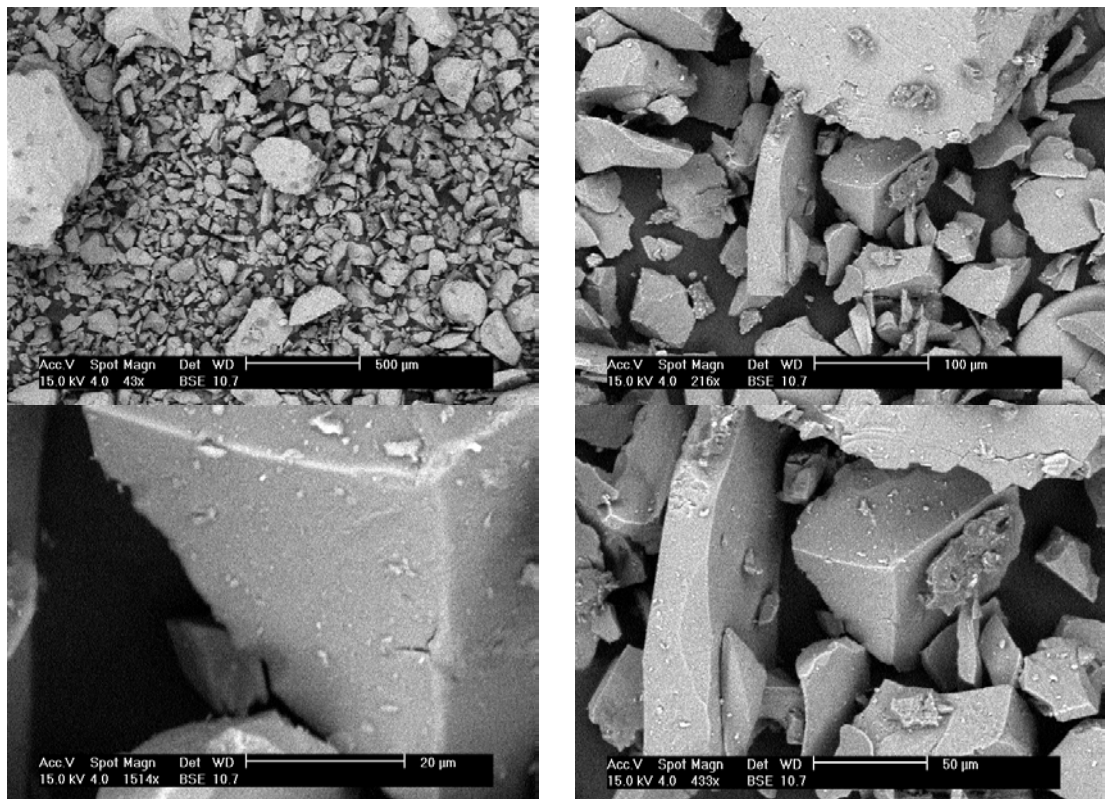
## Perlite: Unexpanded ore

Unexpanded perlite ore was collected as a fine grit (fig. 118).



*Figure 118: Perlite unexpanded ore*

Microscopy of unexpanded perlite ore revealed that it consisted of particles shaped like crushed granite or broken shale, with some particles up to 600  $\mu\text{m}$  in diameter, most between 50  $\mu\text{m}$  and 100  $\mu\text{m}$  and few less than 5  $\mu\text{m}$ . The particles had different shapes, with some having the appearance of being broken from a cubic block, some having the appearance of being chipped or snapped off a sheet (fig. 119).



*Figure 119: Perlite: Unexpanded grey ore*



## **Dunmore latite**

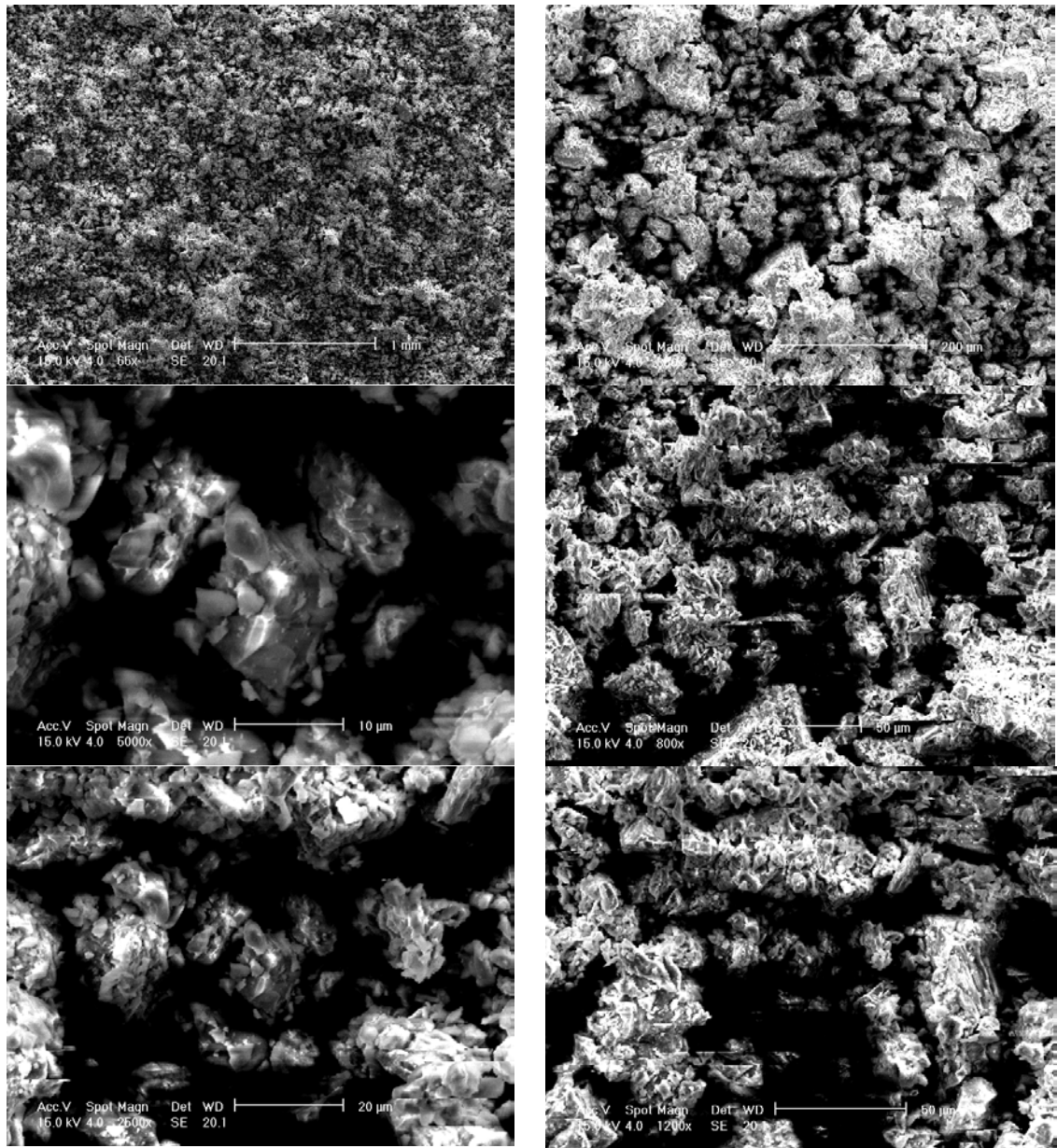
Boral Dunmore dust is a 200-million-year-old latite (Dumitru, 2008), an intermediate igneous rock from the Bumbo flow, near Shellharbour Railway Station (McMeekin, 1985). It was supplied by Boral in fractions less than 75 µm, so crushing was unnecessary. Both Whitfield's (1993) analysis and the analysis from the Geological Survey of NSW supplied by McMeekin (1985) indicated that this olivine latite dust contained almost 7% calcium, so it is expected that inclusions of more than 15% latite dust would have a negative effect on sintering below 1000°C. McMeekin suggests that latite is more useful as a glaze material than a body material because of the calcium, magnesium and iron present.

Boral kindly provided 20 kg of Dunmore latite dust, which had been collected and sieved for experimental use in their laboratories. As received, the dust was a fine brownish-grey powder (fig. 120).



*Figure 120: Dunmore latite as received*

Microscopy revealed that Dunmore latite dust consisted of clumps of irregular gravel-shaped particles, with some as small as 1  $\mu\text{m}$  (fig. 121).



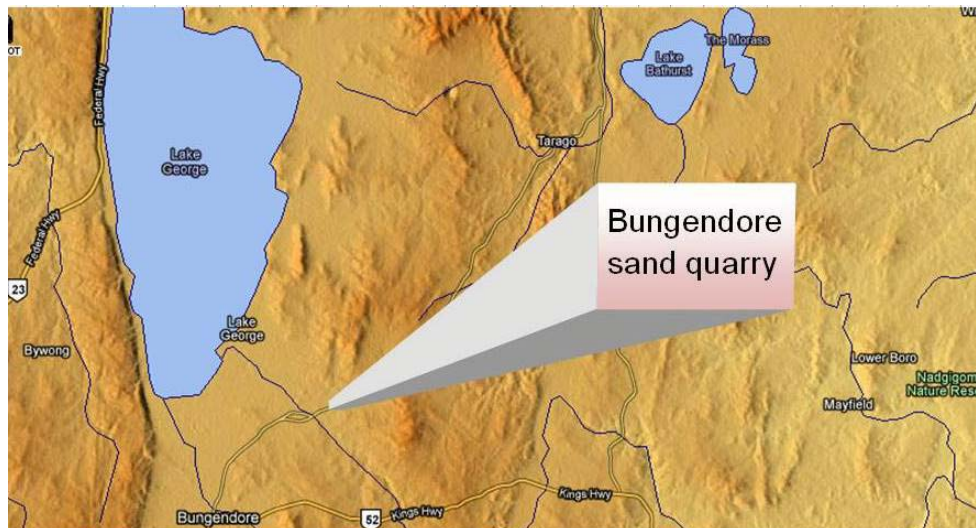
**Figure 121: Dunmore latite**

## Quarry tailings

Quarry tailings were obtained from two sources: Bungendore sand mine and a rock quarry at Marulan.

### Bungendore sand mine tailings

Cemex provided access to their Bungendore (NSW) site, where sand has been mined since 1956. Bungendore quarry has map coordinates of approximately 35°15' south, 149°26' east. It is 28 km along the road from Tarago to Bungendore, approximately 45 km from Canberra and 60 km from Goulburn (fig. 122).



**Figure 122: Relief map showing location of Bungendore sand quarry**

Image adapted from Maps-for-free.com

Excavation produces a mix of clay and sand in approximately equal proportions. This is crushed, washed and separated in a cyclone (fig. 123). The sand is collected for builder's mix and the run-off is flocculated (fig. 124) in a settling pond (fig. 125) to hasten separation of the clay particles from the run-off water, which is re-used. The resultant clay sludge is deposited in 7 m deep silt ponds. The pond surface dries to a depth of up to 30 cm, forming a crust over the remaining clay sludge (fig. 126). These ponds are isolated for safety reasons because the crust will crumble if walked on. The site has 100 acres of these ponds, and the site manager indicated he could supply 160 tonnes per hour of clay sludge, should demand eventuate. Wet and dry samples were obtained.



**Figure 123: Bungendore sand-mining plant**



**Figure 124: Flocculation of Bungendore tailings**



**Figure 125: Flocculated Bungendore tailings settling pond**



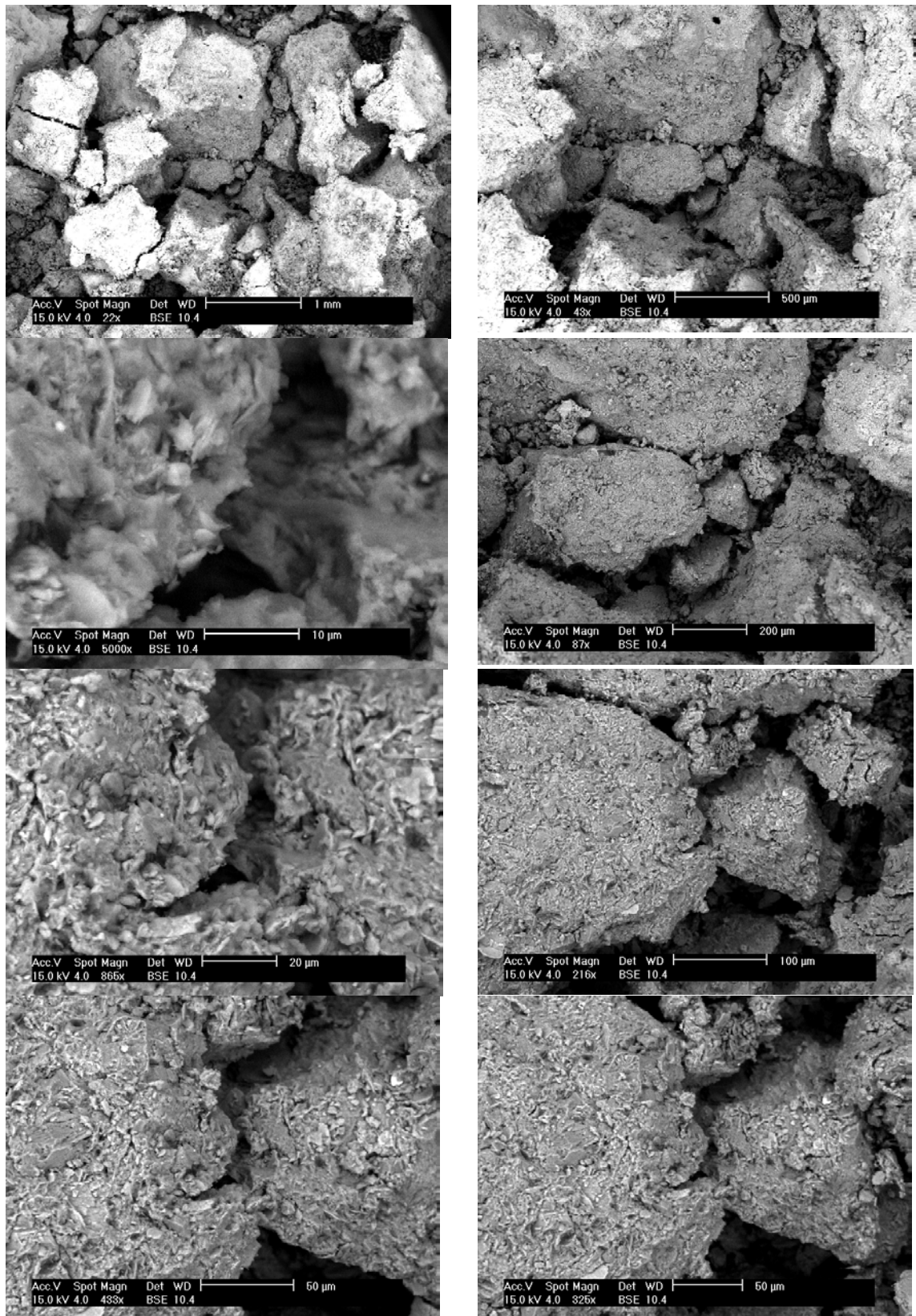
***Figure 126: Bungendore tailings silt pond***

As received on 1 September 2009, the Bungendore sand quarry tailings were yellow-brown pieces with the appearance of dried clay (fig. 127).



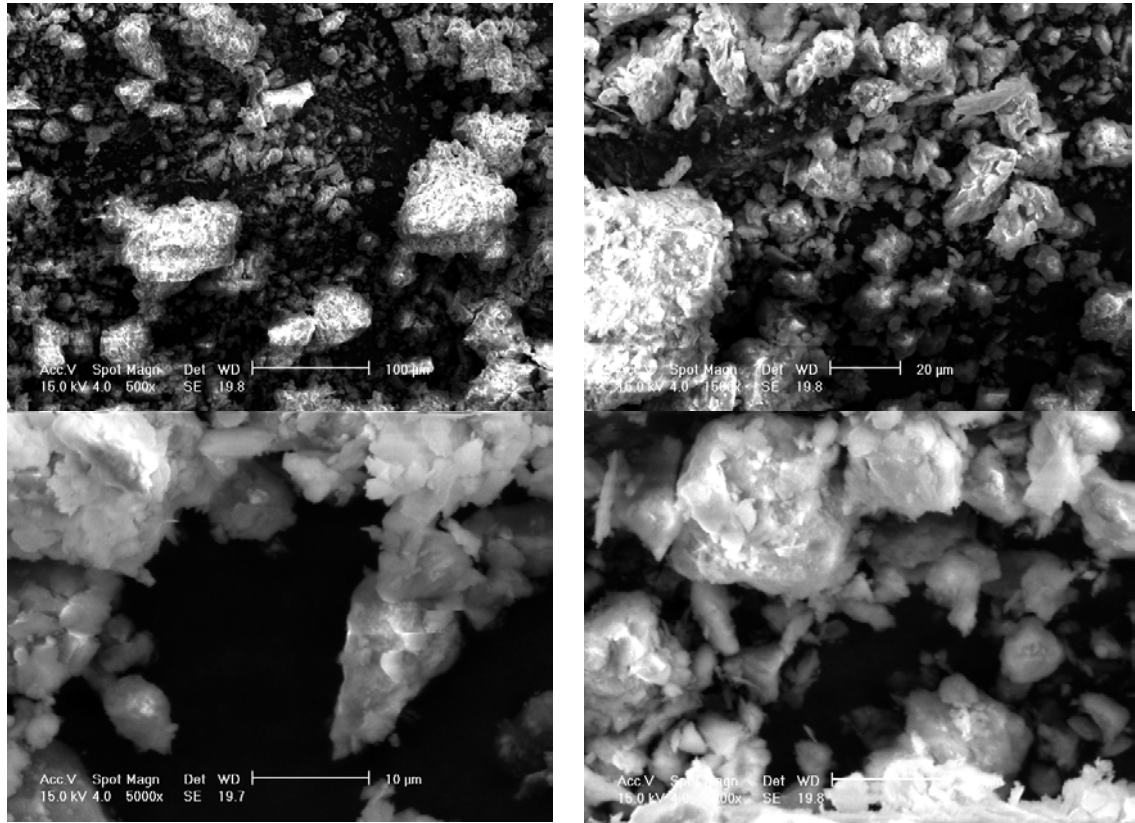
***Figure 127: Bungendore sand quarry tailings as received***

A sample of Bungendore tailings as received was passed through a 40-mesh sieve in order to provide a sample for microscopy, which revealed crumbled agglomerations of particles (fig. 128).



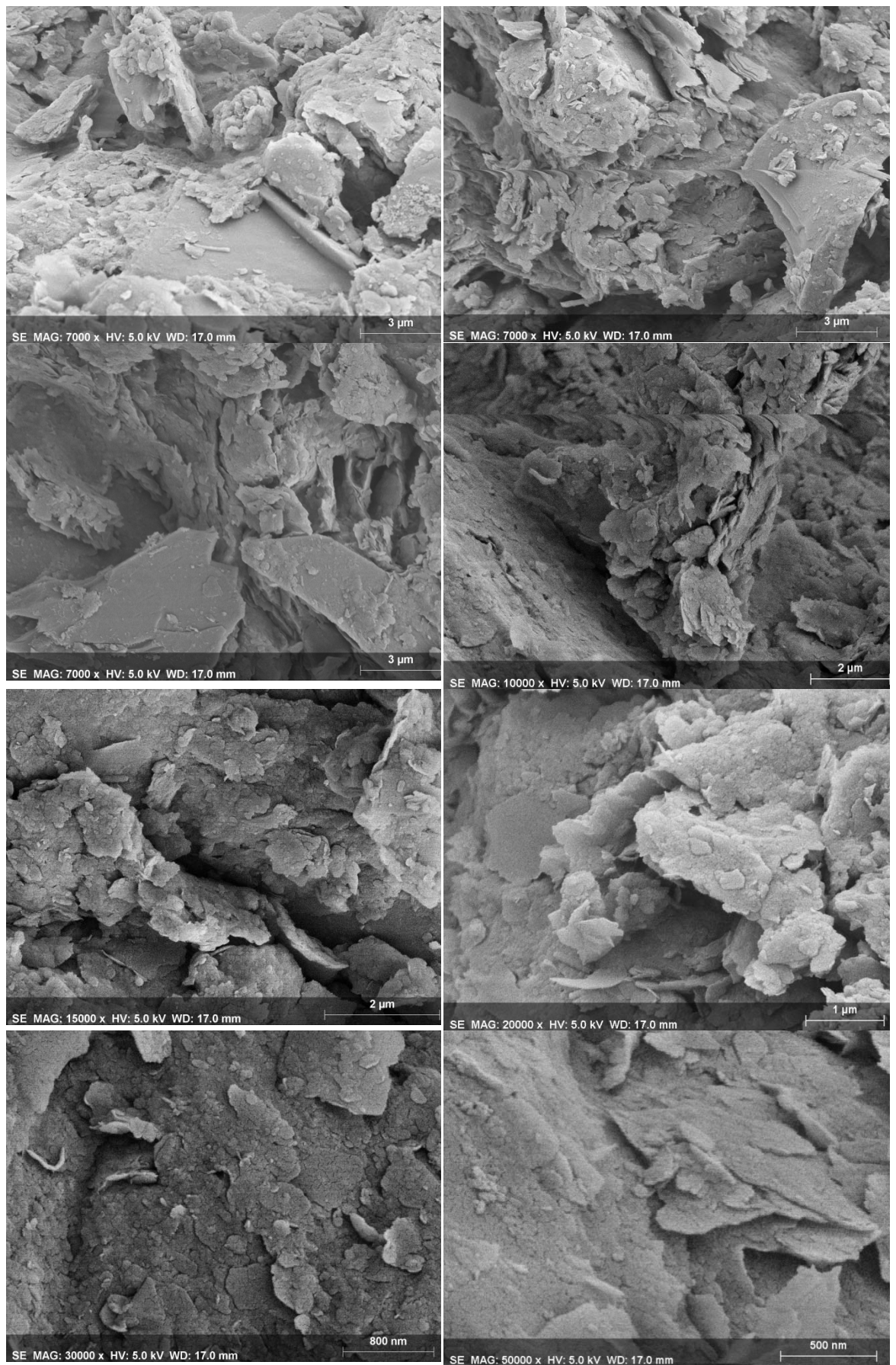
**Figure 128: Bungendore tailings**

When Bungendore tailings were prepared by grinding using a mortar and pestle, it was apparent that the ground agglomerations were comprised of particles, but it was unclear how much smaller the smallest particles were than 1  $\mu\text{m}$  (fig. 129).



**Figure 129: Bungendore tailings hand-ground**

Because the morphology of individual particles was indistinct at the magnifications used, microscopy of Bungendore tailings (as received) was repeated using a Hitachi S-4500 SEM. This enabled the sample to be viewed at multiple sites, with the field narrowed from 3  $\mu\text{m}$  to 500 nm, with magnification increased from 7,000 to 50,000 times. The morphology revealed was consistently of flakes or crumbled plates, with some flakes being up to 10  $\mu\text{m}$  across and with some particles less than 100 nm visible (fig. 130).

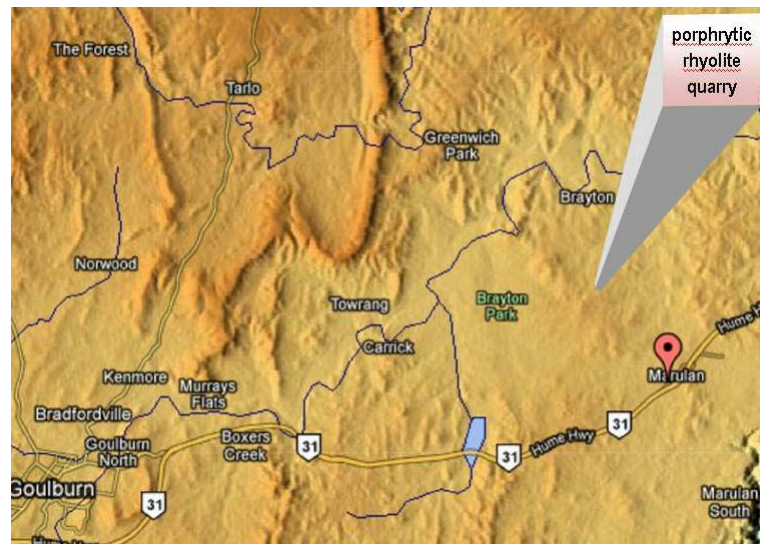


**Figure 130: Narrow field microscopy of Bungendore tailings**



## Marulan quarry tailings

Cemex provided access to their quarry at Marulan, NSW. Marulan is 130 km south of Sydney and 150 km north of Canberra, on the Hume Highway. Coordinates are 34°40' south, 149°59' east (fig. 131).



**Figure 131: Relief map showing location of Marulan quarry**

Image adapted from Maps-for-free.com



**Figure 132: Marulan quarry blasting face**

The rock at Marulan, which is a porphyritic rhyolite, is mined by blasting (fig. 132). The rock is then crushed and washed (fig. 133), and the tailings are collected as run-off containing a fine sludge (fig. 134). The sludge is allowed to settle, then transported to silt ponds for drying (fig. 135), after which it is piled into bunds to provide the required visual barrier for the quarry.



**Figure 133: Marulan quarry crusher and washer**

The site manager indicated that they had sent a sample to a brick maker to see whether there was a potential use, and expressed interest in the current research. Wet and dry samples were obtained on 1 September 2009. Wet samples were obtained from the sludge pond below the crusher (fig. 134).



**Figure 134: Marulan quarry wet sludge pond**

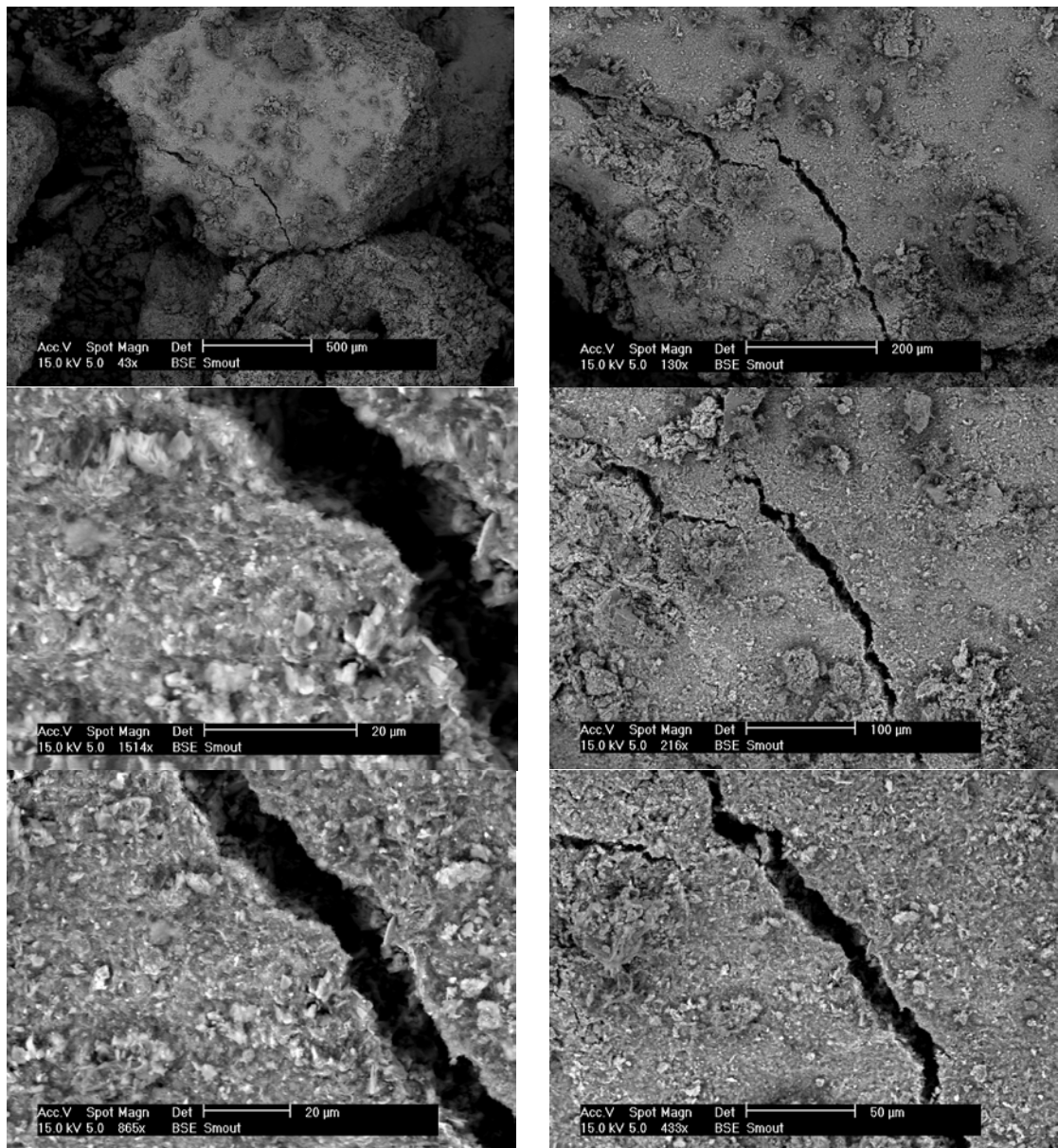
The sludge ponds are left to dry out (fig. 135), and then excavated and piled up in large mounds referred to as bunds (Stone, 2009).



**Figure 135: Marulan quarry dried sludge pond**

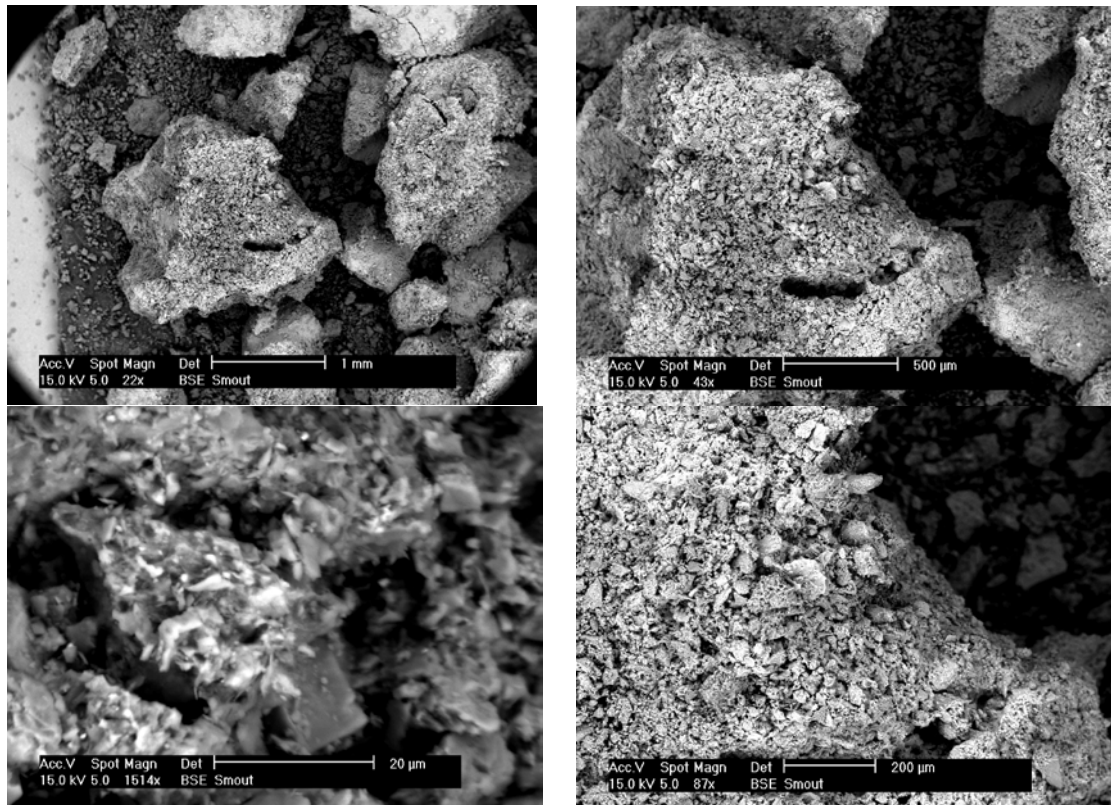
Dry samples were obtained from a bund of dried tailings sludge behind the quarry level designated bench 11.

A sample of Marulan tailings as received was selected for microscopy, which revealed clumps approximately 1 millimetre across, with smaller particles attached and dispersed (fig. 136).



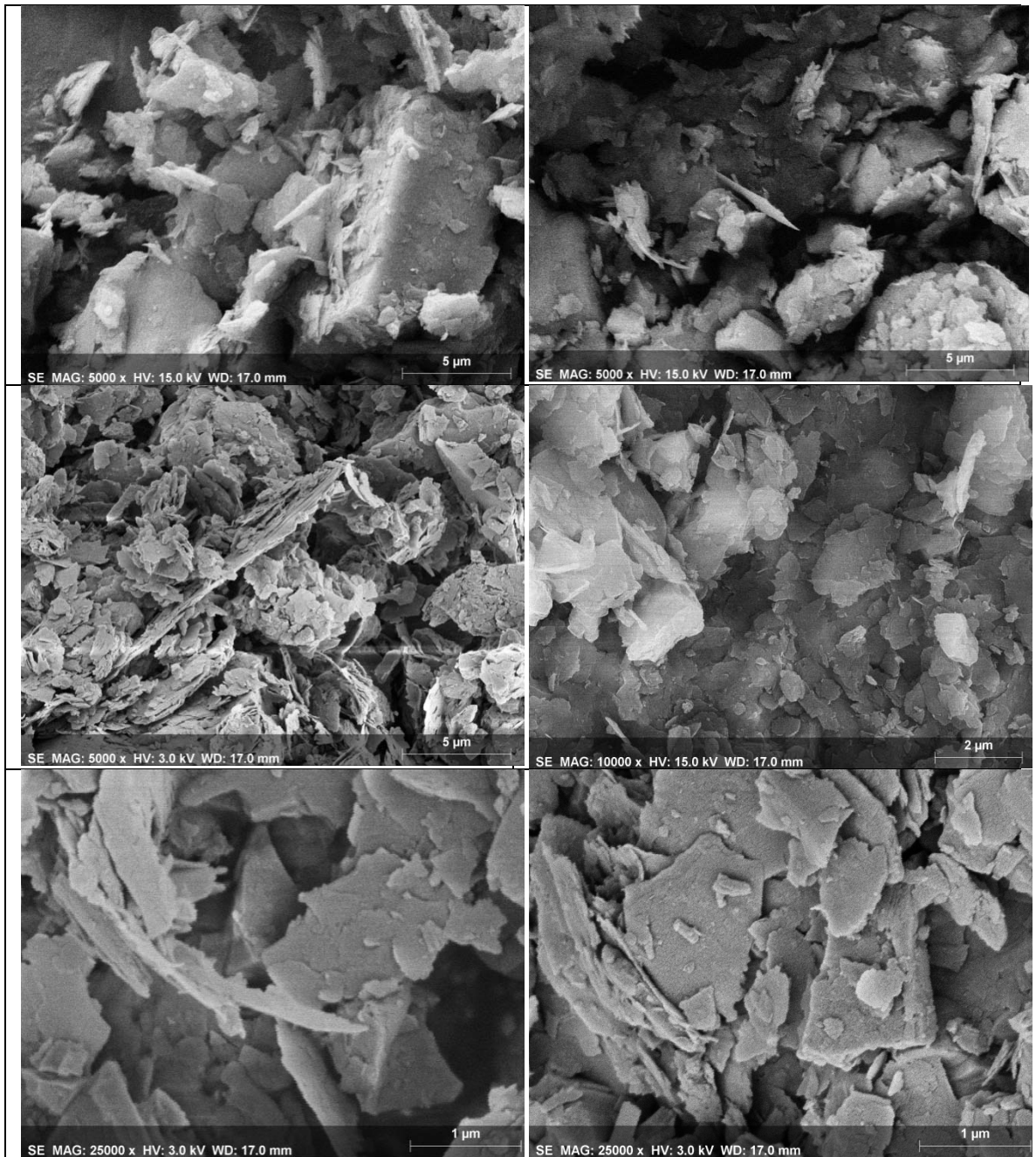
**Figure 136: Marulan tailings, as received**

Increased magnification (figs. 136 and 137) showed no distinct structure to the agglomerated particles.



**Figure 137: Marulan tailings, as received**

Because the morphology of individual particles was indistinct at the magnifications used, microscopy of Marulan tailings (as received) was repeated using a Hitachi S-4500 SEM. This enabled the sample to be viewed at multiple sites, with the field narrowed from 5 µm to 1 µm, with magnification increased from 5,000 to 25,000 times. The morphology revealed was predominantly flakes or crumbled plates, combined with fragments of blocks, as seen in the upper left image (fig. 138).



**Figure 138: Narrow field microscopy of Marulan tailings**

The following chapter investigates how these quarry tailings with fine particle size absorb water and remain in suspension. They are compared with some materials with fine particle size that are regularly used in studio ceramics – ball clay and bentonite.

## Chapter 9: Comparative Observations of Absorption Rates and Suspension in Water: quarry tailings, ball clay and bentonite

Properties of absorption of water and suspension are characteristics that are of interest when raw glazing, when using a clay body for making terra sigillata and when considering means of holding glaze materials in suspension.

In order to make comparative observations of the water absorption and suspension qualities of Marulan and Bungendore quarry tailings, dry crushed tailings were sieved through a 200-mesh sieve, and their speeds of water absorption and settling were compared with two bentonites and one ball clay.

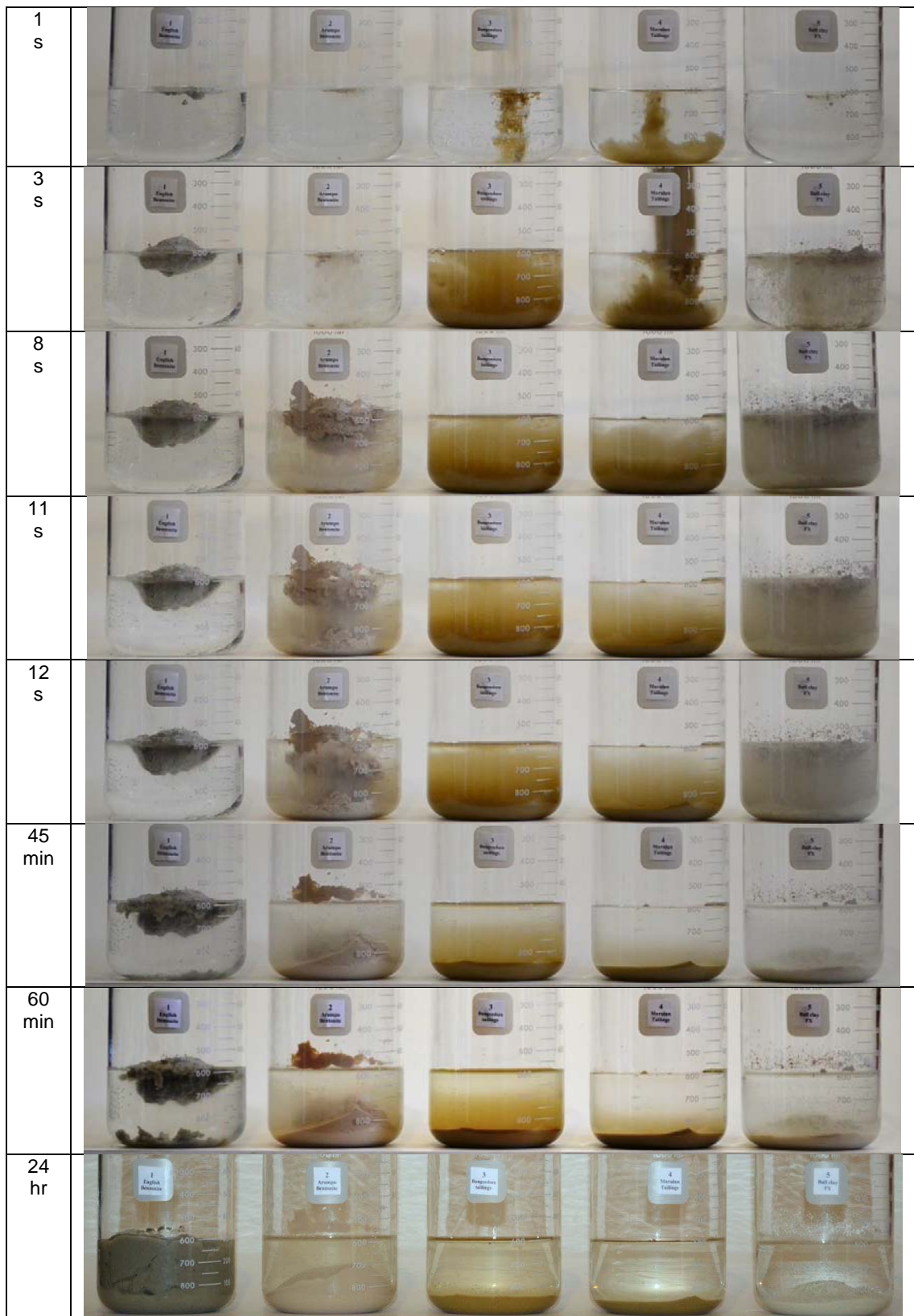
### Absorption

First, 300 ml of distilled water was poured into each of five graduated beakers. The beakers were left to stand so that the interior of the beakers was dry above the water level, and then 50 g of each powder was added simultaneously. At this moment, timing was commenced. For each material, the time elapsed until the last of the powder had sunk below the surface was recorded (table 11).

*Table 11: Elapsed time for absorption of 50 mg in 300 ml water: five clays*

Beaker number	1	2	3	4	5
Clay	English bentonite	Arumpo bentonite	Bungendore tailings	Marulan tailings	ball clay FX
Absorption time	89 min	15 s	upon contact	upon contact	22 s

It was observed that both Bungendore tailings and Marulan tailings sank to the bottom of the beaker upon contact. At least a proportion of each of the other materials remained on top of the water for a period of time. This period was longest for English bentonite. Almost all English bentonite remained at the surface. Particles of ball clay FX began sinking upon contact, but particles also accumulated on the surface and sank successively. With the exception of some material that adhered to the interior wall of the beaker, the entire sample of Arumpo bentonite was submerged after 15 seconds (fig.139).



**Figure 139: Water absorption of (left to right) English Bentonite, Arumpo Bentonite, Bungendore tailings, Marulan tailings, ball clay FX**

## **Comparative absorption of water by English bentonite and Arumpo bentonite**

Based on the detailed characterisation of Arumpo bentonite provided by Churchman and colleagues (2002; summary p. 57 herein), it was expected that English bentonite and Arumpo bentonite would behave differently when added to water, with respect to permeability and swelling. This was partly borne out by observation. The reported low permeability of Arumpo bentonite (Churchman et al., 2002) led to the expectation that Arumpo bentonite powder would be slower to absorb water than would English bentonite. It was observed that the reverse occurred, as shown (fig. 138) and recorded in Table 11. As a result of this finding, it was speculated that the reported low permeability of Arumpo bentonite referred to bentonite in the plastic state.

### **Swelling of English bentonite and Arumpo bentonite after saturation**

The five saturated clays were left in the beakers for 24 hours (fig. 140). It was observed that while most materials appeared to occupy the same volume as they had been observed to occupy after 60 minutes, this was not the case for English bentonite.



**Figure 140: English bentonite, Arumpo bentonite, Bungendore tailings, Marulan tailings, and ball clay FX, 24 hours after saturation**

The English bentonite had swollen to occupy the volume of water in the beaker. By comparison, Arumpo bentonite did not display swelling (see detail in fig. 141). This supported the description of Arumpo bentonite as a non-swelling bentonite (Churchman et al., 2002).





**Figure 141: Water absorption of English (left) and Arumpo bentonites**

Arumpo bentonite is mined 80 km northeast of Mildura, on the NSW side of the Victorian border, where it lies in a five-metre thick band extending over 9 square km (Churchman et al., 2002). Characterisations of Arumpo bentonite performed by Churchman and colleagues indicated that Arumpo bentonite swells much less than Wyoming bentonite, has lower viscosity in aqueous suspensions of the same concentration, and very low permeability to water, even under pressure. Arumpo bentonite was also shown to consist of much smaller particles and to provide far greater external surface area as a consequence. It was reported to consist of 99% smectite/illite, with illite layers randomly interstratified at a ratio of one illite to ten smectites (Churchman et al., 2002). It has unusual properties for a bentonite, including a pH of approximately 4, and the mining company is meeting resistance in having it classified officially as a bentonite (Gardam, 2008).

Although Churchman and colleagues (2002) performed their analyses with environmental barrier applications in mind, their findings indicated characteristics of interest in body formulation. A number of hypotheses arise regarding this clay, which may be classified as a non-swelling bentonite. The minimal swelling when immersed is predictive of lower wet to dry shrinkage,

which has favourable implications for minimising warpage during the drying process. Because of the fine particle size, Arumpo bentonite may contribute to plasticity more than a bentonite of a larger particle size. The low swelling and presumed low shrinkage may allow greater percentage additions than of other bentonites. Mixing may also be easier. The low permeability may result in a requirement for a longer aging period to allow for even penetration of water.

## Suspension

Water was added to each of the beakers containing saturated powder so that each was filled to 800 ml, at which point they were stirred (fig. 142).

























*Figure 142: Stirring of five clay suspensions*

The stirring rods were left in the liquids after stirring to provide an easy visual comparison of the amount of finer material remaining in suspension. The rate and extent of settling was photographed and recorded. The paragraph below describes the rate of settling observed for each, referring to the settling rates of relatively coarser and finer particles within each sample. The observations are made in the order of speed of settling, from fastest to slowest, which corresponds to samples from right to left (fig. 143).

It was observed that the fastest settling occurred with the ball clay, which had settled to the bottom of the beaker within 15 minutes. So little remained in suspension after three minutes that the stirring rod was visible within the liquid. The bulk of the Marulan tailings settled within three minutes, but it was 20

minutes before the stirring rod was visible through the suspension of finer particles. The bulk of the Bungendore tailings settled within 30 minutes, but it was three days before the stirring rod was visible through the suspension of finer particles. Most of the Arumpo bentonite had settled within two hours, but it was four days before the stirring rod was partly visible through the suspension of finer particles (fig. 143). Even after two weeks, the English bentonite remained in suspension, with only a slight amount of translucency in the top 50 ml of liquid indicating there had been minimal settling.

15 s			20 min
30 s			30 min
60 s			45 min
90 s			60 min
2 min			90 min
2.5 min			2 hr
3 min			2.5 hr
4 min			3 hr
5 min			4 hr
10 min			3 days
15 min			4 days

**Figure 143: Settling suspensions of (left to right) English bentonite, Arumpo bentonite, Bungendore tailings, Marulan tailings and Ball clay FX**

The findings of the experiment above suggest that for studio practice:

- English bentonite should be chosen over Arumpo bentonite if long-term glaze suspension is sought.
- Arumpo bentonite has more fine particles held in suspension than the ball clay or the two quarry tailings, so could be expected to contribute more to plasticity.
- Arumpo bentonite swells less than English bentonite, so could be expected to produce less shrinkage and warping if used as a plasticising additive in a clay body.
- English bentonite and ball clay FX, which both display extremes of settling behaviour, would be less suitable for making terra sigillata than would Arumpo bentonite, Bungendore tailings or Marulan tailings.
- Bungendore tailings have more fine particles held in suspension than Marulan tailings, so could be expected to contribute more to plasticity, and would be expected to shrink more during drying.
- Bungendore tailings have more fine particles held in suspension than Marulan tailings, and so could be expected to form a denser body with greater dry strength.

Some of the characteristics of Bungendore and Marulan tailings are explored in the next chapter.

## Chapter 10: Initial Treatment and Handling Experiments with Quarry Tailings

### Preparation

Initial experiments focused on determining how the sand mine and rock quarry tailings might be simply processed to form usable clay bodies, and how those bodies might perform when used alone and in combination. The tailings were in the form of dry lumps of various sizes (figs. 144 and 145).



*Figure 144: Bungendore quarry tailings as received*



*Figure 145: Marulan quarry tailings as received*

The Bungendore and Marulan quarry tailings were each slaked separately in tap water, stirred to a slurry with an electric drill attachment, sieved through 40- and 60-mesh sieves, and hung in cotton bags until they were of workable consistency. The sievings were retained. Sievings from Bungendore tailings (fig. 146, overleaf) contained predominantly pale-coloured grit and pebbles that had been worn so that no sharp edges were present.<sup>9</sup> Sievings from Marulan tailings (fig. 147, overleaf) contained predominantly dark grit and crushed rock with sharp edges. There was twice as much grit and gravel in the Marulan tailings (9% by weight) than there was in the Bungendore tailings (4.5% by weight).

---

<sup>9</sup> The red flecks are paint from the stirring rod.



*Figure 146: Sievings from Bungendore tailings*



*Figure 147: Sievings from Marulan tailings*

Once sufficient moisture was removed to leave the clay slurries in a workable plastic condition, the extent of this workability and plasticity was tested using standard studio techniques that would provide a broad indication of their comparative qualities and potential for further experimentation.

### **Extrusions**

A body consisting of 100% Marulan tailings passed through a 60-mesh sieve was kneaded and loaded into an extruder, and unbroken extrusions were successfully produced (fig. 148).



*Figure 148: Marulan extrusion*

A body consisting of 100% Bungendore tailings passed through a 60-mesh sieve was kneaded and loaded into an extruder, and unbroken extrusions were also successfully produced (fig. 149).



*Figure 149: Bungendore extrusion*

### **Bowls thrown with quarry tailings**

After sufficient moisture had been removed to yield clay of throwing consistency from the slurry that had been sieved through a 60-mesh sieve, small bowls were able to be thrown using 100% Marulan tailings (fig. 150). These bowls were also able to be inverted and have satisfactory foot-rings turned (fig. 151, overleaf).



*Figure 150: Bowl thrown from 100% Marulan tailings*





**Figure 151: Turned foot ring on bowl thrown from 100% Marulan tailings**

Bowls made from 100% Marulan tailings were successfully fired to 900°C (fig. 152).



**Figure 152: Bowl thrown from 100% Marulan tailings and fired to 900° C**

After removing a similar process of preparation, small bowls were able to be thrown and turned using 100% Bungendore tailings (figs. 153 & 154, overleaf).



**Figure 153: Bowl thrown from 100% Bungendore tailings**



**Figure 154: Bungendore bowl showing turned foot ring**

It was noted that a bowl made from Bungendore tailings took twice as long to dry to a leather-hard state as did a bowl made from Marulan tailings.

The two bodies were blended by wedging and kneading to create a body of equal parts Bungendore and Marulan tailings. This 50:50 body was easier to throw than either alone, and dried more quickly than the Bungendore tailings. Figure 155 shows a bowl thrown from equal parts Bungendore and Marulan tailings.



**Figure 155: Bowl of 50% Bungendore, 50% Marulan**

The bowls that had been thrown were fired in an electric kiln to a temperature of 800°C. All bowls retained their forms without cracking, obvious warping or other defects. When fired to 800°C, the clay bodies had a warm terracotta colour (figs. 156–158).



**Figure 156: Bowl thrown from Bungendore tailings fired to 800°C**



**Figure 157: Bowl of 50% Bungendore, 50% Marulan tailings fired to 800°C**



**Figure 158: Bowl of 50% Bungendore, 50% Marulan tailings fired to 800°C**

## **Chapter 11: Triaxial Blend Methodology**

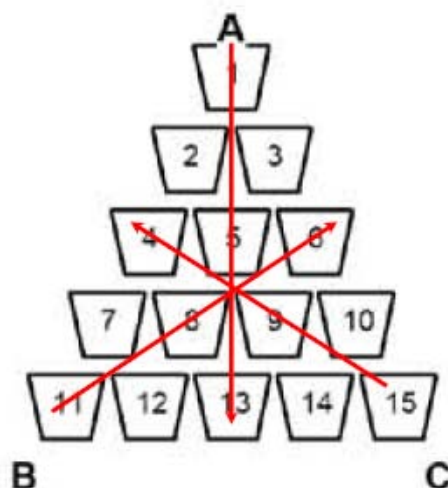
As it had been shown that it was possible to make a usable ceramic body from quarry tailings, the next step was to ascertain whether it was possible to create a low-fire body from these and other recovered materials. Initial experimentation involved blending the quarry tailings with other recovered materials and with proprietary materials expected to assist plasticity or reduce sintering temperature. The blending method adopted is described below.

### **Triaxial blend method**

The method chosen to perform blends was triaxial blending, which is commonly used to blend three ceramic glazes to assess their qualities when combined in different ratios.

In a triaxial blend, batches of equal weight and volume of each of three different glaze recipes are prepared. These three batches are placed at the three corners of a triangle. At these corners, designated A, B, and C, there is a 100% sample of the allocated recipe. The batches at each corner are also systematically mixed with each other in predetermined proportions, based on the number of rows in the triaxial. In a 15-sample triaxial blend, there are five rows of samples from each corner to the opposite side (fig. 159). From the 100% batch at each corner to the row at the opposite side, the proportions decrease in a stepwise fashion: 100%, 75%, 50%, 25%, 0%. The blend recipes are calculated from those proportions.

**Batch Corner Volumes      500 mls**



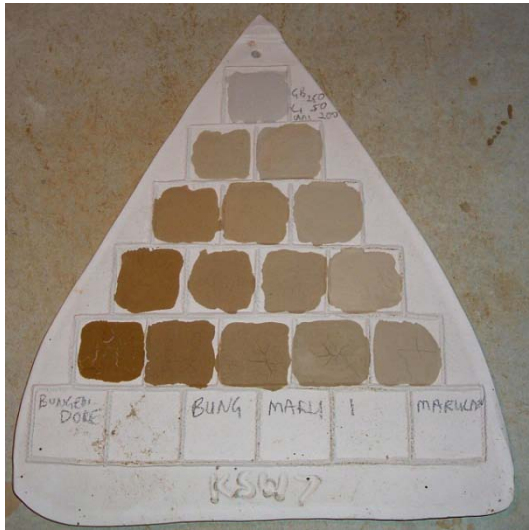
**Figure 159: Diagram of triaxial (15 samples)**  
Adapted from blend printout from Matrix software (Ewing, 2000)

Analysis and characterisation of collected materials did not occur before blending commenced, although in some cases the approximate analyses were available. Named materials with unknown percentage analyses were entered into the matrix glaze calculation program to allow entry of corner recipes for triaxial blends. The resultant worksheets provided the required quantities of the three recipes to be blended for each of the 15 samples to be produced. The required quantities of each corner recipe were mixed with water and sieved, then supplied in the correct proportion to numbered recycled containers (fig. 160), using either a 60-millilitre syringe or a Pyrex measuring cylinder.

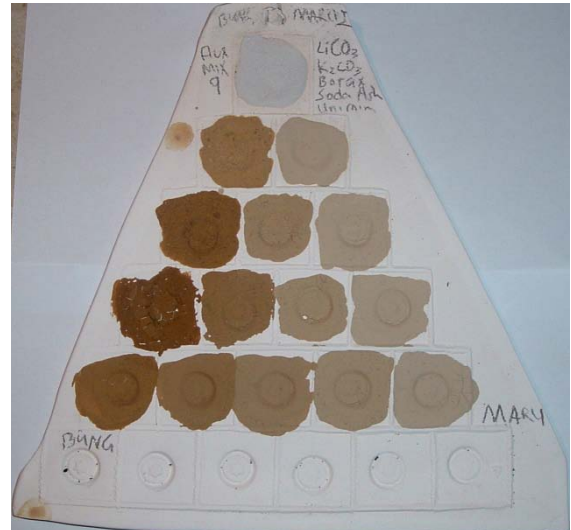


**Figure 160: Triaxial blend preparation (15 sample)**

The samples (Bungendore/Marulan 1, BM1, and Bungendore/Marulan 2, BM2) were mixed by hand, and a layer of each liquid sample was brushed onto the corresponding location on a bisqued triaxial slab (figs. 161 and 162).



**Figure 161: BM1 triaxial for glaze/engobe tests**



**Figure 162: BM2 triaxial for glaze/engobe tests**

The liquid samples were then spread on fibrolite to dry to a plastic state (fig. 163). They were subsequently bagged, labelled and aged for at least a week in preparation for forming.



**Figure 163: Triaxial sample slips drying before kneading and bagging**

## Method of forming body-test samples from triaxial blends

Equipment included a stainless steel laser-cut template, a stainless steel profile with protrusions spaced exactly 50 mm apart, a small hand extruder fitted with a 5 mm x 5 mm die, and a needle-stick tool (fig. 164). The template and profile were designed using Argon® 3D CAD software, and the files were sent to a professional laser-cutting service.



*Figure 164 (clockwise from top left): Template, 50 mm profile, extruder, needle cutter*

### Slab rolling and cutting

The samples were progressively unbagged and kneaded by hand to a uniform consistency. Using a wooden dowel hand-roller, approximately 100 g of each sample was rolled on fibrolite between wooden thickness guides with a thickness of 5 mm. The laser-cut template die was used as a pattern to cut tessellated tile shapes using the needle-stick tool (fig. 165).



*Figure 165: Slab-cutting process*



## Extrusion

The samples were extruded onto fibrolite and cut to lengths of approximately 6 cm (fig. 166). One or more lengths were bent and twisted to attempt to form a loop.



*Figure 166: Extrusion process*

## Marking wet samples for shrinkage calculations

The profile with 50-millimetre-spaced protrusions was used to imprint each slab 'fish' and extruded 'chip' with indentations 50 mm apart (fig. 167) to allow subsequent measurement for calculation of shrinkage.



*Figure 167: 50-millimetre marking process*

## **Observations and ratings used to describe qualities of samples**

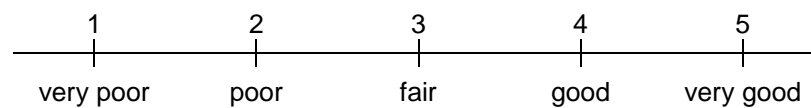
The forming methods used above allowed a number of qualitative observations of each sample, including:

- the amount of settling and separation of the mixed-liquid samples
- the time it took for the liquid samples to dry to kneadable consistency after

being spread on cement board

- whether the kneaded samples exhibited thixotropy, before and after bagging
- the ease with which each sample was rolled out into a slab
- whether the edges of the sample slab were torn by the needle-stick tool
- the ease with which the sample was extruded
- whether the length of sample extrusion tolerated being bent to a loop
- the quality of the extrusion.

Based on observations, extrusion quality was rated on a five-point Likert scale:



The extent to which efflorescence could be observed on the dried samples was also noted.

At this point, a clarification regarding this project's use of the term 'efflorescence' is required, as the term has been used to describe different phenomena.<sup>10</sup> In this project, efflorescence refers to the formation of a visible surface deposit on dried greenware, bisque or vitrified clay that is attributed to salt migration due to body formulation.

---

<sup>10</sup> Brownell (1949, p 375) states:

*The migration of a salt solution through a ceramic body is the direct cause of efflorescence. The salts accumulate on an exposed surface where relatively rapid evaporation takes place. At the points of greatest evaporation these salts are precipitated from solution when the saturation point is exceeded.*

Hansen (2006a) uses the term efflorescence to describe the dried and fired results of the salt migration observed during drying, whereas Brownell (1949) refers only to the effects visible after firing. Brownell bases his use of the term on the generally accepted definitions supplied by Jackson, who states these as:

*Scumming—The formation on the surface of a ceramic body of a deposit of foreign matter during the process of manufacture.*

*Efflorescence—The formation on the surface of a finished ceramic ware of a deposit of foreign matter due to exposure to weather. (Jackson, 1930, p 376)*

Brownell (1949) accepts Jackson's (1930) subsequent recommendation that scumming be used to describe a foreign deposit occurring as a result of kiln gases. He also distinguishes between the post-firing efflorescence that occurs as a result of salt migration where the body has absorbed salts from contact during pre-firing storage, and the post-firing efflorescence on which he concentrates, which is when the origin of the migrating salts is in the body formulation. In both cases, the efflorescence is exacerbated by weathering.

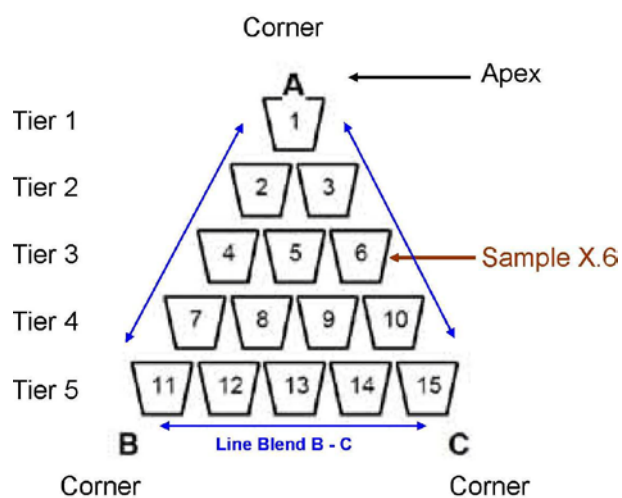
When the samples were dried, the distance between indentations made 50 mm apart after extrusion was measured using a ruler and loupe (fig. 168) to establish approximate shrinkage.



**Figure 168: Measuring dried shrinkage**

### Nomenclature for triaxial blends

When discussing the results of a triaxial blend, it is useful to attend to various patterns that have emerged, as well as individual samples that have resulted from the blending process. The results of triaxial blends are therefore discussed in a number of ways, and an explanation of the nomenclature used is necessary to assist the reader. To achieve this, a 15-sample triaxial blend diagram is overlaid with names for areas of the triaxial that are referred to when describing the results observed (fig. 169).



**Figure 169: Nomenclature for Triaxial 'X'**

Adapted from blend printout from Matrix software (Ewing, 2000)

An entire triaxial is referred to using an alphanumeric descriptor (for example, Triaxial X1). Individual samples are referred to with this descriptor followed by a dot and the numeral representing the sample position (for example, Sample X.6). The three recipes to be blended together are positioned at three corners of the triaxial diagram and referred to as corners A, B and C. Any line of five perimeter samples consisting of two corners and their intermediate blends is referred to as a line blend. These line blends, shown by blue arrows (fig. 169), are referred to using the letters assigned to the corners blended (for example, line blend B–C). Corner A is referred to as the apex of the triaxial. The apex is referred to as Tier 1, and perpendicular rows of samples that contain progressively less of corner A are referred to as Tiers 2–5. Rows that are perpendicular to corner B are referred to as B-tiers and rows that are perpendicular to corner C are referred to as C-tiers.

The following triaxial blends (Chapter 12) were intended to ascertain whether ceramic bodies, engobes or glazes could be produced from the raw materials obtained.

## Chapter 12: Three Triaxial Blends: Workability, drying and shrinkage of samples

When commencing the process of triaxial blending, it is not necessary to have an accurate characterisation of the materials being blended. Observations of workability, drying and shrinkage can be made without having recourse to a percentage analysis. Three triaxial blends were constructed in order to begin the process of making observations to address the proportions of materials that might be included in a low-fire body.

### Triaxial blend: Arumpo Cullet Cold House Fines Latite (ACCL)

A triaxial was constructed to investigate whether it was possible to make a ceramic paste, as a variation on pâte de verre, using predominantly perlite fines or glass cullet fines. Arumpo bentonite was used to provide some plasticity, and Dunmore latite dust was used to include some coarser particles. This triaxial was speculative in nature, as none of the materials had been analysed or utilised previously. The three corner recipes of the triaxial are shown in Table 12.

*Table 12: Triaxial ACCL: Corner recipes*

Triaxial ACCL	A	B	C
		(wt%)	
Arumpo bentonite	30	10	10
Unimin cullet	30		90
Perlite AP10 white	30	90	
Dunmore latite	10		

The sample recipes of triaxial blend ACCL appear in Table 13.

**Table 13: Triaxial ACCL: Blend recipes (wt%)**

Batch Corner Volumes		BLEND RECIPES				
500 mls		Bent	Unim	Perl	Dunm	
	1	30.00	30.00	30.00	10.00	
	2	25.00	22.50	45.00	7.50	
	3	25.00	45.00	22.50	7.50	
	4	20.00	15.00	60.00	5.00	
	5	20.00	37.50	37.50	5.00	
	6	20.00	60.00	15.00	5.00	
	7	15.00	7.50	75.00	2.50	
	8	15.00	30.00	52.50	2.50	
	9	15.00	52.50	30.00	2.50	
	10	15.00	75.00	7.50	2.50	
	11	10.00	----	90.00	----	
	12	10.00	22.50	67.50	----	
	13	10.00	45.00	45.00	----	
	14	10.00	67.50	22.50	----	
	15	10.00	90.00	----	----	

After the corner recipes had been mixed to slurry, apportioned to the sample pots and mixed within the pots, they were brushed onto a bisqued triaxial grid (fig. 170).



**Figure 170: Triaxial ACCL for glaze/engobe test**

The remainder were poured onto cement board to allow absorption of moisture until they were in a malleable condition. They were then bagged into labelled sample bags (fig. 171).



**Figure 171: ACCL Triaxial samples bagged**

After approximately a week, the samples were unbagged in preparation for a series of tests to establish their handling and workability characteristics. This process is documented overleaf.

## Triaxial ACCL: Handling and drying properties

When the triaxial ACCL samples were unbagged, many were no longer in a malleable condition, but had formed wet cakes that could be broken apart. They displayed various degrees of thixotropy when kneaded, with the most extreme thixotropy observed in sample ACCL 1 (figs. 172 and 173).




**Figure 172: ACCL 1 before kneading**





**Figure 173: ACCL 1 after kneading**


The following images (figs. 174–190) show extruded and template-cut samples from triaxial ACCL packed into re-used takeaway food containers ready for transporting. Beside each image is a description of the observed working properties of the body and the extent of efflorescence observed. On some extruded samples, the clay surface roughened into a regular pattern as the unbroken clay extrusion emerged from the extruder nozzle. The result was an intact extrusion with one or more sides formed into a rough surface reminiscent of the bark on the trunk of a palm tree. This feature, henceforth referred to as ‘barking’, increased in a stepwise fashion, moving away from Batch A tier by tier in the triaxial (ACCL 1), where barking was least evident (fig. 174).




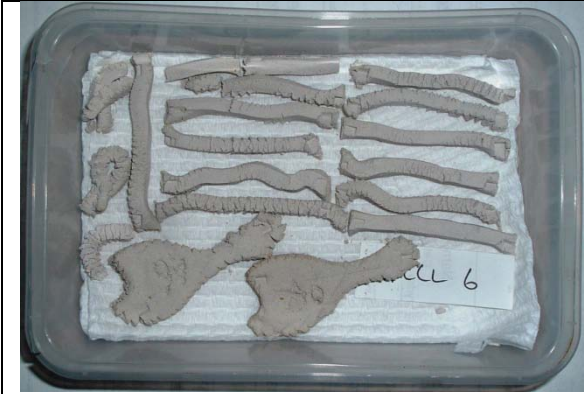
 <p><b>Figure 174: ACCL 1 extrusions and template-cut slabs</b></p>	<b>Extrusion rating</b>	<b>Handling properties (wet) and extent of efflorescence (dry)</b>
	2	Very thixotropic. Template-cut slabs tore at the edges, and at the narrow point, and the slab surface wrinkled. Poor extrusions with occasional barking on one edge, did not crack when twisted. No efflorescence.


 <p><b>Figure 175: ACCL 2 extrusions and template-cut slabs</b></p>	<b>Extrusion rating</b>	<b>Handling properties (wet) and extent of efflorescence (dry)</b>
	2	Marked thixotropy. Template-cut slabs tore at the edges, and the slab surface wrinkled. Poor extrusions with barking on one and sometimes two sides, did not crack when twisted. No efflorescence.


 <p><b>Figure 176: ACCL 3 extrusions and template-cut slabs</b></p>	<b>Extrusion rating</b>	<b>Handling properties (wet) and extent of efflorescence (dry)</b>
	3	Marked thixotropy. Template-cut slabs tore at the edges. Fair but slightly irregular extrusions with occasional barking on one side, did not crack when twisted. No efflorescence.


 <p><b>Figure 177: ACCL 4 extrusions and template-cut slabs</b></p>	<b>Extrusion rating</b>	<b>Handling properties (wet) and extent of efflorescence (dry)</b>
	2	Marked thixotropy. Template-cut slabs tore at the edges, and the slab surface wrinkled during template-cutting. Poor extrusions, with barking on all or most sides, cracked when twisted. No efflorescence.


 <p><b>Figure 178: ACCL 5 extrusions</b></p>	<b>Extrusion rating</b>	<b>Handling properties (wet) and extent of efflorescence (dry)</b>
	2	Marked thixotropy. Poor extrusions, with barking on all or most sides. One in two extrusions cracked when twisted. No efflorescence.


 <p><b>Figure 179: ACCL 6 extrusions and template-cut slabs</b></p>	<b>Extrusion rating</b>	<b>Handling properties (wet) and extent of efflorescence (dry)</b>
	2	Marked thixotropy. Template-cut slabs tore at the edges, and the slab surface wrinkled during template-cutting. Poor extrusions with barking on all or most sides, cracked when twisted. No efflorescence.


 <p><b>Figure 180: ACCL 7 extrusions and template-cut slabs</b></p>	<b>Extrusion rating</b>	<b>Handling properties (wet) and extent of efflorescence (dry).</b>
	1	Moderate thixotropy. Template-cut slabs tore at the edges, the slab distorted and the slab surface wrinkled. Set quickly in extruder barrel so very poor extrusions were produced with great difficulty. The extrusions had barking on all sides, broke easily and cracked when twisted. No efflorescence.


 <p><b>Figure 181: ACCL 8 extrusions and template-cut slabs</b></p>	<b>Extrusion rating</b>	<b>Handling properties (wet) and extent of efflorescence (dry).</b>
	2	Moderate thixotropy. Template-cut slabs tore and distorted at the edges, and the slab outline was poorly defined. Difficult to extrude, producing poor extrusions with barking on all sides, cracked when twisted. No efflorescence.


 <p><b>Figure 182: ACCL 9 extrusions and template-cut slabs</b></p>	<b>Extrusion rating</b>	<b>Handling properties (wet) and extent of efflorescence (dry).</b>
	2	Slight thixotropy. Template-cut slabs tore at the edges, the slab distorted and the slab surface wrinkled. Poor extrusions with barking on all sides, broke easily and cracked when twisted. No efflorescence.


 <p><b>Figure 183: ACCL 10 extrusions and template-cut slabs</b></p>	<b>Extrusion rating</b>	<b>Handling properties (wet) and extent of efflorescence (dry).</b>
	1	Very slight thixotropy. Template-cut slabs tore at the edges, and one broke at the narrow point. Very poor extrusions with barking on two or more sides, broke easily and cracked when twisted. No efflorescence.



 <p><b>Figure 184: ACCL 11</b></p>	<b>Extrusion rating</b>	<b>Handling properties (wet) and extent of efflorescence (dry).</b>
	0	Extreme thixotropy. Sticky. Adhered to roller so unsuitable for making wet slabs. No further ratings of handling properties or efflorescence.

 <p><i>Figure 185: ACCL 11 hand rolled samples</i></p>	<b>Extrusion rating</b>	<b>Handling properties (wet) and extent of efflorescence (dry).</b>
	0	Marked thixotropy. Set quickly in extruder barrel and was strongly resistant to pressure—then fired out pellets instead of connected extrusions. No slab because body grabbed on to roller in chunks. Samples produced by rolling between the fingers. No efflorescence.

 <p><i>Figure 186: ACCL 12 hand rolled samples, extrusions and template-cut slab</i></p>	<b>Extrusion rating</b>	<b>Handling properties (wet) and extent of efflorescence (dry).</b>
	1	Marked thixotropy. Set quickly in extruder barrel so very poor extrusions with pronounced barking on all sides were produced with great difficulty. Some samples produced by rolling between the fingers. Template-cut slabs lost all definition. No efflorescence.

 <p><i>Figure 187: ACCL 13 hand rolled samples, extrusions and template-cut slabs</i></p>	<b>Extrusion rating</b>	<b>Handling properties (wet) and extent of efflorescence (dry).</b>
	1	Moderate thixotropy. Set quickly in extruder barrel so very poor extrusions with barking on all sides were produced with great difficulty. Some samples produced by rolling between the fingers. Template-cut slabs lost definition. No efflorescence.

 <p><b>Figure 188: ACCL 14 hand rolled samples, extrusions and template-cut slabs</b></p>	<b>Extrusion rating</b>	<b>Handling properties (wet) and extent of efflorescence (dry).</b>
	2	Slight thixotropy. Set quickly in extruder barrel so poor extrusions were produced with difficulty. They cracked when twisted. Some samples produced by rolling between the fingers. Template-cut slabs lost definition. No efflorescence.

 <p><b>Figure 189: ACCL 15 before Tylose addition</b></p>  <p><b>Figure 190: ACCL 15 hand-formed samples, extrusions and slab</b></p>	<b>Extrusion rating</b>	<b>Handling properties (wet) and extent of efflorescence (dry).</b>
	3	Not thixotropic. Crumbled when kneading attempted. Had to be pressed to form slab and bars. Addition of 5% by weight 2% Tylose MHB3000 Binder solution allowed kneading and extrusion. Fair extrusions were then produced. Some extrusions had barking on one side. They cracked when twisted. Unable to retain slab shape during template-cutting. No efflorescence.

Triaxial ACCL: Wet to dry shrinkage

The distance between the points marked 50 mm apart on each wet sample was re-measured when the samples were dry. The average measurement (dry) of each sample body on the triaxial blend appears in Table 14, overleaf.

**Table 14: Triaxial ACCL: Dry length at 50 mm wet**

---

**Arumpo cullet cold bag house fines latite (ACCL)**

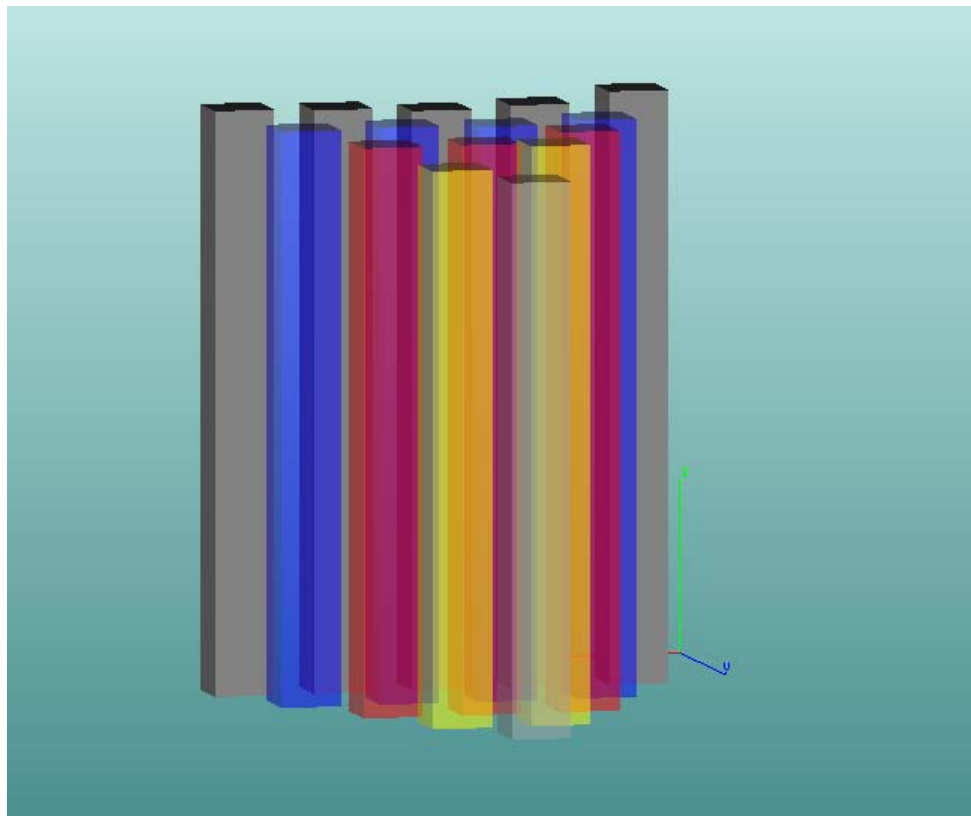
Averaged length of dried samples (mm)

---

1	2	3	4	5	6	7	8	9	10	11	12	13	14	15
49.5	49.0	48.5	48.0	47.5	47.0	46.5	46.0	45.5	45.0	44.5	44.0	43.5	43.0	48.4

---

The averaged dry lengths were entered into a 3D design program to provide an illustration of the extent to which each blend sample had shrunk relative to the others in the blend set. Sample 1 appears at the apex in the foreground of Figure 191.



**Figure 191: Triaxial ACCL: Extrusion length after drying from 50mm**

The average shrinkage of each sample is recorded in Table 15, with samples with the lowest and highest shrinkage printed in red text.

**Table 15: Triaxial ACCL: Wet to dry shrinkage**

---

**ACCL**

Wet to dry shrinkage (%)

---

Sample	1	2	3	4	5	6	7	8	9	10	11	12	13	14	15	15 with Tylose
<b>% shrink</b>	8.0	4.3	7.7	4.1	5.8	5.8	4.3	5.1	4.5	4.9	1.9	3.8	4.1	3.6	3.3	5.5

---

The maximum wet to dry shrinkage observed in blend ACCL was 8% in sample 1, which contained 30% bentonite. The least shrinkage observed was 1.9% in sample 11, which contained 10% bentonite and 90% perlite. The addition of

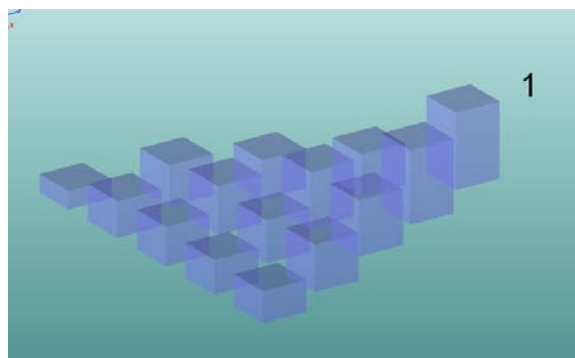
liquid Tylose binder to sample 15 increased shrinkage of the sample by approximately 2%.

As this linear table obscures blend patterns in the data, the data was also arranged in the triaxial format in Table 16.

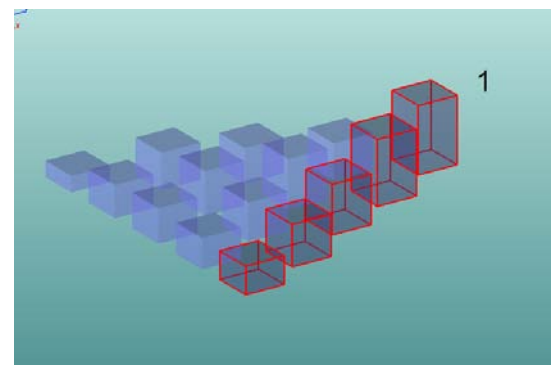
**Table 16: Triaxial ACCL: Wet to dry percentage shrinkage**

<b>ACCL</b>																
Wet to dry shrinkage (%)																
											1					
											8.0					
					2						3					
					4.3						7.7					
				4					5					6		
				4.1					5.8					5.8		
			7				8				9				10	
			4.3				5.1				4.5				4.9	
11			12			13			14			15			(Tylose) (5.5)	
1.9			3.8			4.1			3.6			3.3				

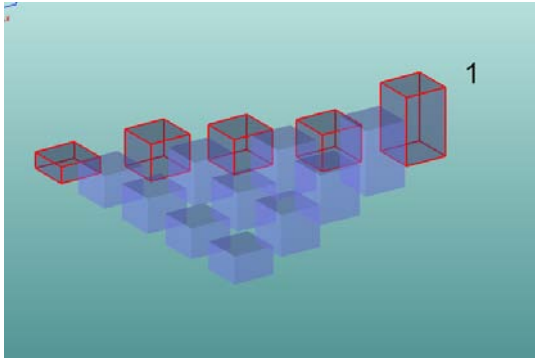
A 3D portrayal of the results appears in Figures 192–195. The numeral 1 identifies the apex of the 15-sample triaxial blend. The samples representing line blends between the apexes of the triaxial are framed.



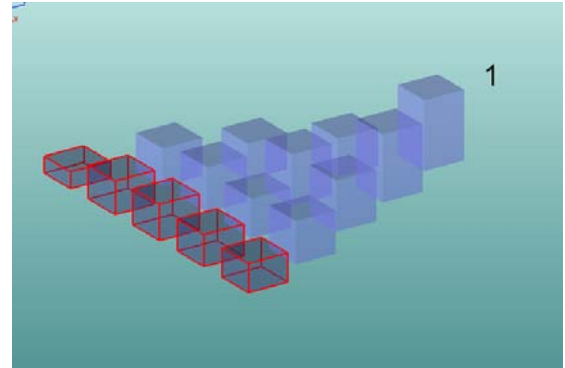
**Figure 192: Triaxial ACCL: Wet to dry shrinkage (%), trimetric view**



**Figure 193: Triaxial ACCL: Wet to dry shrinkage (%), trimetric view, framing samples 1–3–6–10–15**



**Figure 194. Triaxial ACCL.  
Wet to dry percentage shrinkage,  
Trimetric view. Framing samples 1-2-4-7-11**



**Figure 195. Triaxial ACCL.  
Wet to dry percentage shrinkage,  
Trimetric view. Framing samples 11-15**

Wet to dry shrinkage is greatest at ACCL sample 1, which has the most Arumpo bentonite (30%). Shrinkage decreases along both the 1–3–6–10–15 line blend and along the 1–2–4–7–11 line blend, as bentonite content is reduced to 10%. When bentonite is held constant at 10%, more shrinkage occurs when the bentonite is mixed with both cullet and perlite fines than with either alone. The convex curve along the 11–15 line (fig. 195) shows more shrinkage as the remaining mix of cullet and perlite fines approaches equal proportions. The sample with 90% perlite shrank least (1.9%) followed by the sample with 90% cullet (3.3%).

The implications of these results for studio use are considered later, following firing of the samples.



## Triaxial flux mix 1/Bungendore/Marulan (BM1)

Triaxial BM1 was constructed to investigate the properties of Bungendore tailings, Marulan tailings, and a flux mix adapted from previous low-fire glaze tests (Smout, 2008). This flux mix formed glossy glazes below 900°C, so it was reasonable to expect it to lower the sintering temperature of the tailings. In order to include some recycled material in the flux mix, Unimin cullet was used to replace Ferro frit 4064, so the flux mix used for BM1 became:

- Gerstley borate 50
- Lithium carbonate 10
- Unimin cullet 40

The corner recipes of triaxial BM1 appear in Table 17.

*Table 17: Triaxial BM1: Batch corner recipes*

Recipe A	(wt%)	Recipe B	(wt%)	Recipe C	(wt%)
Gerstley borate	50	Bungendore tailings	100	Marulan tailings	100
Lithium carbonate	10				
Unimin cullet 375	40				

The blend diagram and sample recipes of triaxial BM1 appear in Table 18, overleaf.

**Table 18: Triaxial BM1: Blend recipes (wt%)**

Batch Corner Volumes		BLEND RECIPES					
500 mls		Gers	Lith	Unim	Bung	Maru	
		1	50.00	10.00	40.00	----	----
		2	37.50	7.50	30.00	25.00	----
		3	37.50	7.50	30.00	----	25.00
		4	25.00	5.00	20.00	50.00	----
		5	25.00	5.00	20.00	25.00	25.00
		6	25.00	5.00	20.00	----	50.00
		7	12.50	2.50	10.00	75.00	----
		8	12.50	2.50	10.00	50.00	25.00
		9	12.50	2.50	10.00	25.00	50.00
		10	12.50	2.50	10.00	----	75.00
		11	----	----	----	100.00	----
		12	----	----	----	75.00	25.00
		13	----	----	----	50.00	50.00
		14	----	----	----	25.00	75.00
		15	----	----	----	----	100.00


Triaxial BM1: Handling and drying properties


Sample BM1.1 was not tested for handling and drying properties because it contained only flux materials. The handling properties of the 14 blended bodies varied considerably, and a pattern emerged with respect to thixotropy. Thixotropy decreased in a stepwise fashion, moving down the triaxial tier by tier from the apex at samples BM1.2 and BM1.3. Tier 5 (BM1.11 to BM1.15) exhibited no thixotropy.


Some extruded samples were lumpy or had roughened surfaces.


Efflorescence was observed on some samples as they dried.


The images (figs. 196–209) on the following pages show extruded and template-cut samples from triaxial BM1 packed into re-used takeaway food containers ready for transporting. Beside each image is a description of the observed working properties of the body and the extent of efflorescence observed.


	<b>Extrusion rating</b>	<b>Handling properties (wet) and extent of efflorescence (dry)</b>
<p><b>Figure 196: BM1.2 extrusions and template-cut slabs</b></p>	<p>5</p>	<p>Moderate thixotropy. Slabs were template-cut without tearing. Very good extrusions, cracked when twisted. Efflorescence on edges of slabs and isolated specks of efflorescence on ends of some extrusions.</p>


	<b>Extrusion rating</b>	<b>Handling properties (wet) and extent of efflorescence (dry)</b>
<p><b>Figure 197: BM1.3 extrusions and template-cut slabs</b></p>	<p>4</p>	<p>Moderate thixotropy. Slabs were template-cut without tearing. Good extrusions cracked when twisted. Efflorescence on edges of slabs and faces of all extrusions.</p>


	<b>Extrusion rating</b>	<b>Handling properties (wet) and extent of efflorescence (dry)</b>
<p><b>Figure 198: BM1.4 extrusions</b></p>	<p>3</p>	<p>Moderate thixotropy. Fair extrusions were lumpy because of preparation rather than because of the combination of ingredients. Extrusions cracked when twisted. Minimal efflorescence on edges of some samples.</p>


	<b>Extrusion rating</b>	<b>Handling properties (wet) and extent of efflorescence (dry)</b>
<p><b>Figure 199: BM1.5 extrusions and template-cut slabs</b></p>	<p>5</p>	<p>Moderate thixotropy. Slabs were template-cut without tearing. Very good extrusions did not crack when twisted. Sparse efflorescence on edges of all samples.</p>


	<b>Extrusion rating</b>	<b>Handling properties (wet) and extent of efflorescence (dry)</b>
<p><b>Figure 200: BM1.6 extrusions and template-cut slabs</b></p>	<p>4</p>	<p>Moderate thixotropy. Slabs were template-cut without tearing. Good extrusions cracked when twisted. Efflorescence on edges of slabs and isolated specks of efflorescence on ends of some extrusions.</p>


	<b>Extrusion rating</b>	<b>Handling properties (wet) and extent of efflorescence (dry)</b>
<p><b>Figure 201: BM1.7 extrusions and template-cut slabs</b></p>	<p>4</p>	<p>Moderate thixotropy. Slabs were template-cut without tearing. Very good extrusions did not crack when twisted. No dark efflorescence, but unexplained white streaks and speckles on all samples.</p>


	<b>Extrusion rating</b>	<b>Handling properties (wet) and extent of efflorescence (dry)</b>
<p><b>Figure 202: BM1.8 extrusions and template-cut slab</b></p>	<p>3</p>	<p>Moderate thixotropy. Fair extrusions were lumpy because of preparation rather than because of the combination of ingredients. Extrusions cracked when twisted. Minimal efflorescence, but isolated white specks.</p>


	<b>Extrusion rating</b>	<b>Handling properties (wet) and extent of efflorescence (dry)</b>
<p><b>Figure 203: BM1.9 extrusions and template-cut slabs</b></p>	<p>4</p>	<p>Moderate thixotropy. Slabs were template-cut without tearing. Good extrusions cracked when twisted. Efflorescence on parts of slab faces and ends, and edges of most extrusions, and white specks and blotches.</p>


	<b>Extrusion rating</b>	<b>Handling properties (wet) and extent of efflorescence (dry)</b>
<p><b>Figure 204: BM1.10 extrusions and template-cut slabs</b></p>	<p>4</p>	<p>Moderate thixotropy. Slabs were template-cut without tearing. Good extrusions cracked when twisted. Efflorescence on parts of slab faces and ends and edges of most extrusions. Obvious fingerprint efflorescence on extrusion at the bottom.</p>

	<b>Extrusion rating</b>	<b>Handling properties (wet) and extent of efflorescence (dry)</b>
<p><b>Figure 205: BM1.11 extrusions and template-cut slabs</b></p>	<p>5</p>	<p>No thixotropy. Slabs were template-cut without tearing. Very good extrusions cracked when twisted. No efflorescence, but white marks on extrusions and edges of template-cut slabs.</p>

 <p data-bbox="308 595 863 642"><b>Figure 206: BM1.12 extrusions and template-cut slab</b></p>	<p data-bbox="879 203 1034 300"><b>Extrusion rating</b></p>	<p data-bbox="1038 203 1442 300"><b>Handling properties (wet) and extent of efflorescence (dry)</b></p>
	<p data-bbox="879 300 1034 642">5</p>	<p data-bbox="1038 300 1442 642">No thixotropy. Slabs were template-cut without tearing. Very good extrusions. No cracking when twisted. No efflorescence.</p>

 <p data-bbox="308 1093 863 1149"><b>Figure 207: BM1.13 extrusions and template-cut slabs</b></p>	<p data-bbox="879 701 1034 797"><b>Extrusion rating</b></p>	<p data-bbox="1038 701 1442 797"><b>Handling properties (wet) and extent of efflorescence (dry)</b></p>
	<p data-bbox="879 797 1034 1149">5</p>	<p data-bbox="1038 797 1442 1149">No thixotropy. Slabs were template-cut without tearing. Very good extrusions. No cracking when twisted. No efflorescence.</p>

 <p data-bbox="308 1599 863 1641"><b>Figure 208: BM1.14 extrusions and template-cut slabs</b></p>	<p data-bbox="879 1207 1034 1303"><b>Extrusion rating</b></p>	<p data-bbox="1038 1207 1442 1303"><b>Handling properties (wet) and extent of efflorescence (dry)</b></p>
	<p data-bbox="879 1303 1034 1641">5</p>	<p data-bbox="1038 1303 1442 1641">No thixotropy. Slabs were template-cut without tearing. Very good extrusions. No cracking when twisted. No efflorescence.</p>

	<b>Extrusion rating</b>	<b>Handling properties (wet) and extent of efflorescence (dry)</b>
<b>Figure 209: BM1.15 extrusions and template-cut slabs</b>	<p style="text-align: center;">5</p>	<p>No thixotropy. Slabs were template-cut without tearing. Very good extrusions. No cracking when twisted. No efflorescence.</p>

Triaxial BM1: Wet to dry shrinkage

Shrinkage was not measured for sample 1 (flux mix). The greatest wet to dry shrinkage occurred in sample BM.11 (Bungendore tailings), which contracted by 12.4%. The least shrinkage, of 4.3%, occurred in sample BM1.3 (flux mix 75%, Marulan tailings 25%). The next least shrinkage, of 5.8%, occurred in sample BM1.15 (Marulan tailings). The data is arranged in linear format in Table 19. The samples with least and most shrinkage are displayed in red typeface.

**Table 19: Triaxial BM1: Wet to dry shrinkage**

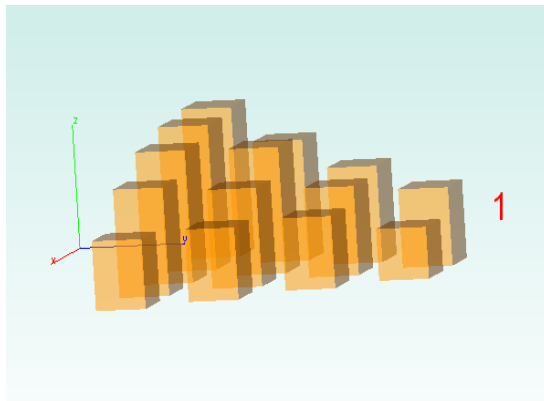
Triaxial BM1: wet to dry shrinkage (%)														
No	2	3	4	5	6	7	8	9	10	11	12	13	14	15
	6.5	4.3	8.0	7.4	6.0	10.0	10.5	8.2	6.0	12.4	12.0	11.0	9.0	5.8

The same data is arranged in triaxial format in Table 20 (overleaf). It can be seen that shrinkage increases along the A–B line blend, and decreases along the B–C line blend.

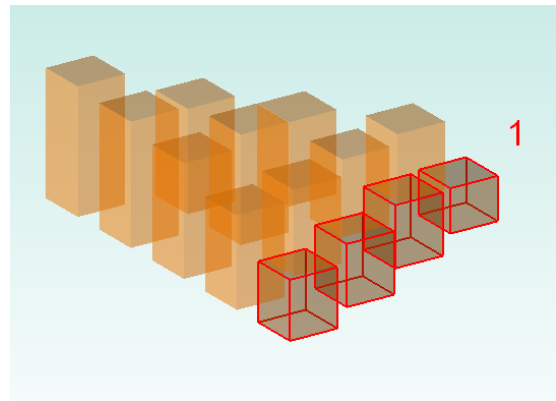
**Table 20: Triaxial BM1: Wet to dry shrinkage**

Triaxial BM1: wet to dry shrinkage (%)														
A														
1														
-														
2                                  3														
6.5                                  4.3														
4                                  5                                  6														
8                                  7.4                                  6														
7                                  8                                  9                                  10														
10                                  10.5                                  8.2                                  6														
11                                  12                                  13                                  14                                  15														
B   12.4                                  12                                  11                                  9                                  5.8   C														

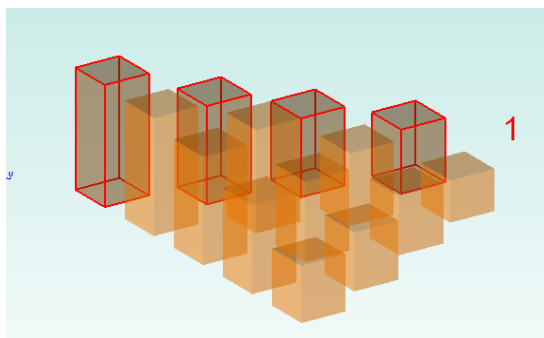
The impact on shrinkage of the proportion of corner recipes was most evident when the shrinkage data was input into a 3D graphical representation using Argon® 3D CAD software. The percentage shrinkage that occurred is shown in Figures 210–213. Corner A of the triaxial is shown by the position of the numeral 1.



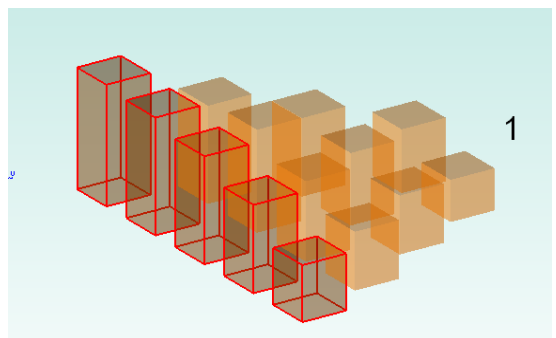
**Figure 210: Triaxial BM1: Wet to dry shrinkage (%), dynamic view**



**Figure 211: Triaxial BM1: Wet to dry shrinkage (%), trimetric view (framing samples 1–3–6–10–15)**



**Figure 212: Triaxial BM1: Wet to dry shrinkage (%), trimetric view (framing samples 1–2–4–7–11)**



**Figure 213: Triaxial BM1: Wet to dry shrinkage (%), trimetric view (framing samples 11–15)**



The relatively high shrinkage of BM.11 (Bungendore tailings) was decreased by partial substitution with inclusions of both other corner recipes (fig. 210).

The inclusion of 75% corner A (BM1.1) flux mix with corner C (BM1.15) Marulan tailings increased shrinkage, but inclusions of 50% or less had no effect (fig. 211).

The inclusion of 25% or more of flux mix from corner A (BM1.1) flux mix reduced shrinkage of corner B (BM1.11) Bungendore tailings, with samples showing a linear decrease with increasing proportions of flux mix (fig. 212).

The inclusion of 25% or more of flux mix from corner C (BM1.15) Marulan tailings reduced shrinkage of corner B (BM1.11) Bungendore tailings, with samples showing a curvilinear trend of shrinkage reduction, with relatively greater impact on shrinkage from increasing proportions of Marulan tailings (fig. 213).

At this stage, the general implications for studio use from triaxial BM1 are that:

- thixotropy and efflorescence result from the flux additions
- bodies without flux additions have better handling properties
- blends of Bungendore and Marulan tailings have lower wet to dry shrinkage when the proportion of Marulan tailings is increased.

### **Triaxial flux mix 2/Bungendore/Marulan (BM2)**

The same blending processes were used in triaxial BM2. The flux mix at corner A was varied but 100% Bungendore tailings was retained at corner B and 100% Marulan tailings was retained at corner C.

Triaxial BM2 was therefore identical to BM1 except that a different flux mix was used. This mix was also adapted a flux mix that had been successfully used for low-fire glaze tests (Smout, 2008). Recycled cullet was used to replace Ferro frit 4194, so the flux mix for BM2 was as shown in recipe A (Table 21, overleaf).

**Table 21: Triaxial BM2: Corner recipes**

Recipe A	(wt%)	Recipe B	(wt%)	Recipe C	(wt%)
Lithium carbonate	10	Bungendore tailings	100	Marulan tailings	100
Pearl ash	25				
Borax	10				
Soda ash	35				
Unimin cullet 375	20				

As samples BM2.11–BM2.15 were of the same formulation as BM1.11–BM 1.15, they were not prepared, and neither was sample BM2.1 (flux mix). As a result, there were nine additional bodies prepared for testing. Percentage by weight of materials in samples BM2.2–BM2.10 is shown in Table 22.

**Table 22: Triaxial BM2: Sample recipes (wt%)**

	Lith	Pear	Bora	Soda	Unim	Bung	Maru
2	7.50	18.75	7.50	26.25	15.00	25.00	-----
3	7.50	18.75	7.50	26.25	15.00	-----	25.00
4	5.00	12.50	5.00	17.50	10.00	50.00	-----
5	5.00	12.50	5.00	17.50	10.00	25.00	25.00
6	5.00	12.50	5.00	17.50	10.00	-----	50.00
7	2.50	6.25	2.50	8.75	5.00	75.00	-----
8	2.50	6.25	2.50	8.75	5.00	50.00	25.00
9	2.50	6.25	2.50	8.75	5.00	25.00	50.00
10	2.50	6.25	2.50	8.75	5.00	-----	75.00

The processes used to prepare plastic samples of the previous triaxial were repeated, and again the samples were bagged and labelled in preparation for tests of handling properties and workability. The results are documented on the following pages.

## Triaxial BM2: Handling and drying properties

BM2.2 was deliquescent. A week after being poured onto fibrolite, it was still wet, so it was dried in a microwave. A day later, it was wet again, exuding an oily liquid (fig. 214), which was evident in greater quantity after three days (fig. 215).



*Figure 214: BM2.2 one day after microwaving to remove moisture*

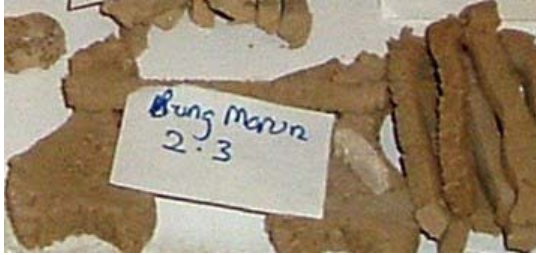



*Figure 215: BM2.2 three days after microwaving, showing liquid run-off*


Sample BM2.2 eventually dried after a month, but was excluded from further investigation.


The handling properties of the remaining eight bodies varied considerably. Thixotropy was present in all samples. This was less so in Tier 4 samples BM2.7–BM2.10 than in Tier 3 samples BM2.4 - BM2.6, or in BM2.3, where thixotropy was most pronounced. Some extruded samples were lumpy or had roughened surfaces. Extrusion quality was again rated on a five-point Likert scale; efflorescence was observed on all samples as they dried.


Figures 216–223 (overleaf) show extruded and template-cut samples from triaxial BM2. Beside each image is a description of the observed working properties of the body and the extent of efflorescence observed.


	Extrusion rating	Handling properties (wet) and extent of efflorescence (dry)
 <p data-bbox="316 510 858 553"><b>Figure 216: BM2.3 extrusions and template-cut slabs</b></p>	3	Pronounced thixotropy. The surface stuck to the fibrolite bench. Indentations lost definition. Felt oily on the hands. Slabs were template-cut with slight edge tearing. Fair extrusions cracked when twisted. White and brown efflorescence on all slabs and extrusions.


	Extrusion rating	Handling properties (wet) and extent of efflorescence (dry)
 <p data-bbox="316 992 858 1037"><b>Figure 217: BM2.4 extrusions and template-cut slabs</b></p>	3	Moderate thixotropy. Felt oily on the hands. Slabs were template-cut without tearing, but cracked at narrow point during template-cutting process. Fair extrusions lost sectional regularity due to thixotropy and cracked when twisted. White and brown efflorescence on all slabs and extrusions.


	Extrusion rating	Handling properties (wet) and extent of efflorescence (dry)
 <p data-bbox="316 1473 858 1516"><b>Figure 218: BM2.5 extrusions and template-cut slabs</b></p>	4	Moderate thixotropy. Felt oily. Slabs were template-cut without tearing. Good extrusions surged from barrel rather than extruding evenly, and some cracked when twisted. White and brown efflorescence on all slabs and extrusions.

	Extrusion rating	Handling properties (wet) and extent of efflorescence (dry)
 <p data-bbox="316 1957 858 2000"><b>Figure 219: BM2.6 extrusions and template-cut slabs</b></p>	4	Moderate thixotropy. Felt oily. Slabs were template-cut with slight edge tearing, and one cracked at narrow point during the template-cutting process. Good extrusions, some of which cracked when twisted. White efflorescence on all slabs and extrusions.

 <p><b>Figure 220: BM2.7 extrusions and template-cut slabs</b></p>	<b>Extrusion rating</b>	<b>Handling properties (wet) and extent of efflorescence (dry)</b>
	4	Minimal thixotropy. Felt slippery. Slabs were template-cut without tearing. Good extrusions cracked when twisted. White and brown efflorescence on all slabs and extrusions.

 <p><b>Figure 221: BM2.8 extrusions and template-cut slabs</b></p>	<b>Extrusion rating</b>	<b>Handling properties (wet) and extent of efflorescence (dry)</b>
	4	Minimal thixotropy. Felt slippery. Slabs were template-cut without tearing. Good extrusions cracked when twisted. White and brown efflorescence on all slabs and extrusions.

 <p><b>Figure 222: BM 2.9 extrusions and template-cut slabs</b></p>	<b>Extrusion rating</b>	<b>Handling properties (wet) and extent of efflorescence (dry)</b>
	4	Minimal thixotropy. Felt slippery. Slabs were template-cut without tearing. Good extrusions cracked when twisted. Brown efflorescence on slabs.

 <p><b>Figure 223: BM2.10 extrusions and template-cut slabs</b></p>	<b>Extrusion rating</b>	<b>Handling properties (wet) and extent of efflorescence (dry)</b>
	4	Minimal thixotropy. Slabs were template-cut without tearing. Good extrusions cracked when twisted. Specks of brown efflorescence on extrusions and edges of slabs.

In summary, with the exception of BM2.2, which was deliquescent, all samples were able to be used to produce slabs and extrusions, but almost all extrusions cracked when twisted. The forming processes were easier for samples BM7–BM10, which contained less flux. The bodies closer to BM2.2, which exuded an oily liquid, felt oily when handled, whereas bodies with less flux (samples B2.7–B2.10) felt slippery when handled. The amount of efflorescence decreased as the proportion of flux decreased.

Triaxial BM2: Wet to dry shrinkage

Shrinkage was not measured for sample BM2.1 (flux mix), or BM2.2, which was deliquescent. The data, including previously obtained shrinkage for BM1.11–BM1.15, are arranged in linear format in Table 23, where the samples with least and most shrinkage are displayed in red typeface.

The least wet to dry shrinkage occurred in sample BM2.6, which contracted by 3.9%. The most shrinkage, at 14.6%, occurred in sample BM2.7.

**Table 23: Triaxial BM2: Wet to dry shrinkage**

---

**Triaxial BM2: wet to dry shrinkage (%)**

---

<b>3</b>	<b>4</b>	<b>5</b>	<b>6</b>	<b>7</b>	<b>8</b>	<b>9</b>	<b>10</b>	<b>11</b>	<b>12</b>	<b>13</b>	<b>14</b>	<b>15</b>
5.3	10.6	9.9	3.9	14.6	11.5	8.5	6.7	12.4	12.0	11.0	9.0	5.8

---

The same data is arranged in triaxial format in Table 24. It is evident that, as with triaxial BM1, shrinkage increases along the A–B line blend, and decreases along the B–C line blend.

**Table 24: Triaxial BM2: Wet to dry shrinkage**

**Triaxial BM2: wet to dry shrinkage (%)**

The diagram shows a triangular arrangement of samples 1 through 15. Point A is at the top, point B is at the bottom left, and point C is at the bottom right. The samples are numbered 1 to 15, with their corresponding shrinkage percentages in yellow boxes. Sample 1 is at the top (A) with 0% shrinkage. Samples 2 and 3 are below it. Samples 4, 5, and 6 form the next row. Samples 7, 8, 9, and 10 form the next row. Samples 11, 12, 13, 14, and 15 form the bottom row (B-C). The shrinkage values are: 1: 0, 2: 0, 3: 5.3, 4: 10.6, 5: 9.9, 6: 3.9, 7: 14.6, 8: 11.5, 9: 8.5, 10: 6.7, 11: 12.4, 12: 12, 13: 11, 14: 9, 15: 5.8.

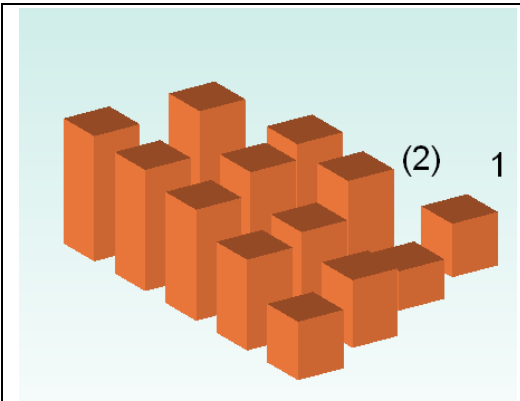
The impact on shrinkage of the proportion of corner recipes was again most evident when the shrinkage data was input into a 3D graphical representation. The percentage shrinkage that occurred is shown in Figures 223–227 (overleaf). Corner A of the triaxial is shown by the position of the numeral 1, and missing sample BM2.2 is represented by bracketed numeral (2).

The relatively high shrinkage of BM2.11 (Bungendore tailings) was decreased by partial substitution with inclusions of both other corner recipes (fig. 224).

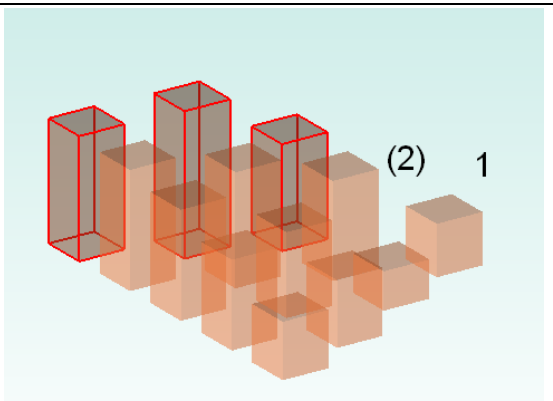
The blending of corner A (BM2.1) flux mix with corner B (BM2.11) Bungendore tailings produced no clear trend as shrinkage was curvilinear (fig. 225).

The blending of corner A (BM2.1) flux mix with corner C (BM2.15) Marulan tailings produced no clear trend as shrinkage was curvilinear (fig. 226).

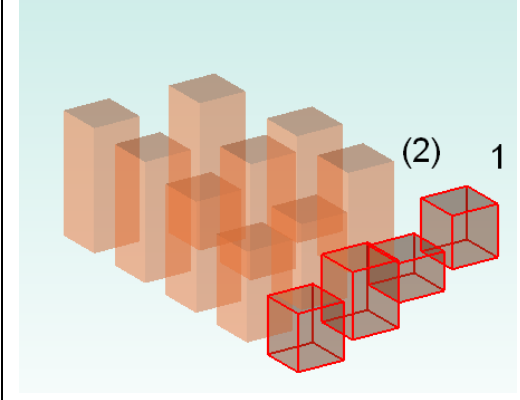
The inclusion of 25% or more of flux mix from corner C (BM1.15) Marulan tailings reduced shrinkage of corner B (BM1.11) Bungendore tailings, with samples showing a curvilinear trend of shrinkage reduction, with relatively greater impact on shrinkage from increasing proportions of Marulan tailings (fig. 227). A more linear trend of increasing shrinkage was observed in Tier 4 samples BM2.7–BM2.10 (fig. 228).



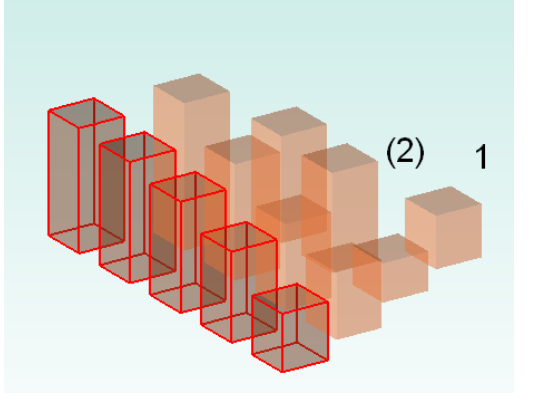
**Figure 224: Triaxial BM2: Wet to dry shrinkage (%), trimetric view**



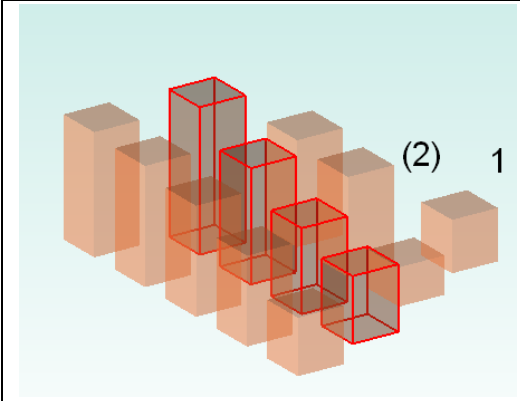
**Figure 225: Triaxial BM2: Wet to dry shrinkage (%), trimetric view, framing samples 4-7-11**



**Figure 226: Triaxial BM2: Wet to dry shrinkage (%), trimetric view, framing samples 3-6-10-15**



**Figure 227: Triaxial BM2: Wet to dry shrinkage (%), trimetric view, framing samples 11-15**



**Figure 228: Triaxial BM2: Wet to dry shrinkage (%), trimetric view, framing samples 7-10**

Now that samples of triaxials ACCL, BM1 and BM2 were dry, it was time to establish how these experimental bodies responded to low-temperature firing. The firing procedures and preliminary results appear in the following chapter.



## Chapter 13: Three Triaxial Blends: Fired shrinkage and appearance after firing to 800°C

All samples from the three triaxial blends documented in Chapter 12 were fired to 800°C to ascertain how they would respond to firing at this temperature.

### Firing procedures

A Tetlow single-phase 15-amp model K4A electric kiln controlled by a Harco electronic timer was used to fire the samples. Unless otherwise specified, all firings documented later herein utilise this equipment. The firing cycle was as follows: a ramp of 60°C per hour from ambient to 300°C, a ramp of 100°C per hour to final temperature, a soak for one hour at top temperature and uncontrolled cooling to opening at 100°C. This schedule is referred to henceforth as the *standard firing schedule*. The controlled ascent in temperature for a firing to 800°C is shown in Figure 229.

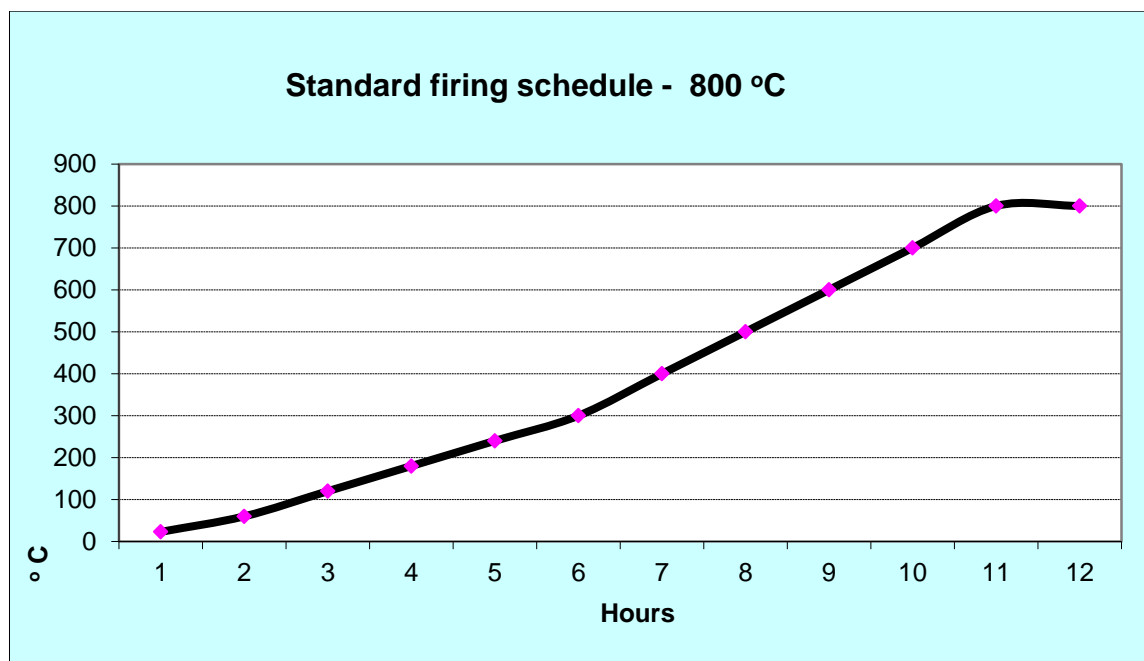


Figure 229: Standard firing schedule

Unmarked samples were labelled and photographed in situ on shelves, to enable identification after firing (e.g. fig. 230), and one extruded example of each sample was placed spanning a gap of approximately 45 mm to determine if slumping occurred during firing (e.g. fig. 231).



**Figure 230: Kiln shelf with labelled samples**



**Figure 231: Slump test set-up**

### **Triaxial ACCL: 800°C**

The composition of triaxial ACCL is shown in Table 13. After firing to 800°C, no sample displayed slumping and all were unfused (fig. 232).



**Figure 232: Triaxial ACCL. Extrusions fired to 800°C**

### **Triaxial ACCL: Shrinkage from dry after firing to 800°C**

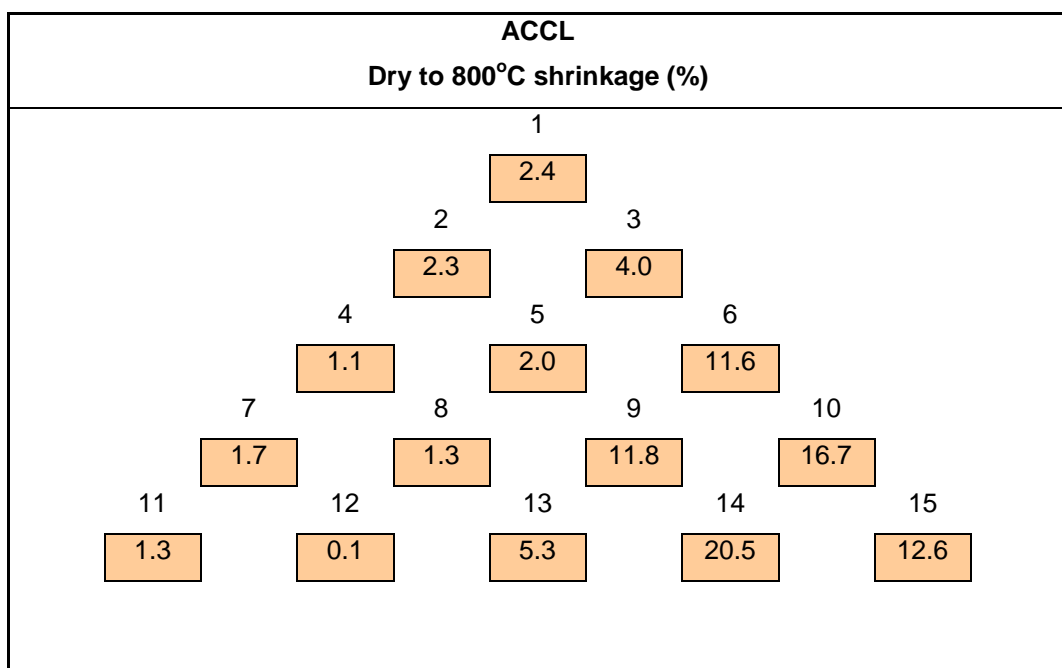
The greatest shrinkage from dry to 800°C was 20.5% for sample 14, and the least was 0.1% for sample 12. Both these samples had 10% bentonite, but the

proportions of perlite and cullet were reversed: sample 12 had 22.5% cullet and 67.5% perlite, while sample 14 had 22.5% perlite and 67.5% cullet. The data in linear format (Table 25) are arranged in the triaxial format in Table 26.

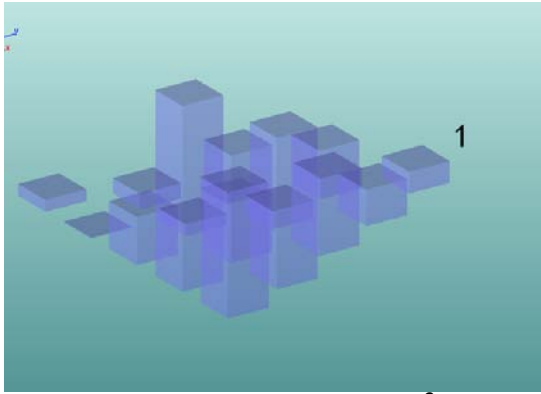
**Table 25: ACCL blend samples: Dry to 800°C shrinkage**

ACCL															
Dry to 800°C shrinkage (%)															
No	1	2	3	4	5	6	7	8	9	10	11	12	13	14	15
%	2.4	2.3	4.0	1.1	2.0	11.6	1.7	1.3	11.8	16.7	1.3	0.1	5.3	20.5	12.6

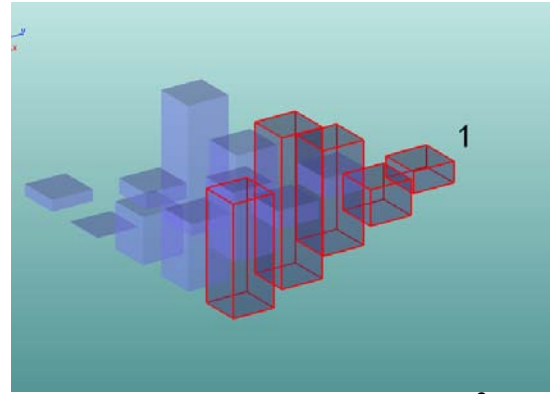
**Table 26: ACCL triaxial: Dry to 800°C shrinkage**



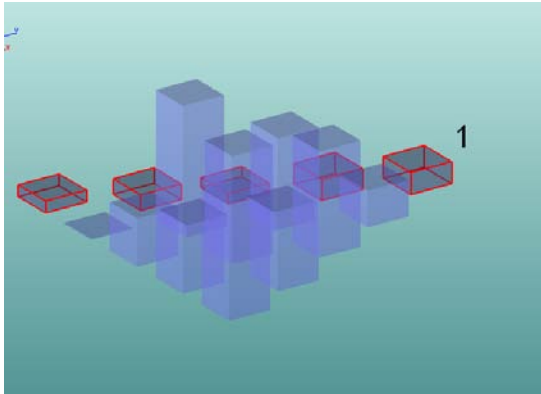
Trimetric views of percentage shrinkage from dry to 800°C across the ACCL triaxial blend are shown in Figures 233–238 (overleaf). There was an almost linear reduction in shrinkage along the 1–2–4–7–11 line blend (fig. 235). There were curvilinear trends across both the 1–3–6–10–15 line blend and the 11–15 line blend (fig. 236 & fig.239), showing that samples with 50–70% cullet and 20–30% perlite shrink more than do samples with 90% cullet and no perlite, or samples with >30% perlite. The apparently anomalous minimal shrinkage (0.1%) of sample 12 continues a straight-line trend of decreasing shrinkage along 3–5–8–12, as shown by the framing (fig. 237). The overall pattern is shown also in dynamic view (fig. 238).



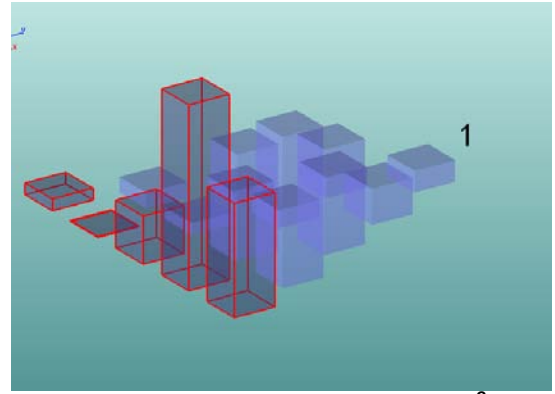
**Figure 233: Triaxial ACCL. Dry to 800°C shrinkage (%), trimetric view**



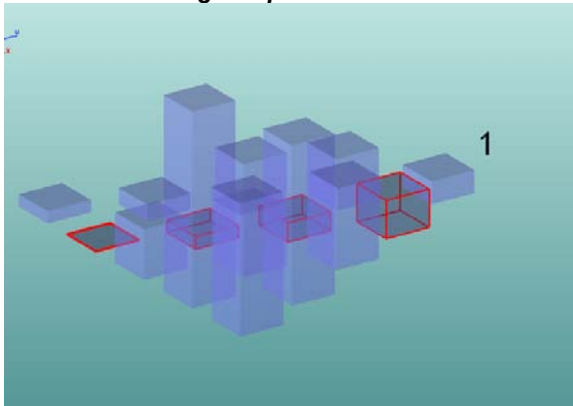
**Figure 234: Triaxial ACCL. Dry to 800°C shrinkage (%), trimetric view. Framing samples 1-3-6-10-15**



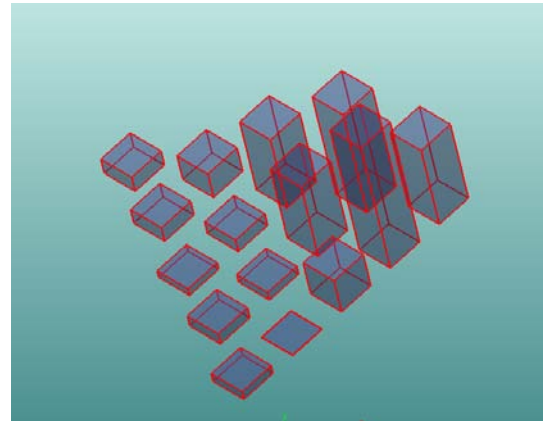
**Figure 235: Triaxial ACCL. Dry to 800°C shrinkage (%), trimetric view. Framing samples 1-2-4-7-11**



**Figure 236: Triaxial ACCL. Dry to 800°C shrinkage (%), trimetric view. Framing samples 11-15**



**Figure 237: Triaxial ACCL. Dry to 800°C shrinkage (%), trimetric view. Framing samples 3-5-8-12**



**Figure 238: Triaxial ACCL. Dry to 800°C shrinkage (%), dynamic view. Framing samples 1(at left)-15(at right)**

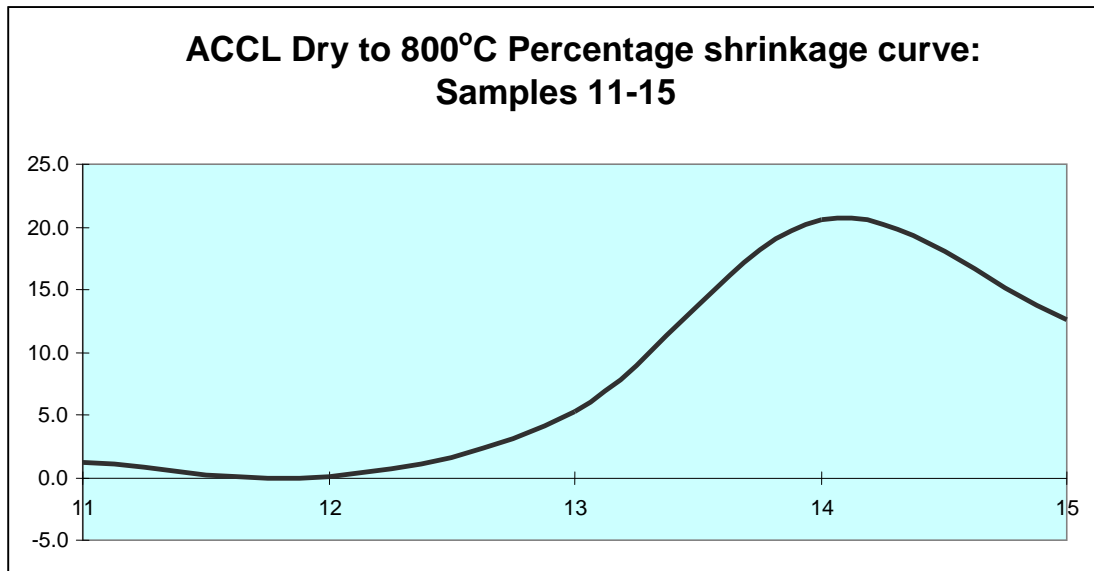


Figure 239: ACCL. Curvilinear shrinkage trend: samples 11–15

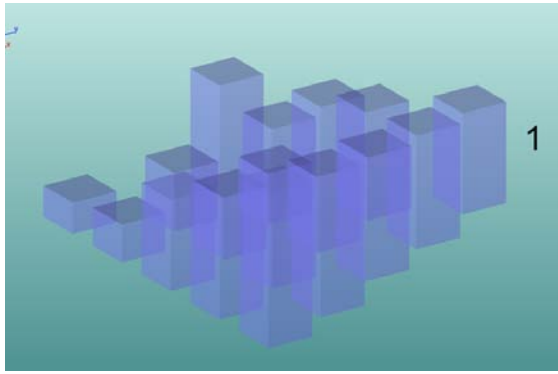
Triaxial ACCL: Shrinkage from wet after firing to 800°C

The combined wet to dry shrinkage and dry to 800°C shrinkage data appear in Table 27.

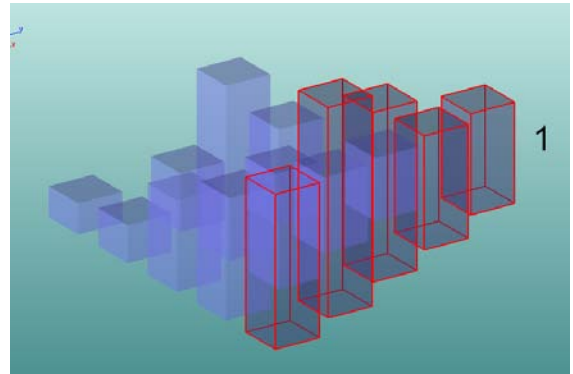
Table 27: ACCL: Wet to 800°C shrinkage

ACCL															
Wet to 800°C shrinkage (%)															
No	1	2	3	4	5	6	7	8	9	10	11	12	13	14	15
%	10.4	6.5	11.7	5.2	7.8	17.4	6.0	6.4	16.4	21.6	3.2	3.9	9.4	24.1	15.9

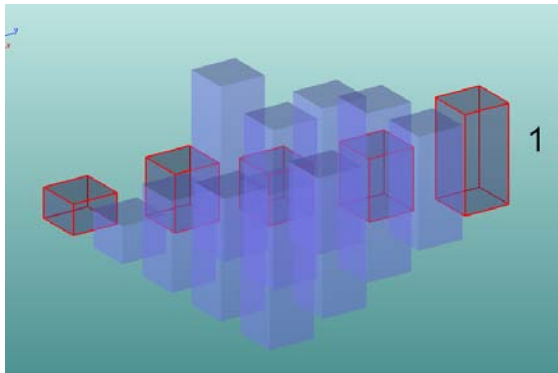
When the wet to 800°C shrinkage data for triaxial ACCL were displayed in 3D, it was apparent that the minimal shrinkage of corner B increased with inclusions of both corner A and corner C, but the shrinkage changes were not in proportion to the blend proportions (figs. 240–244, overleaf).



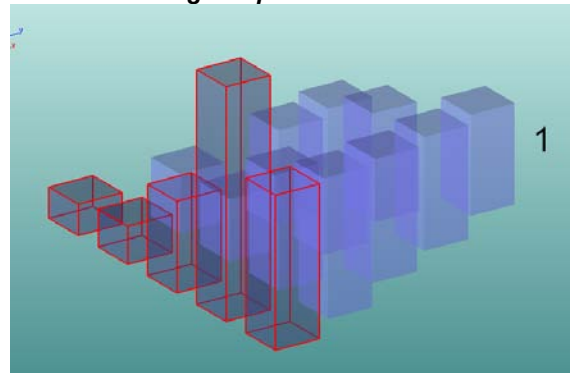
**Figure 240: Triaxial ACCL. Wet to 800°C shrinkage (%), trimetric view.**



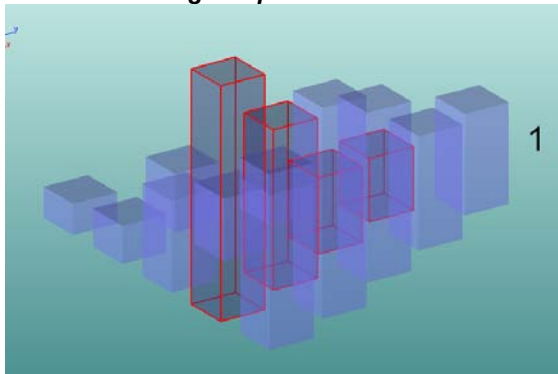
**Figure 241: Triaxial ACCL. Wet to 800°C shrinkage (%), trimetric view. Framing samples 1-3-6-10-15**



**Figure 242: Triaxial ACCL. Wet to 800°C shrinkage (%), trimetric view. Framing samples 1-2-4-7-11**



**Figure 243: Triaxial ACCL. Wet to 800°C shrinkage (%), trimetric view. Framing samples 11-15**



**Figure 244: Triaxial ACCL. Wet to 800°C shrinkage (%), trimetric view. Framing samples 2-5-9-14**

Figure 245 demonstrates the approximate colours of the fired samples, the extent of tearing when cutting slabs, the obviously high shrinkage of sample 14, and the samples (11,12 & 15) with which it was not possible to roll slabs.



**Figure 245: Triaxial ACCL. Fired to 800°C**

After firing to 800°C, the six sample extrusions closest to corner C (90% Unimin cullet, 10% Arumppo bentonite) displayed slumping (fig. 246). The higher the proportion of cullet, the more pronounced the slumping.



**Figure 246: ACCL Triaxial slump tests after firing to 800°C**

After firing to 800°C, sample ACCL11 felt extremely light when held in the hand. This sample was placed in a bowl of water, and was observed to float for a few seconds before absorbing sufficient water to cause it to sink (fig. 247).



**Figure 247: ACCL11 floating ceramic sample**

#### Floating ceramic body (ACCL11; 800°C.)

The floating ceramic body may be useful where extremely lightweight ceramics are required, or where filtration is required.

Perlite AP10 white (wt%)	90
Arumpo bentonite (wt%)	10
COE <sup>11</sup> ( $\times 10^{-6}/^{\circ}\text{C}$ )	9.3
Matrix-estimated melting point ( $^{\circ}\text{C}$ )	1408
Fe <sub>2</sub> O <sub>3</sub> (wt%)	0.05

---

<sup>11</sup> Coefficient of expansion - indicates the amount of expansion and contraction during firing and cooling (Barsoum, 1997).



### Triaxial BM1: Shrinkage from wet, after firing to 800°C

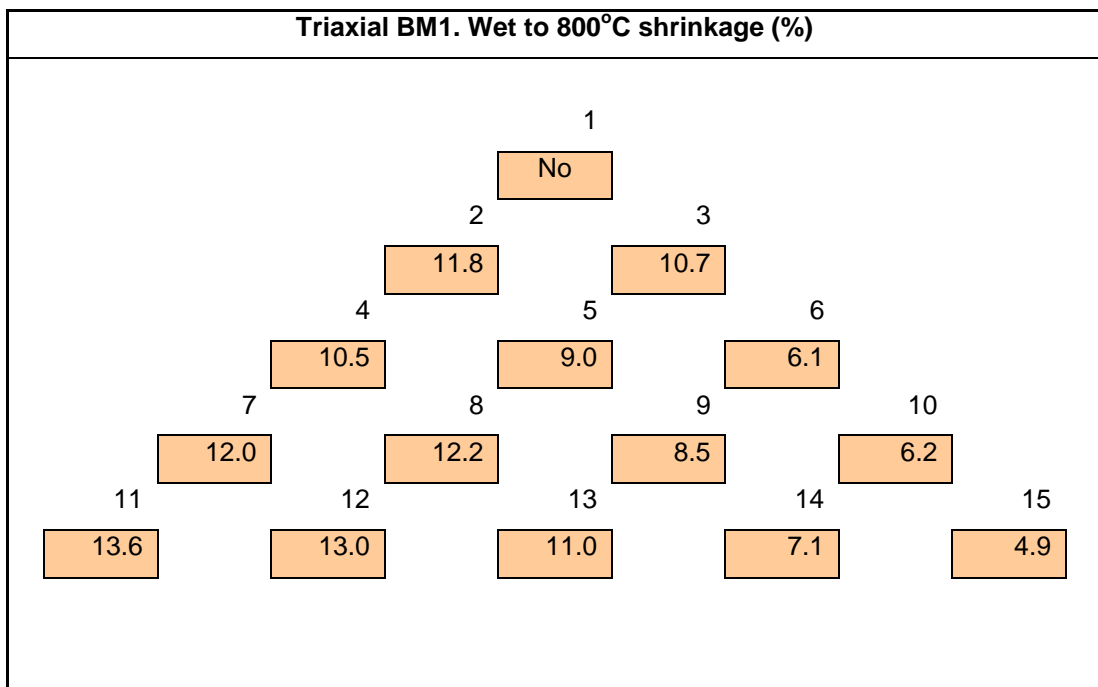
The extruded chips of triaxial BM1 samples were fired to 800°C. The samples with the highest and lowest shrinkage are shown in red (Table 28).

Table 28: Triaxial BM1: Shrinkage from wet to 800°C

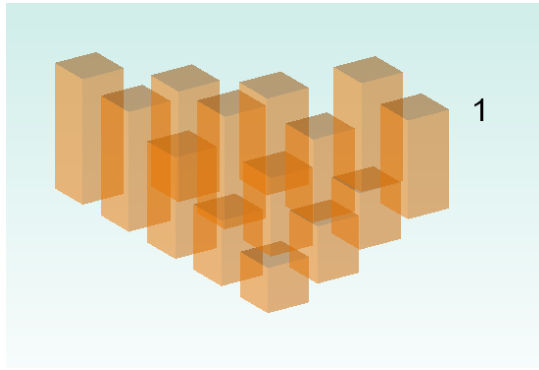
Triaxial BM1													
Wet to 800°C shrinkage (%)													
2	3	4	5	6	7	8	9	10	11	12	13	14	15
11.8	10.7	10.5	9.0	6.1	12.0	12.2	8.5	6.2	13.6	13.0	11.0	7.1	4.9

Bungendore tailings (sample BM1.11) shrunk three times as much as did Marulan tailings (sample BM1.15). The data in Table 29 are arranged in triaxial format showing samples BM1.11 and BM1.15 at corners B and C.

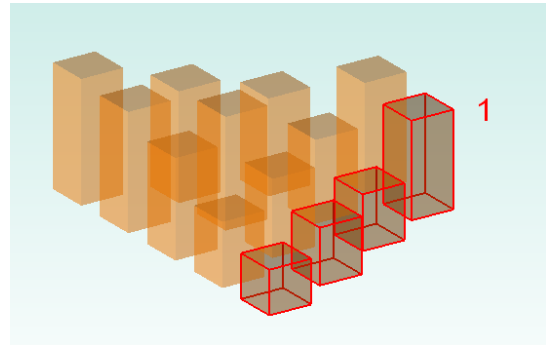
Table 29: Triaxial BM1: Wet to 800°C shrinkage



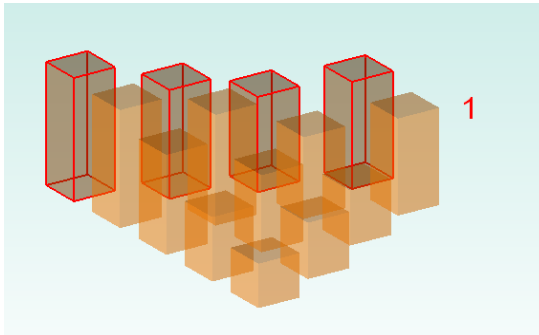
The same data are displayed in 3D in Figures 248–251. There was a linear trend of increase in percentage shrinkage when low shrinkage Marulan tailings (sample BM1.15, corner C) were blended with BM1.1 flux mix (fig. 249) and with high shrinkage Bungendore tailings (at corner B, fig. 251. However, there was a curvilinear decrease in shrinkage when Bungendore tailings were blended with flux mix (fig. 250).



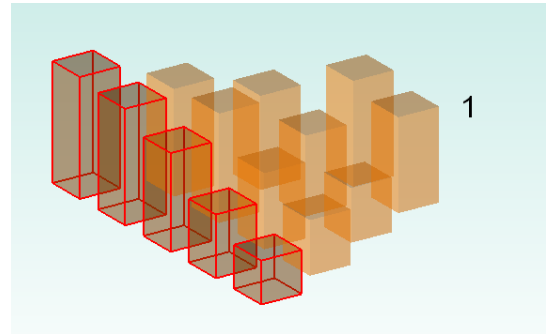
**Figure 248: Triaxial BM1. Wet to 800°C shrinkage (%), trimetric view**



**Figure 249: Triaxial BM1. Wet to 800°C shrinkage (%), trimetric view. Framing samples 3-6-10-15**



**Figure 250: Triaxial BM1. Wet to 800°C shrinkage (%), trimetric view. Framing samples 2-4-7-11**



**Figure 251: Triaxial BM1. Wet to 800°C shrinkage (%), trimetric view. Framing samples 11-15**

Reference back to the wet to dry shrinkage of this triaxial shows that wet to dry shrinkage accounts for most of the shrinkage from wet to fired. Shrinkage from dry to fired is documented in the following section.

### **Triaxial BM1: Shrinkage from dry, after firing to 800°C**

The average shrinkage from dry to 800°C of each sample is recorded in Table 30, with samples showing the lowest and highest shrinkage printed in red.

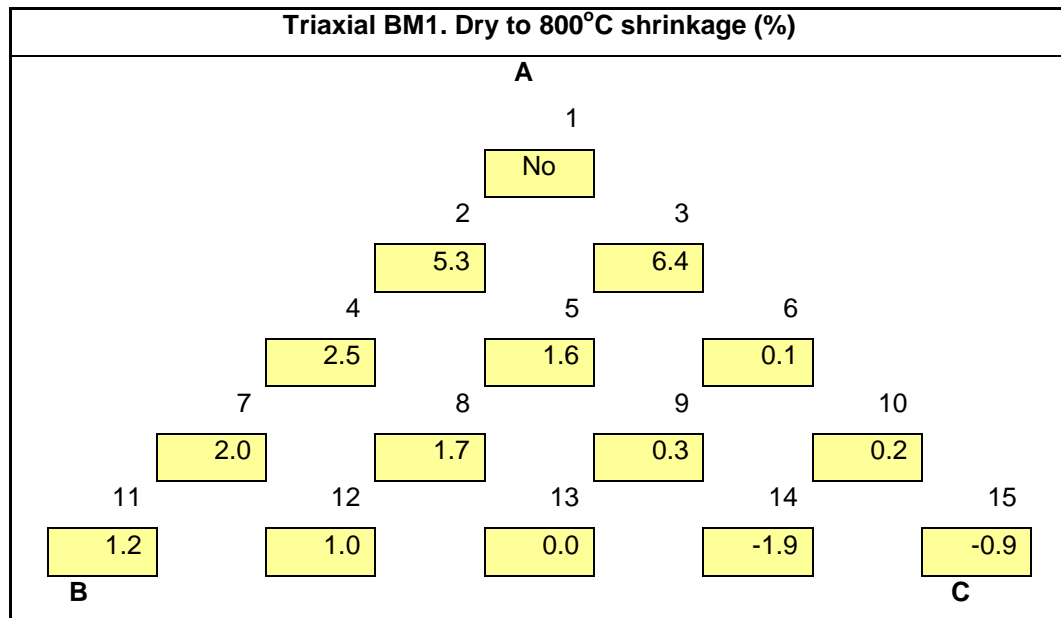
**Table 30: Triaxial BM1: Dry to 800°C shrinkage/expansion**

Triaxial BM1.													
Dry to 800°C shrinkage/expansion (%)													
2	3	4	5	6	7	8	9	10	11	12	13	14	15
5.3	6.4	2.5	1.6	0.1	2.0	1.7	0.3	0.2	1.2	1.0	0.0	-1.9	-0.9

The maximum dry to 800°C shrinkage observed in Blend BM1 was 6.4% in sample 3, which contained 30% bentonite. The least shrinkage observed was

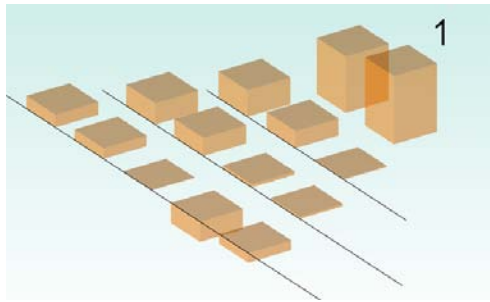
-1.9% in sample 14, which in fact expanded, as did sample 15 to a lesser extent. The likely reasons for this observed expansion are discussed later. The data were arranged also in the triaxial format (Table 31).

**Table 31: Triaxial BM1: Dry to 800°C shrinkage**

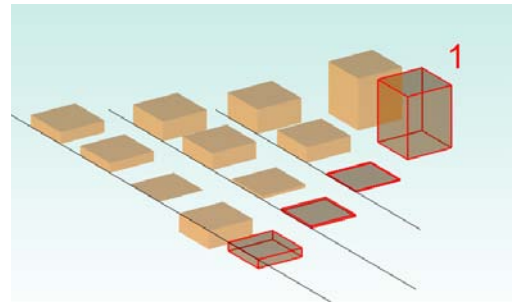


Greater shrinkage occurred closest to the flux mix at corner A, with shrinkage moderated by increasing proportions of Bungendore tailings from corner B, trending to expansion with increasing proportions of Marulan tailings from corner C.

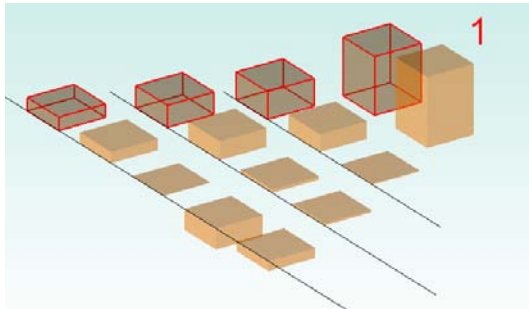
Figures 252–255 (overleaf) show 3D trimetric views of the blend results. The numeral ‘1’ identifies the apex of the 15-sample triaxial blend, and the samples representing line blends between the three corners of the triaxial are framed.



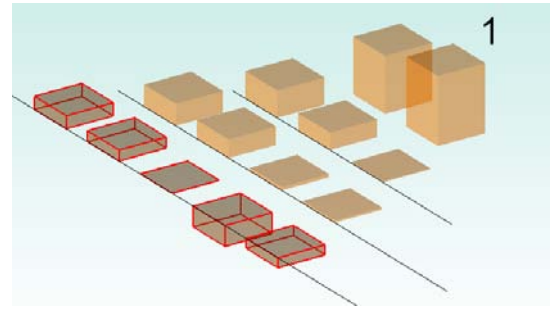
**Figure 252: Triaxial BM1. Dry to 800°C shrinkage (%), trimetric view showing expansion samples 14 & 15**



**Figure 253: Triaxial BM1. Dry to 800°C shrinkage (%), trimetric view. Framing samples 3-6-10-15**



**Figure 254: Triaxial BM1. Dry to 800°C shrinkage (%), trimetric view. Framing samples 2-4-7-11**



**Figure 255: Triaxial BM1. Dry to 800°C shrinkage (%), trimetric view. Framing samples 11-15**

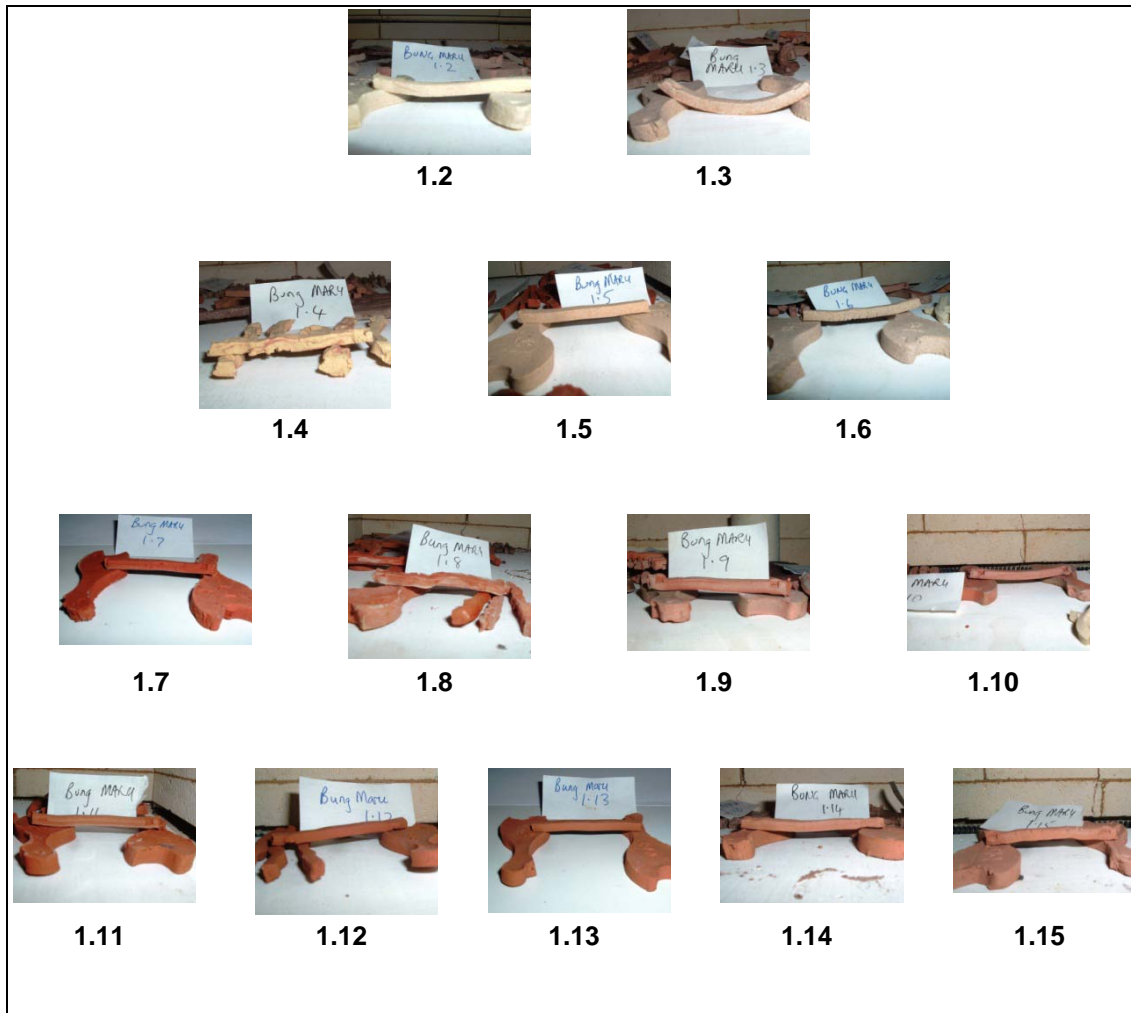
The approximate colours of the samples when triaxial BM1 was fired to 800°C are shown in Figure 256. The sample BM1.1 with the most flux mix (at corner A) was a pale buff pink, darkening with increasing proportions of Bungendore tailings from corner B. The Bungendore tailings were a dark orange/brown. In comparison, the Marulan tailings at corner C were a relatively pale orange/tan. Intermediate samples displayed intermediate shadings.



**Figure 256: Triaxial BM1. Fired to 800°C. Samples 2-15**

## Slumping

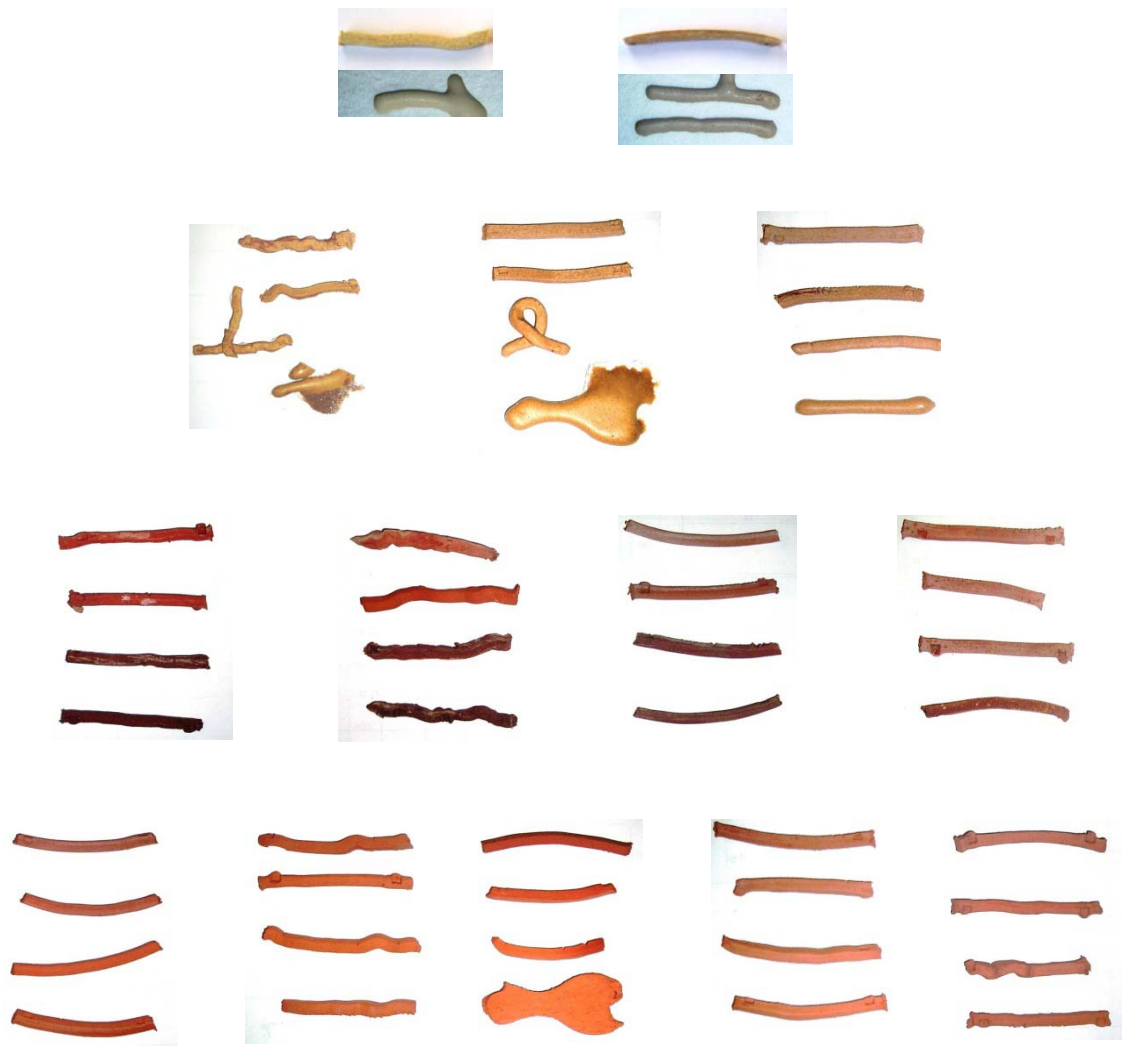
When triaxial BM1 was fired to 800°C, only samples BM1.2 and BM1.3 displayed evidence of slumping (fig. 257).



*Figure 257: Triaxial BM1 slump tests after firing to 800°C: Samples BM1.2- BM1.15.*

## **Triaxial BM1: Fired to 800, 850, 900 and 950°C**

As there was some evidence of slumping after triaxial BM1 was fired to 800°C, tests were also conducted at 850, 900 and 950°C, to ascertain the range of temperatures over which the samples would slump or fuse (fig. 258, overleaf).



**Figure 258: Triaxial BM1: Samples BM1.2–BM1.15 after firing to (from top to bottom) 800, 850, 900 and 950°C**

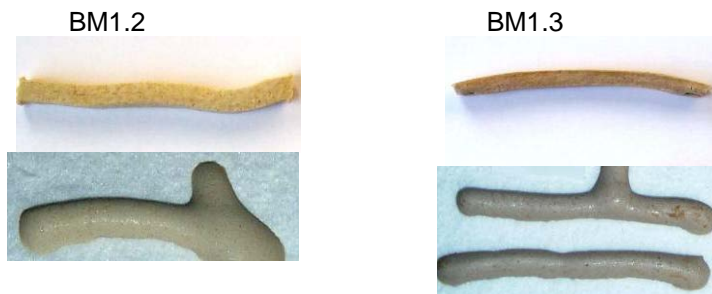
The samples were categorised as having either retained their form, slumped or fused, at each of the four firing temperatures (see Table 32, where blank cells represent samples that retained their form).

**Table 32: Triaxial BM1 slump test result**

<b>Triaxial BM1 slump test results</b>				
	<b>800°C</b>	<b>850°C</b>	<b>900°C</b>	<b>950°C</b>
Sample				
BM1.2	Slumped	Fused	Fused	Fused
BM1.3	Slumped	Fused	Fused	Fused
BM1.4		Slumped	Slumped	Fused
BM1.5		Slumped	Slumped	Slumped
BM1.6			Slumped	Slumped
BM1.7				
BM1.8				
BM1.9				Slumped*
BM1.10				Slumped*
BM1.11				
BM1.12				
BM1.13				
BM1.14				
BM1.15				

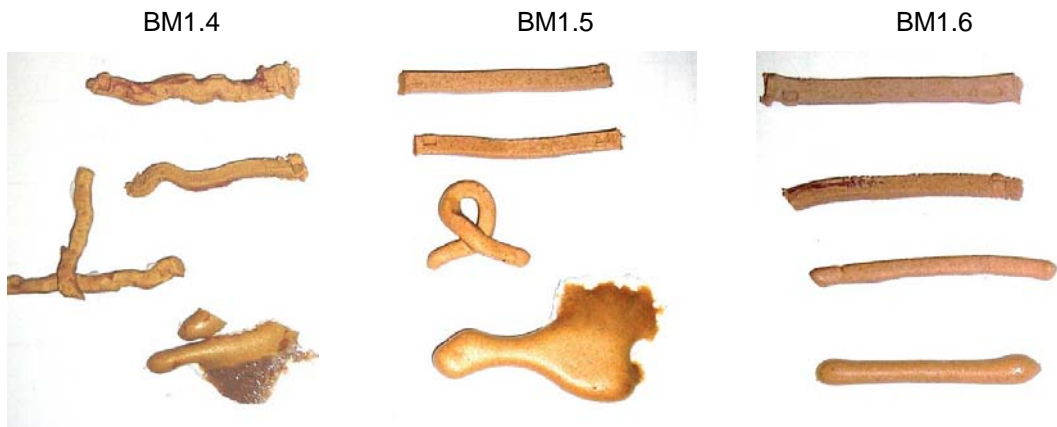
\* = minimal slumping

Enlarged images of selected samples are shown in Figure 259. Samples BM1.2 and BM1.3 were only fired at 800 and 850°C, as they fused onto the ceramic paper at 850°C (fig.259).



**Figure 259: Triaxial BM1 samples BM1.2 and BM1.3 fired to 800 (top) and 850°C**

Samples BM1.4–BM1.15 were fired to 800, 850, 900 and 950°C (figs. 260 and 261). At 950°C, all Tier 3 samples had fused (fig.260), but all Tier 4 samples could be fired to 950°C without fusing (fig.261).



*Figure 260: Samples BM1.7–BM1.10 after firing (from top to bottom) to 800, 850, 900 and 950°C*



*Figure 261: Samples BM1.7–BM1.10 after firing (from top to bottom) to 800, 850, 900 and 950°C*

The results provide convincing evidence that it is possible to create a vitreous ceramic below 1000°C. There was an interesting range of results across the triaxial: some samples fused at 850°C, some slumped at 950°C and some retained their form at 950°C.

### **Triaxial BM2: 800°C**

Triaxial BM2 was fired to 800°C using the standard firing cycle. Samples 315 fired to 800°C are shown in Figures 262 and 263. Sample 3 fused, and samples



4–6 vitrified to the extent that sample pieces that had been in contact had to be broken apart. Sample 7 self-glazed on the fish, but not the chip.

The colours of the samples with most flux were darker than the corresponding samples in triaxial BM1 (fig. 256). BM2.3 was maroon, and Tier 3 samples were tan, with dark holes and white specks (fig 262).



*Figure 262: Triaxial BM2 fired to 800°C. Samples 3–15*



*Figure 263: Triaxial BM2 fired to 800°C. Samples 3–15*

Slump tests of triaxial BM2 after firing to 800°C appear below (fig. 264). The only slumped sample was BM2.3. Samples BM2.4–BM2.6 had fused at contact points, but had not slumped.



Figure 264: Triaxial BM2. Slump tests fired to 800°C: samples BM2.3–BM2.10

Results of further slump tests at higher temperatures are documented below, following the results of shrinkage tests of triaxial BM2 fired to 800°C.

### Triaxial BM2: Shrinkage from dry to 800°C

The dry to 800°C shrinkage data appear in Table 33 (and Table 34, in triaxial format), with samples showing the least and most shrinkage denoted by red numerals. Sample BM2.4 shrank the most, at 2.8%. Sample BM2.14 expanded by 1.9%, as described previously for triaxial BM1.

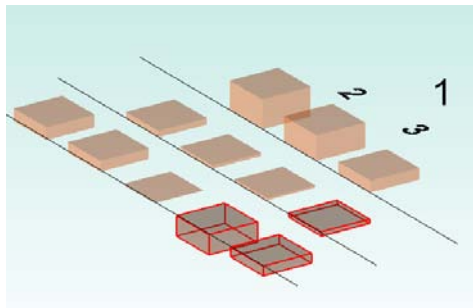
Table 33: Triaxial BM2: Dry to 800°C shrinkage

Triaxial BM2. Dry to 800°C shrinkage (%)														
No	2	3	4	5	6	7	8	9	10	11	12	13	14	15
%	-		2.8	2.4	1.1	0.6	0.3	0.2	-0.4	1.2	1.0	0.0	-1.9	-0.9

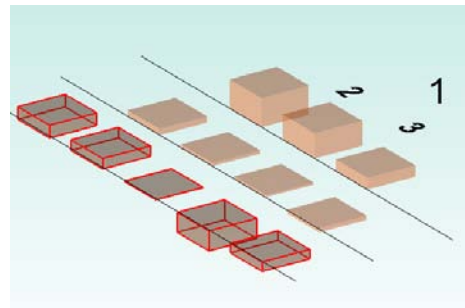
**Table 34: Triaxial BM2: Dry to 800°C shrinkage**

Triaxial BM2. Dry to 800°C shrinkage (%)				
		1		
		No		
	2		3	
	No		fused	
	4	5	6	
	2.8	2.4	1.1	
7		8	9	10
0.6		0.3	0.2	-0.4
11	12	13	14	15
1.2	1.0	0.0	-1.9	-0.9

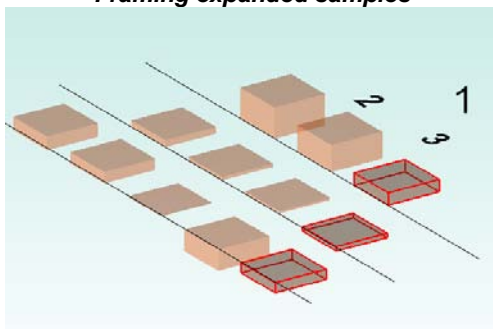
The shrinkage data are displayed so that the extent of shrinkage or expansion is evident from the size of the vertical bars in the triaxial (figs. 265–268). These representations and the data in Table 34 demonstrate that the shrinkage trends along the line blends were not linear. The likely reason for the non-linear trends along the A–B and A–C line blends is addressed when the shrinkage from wet to 800°C is considered below.



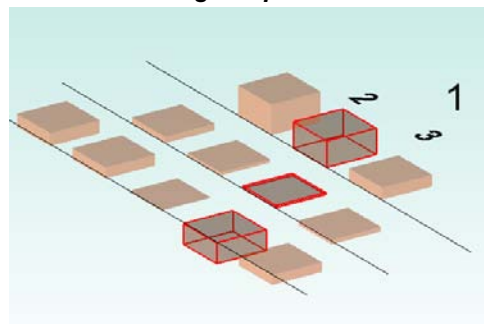
**Figure 265: Triaxial BM2. Dry to 800°C shrinkage (%), trimetric view. Framing expanded samples**



**Figure 266: Triaxial BM2. Dry to 800°C shrinkage (%), trimetric view. Framing samples 11–15**



**Figure 267: Triaxial BM2. Dry to 800°C shrinkage (%), trimetric view. Framing samples 6–10–15**



**Figure 268: Triaxial BM2. Dry to 800°C shrinkage (%), trimetric view. Framing samples 5–9–14**

As shown in Figures 265–268, some of the dried samples shrank when fired to 800°C, and some expanded. Grimshaw's (1971) explanation of the length and volume changes that are irreversible upon cooling divides the causes into manufacturing method (including firing temperature) and the nature of the constituent materials. Since temperature and sample-forming techniques were held constant for BM1 and BM2 triaxials fired to 800°C, the results obtained here are discussed with reference to the varied nature and proportions of the constituent materials, and with reference to information provided earlier regarding sintering and vitrification.

Grimshaw (1971) notes that permanent changes in volume can occur during firing, because of:

- decomposition (in which loss of water or CO<sub>2</sub> results in weight loss and a slight expansion)
- inversional changes (in which a material such as quartz first expands upon heating and forces the surrounding material apart, then upon cooling contracts away from the surrounding material, which remains disrupted)
- crystallisation and densification during solid-state sintering (in which contraction occurs unless there is abnormal particle size growth)
- liquid-phase sintering (in which the liquid fills pores, resulting in contraction)
- bloating (and thus expansion) as a result of gas being liberated from, but trapped within, the clay body.

Grimshaw (1971, p. 805) also notes that inclusion of non-plastic refractory material can act as a 'non-reactive skeleton', which reduces shrinkage.

Grimshaw (1971) provides examples of changes in dry to fired length over 0–1200°C, using a range of ball clays with varying percentages of naturally occurring illite (hydrous mica), and prepared mixtures of china clay, quartz and illite of varied grain size. Of the eight fired samples, only one did not expand at temperatures up to or beyond 950°C. This sample (which had the least silica and illite) expanded to 600°C and then contracted, reaching zero expansion at about 650°C. At 800°C, it had contracted by 0.4% and by 1000°C, it had

contracted by 1%. These experiments showed that in general, greater proportions of silica produce greater expansion due to the quartz inversion. Illite has a stabilising effect up to  $\sim 950^{\circ}\text{C}$ , at which point the alkalis present contribute to liquid-phase sintering (Grimshaw, 1971).

After reviewing the explanations provided by Grimshaw, it became apparent that some slight expansion could be expected to occur from dry to  $800^{\circ}\text{C}$  due to decomposition, quartz inversion and the temperature being lower than that at which sintering would normally commence. Therefore, the contraction recorded on almost all samples in BM1 and BM2 triaxials requires explanation.

The most likely explanation, based on the observation that some samples fused at  $800^{\circ}\text{C}$ , is that the proportion of flux present was sufficient to induce liquid sintering that was progressively less advanced moving from Tiers 1 to 4 of triaxials BM1 and BM2. Tier 5, which was the same in both triaxials, had no added flux, as it was a line blend of Bungendore tailings at corner B, and Marulan tailings at corner C. Why then, would Bungendore tailings display shrinkage when fired to  $800^{\circ}\text{C}$ ? As the densification that accompanies solid-state sintering can occur well before the liquid phase, some densification may have commenced. It was previously noted that using materials with small particle size aids sintering, because the densification process depends on particle-to-particle contact, and the finer the particle size, the greater the surface area available for contact. The suspension settling experiments (fig.143) showed that Bungendore tailings had more fine particles than did Marulan tailings, which may explain the contraction of the Bungendore tailings, but not the Marulan tailings. Also, Bungendore tailings contain only  $\sim 0.5\%$  calcium, while Marulan tailings contain  $\sim 3\%$  calcium (see Chapter 16) and it has been noted previously that calcium concentrations  $>1\%$  inhibit sintering below  $1100^{\circ}\text{C}$  (Hamer, 1975). Hence, the sintering and densification promoted by the presence of smaller particles would also not be inhibited by the presence of excess calcium.

## BM2 Shrinkage from wet to 800°C

The combined wet to dry shrinkage and dry to 800°C shrinkage data appear in Table 35, with the lowest and highest shrinkage rates shown in red. Sample BM2.3 melted, so measurement was not possible. The least shrinkage occurred in sample BM2.6, and the greatest in sample BM2.7.

**Table 35: Triaxial BM2: Wet to 800°C shrinkage**

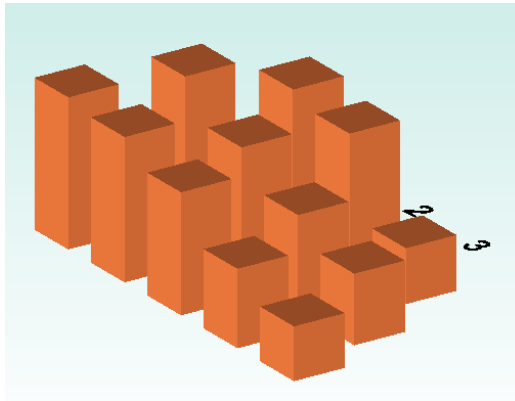
Triaxial BM2. Wet to 800°C shrinkage (%)													
2	3	4	5	6	7	8	9	10	11	12	13	14	15
%	-	13.3	12.3	5.0	15.2	11.8	8.7	6.4	13.6	13.0	11.0	7.1	4.9

Although the samples with the greatest and least shrinkage are consecutively numbered, it is apparent that their compositions are dissimilar when the data are displayed in triaxial format (Table 36).

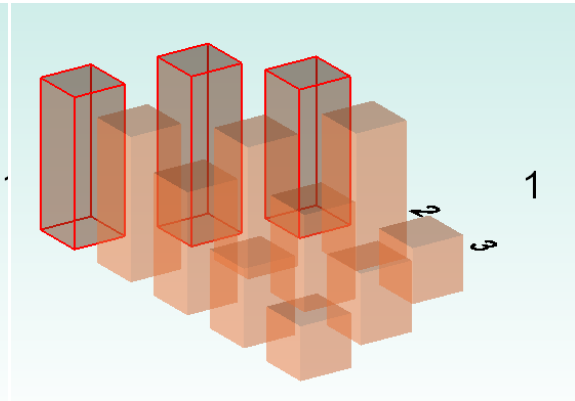
**Table 36: Triaxial BM2: Wet to 800°C shrinkage**  
BM2 Triaxial. Wet to 800°C shrinkage (%)

1														
					-									
				-		Fused								
			13.3		12.3		5.0							
		15.2		11.8		8.7		6.4						
13.6		13		11		7.1		4.9						

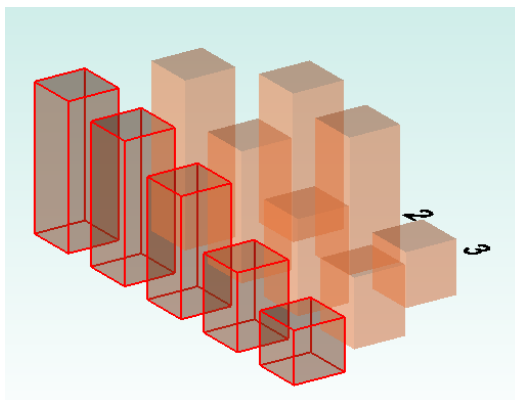
The shrinkage data are displayed so that the extent of shrinkage is evident from the size of the vertical bars in the triaxial (figs. 269–273). From these figures and Table 36 it is apparent that the shrinkage trends along the A-B and A-C blends were not linear.



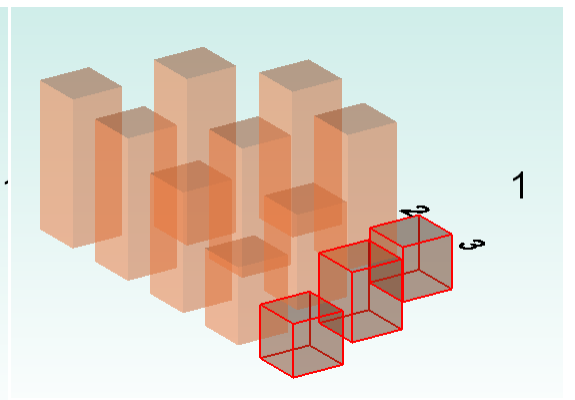
**Figure 269: Triaxial BM2. Wet to 800°C shrinkage (%), trimetric view.**



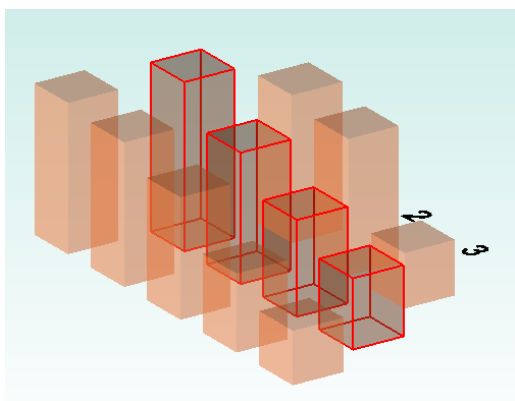
**Figure 270: Triaxial BM2. Wet to 800°C shrinkage (%), trimetric view. Framing samples 4-7-11**



**Figure 271: Triaxial BM2. Wet to 800°C shrinkage (%), trimetric view. Framing samples 11-15**



**Figure 272: Triaxial BM2. Wet to 800°C shrinkage (%), trimetric view. Framing samples 6-10-15**



**Figure 273: Triaxial BM2. Wet to 800°C shrinkage (%), trimetric view. Framing samples 7-10**

The lower than expected shrinkage in Tier 3 samples BM2.4 - BM2.6 may have resulted from bloating. This idea is supported by the presence of multiple holes producing a scoria-like appearance in these samples (fig. 274).



*Figure 274: Samples BM2.4–BM2.6 after firing to 800°C*

### **BM2.7 – BM2.10 after firing to 800, 850, 900 and 950 °C**

At 800°C, BM2.3 had melted and Tier 3 samples had bloated, as seen above (fig.274). Tier 5 samples had already been fired at higher temperatures during experimental firing of triaxial BM1, since they were of identical composition. Accordingly, only Tier 4 samples from triaxial BM2 were fired at higher temperatures, to see how they would respond.

As well as being fired at 850°C, the BM2.7–BM2.10 triaxial samples were fired to three higher temperatures: 900, 950 and 1000°C, using the standard firing schedule introduced in Chapter 13. The fired samples are displayed in Figure 275. All Tier 4 samples of BM2 self-glazed at 950°C.



*Figure 275: Samples BM2.7–BM2.10 after firing (top to bottom) to 800, 850, 900 and 950°C*



The samples were categorised as having either retained their form, bloated, slumped or fused, at each of the four firing temperatures (see Table 37). Blank cells represent samples that retained their form and grey cells represent samples that had fused or bloated at a lower temperature so were not fired at the higher temperatures.

*Table 37: Triaxial BM2 slump test results*

<b>Triaxial BM2 slump test results</b>				
	<b>800°C</b>	<b>850°C</b>	<b>900°C</b>	<b>950°C</b>
Sample				
BM2.3	Fused			
BM2.4	Bloated			
BM2.5	Bloated			
BM2.6	Bloated			
BM2.7				
BM2.8				
BM2.9				
BM2.10				Slumped*
BM2.11				
BM2.12				
BM2.13				
BM2.14				
BM2.15				

\* = minimal slumping

The minimal slumping displayed by sample BM2.10 suggested that this body might be at, or close to, the top of its firing range. Samples BM2.7, BM2.8 and BM2.9 did not slump, but samples BM2.7 and BM2.9 self-glazed at 950°C. These two samples had displayed reasonable workability, so were selected for larger-scale testing. This testing included the making of forms using a pottery wheel (see Chapter 18).

Collectively, the results reported to this point are strongly encouraging: although some experimental clay samples have displayed undesirable characteristics in the raw state, others have displayed acceptable shrinkage and workability

properties. Vitrification has occurred with some samples—in some cases well below the target of 1000°C. There is still a need to know more about the composition of the recovered materials, as this will assist in refining formulation of clays and glazes.

However, at this point in the research there was a temporary diversion from the path of clay and glaze formulation, for process considerations. Two of the agricultural waste products (dry rice husks and freshly shelled corn cobs) required kiln firing to produce ash for use in clay or glaze. This released considerable smoke, and the necessity for electricity use to produce the ash was at odds with the broader aims of the project. Before returning to questions of composition and formulation of clays and glazes, the efforts made to address this dilemma are described. Chapter 14 documents the procurement of simple domestic biomass gasifiers, and the construction and use of a kiln to harvest the energy from gasifying the husks and cobs, while simultaneously producing the required ash.

## Chapter 14: Use of Energy from Rice Husks and Corn Cobs

Ashing the rice husk and corn cobs in the kiln at Sydney College of the Arts was problematic in that it required considerable energy input and produced large amounts of smoke. The aims of this project were to reduce energy input and emissions, so consideration was given to a method of extracting energy from the biomass in a cleaner and more efficient manner, prompting a search for a simple gasifier.

### Obtaining domestic gasifiers

A web search for rice husk gasifiers revealed that Alexis Belonio, of Iloilo University in the Philippines, had developed a stove that successfully gasified rice husks. Through correspondence with Belonio and his marketing manager, a rice husk gasifier stove and a charcoal gasifier stove were obtained from the M.J. Arotech factory in Jakarta. Both stoves use 12-volt fans to assist gasification of feedstock. The rice husk stove was tested by cooking a pot of potatoes for 40 minutes (see fig. 276) according to the instructions in the user manual provided (see Appendix 4).



*Fig 276: Domestic use of rice husk stove*

The ash produced was similar in appearance to that produced by the kiln, but the operation was smoke free and the energy released was used productively. The ash produced could be crushed by hand into a fine, dark grey powder. The next step was to build a kiln that would contain the heat produced from ashing the rice husks.



*Figure 277: Burnt rice husk in biomass gasifier*

### **Biomass kiln construction**

A top-hat kiln was constructed using a rubbish bin and a re-used kiln lid (figs. 278–281). First, the vent hole on the kiln lid was widened to form a burner port (fig. 279). An angle grinder and file were used to cut a 55 mm diameter hole in the side of the bin to receive a re-used cast ceramic spy-hole. A 15 mm hole was drilled to receive the probe from a pyrometer. Two holes were drilled in the base of the bin, and ceramic fibre was cut so that three discs of 25 mm fibre blanket could be anchored to the base of the bin using ceramic anchors and nichrome wire. A layer of ceramic fibre blanket was rolled onto the interior walls of the bin and fixed where the blanket overlapped, using sodium silicate as an adhesive. The centre of the bin lid was cut with an angle grinder. The rim of the

lid was replaced on the bin to support the blanket on the walls when the bin was inverted. The centre of the lid was placed on the exterior of the bin base, over the tied-off ends of nichrome wire, which were covered with a thin layer of fibre blanket. The lid was secured in place with self-tapping screws, so that the handle could be used to lift the inverted bin from the kiln base during loading and unloading.



**Figure 278: Metal rubbish bin**



**Figure 279: Re-used kiln lid**



**Figure 280: Rubbish bin with spy-hole**



**Figure 281: Secured fibre blanket**

### **Firing with rice husks and a gasifier**

The inverted soft-brick kiln lid was supported on two rows of bricks, and the rice husk gasifier placed beneath the burner port (figs. 282 and 283, overleaf).



**Figure 282: Rubbish bin kiln in position**



**Figure 283: Rice husk stove in position**

The top-hat kiln was fired using both the rice husk and charcoal gasifier stoves. The stoves are similar in design, but the charcoal stove is not as tall. It has a smaller reactor chamber and requires a transformer to drive the 12-volt fan used for primary air. The first firing commenced using the rice husk gasifier, which was replaced by the charcoal gasifier when the feedstock was exhausted (fig. 284).



**Figure 284: Charcoal stove in position**

In the first firing, use of a single charge of rice husk raised the temperature to 115°C over a period of 35 minutes. Changeover to the charcoal gasifier took approximately three minutes. Use of a charge of fine-grade charcoal with pieces averaging ~2 cm in diameter increased the temperature to 200°C in 25 minutes, with a rapid increase approximately five minutes after ignition. The temperature dropped to 185°C when the charcoal gasifier charge was exhausted, and replacement with the rice husk gasifier maintained this temperature over the next 30 minutes. Changing back to the charcoal gasifier charged with pieces averaging 8 cm in diameter resulted in a steady loss of temperature for 30 minutes until the larger pieces started to gasify well. When that occurred, the temperature climbed back to 200°C degrees in 20 minutes. The temperature was tracked using a pyrometer (fig. 285).

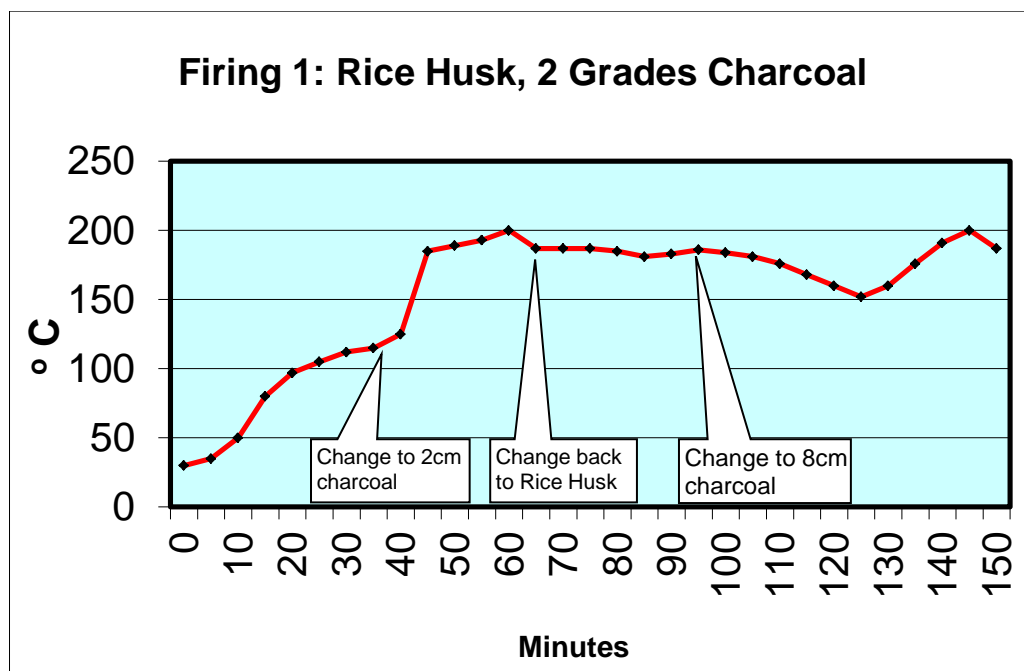


Figure 285: Rice husk and charcoal firing chart

### Burning domestic corn cob waste in a gasifier

Waste corn cobs produced in a domestic kitchen by cooking of whole corn for human consumption were collected over a period of months, and stored loose in a domestic freezer. The collected cobs were then dried using waste heat emanating from a kiln (figs. 286 and 287, overleaf).



**Figure 285: Corn cobs drying on kiln**



**Figure 287: Dried and charred cobs**

Some were then dried further, and some were converted to charcoal by restricting air available during heating to 600°C. The rice husk stove was filled with dried cobs. With this feedstock it was found that introduction of primary air should be delayed until the cobs are well alight. Once this had occurred, the primary air was introduced (figs. 288–291).



**Figure 288: Charcoal stove with dried cobs**



**Figure 289: Cobs burning without primary air**



**Figure 290: Cobs burning with primary air**



**Figure 291: Cobs nearing complete combustion**



Using the rice husk stove filled with dried cobs as a biomass gasifier burner raised the temperature in the top-hat kiln to 142°C. Once they were alight and the primary air introduced, the temperature rise was rapid, climbing 85°C in twenty minutes. Changing to the charcoal stove charged with charcoal averaging 4 cm in diameter produced a gradual rise from 141°C to 178°C over 30 minutes (fig. 292).

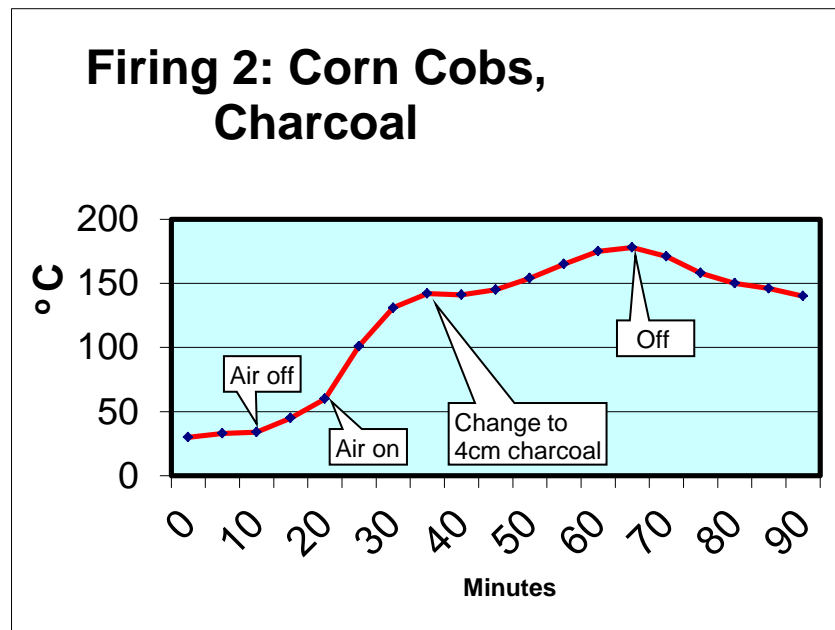


Figure 292: Corn cob and charcoal firing chart

Two processes related to the current project require temperatures of 200°C: the addition of decals to already-glazed ware, and the trial production of sodium silicate from RHA and sodium hydroxide. These two processes potentially could be performed by firing with gasified biomass in the manner described above, if a predominantly oxidising atmosphere is maintained.

### Producing sodium silicate from rice husk ash: Trial 1

Recycled glass containers were used to contain the RHA and commercially available sodium hydroxide, marketed as Drain Clear (fig. 293, overleaf). The process for producing sodium silicate from RHA involved preparing the kiln as shown in Figure 297. The kiln shelf split (fig. 298), so not all mixes were retained after firing.



**Figure 293: Equipment and materials for experimental production of sodium silicate**



**Figure 294: Mix 1: 30g RHA, 100ml Drain Clear, 50ml Water.**



**Figure 295: Mix 2: 30g RHA, 60ml Drain Clear, 90ml Water**



**Figure 296: Mix 3: 30g RHA, 60ml Drain Clear, 140ml Water**



**Figure 297: Three mixes ready for firing**



**Figure 298: Split kiln shelf, spilt mixes**

The sodium silicate produced should be analysed, and the experiment should be repeated using higher fired rice husk ash to remove the carbon. These procedures are out of scope of the current project, but could be the subject of further research.

## Chapter 15: Material Characterisation by X-ray Diffraction

One of the ways of finding out what sort of minerals may be contained in a substance is to employ X-ray Diffraction (XRD). This form of characterisation can be useful because materials with the same chemical composition may be made up of minerals, or phases of minerals, that respond differently to firing (for example quartz phases).

XRD does not provide an accurate quantitative analysis of the composition of a sample, for several reasons (Ling, 2009a). First, only crystalline structures are detected as peaks on the graph, so other materials such as carbon and glasses are omitted from quantification. Second, the search-and-match procedure involves matching the observed peaks with a database compiled from contributions, which may be incomplete. Third, the database presents preferred options and alternatives and the operator must make a visual determination of the proportion of the peaks accounted for by the nominated material, and select the best candidate from the database. To this end, knowledge gleaned from the literature about the class of substances under analysis, and knowledge of the provenance of the samples, is useful in guiding selection of the operator's preferred candidates.

Identification of crystalline structures within the clays and waste materials used was achieved via XRD (Ford, 1967). Neither glassy amorphous materials, nor colourants are identified through this process: in the former no crystals are present and in the latter the colouring agents are small chemical dopants (Ling, 2009a). However, 3D crystalline structures such as alumino-silicates and zeolites can be identified. The size of the crystals is inversely proportional to the width of the peaks on the diffraction graph, and this is more easily interpreted for homogenous substances (Ling, 2009a).

The materials were prepared by hand grinding in a ceramic mortar and pestle, to ensure both fine particle size and homogeneity of dispersion of the compounds of interest through the samples. XRD data were collected on a Panalytical X'Pert Pro diffractometer using Cu  $K\alpha$  (wavelength  $\lambda = 1.5401 \text{ \AA}$ )

radiation. Data were recorded on a PIXcel 2D detector over the range 5–80 °2 $\theta$  in 0.05 °2 $\theta$  steps, with the sample in Bragg-Brentano (flat plate reflection) geometry. The equipment was used courtesy of the Chemistry Department at the University of Sydney.



*Figure 299: Filling sample holders*



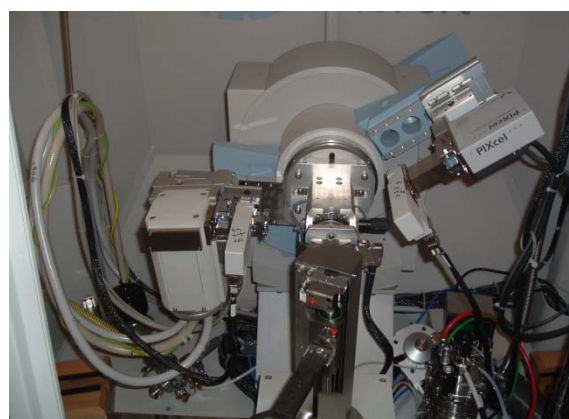
*Figure 300: Prepared sample holders*

Samples were placed into recesses on stainless steel sample holders that had been cleaned with ethanol. Using a glass slide, each sample was compressed to be level with the top of the sample holder, as required by the diffraction process (figs. 299 & 300).

The prepared sample holders were loaded into the rack (fig. 301), the doors were closed and the samples transferred to the sensor plate by a robotic arm (fig. 302).



*Figure 301: Loading samples into rack*



*Figure 302: PANalytical Xpert diffractometer*

The first samples to be analysed were the quarry tailings, which had the appearance of terracotta clays. As such, they were expected to be polymineral substances containing representatives from the silicates; including micas, illites,

kaolinites, chlorites, mixed layer phyllosilicates, feldspars, quartz, carbonates, iron oxide and organic matter (Konta, 1995).

The range of degrees appears as the x-axis on the sample charts shown in Figures 303–317. The y-axis scales the intensity of the diffraction peaks, which is related to the concentration of each crystalline phase in the sample (Brandt & Kinneging, 2005).

Crystalline materials identified by the first XRD search-and-match of Marulan tailings (fig. 303) were quartz, albite and a clay with inclusions of strontium and caesium. The presence of quartz is not surprising as the Marulan quarry tailings are washed from crushed porphyritic<sup>12</sup> rhyolite, the most silica-rich granite-like volcanic rock (Gunn, 1998). Rhyolite contains >66% silica and the balance is predominantly feldspar (Gunn, 1998), which explains the XRD match with albite; a sodium feldspar that frequently occurs in igneous rocks such as granite (Gunn, 1998). The strontium–caesium tecto-alumino-silicate listed was the best match obtained, but a number of similar alumino-silicates were also possible. Accordingly, with the assistance of Ling (2013) the analysis was repeated (see fig. 304). The best match semi-quantitative analysis was quartz 21%, calcite 5%, albite 31%, muscovite 30% and roedderite 13%. Muscovite has the chemical formula  $KAl_2(Si_3Al)O_{10}(OH,F)_2$  and is known as potash mica (Barthelmy, 2010a). Roederrite typically contains 2.28%  $K_2O$ , 4.50%  $Na_2O$ , 14.65%  $MgO$ , 8.70%  $FeO$  and 69.87%  $SiO_2$  (Barthelmy, 2010b) and has been found as inclusions in rhyolite (Petrov, 2005).

XRD of the tailings from the Bungendore sand mine (fig. 305) produced patterns that indicated approximately equal levels of quartz and clay, tentatively identified in the latter case as phengite, an iron-rich alumino-silicate. The iron content is evident in the raw sample, which has colouration similar to yellow iron oxide. The preferred match of the quartz in the XRD database is listed as *quartz low, syn* (with *low* referring to the polymorph alpha quartz that is stable below 573°C (Akhavan, 2005) and *syn* being an abbreviation for synthetic). The quartz crystal in the sample closely matches that obtained by synthetic means. The

---

<sup>12</sup> [i.e. having two distinct crystal sizes ( Nelson, 2004)]

Bungendore tailings diffraction analysis was repeated (fig. 306). A semi-quantitative analysis identified the components as quartz 32%, albite 8% and muscovite 60%.

Boral Dunmore dust was analysed by Whitfield (1993) and described as latite by Dimitru (2008) and as olivine latite or trachyandesite by McMeekin (1985). The initial XRD match for Dunmore latite (fig. 307) was with anorthoclase and an un-named synthetic zeolite. Anorthoclase combines sodium and potassium to form a mixed feldspar, an intermediate classification that distinguishes it from albite (which has >90% sodium feldspar) and orthoclase (which has >90% potassium feldspar) (Hamer, 1975). The XRD database search preferentially matched a synthetic calcium-alumina-silicate zeolite. Further analysis is required to determine if the naturally occurring mineral present is indeed a zeolite (a hydrous framework silicate) or is in fact trachyandesite. Other possibilities include prehnite (a hydrous calcium-aluminium di-octahedral mica of formula  $\text{Ca}_2\text{Al}_2\text{Si}_3\text{O}_{10}(\text{OH})_2$ ; Mineral Data Publishing, 2001), and various other sheet silicates among the micas and smectites.

Perlite is non-crystalline in structure, containing ~0.1% quartz (Australian Vermiculite & Perlite Pty. Ltd., 2004). The lack of crystalline diffraction peaks produced by perlite cold bag house fines (fig. 308) indicates that as expected, this material is almost totally amorphous, being the dust from volcanic glass particles that have been reheated to >870°C. The particles have undergone 4–20-fold volumetric expansion due to formation of minute air-filled glass bubbles (Incon, 1996). Percentage analysis has been provided by Whitfield (1993).

There are almost identical diffraction patterns for the bagasse ash taken from the conveyor belts at different boilers in the sugar mill, and fired to 800°C, indicating that both materials contain silica as 100% of the crystalline component of the samples (figs. 309 & 310). The grey-to-brown colour of the samples indicates the presence of other chemicals, as would be expected in view of the data provided in other research, and further analysis is required to ascertain their identities.

The paucity of crystalline diffraction peaks produced by RHA fired to 800°C (fig. 311) indicates that this material is predominantly amorphous, with a small crystalline component.

The diffraction peaks obtained from corn seeder sludge fired to 800°C (fig. 312) most closely match the cristobalite phase of silica and a synthetic compound named erionite. The match with synthetic erionite is probably caused by the chemical composition, combined with the likely presence of particles in the nanometre size range, resulting from the organic process by which the plant draws mineral nutrients from the ground (Ling, 2009b). Further analysis is required to accurately characterise this ash, especially as there are potential benefits and dangers associated with its use. The potential benefits arise from the presence of alkalis and cristobalite: the alkalis will contribute a useful fluxing effect, while cristobalite has a high coefficient of thermal expansion (Barsoum, 1997) and is added to earthenware bodies to counteract crazing (Hamer, 1975). The potential dangers are from cristobalite, which is a respirable dust, and from any compound that has a similar crystal formation to erionite. Although erionite is unregulated, there is concern in the USA that it may be associated with increased risks of fibrogenic lung disease (North Dakota Department of Health, 2005).

Arumpo Pty Ltd (2005) provided the typical mineralogical composition of Arumpo bentonite as montmorillonite 96%, quartz 3% and anatase 1%. Anatase is natural titanium dioxide (Hamer, 1975). Although titanium dioxide is not identified, the XRD (fig. 313) otherwise matches that composition and accords with the results of the thorough characterisation (fig. 314) performed by Churchman and colleagues (2002) who concluded that 'Arumpo bentonite is largely composed of smectite interstratified with illite' (Churchman et al., p. 208).

The XRD peaks obtained from English bentonite (fig. 315) matched quartz, two sodium montmorillonites and a mixed potassium-sodium-aluminium smectite, which accords with the expected mineralogy of a clay sold as bentonite and with the percentage analysis provided by the retailer (Bath Potters Supplies, 2003) (Table 38).

The compounds listed as matching the XRD peaks obtained from Australian bentonite accounted for all of the chemical analysis in Figure 316, with the exception of iron oxide (which is not reflected) and calcium and potassium, which are both <1% by weight. Australian bentonite was sourced from NSW Pottery Supplies, who buy in bulk from Unimin Australia Ltd. The latter provided a typical chemical analysis of 'ActiveGel' Australian bentonite (Table 39)—'an activated sodium bentonite with high montmorillonite and low grit content' (Unimin Australia Ltd, 2002).

XRD of corn cob ash fired at 800°C for one hour produced peaks that matched with quartz and two phosphates high in potassium and sodium (fig. 317). The XRD analysis of corn seeper sludge suggested that the quartz is most likely to be the cristobalite phase (fig.312). Adesanya and Raheem's (2009) analysis of Nigerian corn cob ash identified aluminium, calcium and magnesium, so further investigation of this sample for the presence of these chemicals is warranted.



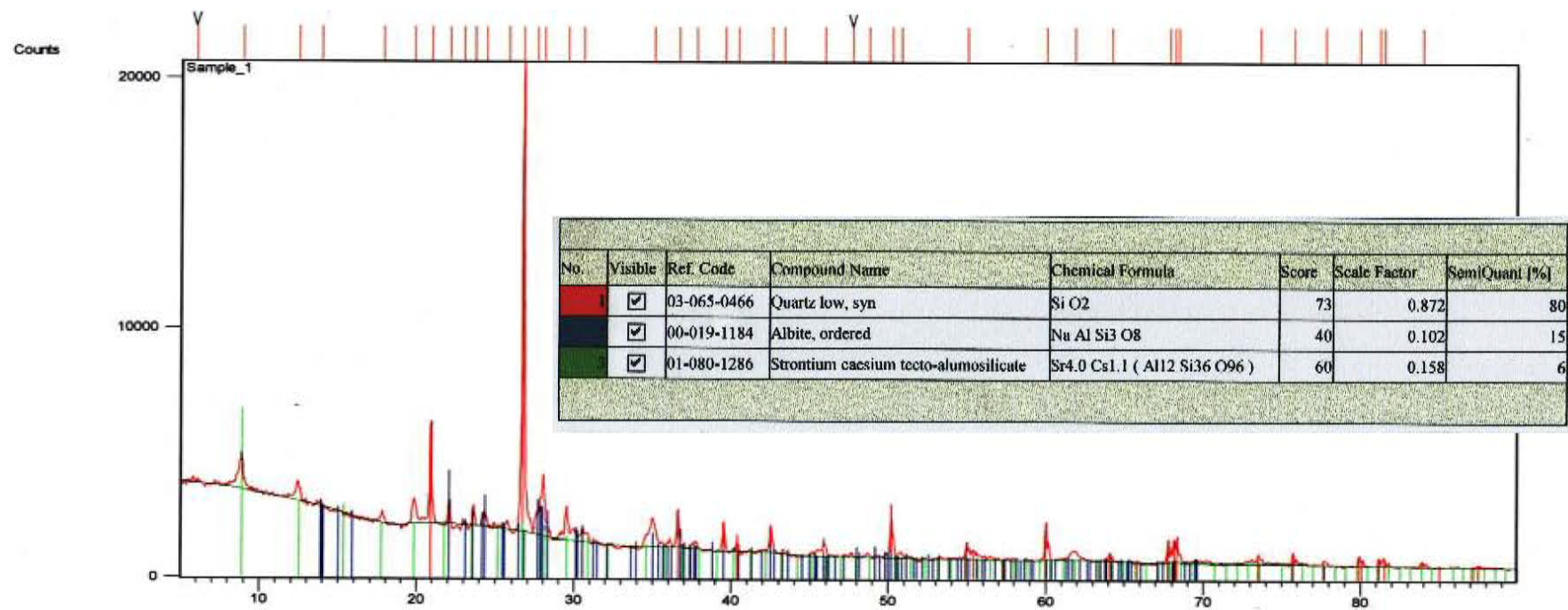


Figure 303: XRD chart: Marulan tailings

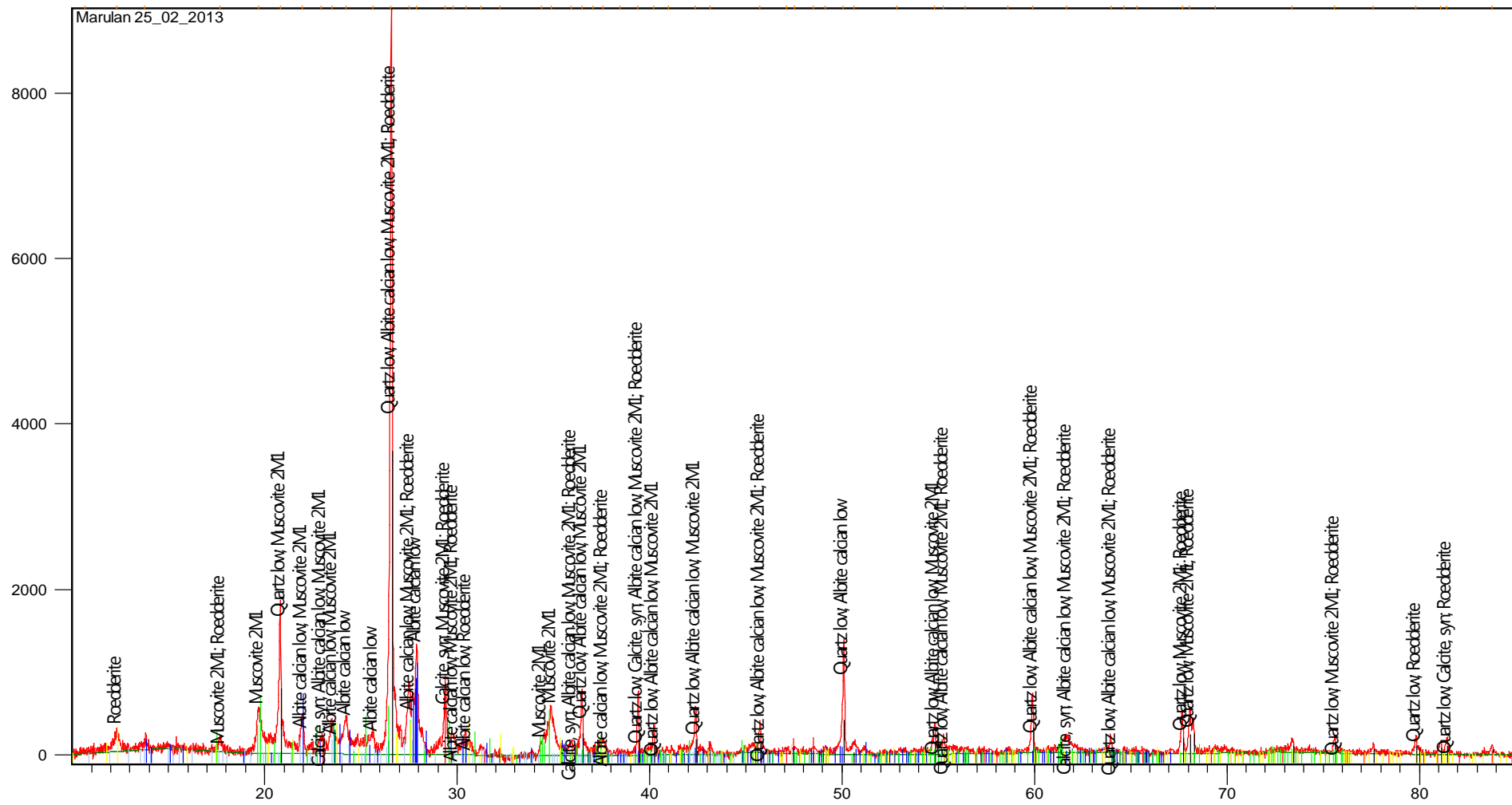


Figure 304: XRD chart: Marulan tailings (re-test)

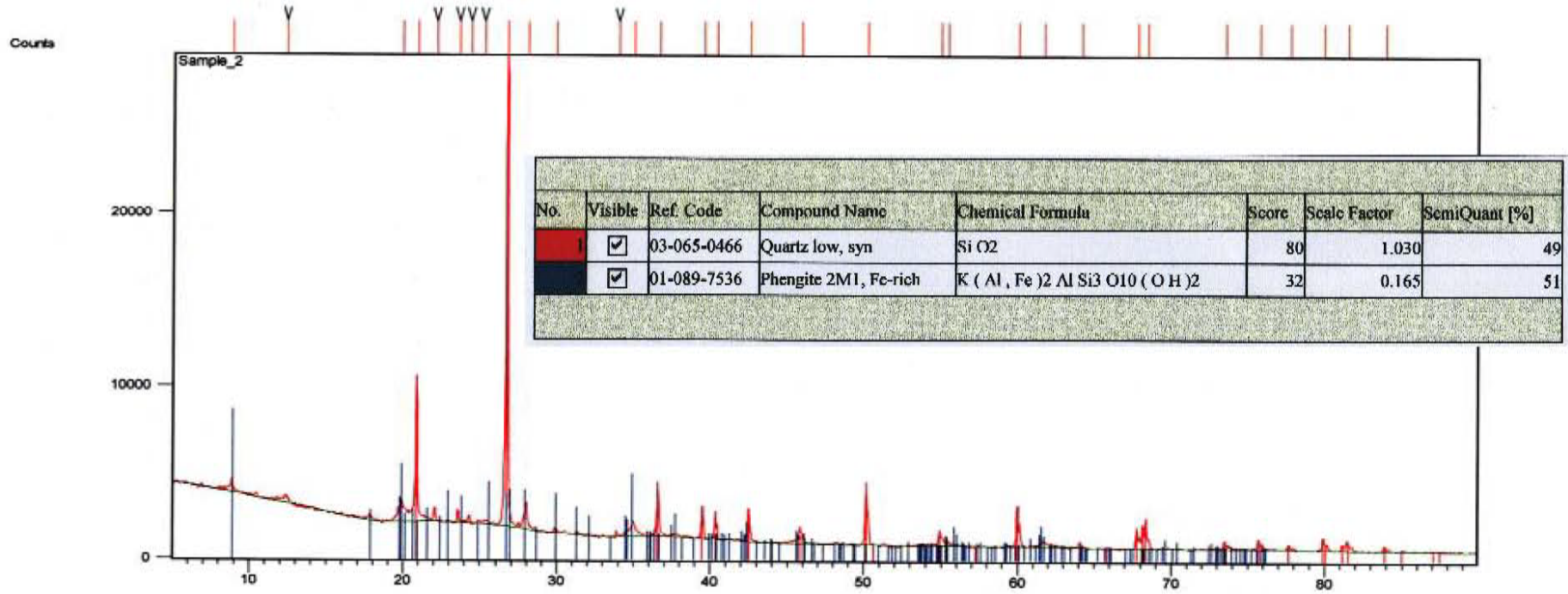


Figure 305: XRD chart: Bungendore tailings

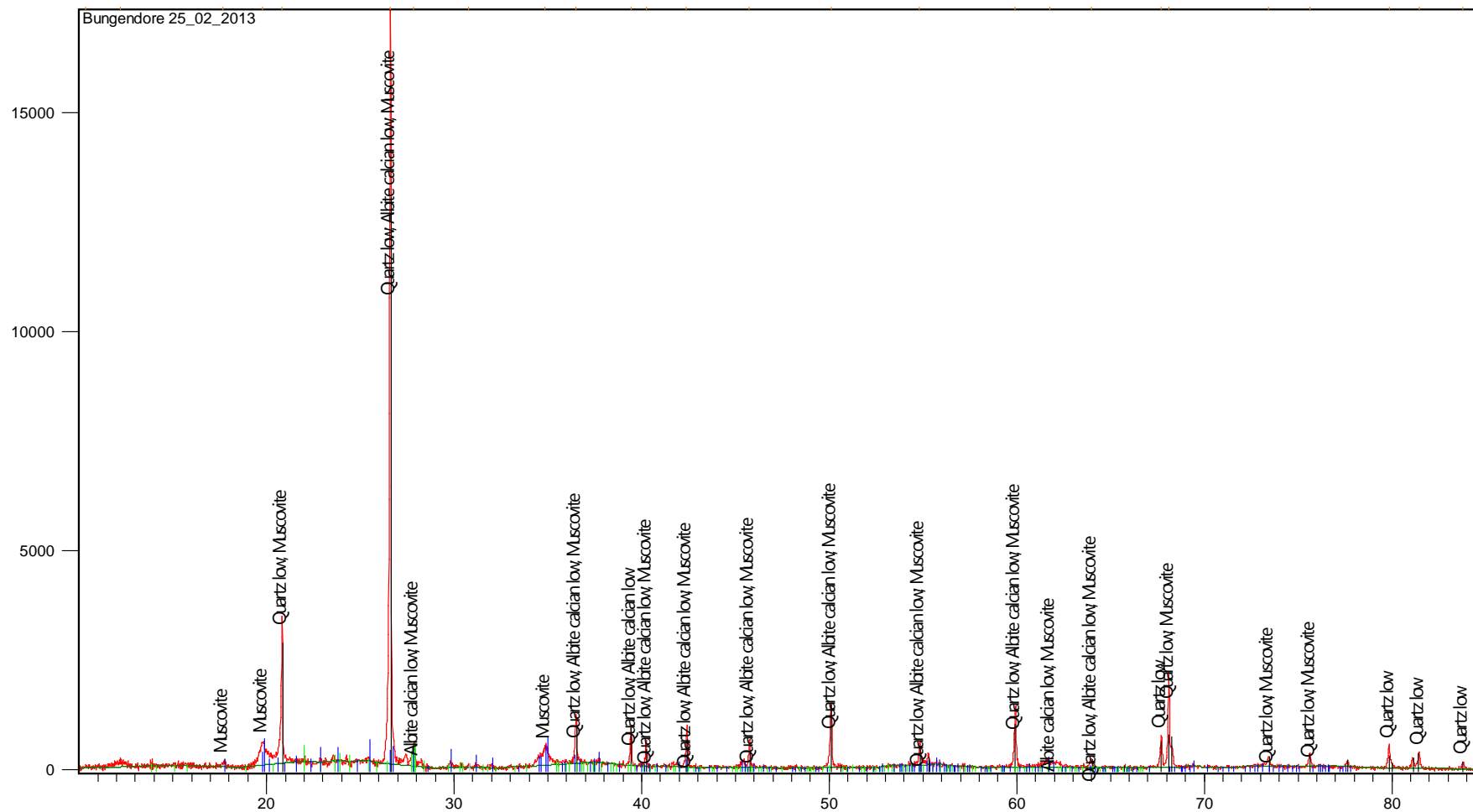


Figure 306: XRD chart: Bungendore tailings (re-test)

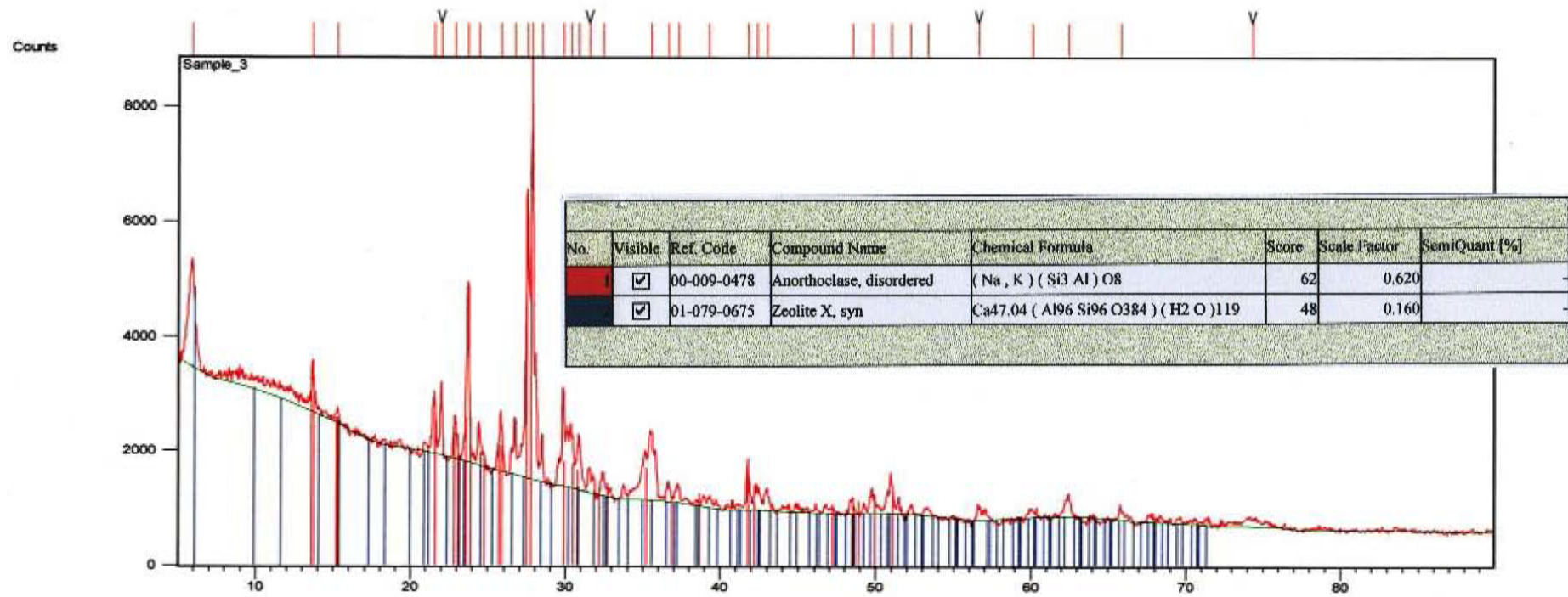


Figure 307: XRD chart: Dunmore latite

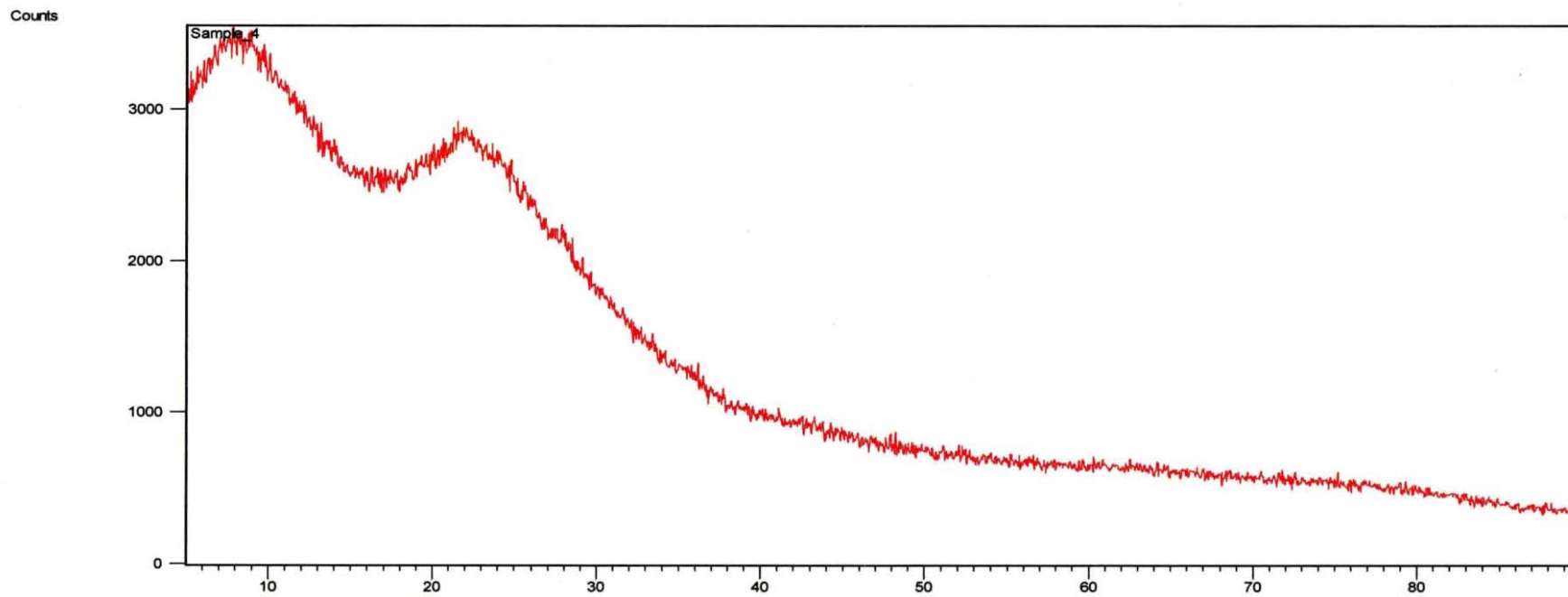


Figure 308: XRD chart: Perlite CBHF AP10 (white)

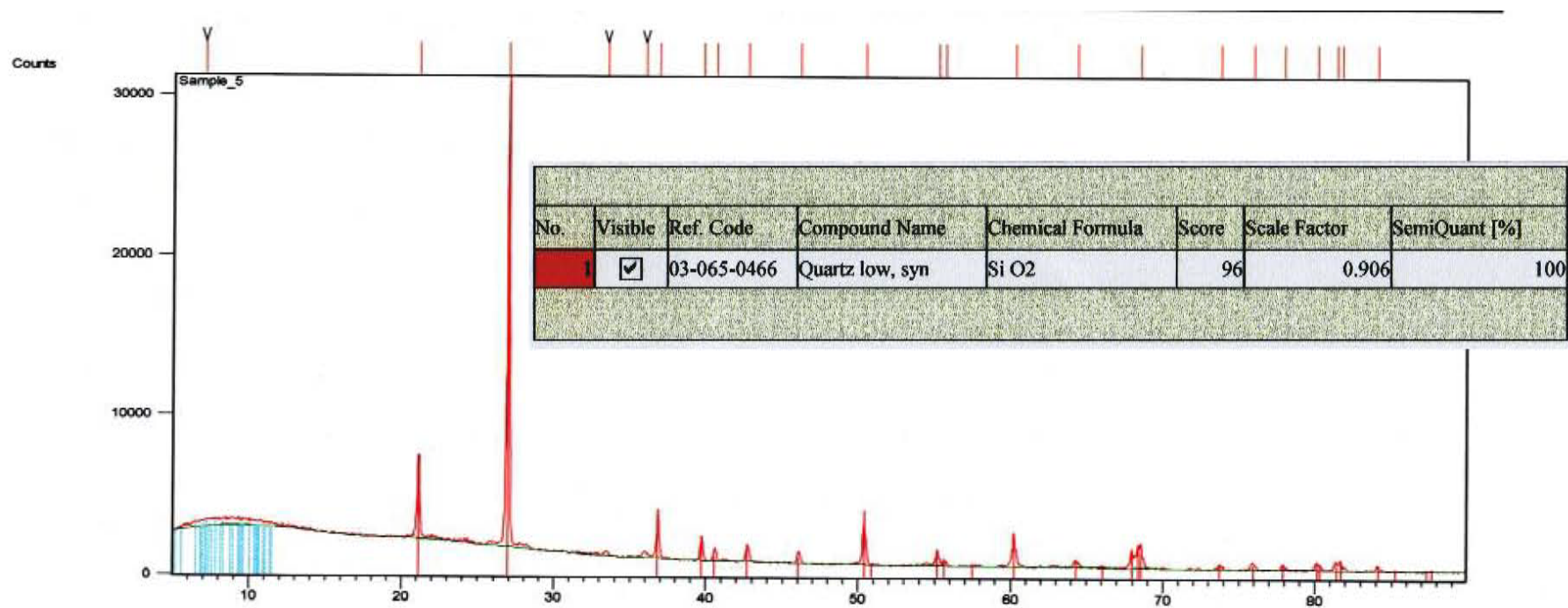


Figure 309: XRD chart: #12 boiler belt ash (1 hour at 800°C)

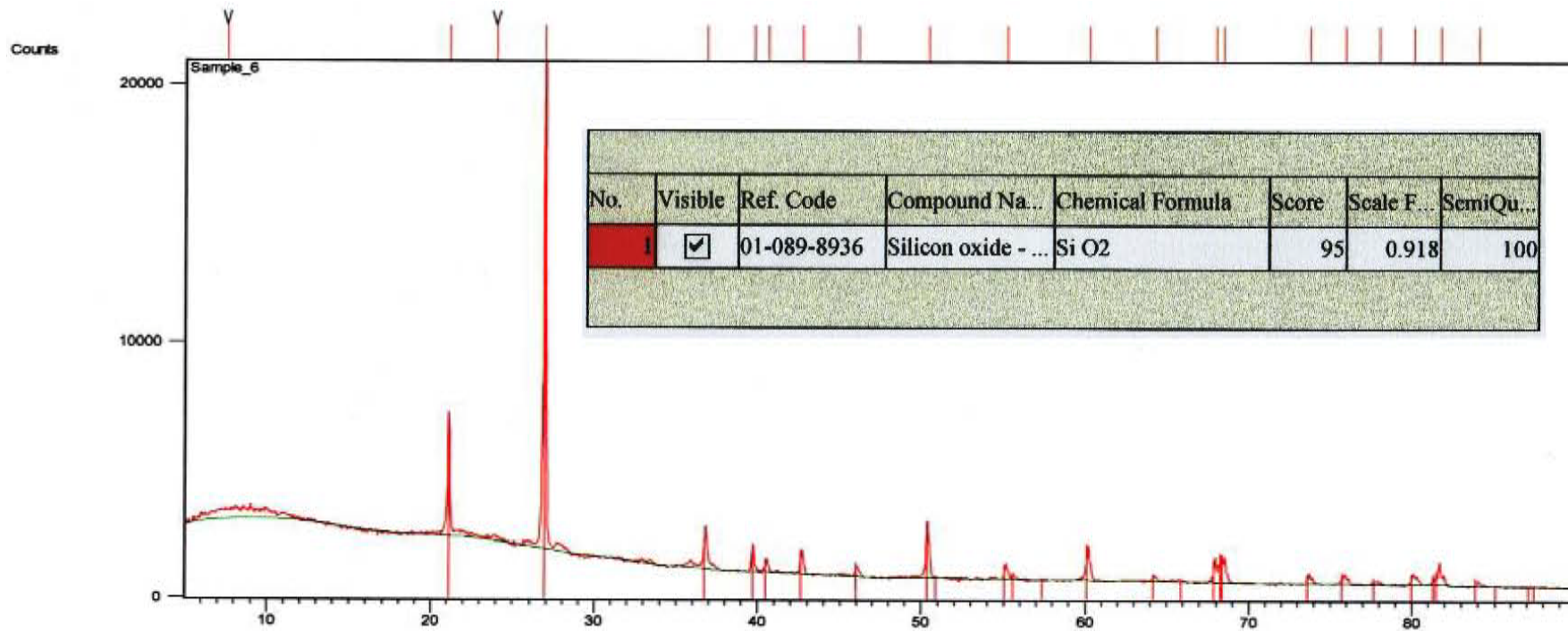
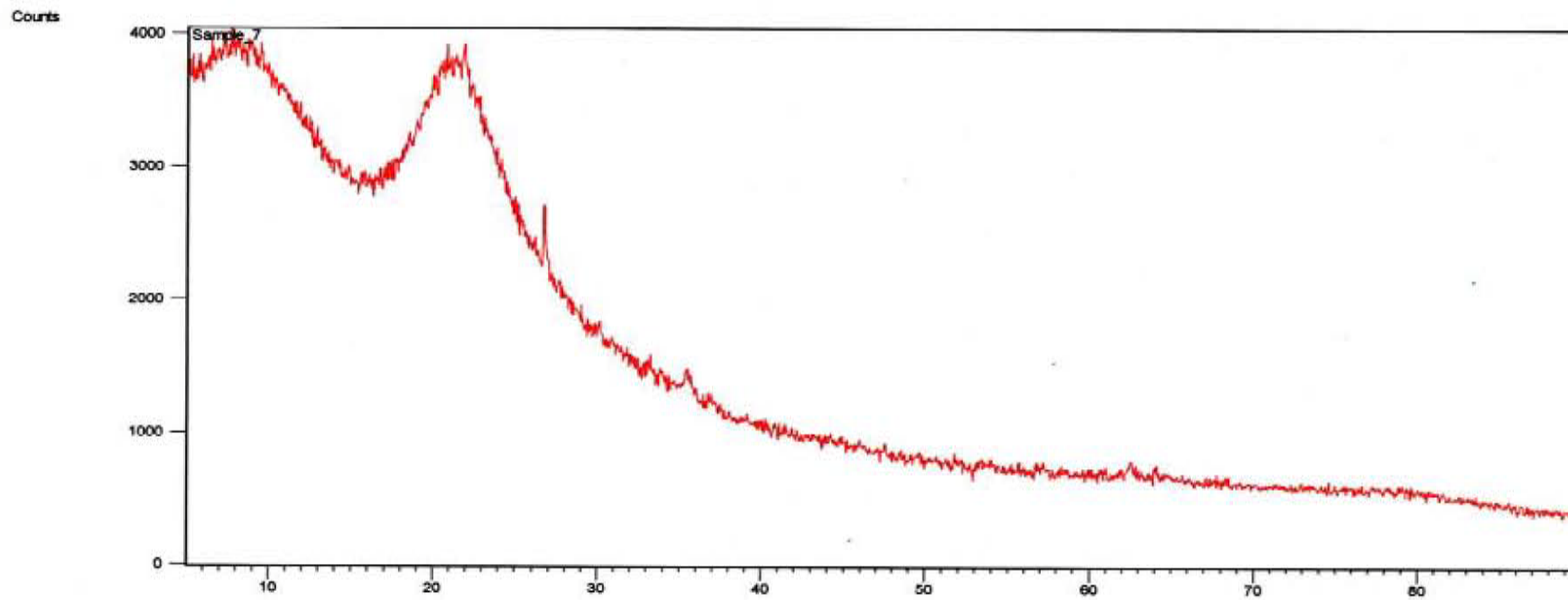


Figure 310: XRD chart: #1 boiler belt ash (1 hour at 800°C)





*Figure 311: XRD chart: RHA (1 hour at 800°C)*

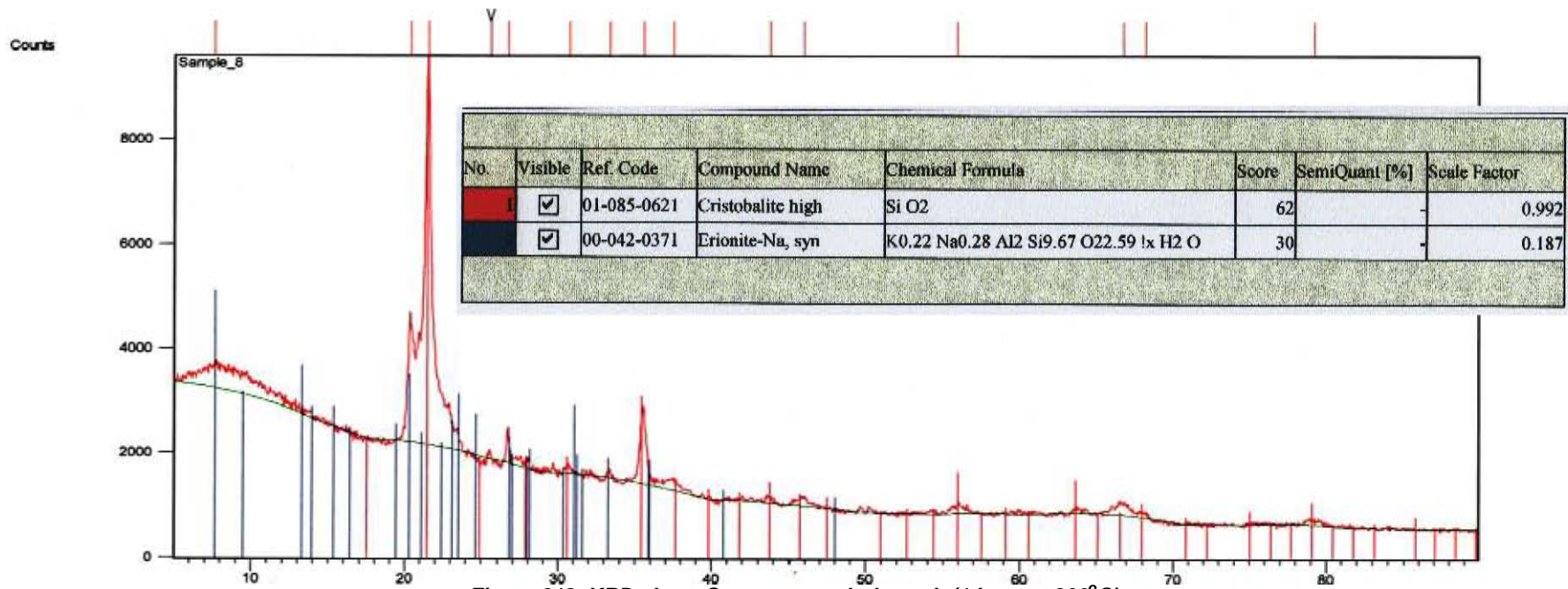


Figure 312: XRD chart: Corn seeper sludge ash (1 hour at 800°C)

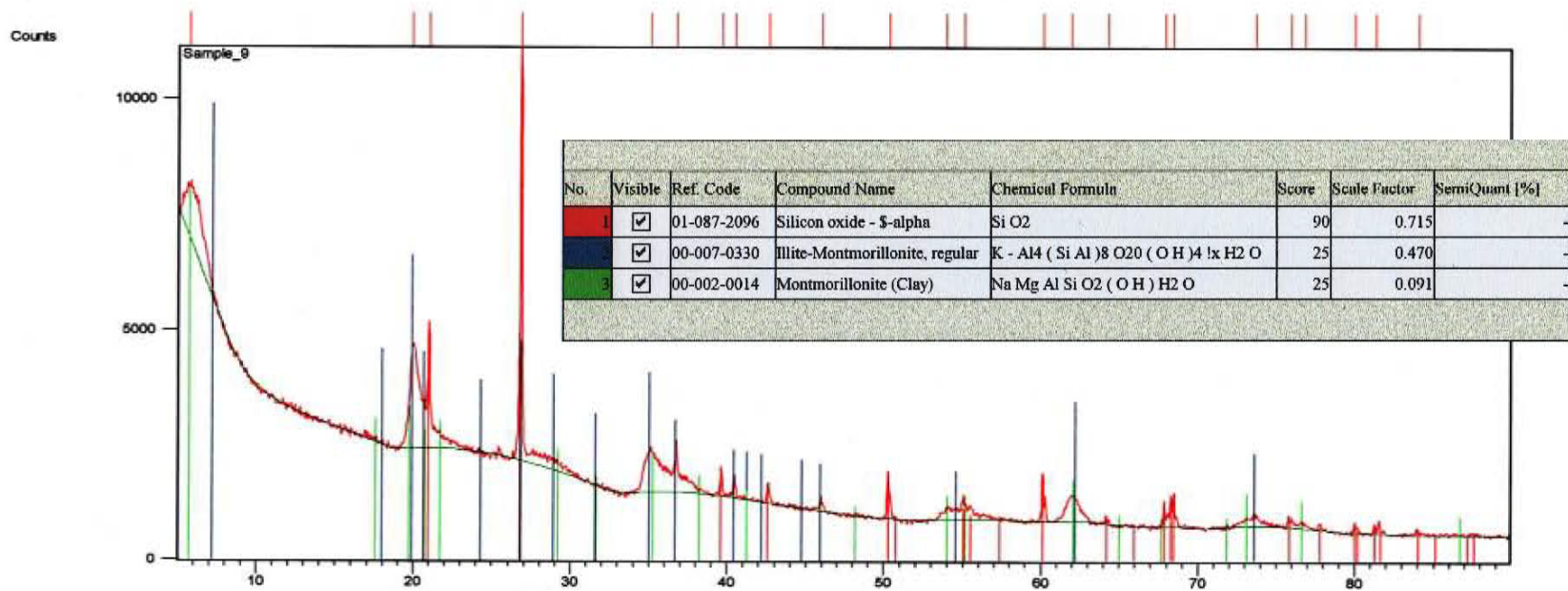


Figure 313: XRD chart: Arumpo bentonite

Sample	Composition (%)			Exchangeable cations (cmol(+) kg <sup>-1</sup> )			EC (mS m <sup>-1</sup> ) (1:5)
	Smectite <sup>a</sup>	Quartz	K <sub>2</sub> O	Mg	Na	CEC	
Arumpo E (E3.80–4.70 m)	>99	0	0.71	55.5	37.0	100	271
Arumpo W (W3.66–4.86 m)	99	0	0.70	44.7	40.7	87	279

Figure 314: Mineralogical and chemical properties of two samples of Arumpo bentonite

Reproduced and adapted from Churchman et al. (2002 p. 204)

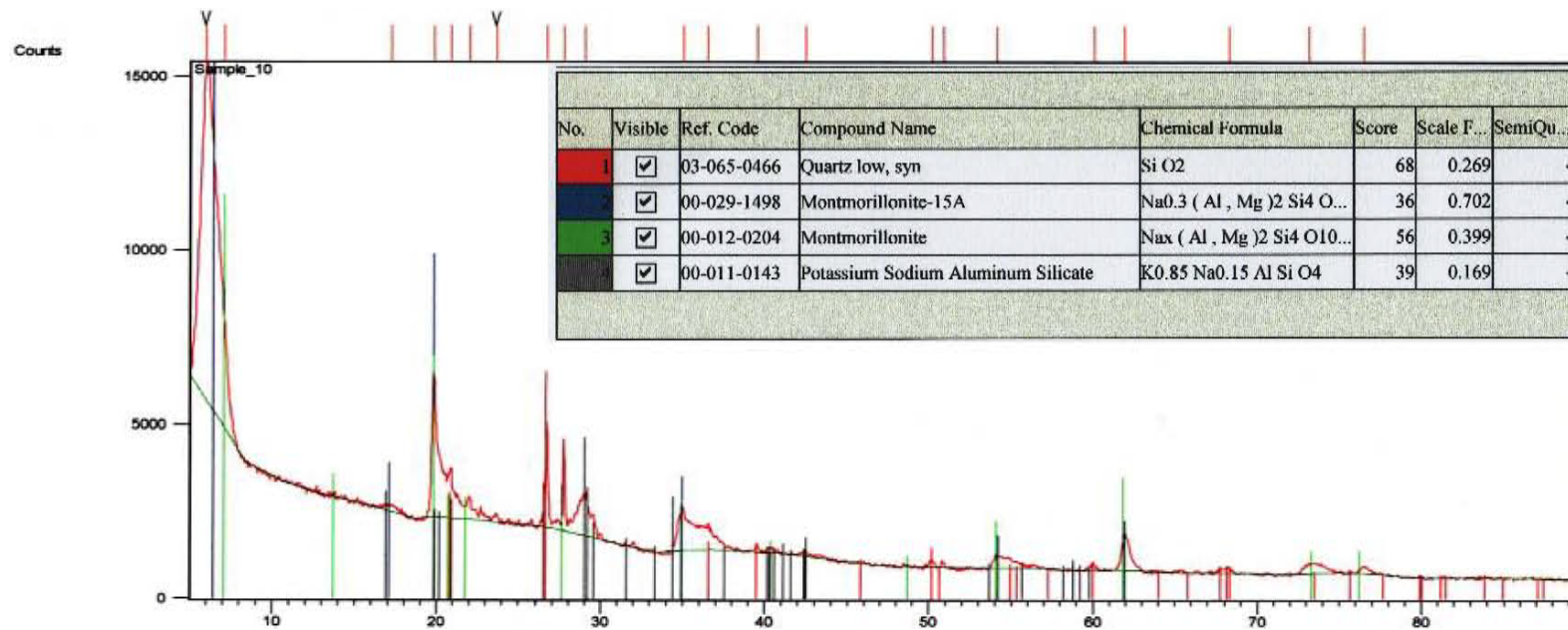


Figure 315: XRD chart: English bentonite

Table 38: Percentage analysis of English bentonite

	SiO <sub>2</sub>	Al <sub>2</sub> O <sub>3</sub>	Fe <sub>2</sub> O <sub>3</sub>	CaO	MgO	K <sub>2</sub> O	Na <sub>2</sub> O	LOI
<b>(wt%)</b>	56.0	16.0	4.6	0.9	3.3	0.4	2.9	5.7

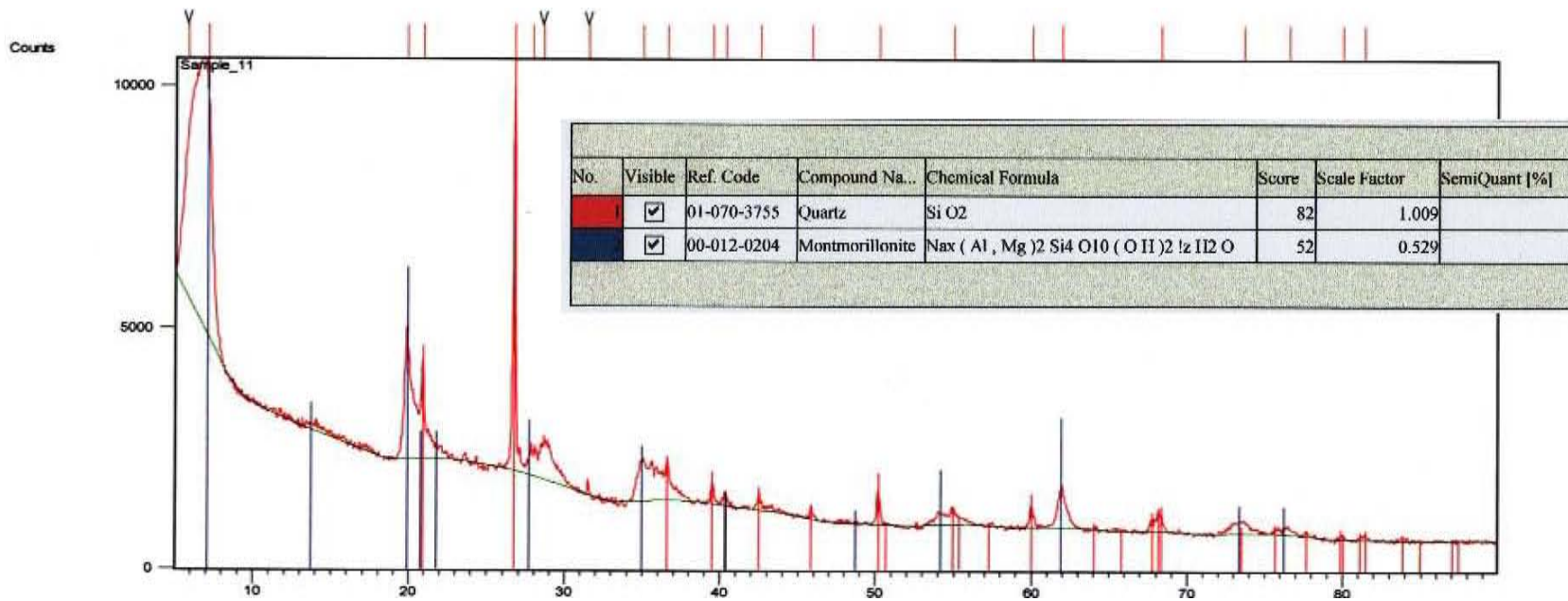


Figure 316: XRD chart: Australian bentonite

Table 39: Typical chemical composition of Australian bentonite

	SiO <sub>2</sub>	Al <sub>2</sub> O <sub>3</sub>	Fe <sub>2</sub> O <sub>3</sub>	CaO	MgO	K <sub>2</sub> O	Na <sub>2</sub> O	LOI <sup>13</sup>
<b>(wt%)</b>	56.00	20.00	4.00	0.49	2.49	0.60	2.76	13.66

<sup>13</sup> LOI is loss on ignition: the percentage weight of water and organic matter that is lost when the material is heated to 750 or 950°C [ASTM International (2006b)].

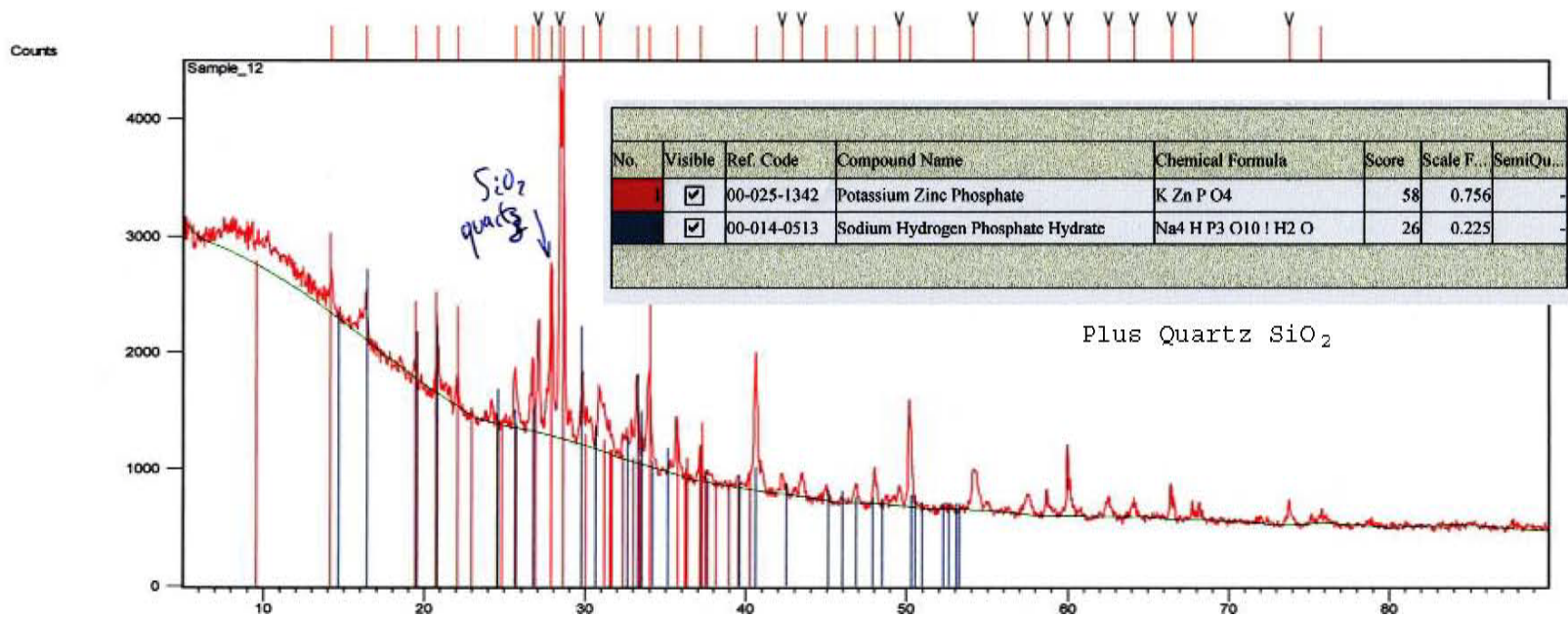


Figure 317: XRD chart: Corn cob ash (1 hour at 800°C)

As mentioned at the beginning of this chapter, XRD does not provide a quantitative analysis of the oxides present in a material. That analysis is provided as a typical percentage analysis, as detailed in Chapter 16.

## Chapter 16: Typical Percentage Analysis of Recovered Materials

It is very useful to obtain a percentage analysis of the oxides present in any material that is being used in ceramics, because this information provides insights into the likely contribution of a material to sintering, facilitates substitution of one material for another, and allows calculations of formulae in a format that is internationally standardised. This standardisation enables independent comparison of formulae despite there being different materials contributing the constituent oxides.

Samples of the collected waste materials were sent to Australian Laboratory Services (ALS) in Brisbane, Australia for analysis (see Table 40). The laboratory provided the following verbal explanation of the level of accuracy of the results:

*The total calculation has a number of assumptions. It does have some inaccuracies, taking into account the loss on ignition. The total calculation is the sum of 24 analytes expressed in the oxides. It normally has an accuracy of  $\pm 0.5\%$ . This form of analysis is a general-purpose analysis and is not specific to any ore type. Perhaps with the sodium, there is a little more error and the calibration only goes to 8%. Acceptable quality control would normally provide totals between 98 and 102%.*

(McCann, B., pers. comm., 2011)

The results from the ALS analysis were entered into the *Matrix* glaze calculation software (Ewing, 2000). The analysis of recycled materials is displayed in oxide percentage format (Table 40).

Entry of these typical percentage analyses into *Matrix* enabled estimation of the COE and melting temperatures of glazes including these recovered materials, and *post hoc* calculation of percentage analyses and Seger formulae for selected glaze, engobe and body tests, as shown in the following chapters.

**Table 40: Percentage analyses of recovered materials**

	KNO	CaO	MgO	BaO	ZnO	PbO	Li2O	SrO	Al2O3	B2O3	P2O5	SiO2	TiO2	ZrO2	K2O	Na2O	Fe2O3
Marulan tailings	6.120	3.040	0.720	0.120					17.650		0.070	61.300	0.300		4.230	1.890	4.490
Bungendore Tailings	2.680	0.630	1.020	0.040				0.010	16.800		0.070	66.300	0.770		1.970	0.710	5.450
Dunmore Latite	7.810	6.410	3.210	0.080				0.090	17.150		0.750	54.100	0.930		3.980	3.830	7.820
Perlite AP10 White CBHF	7.920	0.820	0.250	0.180				0.020	13.200		0.020	74.300	0.120		4.640	3.280	0.810
Corn Seeper sludge calcine	5.130	1.080	0.620	0.030				0.010	42.800		32.700	9.800	0.150		2.510	2.620	5.080
Bagasse Ash #12BB 900calci	1.870	1.160	1.200	0.030				0.010	5.880		1.130	81.500	1.850		1.620	0.250	4.110
Perlite AP10 Grey CBH Fine	8.580	0.540	0.080	0.020					12.650		0.020	74.200	0.140		5.480	3.100	1.340
Perlite unexpanded ore grey	8.280	0.610	0.100	0.020				0.010	12.450		0.030	72.400	0.170		5.250	3.030	1.620
Unimin Cullet 375	13.950	8.720	3.880	0.010				0.010	0.440		0.020	70.300	0.040		0.100	13.850	0.600
Visy Banksmeadow Cullet du	13.780	11.100	0.600	0.030				0.020	1.540		0.020	70.400	0.070		0.430	13.350	0.840
Corn Cob Ash calcined 900	17.690	0.920	4.660	0.010				0.010	0.830		13.000	30.100	0.080		17.100	0.590	27.400
Bagasse Ash #1BB 700calci	2.430	1.180	1.350	0.030				0.010	6.810		1.330	78.100	1.450		2.030	0.400	4.220
Bagasse Ash #1BB 900calci	2.380	1.170	1.340	0.030				0.020	7.630		1.260	80.500	1.450		1.980	0.400	4.110
Rice Husk Ash 800calcined	2.120	0.400	0.240	0.010					0.220		0.390	85.700	0.010		2.070	0.050	2.930



## Chapter 17: Surface Effects: Glaze, slip and engobe tests

In addition to using collected waste materials to develop clay bodies, it was of interest to establish whether these bodies would accept surface coatings, and whether the collected waste materials themselves could be used for surface coatings.

The three most common ceramic surface coatings are glazes, slips and engobes. These terms are defined below.

A *glaze* is 'a layer of glass which is fused into place on a pottery body' (Hamer, 1975, p. 144). Glaze is made of ground minerals in a liquid suspension that will melt when fired at sufficiently high temperatures.

A *slip* is 'a homogenous mixture of clay and water' (Hamer, 1975, p. 274).

An *engobe* can be thought of as a form of surface covering intermediate between a slip and a glaze:

*Engobe is a term of wide meaning often interchangeable with slip but including other materials. An engobe is used to cover clay, produce a buffer layer and give a different surface, texture and colour. It is often halfway between a clay and a glaze in composition and contains materials that are normally considered glaze materials.*

(Hamer, 1975, p. 112)

The first step was to test whether a body made of equal parts Bungendore and Marulan tailings (BM1.13) would accept surface coating. First, a commercially available engobe and a commercially available slip were used to determine if a white surface could be obtained. The engobe was Walker's WEW white earthenware engobe. The slip was Walker's CB1 white earthenware casting slip, with a firing range specified as 1000–1060°C. The WEW engobe and CB1 slip were applied to BM1.13 that had been bisque fired. Both adhered well, before and after firing to 950°C (figs. 318 & 319).



*Figure 318: WEW engobe applied to BM1.13 bisque and fired to 950°C (unglazed)*

*Figure 319: CB1 slip applied to BM1.13 bisque and fired to 950°C (unglazed)*

The next step was to determine whether engobes and glazes could be generated from two triaxials previously used for body tests. Triaxials BM1 and BM2 were used, as detailed below.

### **Triaxials BM1 and BM2: Engobe and glaze tests**

Triaxials BM1 and BM2 were also applied to bisque-fired Keanes' Stoneware No 7 clay. The liquid samples were applied with a loaded brush, onto triangular tiles impressed to receive a 15-part triaxial. The tiles were fired to 900°C using the standard firing cycle.

After firing triaxial BM1 to 900°C (cone 010), inspection revealed a number of possibilities for engobes, including vitreous (glaze-like) engobes and engobes with a range of colours from pale tan to umber (fig. 320, overleaf). The samples on Tier 5 contained only clay, and are therefore classified as slips rather than engobes. These slips did not adhere well to the bisque-fired stoneware body.



Figure 320: BM1 Triaxial fired to 900°C

Perhaps the most promising engobe from triaxial BM1 was produced using sample BM1.2. The description and batch recipe appear below.

Cone 010 vitreous engobe

Sample BM1.2 produced a pale-coloured vitreous engobe that was smooth to the touch and adhered well to the bisque-fired stoneware clay. This engobe contained 55%-recycled materials, including cullet and tailings:

	(wt%)	
Gerstley borate	37.5	
Unimin cullet	30.0	
Bungendore tailings	25.0	
Lithium carbonate	7.5	
Matrix-estimated melting point	1021°C	
COE	10.6	
Fe <sub>2</sub> O <sub>3</sub> (wt%)	1.0	

Triaxial BM2 also was applied to a bisque-fired stoneware clay tile, and fired to 900°C. After firing triaxial BM2 to 900°C (cone 010), inspection revealed few possibilities for engobes, but some potential glazes towards corner A (fig. 321).



*Figure 321: BM2 Triaxial fired to 900°C*

Although BM2.2 displayed some impurities due to specks of undissolved clay, it was glossy and otherwise transparent, and thus was selected for further tests as documented below.







## Glaze tests at 900°C

BM2.2 was the fluid clear glaze obtained from the triaxial BM2. The batch recipe was modified as BM2.2B (see Table 41) to increase the content of tailings at the expense of flux materials.



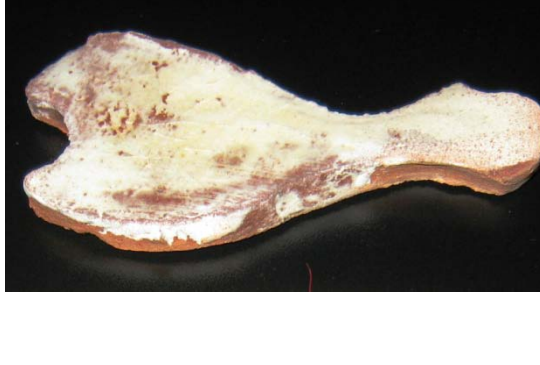



*Table 41: Batch recipes for glazes BM2.2 and BM2.2B*

	<b>BM2.2</b>	<b>BM2.2B</b>
	<b>(wt%)</b>	<b>(wt%)</b>
Lithium carbonate	7.50	6.90
Pearl ash	18.75	17.20
Borax	7.50	6.90
Soda ash	26.25	24.00
Unimin cullet	15.00	13.70
Bungendore tailings	25.00	31.30







Both glazes were applied to raw and bisque clay, and to raw or bisque white engobe or slip, before being fired to 900°C. The engobe was Walker's WEW white earthenware engobe. The slip was Walker's CB1 white earthenware casting slip. The two bodies used were BM1.13 (equal parts of Bungendore and Marulan tailings) and Walker's white raku clay. The images in Figures 322–325 illustrate the results, including the extent of crazing evident on all samples.

BM2.2 glaze applied to raw BM1.13	Detail
	
BM2.2 glaze applied to 800 bisque BM1.13	Detail
	
BM2.2 glaze over raw WEW Engobe applied to 800 bisque BM1.13	Detail
	

**Figure 322: Glaze BM2.2 applied to raw and bisque BM1.13, and over engobe, fired to 900°C**




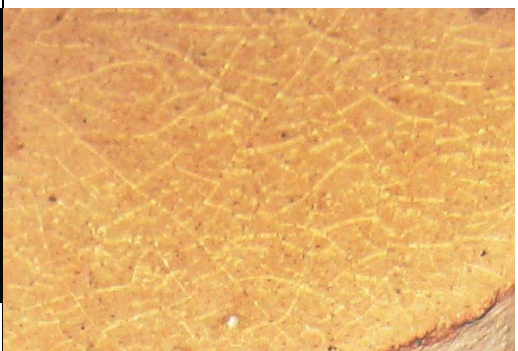
<p>BM2.2 glaze over 950°C bisque-fired WEW Engobe (applied raw to 800°C bisque BM1.13)</p>	<p>Detail</p>
	
<p>BM2.2 glaze over raw CB1 slip applied to 800°C bisque BM1.13</p>	<p>Detail</p>
	
<p>BM2.2 glaze over 950°C bisque-fired CB1 slip (applied raw to 800°C bisque BM1.13)</p>	<p>Detail</p>
	

**Figure 323: Glaze BM2.2 applied to bisque BM1.13, and over raw and bisque engobe, fired to 900°C**

BM2.2b glaze applied to raw BM1.13	Detail
	
BM2.2b glaze applied to 800°C bisque BM1.13	Detail
	
BM2.2b glaze over 950°C bisque-fired WEW Engobe (applied raw to 800°C bisque BM1.13)	Detail
	

**Figure 324: Glaze BM2.2B applied to raw and bisque BM1.13, and over engobe, fired to 900°C**



BM2.2B glaze over 950°C bisqued CB1 slip (applied raw to 800°C bisque BM1.13)	Detail
	
BM2.2B glaze over 800°C bisque WWR	Detail
	

**Figure 325: Glaze BM2.2B applied to high bisque BM1.13 with engobe, and to Walker's white raku body, and fired to 900°C**

These results indicated that:

- BM2.2b, containing 45% recycled materials, made a serviceable glaze at 900°C.
- Under BM2.2b, WEW engobe appeared whiter than CB1 slip.
- Body and/or glaze adjustments were required to eliminate crazing.
- Application of engobes and glazes to raw BM1.13 body did not produce additional glaze defects.
- Further investigation of raw glazing on more complex forms is warranted.

Glaze BM2.2 was applied to bowls made from Bungendore tailings (BM1.1), and mixed Marulan and Bungendore tailings (BM1.13). Both bowls were fired to 900°C, after which they were filled with water and left to stand overnight. High porosity is evident from the seepage occurring (fig. 326).



*Figure 326: BM2.2 glaze on 800°C bisque BM1.13 bowl, seeping after being fired to 900°C, filled with water, and left to stand overnight*

It was obvious that covering the body with glaze did not make the body impervious to water when fired to only 900°C, and so further and larger-scale tests of fluxed bodies was needed. Those tests were conducted following investigation of further possibilities for low-fire engobes reformulated using waste materials.

### **Reformulating engobes using waste materials**

Rhodes (1973, p. 252) provided recipes for a white engobe to be fired between cone 08 and cone 1. This was used as a basis from which to develop engobes for use in NSW. Batch recipes for these were developed using materials available in NSW, including recovered materials (Table 42).

**Table 42: White engobe batch recipe conversions**

Rhodes' material appears on the left. The centre three columns show the percentage by weight for application to damp, dry and bisque-fired clay. The NSW materials appear at the right of the batch recipes. Also shown are coefficients of expansion (COE), estimated melting temperatures and percentages of iron oxides for each engobe

Rhodes ingredients	for application to:			NSW ingredients
	Damp	Dry	Bisque	
	(wt%)	(wt%)	(wt%)	
Kaolin	25	15	5	Eckalite 2
Ball clay	25	15	15	Marulan tailings
Calcined kaolin		20	20	Calcined Eckalite 2
Leadless frit	15	15	15	Unimin cullet 150 µm
Talc	5	5	15	Talc Plustalc N275
Silica (300 mesh)	20	20	20	RHA (800°C)
Zircopax	5	5	5	Zircopax
Borax	5	5	5	Borax
COE	8.47	8.44	7.78	COE
Matrix-estimated melting point (°C)	1339	1358	1291	Matrix-estimated melting point (°C)
Fe <sub>2</sub> O <sub>3</sub> (wt%)	0.07	0.05	0.03	Fe <sub>2</sub> O <sub>3</sub> (wt%)

Adapted from Rhodes (1973) p. 252

## Vitreous engobes

Rhodes (1973, p.253) defined a vitreous engobe as:

*An engobe which has a very low shrinkage because of the small amount of plastic clay in it, and which matures to a dense opaque coating over the ware.*

A number of potential vitreous engobe recipes were developed for this study using the Matrix software (Ewing, 2000). The intention was to develop vitreous engobes that would form an interface between the body and glaze, and mediate the differences in their COE, as well as influencing surface colours and textures.

The purpose of manipulating the COE was to produce a range of engobes so that one could be chosen to approximate the COE of any glaze that was

chosen, in order to improve the fit of the glaze to the ware. The COE of each recipe was manipulated by changing the proportions of talc, Gerstley borate, borax and synthetic cryolite. These materials have very low, medium, high and extremely high COE, respectively.

It was also important to consider the contribution to sintering of the engobes that each material would provide, and to vary the proportions of materials to produce a reasonably narrow range of melting points. This was of necessity a balancing act. For example borax has a high COE, but the lowest melting point of these four materials, whereas talc has the lowest COE and the highest estimated melting point (Table 43).

**Table 43: Coefficients of expansion (COE) and estimated melting temperatures of engobe fluxes**

<b>Material</b>	<b>COE</b>	<b>Estimated melting point (°C)</b>
Talc Plustalc N275	1.62	955
Gerstley borate	10.86	735
Borax	22.33	597
Cryolite synthetic	51.03	674

Although vitreous engobes are usually applied to bisque ware, the intention for this project was to use minimal energy, so the percentage of clay was increased to enable application to raw ware, with the aim of enabling single firing. Eckalite 2 was chosen as the white clay. In two of the engobes, Eckalite 2 was replaced by Marulan tailings. After the Matrix program was used to perform calculations, engobes were formulated with COE ranging from 6.1 to 10.3, and with estimated melting points ranging from 1045 to 1117°C. The batch recipes, COEs, estimated melting temperatures and percentages of iron oxide are shown below (Table 44).

**Table 44: Coefficients of expansion (COE) of experimental engobes**

(wt%)	E1	E2	E3	E4	E5	E6
	Eckalite engobe cone 06 low COE	Eckalite engobe cone 06 high COE	Eckalite engobe cone 08 low COE	Eckalite engobe cone 08 high COE	Marulan engobe cone 08 low COE	Marulan engobe cone 08 high COE
Eckalite 2	30	30	30	30	0	0
Talc Plustalc N275	25	25	20	25	20	20
Gerstley borate	20	10	27	10	27	18
Silica 200	10	8	8	8	8	5
Borax	5	5	5	5	5	5
Zircopax	10	10	10	10	10	10
Cryolite synthetic	0	12	0	12	0	12
Marulan tailings	0	0	0	0	30	30
	100	100	100	100	100	100
<b>COE</b>	6.1	9.4	6.7	10.2	7	10.3
<b>Matrix-estimated melting point (°C)</b>	1114	1117	1078	1064	1058	1045
<b>Fe<sub>2</sub>O<sub>3</sub> (wt%)</b>	0.3	0.3	0.3	0.3	1.6	1.7

Rhodes (1973) suggested that when glazing over raw engobe, the engobe should include some binder, and that glaze application through spraying of glaze is least likely to result in peeling or cracking (Rhodes, 1973). Accordingly, 5% by volume of Tylose was added in liquid form. These engobes were applied to raw test pieces that were partially or bone dry, by dipping, or through use of a rubber bulb slip trailer.

The test pieces using multiple experimental bodies, experimental glazes and experimental engobes are shown in Chapter 29. Meanwhile, documentation of the process of developing experimental low-fire bodies continues. The next chapter describes further tests with two self-glazing bodies from triaxial BM2.

## Chapter 18: Bodies with Self-glazing Properties

Chapter 13 documented the development of two experimental bodies (BM2.7 and BM2.9) that displayed the property of self-glazing when fired to 950°C. The handling properties of these bodies were moderately poor, but the potential benefits of self-glazing suggested that it would be worthwhile experimenting further to see if these bodies could be formed using the traditional studio technique of throwing on the pottery wheel.

Cylinders were thrown on a pottery wheel using BM2.7 and BM2.9.. Both bodies cracked when opening out after centring on the wheel, but were able to be sufficiently consolidated to be formed into the cooling tower forms shown in Figure 327. Although the bodies had the same proportion of flux materials, the BM2.7 towers had more obvious 'whiskers' of efflorescence. This may have occurred because of slower drying of BM2.7, compared with that of the more open BM2.9 body. BM2.9 contained coarser Marulan tailings, allowing faster passage of water through the body, and in turn resulting in less flux migration to the surface.



*Figure 327: Towers thrown from BM2.7 (left) and BM2.9*

Both bodies fused, and the forms partly or completely slumped, when fired at 950°C (fig. 328). There can be no doubt that the bodies have vitrified at 950°C. The BM2.7 towers have more glaze pooling onto the ceramic paper, and the partially obscured BM2.7 tower close to the elements at the rear of the image has deformed. The greater slumping evident in BM2.9 may have occurred for two reasons: (i) faster drying of the BM2.9 body, resulting in less flux migration to the surface and thus more retention of flux in the body, and (ii) more radiant heat from the elements.



*Figure 328: Melted towers at 950°C: BM2.7 (left) and BM2.9*

Both bodies were salty to the taste after firing, and efflorescence was observed on the surface of the fired BM2.7 after three days.

These results suggested that:

- (i) BM2.9 may be useful as a self-glazing or self-sealing body at a lower temperature.
- (ii) These bodies should be reformulated to contain less flux for firing at 950°C.

As will be seen in the following chapter, some bodies with less flux easily withstood firing at 950°C.

## **Chapter 19: Bodies Using Only Recycled Materials**


The experimental bodies used in the preceding chapter contained additions of flux materials that were commercially available and that were not recovered from waste. Whilst it is within the scope of this project to include such materials, it is also important to establish if bodies could be formulated using exclusively recycled or recovered materials. That is the focus of this chapter, beginning with the addition of cullet and perlite fines to Bungendore tailings, and proceeding to addition of cullet to an optimal blend of Bungendore and Marulan tailings.

### **Cullet and perlite additions to Bungendore tailings**

Previous tests showed that BM1.11 (100% Bungendore tailings) had the greatest shrinkage among bodies made from tailings without flux additions. Therefore, it was decided to attempt further densification by adding only recycled wastes. Accordingly, another body was made from Bungendore tailings (90%), Unimin cullet (5%) and AP10 grey perlite cold bag house fines (5%). This body, labelled B1, had shrinkage of 11.8% from wet to dry, compared with 12.4% for 100% Bungendore tailings.

B1 exhibited thixotropic properties. Clay was dried from slip to a state at which resistance to pressure indicated it was ready for preparation by kneading. When kneading commenced, the clay smeared onto the bench rather than adhering to itself, and further drying was required. The cause of the thixotropy was speculated to be both the fine particle size and alkalinity from the sodium content of the perlite fines and the cullet. Additions to counteract thixotropy are investigated in Chapter 25. Meanwhile, the standard handling tests of extruding, cutting slabs and twisting extrusions were undertaken, with results presented below (Figure 329).



 <p><i>Figure 329: B1 extrusions and template-cut slabs</i></p>	<b>Extrusion Rating</b>	<b>Handling properties (wet) and extent of efflorescence (dry)</b>
	<p>5</p>	<p>Moderate thixotropy. Slabs were template-cut with no edge tearing. Very good extrusions, none of which cracked when twisted. No visible efflorescence on slabs and extrusions.</p>

Despite these difficulties, both BM11.1 and BM1 could be used for throwing. BM1.11 was able to be thrown without opening out, although it was somewhat fine and dense, and tended to lack responsiveness. B1 clay opened out quickly and tended to be flabby during the throwing process. The pieces thrown were small cooling tower forms, which were fired to 950°C (fig. 330).



*Figure 330: Towers made from BM1.11 (left) and B1, fired to 950°C*

Shrinkage of BM1.11 was 15.3% from wet to 950°C, while BM1 showed 12.4% shrinkage. This result suggested that a decrease in fired density had been caused by addition of 5% Unimin cullet and 5% AP10 grey perlite cold bag house fines. This was the opposite effect to that intended. The additions had also introduced thixotropy, and thereby worsened the throwing potential of an

already-mediocre throwing body, For these reasons, attention was turned to using an optimal blend of quarry tailings, and using only cullet to attempt increases in densification and vitrification.

### **Cullet addition to an optimal blend of Bungendore and Marulan quarry tailings**

Experiments were conducted to determine the effect of additions of fine cullet to a blend of tailings chosen to produce the best combination of handling and sintering properties. This blend, which consisted of 25% Bungendore tailings and 75% Marulan tailings, was chosen on the basis of the following:

- Bungendore tailings produced 12% shrinkage when drying, and extrusions cracked when twisted.
- Marulan tailings shrank only 6% when drying.
- Bungendore tailings shrank 2.9% from dry to 950°C, whereas Marulan tailings shrank 0.2%.
- Throwing a blend consisting of equal parts Bungendore and Marulan tailings was easier than throwing either alone, so a combined body was preferable.
- Analysis of the two tailings suggested that Marulan tailings would sinter at a lower temperature. The typical analyses were entered into the Matrix software (Ewing, 2000), which indicated that Marulan tailings would melt at a temperature some 90°C lower than would Bungendore tailings.
- Firing a blend of 50% Bungendore tailings and 50% Marulan tailings to 1000°C resulted in a fired body with absorption of 9.9%.

In summary, a blend would be preferable for throwing purposes, and a blend favouring Marulan tailings would shrink less, be less prone to warping and cracking and sinter at a lower temperature, than would a blend favouring Bungendore tailings. Accordingly, a blend of 25% Bungendore tailings and 75% Marulan tailings (represented by BM1.14), was chosen as the body to which cullet was added (BM1.14c). The batch recipes for 1 kg batches of each are presented in Table 45.

**Table 45: Batch recipes: BM1.14 and BM1.14C**

	BM1.14	BM1.14C
	(g)	(g)
Bungendore tailings	250	200
Marulan tailings	750	600
Unimin cullet 150 $\mu$ m	-	200
	1000	1000

Both bodies were easily kneaded, rolled into slabs and cut into test bars. When fired to 1050°C BM1.14c was browner than BM1.14 (fig. 331). Average absorption of BM1.14c was 9%, compared with 12% for BM1.14. Total shrinkage from plastic to 1050°C was 8% for both bodies.



**Figure 331: BM1.14 (top) and BM1.14C fired to 1050°C**

When fired to 1100°C, BM1.14c was browner than BM1.14 and had developed a sheen (fig. 332, overleaf). Average absorption of BM1.14c was 0.3%, compared with 3.2% for BM1.14. Total shrinkage from plastic to 1100°C was 10% for BM1.14c, and 13% for BM1.14.



*Figure 332: BM1.14 (top) and BM1.14C fired to 1100°C*

## Discussion

A blend of 25% Bungendore tailings and 75% Marulan tailings formed an acceptable terracotta body with only 3% absorption at 1100°C, suggesting it should be fired somewhere between 1080°C and 1100°C until higher firing and slump tests determine the top of the firing range. This body uses 100% recovered materials.

### Quarry tailings terracotta body: 1080–1100°C

	(wt%)
Bungendore tailings	25
Marulan tailings	75

Inclusion of 20% fine cullet, and firing to 1100°C reduced the absorption of the body to almost zero. The firing range for this body is thus designated as 1050–1090°C. Since this firing range is lower than that attributed to many commercially available clays, for example those supplied in Australia by Walker Ceramics (Table 2), it can be described as a low-firing terracotta using 100% recycled materials.

Low-firing terracotta body: 1050–1090°C (BM1.14C)

	(wt%)
Bungendore tailings	20
Marulan tailings	60
Unimin cullet 150 µm	20

Further research is needed to establish the extent to which these bodies slump at the top of their stated ranges, and to develop complementary glazes and engobes.

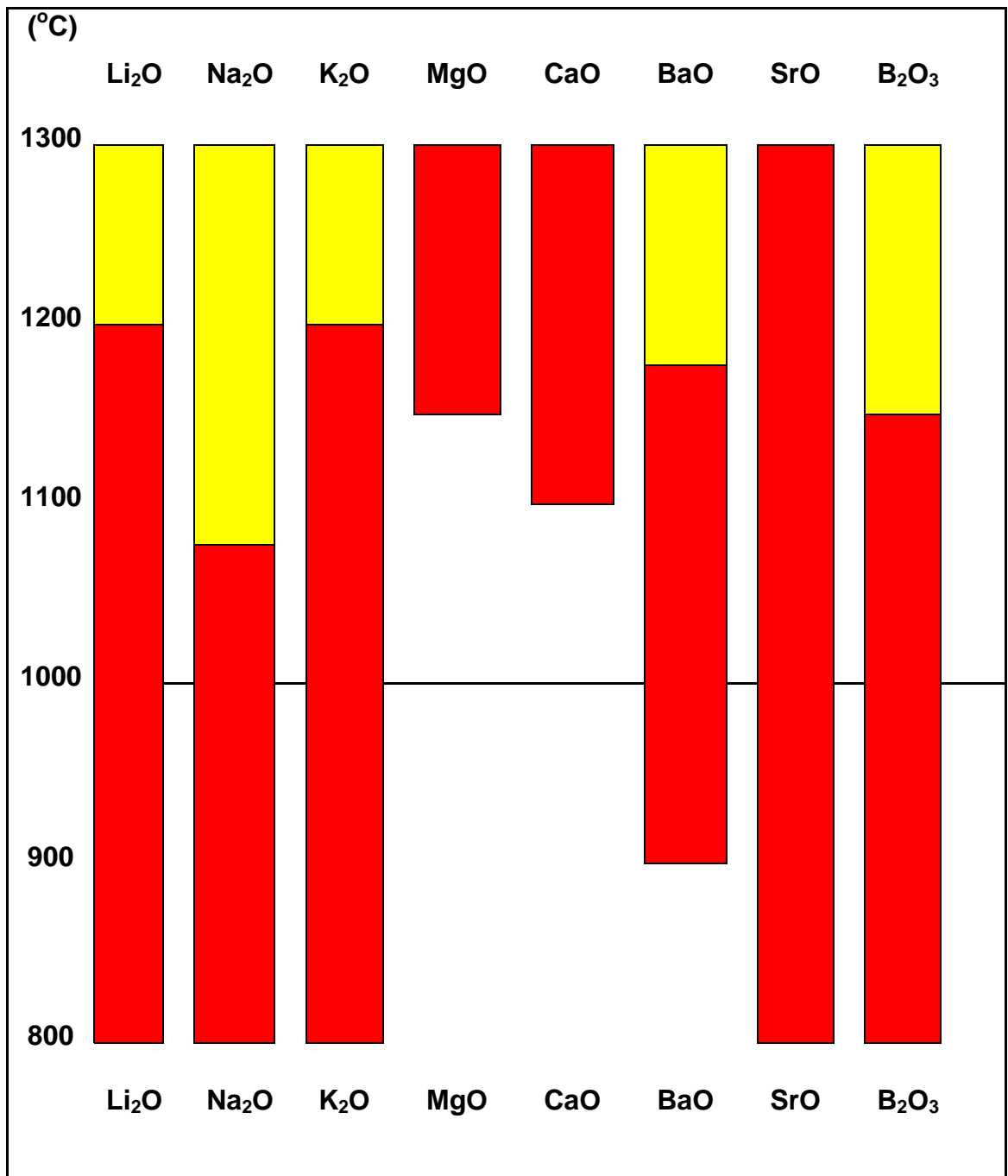
## **Chapter 20: Reformulation to Reduce Flux, Extend Vitrification Range and Decrease Porosity**

No easily workable clay body obtained so far has been vitrified over a range of 50°C. Given that most studio ceramic kilns have temperature variation within a firing, and the aim of this project is to produce a body that could be used by relatively inexperienced ceramicists, a reasonable vitrification range would be preferable to avoid the extremes of sudden slumping or excess porosity.

Sudden slumping of bodies BM2.7 and BM2.9 at 950°C was the result of the high flux content introduced to determine the possibility of bringing about vitrification at low temperature. As vitrification had clearly been accomplished, it was possible to consider which flux materials might be reduced, eliminated or replaced. These considerations were informed by a literature review of physiochemical approaches to reducing sintering temperature (see Chapter 6), and the advantages and disadvantages of the various materials, while bearing in mind that 'small quantities of many fluxes are conducive to a long firing range' (Kraner & McDowell, 1925, p.631).

### **Flux material properties**

It is useful to know the temperature at which a material begins to have a fluxing action. A simplified chart presented in Figure 333 shows red for moderate fluxing action and yellow for strong fluxing action.



**Figure 333: Common flux ranges**  
 adapted from Hamer (1975) p. 337

Information of most relevance in predicting the low-temperature utility of materials containing the major fluxes, and their likely impact on body and glaze properties, is collated in Table 46. The *elements* listed in the column on the left are divided into alkali metals and alkaline earths (Hamer, 1975). The alkali metals, which generally begin their fluxing action at lower temperatures, are at the top of the table and are shaded pink, and the alkaline earths at the bottom are shaded yellow. The intermediate materials containing boron have both fluxing and glass-forming properties, and are shaded blue.

The *source materials* are the most commonly available materials containing the element, and the *formula* shows the other major constituent elements in each source material. The column labelled *oxides into fusion* lists, for each material, which oxides remain in the melt after loss on ignition and reactions during heating.

Tables from the Walker Ceramics Catalogue (2009, p. 71-73) were used to identify the *melting points* of each material when heated in isolation, and the *conversion factors* of the oxides entering fusion. The conversion factor for an oxide represents the percentage of the weight of the original raw material embodied by the oxide remaining in the melt. For example, pearl ash (potassium carbonate) melts at 896°C and 68.3% ends up in fusion, as shown by a conversion factor of 0.683. Similarly, soda ash melts at 852°C and 58.5% goes into the melt, since the conversion factor provided is 0.585. Taken together, the melting points and conversion factors provide an indication of the relative fluxing power of equal weights of the source materials (Walker, 2009). This indication of fluxing power cannot be regarded as constant in all compositions because of various interactive effects, which produce a lower melting point for combined substances than would be predicted by the melting points and proportions of the individual substances (Finkelnburg, 2009). The lowest possible melting temperature achievable for a given combination of materials is referred to as the *eutectic* (Hamer, 1975). The eutectic comparisons of fluxes when combined with  $\text{Al}_2\text{O}_3$  and  $\text{SiO}_2$  appear in Figure 334.

Alkali Eutectic Points	
• Sodina ( $\text{Na}_2\text{-Al}_2\text{O}_3\text{-SiO}_2$ ):	732°C
• Potassia ( $\text{K}_2\text{O-Al}_2\text{O}_3\text{-SiO}_2$ ):	695°C
• Lithia ( $\text{LiO}_2\text{-Al}_2\text{O}_3\text{-SiO}_2$ ):	975°C
Alkaline Earth Eutectic Points	
• Calcia ( $\text{CaO-Al}_2\text{O}_3\text{-SiO}_2$ ):	1170°C
• Baria ( $\text{BaO-Al}_2\text{O}_3\text{-SiO}_2$ ):	1250°C
• Magnesia ( $\text{MgO-Al}_2\text{O}_3\text{-SiO}_2$ ):	1355°C
• Strontia ( $\text{SrO-Al}_2\text{O}_3\text{-SiO}_2$ ):	1400°C

**Figure 334: Eutectic points**

Reproduced from Finkelnburg in *Ceramics Arts Daily* (2009) How glazes melt: In search of the elusive eutectic



The proportional COEs of oxides present determine the overall expansion and contraction rate of a body or glaze (Hamer, 1975). A caveat is that the influence of an oxide does not always correlate with its quantity, as exemplified by B<sub>2</sub>O<sub>3</sub>, which acts to dramatically lower the COE when present in quantities <12%, but increases the COE when present in quantities >15% (Heine, 1972). Knowing the COEs of the body fluxes allows for educated guesses in substitution to adjust glaze fit, should there be defects such as crazing, shivering or dunting (Ewing, 2000).

Knowledge of the relative *surface tensions* of ceramic oxides is used to counteract the phenomenon of crawling, whereby high surface-tension results in the glaze pulling back in beads from the underlying surface (Hamer, 1975).

*Solubility* is an important characteristic of which to be aware, because materials that are soluble will migrate to the surface of the ware during drying—a property that is usually undesirable, as efflorescence and staining can result (Heine, 1972). Soluble salts have an effect on the casting properties of slips (Heine, 1972). The solubility of materials in water is dependent on the temperature of the water, and may increase or decrease as temperature increases. For example, four different MSDS sources were consulted for lithium carbonate, as each used a different reference water temperature. The reported solubility was 15 g/L at 0°C; 13.3 g/L at 20°C; 10 g/L at 20°C and 7.2 g/L at 100°C. Where possible, solubility in water at 20°C has been stated (Table 46).

**Table 46: Flux material properties**

<i>Element</i>	<i>Source material</i>	<i>Formula</i>	<i>Oxides into fusion</i>	<i>Convert factor</i>	<i>Melt point</i>	<i>COE</i>	<i>Surface tension</i>	<i>Soluble g/L 20°C</i>
<b>Lithium</b>	Lithium carbonate	LiCO <sub>3</sub>	Li <sub>2</sub> O	0.405	723	0.67	4.62	13.3
	Petalite	Li <sub>2</sub> O . Al <sub>2</sub> O <sub>3</sub> . 8SiO <sub>2</sub>	Li <sub>2</sub> O Al <sub>2</sub> O <sub>3</sub> SiO <sub>2</sub>	0.049 0.167 0.784	1350	0.67 1.67 0.27	4.62 6.20 3.40	Ins
	Spodumene	Li <sub>2</sub> O . Al <sub>2</sub> O <sub>3</sub> . 4SiO <sub>2</sub>	Li <sub>2</sub> O Al <sub>2</sub> O <sub>3</sub> SiO <sub>2</sub>	0.081 0.274 0.645	1421	0.67 1.67 0.27	4.62 6.20 3.40	Ins

<b>Sodium</b>	Soda ash	Na <sub>2</sub> CO <sub>3</sub>	Na <sub>2</sub> O	0.585	852	3.33	0.70	220
	Cryolite	Na <sub>3</sub> AlF <sub>6</sub>	Na <sub>2</sub> O	0.443	1020	3.33	0.70	0.4
	Sodium silicate	Na <sub>2</sub> SiO <sub>3</sub>	Na <sub>2</sub> O SiO <sub>2</sub>	0.508 0.492	1080	3.33 0.27	0.70 3.40	0.4
	Soda feldspar	Na <sub>2</sub> O . Al <sub>2</sub> O <sub>3</sub> .l. 6SiO <sub>2</sub>	Na <sub>2</sub> O Al <sub>2</sub> O <sub>3</sub> SiO <sub>2</sub>	0.116 0.194 0.688	1250	3.33 1.67 0.27	0.70 6.20 3.40	Ins*
<b>Potassium</b>	Potassium carbonate (pearl ash)	K <sub>2</sub> CO <sub>3</sub>	K <sub>2</sub> O	0.683	896	2.83	0.70	1120
	Potassium dichromate	K <sub>2</sub> Cr <sub>2</sub> O <sub>7</sub>	K <sub>2</sub> O	0.320	400	2.83	0.70	120
	Potash feldspar	K <sub>2</sub> O . Al <sub>2</sub> O <sub>3</sub> . 6SiO <sub>2</sub>	K <sub>2</sub> O Al <sub>2</sub> O <sub>3</sub> SiO <sub>2</sub>	0.169 0.183 0.648	1250	2.83 1.67 0.27	0.70 6.20 3.40	Ins
	Nepheline syenite	K <sub>2</sub> O . 3 Na <sub>2</sub> O . 4Al <sub>2</sub> O <sub>3</sub> . 8SiO <sub>2</sub>	K <sub>2</sub> O Na <sub>2</sub> O Al <sub>2</sub> O <sub>3</sub> SiO <sub>2</sub>	0.080 0.158 0.350 0.412	1200	2.83 3.33 1.67 0.27	0.70 0.70 6.20 3.40	Ins
<b>Boron</b>	Borax (Sodium tetra borate decahydrate )	Na <sub>2</sub> B <sub>4</sub> O <sub>7</sub> . 10H <sub>2</sub> O	Na <sub>2</sub> O B <sub>2</sub> O <sub>3</sub>	0.162 0.365	741	3.33 0.03	0.70 0.80	25
	Gerstley borate	Mix of 2CaO . 3B <sub>2</sub> O <sub>3</sub> .5H <sub>2</sub> O & Na <sub>2</sub> O . 2CaO . 3B <sub>2</sub> O <sub>3</sub> .16H <sub>2</sub> O	CaO B <sub>2</sub> O <sub>3</sub> Na <sub>2</sub> O			1.67 0.03 3.33	4.80 0.80 0.70	Neg**.
	Colemanite	2CaO . 3B <sub>2</sub> O <sub>3</sub> .5H <sub>2</sub> O	CaO B <sub>2</sub> O <sub>3</sub>	0.273 0.508	1472 D 800	1.67 0.03	4.80 0.80	Neg.
<b>Strontium</b>	Strontium carbonate	SrCO <sub>3</sub>	SrO	0.701	D -CO <sub>2</sub> 1350	0.16	4.80	Neg.
<b>Magnesium</b>	Magnesium carbonate	MgCO <sub>3</sub>	MgO	0.478	D 350	0.03	6.60	Neg.
	Talc	3MgO.4SiO <sub>2</sub> .H <sub>2</sub> O	MgO SiO <sub>2</sub>	0.318 0.634		0.03 0.27	6.60 3.40	Neg.
<b>Barium</b>	Barium carbonate	BaCO <sub>3</sub>	BaO	0.777	1360	1.00	3.70	.014
<b>Calcium</b>	Calcium carbonate	CaCO <sub>3</sub>	CaO	0.561	D 825	1.67	4.80	Neg.
	Dolomite	CaCO <sub>3</sub> MgC O <sub>3</sub>	CaO MgO	0.304 0.219	D 730- 760	1.67 0.03	4.80 6.60	28
	Wollastonite	CaSiO <sub>3</sub>	CaO SiO <sub>2</sub>	0.483 0.517	1545	1.67 0.27	4.80 3.40	Ins

\* ins = insoluble

\*\* Neg = negligible

Hamer (1975) supplies melting points for several relatively expensive oxides that may or may not be useful as dopants to aid sintering and extend firing range: phosphorous pentoxide ( $P_2O_5$ , melting at  $580^\circ C$ ) vanadium pentoxide ( $V_2O_5$ ,  $690^\circ C$ ), bismuth oxide ( $Bi_2O_3$ ,  $850^\circ C$ ) and germania ( $GeO_2$ ,  $1115^\circ C$ ).

### **Flux solubility, salt migration and deflocculation**

As noted above, soluble materials will migrate to the surface of the ware during drying, potentially resulting in efflorescence and staining. Soluble salts have an effect on the casting properties of slips.

*Deflocculents* may be present in controlled amounts in casting slips, and will have a negative effect on workability of clays intended to be used as plastic bodies (Walker, 2009). However, inclusion of a deflocculent will potentially reduce the tendency for fine particles to agglomerate and form unusually large grains during sintering (Lange & Kellett, 1989).

Soda ash is a major contributor to efflorescence, and is a deflocculent that has a negative effect on workability, producing rheopexy in the body and limitations in workability where throwers use water (Walker, 2009).

Certain materials may counteract some of the problems associated with deflocculation and salt migration. For example, Zamek (2008) recommends adding 0.3% dry weight magnesium sulphate (epsom salts:  $MgSO_4 \cdot 7H_2O$ ) to flocculate the clay batch after dissolving in water to ensure even dispersal. However, magnesium sulphate will counteract fluxing action when it is fired below  $1150^\circ C$  (Hamer, 1975). The solubility of magnesium sulphate will also exacerbate efflorescence, which can in turn be counteracted with small quantities of barium carbonate (Bennett & Goodrich, 1930). Barium carbonate melts at a relatively high temperature and therefore has little utility as a body flux, but concentrations up to 0.5% are used in earthenware clay bodies to prevent scumming (Bennett & Goodrich, 1930). It is toxic if ingested or inhaled, so the insoluble barium sulphate is an alternative for consideration.

The barium-containing variety of Additive A, a commercially available paper by-product sold in the United States, will achieve increases in plasticity and reductions in efflorescence (Zamek, 2008).

Cryolite is insoluble in water and has a low melting point, so may be a useful source of sodium that does not contribute to efflorescence. Gerstley borate has negligible solubility, but is subject to fluctuations in supply.

## **Chapter 21: Toxicity Considerations**

Information on toxicity is an important factor in the decision to favour a material for body composition. Minimising toxicity is obviously desirable from a safety perspective.

It is not possible to provide a definitive ranking regarding the hazardous nature of materials used in ceramics: available rating systems differ in the rank and pattern of hazard ratings for the same substance. A substance that is listed as a poison in one state or country may not be listed as a poison elsewhere. Material safety data sheets are sometimes incomplete. There is variation among permissible dust exposure limits, and among the figures obtained from animal research into the lethal dose by oral ingestion (oral LD50) for rats.

LD50 is the amount (in mg/kg bodyweight) of a substance that in a single administration kills 50% of animals tested (Canadian Centre for Occupational Health and Safety, n.d.). The rat oral LD50 is higher for some materials sold for human consumption (e.g. potassium chloride sold as a condiment replacement for salt) than for others listed as poisons.

The approach taken in this study was to access multiple sources, list the most conservative hazard ratings, permissible dust exposure limits and rat LD50, and to then eliminate or minimise use of materials that are judged to pose unacceptable risk.

### **Rating and labelling systems**

A variety of rating systems was consulted, and these are outlined below.

## Australian Poison Standards

In Australia, schedules of poisons are updated each year (Commonwealth of Australia, 2012). Three of these are pertinent to the current research:

**Schedule 5. Caution** – Substances with a low potential for causing harm, the extent of which can be reduced through the use of appropriate packaging with simple warnings and safety directions on the label.

**Schedule 6. Poison** – Substances with a moderate potential for causing harm, the extent of which can be reduced through the use of distinctive packaging with strong warnings and safety directions on the label.

**Schedule 7. Dangerous Poison** – Substances with a high potential for causing harm at low exposure and which require special precautions during manufacture, handling or use. These poisons should be available only to specialised or authorised users who have the skills necessary to handle them safely. Special regulations restricting their availability, possession, storage or use may apply. (Commonwealth of Australia, 2012, p. 10)

## Storage requirements classification

Storage requirements are colour coded in the SAF-T-DATA labelling system (J.T. Baker Chemical Co. (1983), (Table 47).

**Table 47: J. T. Baker SAF-T-DATA labelling system: Storage colour codes**

O	ORANGE no serious hazard - may be stored in general storage
B	BLUE health hazard - store in secure poison area
Y	YELLOW reactivity hazard - store in an area isolated from flammables and combustibles
R	RED flammable hazard - store in a flammable liquid storage area
W	WHITE corrosive hazard - store in corrosion-resistant area

Adapted from source: J. T. Baker SAF-T-DATA labelling system.

<http://safety.science.tamu.edu/bakerlabel.html>

## CAS number

The internationally recognised unique registration number assigned by the Chemical Abstracts Service, a division of the American Chemical Society.

## Four hazard categories of health, flammability, reactivity, and contact

Materials are rated from 0 to 4, with 4 indicating the highest level of danger.

**Health:** the capability of the chemical compound to cause personal injury due to inhalation, skin contact, eye contact, or ingestion.

- 0 little or no risk from contact
- 1 can cause significant irritation
- 2 can cause temporary incapacitation or residual injury
- 3 can cause serious or permanent injury
- 4 can be lethal if precautions not observed.

**Flammability** rates the ability to create or sustain a fire.

- 0 the compound will not burn under normal fire conditions
- 1 requires significant source of heat in order to burn
- 2 requires moderate preheating to burn
- 3 solids and liquids that can be ignited under most ambient temperature conditions
- 4 flammable gases and materials that are rapidly vaporised at normal pressures and temperatures and can burn readily.

**Reactivity:** how reactive the compound is under normal laboratory conditions.

- 0 inert
- 4 likely to explode or react violently with air, water, or common substances.

**Contact:** How dangerous physical contact with the compound is under normal workshop conditions.

- 0 little or no risk from contact
- 4 likely to cause severe damage or death when in contact with skin, eyes, or mucous membranes.

Adapted from <http://www.chem.rochester.edu/safety/label.php>

Table 48 contains columns listing i) the material, ii) whether it has been rated as hazardous on the Australian Poison Schedule, and if so the schedule number, iii) the four components of the US Hazard Rating, iv) storage requirements, v) CAS number, vi) solubility, vii) the rat oral LD50 dose, and viii) the permissible dust exposure limits. Blank cells indicate that no data were available.

Table 48: Collated hazard information (part 1)

Source Material	Aust. poison	U.S. hazard rating					CAS No.	Solubility	Ingestion and inhalation	
		Health	Flammability	Reactivity	Contact	Storage			Rat oral LD50 (mg/kg)	Respirable limit (mg/m3)
Lithium carbonate	No	2	0	0	1	O	554-13-2	13.3	525	5
Petalite	No	--	-	-	-	-	1302-66-5	Ins*	-	Si
Spodumene	No	2	0	0		-	1302-37-0	Ins	-	0.1
Soda ash	S5	1	0	1	1	O	497-19-8	220	4090	3
Sodium chloride	No	1	0	1			7647-14-5	360	3000	-
Cryolite	No	3	0	1	2	O	15096-52-3	0.4	2000	2.5
Sodium silicate (powder) (solution)	S5	1	0	0	2	O	1344-09-8	0.4	Miscible	90
	Avoid mist	3	0	0	2		1313-59-3			
Soda feldspar	No	1	0	0	-	-	68476-25-5	Ins	-	5
Potassium carbonate	S5	2	0	1	2	O	584-08-7	1120	1870	-
Potassium chloride	No	3	0	0			7447-40-7	340	2600	-
Potassium dichromate	S6	4	0	2	3	B	7778-50-9	120	25	0.05
Potash feldspar	No	1	0	0		-	68476-25-5	Neg**.	-	Si
Nepheline syenite	No					-	37244-96-5	Neg.	-	5
Borax	S5	2	0	0	2	O	1330-43-4	25	>3500	1
Borax decahydrate	S5	2	0	0	2	O	1303-96-4	60	2600	1
Gerstley borate	No	0	0	0		O	12007-56-6	Neg.	>5000	5
Colemanite	No	0	0	0		O	12007-56-6	Neg.	>5000	5
Strontium carbonate	No	1	0	0	1	O	1633-05-2	Neg.	>2000	.05
Magnesium carbonate	No	1	0	1	1	O	12125-28-9	Neg.	-	15
Talc	No	-	-	-	-	-	14807-96-6	Ins	-	2.5
Barium carbonate	S6**	1	0	0	1	O	7440-39-3	0.014	630	0.5
Barium sulphate	No	1	0	0	0	O	7727-43-7		-	15
Calcium carbonate	No	0	0	0	1	O	1304-76-3	Neg.	500	15
Dolomite	No	1	0	0		-	16389-88-1	28	>5000	15
Wollastonite	No	-	-	-	-	-	13983-17-0	0.1	-	5
Bismuth tri-oxide	S4	1	0	0	1	O	1304-76-3	Ins	5	-
Bismuth sub-carbonate	S4	2	0	0	1	O	5892-10-4	Ins	22	-
Sodium bismuthate	No	2	0	1	2	O	12232-99-4	Ins	420	-
Beryllium sulphate,	S6	3	0	1	2	B	13510-49-1	391	82	.002
Beryllium monoxide	S6	-	-	-	-		1304-56-9	-	-	.002



Phosphorus pentoxide,	No	3	0	3	4	W	1314-56-3			.002
Vanadium pentoxide	No	3	0	1	2	B	1314-62-1	8	10	0.05
Germanium		4	0	2	4	W				

Sources: Digitalfire Hazards Database (2008); Material Safety Data Sheets;

J. T. Baker SAF-T-DATA Labelling System <http://safety.science.tamu.edu/bakerlabel.html>;

US Dept. of Labor Occupational Safety and Health Regulation Tables Z-1 & Z-3 (2004).

\* ins = insoluble

\*\* Neg = negligible

- = no data

Many siliceous ceramic materials have insignificant hazard ratings, other than for respirable dust exposure. The US Department of Labor Occupational Safety and Health Regulation (2004) Tables Z-1 & Z-3 provide formulae to enable calculation of permissible exposure limits for materials that would produce nuisance dusts except for the fact that they contain a phase of silica as a hazardous component. Silica has a reasonably benign amorphous phase, but crystalline phases have low permissible exposure limits for airborne dust. The formulae provided use the same denominator: %SiO<sub>2</sub>+2. The numerators are 80 mg/m<sup>3</sup> for amorphous silica, 10 mg/m<sup>3</sup> for respirable quartz, and 5 mg/m<sup>3</sup> for crystalline silica (cristobalite and tridymite). Respirable limits and formulae for calculating respirable limits (based on percentage of various quartz phases) appear in Table 49.

**Table 49: Collated hazard information (part 2)**

Source material	CAS No.	Respirable limit (mg/m <sup>3</sup> of air)
Silica	14808-60-7	0.1 mg/m <sup>3</sup>
Kaolin	-	15 mg/m <sup>3</sup>
Ball clay	-	15 mg/m <sup>3</sup>
Quartz respirable	14808-60-7	10mg/m <sup>3</sup> / (wt%SiO <sub>2</sub> +2)
Cristobalite, tridymite	14464-46-1	5mg/m <sup>3</sup> / (wt%SiO <sub>2</sub> +2)
Amorphous silica	7631-86-9	80mg/m <sup>3</sup> / (wt%SiO <sub>2</sub> +2)
Bagasse ash	-	0.15 mg/m <sup>3</sup>

Sources: Digitalfire Hazards Database (2008); Material Safety Data Sheets; US Dept. of Labor Occupational Safety and Health Regulation Tables Z-1 & Z-3 (2004).

Mppcf = Millions of particles per cubic foot of air,

Mppcf X 35.3 = million particles per cubic metre = particles per c.c.

\*No exposure standard has been established for this product by the Australian Safety and Compensation Council, formerly known as National Occupational Health and Safety Council. However the following exposure standard applies; Fluorides (as F) TWA = 2.5mg/m<sup>3</sup>.

Materials that have been eliminated from this study because of their hazard profile (Table 48) are listed below, together with the hazard ratings that are most responsible.

### **Eliminated materials**

- Beryllium sulphate, beryllium monoxide and phosphorus pentoxide are extremely toxic, require specialist storage and have permissible exposure limits for airborne dust of only 0.002 mg/m<sup>3</sup>.
- Vanadium pentoxide has a permissible exposure limit for airborne dust of only 0.05 mg/m<sup>3</sup>, and rats died after ingesting only 10 mg/kg of bodyweight.
- Bismuth tri-oxide and bismuth sub-carbonate have rat LD50s of 5 and 22 mg/kg respectively.
- Potassium dichromate has a permissible exposure limit for airborne dust of only 0.05 mg/m<sup>3</sup>, and rats died after ingesting only 25 mg/kg of bodyweight.
- Borax is toxic and should be eliminated or replaced with borax frit.
- Lead was not considered for inclusion due to its toxicity.

### **Materials requiring additional attention to avoid acute injury during glazing, firing or clean-up procedures**

- Universal safety procedures require that dust mask, gloves and goggles be worn when mixing materials in the ceramic studio. Some materials also require extreme caution during glazing, firing or clean-up procedures.
- Sodium silicate has a rat LD50 of 90 mg/kg of bodyweight. Creating a mist from solutions of sodium silicate should be avoided.
- Sodium bismuthate must be used with cold water because it decomposes in hot water and releases toxic fumes.
- Sodium carbonate is an acute irritant, and safety glasses and mask are required.

## **Materials requiring caution to avoid dangers associated with chronic exposure**

Universal safety procedures are advisable in the studio or laboratory. Materials listed below are some of those that contain the quartz phases listed in Table 49 for which care must be taken to consistently follow procedures to avoid respiration of dust above permissible limits:

- Boral Dunmore dust
- Bagasse ash
- RHA
- Bungendore tailings
- Marulan tailings
- Talc

Using the example of talc and the analysis supplied by Unimin Australia the calculation for respirable limit is as follows:

The MSDS provides the exposure standards for constituents silica crystalline-quartz (8hr TWA = 0.1 mg/m<sup>3</sup>) and talc (containing no asbestos fibres, 8hr TWA = 2.5 mg/m<sup>3</sup>). The MSDS provides the amount of crystalline silica as <2%. The applicable formula is 5mg/m<sup>3</sup> divided by (%SiO<sub>2</sub>+2).

$$5\text{mg/m}^3 / (2\% \text{ silica} + 2) = 5/4 = 1.25$$

This is less than the respirable limit provided on some talc material safety data sheets (2.5).

## Chapter 22: Craze Control and Reduction of Porosity

As glazes previously developed had crazed (see Chapter 17) further research was needed to develop a glaze or glazes that utilised waste materials and did not craze on the relevant body, either immediately upon cooling or after a delay. This required an understanding of the role of moisture absorption in contributing to delayed crazing.

Moisture absorption from the air or from contact with water during use can result in an increase in body volume from as low as 0.03% (Fraser, 1986) to between 0.05% and 0.2% (Grimshaw, 1971). A previously compressed glaze can be stretched to the point of crazing (Kingery, Bowen & Uhlmann, 1976).

For any given body, moisture expansion increases with an increase in water absorption, but no direct relationship between water absorption and moisture expansion holds across clay bodies of different compositions (Schurecht & Pole, 1929; Palmer, 1942). Therefore, composition of the body and the amount of absorption must both be considered.

Schurecht and Pole (1929) found that cone 6 clay and feldspar bodies with no added silica had low absorptions and minimal moisture expansions, but developed considerable moisture expansion with additions of >20% silica. Palmer (1942) found that in otherwise identical bodies, replacement of 18% predominantly coarse silica by silica with increasingly finer particle size distributions resulted in successive decreases in moisture absorption and increases in thermal expansion.

Grimshaw (1971, p. 707) attributes moisture absorption to 'rehydration of amorphous crystalline phases ... or absorption of water in alkali-bearing glasses formed at low temperatures'. Schurecht and Pole (1929) reported that in experiments designed to reduce moisture expansion of a cone 5 body, magnesite was more effective than was whiting or iron oxide. Kingery and colleagues (1976) state that moisture expansion can be minimised by vitrification or composition of alkali-free bodies.

Since the fluxes being used to produce vitrification of the bodies in the current research are predominantly alkaline, the implication is that moisture expansion must be prevented through the extent of vitrification achieved. Consideration is also given to literature regarding the inclusion of magnesium.

#### Bodies with magnesia content

Practical experience shows that talc can be added to achieve higher expansion, a better glaze fit, and decreased porosity (Walker, 2009). Talc is predominantly magnesia and silica. The catalytic action of magnesia assists in the conversion of silica quartz to unfused micro-crystalline cristobalite at temperatures over 1000°C and assists in development of an impervious crystalline structure in the fired body (Hamer, 1975). The resultant structure contributes to a watertight body, reduces moisture expansion over time and therefore reduces delayed crazing (Walker, 2009). The amount required is from 5 to 50% (Fraser, 1986). As noted previously, magnesia will counteract fluxing action when it is fired at temperatures below 1150°C (Hamer, 1975). Jones (2006) suggests that adding nepheline syenite to a body increases glass formation to prevent delayed crazing. When nepheline syenite was combined with talc (85:15) ball clay and kaolin, vitrified bodies with <0.3% absorption at cone 02–2 were produced (Lynch & Allen, 1950).

On the basis of the above it was speculated that at temperatures approaching 1000°C, inclusion of talc and nepheline syenite might both increase the firing range and contribute to formation of a micro-crystalline structure that would reduce absorption.

Tichane ( 90; p.289–291) provides, without details of porosity or firing range, the following two lower-firing recipes containing talc:

	<b>Cone 08</b>	<b>Cone 06</b>
Ball clay	70%	60%
Silica (300 mesh)	20%	
Talc	10%	40%

The Digitalfire website (Hansen, 2008), provides a low-fire white talc casting body recipe:

Cone 06–04 ceramic casting slip

Talc	50.0
Ball clay	50.0
Water	45.0 (wt% of dry amount)
Soda ash	0.1 (wt% of dry amount)
Sodium silicate	0.2–0.4 (wt% of dry amount)

Hansen (2008) recommends adding up to 5% bentonite instead of deflocculent for a modelling version of this body, identifies a number of reasons for using a low-fire talc body, points out a number of disadvantages associated with its use, and recommends certain actions to mitigate these negative features (see Table 50, overleaf).

**Table 50: Advantages and disadvantages of cone 06 talc body**

<b>Advantages</b>	<b>Disadvantages</b>	<b>Mitigate by</b>
Fires at cone 06	15% porosity so unhygienic for use as crockery	Fire higher for glass development, but reduced porosity will result in less prevention of crack propagation initiated by free quartz. Add up to 5% CaCO <sub>3</sub> to reduce moisture expansion
Fires white at cone 06, so good for glaze colour development	Very low strength when fired	Fire higher for glass development—but then brittle and darker firing
No warping on firing because no glass development at cone 06	Shivering and crazing because of poor clay/glaze interface	Use a combination of high and low expansion frits and/or fluxes to enable glaze fit adjustment. Test with thermal shock
Excellent workability because of ball clay content	Ball clay contains free quartz with significant volume change at inversion, leading to cracking	Create articles of even wall-thickness to reduce the temperature gradient
Simple formulation	Component change can easily affect the whole body	Use more than one talc and more than one ball clay
Increasing talc can decrease crazing	Increasing talc at the expense of ball clay reduced workability	Add a plasticiser

Compiled from information provided in Hansen (2008)

Kraner and McDowell (1925) note that the eutectic in the MgO:A1<sub>2</sub>O<sub>3</sub>:SiO system can be achieved with the following recipe:

	(wt%)
Talc	58.1
Clay	41.5
Alumina	0.4

This information was utilised in the construction of triaxial BM11, as documented in Chapter 23.

## **Chapter 23:Triaxial BM11**

The results from previous triaxial clay blend trials were sufficient to establish whether the recovered materials would form ceramics, and they provided insight into the relative shrinkages of the quarry tailings and the effects of inclusion of recovered materials on handling and shrinkage. The self-glazing properties observed in samples BM2.7 and BM2.9 at 900°C were of interest, but these samples displayed slumping within a narrow temperature range. A triaxial was required to include the fluxes that contributed to vitrification, while increasing the temperature range, and minimising porosity. The selection of the corner recipes took into account the previously described information on factors affecting sintering, solubility, toxicity, porosity and expansion.

### **Triaxial BM11: Composition**

Sample BM1.2 from triaxial BM1 was used as the starting point for corner A on triaxial BM11. The composition of sample BM1.2 was altered in order to extend the range of fluxes, but reduce the fluxing power and the percentages of fluxes and soluble materials. Sample BM1.2 from triaxial BM1 had the following constituents: Gerstley borate, 37.5; lithium carbonate, 7.5; Unimin cullet 37.5, 30.0 and Bungendore tailings, 25.0.

This 'body' slumped at 800°C, and formed a vitreous engobe at 900°C. It was thixotropic and efflorescent. The thixotropy was thought to result from the particle size and alkalinity of the cullet, and from the presence of alkalis on the lithium carbonate and Gerstley borate.

In an attempt to reduce the thixotropy across triaxial BM11, almost all of the lithium carbonate was replaced by talc. Gerstley borate was reduced in favour of nepheline syenite and cryolite, cullet was reduced and clay increased, and the resultant recipe became corner A on triaxial BM11. This corner A recipe included:



	(wt%)
Bungendore tailings	25
Marulan tailings	10
Unimin cullet 150 $\mu$ m	20
Nepheline syenite	14
Talc (Plustalc N275)	6
Gerstley borate	20
Cryolite (synthetic)	3
Lithium carbonate	2
	100

Corner B was occupied by a recipe calculated to be close to the eutectic for talc and clay reported by Kraner and McDowell (1925):

	(wt%)
Talc Plustalc N275	29
Talc T63B	29
Bungendore tailings	21
Marulan tailings	21

Corner C was occupied by BM1.13:

	(wt%)
Bungendore tailings	50
Marulan tailings	50

The recipe for each sample on the triaxial appears in Table 51 (overleaf).

Table 51: BM11 triaxial blend recipes

BLEND RECIPES (wt%)					N275	63B				
	Bung	Maru	Unim	Neph	Talc	Gers	Cryo	Lith	Talc	
1	25.00	10.00	20.00	14.00	6.00	20.00	3.00	2.00	-----	
2	24.00	12.75	15.00	10.50	11.75	15.00	2.25	1.50	7.25	
3	31.25	20.00	15.00	10.50	4.50	15.00	2.25	1.50	-----	
4	23.00	15.50	10.00	7.00	17.50	10.00	1.50	1.00	14.50	
5	30.25	22.75	10.00	7.00	10.25	10.00	1.50	1.00	7.25	
6	37.50	30.00	10.00	7.00	3.00	10.00	1.50	1.00	-----	
7	22.00	18.25	5.00	3.50	23.25	5.00	0.75	0.50	21.75	
8	29.25	25.50	5.00	3.50	16.00	5.00	0.75	0.50	14.50	
9	36.50	32.75	5.00	3.50	8.75	5.00	0.75	0.50	7.25	
10	43.75	40.00	5.00	3.50	1.50	5.00	0.75	0.50	-----	
11	21.00	21.00	-----	-----	29.00	-----	-----	-----	29.00	
12	28.25	28.25	-----	-----	21.75	-----	-----	-----	21.75	
13	35.50	35.50	-----	-----	14.50	-----	-----	-----	14.50	
14	42.75	42.75	-----	-----	7.25	-----	-----	-----	7.25	
15	50.00	50.00	-----	-----	-----	-----	-----	-----	-----	

### Scaled up triaxial blending for greater sample size

To enable a greater range of clay body tests to be conducted, a larger quantity of each sample was required. The previously published technique for triaxial blending of glazes (Currie, 2000) was scaled up to enable production of sufficient quantities. Three 20-L translucent buckets were graduated using a 1-L graduated cylinder. Ten L of each corner recipe were prepared (fig. 335) so that 2-L quantities of each sample on the 15-sample triaxial were produced, with the intention that 2 kg of each sample would be available for more extensive tests of handling properties, salt migration, absorption, slumping and glaze fit.

The water content of the 15 samples was reduced by pouring the individual blends onto fibre cement sheeting. When they were no longer sloppy, but were still easily indented with pressure from a finger, they were bagged in preparation for the formation of test pieces.



*Figure 335: Scaled up triaxial blending*

### **Sample preparation and observations of handling and drying properties**

Test pieces were formed from the 15 blended bodies obtained. To maintain consistency with previous experiments, the method for preparing extruded samples was used. A quantitative extrusion rating from 1 to 5 was recorded for each sample, and an extrusion was twisted into a loop to provide an indication of plasticity. The triaxial samples were again rolled into slabs. Practice in handling thixotropic bodies resulted in a change from rolling slabs with a bare roller to rolling in a cotton bag, often working from lumps that seemed too hard to roll at all, prior to kneading. Again, a template and needle tool were used to cut shapes to provide an indication of the response of the sample to this forming technique. A qualitative description of how each sample responded to these treatments was recorded, as was any evidence of thixotropy during the kneading and forming processes. Particular attention was paid to the amount of tearing or deformation that occurred as the shapes were cut.



*Figure 336: Extrusions*



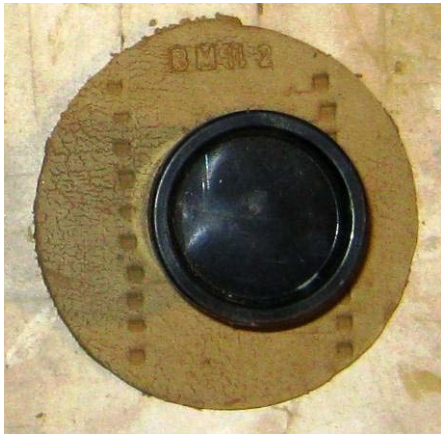
*Figure 337: Slabs cut with needle tool*

The practice of marking extrusions and cut-outs at 50 mm intervals was continued in order to measure shrinkage. In addition, larger sample bars were prepared in accordance with ASTM Standard C373–88 (2006). As well as being stamped with 50 mm separations, these bars were marked at precise 100 mm separations using a set of Kinchrome No 2313 digital vernier calipers (fig. 338), so that shrinkage could be measured in accordance with ASTM Standard C326–09 (2009).

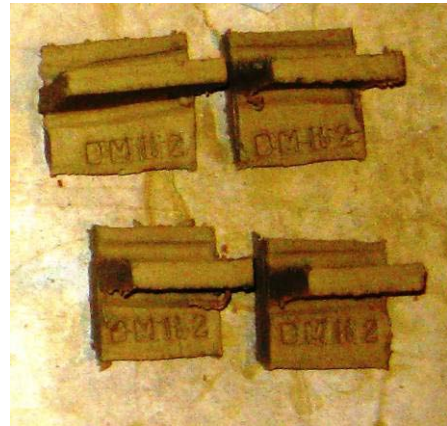


**Figure 338: Bars marked for shrinkage**

In order to examine the tendency of each triaxial sample to produce efflorescence during drying, the method recommended by Hansen (2006b) was employed: 100 mm diameter discs of 6 mm thick clay were cut from slabs of each sample, marked at multiple locations with 50 mm separation, and stamped with the triaxial sample number. A plastic container of smaller diameter was then placed centrally on each clay disc while it was still damp. This served to slow the drying rate of the covered portion of the disc, and to virtually eliminate evaporation from the covered portion (fig. 339). Finally, test tiles were produced in preparation for subsequent glaze tests (fig. 340).



**Figure 339: Efflorescence test disc**



**Figure 340: Test tiles**

A range of test items was produced for each sample (figs. 341 & 342).



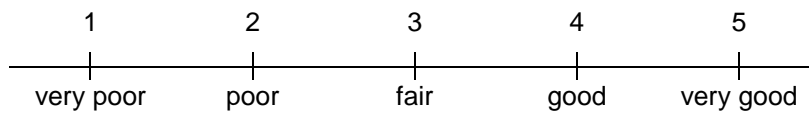
**Figure 341: Triaxial sample range**



**Figure 342: Dried test pieces**






## Triaxial BM11: Handling properties

The handling properties of the 15 bodies varied considerably. Thixotropy decreased in a stepwise fashion moving tier by tier down the triaxial from the apex at Batch A (BM11.1), where thixotropy was most extreme. Tier 5 (BM11.11 to BM11.15) exhibited no thixotropy. Barking decreased in a stepwise fashion moving tier by tier away from Batch B in the triaxial (BM11.11), where barking was most pronounced. There was no barking on samples that did not contain a portion of Batch B. Batch C (BM11.15) produced smooth, plastic extrusions. Extrusion quality was rated on a five-point Likert scale:









The extrusions from each BM11 triaxial sample are pictured in Tables 52–54, alongside a description of their handling properties and extrusion ratings (overleaf).

**Table 52: BM11 triaxial: Handling properties**

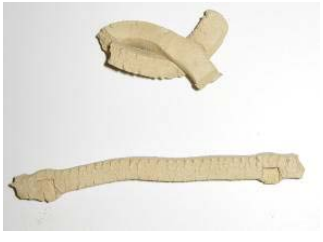


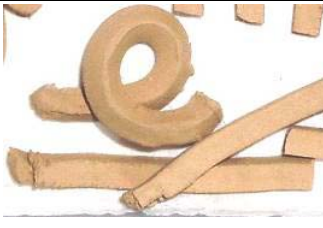
Triaxial sample	Rating	Handling properties (wet)	
11.1	3	Extreme thixotropy. Required cloth between roller and slab to prevent sticking. Slabs were cut without tearing. Reasonably good extrusions were only able to be made from cut slabs as thixotropy made rolled coils too sloppy and sticky to form feedstock for the extruder. Some extrusions lost form during extrusion. Twisted well, but form lost definition.	
11.2	2	Extreme thixotropy. Required cloth between roller and slab to prevent sticking. Slabs were cut without tearing. Reasonably good extrusions were only able to be made from cut slabs as thixotropy made rolled coils too sloppy and sticky to form feedstock for the extruder. Barking on one side of extrusions, and some extrusions lost form during extrusion. Cracked when twisted.	
11.3	3	Extreme thixotropy. Required cloth between roller and slab to prevent sticking. Slabs were cut without tearing. Reasonably good extrusions were only able to be made from cut slabs as thixotropy made rolled coils too sloppy and sticky to form feedstock for the extruder. Some extrusions lost form during extrusion. Twisted well.	
11.4	2	Extreme thixotropy. Required cloth between roller and slab to prevent sticking. Slabs were cut without tearing. Extrusions held form. They were only able to be made from cut slabs as thixotropy made rolled coils too sloppy and sticky to form feedstock for the extruder. Extrusions ranged from good to bad with prominent barking on some. Twisted OK, but was flabby and distorted during twisting.	
11.5	4	Extrusions lost form due to thixotropy but were smooth. Due to extreme thixotropy and moisture content, slab was smeared on to fibro, allowed to dry slightly, rolled and cut off with wire before being cut into slabs. Slabs were cut with no tearing.	



**Table 53: BM11 triaxial: Handling properties (continued)**

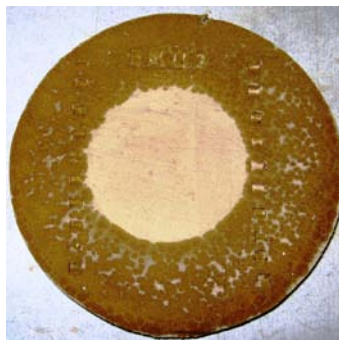
Triaxial sample	Rating	Handling properties (wet)	
11.6	2	Extrusions were lumpy because of poor blending. Due to extreme thixotropy and moisture content, slab was smeared on to fibro, allowed to dry slightly, rolled in cotton bag and cut into slabs. Slabs were cut with no tearing. Split when twisted.	
11.7	3	Most extrusions had marked barking. The body was flabby and short to knead, and exhibited thixotropy as kneading proceeded. Slabs were cut with no tearing. Twists were uncracked.	
11.8	5	Extrusions were very good, and slabs were cut with no tearing. (The slabs were cut and marked wetter than other samples - noted when measuring shrinkage). Thixotropy evident upon kneading. Twisted well.	
11.9	5	Extrusions were very good, and slabs were cut with no tearing. Slight rheopexy and thixotropy were evident, and the body was sticky when kneading. Twisted well.	
11.10	5	Extrusions were very good, and slabs were cut with no tearing. Slight thixotropy was evident, and the body was sticky when kneading. Twisted well.	
11.11	1	Extrusions were very bad, with pronounced barking on all samples and fragility resulting from extreme shortness. Edge tearing when slabs were cut. No thixotropy was evident, and the body needed water addition to make wedging possible. Completely broke when twisted so no twisted pieces were produced.	

**Table 54: BM11 triaxial: Handling properties (continued)**

Triaxial sample	Rating	Handling properties (wet)	
11.12	3	Extrusions were poor, with moderate barking on samples. Slight edge tearing when slabs were cut. Slight rheopexy was evident, and the body was short to knead. Cracked at loop when twisted.	
11.13	4	Extrusions were good, with minor barking on some samples. No edge tearing when slabs were cut. No thixotropy was evident, and the body kneaded well. Extrusion cracked at loop when twisted, as did rolled loop.	
11.14	5	Extrusions were very good, and slabs were cut with no tearing. No thixotropy was evident, and the body kneaded well. Twisted well, but cracked at the loop during drying.	
11.15	5	Extrusions were very good, and slabs were cut with no tearing. No thixotropy was evident, and the body kneaded well. Twisted well.	

### Triaxial BM11: Efflorescence

The extent of efflorescence varied across the triaxial. On the samples on which most efflorescence was visible there was a marked contrast between the portions of the test pieces that had been covered and the portions that had remained uncovered, for example sample BM11.3 (fig. 343).



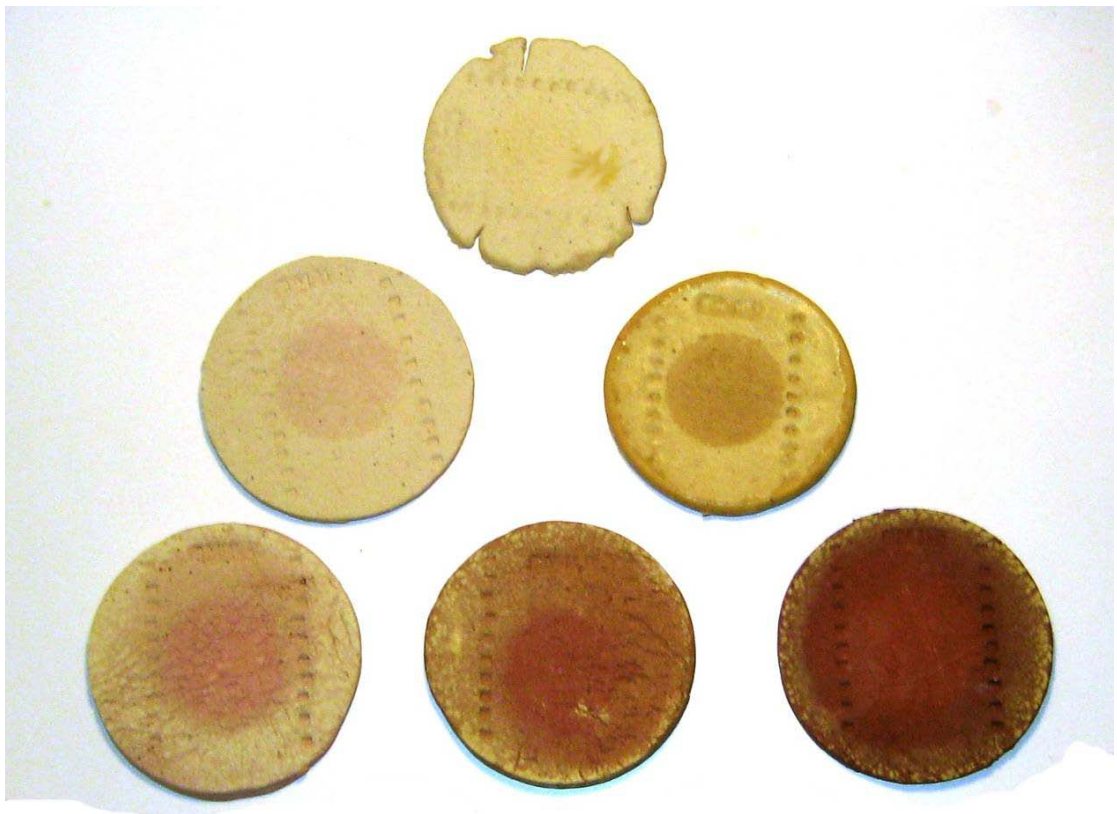
**Figure 343: BM11.3 efflorescence test**

As can be seen in Figure 344, there was no efflorescence on the covered portion of any samples, and the density of the efflorescence on uncovered areas decreased in a stepwise fashion moving tier by tier down the triaxial from the apex A (BM11.1). Sample BM11.1 had a uniform coating of efflorescence ending sharply at the uncoated covered area. Tier 2 samples BM11.2 and BM11.3 had a scattering of uncoated breaks where the underlying body showed through a coating of efflorescence, and a less clear delineation between covered and uncovered areas. Tier 3 samples BM1.1 – BM1.6 were predominantly uncoated, with specks of efflorescence increasing in frequency towards the circumference and decreasing in frequency towards the covered area, so that there was no obvious delineation. Tier 4 samples BM11.7–BM11.10 had minimal efflorescence that showed as isolated specks towards the circumference. Tier 5 samples BM11.11–BM11.15 (not shown) had no visibly evident efflorescence.



**Figure 344: Efflorescence tests: Unfired discs of BM11 triaxial samples 1–10**

The test discs from triaxial BM11 were fired to 900°C using the standard firing cycle. Only samples Bm11.1 – BM11.6 retained visible evidence of the efflorescence that had occurred during drying (fig. 345). On samples BM11.1 and BM11.3, the migrated salts had fluxed the body to the extent that a glaze was formed on the surface. On sample BM11.3 this glaze was more matte on the portion of the surface area that had been uncovered during drying. On both samples there was a loss of surface definition, such that cracks, scratches and indentations were totally or partially obscured. Sample BM11.1 was salty on the tongue one month after firing, indicating ongoing release of unbound salts. This was not discerned on other samples. Samples BM11.2, BM11.4, BM11.5 and BM11.6 displayed evidence of efflorescence, with the covered areas revealing a darker body showing through a speckling of pale yellow efflorescence, and with the efflorescence concentrated towards the perimeter.



**Figure 345: BM11 sample discs fired to 900°C: Extent of efflorescence and self-glazing on samples 1-6**

At 900°C the remaining samples (BM11.7–BM11.15) displayed no visible efflorescence as seen in the two lower rows (fig. 346).



*Figure 346: All BM11 sample discs fired to 900°C: Extent of efflorescence and self-glazing*

### Triaxial BM11: Shrinkage wet to dry

The average shrinkage of each sample is recorded in Table 55. Samples with the highest and lowest shrinkage are in red numerals.

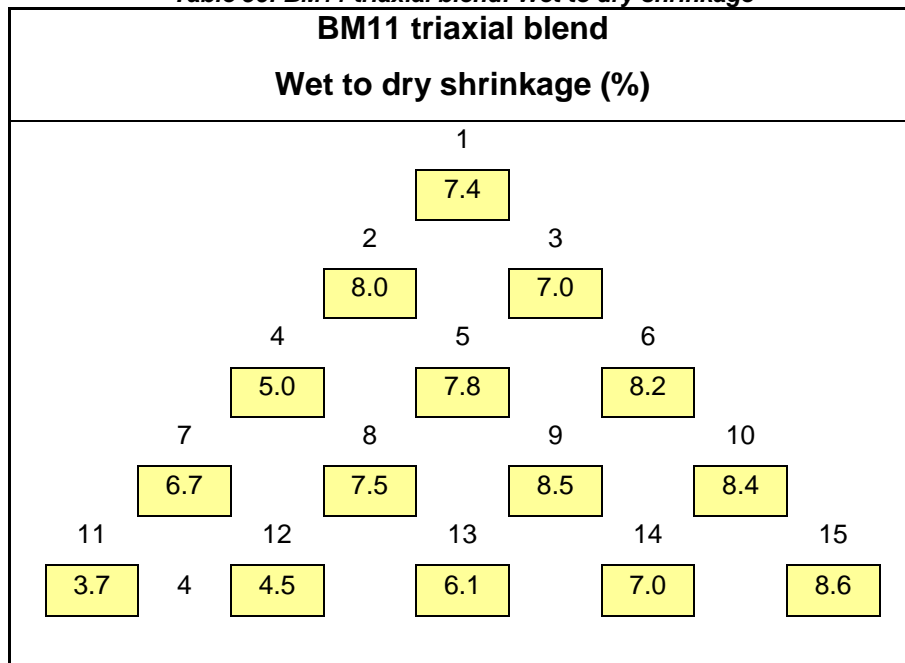
*Table 55: BM11 triaxial blend: Wet to dry shrinkage*

BM11 triaxial blend															
Wet to dry shrinkage (%)															
Sample	1	2	3	4	5	6	7	8	9	10	11	12	13	14	15
% Shrink	7.4	8.0	7.0	5.0	7.8	8.2	6.7	7.5	8.5	8.4	3.7	4.5	6.1	7.0	8.6

The maximum wet to dry shrinkage observed in triaxial blend BM11 was 8.6% in sample 15, which contained equal amounts of Bungendore and Marulan quarry tailings. The least shrinkage observed was 3.7% in sample 11, which

contained 58% talc. When the data were also arranged in the triaxial format (Table 56) and the blend recipes compared, it was apparent that in general, greater proportions of clay produced greater shrinkage, while the opposite was true for talc. This was most evident in samples 11-15 (fig. 347) when the shrinkage data were input into a 3D graphical representation (figs. 344-347). The observed trend continued, but was curvilinear across the sample A-B line blend (fig. 345). It was speculated that the departure from shrinkage in strict proportion to ingredients may have been due to uncontrolled variations in moisture content during bar formation, resulting from variations in thixotropy and drying times in samples 1-10.

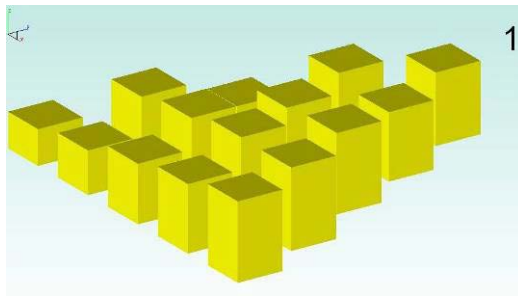
**Table 56: BM11 triaxial blend: Wet to dry shrinkage**



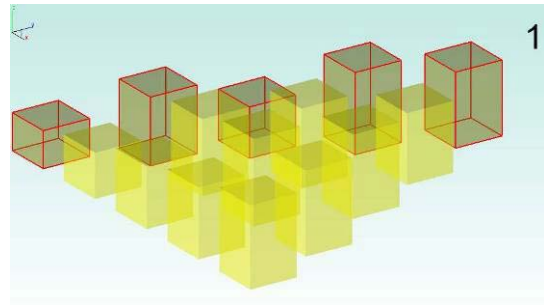
**Triaxial BM11: Fired to 850, 900, 950 and 1000°C**

The BM11 triaxial samples were fired to four different temperatures: 850, 900, 950 and 1000°C using the standard firing schedule. Descriptions and images of each sample follow, preceded by images of each triaxial and associated shrinkage data.

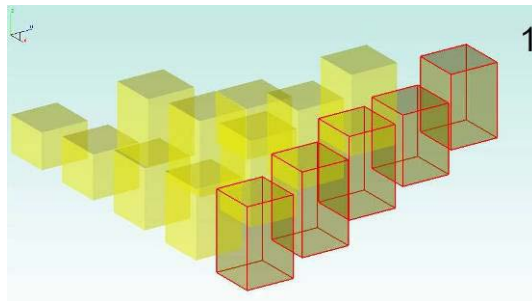
## Triaxial BM11: Fired to 850°C



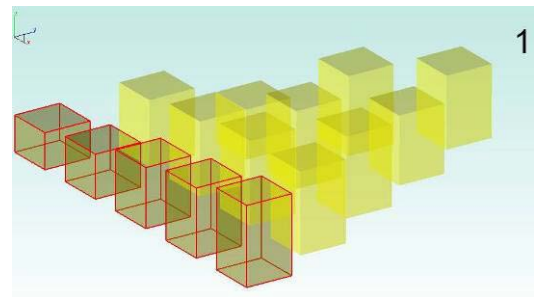
**Figure 347: Triaxial BM11.**  
Wet to dry shrinkage (%), trimetric view



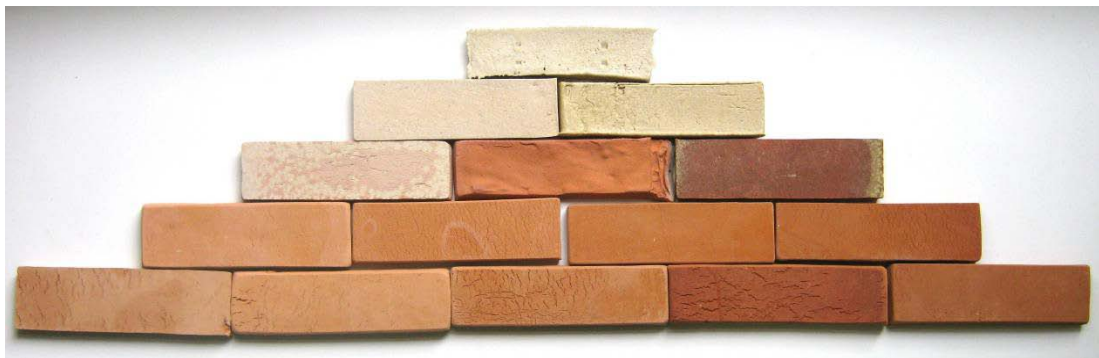
**Figure 348: Triaxial BM11.**  
Wet to dry shrinkage (%), trimetric view.  
Framing samples 1-2-4-7-11



**Figure 349: Triaxial BM11.**  
Wet to dry shrinkage (%), trimetric view.  
Framing samples 1-3-6-10-15



**Figure 350: Triaxial BM11.**  
Wet to dry shrinkage (%), trimetric view.  
Framing samples 11-15



**Figure 351: BM11 triaxial fired to 850°C**

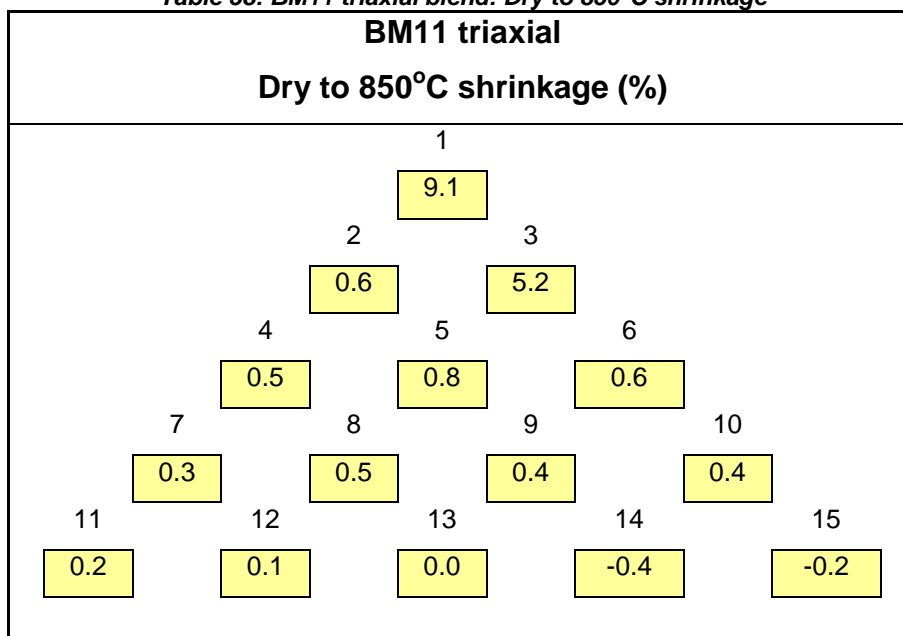
Triaxial BM11 samples were fired to 850°C (fig. 351). The average shrinkage of each sample from dry to 850°C is shown in Table 57, where the percentages for samples with the highest and lowest shrinkage appear in red numerals.

**Table 57: BM11 triaxial blend: Dry to 850°C shrinkage**

BM11 triaxial blend															
Dry to 850°C shrinkage (%)															
Sample	1	2	3	4	5	6	7	8	9	10	11	12	13	14	15
% Shrink	9.1	0.6	5.2	0.5	0.8	0.6	0.3	0.5	0.4	0.4	0.2	0.1	0.0	-0.4	-0.2

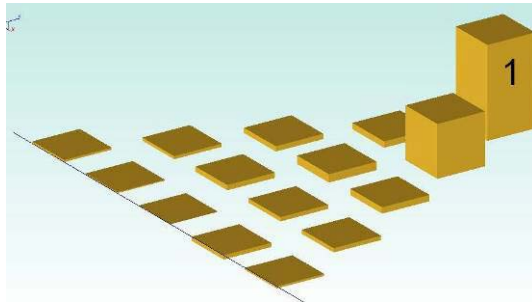
The maximum average dry to 850°C shrinkage observed in triaxial blend BM11 was 9.1% in sample 1, which contained the most flux ingredients. The least shrinkage observed was in fact a slight expansion in sample 14, recorded as shrinkage of -0.4%. When the data were arranged in the triaxial format (Table 58) it was apparent that the only substantial shrinkage was in samples 1 and 3 on the A-C line blend.

**Table 58: BM11 triaxial blend: Dry to 850°C shrinkage**

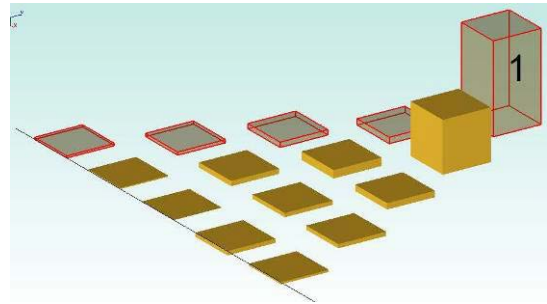


3D graphical representation (figs. 352–355, overleaf) of samples fired to 850°C exposed trends related to the proportions of the corner recipes. High proportions of recipe A produced significant shrinkage that was all but eliminated by replacement with 25% or more of recipe B (fig. 353), and dramatically reduced by replacement with 25% of recipe C (fig. 354). There was a trend from slight contraction to slight expansion along the B-C line blend (fig. 355).

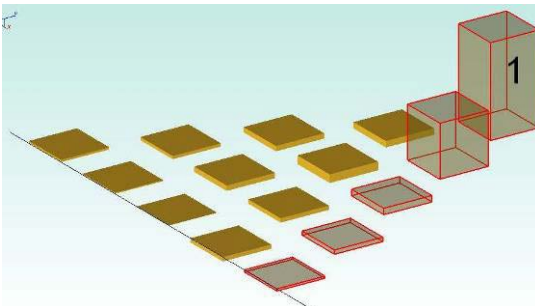




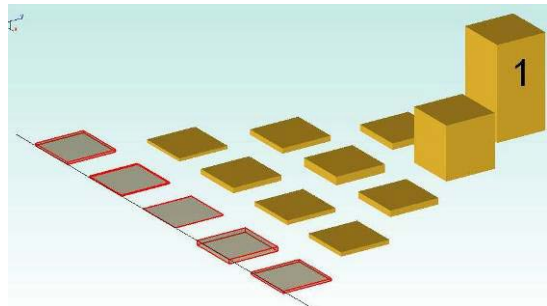
**Figure 352: Triaxial BM11.**  
 Dry to 850°C shrinkage (%), trimetric view



**Figure 353: Triaxial BM11.**  
 Dry to 850°C shrinkage (%), trimetric view.  
 Framing samples 1-2-4-7-11



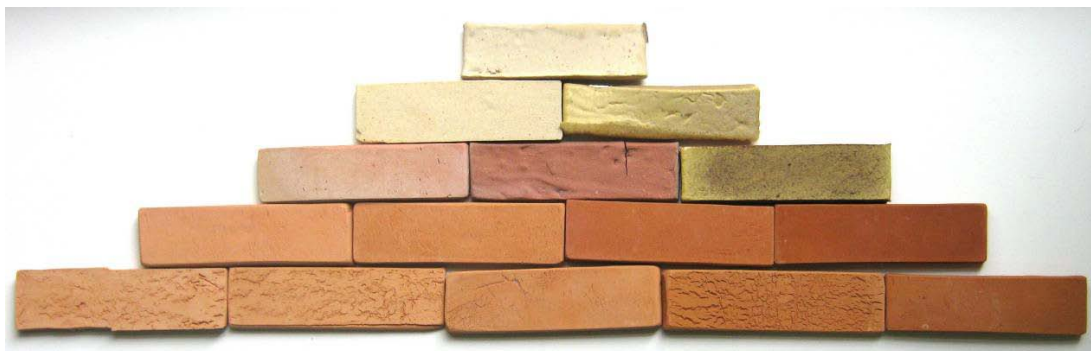
**Figure 354: Triaxial BM11.**  
 Dry to 850°C shrinkage (%), trimetric view.  
 Framing samples 1-3-6-10-15



**Figure 355: Triaxial BM11.**  
 Dry to 850°C shrinkage (%), trimetric view.  
 Framing samples 11-15

### Triaxial BM11: Fired to 900°C

Triaxial BM11 samples were fired to 900°C (fig. 356).



**Figure 356: BM11 triaxial fired to 900°C**

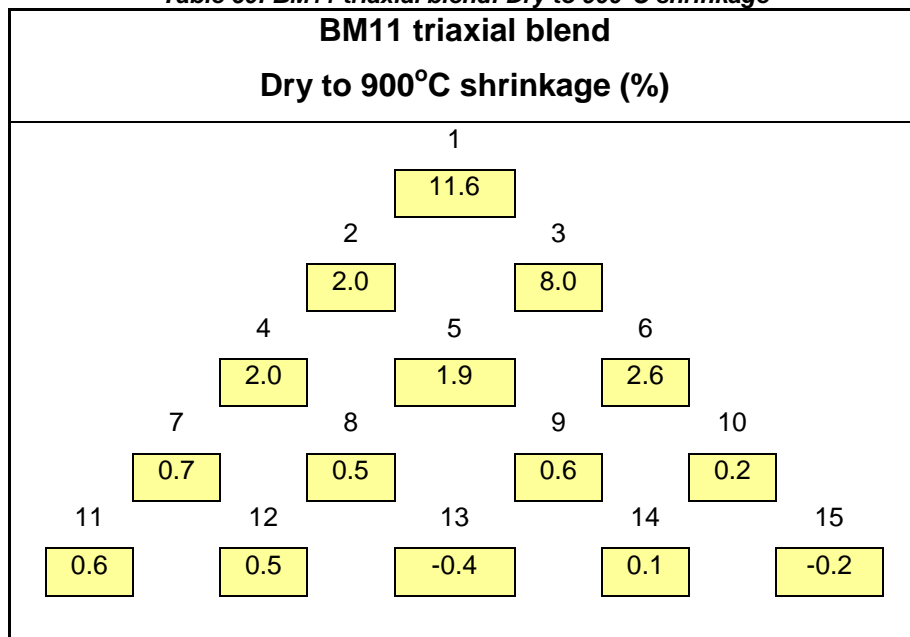
The average shrinkage of each sample from dry to 900°C is shown in Table 59. Samples with the highest and lowest shrinkage are shown in red.

**Table 59: BM11 triaxial blend: Dry to 900°C shrinkage**

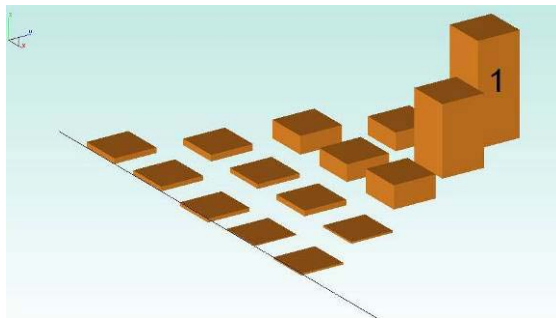
<b>BM11 triaxial</b>															
<b>Dry to 900°C shrinkage (%)</b>															
<b>Sample</b>	<b>1</b>	<b>2</b>	<b>3</b>	<b>4</b>	<b>5</b>	<b>6</b>	<b>7</b>	<b>8</b>	<b>9</b>	<b>10</b>	<b>11</b>	<b>12</b>	<b>13</b>	<b>14</b>	<b>15</b>
<b>% Shrink</b>	11.6	2.0	8.0	2.0	1.9	2.6	0.7	0.5	0.6	0.2	0.6	0.5	-0.4	0.1	-0.2

The maximum average dry to 900°C shrinkage observed in triaxial blend BM11 was 11.6% in sample 1, which contained the most flux ingredients. The least shrinkage observed was in fact a slight expansion in sample 13, recorded as shrinkage of -0.4%. When the data were arranged in triaxial format (Table 60) it was evident that shrinkage had decreased along the A–B and A–C line blends.

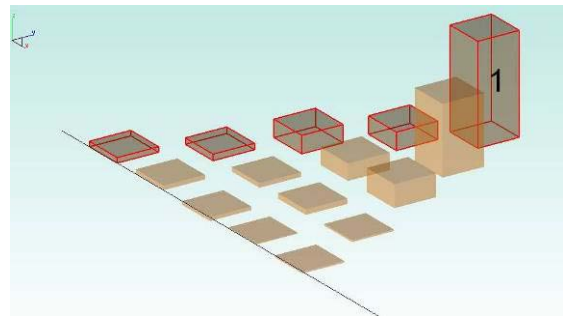
**Table 60: BM11 triaxial blend: Dry to 900°C shrinkage**



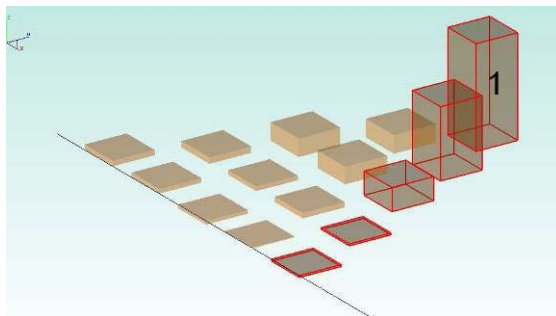
A 3D graphical representation (figs. 357–360, overleaf) of samples fired to 900°C again exposed shrinkage trends related to the proportions of the corner recipes. High proportions of recipe A produced significant shrinkage that was reduced dramatically by replacement with 25% or more of recipe B (fig. 358), and less so by replacement with 25–50% of recipe C (fig. 359). There was a curvilinear trend from slight contraction to slight expansion along the B–C line blend (fig. 360).



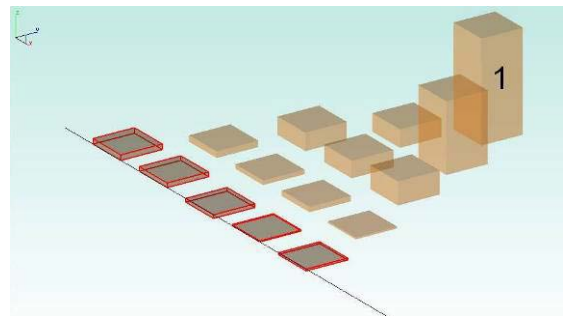
**Figure 357: Triaxial BM11.**  
*Dry to 900°C shrinkage (%), trimetric view*



**Figure 358: Triaxial BM11.**  
*Dry to 900°C shrinkage (%), trimetric view. Framing samples 1-2-4-7-11*



**Figure 359: Triaxial BM11.**  
*Dry to 900°C shrinkage (%), trimetric view. Framing samples 1-3-6-10-15*



**Figure 360: Triaxial BM11.**  
*Dry to 900°C shrinkage (%), trimetric view. Framing samples 11-15*

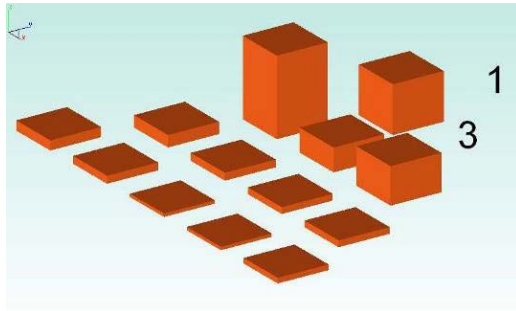
### Triaxial BM11: Fired to 950°C

Because samples 1 and 3 had vitrified at 900°C, they were not fired to 950°C. The remaining 13 samples were fired to 950°C (fig. 361).

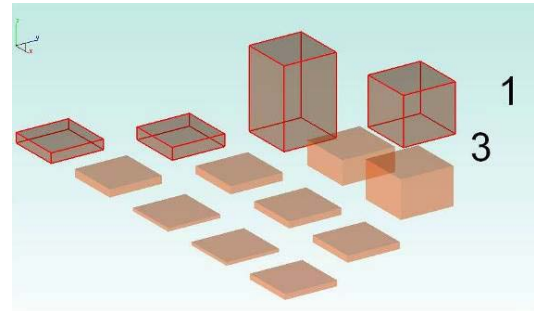


**Figure 361: BM11 triaxial fired to 950°C**

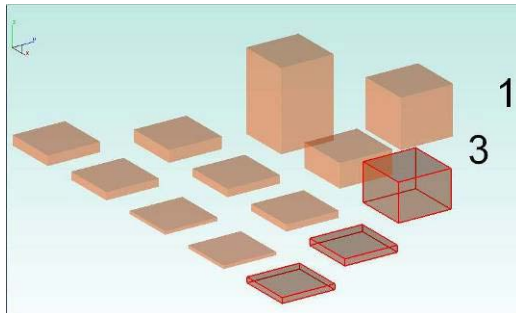




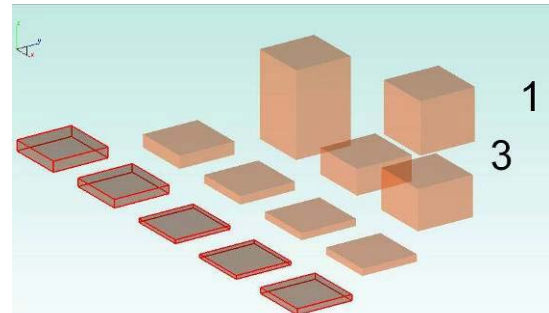
**Figure 362: Triaxial BM11.**  
 Dry to 950°C shrinkage (%), trimetric view



**Figure 363: Triaxial BM11.**  
 Dry to 950°C shrinkage (%), trimetric view. Framing samples 2-4-7-11



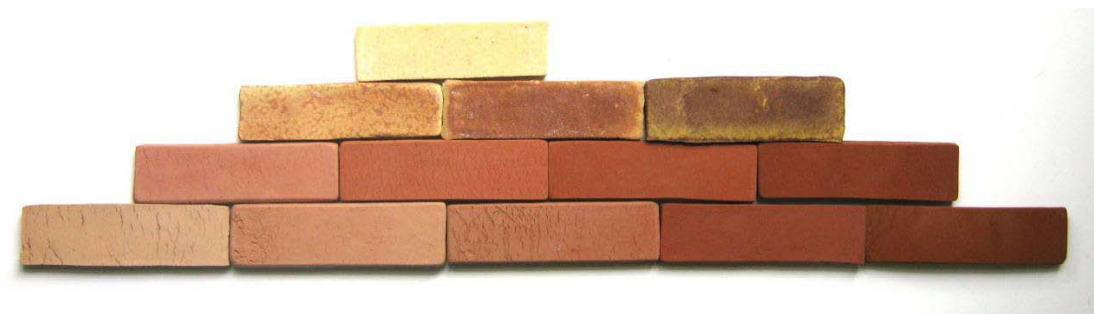
**Figure 364: Triaxial BM11.**  
 Dry to 950°C shrinkage (%), trimetric view. Framing samples 6-10-15



**Figure 365: Triaxial BM11.**  
 Dry to 950°C shrinkage (%), trimetric view. Framing samples 11-15

### Triaxial BM11: Fired to 1000°C

Thirteen samples from triaxial BM11 were fired to 1000°C (fig. 366).



**Figure 366: BM11 triaxial fired to 1000°C**

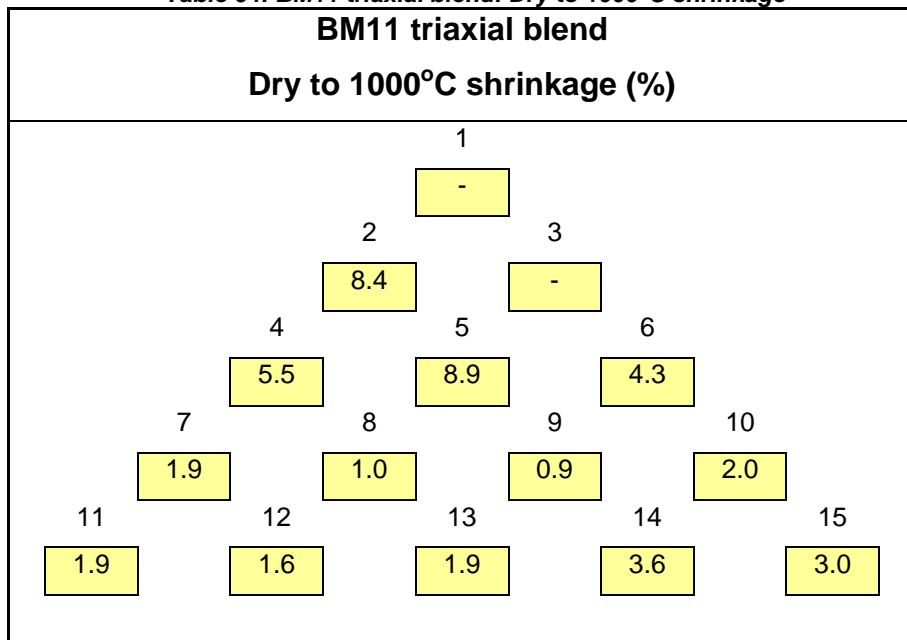
The average shrinkage of each sample from dry to 1000°C is shown in Table 63 (overleaf). Contraction occurred in all 13 remaining samples. Samples with the highest and lowest shrinkage are in red.

Table 63: BM11 triaxial blend: Dry to 1000°C shrinkage

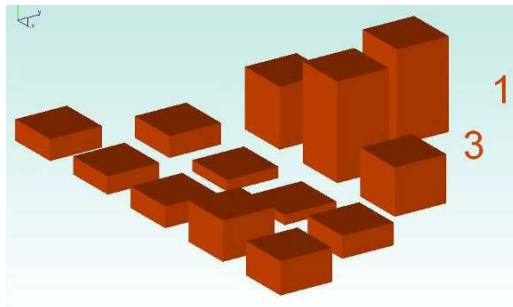
BM11 triaxial Dry to 1000°C shrinkage (%)															
Sample	1	2	3	4	5	6	7	8	9	10	11	12	13	14	15
% Shrink		8.4		5.5	8.9	4.3	1.9	1.0	0.9	2.0	1.9	1.6	1.9	3.6	3.0

The data were also arranged in the triaxial format (Table 64). The highest and lowest shrinkage samples were diagonally adjacent in the triaxial at BM11.5 and BM11.9.

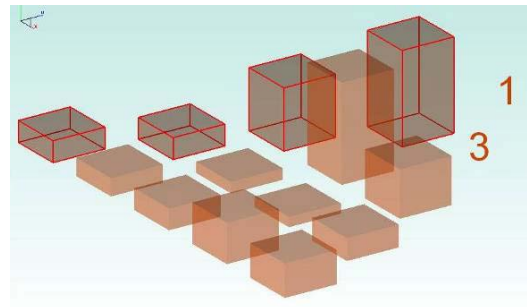
Table 64: BM11 triaxial blend: Dry to 1000°C shrinkage



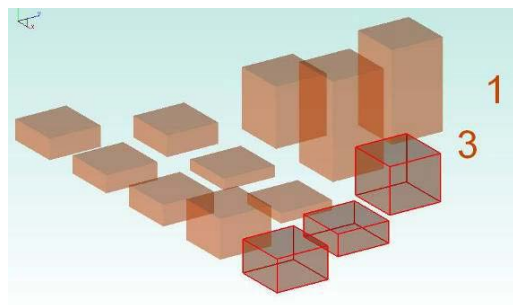
A 3D graphical representation (figs. 367–370, overleaf) of samples fired to 1000°C exposed shrinkage trends only partially related to the proportions of the corner recipes. High proportions of recipe A (not fired to 1000°C) produced significant shrinkage that was reduced by replacement with 25% or more of recipe B (fig. 368) and reduced by replacement with 50–75% of recipe C (fig. 369). The curvilinear trend of increasing contraction along the B–C line blend at 1000°C (fig. 370) reversed the trend observed at 950°C (fig. 363).



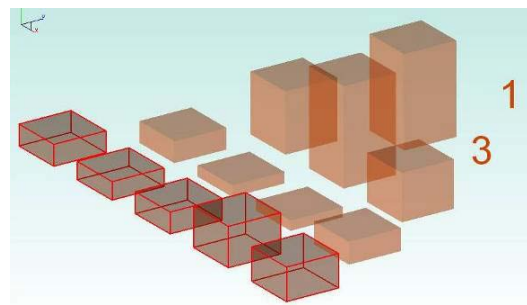
**Figure 367: Triaxial BM11.**  
*Dry to 1000°C shrinkage (%), trimetric view*



**Figure 368: Triaxial BM11.**  
*Dry to 1000°C shrinkage (%), trimetric view. Framing samples 2-4-7-11*



**Figure 369: Triaxial BM11.**  
*Dry to 1000°C shrinkage (%), trimetric view. Framing samples 6-10-15*



**Figure 370: Triaxial BM11.**  
*Dry to 1000°C shrinkage (%), trimetric view. Framing samples 11-15*

## Absorption and porosity

Measures of absorption and porosity were obtained in accordance with ASTM Standard C373–88<sup>14</sup> (2006), and the test for *cold over boiled porosity*<sup>15</sup> recommended by Hansen (2006b). The fired pieces were dried at 150°C, weighed on a Diamond Model 100 digital scale to obtain dry mass, and then soaked in distilled water for 24 hours, (figs. 371 & 372). They were then re-weighed to determine cold saturated mass. The same pieces were then boiled for five hours, cooled and re-weighed to determine boiled saturated mass.

<sup>14</sup> Appendix 5

<sup>15</sup> Appendix 6



**Figure 371: Dried and fired test bars separated with spacers prior to addition of distilled water**



**Figure 372: Dried and fired test bars soaking in distilled water**

In order to determine the volume of the test bars, an apparatus (fig. 373) was built (using mostly discarded items) to make use of Archimedes' displacement principle (Encyclopædia Britannica, 2013). A length of watering system hose was fitted through the base of a compact disc container and a disposable party plate. The container was suspended over a graduated cylinder by positioning it on lengths of wooden slat from a Venetian blind. The container was filled until water overflowed through the hose. Once the overflow had ceased, the fired, boiled and saturated samples were lowered into the container and the displaced water was captured in the graduated cylinder.



**Figure 373: Apparatus for determining volume of fired bars using Archimedes' principle**

Measurements for five examples of each sample body were recorded and entered into a spread sheet. Trends and comparisons within the triaxial, and



across the four firing temperatures, were observed. The following section presents these observations, with reference to images of the fired samples.

Triaxial BM11: Absorption and porosity after firing to 850°C

Table 65 shows the absorption measurements and porosity and cold/boiled calculations for triaxial BM11 at 850°C. The lowest (BM11.1) and highest (BM11.5) values are printed in red.

**Table 65: BM11: Absorption & porosity measurements after firing to 850°C**  
**BM11: Absorption & porosity after firing to 850°C**

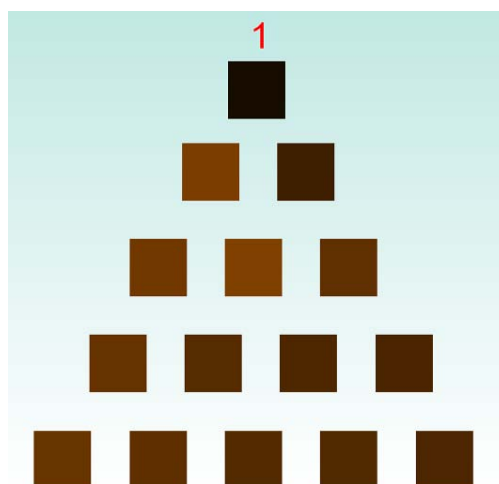
Sample	Absorption (wt%)	Cold / boiled	Apparent porosity (%)
11.1	4.69	0.98	9.44
11.2	25.36	0.96	32.92
11.3	12.69	0.95	19.78
11.4	22.95	0.98	30.73
11.5	26.17	0.98	40.45
11.6	19.77	0.96	27.26
11.7	20.82	0.98	28.24
11.8	17.57	0.98	24.71
11.9	15.72	0.98	22.69
11.10	14.96	0.97	21.35
11.11	21.33	0.99	37.45
11.12	19.10	0.99	34.68
11.13	17.01	0.99	24.93
11.14	16.88	0.98	31.77
11.15	15.40	0.99	26.15

Table 66 shows absorption data in triaxial format. At 850°C the sample with the highest absorption (BM11.5) is in the centre of the triaxial.

**Table 66: Triaxial BM11: Absorption after firing to 850°C**

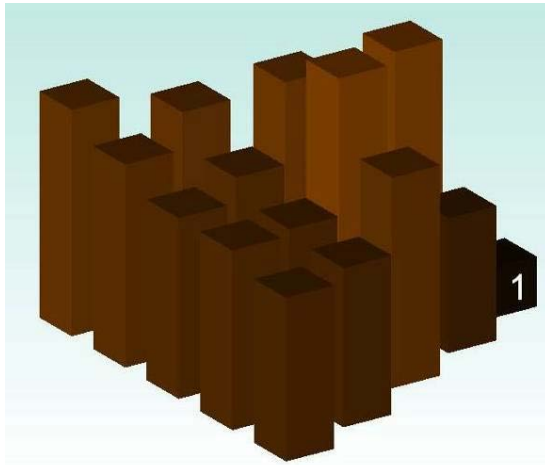
Triaxial BM11: Absorption after firing to 850°C				
		1		
		4.7		
	2		3	
	25.4		12.7	
	4	5	6	
	22.9	26.2	19.8	
7		8		10
20.8		17.6		15.0
11	12	13	14	15
21.3	19.1	17.0	16.9	15.4

To provide a visual representation of absorption in triaxial BM11, the absorption data from Table 66 were used as percentages of brightness to effect translation into transparency ratings (see fig. 374). This translation results in absorption of 0% being represented as pitch black and of 100%, as transparent. The underlying hue is brown. At 850°C, absorption was least at corner A (which is darkest) and greatest in the middle of the triaxial and BM11.5, which is lightest. Further, it can be seen that lighter samples close to corner B had more absorption than did darker samples close to corner C.

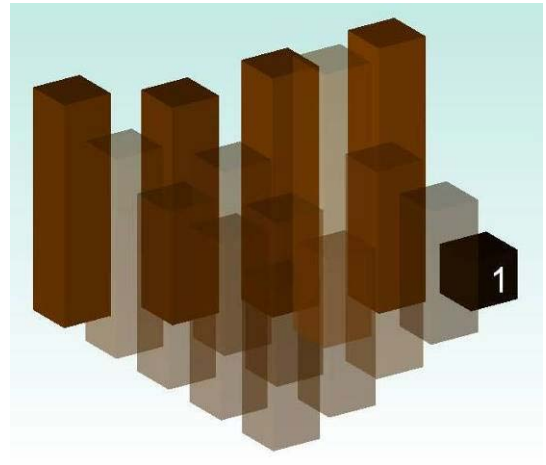


**Figure 374: Triaxial BM11. Absorption at 850°C, top view**

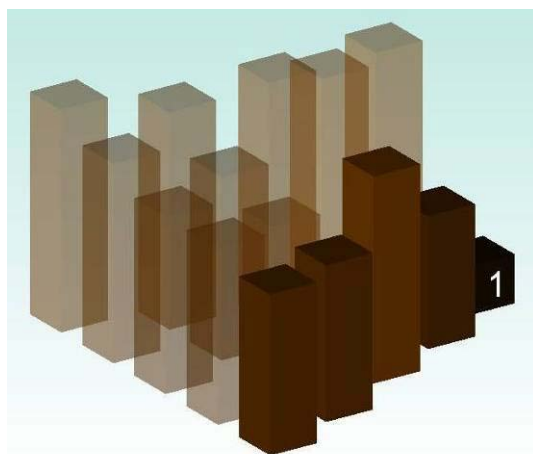
The next series of figures present the absorption depicted by size, as well as by transparency, so that samples with the least absorption are smaller and darker. There was a sharp increase in absorption followed by a gradual decrease along blend line A–B (fig. 375). There was a curvilinear trend from low absorption, to higher and then moderate absorption along blend line A–C (fig. 376) and a linear trend of decreasing absorption along blend line B–C (fig. 377).



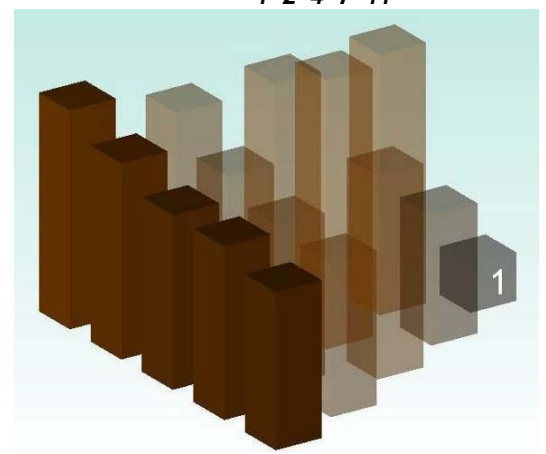
**Figure 375: Triaxial BM11. Absorption at 850°C, trimetric view**



**Figure 376: Triaxial BM11. Absorption at 850°C, trimetric view. Samples 1-2-4-7-11**



**Figure 377: Triaxial BM11. Absorption at 850°C, trimetric view. Samples 1-3-6-10-15**



**Figure 378: Triaxial BM11. Absorption at 850°C, trimetric view. Samples 11-15**

Triaxial BM11: Absorption and porosity after firing to 900°C

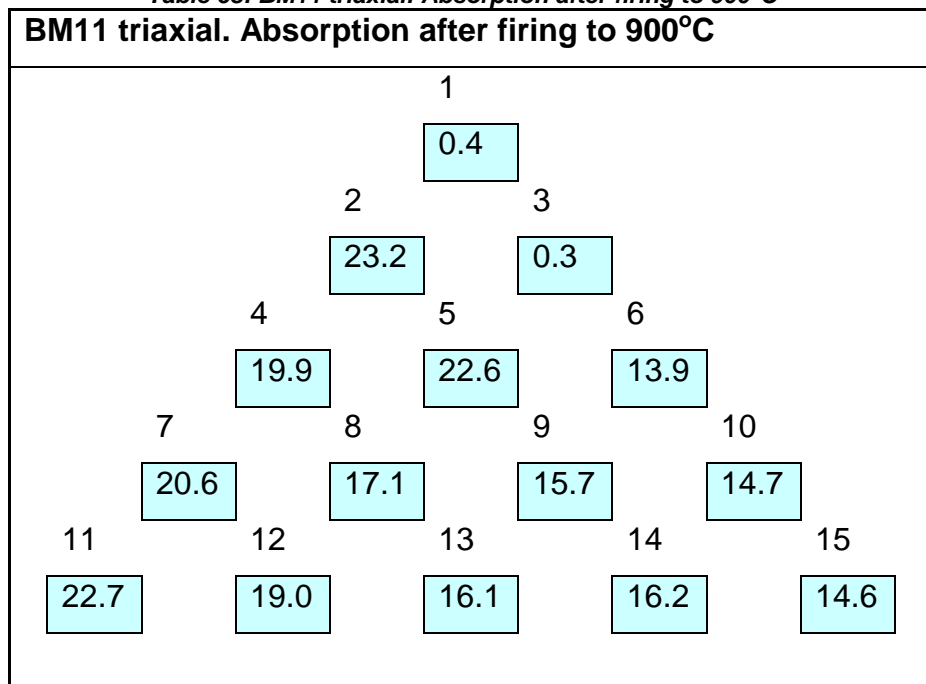
Table 67 (overleaf) shows the absorption and porosity measurements and calculations for triaxial BM11 at 900°C. The adjacent highest (BM11.2) and lowest (BM11.3) results are in red.

**Table 67: Triaxial BM11: Absorption & porosity after firing to 900°C**

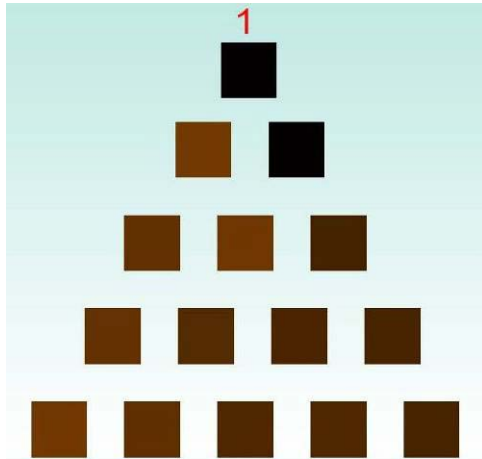
Triaxial BM11: Absorption & porosity after firing to 900°C			
Sample	Absorption (wt%)	Cold / boiled	Apparent porosity (%)
11.1	0.44	1.00	0.99
11.2	23.18	0.94	38.20
11.3	0.30	1.00	0.66
11.4	19.90	0.95	35.22
11.5	22.62	0.95	37.29
11.6	13.93	0.94	26.17
11.7	20.61	0.98	35.69
11.8	17.09	0.98	29.52
11.9	15.65	0.98	28.52
11.10	14.74	0.97	26.56
11.11	22.73	0.98	39.18
11.12	19.01	0.98	34.02
11.13	16.15	0.98	29.03
11.14	16.19	0.99	29.74
11.15	14.65	0.98	27.46

Table 68 shows absorption data in triaxial format. The highest (BM11.2) and lowest (BM11.3) are on the second tier A–B and A–C blend lines, showing extremely different effects of 75% inclusion of corner recipes B (the talc eutectic) and C (the quarry tailings) on recipe A (the high flux recipe).

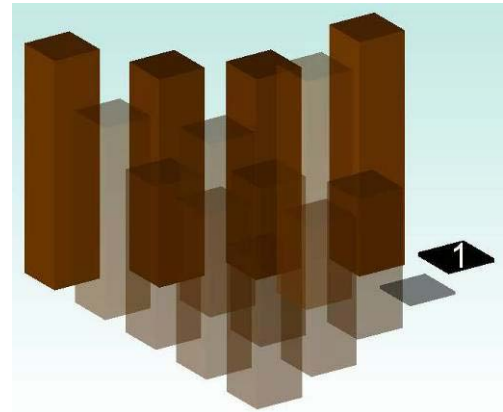
**Table 68: BM11 triaxial: Absorption after firing to 900°C**



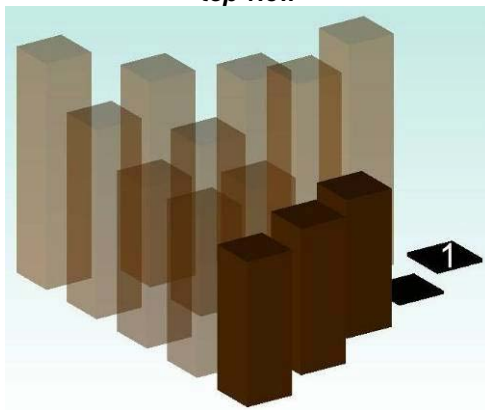
The 2D and 3D graphical representations (figs. 379–382) of samples fired to 900°C again exposed shrinkage trends related to the proportions of the corner recipes. High proportions of recipe A produced very low absorption that was dramatically increased by replacement with 25% or more of recipe B (fig. 380), and reduced by replacement with 25–50% of recipe C (fig. 381). There was a linear trend of reducing absorption along the B–C line blend (fig. 382).



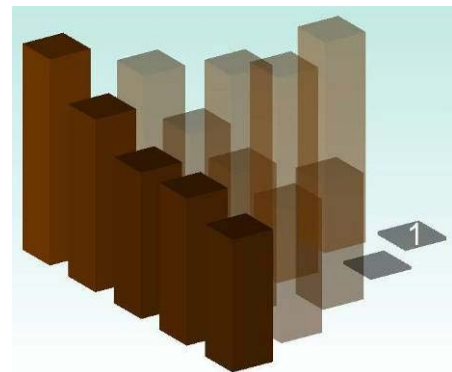
**Figure 379: BM11 triaxial. Absorption at 900°C, top view**



**Figure 380: BM11 triaxial. Absorption at 900°C, trimetric view. Samples 1-2-4-7-11**



**Figure 381: BM11 triaxial. Absorption at 900°C, trimetric view. Samples 1-3-6-10-15**



**Figure 382: BM11 triaxial. Absorption at 900°C, trimetric view. Samples 11-15**

Triaxial BM11: Absorption and porosity after firing to 950°C

Table 69 has absorption and porosity measurements and calculations for triaxial BM11 at 950°C. The lowest (BM11.6) and highest (BM11.11) results are in red.

**Table 69: BM11 triaxial: Absorption & porosity after firing to 950°C**  
**BM11 triaxial. Absorption & porosity after firing to 950°C**

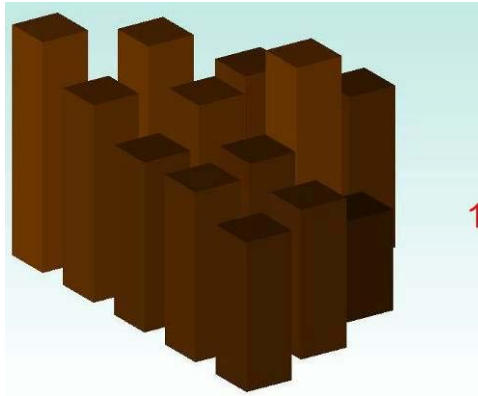
Sample	Absorption (wt%)	Cold / boiled	Apparent porosity (%)
11.1	-	-	-
11.2	15.99	0.95	29.90
11.3	-	-	-
11.4	18.38	0.95	32.65
11.5	22.23	0.95	38.25
11.6	9.96	0.95	20.68
11.7	22.07	0.97	37.72
11.8	19.21	0.97	34.33
11.9	16.41	0.97	32.19
11.10	14.85	0.96	28.06
11.11	22.78	0.98	39.95
11.12	19.52	0.98	35.56
11.13	16.79	0.98	31.40
11.14	16.76	0.78	32.20

Table 70 shows absorption data in triaxial format.

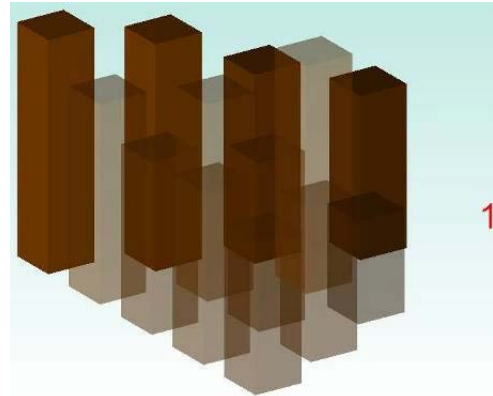
**Table 70: BM11 triaxial: Absorption after firing to 950°C**  
**BM11 triaxial. Absorption after firing to 950°C**

1				
-				
2		3		
16.0		-		
4	5		6	
18.4	22.2		10.0	
7	8	9	10	
22.1	19.2	16.4	14.8	
11	12	13	14	15
22.8	19.5	16.8	16.8	14.8

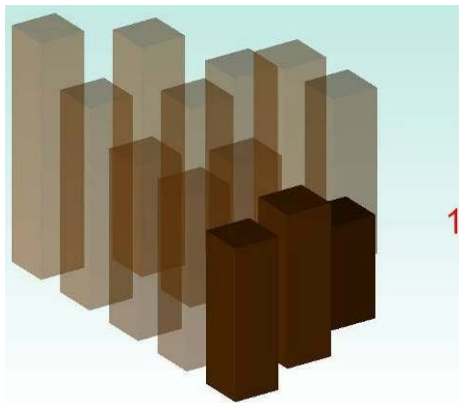
A 3D visual representation of the trends of absorption throughout triaxial BM11 fired to 950°C appears in Figures 383–386.



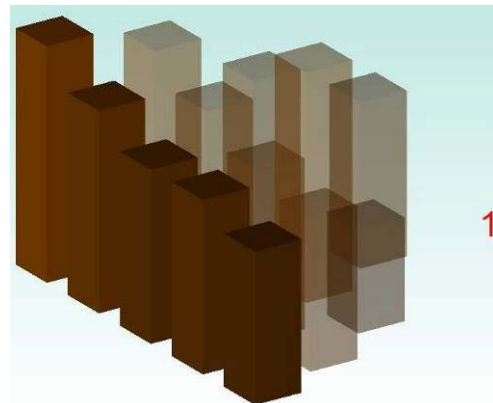
**Figure 383: BM11 triaxial. Absorption at 950°C, trimetric view**



**Figure 384: BM11 triaxial. Absorption at 950°C, trimetric view. Samples 2–4–7–11**



**Figure 385: BM11 triaxial. Absorption at 950°C, trimetric view. Samples 6–10–15**



**Figure 386: BM11 triaxial. Absorption at 950°C, trimetric view. Samples 11–15**

The clearest trend in porosity is the decreasing percentage absorption along the B-C line blend (fig. 385). As none of the samples fired at 950°C had absorption below 10% by weight, the triaxial was fired to 1000°C.

Triaxial BM11: Absorption and porosity after firing to 1000°C

Table 71 (overleaf) shows the absorption and porosity measurements and calculations for triaxial BM11 at 1000°C. The lowest (BM11.6) and highest (BM11.11) results are in red.

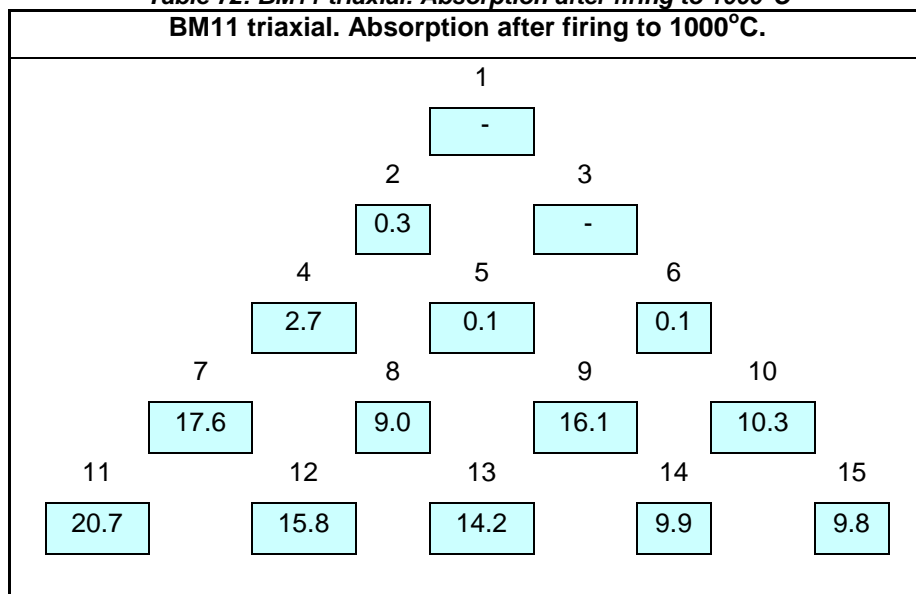
**Table 71: BM11 triaxial: Absorption and porosity after firing to 1000°C**  
**BM11 triaxial. Absorption and porosity after firing to 1000°C**

Sample	Absorption (wt%)	Cold / boiled	Apparent porosity (%)
11.1	-	-	-
11.2	0.29	1.00	0.61
11.3	-	-	-
11.4	2.73	0.98	5.95
11.5.	0.16	1.00	0.31
11.6	0.12	1.00	0.23
11.7	17.62	0.96	32.78
11.8	18.39	0.97	33.33
11.9	16.08	0.96	30.12
11.10	10.28	0.95	19.98
11.11	20.71	0.97	38.21
11.12	15.81	0.97	29.99
11.13	14.22	0.97	27.07
11.14	9.90	0.97	19.09
11.15	9.76	0.97	20.20

The three Tier 3 samples (BM11.4–BM11.6) all had low percentage absorption, with the latter two samples approaching 0%.

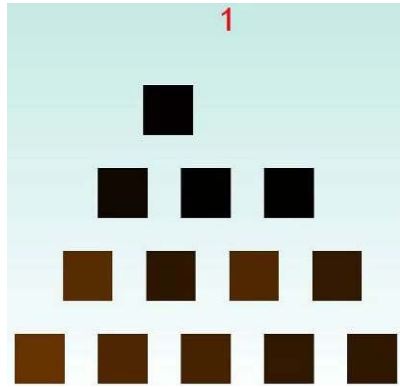
Once again, the data were entered in triaxial format to visualise trends (Table 72). The most obvious trend was towards increasing absorption with increasing proportions of corner B (BM11.11).

**Table 72: BM11 triaxial: Absorption after firing to 1000°C**  
**BM11 triaxial. Absorption after firing to 1000°C.**

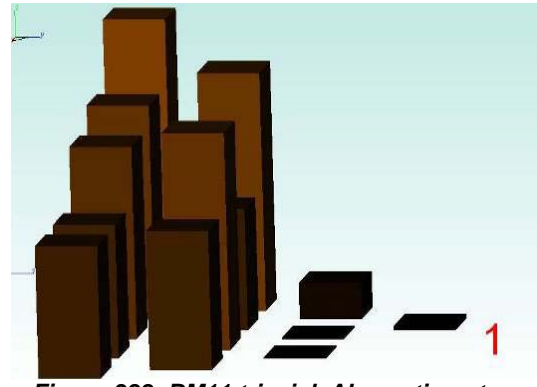




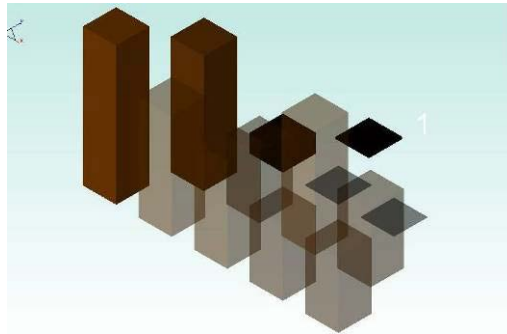
A 2D visual representation of the percentage absorption appears in Figure 387. This is followed by addition of a third dimension of height to represent percentage absorption (figs. 388–392).



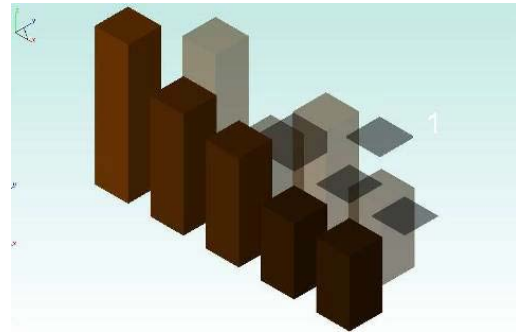
**Figure 387: BM11 triaxial. Absorption at 1000°C**



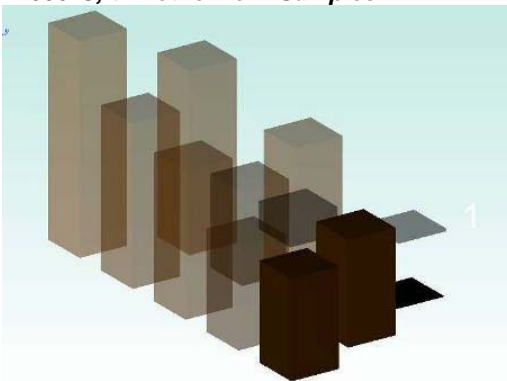
**Figure 388: BM11 triaxial. Absorption at 1000°C**



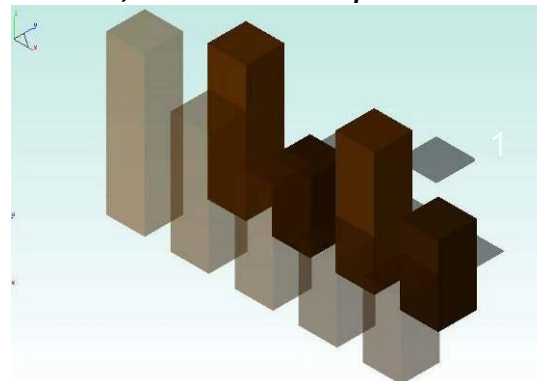
**Figure 389: BM11 triaxial. Absorption at 1000°C, trimetric view. Samples 2-4-7-11**



**Figure 390: BM11 triaxial. Absorption at 1000°C, trimetric view. Samples 11-15**



**Figure 391: BM11 triaxial. Absorption at 1000°C, trimetric view. Samples 6-10-15**



**Figure 392: BM11 triaxial. Absorption at 1000°C, trimetric view. Samples 7-10**

This section of the chapter has focused on inter-sample trends observed within triaxial BM11 at each of four specific firing temperatures. Overall, the results displayed in triaxial format indicate that the inclusion of the talc at corner B (BM11.11) had a negative effect with respect to the desired quality of low

porosity. After firing triaxial BM11 to 1000°C, only three samples had absorption levels consistent with advanced vitrification.

The following section describes intra-sample changes in appearance, density and absorption for each sample from triaxial blend BM11 fired in an oxidising atmosphere at four different firing temperatures: 850, 900, 950 and 1000°C. This has been done in order to document effectively the influence of increasing temperature on each individual sample from triaxial BM11.

## Triaxial BM11: Observations and data across increasing temperatures

Sample BM11.1 fired to an off-white colour at 850 and 900°C (fig. 393). At 850°C, the bars had begun to fuse at the edges. At 900°C, the effloresced surface had started to fuse and smooth over, except where the edges were resting on the kiln shelf and ceramic paper. Bars that were in contact fused together at 900°C. With a volume:mass ratio of 0.45 at 900°C, bars felt denser and heavier than at 850°C. At 900°C the interior of broken samples appeared to be fully vitrified.



Figure 393: BM11.1: 850°C (top) and 900°C

Absorption was 4.7% at 850°C, and 0.4% at 900°C. Porosity was ~9% at 850°C, and ~1% at 900°C. Shrinkage from dry was 9.1% at 850°C and 11.6% at 900°C (fig.394).

BM11.1 was not fired above 900°C.

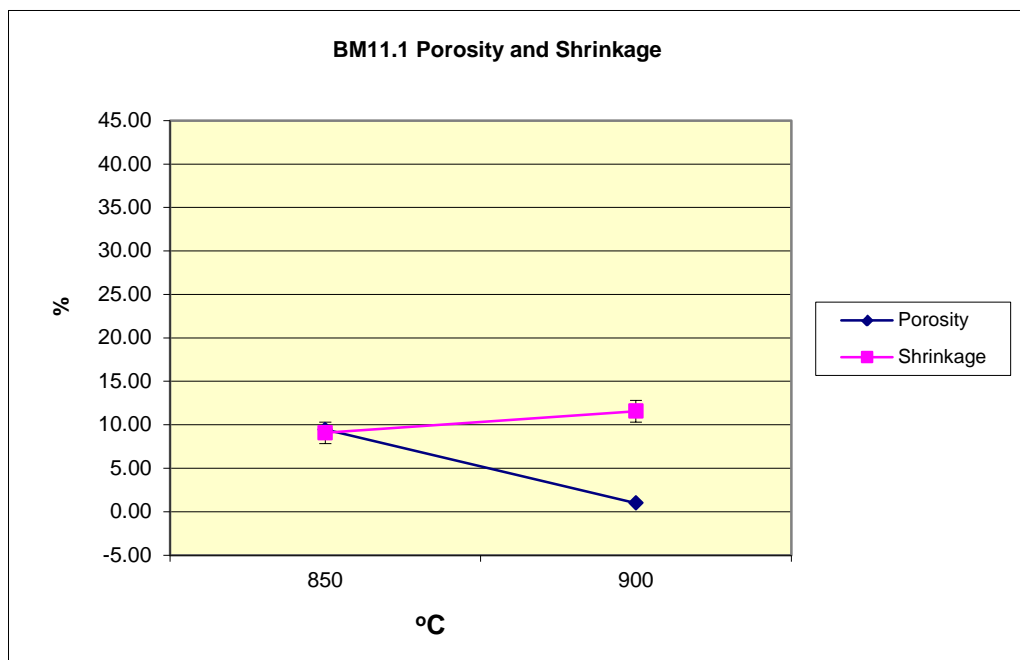
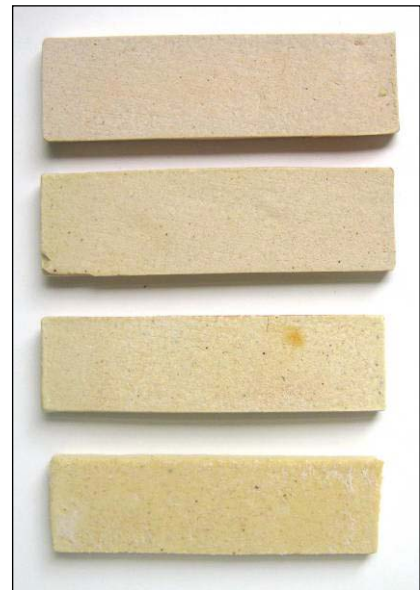


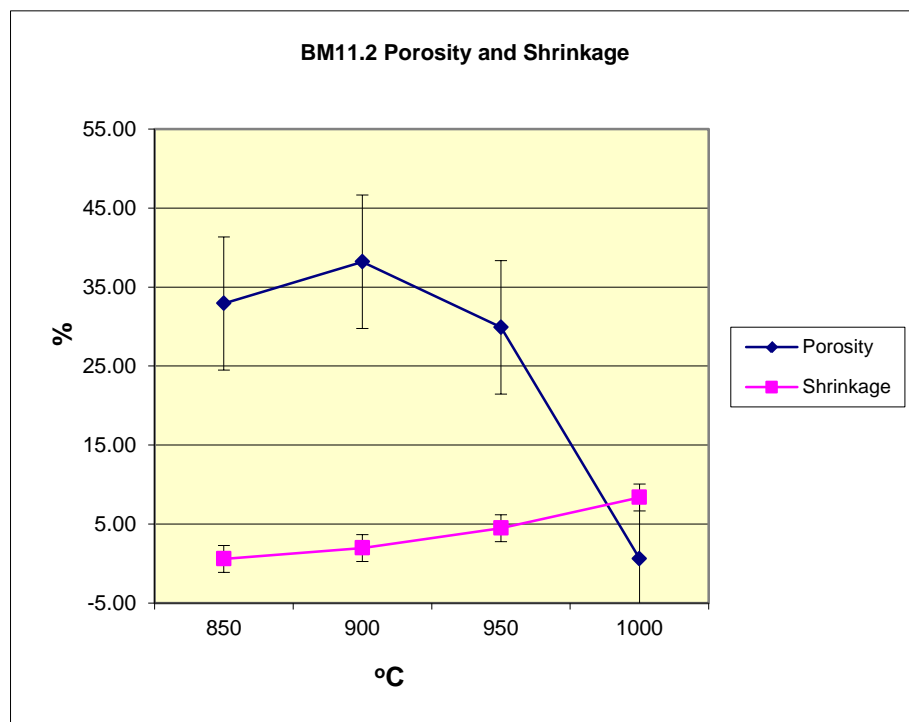
Figure 394: BM11.1 porosity and shrinkage

Sample BM11.2 fired to a pale buff colour at 850°C, becoming progressively more yellow at 900, 950 and 1000°C (fig. 395). No evidence of melting was observed, except at 1000°C, at which point only the edge surface of bars closest to the kiln elements fused, and the bars adhered to the ceramic fibre paper on which they were fired. Weight for size, bars felt light at 850 and 900°C, slightly heavier at 950°C and dense and heavy at 1000°C. The volume:mass ratio was 0.48 at 1000°C.



**Figure 395: BM11.2: 850 (top), 900, 950 and 1000°C**

Absorption decreased from 25.3% at 850°C to .3% at 1000°C. Porosity was ~33% at 850°C, and <1% at 1000°C. Shrinkage from dry was 0.6% at 850°C and 8.4% at 1000°C (fig.396).



**Figure 396: BM11.2 porosity and shrinkage**

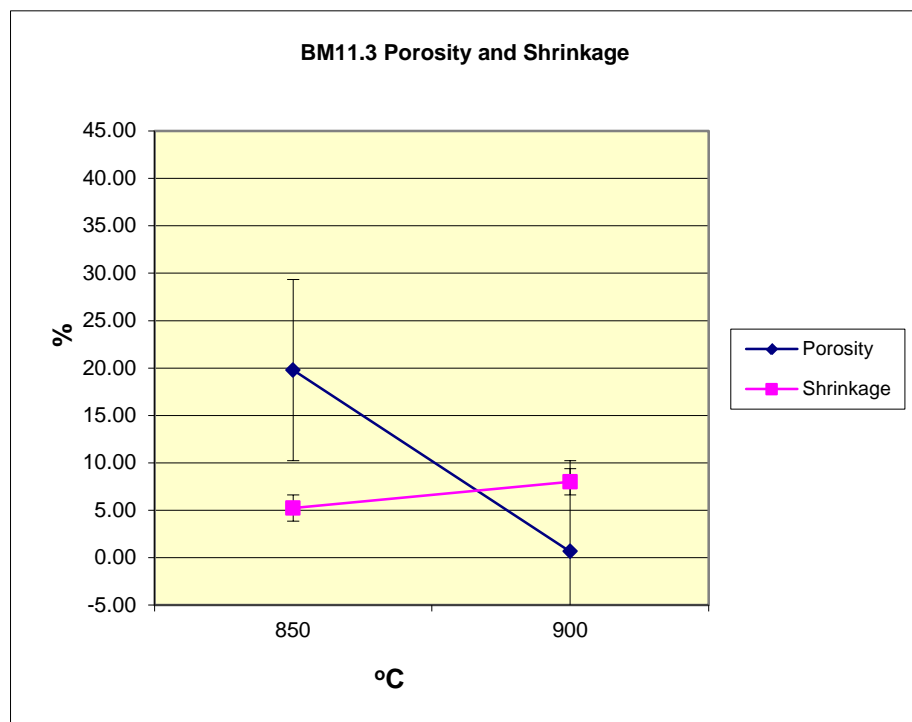
Sample BM11.3 fired to a pale yellow colour at 850°C, becoming more yellow at 900°C. At 850°C, the effloresced surface had started to fuse and smooth over into a matte and bars that were in contact fused together without slumping. At 900°C, the fused effloresced surface had started to flow onto the ceramic paper and the bars adhered to the ceramic fibre paper. Bars that were in contact fused together and slumped. Surfaces that had not effloresced remained unglazed. With a volume:mass ratio of 0.46 at 900°C, bars felt denser and heavier at 900°C than at 850°C, and at 900°C the interior of broken samples appeared to be fully vitrified.



**Figure 397: BM11.3: 850 (top) and 900°C**

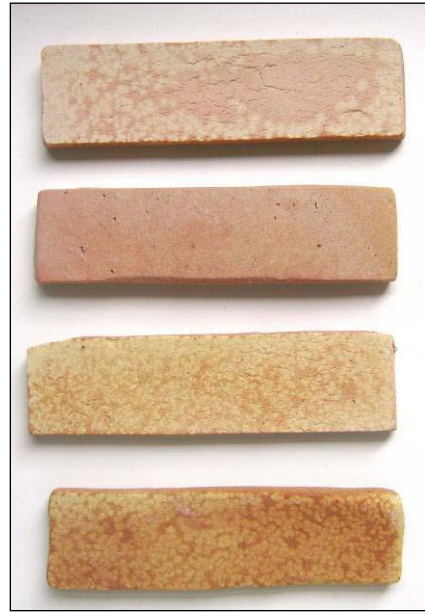
Absorption was 12.7% at 850°C, and 0.3% at 900°C. Porosity was ~20% at 850°C, and <1% at 900°C. Shrinkage from dry was 5.2% at 850°C and 8% at 900°C (fig.398).

BM11.3 was not fired above 900°C.



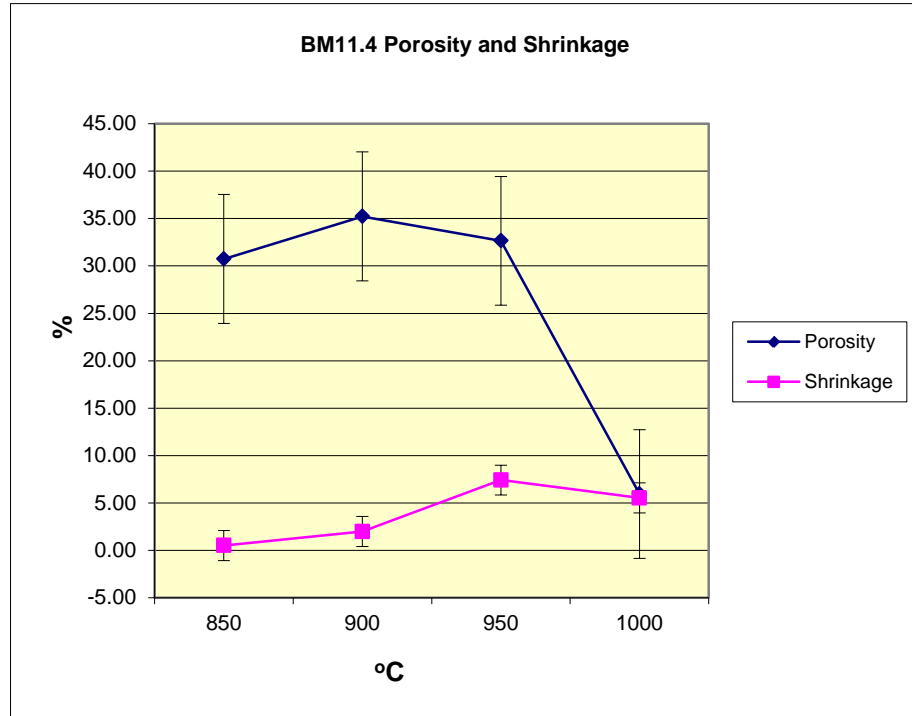
**Figure 398: BM11.3 porosity and shrinkage**

Sample BM11.4 fired to a pale salmon colour with cream speckled efflorescence at 850°C. As firing temperature increased, the underlying body colour darkened to orange and the speckles of efflorescence remained cream (fig. 399). The efflorescence did not form a glaze, remaining similarly 'dry' to the touch at all temperatures. The bar fired to 1000°C felt moderately dense. The volume:mass ratio at 1000°C was 0.46.



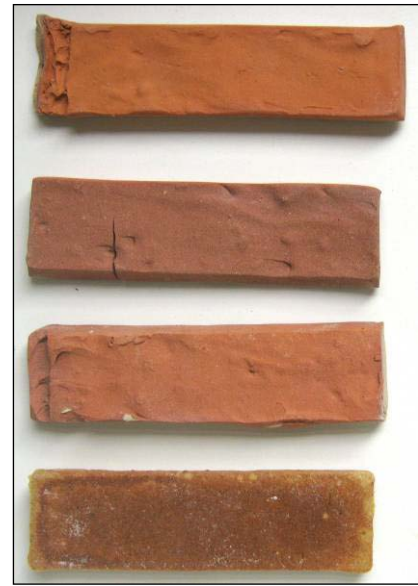
**Figure 399: BM11.4: 850 (top), 900, 950 and 1000°C**

Absorption decreased from 22.9% at 850°C to 2.7% at 1000°C. Porosity was ~31% at 850°C, and ~6% at 1000°C. Shrinkage from dry was 0.5% at 850°C and 5.5% at 1000°C (fig. 400).

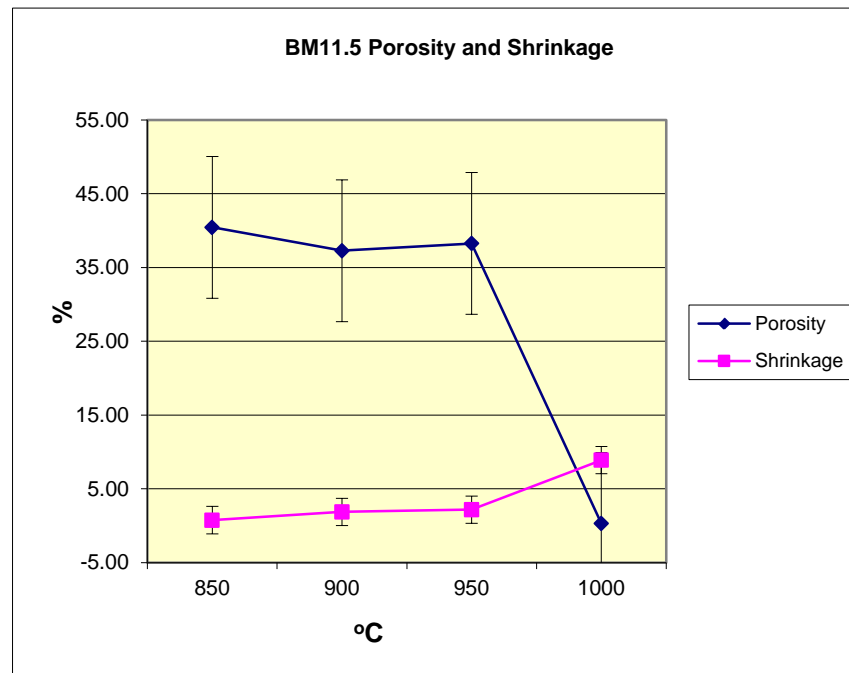


**Figure 400: BM11.4 porosity and shrinkage**

Sample BM11.5 (fig. 401) fired to a terracotta colour at 850°C with cream speckled efflorescence (not shown). As firing temperature increased, the underlying body colour changed in a non-linear manner, first darkening to brown, then becoming lighter again at 950°C. At 1000°C the body was dark tan on the surface in contact with the ceramic paper, and light tan on the top surface. The speckles of efflorescence remained cream. The efflorescence did not form a glaze, remaining similarly 'dry' to the touch at all temperatures, except for a small thicker portion on the edge at the left of the bar fired to 1000°C. The bar fired to 1000°C felt moderately dense. The volume:mass ratio at 1000°C was 0.5. Absorption decreased from 26.2% at 850° to 0.2% at 1000°C. Porosity was ~41% at 850°C, and <1% at 1000°C. Shrinkage from dry was 0.8% at 850°C and 8.9% at 1000°C (fig. 402).



**Figure 401: BM11.5: 850 (top), 900, 950 and 1000°C**

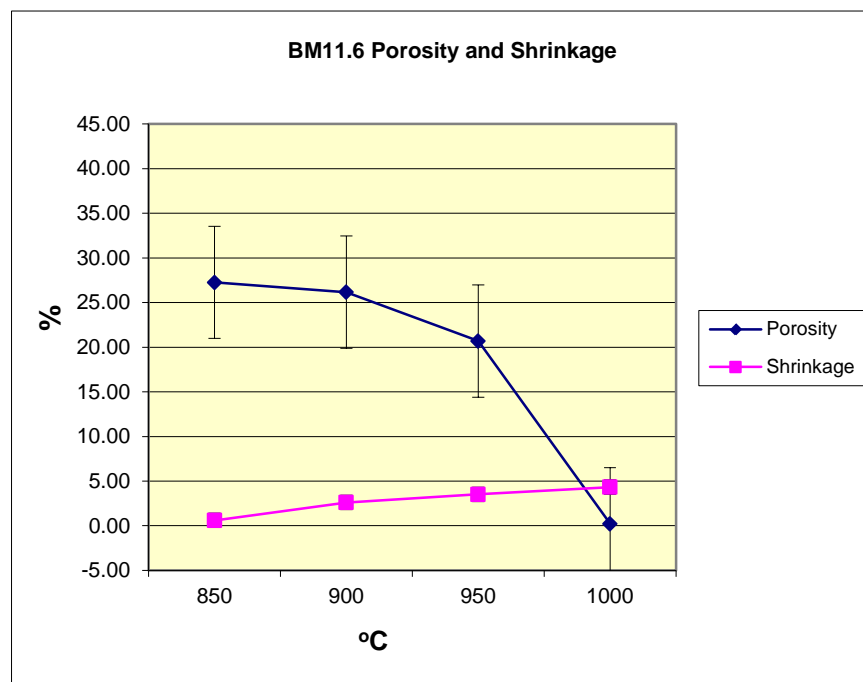


**Figure 402: BM11.5 porosity and shrinkage**

Sample BM11.6 (fig. 403) fired to a liver colour at 850°C with cream speckled efflorescence. As firing temperature increased, the underlying body colour darkened to chocolate brown and the speckles of efflorescence remained cream. Where efflorescence was thicker at the ends of bars a matte glaze developed at temperatures above 900°C. At 1000°C, the entire bar surface had developed a sheen. The edges started to flow onto the ceramic paper and bars that were previously not in contact fused together at the edges. The bar fired to 1000°C felt moderately dense. The volume:mass ratio at 950°C was 0.48, but the volume:mass ratio at 1000°C was 0.55, indicating permanent body expansion between 950 and 1000°C. Absorption decreased from 19.8% at 850°C to 0.1% at 1000°C. Porosity was ~27% at 850°C, and <1% at 1000°C. Shrinkage from dry was 0.6% at 850°C and 4.3% at 1000°C (fig. 404).



**Figure 400: BM11.6: 850 (top), 900, 950 and 1000°C**

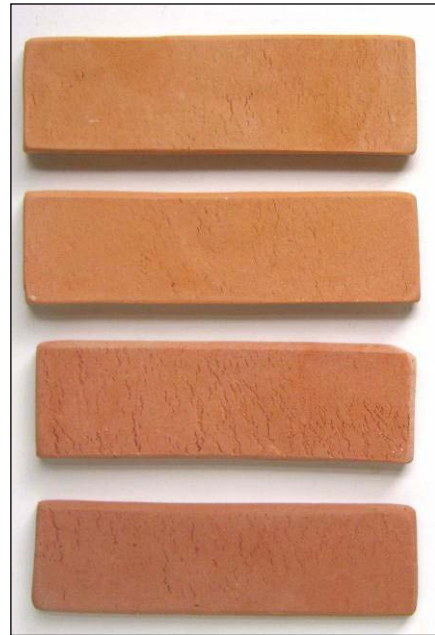


**Figure 404: BM11.6 porosity and shrinkage**

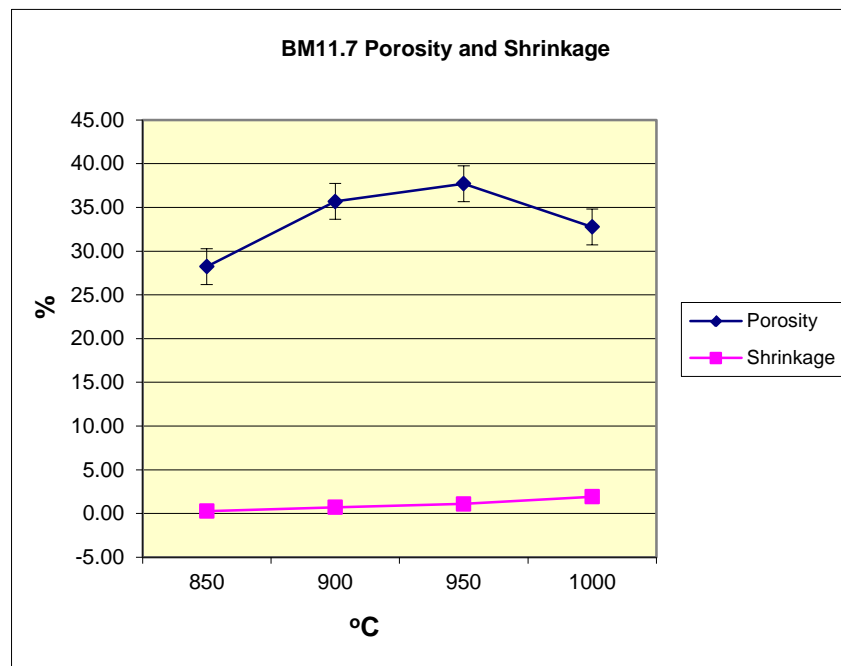


Sample BM11.7 (fig. 405) fired to a deep salmon colour at 850°C. As firing temperature increased, the body colour darkened to a pale dusky terracotta. The bar fired to 1000°C felt light. The volume:mass ratio at 1000°C was 0.55.

In a pattern not observed in previous BM11 samples, absorption increased from 20.8% at 850°C to 22.1% at 950°C, before decreasing to 17.6% at 1000°C. Porosity was ~36% at 850°C, and ~33% at 1000°C. Shrinkage from dry was 0.3% at 850°C and 1.9% at 1000°C (fig. 406).

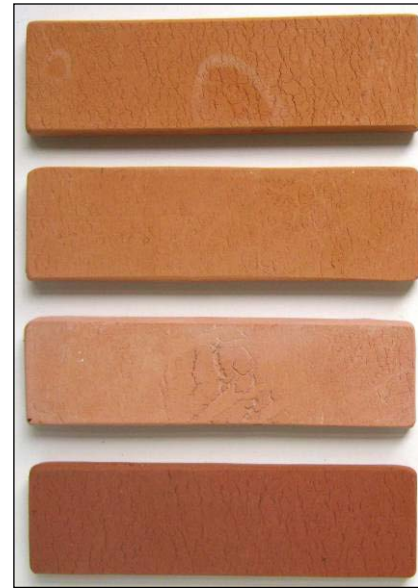


**Figure 405: BM11.7: 850 (top), 900, 950 and 1000°C**



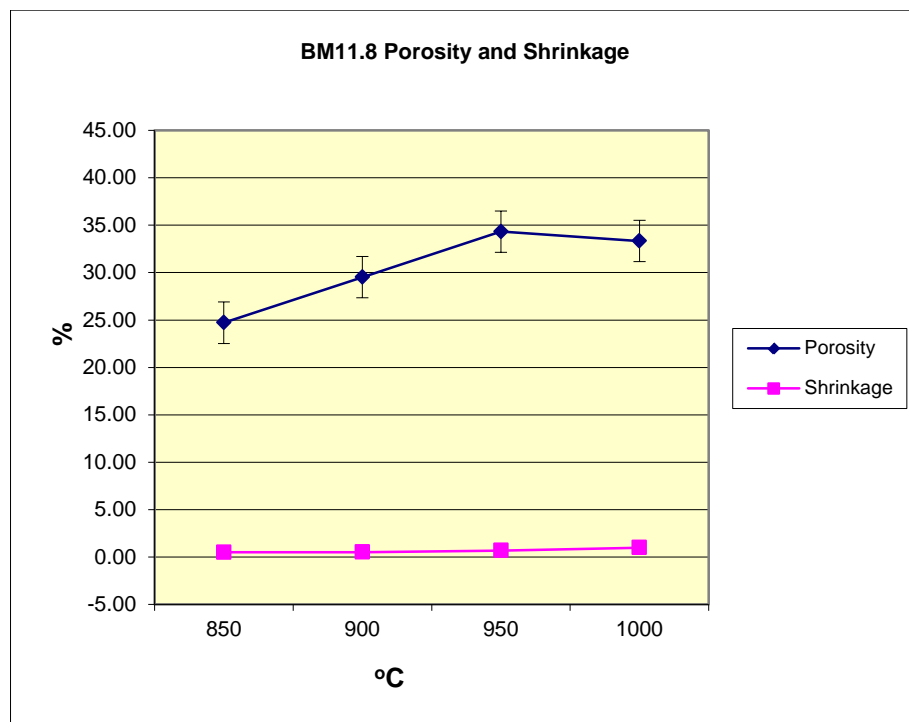
**Figure 406: BM11.7 porosity and shrinkage**

Sample BM11.8 (fig. 407) fired to a deep salmon colour at 850°C. As firing temperature increased to 950°C, the body became paler. At 1000°C this trend was reversed and the body colour darkened to auburn. The bar fired to 1000°C felt light. The volume:mass ratio at 1000°C was 0.55.



**Figure 407: BM11.8: 850 (top), 900, 950 and 1000°C**

In a similar pattern to that observed in BM11.7 samples, absorption increased from 17.6% at 850°C to 19.2% at 950°C, before decreasing to 18.4% at 1000°C. This reflected the direction of colour changes. Porosity was ~25% at 850°C, and ~33% at 1000°C. Shrinkage from dry was 0.5% at 850°C and 1% at 1000°C (fig. 408).



**Figure 408: BM11.8 porosity and shrinkage**

Sample BM11.9 (fig. 409) fired to a dusky terracotta colour at 850°C. As firing temperature increased to 950°C, the body became slightly paler. At 1000°C this trend was reversed and the body colour darkened to auburn. In a similar pattern to that observed in BM11.7 and BM11.8 samples, absorption increased from 15.7% at 850°C to 16.4% at 950°C, before decreasing to 16.1% at 1000°C. This again reflected the direction of colour changes. The bar fired to 1000°C felt light. The volume:mass ratio at 1000°C was 0.53. Porosity was ~23% at 850°C, and ~30% at 1000°C. Shrinkage from dry was 0.4% at 850°C and 0.9% at 1000°C (fig. 410).

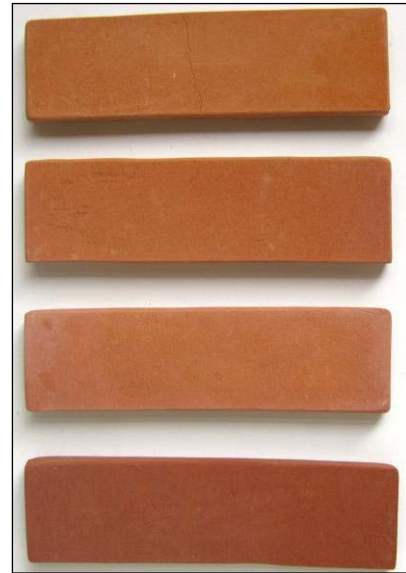


Figure 409: BM11.9: 850 (top), 900, 950 and 1000°C

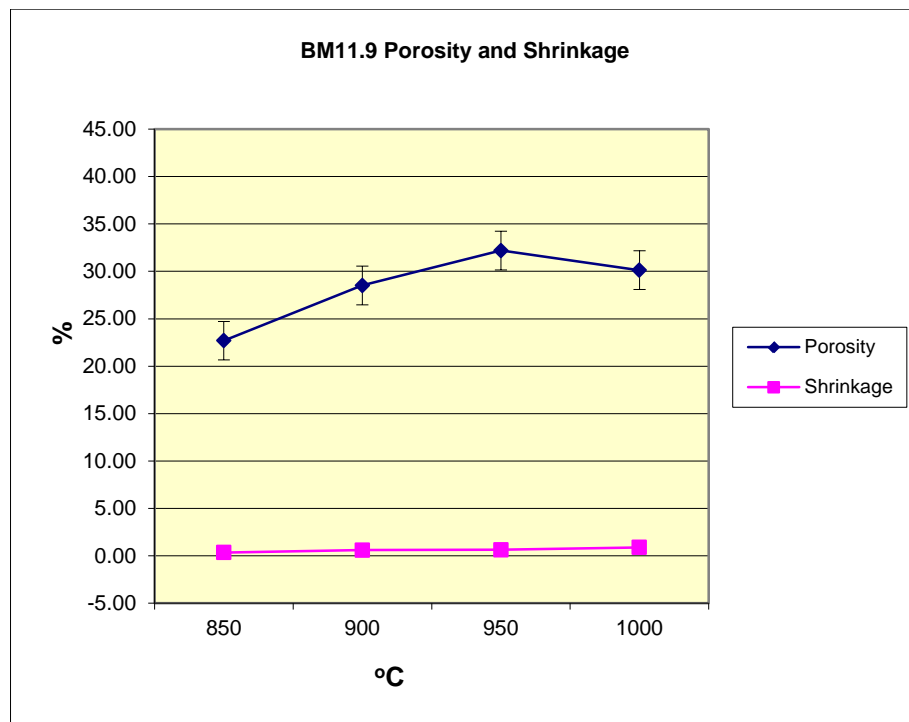
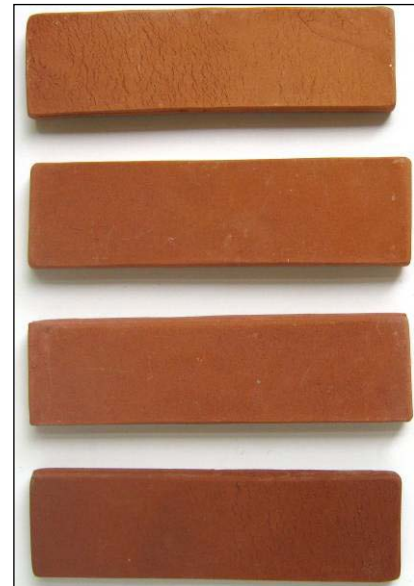
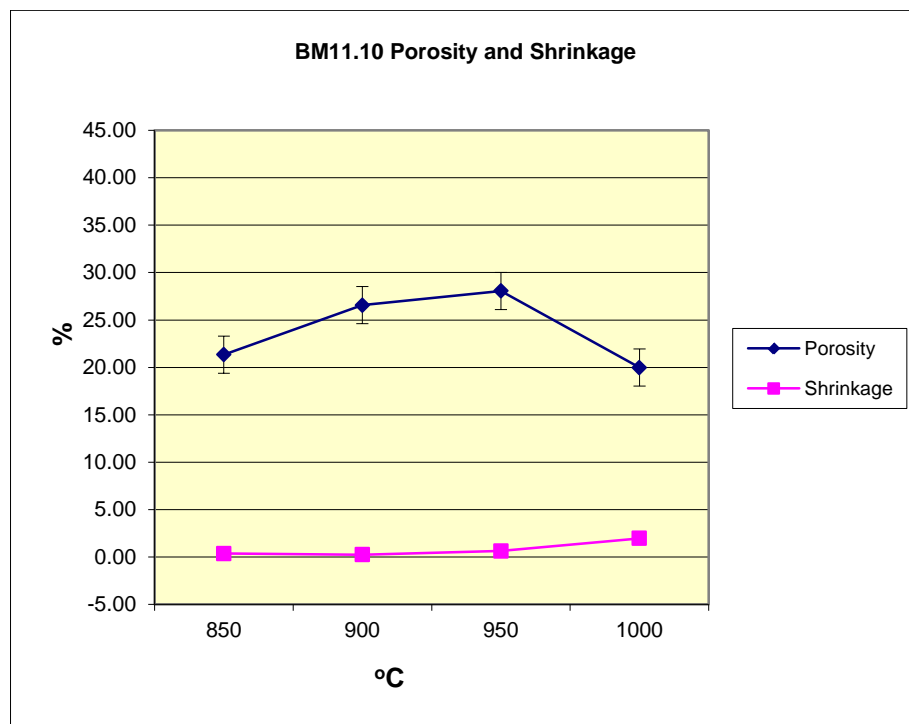


Figure 410: BM11.9 porosity and shrinkage

Sample BM11.10 (fig. 411) fired to a dusky terracotta colour at 850°C. Colour varied little from 850 to 950°C. As firing temperature increased to 1000°C, the body became darker. Changes in absorption followed a similar pattern. Absorption varied little from 15% at 850°C to 14.9% at 950°C. As firing temperature increased to 1000°C, absorption decreased to 10.3%. The volume:mass ratio at 1000°C was 0.51. Porosity was ~21% at 850°C, and ~20% at 1000°C. Shrinkage from dry was 0.4% at 850°C and 2% at 1000°C (fig. 412).



**Figure 411: BM11.10: 850 (top), 900 950 and 1000°C**



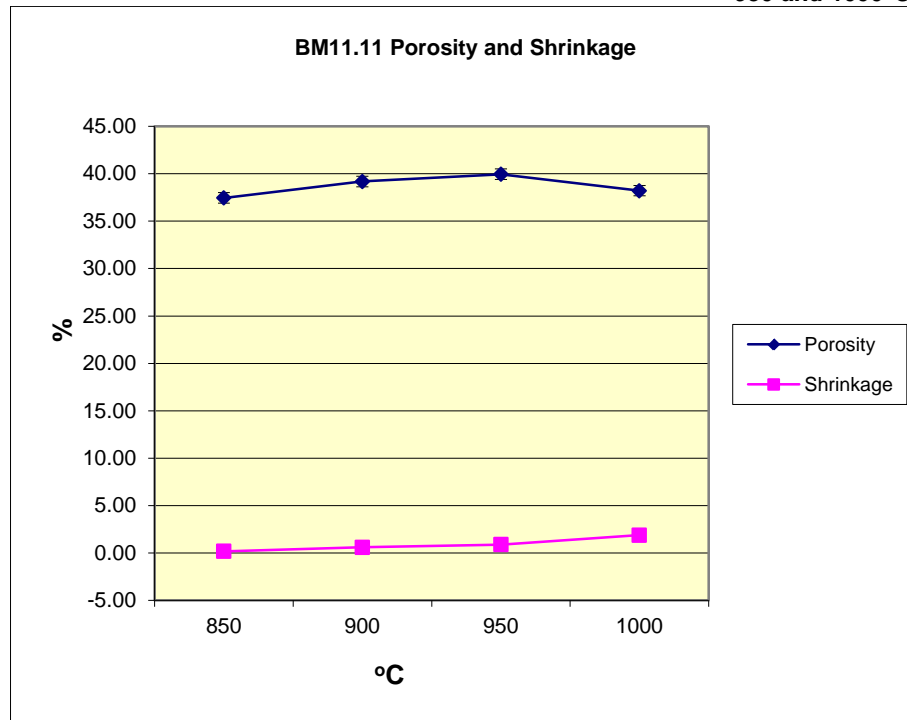
**Figure 412: BM11.10 porosity and shrinkage**

Sample BM11.11 (fig. 413) fired to a pink tan colour at 850°. As firing temperature increased to 950°C, the body became noticeably paler. In a similar pattern to that observed in samples BM11.7–BM11.9 absorption increased slightly from 21.3% at 850°C to 22.8% at 950°C, before decreasing to 20.8% at 1000°C. This again reflected the direction of colour changes.

All bars felt light. The volume:mass ratio at 1000°C was 0.54. Porosity was ~38% at 850°C, and ~38% at 1000°C. Shrinkage from dry was 0.2% at 850°C and 1.9% at 1000°C (fig. 414).



**Figure 413: BM11.11: 850 (top), 900, 950 and 1000°C**



**Figure 414: BM11.11 porosity and shrinkage**

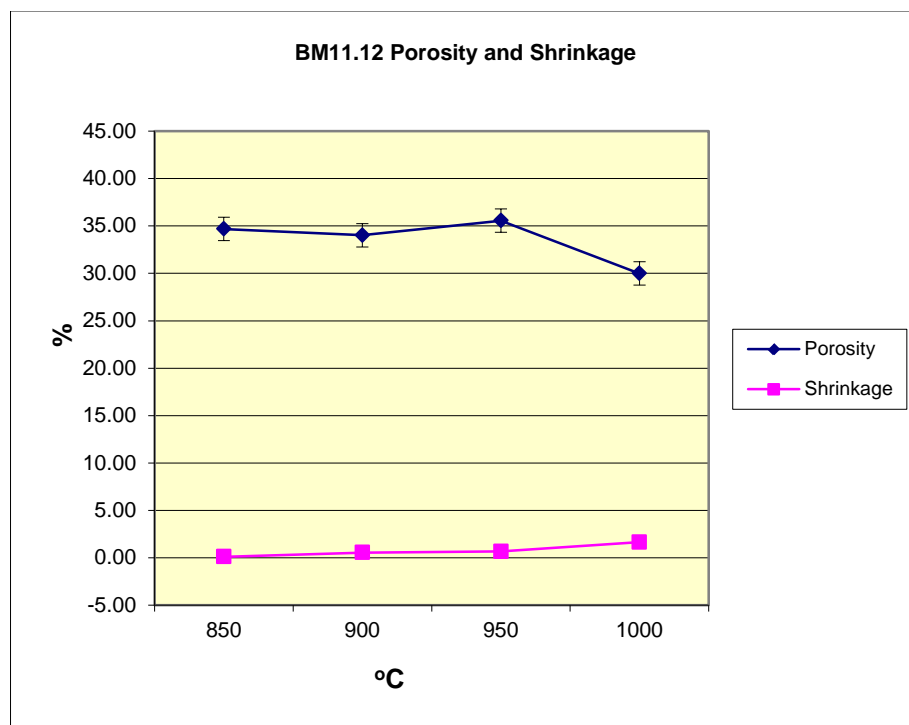
Sample BM11.12 (fig. 415) fired to a pale brown colour at 850°C. As firing temperature increased to 950°C, the body became slightly paler.

In a similar pattern to that observed in samples BM11.7 to BM11.9 absorption increased from 21.3% at 850°C to 22.8% at 950°C, before decreasing to 20.8% at 1000°C. This again reflected the direction of colour changes.

All bars felt light. The volume:mass ratio at 1000°C was 0.53. Porosity was ~35% at 850°C, and ~30% at 1000°C. Shrinkage from dry was 0.1% at 850°C and 1.6% at 1000°C (fig. 416).



**Figure 415: BM11.12: 850 (top), 900, 950 and 1000°C**



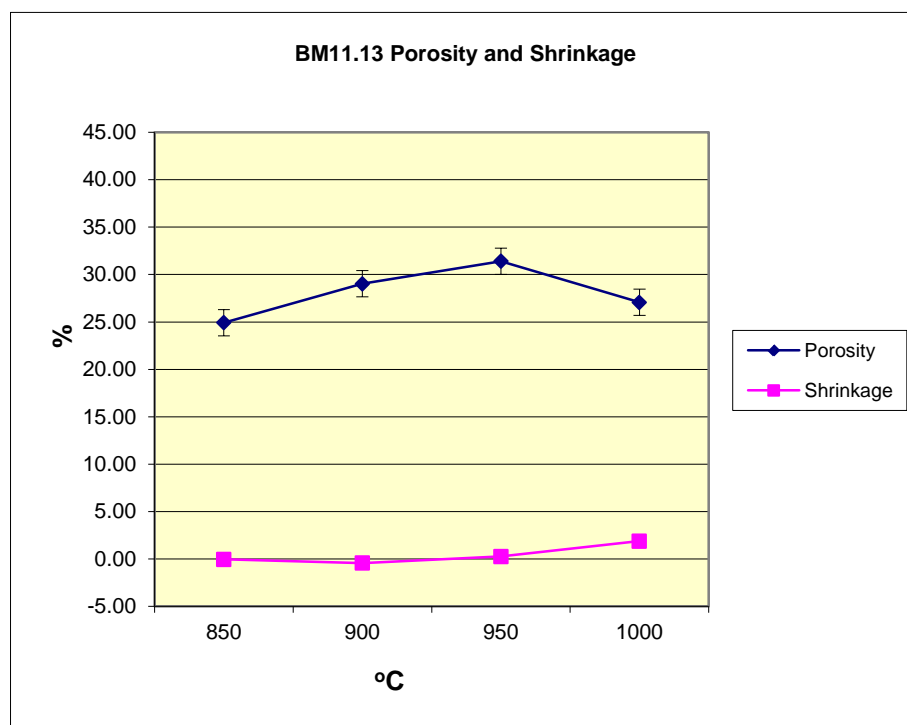
**Figure 416: BM11.12 porosity and shrinkage**

Sample BM11.13 (fig. 417) fired to a dusky terracotta colour at 850°C. As firing temperature increased to 950°C, the body became slightly paler, becoming darker after firing to 1000°C.

Absorption was 17% at 850°C, dipping slightly at 900°C, returning to 16.8% at 950°C, before decreasing to 14.2% at 1000°C. The volume:mass ratio at 1000°C was 0.53. Porosity was ~25% at 850°C, and ~27% at 1000°C. Shrinkage from dry was 0% at 850°C and 1.9% at 1000°C (fig. 418).

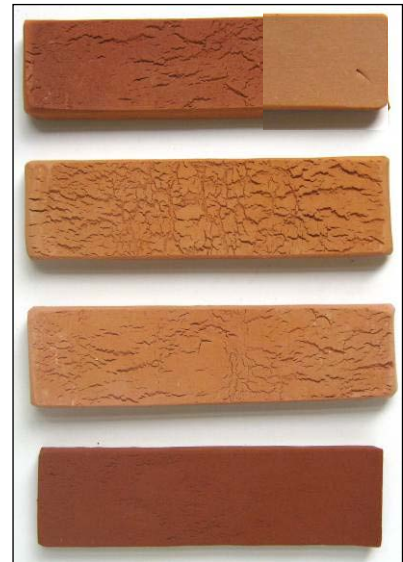


**Figure 417: BM11.13: 850 (top), 900, 950 and 1000°C**

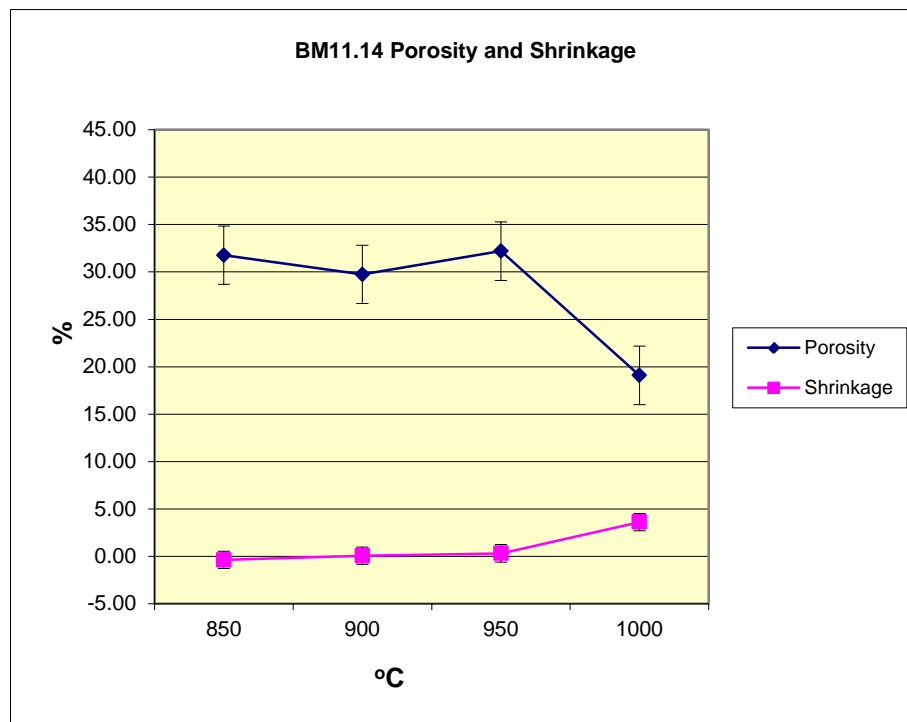


**Figure 418: BM11.13 porosity and shrinkage**

Sample BM11.14 fired to a dusky salmon colour at 850°C. Unlike the bars fired to higher temperatures, the face of the bar fired to 850°C (pictured as an insertion top right in Figure 419) was a paler colour than the base. The body colour changed little as firing temperature increased to 950°C, but darkened to a russet colour at 1000°C. Absorption was 16.9% at 850°C, dipping slightly at 900°C, returning to 16.8% at 950°C, before decreasing to 9.9% at 1000°C. The volume:mass ratio at 1000°C was 0.52. Porosity was ~32% at 850°C, and ~20% at 1000°C. Expansion from dry was 0.4% at 850°C and shrinkage from dry was 3.6% at 1000°C (fig. 420).



**Figure 419: BM11.14: 850 (top), 900, 950 and 1000°C**

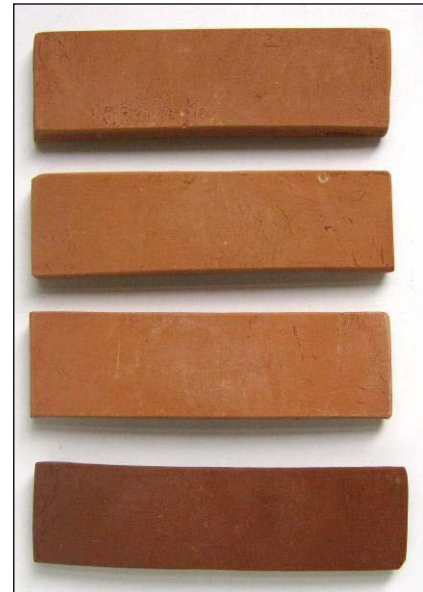


**Figure 420: BM11.14 porosity and shrinkage**

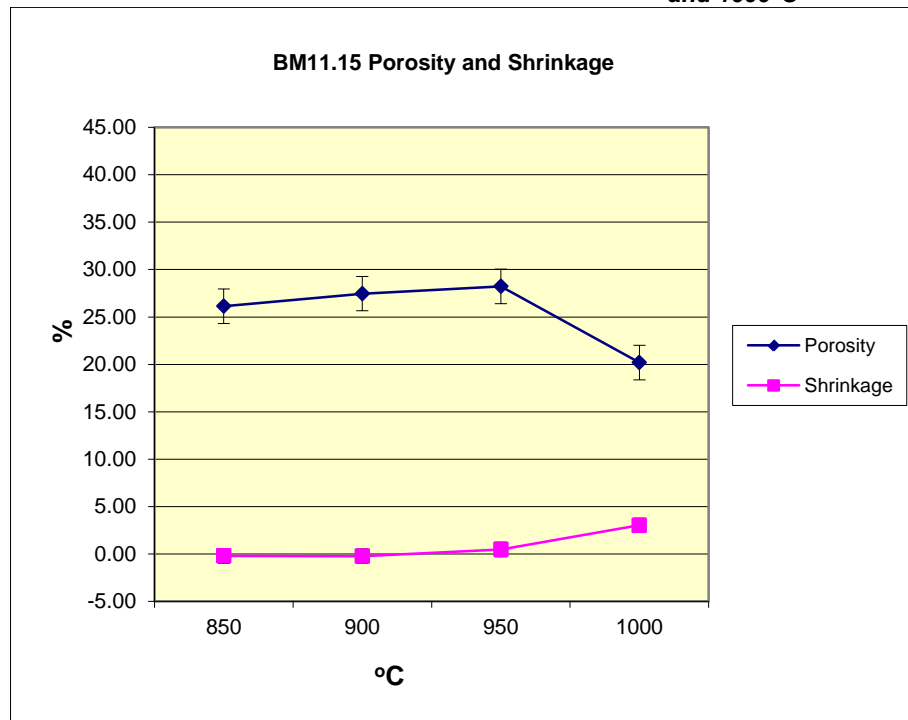


Sample BM11.15 (fig. 421) fired to a dusky terracotta colour at 850°C. As firing temperature increased to 950°C, the body became slightly paler.

Absorption decreased from 15.4% at 850°C to 14.8% at 950°C, before decreasing to 9.3% at 1000°C. The volume:mass ratio at 1000°C was 0.48. Porosity was ~26% at 850°C, and ~20% at 1000°C. Expansion from dry was 0.2% at 850°C and shrinkage from dry was 3.0% at 1000°C (fig. 422).



**Figure 421: BM11.15: 850 (top), 900, 950 and 1000°C**



**Figure 422: BM11.15 porosity and shrinkage**

The results obtained from the investigations documented in this chapter were promising, but demonstrated a continuing trade-off between firing temperature, workability and permeability. The bodies that had low porosity also had undesirable levels of thixotropy, but it was demonstrated that it was possible to use them to make and fire slabs. A highly thixotropic body of almost zero porosity was achieved at 900°C, well within the target range of this study. Other bodies with lower thixotropy had higher absorption, and a question remained as

to how much higher they would need to be fired to minimise absorption. The following chapters continue this exploration of the trade-off between composition, workability, firing temperature and absorption.

## Chapter 24: Further Tests Exploring Properties of Interesting Bodies

Several bodies from the preceding tests were selected for further experimentation, some for firing at different temperatures up to 1100°C, some for experimentation to reduce efflorescence, and some for tests of fired strength. The bodies selected for the experiments documented in this and the following two chapters are listed in Table 73, together with the temperatures at which they were fired.

*Table 73: Bodies selected for further experiment*

	(°C)	850	900	950	1000	1050	1100
BM1.13						✓	✓
BM11.10						✓	✓
BM11.1			✓				
BM11.2				✓	✓		
BM11.3			✓				
BM11.4				✓	✓		
BM11.5				✓	✓		
BM11.6 (+ scum test)				✓	✓	✓	
BM11.6A (+ scum test)				✓	✓		
B20M60C20 (BM1.14c)				✓	✓	✓	✓
B25M75 (BM1.14)				✓	✓	✓	✓

Another series of test pieces was produced to establish more of the properties of these more promising bodies. The properties under investigation included handling requirements, appearance, absorption, shrinkage and fired strength. The properties investigated—the changes to body formulation and the firing temperatures used—were varied based on the previously obtained results. Some bodies that had not vitrified in earlier tests were fired to higher temperatures; one promising terracotta body received a 20% addition of cullet; and one body received additives intended to reduce thixotropy and efflorescence. The procedures involved are described below, beginning with description of the workability issues associated with preparation of slabs from larger quantities of bodies from triaxial BM11.

## **Preparation of larger batches of bodies from triaxial BM11**

A total of 4.5 kg dry weight of bodies BM11.1 – BM11.6 was dry mixed in a closed container and then blunged with a mixer on an electric drill. Each body was then hung in a cotton bag until it was of a suitable consistency for kneading, at which point it was bagged in plastic.

Because of the thixotropic nature of these bodies, kneading and slab formation was achieved in an unorthodox manner. Each body was unbagged when it felt comparatively rigid. Any attempt to knead the body at this stage resulted in it crumbling into smaller damp clumps. These clumps were squeezed through the fingers two to three times, after which they became plastic and soft. These soft, plastic lumps were then slapped together, and a larger plastic mass was built up. Once the desired weight of clay had been accumulated, the entire mass was torn in half and slapped together several times to establish a lump of soft clay of even consistency. This larger lump was then slapped between the hands into a thick slab. The slab was then either placed on a fibre cement work-bench, covered with cotton fabric and hand rolled to an even thickness using 6 mm thick guides, or placed on a slab roller and formed into an even slab.

## **Bodies fired above 1000°C**

Several bodies that had not reached vitrification at lower temperatures were fired to higher temperatures so that their firing ranges could be established.

### **BM11.6**

Although BM11.6 had reached absorption of only 0.1% at 1000°C, it was fired to 1050°C to establish the point at which it began to bloat. After firing to 1050°C, surfaces that had been exposed to the air during drying had the appearance of being coated with a satin matte glaze similar in appearance to a dolomite glaze that had been fired to stoneware temperature (fig. 423). The surface that had rested on cement board during drying was unglazed, but in places had adhered

to the ceramic fibre paper on which it was fired, suggesting advanced sintering. The ceramic fibre was removed with a nylon brush, but fragments remained (fig. 423).



*Figure 423: BM11.6 self-glazed exposed side (top) and unglazed protected side after firing to 1050°C*

After firing to 1050°C, BM11.6 exhibited an average absorption of 0.5%. This represented a slight increase from the 0.1% previously recorded after firing to 1000°C. Apparent porosity of BM11.6 increased from 0.23 after firing to 1000°C, and to 1.19 after firing to 1050°C. The percentage of open pores had doubled from 0.07 to 0.14. These results suggested a change in the microstructure was commencing. However, the average ratio of volume:mass had decreased from 0.55 for bars fired at 1000°C to 0.41 for bars fired at 1050°C, indicating increased density at the higher temperature. Taken together, these results suggest that the top of the firing range for this body is approximately 1040°C. As average absorption at 950°C had previously been established as 10%, the firing range is designated as 980-1040°C. This body utilises 77.5% recovered materials, and may be useful for self-glazed forms that cannot slump. Therefore, it is worthy of further experimentation to see how it would function as a low-fire, self-glazing tile body, with potential for use in building products.

## Low-fire self-glazing tile body: 980–1040°C (BM11.6)

	(wt%)
Bungendore tailings	37.50
Marulan tailings	30.00
Unimin cullet 150 µm	10.00
Nepheline syenite	7.00
Talc Plustalc N275	3.00
Gerstley borate	10.00
Cryolite (synthetic)	1.50
Lithium carbonate	1.00

### BM11.9

BM11.9 was fired to 1100°C (fig. 424).



*Figure 424: Bm11.9 fired to 1100°C*

After firing to 1100°C, the absorption of BM11.9 was 0.2% and the volume:mass ratio was 0.48. The body was chocolate brown. Slump tests are needed to determine if this body is capable of resisting slumping at temperatures approaching 1100°C.

### BM11.10

Previous research showed that after firing to 1000°C, BM11.10 had an average absorption of 10%. Test bars were fired to 1050 and 1100°C, at a rate of 60°C per hour for the first five hours, 100°C per hour until top temperature and a 30-minute soak at top temperature before uncontrolled cooling.

After firing to 1050°C BM11.10 developed a sheen on the surface that had been exposed to air during drying, and as a result, the surface was darker in colour

than the terracotta colour displayed on the surface that had been protected from the air through contact with cement board during drying (fig. 425).



*Figure 425: BM11.10 after firing to 1050°C: Exposed (top) and protected surfaces*

After firing to 1100°C BM11.10 was a chocolate brown colour and had developed a sheen on the surface that had been exposed to air during drying (fig. 426).



*Figure 426: BM11.10 fired to 1100°C: Exposed surface*

Surfaces that had been protected from the air through contact with cement board during drying were unglazed (fig. 427).



*Figure 427: BM11.10 fired to 1100°C: Protected surface*

BM11.10 shrinkage from plastic to dry had already been established as 8.4%. After firing to 1050°C BM11.10 had an average absorption of 4% and an average shrinkage from plastic of 10.6%. After firing to 1100°C, BM11.10 had an average absorption of 1% and an average shrinkage from plastic of 11.1%. This body is worthy of further investigation.

**Low-fire self-glazing body: 980–1100°C (BM11.10) (wt%)**

	(wt%)
Bungendore tailings	43.75
Marulan tailings	32.75
Unimin cullet 150 μm	5.00
Nepheline syenite	3.50
Talc (Plustalc N275)	1.5
Gerstley borate	5.00
Cryolite (synthetic)	1.50
Lithium carbonate	0.5

The tests documented in this chapter have explored the option of increased temperature for selected bodies. The next chapter focuses on attempts to reduce thixotropy and efflorescence in a body with low porosity.



## Chapter 25: Body Additions to Reduce Thixotropy and Efflorescence

In many cases, the bodies previously tested were thixotropic and were therefore not well suited to the standard studio processes of kneading, slab rolling and throwing. While other preparation and construction methods are available for such bodies, it would be useful to have low-firing bodies to which these handling and forming techniques could be applied.

The recommended treatment to reduce thixotropy is the addition of a flocculent (Walker, 2009). Many flocculents are commercially available, but they are often relatively expensive and are frequently only available in large quantities, or, if designed for studio use, by freight from outside Australia. The flocculent chosen for this experiment was one that is available in small quantities in supermarkets throughout Australia and sold as *Epsom salts* (magnesium sulphate:  $\text{MgSO}_4 \cdot 7\text{H}_2\text{O}$ ). It was listed as a flocculent by Zamek (1998), who recommended adding 0.3% dry weight magnesium sulphate to flocculate the clay batch, after first dissolving it in water to ensure even dispersal. A previously mentioned caution regarding the use of magnesium sulphate is that its solubility can lead to efflorescence or scumming. As such, it could be expected to add to the already significant levels of efflorescence in the bodies previously tested.

The thixotropic bodies previously tested frequently displayed considerable salt migration during drying. Different drying conditions produced variations in the extent and direction of salt migration manifesting as efflorescence. These variations resulted in different colouration and surface qualities being displayed on the same test pieces (fig. 428, overleaf).



**Figure 428: Effloresced exposed sides (left) and unaffected protected sides (right) of BM11.2 (top), BM11.4, BM11.5, and BM11.6 (bottom) after firing to 1000°C**

While efflorescence may be intentionally exploited to produce light-coloured surfaces on terracotta bodies, it would also be useful to have the capacity to produce uniform surfaces on a low-fire body if required. The desire for uniformity in the appearance of brick and tile products drove early research into the causes of, and treatments for, efflorescence and scumming (Jackson, 1925).

This research led to the conclusion that where efflorescence was attributed to salt migration, the recommended cost-effective treatment was the addition of barium chloride and barium carbonate, although either could be used alone at greater expense (Bennett & Goodrich, 1930). For the purposes of this research, the use of barium carbonate to reduce efflorescence was preferred because of its ready availability and lower toxicity. Unfortunately, by precipitating the sulphates in order to reduce efflorescence, barium carbonate additions also have the potential to facilitate deflocculation (Tozzi, 2008).

The literature suggests that magnesium sulphate reduces thixotropy but increases efflorescence, and barium carbonate reduces efflorescence but increases deflocculation. Nonetheless, it was hoped that the undesirable side

effects of dosing with magnesium sulphate and barium carbonate would have only a minor influence on the outcome.

Selection of a clay body was required in order to experiment with the recommended addition of 0.65% BaCO<sub>3</sub> (Bennett & Goodrich, 1930) and 0.3% dry weight magnesium sulphate (Zamek, 1998). The body selected was BM11.6, which had the highest clay content (67.5%) and the lowest absorption (0.01%) at 1000°C. The high clay content was chosen because the clay content represented recovered materials, and low absorption was desirable based on the first of Brownell's (1949, p. 386) summary of efflorescence factors, which states:

- (1) A ceramic body with 0% absorption cannot produce efflorescence, and there is probably some practical limit between 6.0 and 0% at which efflorescence will not occur.*
- (2) Slightly soluble as well as extremely soluble salts will cause efflorescence.*
- (3) A ceramic product can contain about 0.270 of extremely soluble salts before efflorescence becomes apparent:*
- (4) A ceramic product can contain about 0.7% of calcium sulphate before efflorescence becomes apparent.*
- (5) Sulphates are the most harmful of the efflorescing salts. The most common sulphates are KAL(SO<sub>4</sub>)<sub>2</sub>, K<sub>2</sub>SO<sub>4</sub>, Na<sub>2</sub>SO<sub>4</sub>, MgSO<sub>4</sub>, and CaSO<sub>4</sub>.*
- (6) Insoluble sulfides in clay materials are common sources of sulfur from which sulphates are formed.*
- (7) Sulphates are formed in a clay material during firing by the combination of various materials with SO<sub>3</sub> and by solid-state reactions involving sulphates.*
- (8) The use of barium compounds cannot prevent the formation of alkali sulphates during the firing process, but barium compounds can prevent the formation of other alkaline-earth sulphates.*
- (9) The cations must be in a form that will allow sulphate formation according to the laws of solid-gas and solid-solid reactions.*

Based on Brownell's (1949) work it was expected that protection from post-firing efflorescence would be best provided by bodies with low absorption.

Body BM11.6 was treated with additions of magnesium sulphate (Epsom salts), which was intended to reduce thixotropy, and barium carbonate to counteract efflorescence. The treated body was designated BM11.6A. The batch recipes of both bodies appear in Table 74.

*Table 74: Batch recipes of BM11.6 and BM11.6A*

	<b>BM11.6</b>	<b>BM11.6A</b>
	<b>(wt%)</b>	<b>(wt%)</b>
Bungendore tailings	37.50	37.50
Marulan tailings	30.00	30.00
Unimin cullet 150 µm	10.00	10.00
Nepheline Syenite	7.00	7.00
Talc (Plustalc N275)	3.00	3.00
Gerstley borate	10.00	10.00
Cryolite (synthetic)	1.50	1.50
Lithium carbonate	1.00	1.00
Epsom salts		0.30
Barium carbonate		0.65
	100.00	100.95

A 1 kg dry batch of BM11.6 was first prepared with an addition of 0.65% BaCO<sub>3</sub>. This was dry mixed in a closed container and then added to water containing 0.3% dry weight magnesium sulphate. The body was then blunged with a mixer on an electric drill, and hung in a cotton bag until it was of a suitable consistency for kneading.

Kneading revealed that BM11.6a was noticeably less thixotropic than BM11.6. This was evidenced by the smaller decrease in viscosity occurring in BM11.6a than in BM11.6 when the treated bodies that had been left standing were agitated through kneading. The treated body was less sticky and fluid, and was therefore easier to knead, with a decreased tendency to stick to the surface. BM11.6a was also more easily rolled into a slab under cotton fabric because the rolling and spreading process had less effect on the consistency, and there was a decreased tendency for the body to adhere to the fabric. Upon drying, the

treated body also displayed none of the efflorescence visible on the untreated body (fig. 429).



**Figure 429: Efflorescence comparison of BM11.6 (top) and BM11.6A treated with barium carbonate to reduce efflorescence**

The bars were fired to 1000°C and the extent of efflorescence was again compared. At 1000°C the untreated body had the appearance of being coated with an off-white engobe that had started to soften on the edges of the bar. The treated body had no visible coating (fig. 430).



**Figure 430: Efflorescence comparison of BM11.6 (top) and BM11.6A fired to 1000°C**

The bars were fired to 1050°C and again the extent of efflorescence was compared. First we have, as previously pictured, samples of BM11.6 with one side heavily self-glazed (fig. 431).



*Figure 431: BM11.6 self-glazed exposed side (top) and unglazed protected side after firing to 1050°C*



*Figure 432: BM11.6A unglazed exposed side (top) and unglazed protected side after firing to 1050°C*

Next we see that when treated with barium carbonate the same body formed no glaze on the exposed surfaces (fig. 432). The slight disparity in colour and the

absence of glaze indicated minimal efflorescence had occurred in the treated body.

This chapter has demonstrated that improvements in workability and reductions in efflorescence can be obtained simultaneously through the addition of barium carbonate and Epsom salts. This is a useful outcome given the list of desirable properties provided earlier (Chapter 5). Also featured among this list of desirable properties is the preference for a body that has good fired strength. This is the focus of the next chapter.

## Chapter 26: Tests of Fired Strength

### Preparation of test pieces for establishing fired strength

In order to establish the fired strengths of the clays developed, the required geometry of test pieces was first discussed with Associate Professor Stuart Reid (Reid, 2011). Reid advised that the size and shape of bars used in this study to establish shrinkage and absorption (approximately 105 × 25 × 5 mm) would be suitable also for a four-point strength test. In addition, fired discs of approximately 120 mm diameter were needed to perform a ring test. Construction of these discs is described below.

Discs were made using an empty *Milo* can with the lid removed and the bottom cut off. The lid was placed on the slab, and the can was placed over this so the sharp rim formed by cutting off the base of the can could be pressed through the clay slab to form a clay disc. The handle of a tennis racket was then used to hold down the lid, and also the clay disc beneath it, as the can was removed. These discs were then fired. An example of a fired disc appears in Figure 433.



Figure 433: Test disc of BM11.2 fired to 950°C



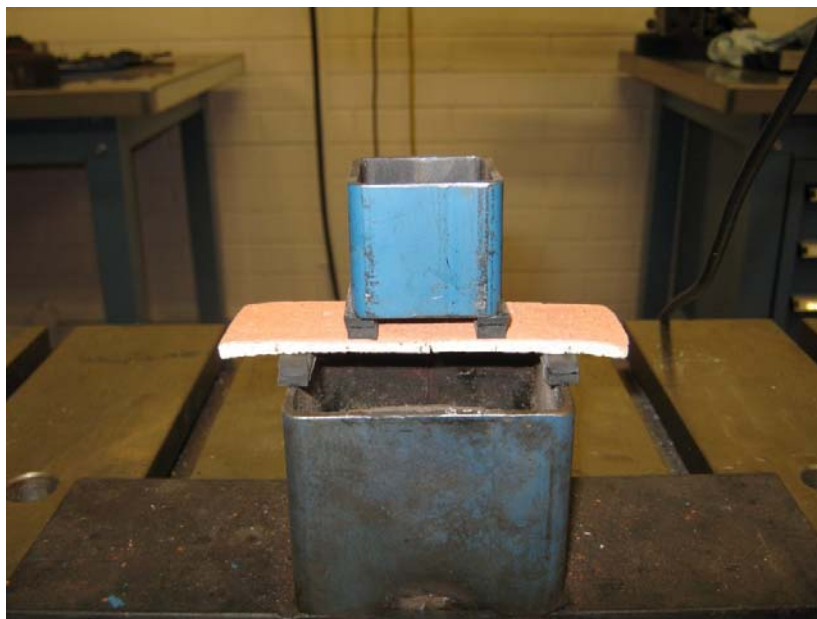
## Strength testing procedure

Testing of ceramic samples was undertaken with the assistance of Professor Stuart Reid and students at the Department of Civil Engineering at the University of Sydney. The apparatus used was a MTS *Sintech 65G* electromechanical tester (fig. 434).



*Figure 434: Apparatus for stress tests*

The pressure at which the sample failed was recorded for both bars and discs. Bars were tested using a four-point stress test (fig. 435).



*Figure 435: Four-point stress test used for bars*

Discs were tested using a ring test (fig. 436).



**Figure 436: Ring stress test used for discs**

Samples were tested on alternate sides to take account of potential variability resulting from warping, cupping and efflorescence. Samples were tested at two different load rates (the rate at which the pressure upon the sample is increased). Raw data with the results from the testing are provided in Appendix 7. These raw data are the time elapsed from commencement of loading until the samples failed. Time elapsed is a difficult measure to relate to strength, so we calculate *equivalent 60-second stress*: the anticipated pressure that would cause the sample to fail after 60 seconds.

The results were provided as average megapascals (MPa). Multiplication by a factor of 10 results in conversion into more familiar units:  $\text{kg/cm}^2$  (Table 75). The values obtained ranged from  $\sim 250 \text{ kg/cm}^2$  to  $\sim 75 \text{ kg/cm}^2$ . Most experimental bodies fired below  $1000^\circ\text{C}$  resisted over  $100 \text{ kg/cm}^2$ , indicating acceptable strength at low temperatures.

BM1.14C was the strongest body, having resisted the most pressure at  $1100^\circ\text{C}$ . BM11.1 also displayed remarkable strength for a body fired  $200^\circ\text{C}$  lower, at  $900^\circ\text{C}$ . WT14, the commercially available body used as a comparative

reference, was the second strongest clay at 1100°C, but had the lowest strength recorded of all samples when it had been fired to 1000°C (Table 76).

**Table 75: Equivalent 60 second stress test: weighted average of bars and disks**

Material	Equivalent 60-second stress (kg/cm <sup>2</sup> )				
	900°C	950°C	1000°C	1050°C	1100°C
BM11.1	172.7	-	-	-	-
BM11.2	95.8 <sup>#</sup>	138.6	119.9	-	-
BM11.3	135.5	-	-	-	-
BM11.4	-	105.8	108.8 <sup>#</sup>	-	-
BM11.5	-	106.1	84.4	-	-
BM11.6	-	106.2	109.4 <sup>#</sup>	179.7 <sup>#</sup>	-
BM11.6a	-	-	141.4	-	-
BM11.10.	-	-	-	128.5	116.9
BM11.13	-	-	-	-	183.7 <sup>#</sup>
BM1.14	-	-	-	115.2 <sup>#</sup>	177.6 <sup>#</sup>
BM1.14C	-	-	-	174.5 <sup>#</sup>	252.2 <sup>#</sup>
Bung	-	-	-	92.4 <sup>#</sup>	103.6 <sup>#</sup>
Marulan	-	-	-	-	154.7 <sup>#</sup>
WT14	-	116.0 <sup>#</sup>	75.3 <sup>*</sup>	162.7 <sup>#</sup>	198.5 <sup>#</sup>

<sup>#</sup> bars only; <sup>\*</sup>discs only

There were two notable results from bodies that had been altered. First, the reformulation of BM1.14 to include 20% cullet resulted in a body (BM1.14c) that was equally as strong as BM1.14, but with a 50°C reduction in firing temperature from 1100 to 1050°C. This suggests considerable energy savings may be possible while retaining desired strength. Second, BM11.6A, which was reformulated from BM11.6 to reduce thixotropy and efflorescence, was stronger than the original body when both were fired to 1000°C. Marulan clay was about 50% stronger than Bungendore clay when both were fired to 1100°C.

Reference back to the porosity of the bodies and comparison with the strength test results showed that in general there was no association between porosity and strength. This was unexpected. For future reference, increasing the number of tests per body and possibly excluding bodies that have bloated may be helpful in confirming a lack of association. Meanwhile, the results documented

in this chapter have given some comfort that low-fired bodies can have acceptable strength.

Next, attention turns to attempts to make casting slips from some of the bodies in triaxial BM11, in the hope that casting might produce a practical means by which low-fire ceramic articles might be formed.

## Chapter 27: Attempts at Producing Casting Slips

In his book *The Essential Guide to Mold Making and Slip Casting*, Andrew Martin writes:

*In contrast to throwing bodies, casting slip clay bodies are generally non-plastic, with a mix of 50% clay and 50% fillers and fluxes, and without any highly plastic elements such as bentonite* (Martin, 2006, p. 117).

Terracotta casting slips are reported to be difficult to deflocculate, due to the water retention of their often highly plastic clay content, the retardant effect of the iron content on the deflocculent, and the comparatively high exchange rates of the clays, which are often present in larger proportions than in whiteware slips (Martin, 2006). However, Martin provides the following recipe for a successful cone 04 terracotta casting slip containing 76.3% clay:

<b>Materials</b>	<b>%</b>
Ball clay	4.8
Redart	47.6
Goldart	23.9
Talc	4.8
Flint	9.5
Frit 3110	9.5
TOTAL	100.1
Water	40
Darvan	0.4 – 0.6

Reproduced from Martin, 2006, p. 151. Redart is an earthenware clay, Goldart is a stoneware clay and Darvan is a deflocculent (Pitelka, 2001).

Martin (2006) notes that choice of clays with a greater predominance of larger particles, and therefore less plasticity, will assist in mitigating water retention. This suggests that Marulan tailings may be more suited to development of a terracotta casting slip than the highly plastic Bungendore tailings.

Attempts were made to form casting slips from BM11.6 and BM11.10. The dry batch recipes were added to the prescribed quantity of water and sodium silicate, and Dispex was added drop by drop. At no stage did the slip deflocculate, so no suitable slip was obtained. Crispin (2012b) suggested that this was due to the amount of alkalis present, which disrupted the flow characteristics of the clay particles.

Further testing of casting slips was abandoned in favour of the more fruitful endeavour of making glazes incorporating waste materials, in order to apply these to bodies incorporating waste materials. This research is documented in the following three chapters.

## Chapter 28: Investigations into Glazes using Recycled Materials

Since the focus of this project is inclusion of industrial and agricultural wastes into glazes and bodies, a number of experiments were conducted to ascertain whether satisfactory glazes could be produced using predominantly recycled materials. The standard firing schedule was used, with a soak of 30 minutes. Glazes were found to suit stoneware, middle fire and lower temperatures, in the hope that use of waste materials such as sugarcane ash and perlite fines might be adopted by a greater number of ceramicists using a range of firing temperatures.

### Glazes developed from triaxial recycle 1

Recycle 1 was a triaxial blend of three untried glaze recipes, containing all, or mostly recycled materials, with the inclusion of Gerstley borate to provide a low-temperature flux and glass former. These three glaze recipes are given in Table 76.

*Table 76: Triaxial R1: Corner recipes*

Recipe A	(wt%)	Recipe B	(wt%)	Recipe C	(wt%)
Gerstley borate	30	Bungendore tailings	10	Bungendore tailings	10
Unimin cullet 375	30	#1 bagasse ash *	90	Perlite fines AP10	10
Bungendore tailings	40			Dunmore latite dust	80

\*(2hr at 700°C)

The recipes and formulae for all samples on the 15-sample triaxial blend are given in Tables 77 and 78, respectively.

**Table 77: Triaxial recycle 1: Blend recipes**

<b>BLEND RECIPES</b>						
	<b>Gers</b>	<b>Unim</b>	<b>Bung</b>	<b>Baga</b>	<b>Perl</b>	<b>Dunm</b>
1	30.00	30.00	40.00	----	----	----
2	22.50	22.50	32.50	22.50	----	----
3	22.50	22.50	32.50	----	2.50	20.00
4	15.00	15.00	25.00	45.00	----	----
5	15.00	15.00	25.00	22.50	2.50	20.00
6	15.00	15.00	25.00	----	5.00	40.00
7	7.50	7.50	17.50	67.50	----	----
8	7.50	7.50	17.50	45.00	2.50	20.00
9	7.50	7.50	17.50	22.50	5.00	40.00
10	7.50	7.50	17.50	----	7.50	60.00
11	----	----	10.00	90.00	----	----
12	----	----	10.00	67.50	2.50	20.00
13	----	----	10.00	45.00	5.00	40.00
14	----	----	10.00	22.50	7.50	60.00
15	----	----	10.00	----	10.00	80.00

Image from Matrix glaze calculation program (Ewing, 2000).

**Table 78: Triaxial recycle 1: Blend formulae**

<b>BLEND FORMULAE</b>																		
	<b>KNO</b>	<b>CaO</b>	<b>MgO</b>	<b>BaO</b>	<b>ZnO</b>	<b>PbO</b>	<b>Li2O</b>	<b>SrO</b>	<b>Al2O3</b>	<b>P2O5</b>	<b>B2O3</b>	<b>SiO2</b>	<b>TiO2</b>	<b>ZrO2</b>	<b>K2O</b>	<b>Na2O</b>	<b>Al:Si</b>	<b>Expan</b>
1	0.338	0.537	0.125	----	----	----	----	----	<b>0.213</b>	----	0.400	<b>2.846</b>	0.012	----	0.028	0.310	13.393	10.43
2	0.339	0.513	0.148	----	----	----	----	----	<b>0.271</b>	0.008	0.368	<b>3.883</b>	0.029	----	0.047	0.292	14.317	9.13
3	0.346	0.499	0.154	----	----	----	----	----	<b>0.304</b>	0.004	0.313	<b>3.032</b>	0.019	----	0.056	0.290	9.957	10.53
4	0.341	0.476	0.183	----	----	----	----	----	<b>0.364</b>	0.022	0.317	<b>5.527</b>	0.054	----	0.077	0.264	15.173	7.93
5	0.349	0.466	0.185	----	----	----	----	----	<b>0.388</b>	0.013	0.259	<b>4.170</b>	0.037	----	0.083	0.266	10.738	9.33
6	0.355	0.459	0.186	----	----	----	----	----	<b>0.405</b>	0.007	0.219	<b>3.235</b>	0.025	----	0.087	0.268	7.987	10.73
7	0.343	0.409	0.247	----	----	----	----	----	<b>0.534</b>	0.046	0.224	<b>8.530</b>	0.101	----	0.132	0.211	15.966	6.63
8	0.354	0.412	0.234	----	----	----	----	----	<b>0.525</b>	0.029	0.170	<b>6.023</b>	0.067	----	0.127	0.227	11.474	8.03
9	0.360	0.413	0.227	----	----	----	----	----	<b>0.519</b>	0.019	0.137	<b>4.491</b>	0.046	----	0.123	0.237	8.649	9.43
10	0.365	0.414	0.221	----	----	----	----	----	<b>0.515</b>	0.012	0.115	<b>3.457</b>	0.032	----	0.121	0.244	6.709	10.83
11	0.350	0.247	0.403	----	----	----	----	----	<b>0.944</b>	0.104	----	<b>15.767</b>	0.213	----	0.265	0.086	16.703	5.43
12	0.363	0.308	0.329	----	----	----	----	----	<b>0.786</b>	0.059	----	<b>9.570</b>	0.124	----	0.210	0.153	12.171	6.83
13	0.369	0.337	0.294	----	----	----	----	----	<b>0.711</b>	0.037	----	<b>6.597</b>	0.082	----	0.184	0.185	9.283	8.13
14	0.373	0.354	0.273	----	----	----	----	----	<b>0.666</b>	0.025	----	<b>4.851</b>	0.057	----	0.169	0.204	7.281	9.53
15	0.375	0.365	0.260	----	----	----	----	----	<b>0.637</b>	0.016	----	<b>3.703</b>	0.040	----	0.158	0.217	5.813	10.93

All samples were applied by brush to Walker's white raku clay. The firing temperatures were varied and the firing atmospheres reflected those thought to be commonly used at the selected temperatures. Samples with high proportions of bagasse ash or latite dust from corner recipes B and C were expected to require stoneware temperatures to form gloss glazes.

Overall, firing glaze triaxial recycle 1 at different temperatures showed (fig. 437) that recipe A fused at the lowest temperature, and was the only sample to form non-dry glazes across all temperatures. Across all temperatures fusion was hindered less by recipe C than by recipe B, which contained 90% sugarcane



ash. Therefore, sugarcane ash was more refractory than a combination of 80 parts latite dust and ten parts perlite fines (totalling 90% of recipe C).



*Figure 437: Triaxial BM11: Glaze/engobe tests at (l to r) 1000, 1100, 1200 and 1280°C*

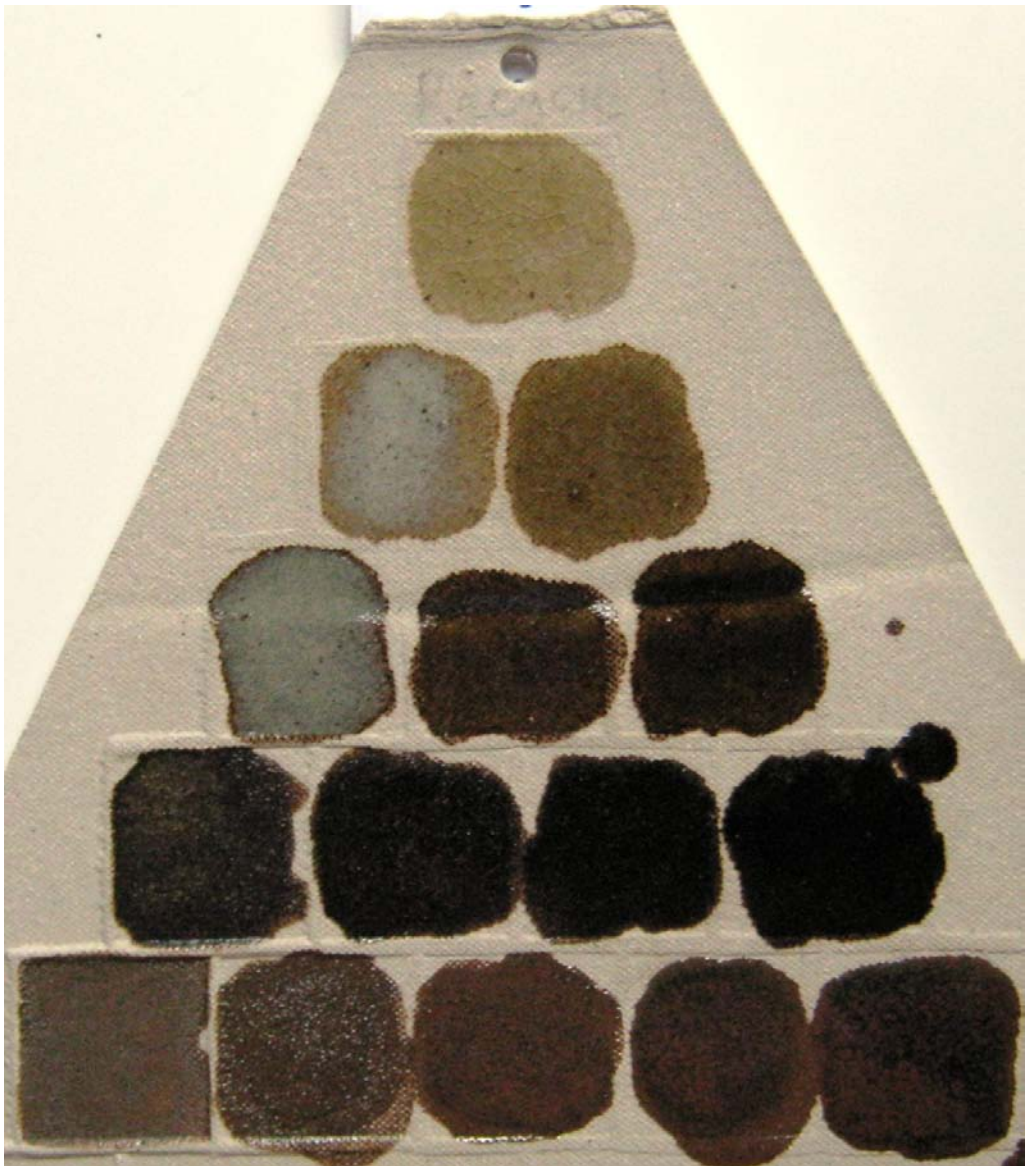
The results from each temperature at which the triaxial was fired appear in more detail below. The triaxial was first gas fired with light reduction to 1280°C (Orton cone 9), with results as seen in Figure 438.

At 1280°C the underlying colour of the glaze samples became progressively darker in a stepwise fashion moving down the triaxial, from an almost transparent pale khaki shown by R1 at Tier 1, to the near blacks of R7–R10 at Tier 4. At Tier 5, samples R11–R15 were all predominantly brown. The uniformity of this stepwise progression appeared to reflect the tier by tier decrease in the combined presence of cullet and Gerstley borate, as all other material proportions varied within tiers. This flux combination accounted for 60% of the glaze sample at Tier 1, 45% at Tier 2, 30% at Tier 3, 15% at Tier 4 and 0% at Tier 5, which had the highest proportion of iron-bearing materials. Marulan tailings contain 4.5% iron oxide; Bungendore tailings, 5.5% iron oxide and Dunmore latite, and 7.8% iron oxide.

When there was an absence of cullet and Gerstley borate in Tier 5, and the proportion of Bungendore tailings was held constant at 10%, the colour across samples R11–R15 was also relatively constant. The brown colouring was largely independent of the proportion of Dunmore quarry latite dust, which increased from 0% at R11 to 80% at R15.

It was apparent from the composition of this triaxial that the underlying brown colouration provided by the Bungendore tailings was strongly mediated by the proportion of flux materials. Before the focus is shifted to the quality of the glaze surfaces, another colour variation is worth mentioning.

Along the A–B line blend, glaze samples R2 and R4 displayed a cloud of pale grey that appeared to float just under the surface where the glaze was thickest. This was most pronounced in glaze sample R4, where the underlying brown colour was obscured on all but the perimeter of the sample. As R2 was distinguished from R3 by the presence of bagasse ash, and the clouding effect was greater at R4 (which contained twice as much ash as did R2) it was apparent that bagasse ash was the ingredient associated with the observed effect. The lack of a similar or greater clouding effect at samples R7 and R11, where the proportions of bagasse ash were even greater, was suspected to relate to the lack of fluidity of those glazes, as discussed below.



*Figure 438: Triaxial recycle 1: Gas fired to 1280°C (light reduction)*

Glossy glaze surfaces were produced by all blend samples, with the exception of sample glaze R11—recipe B, containing 90% ash. The R11 glaze surface was a dull matte. Adjacent glaze samples R7 and R12 both displayed dimples where the flow of the molten glaze surface was insufficiently advanced to completely fill the pinholes resulting from the usual release of gas bubbles through the glaze surface.

All sample glazes could be tested further for use at 1280°C. Three sample glazes were selected as a result of their appearance.

Sample glazes R14 and R15 produced tenmoku-style glazes, but the higher the rock content, the more rapidly the glaze settled, and so sample glaze R14 was the more usable tenmoku-style glaze.

Cone 9 quarry dust tenmoku glaze (R14)

The recipe for this glaze, using entirely recycled materials, was:

Bungendore tailings	10.0
Sugarcane ash	22.5
Perlite fines AP10	7.5
Dunmore latite dust	60.0



The Seger formula, omitting trace elements and with fluxes unified is:

<b>KNO</b>	<b>K<sub>2</sub>O</b>	<b>NaO<sub>2</sub></b>	<b>CaO</b>	<b>MgO</b>	<b>Al<sub>2</sub>O<sub>3</sub></b>	<b>P<sub>2</sub>O<sub>5</sub></b>	<b>B<sub>2</sub>O<sub>3</sub></b>	<b>SiO<sub>2</sub></b>	<b>TiO<sub>2</sub></b>
0.373	0.169	0.204	0.354	0.273	0.666	0.025		4.851	0.057

Alumina:silica ratio	7.28
COE	9.54
Ionic potential	57.3

### Cone 9 quarry dust black glaze (R10)

Sample glaze R10 was an unbroken black gloss containing 92.5% recycled materials.:

Gerstley borate	7.5
Unimin cullet	7.5
Bungendore tailings	17.5
Perlite fines AP10	7.5
Dunmore latite dust	60.0



The Seger formula, omitting trace elements and with fluxes unified is:

<b>KNO</b>	<b>K<sub>2</sub>O</b>	<b>NaO<sub>2</sub></b>	<b>CaO</b>	<b>MgO</b>	<b>Al<sub>2</sub>O<sub>3</sub></b>	<b>P<sub>2</sub>O<sub>5</sub></b>	<b>B<sub>2</sub>O<sub>3</sub></b>	<b>SiO<sub>2</sub></b>	<b>TiO<sub>2</sub></b>
0.365	0.121	0.244	0.414	0.221	0.515	0.012	0.115	3.457	0.032

Alumina:silica ratio	6.71
COE	10.81
Ionic potential	43.2

### Cone 9 sugarcane ash grey glaze (R4)

Sample glaze R4 produced a serviceable-looking ash glaze using 45% calcined sugarcane bagasse ash. This glaze contains 85% recycled materials:

Gerstley borate	15
Unimin cullet	15
Bungendore tailings	25
Sugarcane ash	45

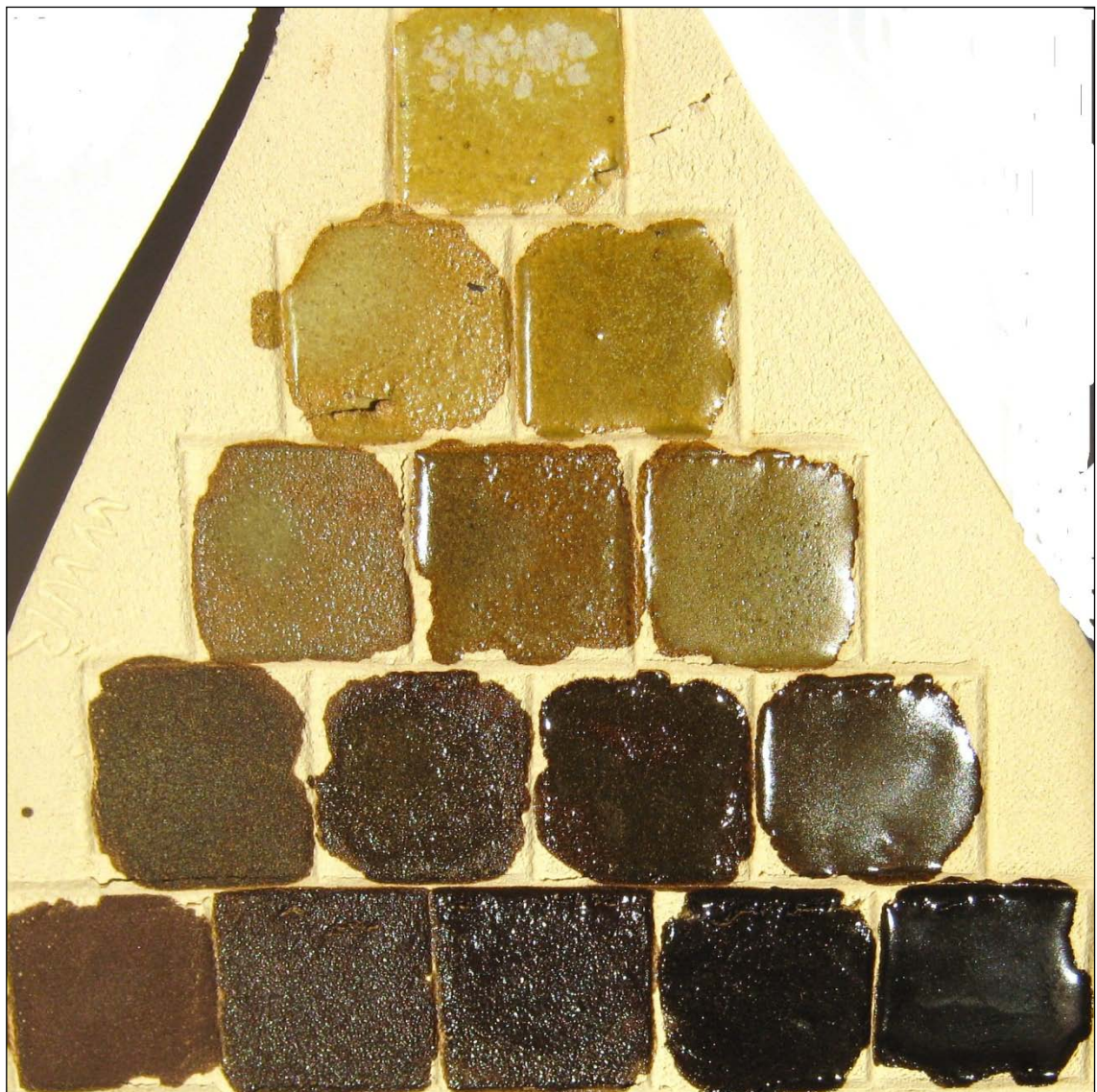


The Seger formula, omitting trace elements and with fluxes unified is:

<b>KNO</b>	<b>K<sub>2</sub>O</b>	<b>NaO<sub>2</sub></b>	<b>CaO</b>	<b>MgO</b>	<b>Al<sub>2</sub>O<sub>3</sub></b>	<b>P<sub>2</sub>O<sub>5</sub></b>	<b>B<sub>2</sub>O<sub>3</sub></b>	<b>SiO<sub>2</sub></b>	<b>TiO<sub>2</sub></b>
0.341	0.077	0.264	0.476	0.183	0.364	0.022	0.317	5.527	0.054

Alumina:silica ratio                      15.17  
COE    7.92  
Ionic potential                                      66.7

As these results indicated potential for glaze formation at lower temperatures, the triaxial was next fired in a predominantly oxidising atmosphere to 1200°C (Orton cone 6). Results are presented in Figure 439.



*Figure 439: Triaxial recycle 1 fired to 1200°C*

At 1200°C the underlying colour of the glaze samples became progressively darker in a stepwise fashion moving down the triaxial, from a pale khaki shown

by R1 at Tier 1, to the chocolate browns at Tier 5 samples R11–R15. As with the triaxial fired to 1280°C, the uniformity of this stepwise colour progression from Tiers 1 to 4 was correlated with the tier by tier decrease in the combined presence of cullet and Gerstley borate.

Glaze sample R1 displayed flakes of paler crystals floating above the underlying pale khaki gloss at the top half of the sample where the glaze was thickest. On sample R2 the glaze was paler where thickest, but no separate flakes were visible to the naked eye. Further research is required to duplicate this effect and ascertain causality.

Along the B–C line blend at Tier 5, the chocolate brown colours produced at 1200°C became progressively darker from R11 to R15. As the Tier 5 proportions of Bungendore tailings were constant at 10%, it is proposed that darker colouring was promoted by glaze maturity resulting from progressively less content of the refractory sugarcane ash moving from R11 (90%) to R15 (0%). This proposition is supported by the following observations regarding glaze surfaces.

At 1200°C, glazes with smooth glossy surfaces were produced by glaze samples R1, R2, R3, R5, R6, R9, R10, R14 and R15. The remaining six samples, which contained 45% or more sugarcane ash, produced rough surfaces. Samples R7 and R11 were fused dry mattes. In samples R4, R8, R12 and R13, the glaze had not flowed to form a smooth surface over the underlying clay, but the rough surfaces reflected the light. The appearance of these glazes was like the surface of a road after rain. The smooth glossy surfaces were like puddles and the fused matte surfaces were like dry tarmac.

All sample glazes could be tested further for use at 1200°C, depending on the surface qualities and colour requirements of the ceramist. However, the five sample glazes along the A–C line blend were selected for potential mid-range domestic ware glazes due to their surfaces and appearances. The darker glazes are less fluid than were the paler glazes.

Cone 5-6 pale khaki gloss (R1)

This fluid glaze has the potential to form flakes of paler crystals floating above the underlying pale khaki gloss where the glaze is thickest. It contains 70% recycled materials:

	(wt%)
Gerstley borate	30
Unimin cullet	30
Bungendore tailings	40



The Seger formula, omitting trace elements and with fluxes unified is:

<b>KNO</b>	<b>K<sub>2</sub>O</b>	<b>NaO<sub>2</sub></b>	<b>CaO</b>	<b>MgO</b>	<b>Al<sub>2</sub>O<sub>3</sub></b>	<b>P<sub>2</sub>O<sub>5</sub></b>	<b>B<sub>2</sub>O<sub>3</sub></b>	<b>SiO<sub>2</sub></b>	<b>TiO<sub>2</sub></b>
0.338	0.028	0.310	0.537	0.125	0.213		0.400	2.846	0.012

Alumina:silica ratio	13.39
COE	10.47
Ionic potential	38.5

Cone 5-6 mid-khaki gloss (R3)

This glaze contains 77.5% recycled materials:

	(wt%)
Gerstley borate	22.5
Unimin cullet	22.5
Bungendore tailings	32.5
Perlite fines AP10	2.5
Dunmore latite dust	20.0



The Seger formula, omitting trace elements and with fluxes unified is:

<b>KNO</b>	<b>K<sub>2</sub>O</b>	<b>NaO<sub>2</sub></b>	<b>CaO</b>	<b>MgO</b>	<b>Al<sub>2</sub>O<sub>3</sub></b>	<b>P<sub>2</sub>O<sub>5</sub></b>	<b>B<sub>2</sub>O<sub>3</sub></b>	<b>SiO<sub>2</sub></b>	<b>TiO<sub>2</sub></b>
0.346	0.056	0.290	0.499	0.154	0.304	0.004	0.313	3.032	0.01

Alumina:silica ratio	9.96
COE	10.58
Ionic potential	39.9



Cone 5-6 khaki gloss (R6)

This glaze contains 85% recycled materials:

	(wt%)
Gerstley borate	15
Unimin cullet	15
Bungendore tailings	25
Perlite fines AP10	5
Dunmore latite dust	40



The Seger formula, omitting trace elements and with fluxes unified is:

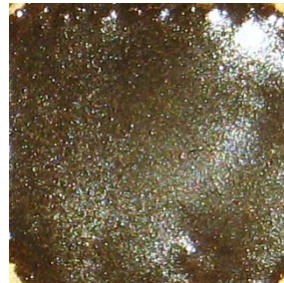
<b>KNO</b>	<b>K<sub>2</sub>O</b>	<b>NaO<sub>2</sub></b>	<b>CaO</b>	<b>MgO</b>	<b>Al<sub>2</sub>O<sub>3</sub></b>	<b>P<sub>2</sub>O<sub>5</sub></b>	<b>B<sub>2</sub>O<sub>3</sub></b>	<b>SiO<sub>2</sub></b>	<b>TiO<sub>2</sub></b>
0.355	0.087	0.268	0.459	0.186	0.405	0.007	0.219	3.235	0.025

Alumina:silica ratio	7.99
COE	10.7
Ionic potential	41.5

Cone 5-6 brown gloss (R10)

This greenish brown gloss glaze contains over 92.5% recycled materials:

	(wt%)
Gerstley borate	7.5
Unimin cullet	7.5
Bungendore tailings	17.5
Perlite fines AP10	7.5
Dunmore latite dust	60.0



The Seger formula, omitting trace elements and with fluxes unified is:

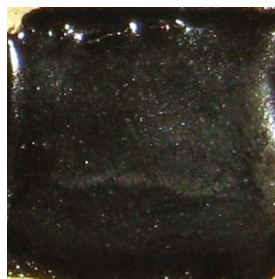
<b>KNO</b>	<b>K<sub>2</sub>O</b>	<b>NaO<sub>2</sub></b>	<b>CaO</b>	<b>MgO</b>	<b>Al<sub>2</sub>O<sub>3</sub></b>	<b>P<sub>2</sub>O<sub>5</sub></b>	<b>B<sub>2</sub>O<sub>3</sub></b>	<b>SiO<sub>2</sub></b>	<b>TiO<sub>2</sub></b>
0.365	0.121	0.244	0.414	0.221	0.515	0.012	0.115	3.457	0.032

Alumina:silica ratio	6.71
COE	10.81
Ionic potential	43.2

### Cone 5-6 deep chocolate gloss (R15)

This dark chocolate brown glaze contains 100% recycled materials:

	(wt%)
Bungendore tailings	10
Perlite fines AP10	10
Dunmore latite dust	80



The Seger formula, omitting trace elements and with fluxes unified is:

<b>KNO</b>	<b>K<sub>2</sub>O</b>	<b>NaO<sub>2</sub></b>	<b>CaO</b>	<b>MgO</b>	<b>Al<sub>2</sub>O<sub>3</sub></b>	<b>P<sub>2</sub>O<sub>5</sub></b>	<b>B<sub>2</sub>O<sub>3</sub></b>	<b>SiO<sub>2</sub></b>	<b>TiO<sub>2</sub></b>
0.375	0.158	0.217	0.365	0.260	0.637	0.016		3.703	0.040

Alumina:silica ratio

COE

Ionic potential

The triaxial was next fired in an oxidising atmosphere to 1100°C. Results are shown below (fig. 440, overleaf). At 1100°C the underlying colour of the glaze samples again became progressively darker in a stepwise fashion moving down the triaxial, from the cream colour shown by R1 at Tier 1, to the dark browns of R7-R10 at Tier 4. Then at Tier 5, samples R11-R15 were all mid-brown. As all other material proportions varied within tiers, the relative uniformity of this stepwise progression again appeared to reflect the tier by tier decrease in the combined presence of cullet and Gerstley borate. At 1100°C glazes along the A-C line blend were slightly darker than glazes along the A-B line blend. This darker colouration was associated with higher proportions of iron-bearing Dunmore latite, absence of the relatively refractory bagasse ash and more advanced fusion of the A-C glazes, as indicated by observation of their surface qualities.

At 1100°C, no glazes with smooth glossy surfaces were produced. Glaze samples R1, R3, and R6 from the A–C line blend produced satin matte surfaces. Adjacent glazes R2, R5 and R10 displayed surfaces that were satin matte where thick, and dry where thin. The remaining nine samples produced dry matte surfaces.



*Figure 440: Triaxial recycle1 fired to 1100°C*

As all of the samples fired to 1100°C adhered well to an immature stoneware body, each of them could be tested further for use at 1100°C, depending on the functionality, surface qualities and required colours. All these features would be expected to vary with changes in the clay body used. Selected glazes appear below.

Each glaze is named and pictured, and the percentage of recycled materials is noted. The glaze recipe is supplied in percentage form. To facilitate comparison with other glazes, the Seger formula is supplied, along with the alumina:silica ratio, the coefficient of thermal expansion and the ionic potential.

### Cone 03 cream matte (R1)

This matte glaze contains 70% recycled materials. It feels slightly drier to touch than do the following two glazes, and is less reflective. It has pinholes visible under magnifying glass. It is made up of:

	(wt%)
Gerstley borate	30
Unimin cullet	30
Bungendore tailings	40



The Seger formula, omitting trace elements and with fluxes unified is:

<b>KNO</b>	<b>K<sub>2</sub>O</b>	<b>NaO<sub>2</sub></b>	<b>CaO</b>	<b>MgO</b>	<b>Al<sub>2</sub>O<sub>3</sub></b>	<b>P<sub>2</sub>O<sub>5</sub></b>	<b>B<sub>2</sub>O<sub>3</sub></b>	<b>SiO<sub>2</sub></b>	<b>TiO<sub>2</sub></b>
0.338	0.028	0.310	0.537	0.125	0.213		0.400	2.846	0.012

Alumina:silica ratio	13.39
COE	10.47
Ionic potential	38.5

Cone 03 mud satin matte (R3)

This satin matte glaze contains 72.5% recycled materials:

	(wt%)
Gerstley borate	22.5
Unimin cullet	22.5
Bungendore tailings	32.5
Perlite fines AP10	2.5
Dunmore latite dust	20.0



The Seger formula, omitting trace elements and with fluxes unified is:

<b>KNO</b>	<b>K<sub>2</sub>O</b>	<b>NaO<sub>2</sub></b>	<b>CaO</b>	<b>MgO</b>	<b>Al<sub>2</sub>O<sub>3</sub></b>	<b>P<sub>2</sub>O<sub>5</sub></b>	<b>B<sub>2</sub>O<sub>3</sub></b>	<b>SiO<sub>2</sub></b>	<b>TiO<sub>2</sub></b>
0.346	0.056	0.290	0.499	0.154	0.304	0.004	0.313	3.032	0.01

Alumina:silica ratio	9.96
COE	10.58
Ionic potential	39.9

Cone 03 olive satin matte (R6)

This satin matte glaze contains 85% recycled materials:

	(wt%)
Gerstley borate	15
Unimin cullet	15
Bungendore tailings	25
Perlite fines AP10	5
Dunmore latite dust	40



The Seger formula, omitting trace elements and with fluxes unified is:

<b>KNO</b>	<b>K<sub>2</sub>O</b>	<b>NaO<sub>2</sub></b>	<b>CaO</b>	<b>MgO</b>	<b>Al<sub>2</sub>O<sub>3</sub></b>	<b>P<sub>2</sub>O<sub>5</sub></b>	<b>B<sub>2</sub>O<sub>3</sub></b>	<b>SiO<sub>2</sub></b>	<b>TiO<sub>2</sub></b>
0.355	0.087	0.268	0.459	0.186	0.405	0.007	0.219	3.235	0.025

Alumina:silica ratio	7.99
COE	10.7
Ionic potential	41.5

### Cone 03 brown dry glaze (R13)

This dry glaze was well adhered to the clay surface, displayed uniform mid-brown colour unaffected by glaze thickness, and did not show brushstrokes. This glaze would be a reasonable starting point for formulation of a series of different coloured cone 03 dry glazes, using a range of oxide colourants and replacing the Bungendore tailings with proportions of non-iron-bearing clay where paler hues are sought. It contains 100% recycled materials:

	(wt%)
Bungendore tailings	10
Sugarcane ash	45
Perlite fines AP10	5
Dunmore latite dust	40



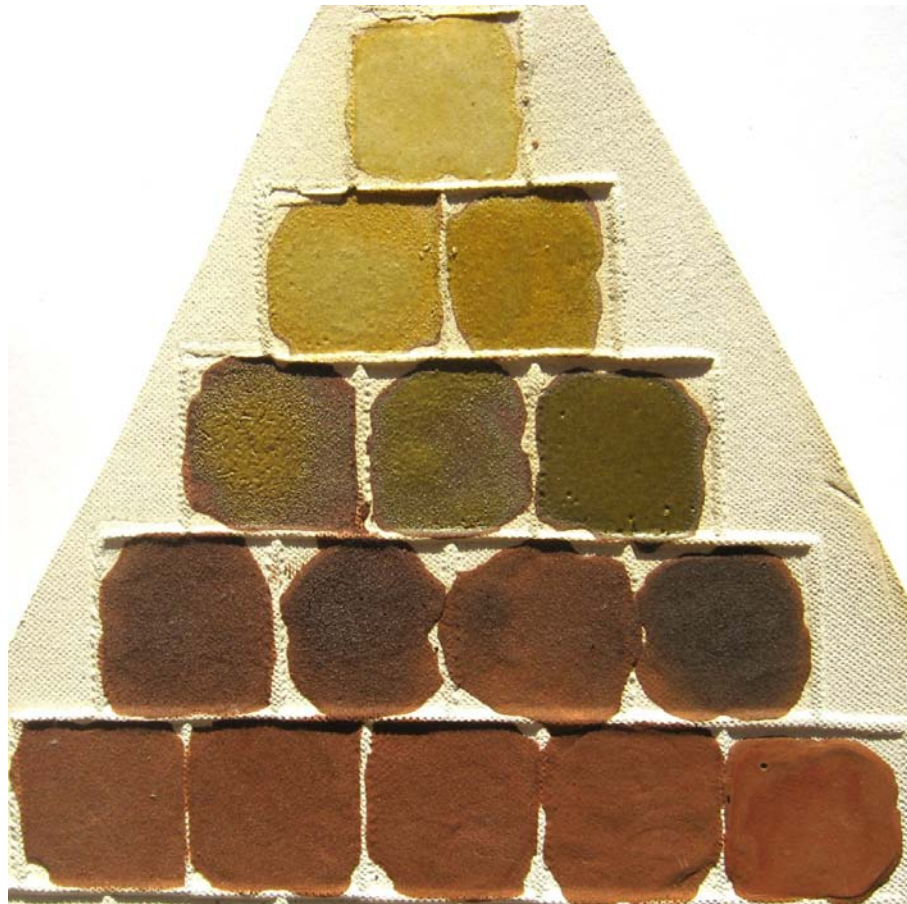
The Seger formula, omitting trace elements and with fluxes unified is:

<b>KNO</b>	<b>K<sub>2</sub>O</b>	<b>NaO<sub>2</sub></b>	<b>CaO</b>	<b>MgO</b>	<b>Al<sub>2</sub>O<sub>3</sub></b>	<b>P<sub>2</sub>O<sub>5</sub></b>	<b>B<sub>2</sub>O<sub>3</sub></b>	<b>SiO<sub>2</sub></b>	<b>TiO<sub>2</sub></b>
0.369	0.184	0.185	0.337	0.294	0.711	0.037		6.597	0.082

Alumina:silica ratio	9.28
COE	8.18
Ionic potential	76.0



Finally the triaxial was fired to 1000°C in an oxidising atmosphere, with results as pictured in Figure 441.



*Figure 441: Triaxial R1 fired to 1000°C*

At 1000°C the triaxial produced a similar tier by tier colour progression to that displayed at higher temperatures, becoming progressively darker in a stepwise fashion moving down the triaxial, from the pale yellow shown by R1 at Tier 1, to the dark browns of R7–R10 at Tier 4. Then at Tier 5, samples R11–R15 were all mid-brown. Colours and surfaces varied most within Tiers 2 and 3.

At 1000°C, Tier 2 glaze samples R2 and R3 formed smooth yellow satin mattes where the application was thickest, but areas of thinner application lost the satin finish and displayed dry brown edges. Tier 3 samples R4–R6 formed olive green mattes with the matte surface increasing in area and degree of maturity from glaze samples R4–R6. On glaze sample R4 the olive green surface was lumpy from the early phase of the melting process, and was surrounded by a substantial area of brown dry surface. On glaze sample R5 the area of dry brown unmelted surface was decreased and the lumpiness of the olive green

area was less pronounced as the melting process was further advanced and the surface perturbations had begun to settle. On glaze sample R6 the surface had begun to flow, the majority of the olive green matte surface appeared smooth to the naked eye, and there was only a thin, dry brown perimeter. At 1000°C, all Tier 4 and 5 glaze samples from R7 to R15 had dry brown surfaces with no evidence of melting except for a faint sheen on the otherwise dry surface at the centre of glaze sample R10.

Cone 06 pale yellow matte glaze (R1)

At 1000°C, sample R1 produced a pale yellow smooth matte glaze reminiscent of a stoneware temperature dolomite matte. The batch recipe for this glaze, which incorporates 70% recycled materials is:

	(wt%)
Gerstley borate	30
Unimin cullet	30
Bungendore tailings	40



The Seger formula, omitting trace elements and with fluxes unified is:

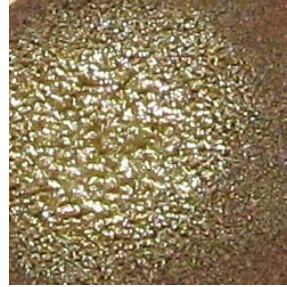
KNO	K <sub>2</sub> O	NaO <sub>2</sub>	CaO	MgO	Al <sub>2</sub> O <sub>3</sub>	P <sub>2</sub> O <sub>5</sub>	B <sub>2</sub> O <sub>3</sub>	SiO <sub>2</sub>	TiO <sub>2</sub>
0.338	0.028	0.310	0.537	0.125	0.213		0.400	2.846	0.012

Alumina:silica ratio	13.39
COE	10.47
Ionic potential	38.50

Cone 06 dry brown/wet olive lichen transition glaze (R4)

This glaze, containing 85% recycled materials, is a dry brown where thin, and an immature lichen-like olive green satin gloss where thick, and is made up of:

	(wt%)
Gerstley borate	15
Unimin cullet	15
Bungendore tailings	25
Sugarcane ash	45



The Seger formula, omitting trace elements and with fluxes unified is:

<b>KNO</b>	<b>K<sub>2</sub>O</b>	<b>NaO<sub>2</sub></b>	<b>CaO</b>	<b>MgO</b>	<b>Al<sub>2</sub>O<sub>3</sub></b>	<b>P<sub>2</sub>O<sub>5</sub></b>	<b>B<sub>2</sub>O<sub>3</sub></b>	<b>SiO<sub>2</sub></b>	<b>TiO<sub>2</sub></b>
0.341	0.077	0.264	0.476	0.183	0.364	0.022	0.317	5.527	0.054

Alumina:silica ratio	15.17
COE	7.92
Ionic potential	66.7

### Cone 06 dry brown glaze (R8)

This dry glaze, containing 92.5% recycled materials, has a tough surface that displays subtle cracking where thick. This glaze would be a reasonable starting point for formulation of a series of different coloured cone 06 dry glazes, with the recipe:

	(wt%)
Gerstley borate	7.5
Unimin cullet	7.5
Bungendore tailings	17.5
Sugarcane ash	45.0
Perlite fines AP10	2.5
Dunmore latite dust	20.0



The Seger formula, omitting trace elements and with fluxes unified is:

<b>KNO</b>	<b>K<sub>2</sub>O</b>	<b>NaO<sub>2</sub></b>	<b>CaO</b>	<b>MgO</b>	<b>Al<sub>2</sub>O<sub>3</sub></b>	<b>P<sub>2</sub>O<sub>5</sub></b>	<b>B<sub>2</sub>O<sub>3</sub></b>	<b>SiO<sub>2</sub></b>	<b>TiO<sub>2</sub></b>
0.354	0.127	0.227	0.412	0.234	0.525	0.029	0.170	6.023	0.067

Alumina:silica ratio	11.47
COE	8.05
Ionic potential	71.0

Many glazes warrant further testing at higher temperatures, which is beyond the scope of this project. However, the results obtained at the highest temperatures used here do indicate that sugarcane ash, Bungendore tailings, perlite fines and latite dust are potentially saleable glaze materials. Several glazes also exhibit potential for use at lower temperatures. Use on a terracotta earthenware body at lower temperatures would be expected to affect the colour and surface qualities of the more fused glazes.

## Ionic potential

The Matrix glaze software program makes use of Pauling's theory of ionic potential (Ewing, 2000). According to Cardew (1977 p. 301–2):

*ionic potential = valency/ionic radius, where valency is the number of hydrogen atoms with which the element will combine and the ionic radius is the radius of the sphere formed by a neutron and its circulating electrons.*

Theoretically, the lower the ionic potential, the more readily a glaze will melt. To test this theory, the ionic potentials of triaxial recycle 1 were placed in the triaxial format (Table 79). The pattern of values was compared with the pattern of melts observed when the triaxial was fired (fig. 442). The pattern of melts corresponded with the values obtained for the triaxial recipes, indicating that ionic potential could be used as a comparative indication of the extent to which glazes would melt at a given temperature.

**Table 79: Triaxial recycle 1: Ionic potentials**

Recycle 1 triaxial: Ionic potentials				
		1		
		38.5		
	2		3	
	49.4		39.9	
	4	5	6	
	66.7	51.7	41.5	
	7	8	9	10
	98.2	71.0	54.4	43.2
11	12	13	14	15
174.2	107.8	76.0	57.3	45.0



**Figure 442: Triaxial recycle 1**

## Low-fire glazes

A high COE glossy glaze that melted below 950°C was developed earlier in the study (glaze 2.2b). A satin matte glaze for 1100°C containing all recycled materials was also developed (Recycle 1). A series of triaxials was required to develop a range of glazes using recycled materials and fluxes with varying properties.

The typical percentage analyses obtained for the recovered materials and bentonites were entered into the Matrix glaze development program, so they were available to use as raw materials when attempting to formulate glazes for low temperatures. The Matrix program uses the typical analysis of each material to determine the COE and estimated melting temperature of that material. These are listed in Table 80.

**Table 80: Expansion coefficients and estimated melting temperatures of analysed raw materials**

Raw material	Matrix values	
	COE	Melting temp (est. °C)
Corn cob ash	17.35	948
Unimin <150 µm cullet	14.1	1150
Visy conveyor belt cullet dust	14.47	1168
Dunmore latite	11.55	1216
Corn seeper sludge ash	14.16	1246
Marulan tailings	9.84	1359
Australian bentonite	8.51	1369
English bentonite	8.21	1396
Unexpanded grey perlite ore	9.77	1402
Perlite CBHF AP10 grey	9.8	1403
Perlite AP10 white	9.58	1407
Arumpo bentonite	6.86	1416
Bungendore tailings	7.12	1449
#1 boiler belt ash	5.31	1456
#12 boiler belt sugarcane ash	4.77	1472
RHA	3.99	1508

Knowledge of the COEs and estimated melting temperature of these materials was useful in attempting to formulate glazes that had low firing temperatures and low COEs. A similar table of flux materials (Table 81) shows that some of the sodium- and potassium-based fluxes have low melting points but high expansion coefficients. Gerstley borate and lithium carbonate both have low melting points and relatively low COEs, and so these two materials were viewed as most promising for the purposes of this research. At this point, Ferro lead-based frit 4364 was rejected due to the lead content, but frit 4364 could be considered in future research due to its low melting point and expansion coefficient.

**Table 81: Expansion coefficients and estimated firing temperatures of selected fluxes and frits**  
Matrix values

	Matrix values	
	COE	Melting temp (est. °C)
Potassium carbonate	61.6	597
Sodium carbonate	61.6	597
Borax	22.33	597
Cryolite synthetic	51.03	674
Lithium carbonate	6.7	723
Gerstley borate	10.86	735
Lead bisilicate	7.8	767
Ferro 4364 lead	7.72	774
Ferro 4064 lead	7.72	774
Ferro 3304 lead	8.05	828
Ferro 3417 lead	7.69	873
Ferro 5301	21.9	957
Ferro 4194	21.9	957
Ferro 3124	10.62	1050
Ferro 4124	10.62	1050
Ferro 3224	7.27	1052
Ferro 938	9.35	1071
Ferro 4712	10.29	1101

The glaze recipes given in Table 82 attempted to balance relatively high proportions of recovered materials, with relatively low COEs at relatively low temperatures. With the exception of recipes based on 2.2b, these glazes were used as the corner recipes on a series of four triaxial blends, as shown below.

**Table 82: Expansion coefficients and estimated firing temperatures of low-fire glaze recipes**

Glaze recipes	Matrix values		Triaxial No.			
	COE	Firing temp (est. °C)	1	2	3	4
BM2.2b	27.94	931				
Marulan	10.41	932				C
Corn ash 1	16.14	938	B			
Bungendore	9.22	953				A
Corn and sugar ash	11.71	965			A	
Lithium 60 low c.o.e.	7.73	974	C	B		
Rice husk	7.94	980		C	C	
Low-fire rock	10.92	994			B	B
Sugarcane ash	8.18	1000		A		
BM2.2b plus RHA20	23.47	1024				
Recycle1_#1_A (R1)	10.47	1096	A			

### Low-fire triaxial 1

The batch recipes of the three corner recipes are given in Table 83.

**Table 83: Glaze triaxial low-fire 1: Corner recipes**

Recipe A (Recycle 1)	(wt%)	Recipe B (Low-fire corn ash 1)	(wt%)	Recipe C (Lithium 60 low c.o.e. 7.73)	(wt%)
Gerstley borate	30	Gerstley borate	10	Gerstley borate	20
Unimin cullet 375	30	Corn cob ash	85	Corn cob ash	5
Bungendore tailings	40	Marulan tailings	5	Marulan tailings	4
				Lithium carbonate	60
				#1BB sugar cane ash	11



Recipe A (R1) has already been described and pictured earlier. Recipe B (Low-fire corn ash 1), which was predicted to melt at 938°C, fired to a rough dry chocolate matte at 950°C, and gave no sign of melting until 1100°C, when it formed a very rough metallic glaze (fig. 443).



*Figure 443: Low-fire corn ash 1 at (l to r) 950, 1000, 1050 and 1100°C*

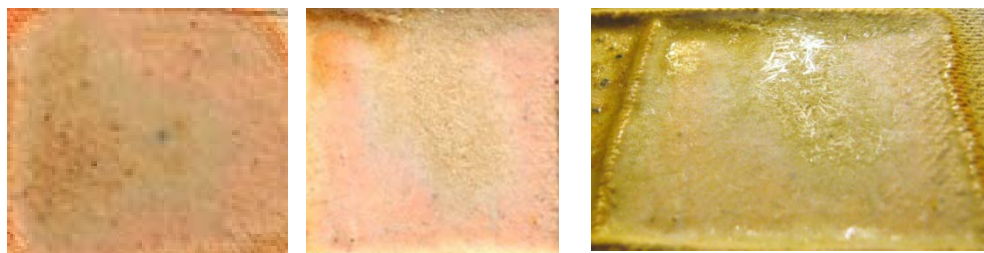
It was noted during the preparation of these glazes that the consistency of the corn ash was problematic. The majority would not pass through an 80-mesh sieve, and attempts at sieving this glaze were eventually abandoned. This explains the speckling evident in the fired triaxials (figs. 444 & 445).

Further inspection and grinding of the samples of ash calcined at different temperatures revealed that corn cob ash calcined at 800°C or above was very resistant to grinding as the particles had sintered. Ash calcined at 700°C contained charcoal fragments that were also resistant to grinding. The optimum temperature for removing charcoal preceding sintering was established to be 750°C.

Recipe C formed a glaze at 950 and 1000°C, as described below.

950–1000°C (cone 08–06) lithium crystal glaze (L1.15)

Recipe C (lithium 60 low COE 7.73), which was expected to melt at 974°C, melted at 950°C and formed a matte glaze with reflective needle-shaped crystals that were 2–3 mm in length (fig. 444). At 1000°C the needle-shaped crystals were up to 6 mm long (fig. 444).



*Figure 444: Lithium 60 low COE at 950°C (left), and 1000°C (centre & right)*

The batch recipe is:

	(wt%)
Gerstley borate	20
Corn cob ash	5
Marulan tailings	4
Lithium carbonate	60
Sugarcane ash	11

The Seger formula, omitting trace elements and with fluxes unified is:

<b>KNO</b>	<b>K<sub>2</sub>O</b>	<b>NaO<sub>2</sub></b>	<b>CaO</b>	<b>MgO</b>	<b>LiO<sub>2</sub></b>	<b>Al<sub>2</sub>O<sub>3</sub></b>	<b>P<sub>2</sub>O<sub>5</sub></b>	<b>B<sub>2</sub>O<sub>3</sub></b>	<b>SiO<sub>2</sub></b>	<b>TiO<sub>2</sub></b>
0.015	0.006	0.009	0.039	0.005	0.941	0.007	0.003	0.039	0.127	0.001

Alumina:silica ratio 18.432

COE 7.74

The recipes of all samples in triaxial low-fire 1 are shown in Table 84.

**Table 84: Glaze triaxial low-fire 1: Blend recipes**

	<b>Gers</b>	<b>Unim</b>	<b>Bung</b>	<b>Corn</b>	<b>Maru</b>	<b>LiCO</b>	<b>Baga</b>
1	30.00	30.00	40.00	----	----	----	----
2	25.00	22.50	30.00	21.25	1.25	----	----
3	27.50	22.50	30.00	1.25	1.00	15.00	2.75
4	20.00	15.00	20.00	42.50	2.50	----	----
5	22.50	15.00	20.00	22.50	2.25	15.00	2.75
6	25.00	15.00	20.00	2.50	2.00	30.00	5.50
7	15.00	7.50	10.00	63.75	3.75	----	----
8	17.50	7.50	10.00	43.75	3.50	15.00	2.75
9	20.00	7.50	10.00	23.75	3.25	30.00	5.50
10	22.50	7.50	10.00	3.75	3.00	45.00	8.25
11	10.00	----	----	85.00	5.00	----	----
12	12.50	----	----	65.00	4.75	15.00	2.75
13	15.00	----	----	45.00	4.50	30.00	5.50
14	17.50	----	----	25.00	4.25	45.00	8.25
15	20.00	----	----	5.00	4.00	60.00	11.00

These glazes were brushed onto Walker's white raku clay and fired in oxidation to 950 and 1000°C. The appearance and surface qualities of the glazes were relatively stable across this temperature range. These are described and pictured on the following pages (figs. 445 & 446).



**Figure 445: Glaze triaxial low-fire 1, 1000°C**

At 1000°C recycle 1 glaze (R1) at corner A (L1.1) formed a pale yellowcream satin matte. The corn cob ash glaze (L1.11) at corner B produced a dry and rough dark chocolate matte. This glaze was well adhered to the clay surface, with no flaking evident. The blend of corners A and B produced glaze surfaces that were tough, dry, and matte, with a light sheen only evident on L1.7. The dark colouration contributed by the corn ash glaze became increasing lighter and then speckled as its proportion was decreased. The brown colouration provided by the iron content in the corn cob ash at corner C also contributed speckling to samples L1.5, 8, 9, 13 and 14.

The lithium carbonate glaze at corner C (L1.15) formed an opaque matte where thinly applied, with a mass of needle-shaped crystals visible where the glaze was thick. This matte surface at corner C was caused by crystallisation of the L1.15 surface during cooling, rather than by immaturity of melt. This conclusion was based on three factors: the melting points of the L1.15 constituent materials, the visibility of the crystals formed and the glossy surface observed on the glaze at the mid-point of the A-C line blend, as seen in Figure 44 5 and described below.

This mid-blend glossy glaze (L1.6) had equal parts of two matte glazes: L1.15 and L1.1 (R1). R1 glaze was observed earlier to require higher temperatures to develop more gloss. Blending R1 with L1.15 along the A-C line blend produced transparent, crazed, increasingly glossy glazes at samples L1.3 and L1.6, showing that increasing additions of L1.15 lowered the melting temperature. Sample L1.10 was a crazed opaque satin matte, showing the transition to a crystallised melt.

Along the BC line blend, the colouration progressed from dark chocolate brown to cream (fig. 445). The surfaces developed more sheen as the proportion of corn ash glaze decreased, and then at sample L1.14 the impact of the crystallisation contributed by the lithium glaze became evident.

The triaxial was held at an angle to the light so the camera would record the degree of reflectivity of the surfaces. The image in Figure 446 shows the triaxial fired to 1000°C.

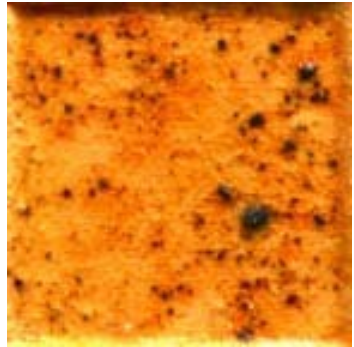


**Figure 446: Reflectivity of glazes in triaxial low-fire 1 after firing to 1000°C**

950–1000°C (cone 08–06) corn ash glaze (L1.5)

This satin to gloss glaze, containing 85% recycled materials, would be a reasonable starting point for formulation of a series of different coloured cone 08–06 glazes. It should show interesting variation in response to temperature given that it was glossier at 950°C than at 1000°C. It is made up of:

	(wt%)
Gerstley borate	22.50
Unimin cullet	15.00
Bungendore tailings	20.00
Corn cob ash	22.50
Marulan tailings	2.25
Lithium carbonate	15.00
Sugarcane ash	2.75



The Seger formula, omitting trace elements and with fluxes unified is:

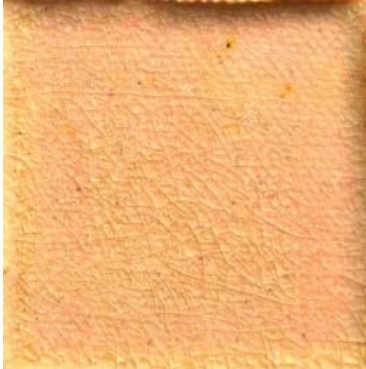
<b>KNO</b>	<b>K<sub>2</sub>O</b>	<b>NaO<sub>2</sub></b>	<b>CaO</b>	<b>MgO</b>	<b>LiO<sub>2</sub></b>	<b>Al<sub>2</sub>O<sub>3</sub></b>	<b>P<sub>2</sub>O<sub>5</sub></b>	<b>B<sub>2</sub>O<sub>3</sub></b>	<b>SiO<sub>2</sub></b>	<b>TiO<sub>2</sub></b>
0.056	0.009	0.047	0.102	0.020	0.821	0.033	0.002	0.085	0.473	0.002

Alumina:silica ratio                      14.312  
COE    9.03



950–1000°C (cone 08–06) transparent gloss (L1.6)

This low-fire transparent gloss glaze contains 45% recovered materials. As can be seen below, this glaze crazes when applied to Walker's white raku clay, but as this glaze is very glossy at 950°C, it shows potential for use as a raku glaze base. Substitution of RHA for corn cob ash may reduce crazing.

	(wt%)	
Gerstley borate	25.0	
Unimin cullet	15.0	
Bungendore tailings	20.0	
Corn cob ash	2.5	
Marulan tailings	2.0	
Lithium carbonate	30.0	
Sugarcane ash	5.5	

The Seger formula, omitting trace elements and with fluxes unified is:

<b>KNO</b>	<b>K<sub>2</sub>O</b>	<b>NaO<sub>2</sub></b>	<b>CaO</b>	<b>MgO</b>	<b>LiO<sub>2</sub></b>	<b>Al<sub>2</sub>O<sub>3</sub></b>	<b>P<sub>2</sub>O<sub>5</sub></b>	<b>B<sub>2</sub>O<sub>3</sub></b>	<b>SiO<sub>2</sub></b>	<b>TiO<sub>2</sub></b>
0.056	0.009	0.047	0.102	0.020	0.821	0.033	0.002	0.085	0.473	0.002

Alumina:silica ratio                      14.312

COE    9.03



950–1000°C (cone 08–06) transparent gloss (L1.3)

This low-fire transparent gloss glaze contains 57.5% recovered materials. As can be seen below, this glaze crazes when applied to Walker’s white raku clay, but less than does L1.6. Substitution of RHA for corn cob ash or application to a higher expansion body may reduce crazing.

	(wt%)
Gerstley borate	27.50
Unimin cullet	22.50
Bungendore tailings	30.00
Corn cob ash	1.25
Marulan tailings	1.00
Lithium carbonate	15.00
Sugarcane ash	2.75



The Seger formula, omitting trace elements and with fluxes unified is:

<b>KNO</b>	<b>K<sub>2</sub>O</b>	<b>NaO<sub>2</sub></b>	<b>CaO</b>	<b>MgO</b>	<b>LiO<sub>2</sub></b>	<b>Al<sub>2</sub>O<sub>3</sub></b>	<b>P<sub>2</sub>O<sub>5</sub></b>	<b>B<sub>2</sub>O<sub>3</sub></b>	<b>SiO<sub>2</sub></b>	<b>TiO<sub>2</sub></b>
0.114	0.013	0.101	0.190	0.042	0.655	0.069	0.002	0.149	0.955	0.004

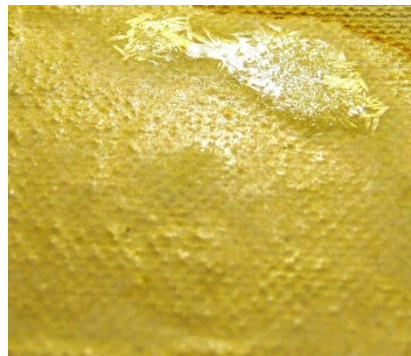
Alumina:silica ratio                      13.741

COE    9.73

950–1000°C (cone 08–06) crystalline matte (L1.10)

This low-fire cream crystalline matte glaze contains 33.5% recovered materials. At 950°C it formed reflective needle-shaped crystals where thick. These crystals were not visible at 1000°C, when a more uniform matte was produced. The fluidity of glazes within the line blend suggests this glaze may run down vertical surfaces.

	(wt%)
Gerstley borate	22.50
Unimin cullet	7.50
Bungendore tailings	10.00
Corn cob ash	3.75
Marulan tailings	3.00
Lithium carbonate	45.00
Sugarcane ash	8.25



The Seger formula, omitting trace elements and with fluxes unified is:

<b>KNO</b>	<b>K<sub>2</sub>O</b>	<b>NaO<sub>2</sub></b>	<b>CaO</b>	<b>MgO</b>	<b>LiO<sub>2</sub></b>	<b>Al<sub>2</sub>O<sub>3</sub></b>	<b>P<sub>2</sub>O<sub>5</sub></b>	<b>B<sub>2</sub>O<sub>3</sub></b>	<b>SiO<sub>2</sub></b>	<b>TiO<sub>2</sub></b>
0.030	0.007	0.023	0.062	0.010	0.898	0.016	0.003	0.056	0.253	0.002

Alumina:silica ratio                      15.413

COE    8.33

950–1000°C (cone 08–06) corn ash matte (L1.8)

This matte glaze, containing 43.75% corn ash as the major component, and 87.5% recovered materials, had a speckled golden colour and unchanged matte surface at 950 and at 1000°C.

	(wt%)
Gerstley borate	17.50
Unimin cullet	7.50
Bungendore tailings	10.00
Corn cob ash	43.75
Marulan tailings	3.50
Lithium carbonate	15.00
Sugarcane ash	2.75



The Seger formula, omitting trace elements and with fluxes unified is:

<b>KNO</b>	<b>K<sub>2</sub>O</b>	<b>NaO<sub>2</sub></b>	<b>CaO</b>	<b>MgO</b>	<b>LiO<sub>2</sub></b>	<b>Al<sub>2</sub>O<sub>3</sub></b>	<b>P<sub>2</sub>O<sub>5</sub></b>	<b>B<sub>2</sub>O<sub>3</sub></b>	<b>SiO<sub>2</sub></b>	<b>TiO<sub>2</sub></b>
0.159	0.110	0.049	0.116	0.081	0.644	0.036	0.053	0.093	0.704	0.002

Alumina:silica ratio                      19.515

COE    12.13

950–1000°C (cone 08–06) corn ash camouflage matte (L1.13)

This variegated matte glaze contains 45% corn ash and 55% recovered materials. It displays islands of dark brown matte appearing on the surface of a wrinkled, reflective tan surface that dries to a speckled matte where thin. The separation of colours was more pronounced at 950 than at 1000°C.

	(wt%)
Gerstley borate	15.0
Corn cob ash	45.0
Marulan tailings	4.5
Lithium carbonate	30.0
Sugarcane ash	5.5



The Seger formula, omitting trace elements and with fluxes unified is:

<b>KNO</b>	<b>K<sub>2</sub>O</b>	<b>NaO<sub>2</sub></b>	<b>CaO</b>	<b>MgO</b>	<b>LiO<sub>2</sub></b>	<b>Al<sub>2</sub>O<sub>3</sub></b>	<b>P<sub>2</sub>O<sub>5</sub></b>	<b>B<sub>2</sub>O<sub>3</sub></b>	<b>SiO<sub>2</sub></b>	<b>TiO<sub>2</sub></b>
0.086	0.070	0.015	0.056	0.045	0.813	0.012	0.035	0.050	0.320	0.001

Alumina:silica ratio                      25.979

COE    11.33

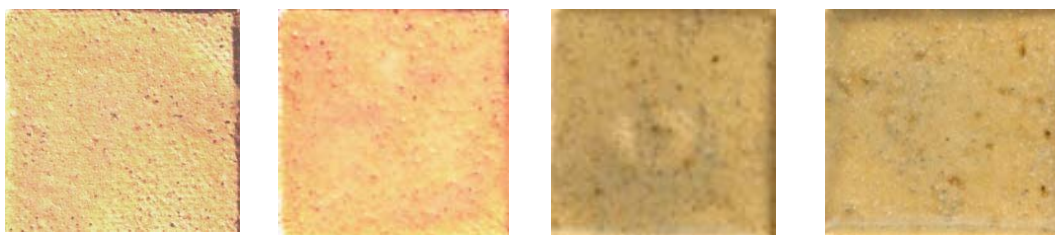
## Low-fire triaxial 2

The batch recipes of the three corner recipes are given in Table 85.

**Table 85: Glaze triaxial low-fire 2: Corner recipes**

Corner A (low-fire sugarcane ash) (wt%)		Corner B (lithium 60 low COE 7.73) (wt%)		Corner C (low-fire RHA ) (wt%)	
Bungendore tailings	5	Gerstley borate	20	Bungendore tailings	3
Gerstley borate	55	#1BB sugar cane ash	11	Gerstley borate	60
Sugarcane ash	40	Lithium carbonate	60	Rice husk ash	37
		Corn cob ash	5		
		Marulan tailings	4		

Corner A (low-fire sugarcane ash), which was predicted to melt at 1000°C, was a dry pale matte at 950°C, and a lightly speckled pale gloss at 1000°C, maintaining similar surface qualities up to 1100°C (fig. 448).



**Figure 448: Low-fire sugarcane ash at (l to r) 950, 1000, 1050 and 1100°C**

### Sugarcane ash glaze (L2.1)

950°C (cone 08) matte & 1000–1100°C (cone 06–03) gloss

	(wt%)
Bungendore tailings	5
Gerstley borate	55
Sugarcane ash	40

The Seger formula, omitting trace elements and with fluxes unified is:

KNO	K <sub>2</sub> O	NaO <sub>2</sub>	CaO	MgO	LiO <sub>2</sub>	Al <sub>2</sub> O <sub>3</sub>	P <sub>2</sub> O <sub>5</sub>	B <sub>2</sub> O <sub>3</sub>	SiO <sub>2</sub>	TiO <sub>2</sub>
0.199	0.033	0.166	0.751	0.050	-	0.119	0.013	0.774	2.534	0.026

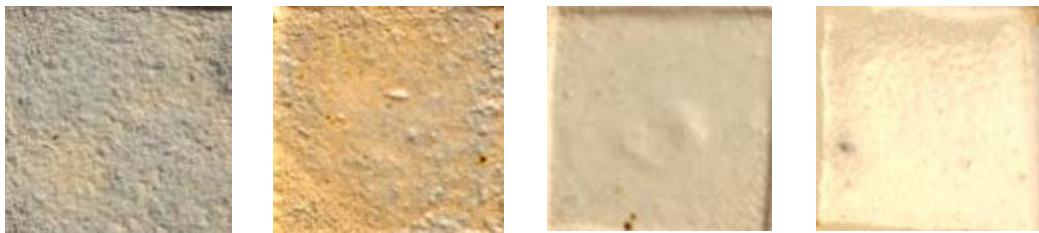
Alumina:silica ratio                      21.285

COE    8.13

The corner B recipe was described and pictured earlier.

Corner C (low-fire RHA), which was predicted to melt at 980°C, formed glazes with different qualities as temperature increased (fig. 449). It formed a light grey dry matte at 950°C. This became slightly paler at 1000°C and formed a satin matte where thin. After firing to 1050°C it was a uniform cream satin matte, and after firing to 1100°C it was a white gloss.

**Figure 449: Low-fire RHA glaze at (l to r) 950, 1000, 1050 and 1100°C**



### **Rice husk ash glaze (L2.15)**

950–1000°C (cone 08–06) matte

1050–1100°C (cone 05–03) satin to gloss

	<b>(wt%)</b>
Bungendore tailings	3
Gerstley borate	60
RHA	37

The Seger formula, omitting trace elements and with fluxes unified is:

<b>KNO</b>	<b>K<sub>2</sub>O</b>	<b>NaO<sub>2</sub></b>	<b>CaO</b>	<b>MgO</b>	<b>LiO<sub>2</sub></b>	<b>Al<sub>2</sub>O<sub>3</sub></b>	<b>P<sub>2</sub>O<sub>5</sub></b>	<b>B<sub>2</sub>O<sub>3</sub></b>	<b>SiO<sub>2</sub></b>	<b>TiO<sub>2</sub></b>
0.200	0.030	0.171	0.790	0.010	-	0.019	0.003	0.838	2.521	0.001

Alumina:silica ratio                      129.99

COE    7.92

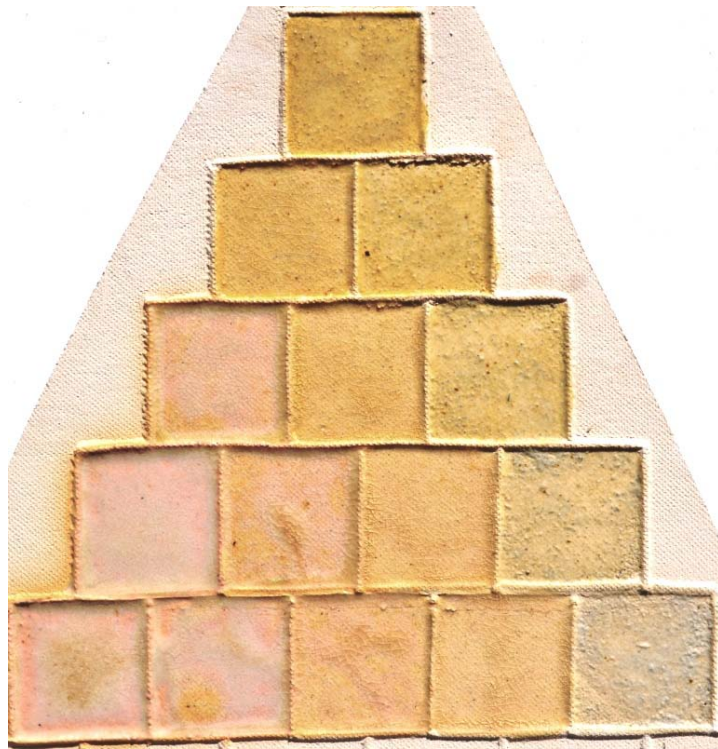
Images of low-fire triaxial 2 fired to 950 and 1000°C are shown in Figures 450–452.



*Figure 450: Low-fire 2 triaxial after firing to 950°C*

The glazes highest in lithium carbonate displayed a pale pink colour. Glazes higher in sugarcane ash tended towards pale khaki, and glazes with most RHA were light grey.

At 1000°C, (fig.451) the glossiest glazes were those containing 15% lithium carbonate.



**Figure 451: Low-fire 2 triaxial after firing to 1000°C**

The same triaxial was held at an angle to the camera to show reflectivity (fig. 452).



**Figure 452: Low-fire 2 triaxial after firing to 1000°C showing reflectivity**

Two glazes from the triaxial were considered worth noting for potential use, and are presented below.



950–1000°C (cone 08–06) RHA transparent gloss (L2.14)

This glossy glaze, containing 27.75% RHA and 35% recovered materials, displayed fine crazing, despite having a relatively low COE. It was less glossy at 950°C and very glossy at 1000°C, suggesting it could tolerate higher proportions of RHA at the higher temperature. This addition could be expected to reduce crazing. Crazing may also be reduced by the use of a high expansion engobe or body.

	(wt%)
Bungendore tailings	2.25
Gerstley borate	50.00
Sugarcane ash	2.75
Lithium carbonate	15.00
Corn cob ash	1.25
Marulan tailings	1.00
RHA	27.75



The Seger formula, omitting trace elements and with fluxes unified is:

<b>KNO</b>	<b>K<sub>2</sub>O</b>	<b>NaO<sub>2</sub></b>	<b>CaO</b>	<b>MgO</b>	<b>LiO<sub>2</sub></b>	<b>Al<sub>2</sub>O<sub>3</sub></b>	<b>P<sub>2</sub>O<sub>5</sub></b>	<b>B<sub>2</sub>O<sub>3</sub></b>	<b>SiO<sub>2</sub></b>	<b>TiO<sub>2</sub></b>
0.070	0.013	0.057	0.260	0.006	0.664	0.011	0.003	0.274	0.833	0.001

Alumina:silica ratio                      78.625  
COE    7.83

950–1000°C (cone 08-06) rice husk/sugarcane ash glaze (L2.6)

This glaze contains 42.5% recovered materials. It requires firing to cone 06 to become moderately glossy. It is a dry matte at 950°C.

	(wt%)
Bungendore tailings	4.0
Gerstley borate	57.5
Sugarcane ash	20.0
RHA	18.5



The Seger formula, omitting trace elements and with fluxes unified is:

<b>KNO</b>	<b>K<sub>2</sub>O</b>	<b>NaO<sub>2</sub></b>	<b>CaO</b>	<b>MgO</b>	<b>LiO<sub>2</sub></b>	<b>Al<sub>2</sub>O<sub>3</sub></b>	<b>P<sub>2</sub>O<sub>5</sub></b>	<b>B<sub>2</sub>O<sub>3</sub></b>	<b>SiO<sub>2</sub></b>	<b>TiO<sub>2</sub></b>
0.200	0.031	0.168	0.771	0.030		0.069	0.008	0.806	2.526	0.014

Alumina:silica ratio                      36.617

COE    8.02

### Low-fire triaxial 3

The batch recipes of the three corner recipes are given in Table 86.

*Table 86: Glaze triaxial low-fire 3: Corner recipes*

Corner A (corn and sugarcane ash)	(wt%)	Corner B (rock)	(wt%)	Corner C (RHA)	(wt%)
Bungendore tailings	2.5	Bungendore tailings	8.0	Bungendore tailings	3.0
Gerstley borate	34.0	Gerstley borate	42.0	Gerstley borate	60.0
Sugarcane ash	21.0	Dunmore latite dust	50.0	Rice husk ash	37.0
Corn cob ash	42.5				

#### 950–1000°C (cone 08–06) corn/sugarcane ash sandy matte (L3.1)

Corner A (low-fire corn/sugarcane ash), which was predicted to melt at 965°C, fired to a dry speckled sandy matte at 950°C, and a slightly darker dry speckled sandy matte at 1000°C. With increases in temperature, it became lighter in colour, but had not matured into a uniform glaze at 1100°C (fig. 453). At 1100°C there were opaque, slightly raised clumps of glossy glaze on a background of gloss. Higher-temperature firing would be required to produce a uniform gloss.



*Figure 453: Low-fire corn/sugarcane ash at (l to r) 950, 1000, 1050 and 1100°C*

The Seger formula, omitting trace elements and with fluxes unified is:

KNO	K <sub>2</sub> O	NaO <sub>2</sub>	CaO	MgO	LiO <sub>2</sub>	Al <sub>2</sub> O <sub>3</sub>	P <sub>2</sub> O <sub>5</sub>	B <sub>2</sub> O <sub>3</sub>	SiO <sub>2</sub>	TiO <sub>2</sub>
0.370	0.263	0.107	0.448	0.182	-	0.069	0.131	0.441	1.966	0.013

Alumina:silica ratio 28.555

COE 11.72



## Low-fire triaxial 4

In this triaxial two simple quarry tailings glazes were blended with the simple rock glaze. The batch recipes of the three corner recipes are given in Table 87

*Table 87: Glaze triaxial low-fire 4: Corner recipes*

Corner A Low-fire Bungendore	(wt%)	Corner B Low-fire rock	(wt%)	Corner C Low-fire Marulan	(wt%)
Bungendore tailings	40	Bungendore tailings	8	Marulan tailings	40
Gerstley borate	60	Gerstley borate	42	Gerstley borate	60
		Dunmore latite dust	50		

After firing to 950°C, all the glazes had matte surfaces, and colour varied according to the proportion of corner glazes present. Glazes containing proportions of the low-fire rock glaze (Corner B) clearly showed variation in application thickness. The glazes along the A–C line blend were more uniform in appearance (fig. 455).



*Figure 455: Low-fire 4 triaxial at 950°C*

After firing to 1000°C, all the glazes had satin matte surfaces, and colour varied according to the proportion of corner glazes present. Glazes containing proportions of the low-fire rock glaze (Corner B) showed less variation in application thickness than they had when fired to 950°C. The glazes along the A–C line blend were becoming glossy (fig. 456).



**Figure 456: Low-fire 4 triaxial at 1000°C**

After firing to 1050°C, all the glazes had glossy surfaces, and colour varied according to the proportion of corner glazes present. Some glazes (L4.3, L4.8, & L4.13) displayed pinholes where they were very thick (fig. 457).



**Figure 457: Low-fire 4 triaxial at 1050°C**







## Chapter 29: Glaze, Engobe and Body Interactions

Glazes with a range of different surface qualities were selected for testing on different combinations of body and slip at increasing temperatures. At 850°C glaze 1 formed a rough white glaze that crawled on BM11.1 and varied little on other surfaces tested (fig. 461). Glaze 2 (Marulan RHA 845 coe 9.7) also crawled on BM11.1. It developed a sheen on BM11.5.















850°C	BM11.1	ACCL11	BM11.5	E3 (Eckalite c08 low expansion) on BM11.3	E4 (Eckalite c08 high expansion) on BM11.3	E5 (Marulan c08 low expansion) on BM11.3	E6 (Marulan c08 high expansion) on BM11.3
<b>Glaze 1</b> Marulan 830 coe 10.6							
<b>Glaze 2</b> Marulan RHA 845 coe 9.7							

Figure 461: Glaze 1 and 2 on different combinations of body and slip, fired to 850°C

At 850°C, glaze three formed a crazed green-tinged satin translucent gloss where thick (fig. 462). There were few differences in appearance when this glaze was applied over the different engobes. The additional iron present in BM11.5 contributed to the glaze being a tan colour on that body. In contrast, glaze 4 masked the colour of BM11.5.















850°C	BM11.1	ACCL11	BM11.5	E3 (Eckalite c08 low expansion) on BM11.3	E4 (Eckalite c08 high expansion) on BM11.3	E5 (Marulan c08 low expansion) on BM11.3	E6 (Marulan c08 high expansion) on BM11.3
<b>Glaze 3</b> Marulan 850 coe 8							
<b>Glaze 4</b> Marulan 850 coe 10.5							

Figure 462: Glaze 3 and 4 on different combinations of body and engobe, fired to 850°C

There were dramatic differences between the above two glazes when they were fired to 900°C on the four different bodies shown (fig. 463). For example the surfaces of Glaze 4 were progressively less melted on bodies with progressively less flux material. BM11.1 has the most body flux and BM11.5 has the least. ACCL11 is the perlite body that floated.

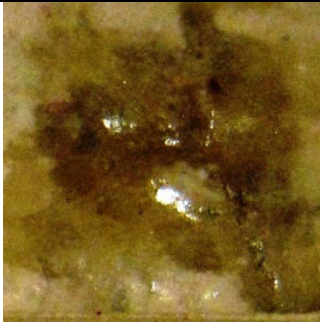
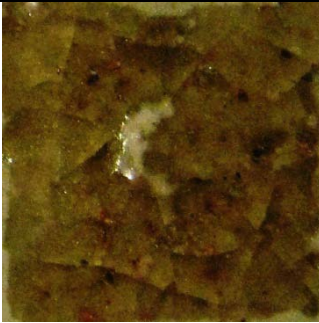
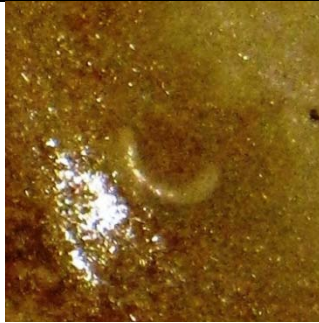

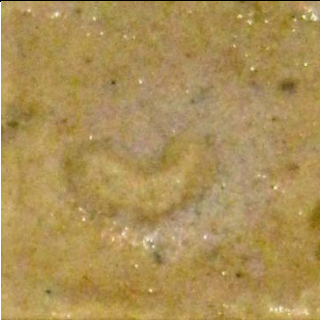



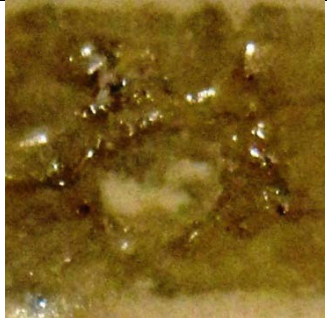
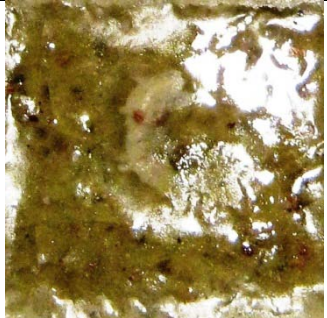


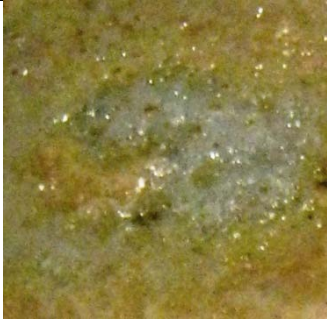



900°C	BM11.1	BM11.3	BM11.5	ACCL11
<b>Glaze 3</b> Marulan 850 coe 8				
<b>Glaze 4</b> Marulan 850 coe 10.5				

Figure 463: Glaze 3 and 4 on four different bodies, 900°C.

There were also dramatic differences within glazes 5 and 6 when they were fired to 900°C on the four different bodies shown (fig. 464). It was clear from these results that glaze/body interactions were occurring at 900°C.

900°C	BM11.1	BM11.3	BM11.5	ACCL11
<b>Glaze 5</b> Marulan 900 c.o.e. 8				
<b>Glaze 6</b> Marulan RHA 912 c.o.e. 9				

*Figure 464: Glaze 5 and 6 on four different bodies, 900°C*

The firing temperature was increased to 950°C for the next tests (figs. 465 & 466). Glaze 7 displayed crawling. The application of different engobes to BM11.5 made no difference to the glaze colour but the surface was slightly more matte.

<b>950°C</b>	<b>BM11.2</b>	<b>BM11.4</b>	<b>BM11.5</b>	<b>E3 (Eckalite c08 low expansion) on BM11.5</b>	<b>E4 (Eckalite c08 high expansion) on BM11.5</b>	<b>E5 (Marulan c08 low expansion) on BM11.5</b>	<b>E6 (Marulan c08 high expansion) on BM11.5</b>
<b>Glaze 7</b> Pale yellow matte glaze (R1)							
<b>Glaze 8</b> Low-fire Bungendor e (L4.1)							
<b>Glaze 9</b> Low-fire Marulan (L4.15)							
<b>Glaze 10</b> RHA transparent gloss (L2.14)							
<b>Glaze 11</b> Lithium 60 low c.o.e.							

Figure 465: Glazes 7–11 on selected bodies and engobes, 950°C





























950°C	BM11.2	BM11.4	BM11.5	E3 (Eckalite c08 low expansion) on BM11.5	E4 (Eckalite c08 high expansion) on BM11.5	E5 (Marulan c08 low expansion) on BM11.5	E6 (Marulan c08 high expansion) on BM11.5
<b>Glaze 12</b> Low-fire RHA							
<b>Glaze 13</b> Transparent gloss (L1.3)							
<b>Glaze 14</b> Low-fire sugarcane ash							
<b>Glaze 15</b> Crystalline matte (L1.10)							

Figure 466: Glazes 12–15 on selected bodies and engobes, 950°C

The firing temperature was increased to 980°C for the next tests (figs. 467–469). Glaze 7 again displayed crawling. Again the application of different engobes to BM11.5 made no difference to the glaze colour but the surface was slightly more matte.




























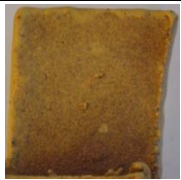




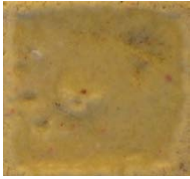


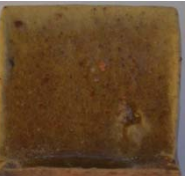



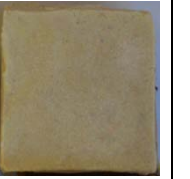
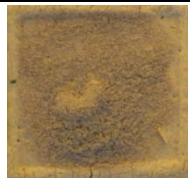




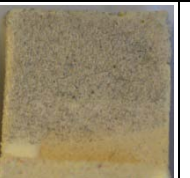
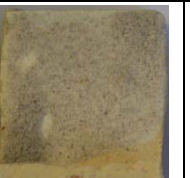


















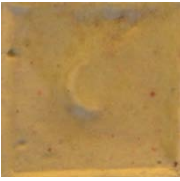





980°C	BM11.2	BM11.4	BM11.5	BM11.6A	E3 (Eckalite c08 low expansion) on BM11.5	E4 (Eckalite c08 high expansion) on BM11.5	E5 (Marulan c08 low expansion) on BM11.5	E6 (Marulan c08 high expansion) on BM11.5
<b>Glaze 7</b> Pale yellow matte glaze (R1)								
<b>Glaze 8</b> Low-fire Bungend ore (L4.1)								
<b>Glaze 9</b> Low-fire Marulan (L4.15)								
<b>Glaze 10</b> RHA transparent gloss (L2.14)								

Figure 467: Glazes 7–10 on selected bodies and engobes, 980°C

<b>980°C (Cone 0)</b>	<b>BM11.2</b>	<b>BM11.4</b>	<b>BM11.5</b>	<b>BM11.6A</b>	<b>E3 (Eckalite c08 low expansion) on BM11.5</b>	<b>E4 (Eckalite c08 high expansion) on BM11.5</b>	<b>E5 (Marulan c08 low expansion) on BM11.5</b>	<b>E6 (Marulan c08 high expansion) on BM11.5</b>
<b>Glaze 11</b> Lithium 60 low c.o.e.								
<b>Glaze 12</b> Low-fire RHA								
<b>Glaze 13</b> Transparent gloss (L1.3)								
<b>Glaze 14</b> Low-fire sugarcane ash								

*Figure 468: Glazes 11–14 on selected bodies and engobes, 980°C*



<b>980°C</b>	<b>BM11.2</b>	<b>BM11.4</b>	<b>BM11.5</b>	<b>E3 (Eckalite c08 low expansion) on BM11.5</b>	<b>E4 (Eckalite c08 high expansion) on BM11.5</b>	<b>E5 (Marulan c08 low expansion) on BM11.5</b>	<b>E6 (Marulan c08 high expansion) on BM11.5</b>
<b>Glaze 15</b> Crystalline Matte (L1.10)							

*Figure 469: Glaze 15 on selected bodies and engobes, 980°C*

The firing temperature was increased to 1000°C for the next tests (figs. 470–472). Glaze 7 displayed crawling. Again the application of different engobes to BM11.5 made no difference to the glaze colour and again the surface was slightly more matte. There were some interesting glaze/body interactions on BM11.6A at 1000°C. The edges of the test tiles softened and the glaze became slightly more fluid.

1000°C	BM11.2	BM11.4	BM11.5	BM11.6A	E3 (Eckalite c08 low expansion) on BM11.5	E4 (Eckalite c08 high expansion) on BM11.5	E5 (Marulan c08 low expansion) on BM11.5	E6 (Marulan c08 high expansion) on BM11.5
<b>Glaze 7</b> Pale yellow matte glaze (R1)								
<b>Glaze 8</b> Low-fire Bungendore (L4.1)								
<b>Glaze 9</b> Low-fire Marulan (L4.15)								
<b>Glaze 10</b> RHA transparent gloss (L2.14)								

Figure 470: Glazes 7–10 on selected bodies and engobes, 1000°C















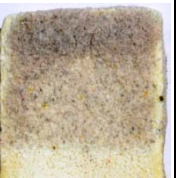

















<b>1000°C (Cone 06)</b>	<b>BM11.2</b>	<b>BM11.4</b>	<b>BM11.5</b>	<b>BM11.6A</b>	<b>E3 (Eckalite c08 low expansion) on BM11.5</b>	<b>E4 (Eckalite c08 high expansion) on BM11.5</b>	<b>E5 (Marulan c08 low expansion) on BM11.5</b>	<b>E6 (Marulan c08 high expansion) on BM11.5</b>
<b>Glaze 11</b> Lithium 60 low c.o.e.								
<b>Glaze 12</b> Low-fire RHA								
<b>Glaze 13</b> Transparen t gloss (L1.3)								
<b>Glaze 14</b> Low-fire sugarcane ash								

Figure 471: Glazes 11–14 on selected bodies and engobes, 1000°C


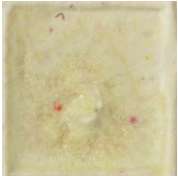





1000°C	BM11.2	BM11.4	BM11.5	E3 (Eckalite c08 low expansion) on BM11.5	E4 (Eckalite c08 high expansion) on BM11.5	E5 (Marulan c08 low expansion) on BM11.5	E6 (Marulan c08 high expansion) on BM11.5
<b>Glaze 15</b> Crystalline matte (L1.10)							

Figure 472: Glaze 15 on selected bodies and engobes, 1000°C

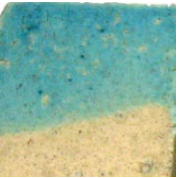



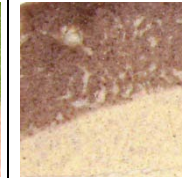
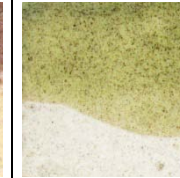
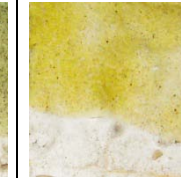
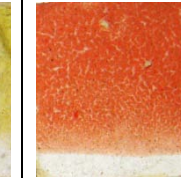



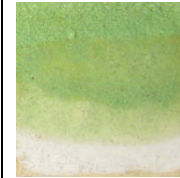


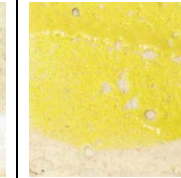
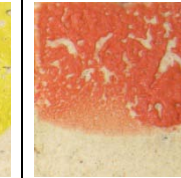
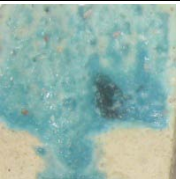
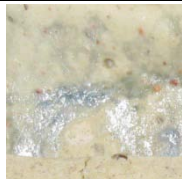

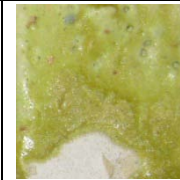
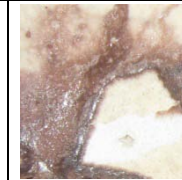


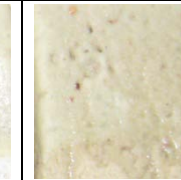
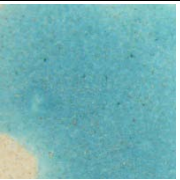

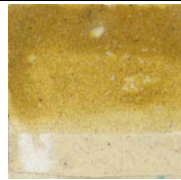
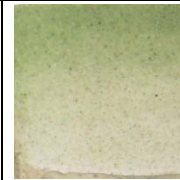

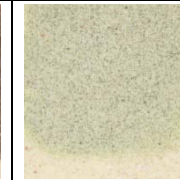
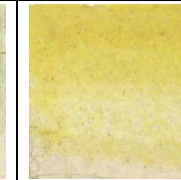
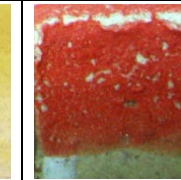
### Colourant additions to selected glazes

Fromme (1994) suggests that the most productive limits for metal oxides chosen for glaze colourants are as follows:

Cobalt carbonate	0.25% to 2%
Red iron oxide	1.00% to 11%
Copper carbonate	1.50% to 6%
Chrome oxide	1.50% to 5%
Manganese dioxide	1.00% to 5.75%
Nickel oxide	0.50% to 3.50%

These limits were observed when choosing colourant additions for testing. Two commercially available stains were also used: Walker's lobster red stain, and Walker's FW5400 bright yellow stain.

Glazes shown (fig. 473) were applied to raw Marulan cone 08 high expansion engobe, over raw BM11.3 and fired to 850°C (cone 013) in oxidation. The engobe chosen was the engobe with the lowest predicted melting point.

<b>850°C (cone 013)</b>	<b>3% copper carbonate</b>	<b>0.25% cobalt carbonate</b>	<b>3% red iron oxide</b>	<b>0.5% chrome oxide</b>	<b>3% manganese dioxide</b>	<b>3% nickel oxide</b>	<b>8% yellow stain</b>	<b>8% red stain</b>
<b>Glaze 1</b> Marulan 830 c.o.e. 10.6								
<b>Glaze 2</b> Marulan RHA 845 c.o.e. 9.7								
<b>Glaze 3</b> Marulan 850 c.o.e. 8								
<b>Glaze 4</b> Marulan 850 c.o.e. 10.5								

**Figure 473: Colourant additions to glazes applied to raw Marulan cone 08 high expansion engobe, over raw BM11.3, 850°C**

## BM11.3A

As a result of the slumping in evidence when BM11.3 was fired to 900°C, a body was prepared to have some of the properties of BM11.3 and some of the properties of BM11.6, which was the next body along the A-C line blend in triaxial BM11. Bm11.3 had 0% porosity at 900°C (fig. 397). BM11.6 had approximately 26% porosity at 900°C, reducing to 0.1% porosity at 1000°C. The new body, labelled BM11.3A was formulated with the intention of avoiding slumping at 900°C, and of having zero porosity at a temperature above 900°C but below 1000°C. It contained 75% BM11.3 and 25% BM11.6, with appropriate additions of magnesium sulphate and barium carbonate to improve workability and reduce efflorescence. A second body labelled BM11.6B was formulated with the intention of avoiding slumping at 950°C, and of having low porosity between 950°C and 1000°C. It contained 25% BM11.3 and 75% BM11.6, again with appropriate additions of magnesium sulphate and barium carbonate.

**Table 89: Batch recipes BM11.3A and BM11.6B**

	<b>BM11.3A</b>	<b>BM11.6B</b>
	<b>(wt%)</b>	<b>(wt%)</b>
Bungendore tailings	32.81	35.94
Marulan tailings	22.50	27.50
Unimin cullet 150	13.75	11.25
Nepheline syenite 200	9.63	7.88
Talc Plustalc N275	4.13	3.38
Gerstley borate	13.75	11.25
Cryolite synthetic	2.06	1.69
Lithium carbonate	1.38	1.13
	<b>100</b>	<b>100</b>
Epsom salts	0.3	0.3
Barium carbonate	0.65	0.65

The Seger formula of BM11.3A, omitting trace elements and with fluxes unified (as if for a glaze) is:

<b>KNO</b>	<b>K<sub>2</sub>O</b>	<b>NaO<sub>2</sub></b>	<b>CaO</b>	<b>MgO</b>	<b>BaO</b>	<b>Al<sub>2</sub>O<sub>3</sub></b>	<b>P<sub>2</sub>O<sub>5</sub></b>	<b>B<sub>2</sub>O<sub>3</sub></b>	<b>SiO<sub>2</sub></b>	<b>TiO<sub>2</sub></b>
0.330	0.072	0.258	0.300	0.210	0.011	0.386		0.187	3.025	0.013

Alumina:silica ratio                      7.84  
 COE    10.50  
 Estimate firing temp (as glaze)    1200°C

The Seger formula of BM11.3A, omitting trace elements and with alumina unified (in keeping with convention for a clay) is:

<b>KNO</b>	<b>K<sub>2</sub>O</b>	<b>NaO<sub>2</sub></b>	<b>CaO</b>	<b>MgO</b>	<b>BaO</b>	<b>Al<sub>2</sub>O<sub>3</sub></b>	<b>P<sub>2</sub>O<sub>5</sub></b>	<b>B<sub>2</sub>O<sub>3</sub></b>	<b>SiO<sub>2</sub></b>	<b>TiO<sub>2</sub></b>
0.854	0.185	0.668	0.776	0.543	0.028	1.000		0.484	7.835	0.034

The Seger formula of BM11.6B, omitting trace elements and with fluxes unified (as if for a glaze) is:

<b>KNO</b>	<b>K<sub>2</sub>O</b>	<b>NaO<sub>2</sub></b>	<b>CaO</b>	<b>MgO</b>	<b>BaO</b>	<b>Al<sub>2</sub>O<sub>3</sub></b>	<b>P<sub>2</sub>O<sub>5</sub></b>	<b>B<sub>2</sub>O<sub>3</sub></b>	<b>SiO<sub>2</sub></b>	<b>TiO<sub>2</sub></b>
0.340	0.088	0.252	0.299	0.209	0.012	0.470		0.172	3.506	0.017

Alumina:silica ratio                      7.46  
 COE    10.01  
 Estimate firing temp (as glaze)    1230°C

The Seger formula of BM11.6B, omitting trace elements and with alumina unified (convention for a clay) is:

<b>KNO</b>	<b>K<sub>2</sub>O</b>	<b>NaO<sub>2</sub></b>	<b>CaO</b>	<b>MgO</b>	<b>BaO</b>	<b>Al<sub>2</sub>O<sub>3</sub></b>	<b>P<sub>2</sub>O<sub>5</sub></b>	<b>B<sub>2</sub>O<sub>3</sub></b>	<b>SiO<sub>2</sub></b>	<b>TiO<sub>2</sub></b>
0.724	0.188	0.536	0.635	0.445	0.026	1.000		0.367	7.459	0.035

Glazes shown below (fig. 474) were applied to raw Marulan cone 08 high expansion engobe (E6), over raw BM11.3A and fired to 900°C in oxidation. In every case the glaze had a similar appearance when applied over BM11.3A with or without engobe, but in the latter case the glaze was smoother to touch.

There was an interaction between glazes and BM11.3A at 900°C, with the body softening at the edges, and with this effect being more noticeable with the more fluid glazes, which appeared to leach material from the top of the test tiles for glazes 3 and 5 (fig. 474) below. The presence of the engobe inhibited this effect, indicating it was more refractory than the body







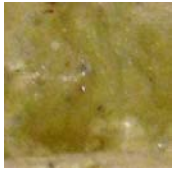














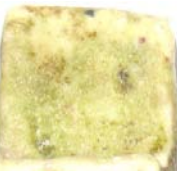










900°C	3% copper carbonate	0.25% cobalt carbonate	3% red iron oxide	0.5% chrome oxide	3% manganese dioxide	3% nickel oxide	8% yellow stain	8% red stain
<b>Glaze 3</b> Marulan 850 c.o.e. 8								
<b>Glaze 4</b> Marulan 850 c.o.e. 10.5								
<b>Glaze 5</b> Marulan 900 c.o.e. 8								
<b>Glaze 6</b> Marulan RHA 912 c.o.e. 9								

Figure 474: Colourant additions to glazes applied to raw Marulan cone 08 high expansion engobe (E6), over raw BM11.3A, 900°C



Glaze colour runs were also performed at 950°C, using BM11.2. Again a range of interesting glaze/body reactions occurred (figs. 475 & 476).






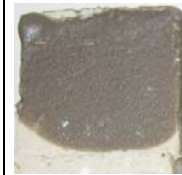






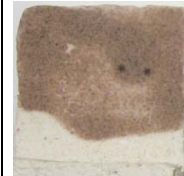
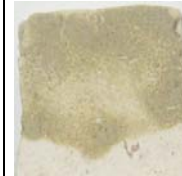

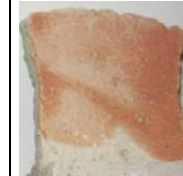






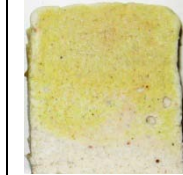
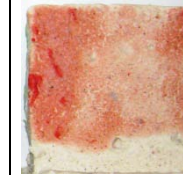




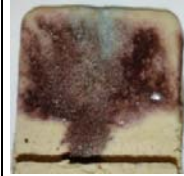


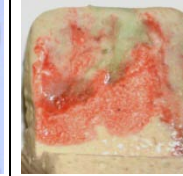
950°C	3% copper carbonate	0.25% cobalt carbonate	3% red iron oxide	0.5% chrome oxide	3% manganese dioxide	3% nickel oxide	8% yellow stain	8% red stain
<b>Glaze 7</b> Pale yellow matte glaze (R1)								
<b>Glaze 8</b> Low-fire Bungendor e (L4.1)								
<b>Glaze 9</b> Low-fire Marulan (L4.15)								
<b>Glaze 10</b> RHA transparent gloss (L2.14)								

Figure 475: Colourant additions to glazes 7–10 applied to raw BM11.2, 950°C

950°C	3% copper carbonate	0.25% cobalt carbonate	3% red iron oxide	0.5% chrome oxide	3% manganese dioxide	3% nickel Oxide	8% yellow stain	8% red stain
<b>Glaze 11</b> Lithium 60 low c.o.e.								
<b>Glaze 12</b> Low-fire RHA								
<b>Glaze 13</b> Transparent gloss (L1.3)								
<b>Glaze 14</b> Low-fire sugarcane ash								
<b>Glaze 15</b> Crystalline matte (L1.10)								

Figure 476: Colourant additions to glazes 11–15 applied to raw BM11.2, 950°C

The 950°C colour runs were repeated using BM11.6B (figs. 477 & 478). Less glaze/body interaction occurred. Glaze 13 was a vibrant, almost craze-free gloss. Glaze 12 and glaze 14 were interesting because of their different colour responses to copper, cobalt and chrome, and their well-sintered, predominantly dry surfaces.

950°C	3% copper carbonate	0.25% cobalt carbonate	3% red iron oxide	0.5% chrome oxide	3% manganese dioxide	3% nickel Oxide	8% yellow stain	8% red stain
<b>Glaze 7</b> Pale yellow matte glaze (R1)								
<b>Glaze 8</b> Low-fire Bungendore (L4.1)								
<b>Glaze 9</b> Low-fire Marulan (L4.15)								
<b>Glaze 10</b> RHA transparent gloss (L2.14)								

Figure 477: Colourant additions to glazes 7–10 applied to raw BM11.6B, 950°C

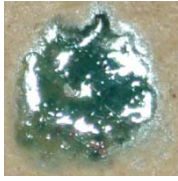
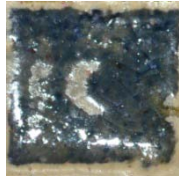

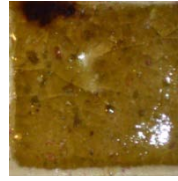
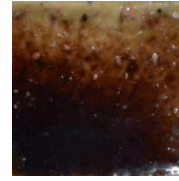
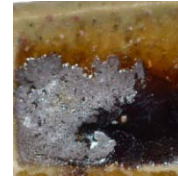

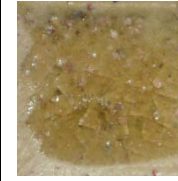
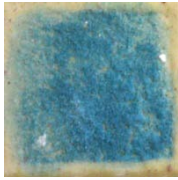
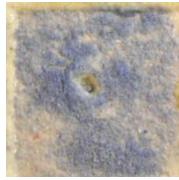





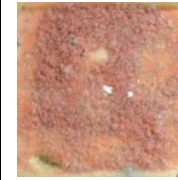
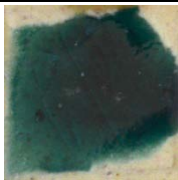

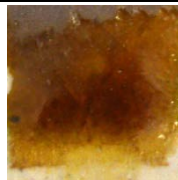
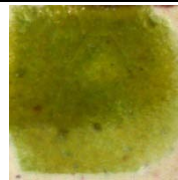
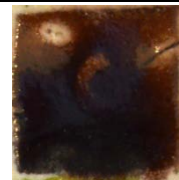
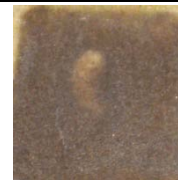










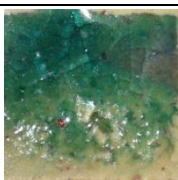
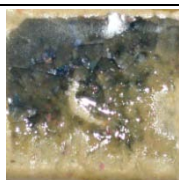


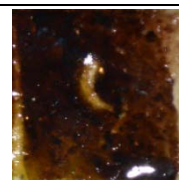
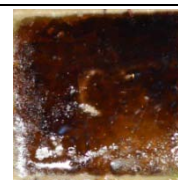

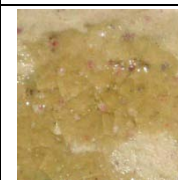
<b>950°C</b>	<b>3% copper carbonate</b>	<b>0.25% cobalt carbonate</b>	<b>3% red iron oxide</b>	<b>0.5% chrome oxide</b>	<b>3% manganese dioxide</b>	<b>3% nickel oxide</b>	<b>8% yellow stain</b>	<b>8% red stain</b>
<b>Glaze 11</b> Lithium 60 low c.o.e.								
<b>Glaze 12</b> Low-fire RHA								
<b>Glaze 13</b> Transparent gloss (L1.3)								
<b>Glaze 14</b> Low-fire sugarcane ash								
<b>Glaze 15</b> Crystalline matte (L1.10)								

Figure 478: Colourant additions to glazes 11–15 applied to raw BM11.6B, 950°C

The glazes were most vibrant when the BM11.6B colour runs were repeated at 1000°C (figs. 479 & 480). Less glaze/body interaction occurred. Glaze 13 was a vibrant, almost craze-free gloss. Glaze 12 and glaze 14 were interesting because of their different colour responses to copper, cobalt and chrome, and their well-sintered, predominantly dry surfaces.

































1000°C	3% copper carbonate	0.25% cobalt carbonate	3% red iron oxide	0.5% chrome oxide	3% manganese dioxide	3% nickel oxide	8% yellow stain	8% red stain
<b>Glaze 7</b> Pale yellow matte glaze (R1)								
<b>Glaze 8</b> Low-fire Bungendore (L4.1)								
<b>Glaze 9</b> Low-fire Marulan (L4.15)								
<b>Glaze 10</b> RHA transparent gloss (L2.14)								

Figure 479: Colourant additions to glazes 7–11 applied to raw BM11.6A, 1000°C

1000°C	3% copper carbonate	0.25% cobalt carbonate	3% red iron oxide	0.5% chrome oxide	3% manganese dioxide	3% nickel oxide	8% yellow stain	8% red stain
<b>Glaze 12</b> Low-fire RHA								
<b>Glaze 13</b> Transparent gloss (L1.3)								
<b>Glaze 14</b> Low-fire sugarcane ash								
<b>Glaze 15</b> Crystalline matte (L1.10)								

Figure 480: Colourant additions to glazes 12–15 applied to raw BM11.6A, 1000°C

The previous few pages have catalogued a library of low-fire bodies glazed with a muted pastel palette that became increasingly vibrant and earthy as temperature increased to 1000°C. The results were often specific to the bodies glazed. Those tiles that were fired flat may well have vitrified and so it was prudent to explore the extent to which some of these bodies might slump.

## Chapter 30: Slump Tests for Selected Bodies

Bodies with added flux can be susceptible to slumping, so it was necessary to establish whether, within the BM11 series, there was a body or bodies that would display visible clay/glaze interaction but would resist slumping at the chosen firing temperature.

A number of slump tests were conducted. Results are displayed below (Table 90). The best fit was BM11.2. This body is relatively high flux and almost white. It resisted slumping at 980°C and interacted relatively strongly with low-fire glazes. It also had absorption of 0.3% at 1000°C.

BM11.3, which was next to BM11.2 on the triaxial, slumped at 850°C.

BM11.4 and BM11.5 both withstood temperatures of 1000°C without slumping. At this temperature, BM11.4 had absorption of 2.7% and BM11.5 had absorption of 0.2%. The whiteness of these bodies is also an advantage for colour development in glazes.

BM11.6 was beginning to slump at 1000°C. At this temperature, BM11.6 had only 0.1% absorption, so it could be fired slightly lower or used on forms that are more self-supporting.



















BM11.6A slumped badly at 1000°C, and as absorption was 13% at 950°C, this body has less prospect of successful use.

BM11.6B successfully withstood 1000°C without slumping, but absorption was 7%.

BM11.6C began slumping at 950°C.

All slump tests are pictured overleaf (Table 90).

Table 90: Slump tests for selected bodies

	900°C.	950°C	980°C
BM11.2	-		
BM11.3		-	-
	900°C.	950°C	1000°C
BM11.4			
BM11.5			
BM11.6			
BM11.6A	-	-	
BM11.6B	-		
BM11.6C			

- Empty cells were not tested, - expected results obtained from adjoining cells



## **Chapter 31: Studio Tests using Bodies and Glazes Developed**

As a range of experimental bodies had been developed, it was important to establish whether they were amenable to the traditional studio processes of throwing, turning, glaze application and firing. This chapter documents attempts to produce ware by these methods, using experimental bodies and combinations of experimental and proprietary bodies.

### **BM11.6A**

A number of bowls were thrown from freshly kneaded BM11.6A, and turned using standard turning tools. These bowls (figs. 481–486) were bisque-fired to a temperature of 700°C, some 200–300 °C lower than conventional bisque firing. This was to establish whether they would be sufficiently strong, and yet sufficiently porous to be suitable for glaze application by filling with, and immersing in, glazes for low-firing. A number of features of the clay body were revealed and are discussed with reference to the images below.

The exterior of the bowl has efflorescence on the surface, but the interior does not (fig. 481). This matches the results from tests where the surface most exposed to the air was the surface that had the most efflorescence. In the case of the bowl, it is probable that the air inside the bowl was more captive and retained more moisture than the air passing the exterior of the bowl. The foot ring does not have efflorescence on the surface (fig. 482). Drying in this area was also restricted by contact with the bench surface during drying.



*Figure 481: Bowl thrown from BM11.6A, bisque fired to 700°C*



*Figure 482: Bowl: BM11.6A, bisque fired to 700°C, showing turned foot ring*

In addition to the properties mentioned above, the body could be roughly thrown, and lumps could result from failure to achieve a homogenous mix during kneading (fig. 483).



*Figure 483: Bowl thrown from BM11.6A, bisque fired to 700°C*

Efflorescence has formed on an exposed throwing ridge on the interior of the bowl and on the exposed ridge delineating the exterior of the bowl from the foot ring, as a result of faster drying of these surfaces (fig. 484).



*Figure 484: Bowl: BM11.6A, bisque fired to 700°C, showing turned foot ring*

The rim dried fastest, and being relatively thin compared with the rest of the bowl, formed a thick layer of efflorescence (fig. 485).



*Figure 485: Bowl thrown from BM11.6A, bisque fired to 700°C*

It is also evident that the efflorescence has formed without a clear delineation between where the bowl was turned and where the wall was thrown (fig. 486), indicating that the majority of efflorescence occurred when the clay body had already been turned. This is also evident in the preceding images.



*Figure 486: Bowl: BM11.6A, bisque fired to 700°C, showing turned foot ring*

All the bowls bisque fired at 700°C were strong but porous, rendering them suitable for glaze application.

### Glazing and firing

Glaze 17 (cone 08 clear gloss) was based on Glaze 13 with sugarcane ash increased by 1.25% to replace corn cob ash.

<b>Cone 08 clear gloss:</b>	(wt%)
Gerstley borate	27.50
Unimin cullet	22.50
Bungendore tailings	30.00
Sugarcane ash	4.00
Marulan tailings	1.00
Lithium carbonate	15.00
	100.00

The Seger formula, omitting trace elements and with fluxes unified is:

<b>KNO</b>	<b>K<sub>2</sub>O</b>	<b>NaO<sub>2</sub></b>	<b>CaO</b>	<b>MgO</b>	<b>Al<sub>2</sub>O<sub>3</sub></b>	<b>LiO<sub>2</sub></b>	<b>B<sub>2</sub>O<sub>3</sub></b>	<b>SiO<sub>2</sub></b>	<b>TiO<sub>2</sub></b>
0.111	0.010	0.101	0.191	0.040	0.071	0.657	0.149	0.972	0.005

Alumina:silica ratio 13.74

COE 9.63

Ionic potential 14.2

Additions were based on previous colour runs (fig.478).

Cobalt carbonate	0.25	cone 08 blue gloss (Glaze 17.2)
Chrome oxide	0.50	cone 08 green gloss (Glaze 17.4)

The bowls were glazed with the above two glazes. For ease of reference the bowls are numbered 1–4 for the description of the glazing process. Bowls 1 and 2 had Glaze 17.4 poured inside, and each bowl was tilted and rotated before the excess glaze was poured out. The lips were sponged clean and the exteriors had no glaze applied. Bowls 3 and 4 had Glaze 17.2 poured inside them. The excess was poured out and after approximately five minutes, when Glaze 17.2 was sufficiently dry, each bowl was held by the foot ring and lowered into Glaze 17.4 so that glaze was applied to the interior and exterior lip of the bowls. The bowls were sufficiently robust for ease of handling, and glaze thickness, adhesion and drying time were all satisfactory.

The bowls were fired to 940°C or 950°C in oxidising atmospheres in electric kilns controlled by Harco Kiln controllers, using a ramp of 60°C per hour to 500°C, and 100°C per hour to peak temperature, with a 15-minute soak at top temperature and unforced cooling. Orton cone 08 was touching and slumping in the kiln fired to 940°C (fig. 487), and was more slumped in the kiln fired to 950°C (fig. 488). The temperature for cone 08 is nominally 855°C when fired at 150°C per hour. The extent of slumping of the cones at the lower temperatures reflects the heat work from the slower firing schedule.



*Figure 487: Cone 08 after reading 940°C*



*Figure 488: Cone 08 after reading 950°C*

The images below reveal a number of fired properties of body and glaze.

The sheen on the exterior of the rim in the centre of the image (fig. 489) shows that the exterior of Bowl 1 has self-glazed. Impurities in the body are visible as specks of colour. There was a coating of green gloss glaze on the interior.



*Figure 489: Bowl 1 thrown from BM11.6A, fired to 940°C, Glaze 17.4*

The gloss glaze, in this case coloured with chrome oxide, has run, forming streaks and a darker pool in the hollow of the bowl (fig. 490).



*Figure 490: Bowl 1 thrown from BM11.6A, fired to 940°C, Glaze 17.4*

The self-glazed rim of Bowl 2 (fig. 491) has a slightly greater sheen than was evident on Bowl 1 (fig. 490). Bowl 2 was fired at higher temperature, by 10°C.



*Figure 491: Bowl 2 thrown from BM11.6A, fired to 950°C, Glaze 17.4*

The gloss glaze has also formed streaks and a darker pool in the hollow of Bowl 2 (fig. 492).



*Figure 492: Bowl 2 thrown from BM11.6A, fired to 950°C, Glaze 17.4*



The extent of self-glazing on the exterior and the convenient lack of self-glazing on the foot ring is visible on Bowl 2 (fig. 493). Glaze has formed without a clear delineation between where the bowl was turned and where the wall was thrown, reflecting the pattern of efflorescence formed during drying.



*Figure 493: Bowl 2: BM11.6A, fired to 950°C, Self-glazed exterior, unglazed foot ring*

Bowl 3 was fired to 940°C with Glaze 17.2 inside, and Glaze 17.4 applied to the interior and exterior lip. It can be seen in the foreground (fig. 494) that the lump on the lip of the bowl that was clearly evident on the bisque-fired bowl (fig. 487) is much less evident after glaze firing. Observation showed this to be partly due to subsidence of the lump resulting from interaction of the body and glaze, and partly due to the remaining lump being covered with a layer of glaze.



*Figure 494: Bowl 3: BM11.6A fired to 940°C. Glazes 17.2 (interior) and 17.4 (rim)*

The blue glaze 17.2 has become fluid and pooled slightly in the hollow of Bowl 3 (fig. 495). Streaks of the paler green glaze can be seen running down from the lip into the bowl, beyond the zone where the two glazes overlapped during application.



*Figure 495: Bowl 3: BM11.6A fired to 940°C. Glazes 17.2 (interior) and 17.4 (rim)*

Bowl 3 is shown inverted (fig. 496). As observed for Bowl 2, the foot ring remained conveniently unglazed. The extent of self-glazing on the exposed ridge delineating the foot ring resulted from the amount of efflorescence accumulated on that ridge after turning.



*Figure 496: Bowl 3: BM11.6A, 940°C. Self-glazed exterior, unglazed foot ring. Glaze 17.4 (rim)*

The fluidity of Glaze 17.4 is obvious on the lip of Bowl 4 (fig. 497). A line of pooled glaze is evident where the applied glaze meets the self-glazed surface. Crazeing is evident.



*Figure 497: Bowl 4: BM11.6A fired to 950°C. Glazes 17.2 (interior) and 17.4 (rim)*

A thinner application of Glaze 17.2 avoided pooling, with some throwing lines showing in the hollow of the bowl (fig. 498).



*Figure 498: Bowl 4: BM11.6A fired to 950°C. Glazes 17.2 (interior) and 17.4 (rim)*

When the same bowl is seen turned upside down (fig. 499) cracks are apparent in the self-glazed area near the foot ring. Inspection revealed them to be cracks extending through the glaze-body interface, but not through the wall of the vessel. More extensive self-glazing on this bowl, resulting from leaving the bowl inverted on the wheel for a period during drying, was accompanied by more adhesion of alumina hydrate to the foot ring.



*Figure 499: Bowl 4: BM11.6A, 950°C. Glaze 13.4 (rim). Self-glazed exterior, unglazed foot ring*

These bowls all held water without seeping when left overnight. However, since this body had an absorption of approximately 10% when tested at 950°C, it is likely that over time the glazes will craze.

As BM11.6B had been developed to be a lower absorption body, and BM1.14C had proved to have low absorption and high strength, larger numbers of these two bodies were required for further testing.

## Scaled up production of BM1.14C and BM11.6B

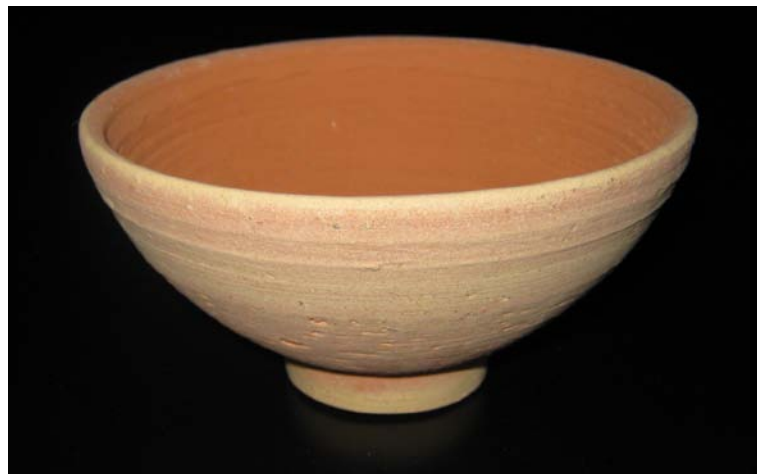
100 kg batches of BM1.14C and BM11.6B were prepared using a Soldner clay mixer and a Venco de-airing pug mill. The extruded pugs were bagged and the bags were sealed and labelled and stored in plastic bins (fig.500).



*Figure 500: Bagged and labelled pugs of experimental clays*

## Ware produced using BM11.6B

The next step was to make some ware from BM11.6B. Assistance was kindly provided by Geoff Crispin, who provided a report on the properties of BM11.6B (Appendix 8). Crispin threw and turned some articles, and examples of these following firing to 800°C are pictured (figs. 501 & 502).



*Figure 501: Bowl thrown by Geoff Crispin from BM11.6B, bisque fired to 800°C*



*Figure 502: Vase by Geoff Crispin from BM11.6B, bisque fired to 800°C*

The ware was then fired to 975°C, using the standard firing cycle. Although previous slump tests had seen BM11.6B withstand 980°C without slumping, the bowl, which was approximately 3 mm thick at the top of the foot ring,

slumped and cracked open (fig. 503). Glaze 13, with an addition of 4% copper carbonate, pooled in the hollow of the bowl.



*Figure 503: Bowl by Geoff Crispin. BM11.6B, glazed with 13.1 and fired to 975°C*

Another Crispin bowl (fig. 504) slumped less, and the matt glaze 7.3 did not run.



*Figure 504: Bowl by Geoff Crispin. BM11.6B, glazed with 7.4 and fired to 975°C*

I also threw a number of bowls from BM11.6B and bisque fired them at 700°C. Two glazes were adapted from Glaze 17, with the intention of reducing the fluidity at cone 08.

### **Cone 08 glaze (Glaze 18)**

Glaze 18 contained an addition of 4% RHA, thereby increasing the silica content.

	(wt%)
Gerstley borate	27.50
Unimin cullet	22.50
Bungendore tailings	30.00
Sugarcane ash	4.00
Marulan tailings	1.00
Lithium carbonate	15.00
	<b>100.00</b>
Plus rice husk ask	4.00

When coloured with 0.5% chrome oxide, applied to BM11.6B, and fired to cone 08, Glaze 18 formed a gloss without pooling in the centre of the bowl (fig. 505).



*Figure 505: Bowl 5: BM11.6B, 950°C. Glaze 18.4*



The Seger formula, omitting trace elements and with fluxes unified is:

<b>KNO</b>	<b>K<sub>2</sub>O</b>	<b>NaO<sub>2</sub></b>	<b>CaO</b>	<b>MgO</b>	<b>Al<sub>2</sub>O<sub>3</sub></b>	<b>LiO<sub>2</sub></b>	<b>B<sub>2</sub>O<sub>3</sub></b>	<b>SiO<sub>2</sub></b>	<b>TiO<sub>2</sub></b>
0.112	0.011	0.101	0.191	0.041	0.071	0.656	0.149	1.045	0.005

Alumina:silica ratio 14.78

COE 9.42

Ionic potential 15.0

### **Cone 08 glaze (Glaze 19)**

Glaze 19 was formulated to have an alumina:silica ratio mid-way between Glaze 17 and Glaze 18, but with a COE slightly lower than Glaze 18.

The Seger formula, omitting trace elements and with fluxes unified is:

<b>KNO</b>	<b>K<sub>2</sub>O</b>	<b>NaO<sub>2</sub></b>	<b>CaO</b>	<b>MgO</b>	<b>Al<sub>2</sub>O<sub>3</sub></b>	<b>LiO<sub>2</sub></b>	<b>B<sub>2</sub>O<sub>3</sub></b>	<b>SiO<sub>2</sub></b>	<b>TiO<sub>2</sub></b>
0.107	0.012	0.095	0.187	0.038	0.074	0.668	0.149	0.990	0.005

Alumina:silica ratio 13.45

COE 9.39

Ionic potential 14.5

Glaze 19 contains 56% recycled materials:

	(wt%)
Gerstley borate	27.00
Unimin cullet	20.00
Bungendore tailings	30.00
Sugarcane ash	4.00
Marulan tailings	2.00
Lithium carbonate	15.00
RHA	2.00
	<b>100.00</b>

When applied to BM11.6B, and fired to cone 08, Glaze 19 formed a low sheen glaze with low fluidity (fig. 506).



*Figure 506: Bowl 6: BM11.6B, 950°C. Glaze 19 without colourant addition*

Addition of 4% copper carbonate produced a blue glaze where applied sufficiently thickly (fig.507).



*Figure 507: Bowl 7: BM11.6B, 950°C. Glaze 19 with 4% copper carbonate*

## **Blends with a proprietary body**

As discussed earlier, the main workability problem of the low-fire bodies developed was their tendency to set after being extruded from the pug mill, bagged and stored. An option for managing this tendency would be to use a combined mixing/extruding mill such as the Peter Pugger, which enables mixing of material of varying consistency. A second option is to compromise on the extent to which firing temperature is lowered by blending the low-firing bodies with a proprietary body. This second option is explored in this chapter, using Walker's middle fire (WMF) as the proprietary body, chosen for its porosity of approximately 3% at 1178°C (Appendix 9).

The two bodies that were mixed were the two bodies of which 100 kg had been produced—BM11.6B and BM1.14C. First, each body was blended in a 50:50 ratio with WMF. These blends were then mixed in a 50:50 ratio with the experimental body, and then with WMF. A 20:80 blend of BM11.6B:WMF was also mixed. Sample bars were cut, marked at 100 mm with digital calipers, and fired to three temperatures using the standard firing cycle: 1000, 1050 and 1100°C. A sample of each blend was also bagged and stored to enable assessment of malleability after 6 weeks.

It was predicted that:

1. Increasing the proportion of WMF would increase the duration of time over which the body retained malleability.
2. Increasing the proportion of WMF would increase porosity at a given temperature from 1000 to 1100°C.
3. Increasing the proportion of WMF would decrease the shrinkage at a given temperature from 1000 to 1100°C.

The range of bodies appears, with a description of malleability 6 weeks after blending and bagging, in Table 91.

**Table 91: Experimental and proprietary blends. Malleability 6 weeks after blending and bagging**

<b>BM11.6B</b>	<b>WMF</b>	<b>Malleability 6 weeks after blending &amp; bagging</b>
75	25	Very firm. Able to be dented with thumb pressure. Short, but did not crumble when manipulated. Softened to kneadable state without crumbling.
50	50	Firm. Able to be dented with finger pressure. Softened quickly to kneadable state. No crumbling.
25	75	Firm, but immediately kneadable. No crumbling.
20	80	Firm, but immediately kneadable. No crumbling.
<b>BM1.14C</b>	<b>WMF</b>	<b>Malleability 6 weeks after blending &amp; bagging</b>
75	25	Very firm. Able to be dented with thumb pressure. Softened to kneadable state without crumbling.
50	50	Firm, easily dented with finger pressure. Softened quickly to kneadable state. No crumbling.
25	75	Soft and immediately kneadable. No crumbling.

Fired samples were measured for shrinkage and the average shrinkage at 1000, 1050 and 1100°C was recorded (Table 92).

**Table 92: Wet to fired shrinkage BM11.6B & BM1.14C blended with WMF**

<b>Wet to fired shrinkage (%) BM11.6B &amp; BM1.14C blended with WMF</b>							
	<b>% BM11.6B</b>				<b>% BM1.14C</b>		
	<b>75</b>	<b>50</b>	<b>25</b>	<b>20</b>	<b>75</b>	<b>50</b>	<b>25</b>
<b>1000°C</b>	7.5	7.0	6.4	6.5	6.2	5.8	6.2
<b>1050°C</b>	11.0	10.3	8.2	8.1	8.1	7.2	8.0
<b>1100°C</b>	11.2	10.8	9.2	9.1	8.8	8.4	8.7

For BM11.6B blends, increasing the proportion of WMF decreased the shrinkage at all three temperatures, as predicted. Contrary to predictions, at all three temperatures the blend containing 50% BM1.14C shrank less than the blends containing 25 or 75% BM1.14C.

Measures of absorption and porosity were obtained in accordance with ASTM Standard C37388 (2006). The fired pieces were dried at 160 °C, weighed on a Diamond Model 100 digital scale to obtain dry mass, and then boiled in distilled water for five hours, soaked for 24 hours and re-weighed.

The average porosity at 1000, 1050 and 1100°C was calculated and recorded (Table 93).

**Table 93: Average apparent porosity. BM11.6B & BM1.14C blended with WMF**

Porosity BM11.6B & BM1.14C blended with WMF							
	(wt%) BM11.6B				(wt%) BM1.14C		
	75	50	25	20	75	50	25
1000°C	29.4	27.7	29.8	31.0	28.4	26.5	28.6
1050°C	3.3	12.4	25.3	23.6	21.8	22.4	24.8
1100°C	1.3	4.3	18.0	18.1	9.6	14.7	19.3

Average absorption of <2% was recorded for samples with 50% BM11.6B fired to 1100°C, so this blended body may be useful for making vitreous ware at this temperature. A number of forms were easily thrown, indicating potential for further research with this blended body (fig508).



Figure 508. BM11.6B 50: 50 WMF blend fired to 900°C. 15x20cm

## Conclusion

This research has demonstrated that it is possible to produce vitrified studio ceramics below 1000°C, incorporating industrial and agricultural wastes from NSW, Australia. Clay bodies have been produced incorporating quarry tailings and glass cullet, and low-temperature glazes have been produced incorporating these same ingredients combined with sugarcane ash, corn cob ash, RHA, rock dust, and perlite fines. The triaxial blending method usually reserved for glaze development has been scaled up to adapt it for clay body formulation. Novel methods of displaying data in triaxial format to expose trends in shrinkage and absorption were developed, and 3D design software was employed creatively to make these trends visible at a glance.

A survey of the literature and discussion with ceramists indicated that some success had been achieved in reducing sintering temperatures industrially, in studio ceramics, and in advanced ceramics; and in some cases the bodies developed had incorporated industrial, agricultural or urban waste. This research has contributed to the field through the combination of techniques and materials used to develop a studio ceramic of low porosity and acceptable strength below 1000°C. In addition, the documentation of dramatic interaction of novel bodies and glazes at relatively low temperatures represents a contribution to the field.

Several bodies incorporating industrial wastes were formulated and fired at a range of temperatures. These bodies were tested for absorption using standardised methods, and a number of bodies were selected for further development. Engobes and glazes incorporating agricultural and industrial waste were formulated and tested on selected bodies at a range of temperatures.

One major aim of the research was to demonstrate that it is possible to reduce energy input requirements, and this has been achieved by developing a vitrified ceramic at 950°C. Studio ceramics frequently undergo preliminary

bisque firing at this temperature to produce ware that is strong enough to withstand the glazing process. The bodies produced were able to be bisque fired at 700°C. As a result there are energy savings at both bisque and glaze firings. For some forms, bisque firing was unnecessary due to the composition of the clay bodies. The relatively fine particle size of the quarry tailings resulted in bodies that were slow to absorb water when the objects made were approaching dryness at room temperature. Raw glazing was therefore possible and bisque firing was avoided altogether.

The preparation and application of glaze does of course involve some energy input, time, labour, storage and expense. Further energy input reductions are achieved if glazing is avoided, and in this sense the discovery of a vitrified self-glazing body was a valuable outcome of the research. The ability of this body to produce vitrified glazed ceramics from raw articles placed in the kiln and fired to 1000°C shows potential for industrial, as well as studio applications, especially as the underside of the articles remained glaze free.

Despite these advances, there were some limitations to the utility of the bodies developed. The most significant were related to the thixotropy of the body, causing flabbiness when throwing, and a tendency to set hard when packaged in sealed bags. This latter quality, as exemplified by the body labelled BM11.6B, demanded that considerable time and effort was expended in returning the body to a malleable condition after storage. Once that had been achieved, it was possible to make ceramic articles using hand-forming methods, including slab building of forms.

Geoff Crispin also kindly persevered with the bagged plastic clay, and demonstrated that the low-firing body could be thrown and turned, but documented a range of problematic qualities that would discourage choice of this clay for wheel work (Appendix 8). Most problematic were thixotropy and inclusion of coarse particles, which can result in abrasion on hands and forming equipment (Shelton, 1929). Screening or dry ball-milling might eliminate coarse particles, and further research should investigate alternative methods of reducing thixotropy.

It may also be possible to further adjust studio processes to accommodate the limitations of the clay. One possibility explored was slip casting. Unfortunately, earthenware clays are difficult to cast and the flux additions in the experimental clays interfered with the flow properties to the extent that formulation of casting slip was abandoned.

Realistically, the limitation associated with bagging plastic thixotropic clay requires that the bodies developed for the lowest temperatures must be used within hours of blending. The alternative is to laboriously crumble and knead the set clay by hand, or machine process it until it has been sufficiently agitated to become malleable again. As this is impractical for a studio not equipped with appropriate mixing and extruding machinery, and is inconvenient even if the studio is so equipped, it is unlikely that the lowest firing clays could be marketed in plastic form to the average ceramist.

The solution explored was dry batch and wet batch blending. Using this method, large batches of mixed powder were produced for a thixotropic body. Wet batches were mixed with so much water that they did not set too hard when stored, after which they were kneaded on the bench with a quantity of dry batch powder until the right consistency for throwing was obtained. This method was successfully employed to prepare low-firing bodies for throwing and other forming methods. This leaves open the possibility for marketing companion packs of carefully quantified slip and powder.

The workability limitations imposed by thixotropy placed certain restrictions on the manner in which the lowest firing clays could be used, so they were also blended with proprietary clay. This demonstrated that it was possible to arrive at a compromise whereby low porosity below 1100°C was achieved by blends that were capable of remaining malleable when stored.

Another consideration is the cost and environmental impact of the flux materials used to lower the absorption of the clay bodies. Glass cullet is relatively inexpensive and can be obtained as a waste material, but fluxes



such as lithium carbonate and cryolite are more expensive and are industrially produced. While the toxicity of materials was considered and highly toxic materials eliminated, there has been no analysis of the life cycle effects from mining to the point of purchase of these materials. It is beyond the scope of this project to consider the many factors involved, or to calculate the extent to which the effect of these bought materials is offset by the low cost and environmental benefit of using waste materials. However, there was broad consideration of environmental economics, and use of the more expensive processed materials was minimised.

As the project resulted in the recovery and transformation of waste, but in no way beautified or added meaning to the sites from which that waste was recovered, there is arguably little distinction between the approach taken here and the use of found objects, except that more processing is occurring. Nonetheless, the inclusion of cullet and quarry tailings as usable waste instead of materials requiring production reduces impact on the environment, achieving both reclamation and prevention. The process has been re-designed to incorporate waste, and reduce firing cost and emissions. If low-fire vitrified ceramics is adopted solely by the researcher, it will represent an energy-conscious choice within studio practice. If other ceramicists or industries such as brick manufacturers see an economic benefit in compositions that fire at lower temperatures, there will be a corresponding reduction in carbon emissions.

It was noted by Sharma (2011) that calculations of environmental economics will follow invention of a new process or material once others learn of the invention and consider the applications. Future research could include an analysis of the 'green' credentials of any similar compositions developed, and the feasibility of their use and commercial production. Inevitably, commercial considerations influenced by government policies such as Australia's carbon tax will determine the extent to which low-firing clays are developed and used.

I have recently been approached by a private company interested in providing product to NSW brickworks to lower the firing temperature, firing costs and emissions associated with firing. This work will commence following submission of this thesis.

Further avenues of research that could be explored include scaling up the gasification of biomass such as corn cobs and rice husks, using the gas to fire kilns and using the ash for inclusion in ceramic glazes. In the case of rice husk, production of various phases of silica or of sodium silicate may be viable uses of the ash produced.

The accidental discovery of a floating ceramic also has potential that could be explored in future research. Sealing the surface may allow the ceramic to float indefinitely.

One intention of undertaking the technical challenge of developing low-fired vitreous ceramics was to bring about a transformation of studio practice. Conducting this cross-disciplinary research within a contemporary arts research community has led to another transformation. My studio practice was previously aligned with the decorative arts, with an emphasis on formalism, and solely used ceramics. The community of ideas and influences that I have been exposed to has enabled me to develop a much more conceptual approach, and make art works in a wide variety of media. Some of those art works have been documented throughout this thesis.

It has been an extremely enjoyable and engaging process.

## List of Plates

Plate 1. Brett Smout Thin Air Bottling. 2010. South Coast, NSW, Australia.  
(Rigg, W.)

Plate 2. Brett Smout Thin Air Bottling (2). 2010. South Coast, NSW, Australia.

Plate 3. Thin Air 'marketing shots'

Plate 4. Thin Air 'marketing shots' 2

Plate 1. Brett Smout Crack Wrap 2010

Plate 6. Destruction of Tinsley Cooling Towers [Siandara (2008)]

Plate 7. Wallerawang, NSW cooling tower

Plate 8. Pylon at Wallerawang, NSW.

Plate 9. Pylon at Sherbrook, NSW.

Plate 10. Pylon at Auckland, NZ.

Plate 11. Pylon at Sherbrook, NSW.

Plate 12. Shukhov Oka Towers 1988. ( Kazus, I.)

Plate 13. Shukhov Oka Tower 2006 (Tomilov, V.)

Plate 14. Shukhov tower destroyed (Mihadzr, 2005c)

## References

- Abdrakhimov, D. V., Abdrakhimova, E. S. & Abdrakhimov, V. Z. (1999). Sintering quality of clay materials. *Glass and Ceramics*. 56 (5) p.190–193.
- Acchar, W., Vieira, F. A. & Segadães, A. M. (2006). Using ornamental stone cutting rejects as raw materials for red clay ceramic products: properties and microstructure development. *Materials Science and Engineering A* (435–436) p. 606–610.
- Adamis, Z. & Williams, R. B. (2005). *Bentonite, Kaolin, and Selected Clay Minerals*. [Online] Geneva: World Health Organization. Available from: [www.inchem.org/documents/ehc/ehc/v231eh02.gif](http://www.inchem.org/documents/ehc/ehc/v231eh02.gif). [Accessed: 12 August 2008].
- Adesanya, D. & Raheem, A. (2009). Development of corn cob ash blended cement. *Construction and Building Materials*. 23 (1) p. 347–352.
- Adylov G., Kulagina, N. A., Mansurova, E. P., Rumi, M. & Sh. A. Faiziev, S. A. (2005). Lightweight dinas refractories based on rice husk ash. *Refractories and Industrial Ceramics*. 46 (3) p. 187–188.
- Ahmed, Y. M. Z., Ewais, E. M. & Zaki, Z. I. (2008). Production of porous silica by the combustion of rice husk ash for tundish lining. *Journal of University of Science and Technology Beijing, Mineral, Metallurgy, Material*. 15 (3) p. 307–313.
- Aineto, M., Acosta, A. & Iglesias, I. (2006). The role of a coal gasification fly ash as clay additive in building ceramic. *Journal of the European Ceramic Society*. 26 (16) p. 3783–3787.
- Akhavan, A. C. (2005). *The quartz page*. [Online]. [http://www.quartzpage.de/gen\\_mod.html](http://www.quartzpage.de/gen_mod.html) [Accessed 3 March, 2013].
- Alcock (2009) Image of Greenpeace slogans beamed onto Loy Yang Power station in Victoria. [Online] Available from: <http://www.greenpeace.org.au/climate/GI-GlobalLeadership.html> [Accessed 1 April 2010].

- American Ceramic Society (2005). Word of the month: vitrification. *Ceramics Monthly*. 53 (10) p. 28.
- Anastas, P. T. & Warner, J. C. (1998). *Green Chemistry: Theory and Practice*. New York: Oxford University Press.
- Anastas, P. & Zimmerman, J. (2003). Design through the 12 principles of green engineering. *Environmental Science and Technology*. 37 (5) p. 94a–101a.
- Anderson, M. (2002). Encouraging prospects for recycling incinerated sewage sludge ash into clay-based building products. *Journal of Chemical Technology and Biotechnology*. 77 (3) p. 352–360.
- An Inconvenient Truth*. (2006). Film. Directed by D. Guggenheim. [DVD] US: Lawrence Bender Productions, Participant Productions.
- Anonymous (2009). Acid seas no go for Nemo. *New Scientist* 61 (7 February) p. 6.
- ASTM Standard C326–09 (2009). *Standard Test Method for Drying and Firing Shrinkages of Ceramic Whiteware Clays*. [CD] ASTM International, West Conshohocken, PA, 2003.
- ASTM Standard C242 - 12 (2007). *Standard Terminology of Ceramic Whitewares and Related Products* [Online] DOI: 10.1520/C0242-12 ASTM International, West Conshohocken, PA, 2003.
- ASTM standard C 373–88 (2006). *Standard Test Method for Water Absorption, Bulk Density, Apparent Porosity, and Apparent Specific Gravity of Fired Whiteware Products*. [Online] Available from: <http://www.astm.org/Standards/C373.htm> [Accessed 27 May 2009] ASTM International, West Conshohocken, PA, 2003.
- Austen, K. (2011). Beautiful waste. *New Scientist* 2831 (24 September) p. 62.
- Austin, C. R. & Brooks, S. J. (1941). Study of eutectic fluxes in semi-vitreous and vitreous whiteware bodies. *Journal of the American Ceramic Society* 24 (5) p.155–159.

- Australian Government Bureau of Meteorology & Commonwealth Scientific and Industrial Research Organisation. (2012). *State of the Climate, 2012*. [Online] Available from: [www.csiro.au/State-of-the-Climate-2012](http://www.csiro.au/State-of-the-Climate-2012) [Accessed 1 February, 2013]
- Australian Perlite Ltd. (n.d.) *Typical Analysis of Perlite*. [Online] Available from: <http://www.australianperlite.com/perlite.htm> [Accessed: 10 May 2009].
- Australian Vermiculite and Perlite Ltd. (2004). *Perlite Material Safety Data Sheet*. [Online] Available from: <http://www.australianperlite.com/materialsafety/perlite/> [Accessed: 10 May 2009].
- Avalova, E. V. (1979). Methods of extending the narrow vitrification range of clays. *Glass and Ceramics* 36 (8) p. 450–452.
- Bailey S. W. (1980). Structures of layer silicates. In: Brindley, G. W. & Brown, G. (eds) *Crystal Structures of Clay Minerals and their X-ray Identification*. London: Mineralogical Society. (Monograph No. 5). Cited by Adamis, Z. & Williams, R. B. (2005). *Bentonite, Kaolin, and Selected Clay Minerals*. [Online] Geneva: World Health Organization. Available from: [www.inchem.org/documents/ehc/ehc/v231eh02.gif](http://www.inchem.org/documents/ehc/ehc/v231eh02.gif). [Accessed: 12 August 2008].
- Baklouti, S., Chartier T. & Baumard, J. (1997). Mechanical properties of dry-pressed ceramic green products: the effect of the binder. *Journal of the American Ceramic Society*. 80 (8) p. 1992–1997.
- Balkyavichus, V., Valyukyavichus, C., Shpokauskas, A., Laukaitis, A. & Pyatrikaitis, F. (2003). Sinterability of low-melting illite-bearing clays. *Glass and Ceramics*. 60 (5) p.179–182.
- Bamford, R. (2010). Clean, green, lumpy & brown: challenges, opportunities & persistent values in ceramics. *Celsius*.1 1 p.165–171. [Online] Available from: [www.usyd.edu.au/sca/research/projects/celsiusjournal](http://www.usyd.edu.au/sca/research/projects/celsiusjournal) [Accessed: 1 September 2012].

- Barabanov, A. I., Tagil'tseva, N. O., Elyukova, N. V., Khalilev, V. D. & Zaitsev, G. P. (2005). Low-melting crystallizable borophosphate glass binders. *Glass and Ceramics*. 62 (11–12) p. 341–343.
- Barbieri, L., Bonamartini, A. & Lancellotti, I. (2000). Alkaline and alkaline-earth silicate glasses and glass-ceramics from municipal and industrial wastes. *Journal of the European Ceramic Society*. 20 (14–15) p. 2477–2483.
- Barbieri, L., Ferrari, A.M., Lancellotti, I., Leonelli, C., Rincòn, J., & Romero, M. (2000). Crystallization of (Na<sub>2</sub>O;MgO);CaO;Al<sub>2</sub>O<sub>3</sub>;SiO<sub>2</sub> Glassy Systems Formulated from Waste Products. *Journal of the American Ceramic Society* 83(10): 2515-2520.
- Barroso, J., Barreras, F., Amaveda, H. & Lozano, A. (2003). On the optimization of boiler efficiency using bagasse as fuel. *Fuel*. 82(12) p. 1451–1463.
- Barry, P. (2006). Zooplankton survey plumbs the depths. *New Scientist Life*. [Online]. Available from: <http://www.newscientist.com/article/dn9108-zooplankton-survey-plumbs-the-depths.html> [Accessed: 30 November 2009].
- Barsoum, M. W. (1997). *Fundamentals of Ceramics*. New York: McGraw Hill.
- Barthelmy, D. (2010a). Muscovite Mineral Data. *Mineral News* [Online] Available from: <http://www.webmineral.com/data/Muscovite.shtml> [Accessed 27 February 2013].
- Barthelmy, D. (2010b). Excalibur Mineral Corp. Albite Mineral Data. *Mineral News* [Online] Available from: <http://webmineral.com/data/Albite.shtml> [Accessed 27 February 2013].
- Basegio, T., Berutti, F., Bernardes, A. & Bergmann, C. P. (2002). Environmental and technical aspects of the utilisation of tannery sludge as a raw material for clay products. *Journal of the European Ceramic Society*. 22 (13) p. 2251–2259.

- Bath Potters Supplies (2003). *Percentage weight analysis. Bentonite*. Unpublished.
- Beardsley, J. (1998). *Earthworks and Beyond: Contemporary Art in the Landscape*. New York: Abbeville Press.
- Beaumont, L. (2006). *Hot with a chance of a late storm*. [Photograph] The Glue Society, Bondi. [Online] Available from: <http://www.sculpturebythesea.com> [Accessed: 16 June 2008].
- Beechey, D. (2012). *The Seashells of New South Wales*. Release 16, 1 January, 2012. [Online] Available from: <http://seashellsofnsw.org.au/index.htm> [Accessed: 3 March 2012].
- Belonio, A. (2005). *Rice Husk Stove Improved*. [Online] Available from: <http://www.pcarrrd.dost.gov.ph/consortia/wesvarrdec/postharvest.htm> [Accessed: 30 September 2009].
- Bemis, R. A., Shiloh, K. & Ellingson, W. A. (1996). Nondestructive evaluation of thermally shocked silicon carbide by impact-acoustic resonance. *Journal of Engineering for Gas Turbines and Power*. 118 (3) p. 491–494 doi:10.1115/1.2816673
- Bennett, A. L & Goodrich H. R. (1930). The reactivity test for determining the value of barium carbonate as a scum preventative. *Journal of the American Ceramic Society*. 13 (7) p. 461–469.
- Bennett, J. (2008). *Paper clay information, how to make it and how to use it*. [Online] Available from: <http://www.jerrybennett.net/paperclay.html> [Accessed: 12 September 2008].
- Bernard, J., Benčan, A., Rojac, T., Holc, J., Malič, B. & Kosec, M. (2008). Low-temperature sintering of K<sub>0.5</sub>Na<sub>0.5</sub>NbO<sub>3</sub> ceramics. *Journal of the American Ceramic Society*. 91 (7) p. 2409–2411.
- Bijvoet, M. (1997). *Art as Inquiry: Toward New Collaborations between Art, Science, and Technology*. New York: Peter Lang.
- Binrock, M. (2006). *Fragile Ecologies* by Elizabeth Stanek, Andrea Thompson, and Valerie Ortani. (Simmons, M). [Photo Gallery] Available from: [mike.binrock.net/tags/sculpture](http://mike.binrock.net/tags/sculpture) [Accessed: 1 February 2009].



- Bondioli, F., Andreola, F., Barbieri, L., Manfredini, T. & Ferrari, A. M. (2007). Effect of rice husk ash (RHA) in the synthesis of (pr,zr)SiO<sub>4</sub> ceramic pigment. *Journal of the European Ceramic Society*. 27 (12) p. 3483–3488.
- Booth D. (2011). Fish behaving badly. *UTSpeaks Public Forum*. 28 September 2011. University of Technology, Sydney.
- Bottlecyclor Glass Management Ltd. (2007). *Recycling of glass bottles with bottlecyclor*. [Online]. Available from: [http://www.bottlecyclor.com/Content\\_Common/pg-Environment.seo](http://www.bottlecyclor.com/Content_Common/pg-Environment.seo) [Accessed: 8 April 2010].
- Boyle, B. (2010). *Australian Coal Export Forecast to 2015- Responding to strong demand from China and India*. AustCoal Consulting Alliance Client Briefing
- Brahic, C. & Le Page, M. (2007). Climate myths: ice cores show CO<sub>2</sub> increases lag behind temperature rises, disproving the link to global warming. *New Scientist*. [Online]. Available from: <http://www.newscientist.com/article/dn11659-climate-myths-ice-cores-show-co2-increases-lag-behind-temperature-rises-disproving-the-link-to-global-warming.html?full=true> [Accessed: 10 November 2009].
- Brandt, C. G. & Kinneging, A. J. (2005). *X-Ray Powder Diffraction. A Practical Guide to Quantitative Phase Analysis*. Almelo: PANalytical B.V.
- Briggs, A. (2008). Commenting on *Flickr* [Online] Available from: <http://www.flickr.com/photos/wsogmm/2791798478/in/photostream/> [Accessed: 12 December 2008].
- Bronzeoak Ltd (2003). *Rice husk ash market study*. Report carried out under contract as part of the DTI New and Renewable Energy Programme. UK. [Online] Available from: <http://webarchive.nationalarchives.gov.uk/+http://www.berr.gov.uk/files/file15138.pdf> [Accessed 13 August 2011].
- Brown, P. (2008). Granites of Australia Ltd. Personal Communication. 22 October 2008.

- Brownell, W. E. (1949). Fundamental factors influencing efflorescence of clay products. *Journal of the American Ceramic Society*. 32 (5) p. 375–389.
- California State University WorldArt Kiosk (n.d.) Kessel, K. (n.d.) Heizer, M. *Double Negative*. View from end of one slot to other. 1969–1970 California State University WorldArt Kiosk. [Online] Available from: <http://worldart.sjsu.edu/VieO640?sid=2599&x=621874> [Accessed: 10 May 2009].
- Canadian Centre for Occupational Health and Safety (n.d.). *What is LD50 and LC50?* [Online] Available from: [www.ccohs.ca/oshanswers/chemicals/LD50](http://www.ccohs.ca/oshanswers/chemicals/LD50) [Accessed: 14 February 2010].
- Cardew, M. (1977). *Pioneer Pottery*. London: Longman.
- Catarino, L., Sousa, J., Martins, I. M., Vieira, M. T. & Oliveira, M. M. (2003). Ceramic products obtained from rock wastes. *Journal of Materials Processing Technology*. (143–144) Proceedings of the International Conference on the Advanced Materials Processing Technology, 2001. p. 843–845.
- Ceramics Today (nd). Egyptian Paste. [Online] <http://www.ceramicstoday.com/articles/092501.htm> [Accessed 2 September, 2012].
- Chai, Y., Chang, Y., Hsiao, Y. & Lian, Y. (2008). Effects of borosilicate glass addition on the structure and dielectric properties of ZnTiO<sub>3</sub> ceramics. *Materials Research Bulletin*. 43 (2) p. 257–263.
- Chandrasekhar, S., Satyanarayana, K., Pramada, P., Raghavan, P. & Gupta, T. (2003). Review: processing, properties and applications of reactive silica from rice husk—an overview. *Journal of Materials Science*. 38 (15) p. 3159–3168.
- Chang, Y., Lin, C. & Chen, H. (2001). Rice hull ash structure and bleaching performance produced by ashing at various times and temperatures. *Journal of the American Oil Chemists Society*. 78 (6) p. 657–660.

- Chin, M. (2001). Interview. *Art 21* [Online] Available from:  
<http://www.pbs.org/art21/artists/chin/clip2.html> [Accessed: 2 October 2011].
- Chin, M. (n.d.). *Revival Field*. [Online]. Available from:  
<http://melchin.org/oeuvre/revival-field> [Accessed: 2 October, 2011].
- Christiansen, R. (2008). Soil tilth lab studies corn stover harvesting. *Biomass Magazine* (November) [Online] Available from:  
[http://www.biomassmagazine.com/article.jsp?article\\_id=2178&q=potassium](http://www.biomassmagazine.com/article.jsp?article_id=2178&q=potassium) [Accessed: 5 March 2009].
- Churchman, G. J., Askary, M., Peter, P., Wright, M., Raven, M. D. & Self, P. G. (2002). Geotechnical properties indicating environmental uses for an unusual Australian bentonite. *Applied Clay Science*. 20 (4–5) p.199–209.
- Colson, F. A. (1975). *Kiln Building with Space-age Materials*. Melbourne: Van Nostrand Reinhold.
- Commonwealth of Australia Department of Climate Change and Energy Efficiency (2007). *The National Greenhouse and Energy Reporting Act 2007 (the NGER Act)*. Available from:  
<http://www.climatechange.gov.au/reporting> [Accessed: 30 September 2011].
- Commonwealth of Australia Department of Climate Change and Energy Efficiency (2009). Energy Rating label [Image] Available from:  
<http://www.energyrating.gov.au> [Accessed: 30 September 2009].
- Commonwealth of Australia Department of Health and Aging, Therapeutic Goods Administration (2012). *Poisons Standard 2012. Standard for the Uniform Scheduling of Medicines and Poisons No. 3 (SUSMP 3)* ISBN: 978-1-74241-735-6. [Online] Available from:  
<http://.comlaw.gov.au/Details/F2012L01200>. [Accessed: 29 July 2012].

- Commonwealth of Australia Department of Resources, Energy and Tourism (2012) *Australia's Coal Industry: Australian coal production and exports* [Online] Available from: [http://www.ret.gov.au/resources/mining/australian\\_mineral\\_commodities/coal/Pages/australia\\_coal\\_industry.aspx](http://www.ret.gov.au/resources/mining/australian_mineral_commodities/coal/Pages/australia_coal_industry.aspx) [Accessed 14 April, 2012].
- Commonwealth Scientific and Industrial Research Organisation (2008). *Cape Grim Baseline Air Pollution Station* [online]. Available from: <http://www.csiro.au/places/pps64.html> [Accessed: 30 September 2009].
- Connor, J. & Stefanova, K. (2012). *Climate of the Nation 2012. Australian Attitudes on Climate Change*. The Climate Institute. Sydney. [Online] Available from: [www.climateinstitute.org.au](http://www.climateinstitute.org.au) [Accessed 3 September 2012].
- Conrad, J. W. (1981). *Contemporary Ceramic Formulas*. New York: Macmillan.
- Cooper English, E. (2000). "Arkhitektura i mnimosti": The origins of Soviet avant-garde rationalist architecture in the Russian mystical-philosophical and mathematical intellectual tradition". [Online] <http://repository.upenn.edu/dissertations/AAI9989589> [Accessed 25 November, 2012].
- Cote, R. P. & Smolenaars, T. (1997). Supporting pillars for industrial ecosystems. *Journal of Cleaner Production*. 5 (1–2) p. 67–74.
- Cote, R. P. (2003). *A Primer on Industrial Ecosystems: a Strategy for Sustainable Industrial Development*. Halifax: Eco-Efficiency Centre, School for Resources and Environmental Studies, Dalhousie University.
- Courtney, P. (2008). *Renewable Energy Revolution for NSW Cane Growers*. [Online] Saturday 9 February. Available from: <http://www.abc.net.au/am/content/2008/s2158472.Htm> [Accessed: 8 April 2008].
- Cowan, R. (1989). *Technical Notes for the Craft Potter*. 8th Ed. Waitara, New South Wales: Russell Cowan Pty Ltd.

- Crispin, G. (2008). *Obtaining Illitic Clay*. [Online] Wed Aug 27 21:21:24 EST 2008 Australian Ceramics Discussion List. .Available from: [australianceramicsdiscussionlist@australianceramics.com](mailto:australianceramicsdiscussionlist@australianceramics.com) [Accessed: 1 September 2008].
- Crispin, G. (2012a). Personal communication. 14 March, 2012.
- Crispin, G. (2012b). *Report on Clay Body*. Unpublished.
- Crosby, A. (curator) (2007). Yanti, Hardono, Kehidupan & Padi. (artists). *Sisa: re-use, collaborations and cultural activism from Indonesia. published on the occasion of the exhibition at the UTS Gallery, 6 November –7 December 2007*. Presented as part of, and with support from, GANG Festival 07-08. University of Technology, Sydney.
- Cubby, B. (2009). Climate emails: a dirty war swirls around 'swindle'. *Sydney Morning Herald* [Online] Available from: <http://www.smh.com.au/opinion/society-and-culture/climate-emails-a-dirty-war-swirls-around-swindle-20091209-kk69.html> [Accessed 13 September 2010].
- Cui, X. & Zhou, J. (2008). A simple and an effective method for the fabrication of densified glass-ceramics of low temperature co-fired ceramics. *Materials Research Bulletin*. 43 (6) p.1590–1597.
- Currie, I. (2000). *Revealing Glazes Using The Grid Method*. Maryvale, Qld: Bootstrap Press.
- Dahlsen, J. (2001–2010). *John Dahlsen. Environmental Artist and Contemporary Painter*. [Online] Available from: <http://www.johndahlsen.com/index.html> [Accessed: 2 October 2011].
- Dahlsen, J. (n.d.). Interview. Sunflowers Art Association. [Online] Available from: <http://www.sunflowers-art.com/wp-content/uploads/A-short-interview-with-John-Dahlsen.pdf> [Accessed: 2 October 2011].
- Dan, T., Chand, C. & Rohatgi, P. (1987). Effect of glass, rice-husk ash and wollastonite on transverse strength of porcelain. *Journal of Materials Science Letters*. 6 (3) p. 277–280.

- Dananaj, I., Frankovská, J. & Janotka, I. (2005). The influence of smectite content on microstructure and geotechnical properties of calcium and sodium bentonites. *Applied Clay Science*. 28 (1–4), p. 223–232.
- Das, T. (2005a) Sustainability and Sustainable Development. In: Das, T. (ed.) *Toward Zero Discharge: Innovative Methodology and Technologies for Process Pollution Prevention*. New Jersey: John Wiley & Sons.
- Das, T. (2005b). Fundamentals of Life Cycle Assessment. In: Das, T. (ed.) *Toward Zero Discharge: Innovative Methodology and Technologies for Process Pollution Prevention*. New Jersey: John Wiley & Sons.
- Dellow, J. (2009). *Carbon emissions and wood firing?* [Online] 23 May 2009. Australian Ceramics Discussion List. Available from: [australianceramicsdiscussionlist@australianceramics.com](mailto:australianceramicsdiscussionlist@australianceramics.com) [Accessed: 23 May 2009].
- Dembosky, A. (2008). Art the garbage man can appreciate. *New York Times*. 8 September. p. B2 [Online] Available from: <http://www.nytimes.com/2008/09/08/nyregion/08trash.html> [Accessed: 30 September 2009].
- Denes, A. (2011). Comments on City of Kent, Washington [Online] Available from: <http://146.129.252.5/content.aspx?id=7470> [Accessed: 2 October 2011].
- Denning, (2007). China's Appetite for Australian Coal Up 51% in 2006. *Daily Reckoning* [Online] Available from: <http://www.dailyreckoning.com.au/china-aussie-coal/2007/01/16/> [Accessed 26 October, 2011].
- Dhir, R., Limbachiya, M. & Dyer, T. (eds) (2001). *Recycling and reuse of glass cullet: Proceedings of the International Symposium Organised by the Concrete Technology Unit and Held at the University of Dundee, Scotland, UK on 19–20 March 2001*. London: Thomas Telford.

- Digitalfire (2008). *Hazards Database*. [Online] Available from:  
<http://69.64.69.57/4sight/hazards/> [Accessed: 3 February 2010].
- Dimitru, I. (2009) Personal communication. Boral, NSW, 11 October, 2008.
- Doering, O. C., O'Hare, T. J. & Peart, R. M. (1979). Small scale gasification of biomass: the case of corn cob gasifiers. *Energy*. 4 (2) p. 235–248.
- Dondi, M., Guarini, G., Raimondo, M. & Venturi, I. (2002). Orimulsion fly ash in clay bricks—part 2: technological behaviour of clay/ash mixtures. *Journal of the European Ceramic Society*. 22 (11) p. 1737.
- Douda, H. (1920). The effect of wet grinding, screening, and electrolytes and dextrine on clays of low plasticity and strength. *Journal of the American Ceramic Society*. 3 (11) p. 885–892.
- Dumitru, I. (2008). Personal Communication. 30 October, Boral Sydney, Australia.
- Dyer, T. & Dhir, R. (2001). Use of glass cullet as a cement component in concrete. In: Khir, R., Limbachiya, M. & Dyer, D. (eds) *Recycling and reuse of glass cullet: Proceedings of the International Symposium Organised by the Concrete Technology Unit and Held at the University of Dundee, Scotland, UK on 19–20 March 2001*. London: Thomas Telford.
- Encyclopaedia Britannica (n.d.) *Mohs Hardness* [Online] Available from:  
<http://www.britannica.com/EBchecked/topic/387714/Mohs-hardness> [Accessed: 24 February 2013].
- Encyclopaedia Britannica (2013) Archimedes' principle. *Encyclopædia Britannica Online*. Available from:  
<http://www.britannica.com/EBchecked/topic/32827/Archimedes-principle> [Accessed 27 February 2013].
- Erauw J. P., Vander Gucht, A. & Cambier, F. (2004). Assessment of impact acoustic resonance as a non-destructive testing method for advanced ceramic parts. *Key Engineering Materials*. 264–268, p. 921–924.

- Ewing, L. (2000). *Matrix glaze calculation software*. Otago: Otago Polytechnic.
- Farrell, B. (2008). Personal communication on the occasion of site visit. Broadwater Sugar Mill, Ballina NSW. 12 December 2008.
- Farrow, C. (1987). Paper/clay, *Artists Newsletter*. UK (April) p. 20–21.
- Ferrari, S. & Gualtieri, A. F. (2006). The use of illitic clays in the production of stoneware tile ceramics. *Applied Clay Science*. 32 (1) p. 73–81.
- Finkelburg, D. (2009). How glazes melt: in search of the elusive eutectic. *Ceramics Arts Daily* 9 December 2009. [Online]. Available from: <http://ceramicartsdaily.org/ceramic-glaze-recipes/glaze-chemistry-ceramic-glaze-recipes-2/how-glazes-melt-in-search-of-the-elusive-eutectic/> [Accessed: 31 January, 2010].
- Foletto E., Gratieri E., de Oliveira L. & Jahn, S. (2006). Conversion of rice hull ash into soluble sodium silicate. *Materials Research*. 9 (3) p. 335–338.
- Ford, W. (1967). *The Effect of Heat on Ceramics*. London: Maclaren
- Fowler, N. (2011). Interviewing Nichols, M. Alternatives to clay bricks and cement. *Science Show*. 2 April. ABC Radio National. [Podcast]. Available from: <http://www.abc.net.au/rn/scienceshow/stories/2011/3180096.htm#transcript> [Accessed: 4 April 2011].
- Fraser, H. (1986). *Ceramic Faults and their Remedies*. London: A & C Black.
- Fresh, T., Garner, C., Connors, C. & Keyes, P. (1978). Firing with sunlight. In: Williams, G., Sabin, P. & Bodine, S. (eds). *Studio Potter Book*. Melbourne: Van Nostrand Reinhold.
- Fromme, R. (1994). *Notes on Lead, Sodium, Potassium & Lithium: The Low Melting Fluxes or Bases (RO, R2O)*. [Online] Available from: [http://ceramics.sdsu.edu/articles/glaze\\_tech/basic\\_flux\\_oxides.htm#anchor1094191](http://ceramics.sdsu.edu/articles/glaze_tech/basic_flux_oxides.htm#anchor1094191) [Accessed 24 May 2010].
- Fuzi, L. (2006). Paper, clay, paperclay. *Ceramics Technical*. (23) p. 29–31.



- Ganesan, K., Rajagopal, K. & Thangavel, K. (2007). Evaluation of bagasse ash as supplementary cementitious material. *Cement and Concrete Composites*. 29 (6) p. 515–524.
- Gardam, M. (2008). Personal communication. Arumpo Pty Ltd. 30 October 2008.
- Garforth, A. (2009). *Moss Graffiti*. [Online] Available from: Environmental Graffiti.com <http://www.environmentalgraffiti.com/featured/moss-grass-graffiti/2147>. [Accessed: 20 May 2010].
- Gault, R. (1998) *Paperclay*. London: A & C Black.
- Gibson (2011) Image: *Make a wish* Elpida Hadzi-Vasileva: 2011, London. *New Scientist* 2831, 24 September 2011, p. 62.
- Gill, S. (2011). *Art and Ecology - Joseph Beuys*. [Online]. 22 September 2011. Available from: Lights going on.com <http://www.lightsgoingon.com/2011/09/art-and-ecology-joseph-beuys/> [Accessed: 1 November 2011].
- Glick, J. (1978). Some proposals concerning the use of waste heat. In: Williams, G., Sabin, P. & Bodine, S. (eds). *Studio Potter Book*. Melbourne: Van Nostrand Reinhold.
- Goldate, S. (2008). Paperslip. *Ceramics Today* [Online]. Available from: [http://www.ceramicstoday.com/articles/paper\\_slip.htm](http://www.ceramicstoday.com/articles/paper_slip.htm) [Accessed: 25 October 2008].
- Goldsworthy, A. (2007). *White Walls* Galerie Lelong. *This week in New York* [Online] Available from: [twi-ny.com/twiny.06.06.07.html](http://twi-ny.com/twiny.06.06.07.html) [Accessed: 2 November 2009].
- Gompertz, W. (2012). *What are you looking at? 150 years of modern art in the blink of an eye*. Penguin, England.
- Gonzalez-Murillo, (2007). *Physical properties of unfired, extruded clays reinforced with low cost additives*. Bath: University of Bath.

- Graddy, S.E. (2005). *Creative and Green: Art, Ecology, and Community*. A Thesis Submitted in partial fulfilment of the Requirements of the University of Southern California for the Degree of Master of Public Art Studies. University of Southern California. [Online]. Available from: [http://greenmuseum.org/generic\\_content.php?ct\\_id=238](http://greenmuseum.org/generic_content.php?ct_id=238) [Accessed: 2 November 2009].
- Green, D. J., Guillon, O. & Rodel, J. (2008). Constrained sintering: a delicate balance of scales. *Journal of the European Ceramic Society*. 28 (7) p.1451–1466.
- Greenpeace (2009). *Where is Australia's Global Leadership?* [Online] Available from: <http://www.greenpeace.org.au/climate/GI-GlobalLeadership.html> [Accessed: 2 March 2010].
- Grimshaw, R. A. (1971). *The Chemistry and Physics of Clays and other Allied Ceramic Materials*. 4th Ed. London: Ernest Benn.
- Guan, E., Chen, W. & Luo, L. (2007). Low firing and microwave dielectric properties of BaTi4O9 with B2O3–ZnO–La2O3 glass addition. *Ceramics International*. 33 (6) p.1145–1148.
- Gunn, B. (1998). *Rhyolites, trachytes and phonolites*. [Online] Available from: <http://www.geokem.com/rhyolites-trachytes.html> [Accessed, 17 October, 2011].
- Guy, J. (2009). Bad manners and family dinners: a key to the future. *Celsius*. (1). p. 209–216. [Online]. Available from: [www.usyd.edu.au/sca/research/projects/celsiusjournal](http://www.usyd.edu.au/sca/research/projects/celsiusjournal) [Accessed: 1 September 2012].
- Haldy, N. L., Wright, J. H. & Todd, F. C. (1947). Translucency meter for use in whiteware research. *Journal of the American Ceramic Society*. 30 (5) p.153–159.
- Hamer, F. (1975). *The Potter's Dictionary of Materials and Techniques*. Cambridge, UK: Cambridge University Press.
- Hansen, T (2003). Test Dry strength round bars. Digitalfire database. [Online] Available from: [http://digitalfire.com/4sight/tests/ceramic\\_test\\_dry\\_strength\\_round\\_bars.html?logout=yes](http://digitalfire.com/4sight/tests/ceramic_test_dry_strength_round_bars.html?logout=yes) [Accessed, 11 October, 2011].

- Hansen, T. (2006a). Soluble Salts - SOLU. *Digitalfire Test Procedure Database* [Online] Available at:  
[http://digitalfire.com/4sight/tests/ceramic\\_test\\_soluble\\_salts.html](http://digitalfire.com/4sight/tests/ceramic_test_soluble_salts.html)  
 [Accessed: 2 October 2009].
- Hansen, T. (2006b). Test for cold over boiled porosity. *Digitalfire Test Procedure Database* [Online] Available at:  
[http://digitalfire.com/4sight/tests/ceramic\\_test\\_cold\\_over\\_boiled\\_porosity.html](http://digitalfire.com/4sight/tests/ceramic_test_cold_over_boiled_porosity.html) [Accessed: 2 October 2009].
- Hansen, T. (2006c). Troubleshooting ceramic process problems and links. *Digitalfire Ceramic Troubleshooting Database*. [Online] Available at: <http://digitalfire.com/4sight/troubleshooting/index.html>  
 [Accessed: 10 October, 2011].
- Hansen, T. (2008). Low fire white talc casting body recipe. *Digitalfire*. [Online] Available at: <http://digitalfire.com> [Accessed: 24 January 2010].
- Harrison M. (2008). *From waste to want? Sustainable design: recycled materials, macadamia shell*. [Online] Available from:  
[http://www.powerhousemuseum.com/smartworks/symposium\\_speakers.asp](http://www.powerhousemuseum.com/smartworks/symposium_speakers.asp) [Accessed: 2 February 2011].
- Harrison. S. (1989) *Ecological Consequences*. [Online] Available from:  
<http://www.hotnsticky.com.au/articles/ecologicalconsequences.pdf>  
 [Accessed 19 April, 2011].
- Harrison, S. (1992) *Full Circle*. [Online] Available from:  
<http://www.hotnsticky.com.au/articles/Fullcircle.pdf> [Accessed 19 April, 2011].
- Harrison, S. (2007). From the ground up: new work from an old landscape. *Ceramics Art and Perception*. (24) p.45-52. [Online] Available from: <http://www.ceramicart.com.au/articles/CT24.htm> [Accessed: 3 April 2008].
- Harrison, S. (2009). *Cool solutions for a warming planet. Some thoughts on sustainability*. [Online] Available from:  
[www.hotnsticky.com.au/articles/sustainability.pdf](http://www.hotnsticky.com.au/articles/sustainability.pdf) [Accessed: 28 May 2009].

- Hay, G. (1996). More on paperclay. *Ceramics Technical*. (3) p. 22–28.
- Hee, D. (2003) Image: *Ken Yonetani installing tiles* [Online] Available from: <http://www.kenyonetani.com/Kenworksfumie-tiles.html> [Accessed 29 April, 2011].
- Hee, D. (2003) Image: *Yonetani's tiles at CSIRO Discovery, Canberra, 2003*. [Online] Available from: <http://www.kenyonetani.com/Kenworksfumie-tiles.html> [Accessed 29 April, 2011].
- Hee, D. (2003) Image: *Yonetani's tiles at CSIRO Discovery, Canberra, Australia. 2003* [Online] Available from: <http://www.kenyonetani.com/Kenworksfumie-tiles.html> [Accessed 29 April, 2011].
- Heine, V. (1972). *Ceramic Training Notes*. Crown Lynn Potteries. Auckland, New Zealand. Unpublished
- Henderson, C. (2006). Ocean acidification: the other CO<sub>2</sub> problem. *New Scientist*. 2563 (5 August) p. 28–33.
- Henderson, M. & Cohen, K. (1964). Image: *Oil*. Mel Henderson: 1964 San Francisco Bay. California. U.S.A. [Online] Available from: <http://worldart.sjsu.edu/VieO53299?sid=2624&x=626473> [Accessed 24 November, 2009].
- Henstock, M. E. (1976). New products from waste. *Conservation and Recycling* 1 (1) p. 161–166.
- Hill, E. C. (1922). The effect of some fluxes on the absorption and transverse strength of a terra cotta body. *Journal of the American Ceramic Society*. 5 (11) p. 832–837.
- Hocking, M. (1994). Reusable and disposable cups: an energy-based evaluation. *Environmental Management*. 18 (6) p. 889–899.
- Holmes, G. G. (1983). *Bentonite and Fullers Earth in New South Wales*. Sydney: New South Wales Department of Mineral Resources.

- Hopcroft, R. (2006). Image of *Clio pyramidata* in Barry, P. Zooplankton survey plumbs the depths. *New Scientist Life*. (4 May) [Online] Available from: <http://www.newscientist.com/article/dn9108-zooplankton-survey-plumbs-the-depths.html> [Accessed: 30 April 2009].
- Horne, G. (2008). Personal Communication. 19 December 2008. Visy Glass Recycling Plant, Banksmeadow, Australia.
- Howard, D. (2009). *Carbon emissions and wood firing?* [Online] 20 May 2009. Australian Ceramics Discussion List. Available from: [australianceramicsdiscussionlist@australianceramics.com](mailto:australianceramicsdiscussionlist@australianceramics.com) [Accessed: 23 May 2009].
- Incon. (1996). Perlite.net [Online] Available from: <http://www.perlite.net/> [Accessed: 10 May 2009].
- Irvine, J. (2008). RBA Chief warns: get used to being greener, poorer. *Sydney Morning Herald*. (5 April) p. 1.
- Jackson, F G. (1925). A descriptive bibliography of scumming and efflorescence. *Journal of the American Ceramic Society*, 8 (8): p. 376–401.
- Jaouen, L. (nd). Open Porosity. *Acoustical Porous Material Recipes* [Online] <http://apmr.matelys.com/Parameters/OpenPorosity.html> [Accessed 5 March, 2013].
- Jeoung-Ah, K. (2006). The characterisation of paper-composite porcelain in a green state. *Journal of the European Ceramic Society*. 26 (6) 1023–1034.
- Johnston, C. (2009). *Carbon emissions and wood firing?* [Online] 25 May 2009. Australian Ceramics Discussion List. Available from: [australianceramicsdiscussionlist@australianceramics.com](mailto:australianceramicsdiscussionlist@australianceramics.com) [Accessed: 25 May 2009].
- Jones, B. (2011). *Climate change debate? Pity about the science*. Ockham's Razor. ABC Radio National. 2 October 2011.
- Jones, D. (2006). Dust to mud–mud to dust. David Jones reports on the installation 'Fragile Ecologies' *Ceramics Technical*. (23) p. 11–14.

- J.T. Baker Chemical Co. (1983) *Analytical Chemistry* 55 (2), p. 333A.
- Kastner, J. (1998). *Land and Environmental Art*. London: Phaidon.
- Kazus, I. (1988). *Shukhov Tower* [Photograph] [Online] Available from: [http://en.wikipedia.org/wiki/File:Shukhov\\_Oka\\_Towers\\_1988\\_photo\\_by\\_Igor\\_Kazus.jpg](http://en.wikipedia.org/wiki/File:Shukhov_Oka_Towers_1988_photo_by_Igor_Kazus.jpg) [Accessed: 2 April 2010].
- Kim, M., Lim, J., Nahm, S., Paik, J. & Lee, H. (2007). Low temperature sintering of BaCu(B<sub>2</sub>O<sub>5</sub>)-added BaO–Re<sub>2</sub>O<sub>3</sub>–TiO<sub>2</sub> (Re = Sm, nd) ceramics. *Journal of the European Ceramic Society*. 27 (8–9) p. 3033–3037.
- Kingery, W. D., Bowen, H. K. & Uhlmann, D. R. (1976). *Introduction to Ceramics*. 2nd Ed. New York: John Wiley and Sons.
- Kirk, C. (2001). A glass artist's profile using recycled glass techniques—Pate de Verre. In: Dhir, R., Limbachiya, M. & Dyer, T. (eds) *Recycling and reuse of glass cullet: Proceedings of the International Symposium Organised by the Concrete Technology Unit and Held at the University of Dundee, Scotland, UK on 19–20 March 2001*. London: Thomas Telford.
- Kleypas, J. A., Feely, R. A., Fabry, V. J., Langdon, C., Sabine, C. L. & Robbins, L. L. (2006). *Impacts of Ocean Acidification on Coral Reefs and Other Marine Calcifiers: A Guide for Future Research*. Report from a workshop sponsored by the National Science Foundation, the National Oceanic and Atmospheric Administration, and the U.S. Geological Survey 18–20 April 2005, St. Petersburg, FL.
- Kobayashi, Y. & Kato, E. (1994). Low-temperature fabrication of anorthite ceramics. *Journal of the American Ceramic Society*. 77 (3) p. 833–834.
- Koenig, C. (1942). Low-temperature vitreous bodies. *Journal of the American Ceramic Society*. 25 (9) p. 230–236.
- Konta, J. (1995). Clay and man: clay raw materials in the service of man. *Applied Clay Science*. 10 (4) p. 275–335.
- Koval'chenko, N. A. & Pavlenko, Z. V. (2006). Waste-bearing decorative glazes for facade ceramics. *Glass and Ceramics*. 63 (1) p. 26–28.

- Kraner, H. M. & McDowell, S. J. (1925). Talc as the principal body ingredient in vitrified ceramic bodies. *Journal of the American Ceramic Society*. 8 (10) p. 626–635.
- Kawamura Chemical Company Ltd. (n.d.) Chemical formula and melting point of Seger cone. [Online] Available at: <http://kawamura-chemical.co.jp/jpn/21kagakushiki.htm> [Accessed: 20 September 2009].
- Kurama, S. & Kurama, H. (2008). The reaction kinetics of rice husk based cordierite ceramics. *Ceramics International*. 34 (2) p. 269–272.
- Krupa, A. A., Gorodov, V. S., Zyatkevich, D. P., Ovcharenko, I. V. & Tkach, V. V. (1997). Stepping up the sintering rate of china through the use of firing wastes treated by a plasma-chemical method. *Glass and Ceramics*. 54(1) p.63-65.
- Lancellotti, I., Barbieri, L., Corradi, A., Brusatin, G., Scarinci, G. & Colombo, P. (2001). Glass cullet: scrap or new raw material? In: Khir, R., Limbachiya, M. & Dyer, D. (eds) In: *Recycling and reuse of glass cullet: Proceedings of the International Symposium Organised by the Concrete Technology Unit and Held at the University of Dundee, Scotland, UK on 19–20 March 2001*. London: Thomas Telford.
- Lange, F. F. & Kellett, B. J. (1989). Thermodynamics of densification: II, grain growth in porous compacts and relation to densification. *Journal of the American Ceramic Society*. 72 (5) p. 735–741.
- Leach, B. (1976). *A Potter's Book*. 3rd Ed. London: Faber & Faber.
- Levitskii, I. A. & Papko, L. F (1994). Colored glazes based on tannery ash. *Glass and Ceramics*. 51 (5) p. 4–7.
- Ligthart, T. & Ansems, A. (2007). Single use or reusable (coffee) rinking systems: an environmental comparison. Appeldoorn: TNO Built Environment and Geosciences Publications.
- Lim, J., Jeong, Y. H., Nguyen, N., Nahm, S., Paik, J., Kim, J. & Hwack-Joo, L. (2007). Low temperature sintering of the Ba<sub>2</sub>Ti<sub>9</sub>O<sub>20</sub> ceramics using B<sub>2</sub>O<sub>3</sub>/CuO and BaCu(B<sub>2</sub>O<sub>5</sub>) additives. *Journal of the European Ceramic Society*. 27 (8–9) p. 2875–2879.

- Ling, C. (2009a). Personal communication. University of Sydney. 12 May 2009.
- Ling, C. (2009b). Personal communication. University of Sydney. 19 May 2009.
- Ling, C. (2013) *XRD results for Marulan and Bungendore tailings*. PhD associate supervision 1 March, 2013.
- Lipton, A. & Watts, P. (2004). Ecoart: ecological art. In: Strelow, H., Prigann, H. & David, V. (eds) *Ecological Aesthetics: Art in Environmental Design: Theory and Practice*. Basel: Birkhäuser.
- Lynch, E. D. & Allen, A. W. (1950). Nepheline syenite-talc mixtures as a flux in low-temperature vitrified bodies. *Journal of the American Ceramic Society*. 33 (4) p. 117–130.
- Manacorda, F. (ed.) (2009). *Radical Nature. Art and Architecture for a Changing Planet 1969-2009*. Cologne: Walther König.
- Manson, M. E. (1931). Sodium silicate, a new enamel raw material. *Journal of the American Ceramic Society*. 14 (7) p. 490–494.
- Martin, A. (2006). *The Essential Guide to Mold Making and Slip Casting*. New York: Sterling Publishing.
- Mason, H. (1967). Why do we make pots? *New Zealand Potter*. 9 (2) p. 33–35.
- McCann, B. (2011). Personal Communication by telephone. 18 January 2011. Australian Laboratory Services. Brisbane.
- McConville, C. J. & Lee, W. E. (2005). Microstructural development on firing illite and smectite clays compared with that in kaolinite. *Journal of the American Ceramic Society*. 88 (8) p. 2267–2276.
- McEwan, L. (2007). Seeds of discontent. *Ceramics Technical*. (25) p. 65–68.
- McMeekin, I. (1985). *Notes for Potters in Australia: Raw Materials and Clay Bodies*. 3rd Ed. Kensington: University of New South Wales Press.
- Menezes, R. R., Ferreira, H. S., Neves, G. A., Lira, H. d. L. & Ferreira, H. C. (2005). Use of granite sawing wastes in the production of ceramic bricks and tiles. *Journal of the European Ceramic Society*. 25 (7) p. 1149–1158.



- Mihadzr, (2005). *Shukhov Tower Destroyed* [Photograph] [Online] Available from:  
[http://en.wikipedia.org/wiki/File:Oka\\_Shukhov\\_tower\\_2005\\_destroyed\\_3.jpg](http://en.wikipedia.org/wiki/File:Oka_Shukhov_tower_2005_destroyed_3.jpg) [Accessed: 2 April 2010].
- Miller, A. (1994). *Slipping into paperclay: a research paper*. [Online] Available from: <http://www.grahamhay.com.au/miller1994.html> [Accessed: 10 August 2008].
- Miller, J. (2012). Climate change: generation X attitudes, interest, and understanding. *The Generation X Report. A quarterly Research Report from the Longitudinal Study of American Youth*. 1 (3). University of Michigan. [Online] Available from: <http://www.sampler.isr.umich.edu/wp-content/uploads/2012/07/GenXReport.pdf> [Accessed: 1 September, 2012].
- Mineral Data Publishing (2001) *Prehnite* [Online] Available from: <http://rruff.info/doclib/hom/prehnite.pdf> [Accessed 24 November, 2011].
- Modesto, C. & Bernardin, A. (2008). Determination of clay plasticity: indentation method versus Pfefferkorn method. *Applied Clay Science*. 40 (1-4) p. 15–19.
- Mombass (1979) Image from *Photobucket* [Online] Available from: <http://s273.photobucket.com/profile/mombass/uploads#!cpZZ4QQtpPZZ28> [Accessed 14 March, 2013].
- Moore, F. (1963). Two instruments for studying the plasticity of clays. *Journal of Scientific Instruments*. 40 (5) p. 228.
- Munday, P. L., Dixon, D. L., Donelson, J. M., Jones, G. P., Pratchett, M. S., Devitsina, G. V. & Døving, K. B. (2009). Ocean acidification impairs olfactory discrimination and homing ability of a marine fish. *Proceedings of the National Academy of Sciences*. 106 (6) p. 1848–1852.
- Mustafi, S., Ahsan, M., Dewan, A., Ahmed, S., Khatun, N. & Absar, N. (2011). Effect of waste glass powder on physio-mechanical properties of ceramic tiles. *Bangladesh Journal of Scientific*

*Research*. 24 (2) p. 169–180.

Naskar, M. & Chatterjee, M. (2005). A novel process for the synthesis of lithium aluminum silicate powders from rice husk ash and other water-based precursor materials. *Materials Letters*. 59 (8–9) p. 998–1003.

National Oceanic & Atmospheric Administration, Earth System Research Laboratory, Global Monitoring Division. (2011a). *Trends in atmospheric carbon dioxide*. US Department of Commerce.

[Online]. Available from:

[ftp://ftp.cmdl.noaa.gov/ccg/co2/trends/co2\\_weekly\\_mlo.txt](ftp://ftp.cmdl.noaa.gov/ccg/co2/trends/co2_weekly_mlo.txt)

[Accessed: 30 March 2012].

National Oceanic & Atmospheric Administration, Earth System Research Laboratory, Global Monitoring Division. (2011b). Chart: *CO2 Cape Grim Australia Time series since 1984*. [Online] Available from:

<http://www.esrl.noaa.gov/gmd/dv/iadv/graph.php?code=CGO&program=ccgg&type=ts> [Accessed: 30 March 2012].

National Oceanic & Atmospheric Administration, Earth System Research Laboratory, Global Monitoring Division. (2012). Chart: *CO2 Cape Grim Australia Time series since 1984*. [Online] Available from:

<http://www.esrl.noaa.gov/gmd/dv/iadv/graph.php?code=CGO&program=ccgg&type=ts> [Accessed: 30 March 2012].

Nelson, S. (2004). Textures of Igneous Rocks [Online] Available from:

[http://www.tulane.edu/~sanelson/eens212/textures\\_igneous\\_rocks.htm](http://www.tulane.edu/~sanelson/eens212/textures_igneous_rocks.htm) [Accessed 10 July, 2011].

Newbert, C. (2009). Image of clown fish. Minden Pictures/FLPA

accompanying uncredited article: Acid seas no go for Nemo. *New Scientist*. (7 February) p. 6.

Nisbet, M. (2011). Climate shift: clear vision for the next decade of public debate. American University School of Communication. [Online].

Available from: <http://climateshiftproject.org/report/climate-shift-clear-vision-for-the-next-decade-of-public-debate/#the-economy-and-our-finite-pool-of-worry> [Accessed: 1 September 2011].

- North Dakota Department of Health (2005). *Erionite*. [Online] Available from: Environmental health and Safety <http://www.ndhealth.gov/EHS/erionite/> [Accessed: 25 May 2009].
- Norton, F. H. & Hodgdon, F. (1931). The influence of time on the maturing temperature of whiteware bodies. *Journal of the American Ceramic Society*. 14 (3) p. 177–191.
- Novotny, R., Hoff, A. & Schuertz, J. (1991). *Process for hydrothermal production of sodium silicate solutions*. United States Patent 5,000,933.
- Ol'khovskii, I. & Sartakov, Y. (1964). Rice husks as a combustible addition for making lightweight refractories. *Refractories January–February, 1964, Volume 5, (1-2)*, p. 92-95. Uncredited translation from *Ogneupory*. 2 p. 89–92.
- Özel, E., Kurama, S. & Ay, N. (2002). How active silica affects slip properties of sanitary ware. *Ceramic Bulletin*. [Online] Available from: [www.ceramicbulletin.org](http://www.ceramicbulletin.org) [accessed 2 March, 2011].
- Palmer, W. E. (1942). Influence of flint particle size on permanent moisture and thermal expansion in porous earthenware bodies. *Journal of the American Ceramic Society*. 25 (14) p. 413–416.
- Park, Y. J. & Heo, J. (2002). Conversion to glass-ceramics from glasses made by MSW incinerator fly ash for recycling. *Ceramics International*. 28 (6) p. 689–694.
- Pask, J. (1953) Measurement of Dry Strength of Clay Bodies. *Journal of The American Ceramic Society*. 36 (9) p. 313-318.
- Pauley, K. (2008). Personal communication. Norskeskog, Australia.
- Peterson, B. (2012). How to choose a pottery clay. *The New York Times*. *About.com* [Online]. Available from: <http://pottery.about.com/od/understandclays/tp/chooseclay.htm> [Accessed: 3 September 2012].
- Petrov, A. (2005) *Mother Nature's Violent & Poisonous Underworld*. [Online]. <http://www.mineraldreams.com/articles/2005-petrov-io-jima.pdf> [Accessed 3 March, 2013].

- Pitelka, V. (2001). *Clay: a Studio Handbook*. Westerville: American Ceramic Society.
- Porritt, J. (2009). Foreword. In: Manacorda, F. (ed.) *Radical Nature. Art and Architecture for a Changing Planet*. 1969–2009. Cologne: Walther König.
- Prasad, C. S., Maiti, K. N. & Venugopal, R. (2001). Effect of RHA in whiteware compositions. *Ceramics International*. 27 (6) p. 629–635.
- Proctor, A. (1990). X-Ray Diffraction and Scanning Electron Microscope Studies of Processed Rice Hull Silica. *Journal of the American Oil Chemists Society*. 67 (9) p. 576–583.
- Rahman, M. A. (1987). Properties of clay-sand-RHA mixed bricks. *International Journal of Cement Composites and Lightweight Concrete*. 9 (2) p. 105–108.
- Rama Rao, G., Sastry, A. & Rohatgi, P. (1989). Nature and reactivity of silica available in rice husk and its ashes. *Bulletin of Materials Science*. 12 (5) p. 469–479.
- Rambaldi, E., Carty, W. M., Tucci, A. & Esposito, L. (2007). Using waste glass as a partial flux substitution and pyroplastic deformation of a porcelain stoneware tile body. *Ceramics International*. 33 (5) p. 727–733.
- Rawlings, R. D., Wu, J. P. & Boccaccini, A. R. (2006). Glass-ceramics: their production from wastes—a review. *Journal of Materials Science*. 41 (3) p. 733–761.
- Real C., Alcala, M. D. & Criado, J. M. (1996). Preparation of silica from rice husks. *Journal of the American Ceramic Society*. 79 (8) p. 2012–2016.
- Reid, S. (2011). *Strength tests of glass and ceramics*. [Interview] 20 April 2011. University of Sydney Department of Civil Engineering.
- Rhodes, D. (1973). *Clay and Glazes for the Potter*. Philadelphia: Chilton Book Co.
- Roberts, J. (1966). Radio criticism cited in *New Zealand Potter*. 9 (1) p. 25.

- Royal Stafford Tableware Ltd. (2012). *Production Techniques: Biscuit firing and kilns*. [Online] Available from: <http://www.royalstafford.co.uk/Biscuit.htm> [Accessed: 29 August, 2012].
- Rudd, K. (2007). *Address to Australian Labor Party National Climate Change Summit. Canberra, Australia*. [Online video] 31 March 2007. Available from: [www.youtube.com/watch?v=CqZvpRjGtGM](http://www.youtube.com/watch?v=CqZvpRjGtGM) [Accessed: 4 April 2010].
- Ryan, W. (1978). *Properties of Ceramic Raw Materials*. 2nd Ed. Oxford: Pergamon Press.
- Rye, O. (2009). *Burning Wood*. [Online] 20 May 2009. Australian Ceramics Discussion List. Available from: [australianceramicsdiscussionlist@australianceramics.com](mailto:australianceramicsdiscussionlist@australianceramics.com) [Accessed: 20 May 2009].
- Saboya, Jr. F., Xavier, G. C. & Alexandre, J. (2007). The use of the powder marble by-product to enhance the properties of brick ceramic. *Construction and Building Materials*. 21 (10) p. 1950–1960.
- Savard, M. & Speyer, R. (1993). Effects of particle size on the fusion of soda–lime–silicate glass containing NaCl. *Journal of the American Ceramic Society*. 76 (3) p. 671–677.
- Saxe, C. W. & Buckner, O. S. (1915). The bonding strengths of a number of clays between normal temperature and red heat. *Journal of the American Ceramic Society*. 1 (1) p. 113-133.
- Schimmel, G., Kotzian, M., Panter H., & Tapper, A. (1993) *Process for producing amorphous sodium silicate*. United States Patent US005229095A.
- Schurecht, H. G. & Pole, G. R. (1929). Effect of water in expanding ceramic bodies of different compositions. *Journal of the American Ceramic Society*. 12 (9) p. 596–614.
- Seattle Pottery Supply (1999). *REPORT NO. GL-99-1: Glass Clay Body Flux* [Online] Available from: <http://www.cwc.org/glass/gl991rpt.pdf> [Accessed 23 June, 2010].
- Seega, B. (Producer). (2009, October 18). Professor Ian Pilmer replies to

- his critics. *Ockham's Razor* [Audio podcast]. Available from: <http://www.abc.net.au/rn/ockhamsrazor/stories/2009/2716078.htm> [Accessed 17 July, 2010].
- Sharma, D. (2011). Personal communication. Conversation in the lift about environmental economics. University of Technology, Sydney, 7 October, 2011.
- Sharma, R, Phanikumar B., & Varapasada Rao, B. (2008) Engineering behavior of a remolded expansive clay blended with lime, calcium chloride, and rice-husk ash. *Journal of Materials in Civil Engineering* 20(8) p. 509–515.
- Shatrov, S. (2009). *Carbon Emissions and Wood Firing?* [Online] 21 May 2009. Australian Ceramics Discussion List. Available from: [australianceramicsdiscussionlist@australianceramics.com](mailto:australianceramicsdiscussionlist@australianceramics.com) [Accessed: 23 May 2009].
- Shaw, K. (1972). *Science for Craft Potters and Enamellers*. Sydney: AH & AW Reed.
- Shelton, G. (1929). Pyrophyllite, a new ceramic raw material. *Journal of the American Ceramic Society*. 12 (2) p. 79–82.
- Shil'tsina, A. & Selinov, V. (2000). Utilisation of waste. Ceramic tiles made of granular technogenic raw materials. *Glass and Ceramics*. 57 (7–8) p. 252–256.
- Shinohara, Y. & Kohyama, N. (2004). Quantitative analysis of tridymite and cristobalite crystallised in RHA by heating. *Industrial Health*. 42 (2) p. 277–285.
- Siandara, (2008). *Sheffield Tinsley towers demolition* photo stream on *Flickr* [Online] Available from: <http://www.flickr.com/photos/67611923@N00/sets/72157606918402173> [Accessed: 3 October, 2010].
- Simpson, B. (1983–1991). Hudson River Purge. [Online] Available from: <http://www.bustersimpson.net/hudsonriverpurge/> [Accessed: 1 October 2010].
- Simpson, J. (1967). Criticism. *New Zealand Potter*. 9 (2) p. 5.
- Smith, A. S. (2004). To demonstrate commercial viability of incorporating

ground glass in bricks with reduced emissions and energy savings.  
The Waste & Resources Action Programme, Oxon, UK.

- Smout, B. (2005). Designing at UTS–fused deposition modelling for slip cast mould making at the University of Technology, Sydney. *Journal of Australian Ceramics*. 44 (2) p.94-95.
- Smout, B. (2008). Low-fire glazes. Unpublished.
- Smout, B. (2009). Image of Porcelain vases inspired by seashells. Unpublished.
- Smout, B. (2011). Transformations, Clay and Our Environment. In: Lange, P. & Newby, S. (eds). *Playing with Fire*. Auckland: Centre for New Zealand Art Research and Discovery, National Institute of Creative Arts and Industries, University of Auckland.
- Spires, T. (2008). Personal communication. Telephone call to Sunrice, Leeton NSW. 13 August 2008.
- Spode U.K. Ltd. (n.d.). *Spode Museum Website* [Online] Available from: <http://www.spodemuseumtrust.org/index.html> [Accessed: 2 March 2010].
- Stairs, G. (1997). Post to 'woooo!!! fired strength surprise' thread! *Clayart* Wednesday 5 March 1997 [Online] Available from: <http://www.potters.org/subject10058.htm> [Accessed: 15 October 2009].
- Stapley, R. (2008). Personal Communication. Factory Manager. Simplot Pty Ltd, Bathurst NSW Australia. 1 December 2008.
- Stern, N. (2009). Decision time. *New Scientist*. 2692 (24 January) p. 26.
- Stichting Disposables Benelux (2007). *Single use cups are the winners!* [Online] Available from: <http://www.prodisposables.nl/nl/file/20110104173451/5/Brochure-with-a-summary-of-the-research.html> [Accessed: 5 September, 2012].
- Strelow, H., Prigann, H. & David, V. (eds) (2004). *Aesthetics of Ecology: Art in Environmental Design : Theory and Practice*. Basel: Birkhauser.

- Stone, W. (2009) Personal Communication. Site visit, Cemex, Marulan, Australia, 1 September 2009.
- Sujirote, K. & Leangsuwan, P. (2003). Silicon carbide formation from pretreated rice husks. *Journal of Materials Science*. 38 (23) p. 4739–4744.
- Tandoc, E. (2009) The Belonio Rice Husk Stove. *Philippine Daily Inquirer* 15 February 2009. [Online] Available from: <http://www.iloiloviews.com/the-belonio-rice-husk-stove.html> [Accessed 30 September 2009].
- Tavornpanich, T., Souza, G. P. & Lee, W. E. (2005). Microstructural evolution on firing soda & lime & silica glass fluxed whitewares. *Journal of the American Ceramic Society*. 88 (5) p.1302–1308.
- Taylor, J. R. & Bull, A.C. (1986). *Ceramics Glaze Technology*. New York: Pergamon Press (on behalf of the Institute of Ceramics).
- Teixeira, S. R., de Souza, A. E., de Almeida Santos, G. T., Peña, A. F. V. & Miguel, A. G. (2008). Sugarcane bagasse ash as a potential quartz replacement in red ceramic. *Journal of the American Ceramic Society*. 91 (6) p. 1883–1887.
- Thurn, H. (1945). Use of wood ash in a low-fire mat glaze. *Journal of the American Ceramic Society* 28(9): 261-264.
- Tichane, R. (1990). *Clay Bodies*. New York: New York Glaze Institute.
- Tiffany, M. (2004) Image: *Scanning Electron Micrographs of Diatoms*. (a) *Biddulphia reticulata*. (b) *Diploneis sp.* (c) *Eupodiscus radiatus*. (d) *Melosira varians*. [Online] Available from: <http://en.wikipedia.org/wiki/File:Diatoms.png> San Diego State University. [Accessed 23 June, 2011].
- Tomilov, V. (2006).Image: *Shukhov Tower* [Online] Available from: [http://en.wikipedia.org/wiki/File:Shukhov\\_Tower\\_photo\\_by\\_Vladimir\\_Tomilov.jpg](http://en.wikipedia.org/wiki/File:Shukhov_Tower_photo_by_Vladimir_Tomilov.jpg) [Accessed: 2 April 2010].
- Torres, P., Fernandes, H. R., Olhero, S. & Ferreira, J. M. F. (2009). Incorporation of wastes from granite rock cutting and polishing industries to produce roof tiles. *Journal of the European Ceramic Society*. 29 (1) p. 23–30.



- Toya, T., Kameshima, Y., Nakajima, A. & Okada, K. (2006). Preparation and properties of glass-ceramics from kaolin clay refining waste (Kira) and paper sludge ash. *Ceramics International*. 32 (7) p. 789–796.
- Tozzi, N. (2003) Deflocculants: A Detailed Overview [Online] Available from: [digitalfire.com/4sight/education/deflocculants\\_a\\_detailed\\_ove](http://digitalfire.com/4sight/education/deflocculants_a_detailed_ove) [Accessed 2 December, 2010].
- Tsai, D. (1991). Pressure buildup and internal stresses during binder burnout: numerical analysis. *American Institute of Chemical Engineers Journal*. 37 (4) p. 547–554.
- Ueda, T., Kunimitsu Y. & Shinogi, Y. (2007) .Potential conflicts for the re-use of rice husk in Thailand. *Paddy Water Environment*. 5 p. 123–129.
- Unimin Australia Ltd. (2002). Australian Bentonite Product Profile *ActiveGel* 150 (Issue E) p.1
- United States Department of Labor (2004). *Occupational Safety and Health Regulation Tables Z-1 & Z-3*. [Online] Available from: <http://www.osha.gov/pls/oshaweb> [Accessed: 5 February 2010].
- VanCott, R. (2009). Your mug and the environment. *Powering down* blog. [Online] Available from: <http://www.pbs.org/wgbh/nova/energy/poweringdown/2009/01/coffee-cup-contest.html> [Accessed: 25 January, 2009].
- Van der Drift, A. & Olsen, A (1999). *Conversion of Biomass, Prediction and Solution Methods for Ash Agglomeration and Related Problems*. Petten: Energy Research Foundation.
- Vaux, J. (2009). *Carbon emissions and wood firing?* 20 May 2009 [Online] Australian Ceramics Discussion List Available from: [australianceramicsdiscussionlist@australianceramics.com](mailto:australianceramicsdiscussionlist@australianceramics.com) [Accessed: 20 May 2009].
- Voiland, A. (2010). 2009: Second warmest year on record; end of warmest decade. National Aeronautics and Space Administration. Goddard Institute for Space Studies. [Online] Available from: <http://www.giss.nasa.gov/research/news/20100121/> [Accessed: 1 November 2011].

- Wajima, T., Haga, M., Kuzawa, K., Ishimoto, H., Tamada, O., Ito, K., Nishiyama, T., Downs, R., & Rakovan, J.. (2006). Zeolite synthesis from paper sludge ash at low temperature (90°C) with addition of diatomite. *Journal of Hazardous Materials*. 132 (2–3) p. 244–252.
- Walker Ceramics (2009). *Conversion factors and melting points of common materials*. [Online] Available from: <http://www.walkerceramics.com.au> [Accessed 14 May 2009].
- Walker, D. (2009). Personal Communication. Melbourne, Australia. 17 October, 2009.
- Walker, D. (2010). *Cones* [Online] Available from: <http://walkerceramics.com.au/cones.htm> [Accessed, 1 March 2011].
- Ward, L., & Terry, P. (2011). Nambassa: A 25 years commemorative archival website [Online] Available from: <http://www.nambassa.com/> [Accessed 1 March 2013].
- Watari, T., Nakata, A., Kiba, Y., Torikai, T. & Yada, M. (2006). Fabrication of porous SiO<sub>2</sub>/C composite from rice husks. *Journal of the European Ceramic Society*. 26 (4–5) p. 797–801.
- Whitfield, D. (1985). *Sand Sashing Tailings –their Nature and Potential for Use in Earthenware and Stoneware Bodies*. A Thesis Submitted in partial fulfilment of the Requirements of the University of New South Wales for the Degree of Master of Science. Sydney: University of New South Wales.
- Whitfield, D. (1993). *The Potential for Utilisation of Some Solid Industrial Process Wastes as Raw Materials in the Manufacture of Ceramic Building Products*. A Thesis Submitted in partial fulfilment of the Requirements of the University of New South Wales for the Degree of Doctor of Philosophy. Sydney: University of New South Wales.
- Wilkinson, M. & Cubby, B. (2008). Recycling illusion exposed. *Sydney Morning Herald*. (7 April) p. 1.
- Wilson-Foster, J. (nd). *Julie Wilson-Foster: Australian Contemporary Environmental Artist*. [Online] Available from: <http://www.jwf-artist.com/> [Accessed: 10 November 2009].

- Winter, K. (2009). Carbon Emissions... [Online]. *Australian Ceramics Discussion List*. Available from:  
 australianceramicsdiscussionlist@australianceramics.com  
 [Accessed: 22 May 2009].
- Winter, K. (2009). Burning wood. [Online] 20 May 2009. *Australian Ceramics Discussion List* Available from:  
 australianceramicsdiscussionlist@australianceramics.com  
 [Accessed: 20 May 2009].
- Worrall, W. E. (1986). *Clays and Ceramic Raw Materials*. 2nd Ed. London: Elsevier Applied Science Publishers.
- Yonetani, K. (2004). Images of Yonetani's fumie tiles. [Online] Available from: <http://www.kenyonetani.com/Kenworksfumie-tiles.html>  
 [Accessed: 8 June 2009].
- Yonetani, K. (2008). PhD Colloquium presentation convened by Ross Gibson, Sydney College of Arts, University of Sydney, Australia.
- Yonetani, K & J. (2011). Image: *Still life – the food bowl*. Ken & Julia Yonetani [Online] Available from:  
<http://www.artabase.net/exhibition/3319> [Accessed 12 April, 2012].
- Yugai, N. (2001). Ceramic mixtures containing cullet for decorative majolica. *Glass and Ceramics*. 58 (9) p. 320–321.
- Yun, Y. -H., Kim, S. -B., Kang, B. -A. & Oh, J. -S. (2002). Chemical durability of waste fluorescent glass and shell-derived glass-ceramics. *Journal of Materials Synthesis and Processing*. 10 (1) p. 37–42.
- Zamek, J. (1998). Additives for glazes and clay bodies. *Ceramics Monthly*. December (61–62) p. 86–91.
- Zamek, J. (2007). Glazes: materials, mixing, testing and firing. *Ceramics Monthly*. (54) Supplementary Buyers Guide, p. 6–8.
- Zimmerman, K. (2012). Pareidolia: Seeing Faces in Unusual Places. *Live Science* [Online] Available from <http://www.livescience.com/25448-pareidolia.html> [Accessed 18 May, 2013].

## Appendices

### Appendix 1: Orton standard cones: temperature equivalents & Seger cone formulae

ORTON Standard Pyrometric CONES							
TEMPERATURE EQUIVALENT when heated at 150°C/hr							
<u>Cone</u>	<u>Temp.</u>	<u>Cone</u>	<u>Temp.</u>	<u>Cone</u>	<u>Temp.</u>	<u>Cone</u>	<u>Temp.</u>
022	600	013	852	04	1060	5	1196
021	614	012	884	03½	1080	6	1222
020	635	011	894	03	1101	7	1240
019	683	010	900	02	1120	8	1263
018	717	09	923	01	1137	9	1280
017	747	08	955	1	1154	10	1305
016	792	07	984	2	1162	11	1315
015	804	06	999	3	1168	12	1326
014	838	05	1046	4	1186	13	1346

### Seger cone formulae to 790°C–1000°C

015a	0.432 Na <sub>2</sub> O 0.432 CaO 0.136 MgO	0.34 Al <sub>2</sub> O <sub>3</sub>	2.06 SiO <sub>2</sub> 0.86 B <sub>2</sub> O <sub>3</sub>	790
014a	0.385 Na <sub>2</sub> O 0.385 CaO 0.230 MgO	0.34 Al <sub>2</sub> O <sub>3</sub>	1.92 SiO <sub>2</sub> 0.77 B <sub>2</sub> O <sub>3</sub>	815
013a	0.343 Na <sub>2</sub> O 0.343 CaO 0.314 MgO	0.34 Al <sub>2</sub> O <sub>3</sub>	1.78 SiO <sub>2</sub> 0.69 B <sub>2</sub> O <sub>3</sub>	835
012a	0.345 Na <sub>2</sub> O 0.314 CaO 0.314 MgO	0.365 Al <sub>2</sub> O <sub>3</sub>	2.04 SiO <sub>2</sub> 0.68 B <sub>2</sub> O <sub>3</sub>	855
011a	0.349 Na <sub>2</sub> O 0.340 CaO 0.311 MgO	0.4 Al <sub>2</sub> O <sub>3</sub>	2.38 SiO <sub>2</sub> 0.68 B <sub>2</sub> O <sub>3</sub>	880
010a	0.338 Na <sub>2</sub> O 0.011 K <sub>2</sub> O 0.338 CaO 0.313 MgO	0.423 Al <sub>2</sub> O <sub>3</sub>	2.626 SiO <sub>2</sub> 0.675 B <sub>2</sub> O <sub>3</sub>	900
09a	0.336 Na <sub>2</sub> O 0.018 K <sub>2</sub> O 0.335 CaO 0.311 MgO	0.468 Al <sub>2</sub> O <sub>3</sub>	3.087 SiO <sub>2</sub> 0.671 B <sub>2</sub> O <sub>3</sub>	920
08a	0.279 Na <sub>2</sub> O 0.038 K <sub>2</sub> O 0.369 CaO 0.314 MgO	0.543 Al <sub>2</sub> O <sub>3</sub>	2.691 SiO <sub>2</sub> 0.559 B <sub>2</sub> O <sub>3</sub>	940
07a	0.261 Na <sub>2</sub> O 0.055 K <sub>2</sub> O 0.391 CaO 0.293 MgO	0.554 Al <sub>2</sub> O <sub>3</sub>	2.984 SiO <sub>2</sub> 0.521 B <sub>2</sub> O <sub>3</sub>	960
06a	0.247 Na <sub>2</sub> O 0.069 K <sub>2</sub> O 0.407 CaO 0.277 MgO	0.561 Al <sub>2</sub> O <sub>3</sub>	3.197 SiO <sub>2</sub> 0.493 B <sub>2</sub> O <sub>3</sub>	980
05a	0.229 Na <sub>2</sub> O 0.086 K <sub>2</sub> O 0.428 CaO 0.257 MgO	0.571 Al <sub>2</sub> O <sub>3</sub>	3.467 SiO <sub>2</sub> 0.457 B <sub>2</sub> O <sub>3</sub>	1000

Adapted from <http://kawamura-chemical.co.jp/jpn/21kagakushiki.htm>

## Appendix 2: Norkse Skog paper sludge analysis

### EMP 37 - Recycled Fibre Biosolids Testing

Month	pH	Organic Carbon mg/kg	Total Solids %	Total Phos mg/kg	TKN as N mg/kg	Arsenic mg/kg	Cadmium mg/kg	Chromium mg/kg	Cobalt mg/kg	Copper mg/kg	Lead mg/kg	Magnesium mg/kg	Mercury mg/kg	Nickel mg/kg	Potassium mg/kg	Selenium mg/kg	Sodium mg/kg	Zinc mg/kg	Calcium mg/kg
Jul-07	8.0	27900	40.0	300	2500	0.0	0.0	10.0	3.7	160	2.8	1800	0.0	1.1	410	0.0	1100	31	90000
Aug-07	8.2	377000	22.0	300	3500	0.0	0.0	11.0	3.2	200	3.2	1800	0.0	8.0	1100	0.7	1800	21	80000
Sep-07	8.2	320000	31.0	400	2700	0.0	0.0	9.0	2.4	160	4.5	1900	0.0	4.6	600	0.0	1400	15	91000
Oct-07	6.7	320000	32.0	2300	3100	0.5	0.0	4.4	0.6	18	1.1	740	0.0	14.0	1400	0.0	1400	30	9100
Nov-07	7.7	310000	33.0	260	220	0.0	0.0	4.9	2.1	97	3.8	2100	0.0	3.1	730	0.0	1100	11	97000
Dec-07	7.2	440000	44.0	1200	2800	0.5	0.0	3.7	0.0	63	1.8	770	0.0	2.3	1300	0.0	750	26	33000
Jan-08	8.8	280000	42.0	210	3100	0.0	0.0	6.4	3.0	150	2.1	1900	0.1	8.3	880	0.0	1100	12	90000
Feb-08	7.7		42.0	360	2100	0.0	0.0	3.3	2.3	130	2.3	2400	0.0	0.0	1500	0.0	1900	9	140000
Mar-08	7.6	360000	36.0	200	2700	0.0	0.0	4.8	2.6	160	2.6	1300	1.0	9.6	820	0.0	890	12	76000
Apr-08	6.9	180000	32.0	240	3200	0.0	0.0	5.0	0.0	210	0.0	1500	0.0	0.0	300	6.0	1100	25	90000
May-08	7.9	6600	39.0	220	2900	0.0	0.0	4.1	3.3	130	2.8	2200	0.0	8.2	1100	0.0	930	19	110000
Jun-08	8.0	460000	44.0	240	2100	0.0	0.0	0.0	0.0	160	0.0	1600	0.0	0.0	770	0.0	870	16	91000
<b>Average</b>	7.7	280136	36.4	519	2577	0.1	0.0	5.6	1.9	137	2.2	1668	0.1	4.9	909	0.6	1195	18.9	83092
<b>Std Dev</b>	0.6	150403	6.6	624	852	0.2	0.0	3.1	1.4	55	1.4	521	0.3	4.6	380	1.7	363	7.6	33667
<b>Max</b>	8.8	460000	44.0	2300	3500	0.5	0.0	11.0	3.7	210	4.5	2400	1.0	14.0	1500	6.0	1900	31.0	140000
<b>Min</b>	6.7	6600	22.0	200	220	0.0	0.0	0.0	0.0	18	0.0	740	0.0	0.0	300	0.0	750	9.0	9100

### EMP 38 - Waste Water Treatment Plant Biosolids Testing

Month	pH	Organic Carbon mg/kg	Total Solids %	Total Phos mg/kg	TKN as N mg/kg	Arsenic mg/kg	Cadmium mg/kg	Chromium mg/kg	Cobalt mg/kg	Copper mg/kg	Lead mg/kg	Magnesium mg/kg	Mercury mg/kg	Nickel mg/kg	Potassium mg/kg	Selenium mg/kg	Sodium mg/kg	Zinc mg/kg	Calcium mg/kg
Jul-07	7.5	486000	17.0	1600	19500	0.0	0.0	4.3	0.6	44	1.3	600	0.0	1.3	100	0.0	1100	25	12000
Aug-07	7.5	523000	20.0	1200	13000	0.5	0.0	10.0	2.1	54	1.5	1100	0.0	5.5	1700	0.7	1600	24	19000
Sep-07	7.7	410000	28.0	650	6500	0.0	0.0	5.9	1.1	89	3.5	1200	0.1	2.4	1300	0.0	520	15	63000
Oct-07	6.3	560000	17.0	290	29000	0.0	0.0	17.0	5.5	130	4.3	2200	0.0	8.4	590	0.0	1100	35	75000
Nov-07	7.1	530000	15.0	920	15000	0.0	0.0	3.2	0.0	42	1.6	550	0.0	1.0	1400	0.0	1600	18	20000
Dec-07	6.9	260000	25.0	300	18000	0.0	0.0	8.4	2.6	150	3.0	2300	0.0	6.8	1100	0.0	890	12	110000
Jan-08	7.7	380000	21.0	730	13000	0.5	0.6	3.8	0.6	20	6.3	380	0.2	2.7	1100	0.0	920	19	10000
Feb-08	7.5		28.0	600	8400	0.0	0.0	2.0	0.7	40	0.9	1000	0.0	1.2	1800	0.0	1100	9	4900
Mar-08	6.9	38000	17.0	3100	48000	1.9	0.1	5.8	0.9	34	1.2	850	1.8	3.0	1900	0.0	1800	36	19000
Apr-08	6.9	250000	23.0	1200	14000	0.0	0.0	0.0	0.0	140	0.0	1200	0.0	0.0	820	7.0	1000	38	59000
May-08	7.2	390000	22.0	1400	27000	0.0	0.0	3.0	1.0	29	1.1	720	0.0	2.6	1500	0.0	820	29	14000
Jun-08	7.3	640000	20.0	2900	28000	0.0	0.0	8.0	0.0	150	0.0	1100	0.0	0.0	1400	0.0	1700	43	31000
<b>Average</b>	7.2	406091	21.1	1241	19950	0.2	0.1	6.0	1.3	77	2.1	1100	0.2	2.9	1226	0.6	1179	25.3	36408
<b>Std Dev</b>	0.4	172035	4.3	918	11513	0.6	0.2	4.5	1.6	52	1.9	600	0.5	2.7	524	2.0	402	11.0	32774
<b>Max</b>	7.7	640000	28.0	3100	48000	1.9	0.6	17.0	5.5	150	6.3	2300	1.8	8.4	1900	7.0	1800	43.0	110000
<b>Min</b>	6.3	38000	15.0	290	6500	0.0	0.0	0.0	0.0	20	0.0	380	0.0	0.0	100	0.0	520	9.0	4900

## Appendix 3: Cullet technical data

### TECHNICAL DATA

# CULLET

Glass 150

#### FEATURES

#### SANDGATE, NEW SOUTH WALES

A finely ground glass powder produced from low grade cullet. Typically used in abrasive and ceramic applications. Also used as a low temperature flux in brick manufacture.

Glass Cullet 150 is tested and controlled to rigorous standards which ensure consistent chemical and physical properties resulting in predictable and repeatable performance. Sibelco Australia actively manages a Quality Management System certified to ISO9001:2008.

The following properties may help you to determine the suitability of the product to best suit your application.

Sandgate Cullet 150 (01/11)

#### SPECIFICATION

**Sizing** 5% maximum + 150 microns

*Note: This product is manufactured to the requirements of the process specifications above. Typical properties are a consequence of the process, nature of raw material and are measured at a lower frequency than the specified properties. These results are an average of historical data.*

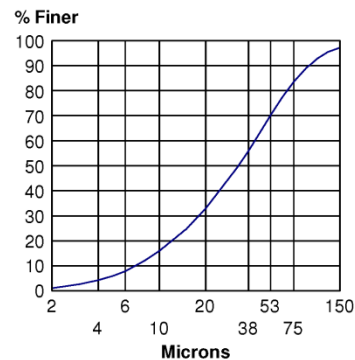
#### CHEMICAL AND ANALYTICAL DATA

Mean Values. These Do Not Represent A Specification

Mean Percent by Weight		(UAL 8.5)	
Silica	(SiO <sub>2</sub> )		<b>72</b>
Alumina	(Al <sub>2</sub> O <sub>3</sub> )		<b>0.3</b>
Potash	(K <sub>2</sub> O)		<b>0.1</b>
Soda	(Na <sub>2</sub> O)		<b>14.0</b>
Lime	(CaO)		<b>9.0</b>
Ferric Oxide	(Fe <sub>2</sub> O <sub>3</sub> )		<b>0.5</b>
Titania	(TiO <sub>2</sub> )		<b>&lt;0.1</b>
Magnesia	(MgO)		<b>4.0</b>
Loss on Ignition	(1000°C)	UAL 2.3	<b>0.4</b>
Specific Gravity		UAL 2.13	<b>2.50</b>
pH	(20% Slurry)	UAL 2.11	<b>11</b>
Bulk Density (compacted)	(g/cm <sup>3</sup> )	UAL 2.10(a)	<b>1.3</b>

#### PARTICLE SIZE ANALYSIS

Mean Values. These Do Not Represent A Specification



#### ORDERING INFORMATION

Shipping Point: Sandgate, New South Wales  
Availability: 25 kg Multi-Wall Paper Bags / Bulk Bags

**DISCLAIMER:** Ranges and values of trial sample testing or on a Technical Information Sheet are typical or expected ranges and are not guaranteed ranges. You must satisfy yourself that the product is suitable for the purpose for which you intend to use it. Sibelco makes no representations as to suitability, fitness or merchantability.

**HAZARD WARNING:** Avoid creating dust when handling, using or storing the product. Use only with adequate ventilation to keep exposure low. Undertake health and safety risk assessments on safe methods of handling and use appropriate to your workplace. To prevent inhalation of airborne dust, wear respiratory protection in accordance with Australian Standard AS1715 and AS1716. To prevent potential irritation to eyes, wear eye protection in accordance with Australian Standard AS1337.

Please refer to the relevant Sibelco Australia Limited Material Safety Data Sheet (MSDS) for health hazard information before opening or using this product and take care when disposing of the empty bag/container (as it may contain product residue). If you do not have an MSDS, please ring the ACOHS 24 hour emergency phone number 1800 638 556 and you will be sent one.

#### FOR PRODUCT INFORMATION AND CUSTOMER SERVICE

AUST: Adelaide +61 8 8240 8200 Brisbane +61 7 3909 4500 Melbourne +61 3 9586 5400  
Sydney +61 2 9637 7066 Perth +61 8 9362 1411 Newcastle +61 2 4028 9300  
NZ Auckland +64 9 914 7010 Visit our website [www.sibelco.com.au](http://www.sibelco.com.au)



ACN 000 971 844

BARYTES • BENTONITE • CLAY • DOLOMITE • FELDSPAR • ILMENITE • LIME • LIMESTONE • MAGNETITE • NEPH SYENITE • RUTILE • SILICA • TALC • ZIRCON

## Appendix 4: Rice husk gasifier stove operating instructions

**SPECIFICATIONS / SPESIFIKASI**

<b>Model</b>	<b>RHGS-15D</b> Patent no. S00200800240 December 16, 2008
<b>Fuel / Bahan Bakar</b>	<b>RICE HUSK / Sekam Padi</b>
<b>Fuel Consumption rate/hr</b> Pemakaian Bahan Bakar /Jam	1 kg
<b>Flame Color</b> Warna Api	Blue--pink / Biru-jingga
<b>Power Output (Kw)</b> Tenaga yang Dihasilkan (Kw)	1.1
<b>Start-up time (min)</b> Waktu untuk menyalakan (menit)	1
<b>Time to boil water</b> Waktu untuk memasak Air	8 mins for 1.5 liters of water 8 menit untuk 1.5 liter
<b>Operating time</b> Lama Penggunaan	45 minute 45 menit
<b>Overall dimension</b> Ukuran	30 x 30 x 80

**Safety Guidelines / Petunjuk keselamatan**

Do not operate near children / *Jaukan dari anak-anak*  
 Do not use other fuel / *Dilarang menggunakan bahan bakar lain*  
 Use 220 V outlet only / *Gunakan listrik 220 V*  
 Disconnect Fan from outlet after using / *Matikan kipas setelah digunakan*  
 Discharge char properly / *Buang arang sekam setelah digunakan*


PT. MINANG JORDANINDO APPROTECH

PT. MINANG JORDANINDO APPROTECH

# User's Manual

(Petunjuk Penggunaan)

**RHGS-15D**



**Product Component / Bagian—Bagian Kompor**



Support Legs / Kaki Penyangga



AC Fan / Kipas

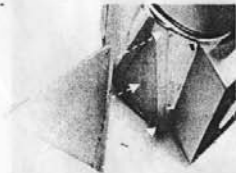


Reactor / Ruang Bakar



Casing / Badan Kompor

**Pre-operating procedure /  
Prosedur Sebelum Penggunaan**



Install Support leg /  
Pemasangan Kaki



Operator's Manual /  
Petunjuk Penggunaan  
Buku Panduan

**Operating Procedure / Cara Penggunaannya**

1. Fill the stove with fuel



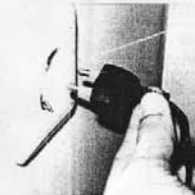
Masukan sekam padi

2. Prepare at least 1 inch space for the igniter



Isi hingga hampir Mencapai  
Penuh 3.5 cm

3. Turn on the AC Fan



Hidupkan Kipas

4. Make sure the top layer is burning



Pastikan Daun Kering Dan Sekam  
Pada bagian atas terbakar

**Note \***

For easy ignition, Put dry chunk coconut or palm leaf or spray kerosene

Agar lebih mudah untuk pembakaran, Letakan daun kelapa kering / daun palem raja kering atau semprotkan sedikit minyak tanah



# Appendix 5: ASTM standard C-373



Designation: C 373 – 88 (Reapproved 2006)

## Standard Test Method for Water Absorption, Bulk Density, Apparent Porosity, and Apparent Specific Gravity of Fired Whiteware Products<sup>1</sup>

This standard is issued under the fixed designation C 373; the number immediately following the designation indicates the year of original adoption or, in the case of revision, the year of last revision. A number in parentheses indicates the year of last reapproval. A superscript epsilon ( $\epsilon$ ) indicates an editorial change since the last revision or reapproval.

### 1. Scope

1.1 This test method covers procedures for determining water absorption, bulk density, apparent porosity, and apparent specific gravity of fired unglazed whiteware products.

1.2 *This standard does not purport to address all of the safety concerns, if any, associated with its use. It is the responsibility of the user of this standard to establish appropriate safety and health practices and determine the applicability of regulatory limitations prior to use.*

### 2. Significance and Use

2.1 Measurement of density, porosity, and specific gravity is a tool for determining the degree of maturation of a ceramic body, or for determining structural properties that may be required for a given application.

### 3. Apparatus and Materials

3.1 *Balance*, of adequate capacity, suitable to weigh accurately to 0.01 g.

3.2 *Oven*, capable of maintaining a temperature of  $150 \pm 5^\circ\text{C}$  ( $302 \pm 9^\circ\text{F}$ ).

3.3 *Wire Loop, Halter, or Basket*, capable of supporting specimens under water for making suspended mass measurements.

3.4 *Container*—A glass beaker or similar container of such size and shape that the sample, when suspended from the balance by the wire loop, specified in 3.3, is completely immersed in water with the sample and the wire loop being completely free of contact with any part of the container.

3.5 *Pan*, in which the specimens may be boiled.

3.6 *Distilled Water*.

### 4. Test Specimens

4.1 At least five representative test specimens shall be selected. The specimens shall be unglazed and shall have as much of the surface freshly fractured as is practical. Sharp

edges or corners shall be removed. The specimens shall contain no cracks. The individual test specimens shall weigh at least 50 g.

### 5. Procedure

5.1 Dry the test specimens to constant mass (**Note 1**) by heating in an oven at  $150^\circ\text{C}$  ( $302^\circ\text{F}$ ), followed by cooling in a desiccator. Determine the dry mass,  $D$ , to the nearest 0.01 g.

**NOTE 1**—The drying of the specimens to constant mass and the determination of their masses may be done either before or after the specimens have been impregnated with water. Usually the dry mass is determined before impregnation. However, if the specimens are friable or evidence indicates that particles have broken loose during the impregnation, the specimens shall be dried and weighed after the suspended mass and the saturated mass have been determined, in accordance with 5.3 and 5.4. In this case, the second dry mass shall be used in all appropriate calculations.

5.2 Place the specimens in a pan of distilled water and boil for 5 h, taking care that the specimens are covered with water at all times. Use setter pins or some similar device to separate the specimens from the bottom and sides of the pan and from each other. After the 5-h boil, allow the specimens to soak for an additional 24 h.

5.3 After impregnation of the test specimens, determine to the nearest 0.01 g the mass,  $S$ , of each specimen while suspended in water. Perform the weighing by placing the specimen in a wire loop, halter, or basket that is suspended from one arm of the balance. Before actually weighing, counterbalance the scale with the loop, halter, or basket in place and immerse in water to the same depth as is used when the specimens are in place. If it is desired to determine only the percentage of water absorption, omit the suspended mass operation.

5.4 After the determination of the suspended mass or after impregnation, if the suspended mass is not determined, blot each specimen lightly with a moistened, lint-free linen or cotton cloth to remove all excess water from the surface, and determine the saturated mass,  $M$ , to the nearest 0.01 g. Perform the blotting operation by rolling the specimen lightly on the wet cloth, which shall previously have been saturated with water and then pressed only enough to remove such water as will drip from the cloth. Excessive blotting will introduce error

<sup>1</sup> This test method is under the jurisdiction of ASTM Committee C21 on Ceramic Whitewares and Related Products and is the direct responsibility of Subcommittee C21.03 on Methods for Whitewares and Environmental Concerns.

Current edition approved Feb. 15, 2006. Published February 2006. Originally approved in 1955. Last previous edition approved in 1999 as C 373 – 88 (1999).

by withdrawing water from the pores of the specimen. Make the weighing immediately after blotting, the whole operation being completed as quickly as possible to minimize errors caused by evaporation of water from the specimen.

## 6. Calculation

6.1 In the following calculations, the assumption is made that 1 cm<sup>3</sup> of water weighs 1 g. This is true within about 3 parts in 1000 for water at room temperature.

6.1.1 Calculate the exterior volume,  $V$ , in cubic centimetres, as follows:

$$V = M - S \quad (1)$$

6.1.2 Calculate the volumes of open pores  $V_{OP}$  and imperious portions  $V_{IP}$  in cubic centimetres as follows:

$$V_{OP} = M - D \quad (2)$$

$$V_{IP} = D - S \quad (3)$$

6.1.3 The apparent porosity,  $P$ , expresses, as a percent, the relationship of the volume of the open pores of the specimen to its exterior volume. Calculate the apparent porosity as follows:

$$P = [(M - D)/V] \times 100 \quad (4)$$

6.1.4 The water absorption,  $A$ , expresses as a percent, the relationship of the mass of water absorbed to the mass of the dry specimen. Calculate the water absorption as follows:

$$A = [(M - D)/D] \times 100 \quad (5)$$

6.1.5 Calculate the apparent specific gravity,  $T$ , of that portion of the test specimen that is impervious to water, as follows:

$$T = D/(D - S) \quad (6)$$

6.1.6 The bulk density,  $B$ , in grams per cubic centimetre, of a specimen is the quotient of its dry mass divided by the exterior volume, including pores. Calculate the bulk density as follows:

$$B = D/V \quad (7)$$

## 7. Report

7.1 For each property, report the average of the values obtained with at least five specimens, and also the individual values. Where there are pronounced differences among the individual values, test another lot of five specimens and, in addition to individual values, report the average of all ten determinations.

## 8. Precision and Bias

8.1 This test method is accurate to  $\pm 0.2$  % water absorption in interlaboratory testing when the average value recorded by all laboratories is assumed to be the true water absorption. The precision is approximately  $\pm 0.1$  % water absorption on measurements made by a single experienced operator.

## 9. Keywords

9.1 apparent porosity; apparent specific gravity; bulk density; fired whiteware products; water absorption

*ASTM International takes no position respecting the validity of any patent rights asserted in connection with any item mentioned in this standard. Users of this standard are expressly advised that determination of the validity of any such patent rights, and the risk of infringement of such rights, are entirely their own responsibility.*

*This standard is subject to revision at any time by the responsible technical committee and must be reviewed every five years and if not revised, either reapproved or withdrawn. Your comments are invited either for revision of this standard or for additional standards and should be addressed to ASTM International Headquarters. Your comments will receive careful consideration at a meeting of the responsible technical committee, which you may attend. If you feel that your comments have not received a fair hearing you should make your views known to the ASTM Committee on Standards, at the address shown below.*

*This standard is copyrighted by ASTM International, 100 Barr Harbor Drive, PO Box C700, West Conshohocken, PA 19428-2959, United States. Individual reprints (single or multiple copies) of this standard may be obtained by contacting ASTM at the above address or at 610-832-9585 (phone), 610-832-9555 (fax), or service@astm.org (e-mail); or through the ASTM website (www.astm.org).*

## Appendix 6: Cold Over Boiled Porosity—COVB

Reprinted from:

[http://digitalfire.com/4sight/tests/ceramic\\_test\\_cold\\_over\\_boiled\\_porosity.html](http://digitalfire.com/4sight/tests/ceramic_test_cold_over_boiled_porosity.html)

Clay products both structural and artistic that will be used outside must be able to survive the stresses of freeze–thaw. Porous ceramics absorb water and freezing temperatures that cause this absorbed water to expand tend to break down the matrix, eventually crumbling it.

Some technicians assume that if absorption is below a certain amount, a fired clay is durable for outdoor use. However, any fired clay with more than 0% absorption demonstrates water penetration and is theoretically susceptible to freeze–thaw damage (although for practical purposes if a body is <0.5% normal porosity there is usually no concern).

A fired clay has both absorbency and porosity. A fired piece will naturally absorb a certain amount of water to fill the pores (open porosity). However clay matrixes also have capillary-like networks which normal soaking does not fill (closed porosity). This auxilliary network allows fired ceramics to survive freeze–thaw because the expansion of the water has somewhere to go.

This test is based on the principle that a sample of clay boiled in water will absorb more water than one that is soaked, because for the former, the entire network is filled, for the latter only the pores. This test compares the cold soaking absorption or open porosity (C) of a clay with its boiled absorption or closed porosity (B). The structural ceramic industry requires a C/B result of less than 0.78 in order to pass CSA and ASTM specs for outdoor use.

This test depends on bars as made in the SHAB test. Prepare bars using the SHAB standard procedures altering the boiling and weighing aspect as follows:

Weigh the bars after a 24 hour soak, boil them for five hours and allow them to cool to room temperature, then weigh again. Be careful to blot the bars well on an absorbent towel. In the case of some dense bodies it is possible for the

boiling process to clear the pores somewhat so that the boiled bar will be lighter than the soaked one. Such cases are considered a pass.

### **Variables**

#### **24HR - Value (C)**

This is a calculation of the C value for this test, i.e. the absorption of a clay sample if soaked for 24 hours in cold water.

#### **5HR - Value (C)**

This is a calculation of the B value, i.e. the absorption of a clay bar if soaked for 24 hours and boiled for five hours.

#### **SCOE - Value (C)**

This is a calculation of the C/B value, the cold water absorption divided by the boiling water absorption.

#### **DRWT - Value (V)**

The weight of a dry test specimen of the fired clay.

#### **24WW - Value (V)**

The weight of a specimen that has been soaked for 24 hours in room temperature water and wiped clean of all surface water.

#### **5BW - Value (V)**

The weight of a specimen that has been soaked for 24 hours, boiled for five hours and wiped clean of all surface water.

## Appendix 7: Data from strength tests

Weighted average of bars and disks

Material	Temperature *C				
	900	950	1000	1050	1100
BM11.1	17.27344	-	-	-	-
BM11.2	9.241519	13.86502	11.99915	-	-
BM11.3	13.97369	-	-	-	-
BM11.4	-	10.58035	10.88438	-	-
BM11.5	-	10.61391	8.449156	-	-
BM11.6	-	10.62163	10.94503	17.97318	-
BM11.6a	-	-	14.14872	-	-
BM11.10.	-	-	-	12.85233	11.69882
BM11.13	-	-	-	-	18.37699
BM1.14	-	-	-	11.52133	17.76299
BM1.14C	-	-	-	17.45699	25.22159
Bung	-	-	-	9.241519	10.36318
Marulan	-	-	-	-	15.47519
WT14	-	11.60748	7.533367	16.27308	19.85934

## **Appendix 8: Report on clay body BM11.6B—Geoff Crispin**

Clay body is on the extreme end of thixotropy.

This leads to some practical problems.

Clay as supplied had been put through a pugmill and so when kneaded the clay remained even through the mixing process.

It required several days of gradual drying to reduce the stickiness to a level where the clay could be thrown on a wheel.

When recycling of scraps after attempting to make pots was attempted this proved to be a long drawn out process with lumps proving to be difficult to break down.

### **Throwing proved to be a challenge.**

I was able to make some small bowls 1 1/2 lbs and 3lbs.

When I tried to make taller forms out of approx 4-5lbs it proved to be very difficult.

The clay would not rise as you would expect from a standard throwing clay. The clay would shear suddenly and unevenly meaning that the walls of the shape quickly became uneven and the shape would not remain centered.

The only way to do this was to leave the walls very thick and subsequently turn down the walls to a lessor thickness.

Normally for a throwing body the standard is 1 1/2 lbs will make a 10 inch cylinder that you can still get your hand inside.

This clay body will not allow that to be done.

The clay tends to shear under pressure and give way suddenly.

This is typical of some interference with the layer of water around clay crystals that support plasticity.

It is very different for example from throwing traditional porcelain where the body is flabby and resistant to being drawn up due to the clay mineralogy (primary kaolin), and fineness of components.

### **Comments on turning**

Normally the expectation is that clay will be removed by a turning tool easily. In this tested example the clay tended to smear rather than be cut cleanly by the various tools used. This to some extent is due to the uneven drying where the surface can be firm but underneath the body rapidly becomes softer as the cut deepens. Thixotrophy which leads to uneven drying appears to be at fault.

### **Comments on clay mineralogy**

If a clay has a majority of montmorillonite minerals then the clay from my experience can be thrown and made extremely thin, making a 1 1/2lb cylinder to over 12 inches. It is important to note that commercial bentonites are usually treated with sodium and then they reflect the problems discussed above about shearing and lack of responsiveness.

Illitic clays are also usually very plastic but when a belly is applied they can often split and shatter into pieces. This is assumed to be to do with interference with water around the clay crystals, possibly from sodium again or calcium.

### **Comment of clay body construction**

Non-plastics in the clay body are usually ground down and so particles are regular in shape. The non-plastic components in the body provided are sharp and angular and so from a throwing point of view will cause damage to skin from abrasion.

### **Comments on assemblage of pieces**

Due to the thixotropic nature of the body it leads to uneven drying and so several problems arise.

1. Turning footrings on bowls tends to the formation of cracks in the area between the bowl body and the footring. These are caused by the exposure of the damper clay underneath the dryer hard skin on the surface.
2. Adding handles to a mug for example will face the same problems with cracks appearing where the handle joins the existing form. This would apply to constructed pieces as well. It may be that paper clay type reinforcement may be needed on joints to overcome this problem.

### **Overall Comments**

I did my own test on drying shrinkage and it was about 5%, which is good as a general rule, but the unevenness is what creates problems.

I would suggest that probably the best use of this body would be moulding under pressure in a powered form with minimal moisture to get around the thixotropy problem and others I have outlined.

I made no attempt to make slab formed pieces.  
At this point no glazing has been carried out.

Geoff Crispin  
6/3/2012

## Appendix 9: WMF technical data



### White Midfire

**Code: AA175**

#### Description

A superb super white midfire body for throwing and pressing with precise thermal expansion for accurate glaze fit. This body is designed to be used as a vitreous midfire body at 1200-1220°C.

**Mesh** : 80#

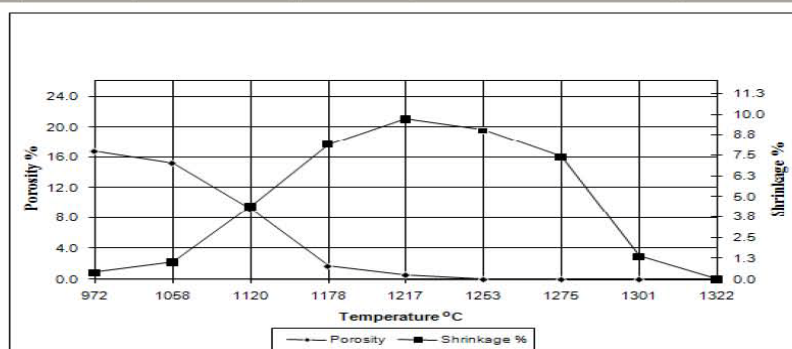
#### Recommended Firing

Bisque	Glaze Middle Fire
1000° C to 1060° C	1200° C to 1220° C

#### Coefficient of Expansion

Sample fired at 1100° C, Orton cone 03. Linear expansion is 0.290% at 500° C and coefficient is 63.66 x 10<sup>-7</sup> from 200° C to 500° C

Chemical Analysis		Shrinkage (fired)			
SiO <sub>2</sub>	64.59%	Wet to dry	2.3%	± 0.5%	
Al <sub>2</sub> O <sub>3</sub>	21.18%	Dry to bisque	0.2%	± 0.2%	
TiO <sub>2</sub>	0.37%	Bisque to glaze	1.0%	± 0.5% at 1100° C	
Fe <sub>2</sub> O <sub>3</sub>	0.40%	Bisque to glaze	5.0%	± 0.5% at 1250° C	
CaO	0.86%				
MgO	0.98%				
		Water absorption			
Na <sub>2</sub> O	1.00%	Biscuit	1000° C	Orton Cone 06	14%
K <sub>2</sub> O	3.87%	Fired	1225° C	Orton Cone 6	less than 2%
L.O.I.	6.76%	Fired	1250° C	Orton Cone 7	0%



#### Glazes

Use our standard clear lead free glaze for White Midfire. EN/EO/EL 250

#### Presentation

Fully de-aired 10 kilogram block wrapped in recyclable polythene bags.

Moisture content of standard clay is 22% to 24%, PR 3 to 4.

Other moisture contents are available on special request using our Penetrometer Readings (PR) outlined below.

#### Preparation

Crude clays are blunged, sieved and passed over rare earth magnets, then stored in constantly agitated farm tanks. Final body blend is made with millimetre accuracy with powdered raw materials being added and agitated in. With this manufacturing method we can ensure reproducible recipe formulation to within 0.1%. Final body in liquid form is sieved and passed over rare earth magnets once again and then filter pressed. Filter pressed clays are then stock piled in cake form and allowed to age. Extruding takes place through a de-airing pugmill and clay is sealed airtight in polythene bags which can be stored indefinitely.

**Victoria** 2/21 Research Drive Croydon South 3136 Phone 03 87616322 Fax 03 87616344 Email [sales@walkerceramics.com.au](mailto:sales@walkerceramics.com.au)  
**NSW** Phone 03 87616322 Fax 03 87616344 Email [nsw@walkerceramics.com.au](mailto:nsw@walkerceramics.com.au)  
**ACT** 289 Canberra Avenue Fyshwick 2609 Telephone 02 6280 5700 Fax 02 6280 5705 Email [act@walkerceramics.com.au](mailto:act@walkerceramics.com.au)  
**Queensland** Feeneys Clay 55 Tiger St West Ipswich 4305 Phone 03 87616322 Fax 87616344 Email [qld@walkerceramics.com.au](mailto:qld@walkerceramics.com.au)  
 TOLL FREE 1800 692529 OR 1800 OZCLAY  
 Ozclay Pty Ltd trading as Walker Ceramics (Australia) ABN 30 456 822 810  
 Website [www.walkerceramics.com.au](http://www.walkerceramics.com.au)



## Appendix 10. Conceptual Artworks Developed from the Research

The development of a number of conceptual artworks is described on the following pages. These works explore the themes of the environment, energy, consumption and waste. In order to demonstrate the cross-disciplinary nature of the research, the thesis is interspersed with accounts of how these conceptual artworks emerged from the research experience, materials and motivating concerns. Each work is pictured, and in some cases there are accompanying images related to the development of the work. These are listed as plates:

- Plate 1. Brett Smout *Thin Air* Bottling. 2010. South Coast, NSW, Australia. (Rigg, W.)
- Plate 2. Brett Smout *Thin Air* Bottling (2). 2010. South Coast, NSW, Australia.
- Plate 3. *Thin Air* 'marketing shots'
- Plate 4. *Thin Air* 'marketing shots' 2
- Plate 5. Brett Smout *Crack Wrap* 2010
- Plate 6. Destruction of Tinsley Cooling Towers [Siandara (2008)]
- Plate 7. Wallerawang, NSW cooling tower
- Plate 8. Pylon at Wallerawang, NSW.
- Plate 9. Pylon at Sherbrook, NSW.
- Plate 10. Pylon at Auckland, NZ.
- Plate 11. Pylon at Sherbrook, NSW.
- Plate 12. Shukhov Oka Towers 1988. ( Kazus, I.)
- Plate 13. Shukhov Oka Tower 2006 (Tomilov, V.)
- Plate 14. Shukhov tower destroyed (Mihadzr, 2005c)



**Screaming Cans**

## ***Screaming Cans***

900 x 650mm, Aluminium cans, digital print

The mining engineering scientist Ian Pilmer claims that recognising the anthropogenesis of climate change (i.e. attributing climate change to human activity) is misinterpretation of data, asking: 'If such warmings and coolings took place in the historical past before industrialisation, why is the most recent warming now due to human activity?' (Seega, 2009). The tendency to see patterns in random data is referred to as apophenia, and one form of apophenia is pareidolia, a psychological phenomenon that involves misinterpretation of an image, (Zimmerman, 2012). These concepts (anthropogenesis and pareidolia,) came together in a number of my works linking inanimate objects with the themes of energy use, consumption and waste. These works began accidentally with the advent of *Screaming Cans*.

Being mindful of the amount of embodied energy contained in aluminium cans, I was in the process of collecting energy drink cans. I was removing the ring-pull tabs in the hope that a use for them would present itself. After I removed the ring-pull tabs I placed the cans in cardboard boxes. It was when I stacked them in a box with their open tops facing up that I realised they looked like round faces with mouths that were hungry, screaming, gluttonous, benign and insatiable all at once. These mouths were not visible when the ring-pulls were still attached as they obscured the top of the 'mouth'. I photographed groups of these cans. On some of them I repositioned the ring-pull horizontally across the top of the can above the mouth to represent eyes or glasses. On some of them I hid the 'tongue' that was bent inside the can during the opening process, and on some I left it visible. On some the residue of the drink appeared as globs of sweat-like moisture around the perimeter of the face. Photographing these cans as 'humans' draws attention to them as articles of value – worth a second look. The manner in which they are packed in for transportation and the sense of anxiety that is portrayed by their expressions reflects concern over their destination.



**Switch**

## **Switch**

720mm x 550mm x 110mm, Acrylic sheet, neon tube, household light switch, electrical components.

A number of considerations and experiences lie behind the creation of this work, which was exhibited in 2012. It is intended to bring the viewer to consider the connection between the everyday use of electricity and CO2 emissions. A neon sign reading CO2 is mounted on the front of a shiny black box, and connected via a transformer to mains power. A switch is mounted on the front of the box. The viewer has the choice of switching the light off, thereby foregoing the pleasure of viewing the neon sign, or switching it on, thereby contributing to carbon emissions.

The glow of red neon is produced by electrical energisation of trapped neon gas. Other gases could have been used, as many gases can be energised by electricity, and a range of different colours can be produced. The choice of the gas contained in the glass lettering was based on the colour it would produce, rather than on the actual gas to which the sign refers. Although it would have been equally possible to use glass tube lettering containing carbon dioxide, this would have produced white light. White has associations with cleanliness, goodness, and rescue. The choice of red neon was made because red is associated with allure, blood, and danger. The black box has associations with concealment, unknown workings, recording of actions, and disaster survival. The glossy surface allows the viewer to be dimly reflected.

The light switch chosen was of the type that is ubiquitous across Australia, in order that viewers would have had the experience of using just such a switch in their everyday lives. The single light switch was mounted on the box to make it obvious that the viewer could control the operation of the work. That was what happened when the work was exhibited, with some viewers interacting with the work and making the decision to switch on or off.



*Human*

## ***Human***

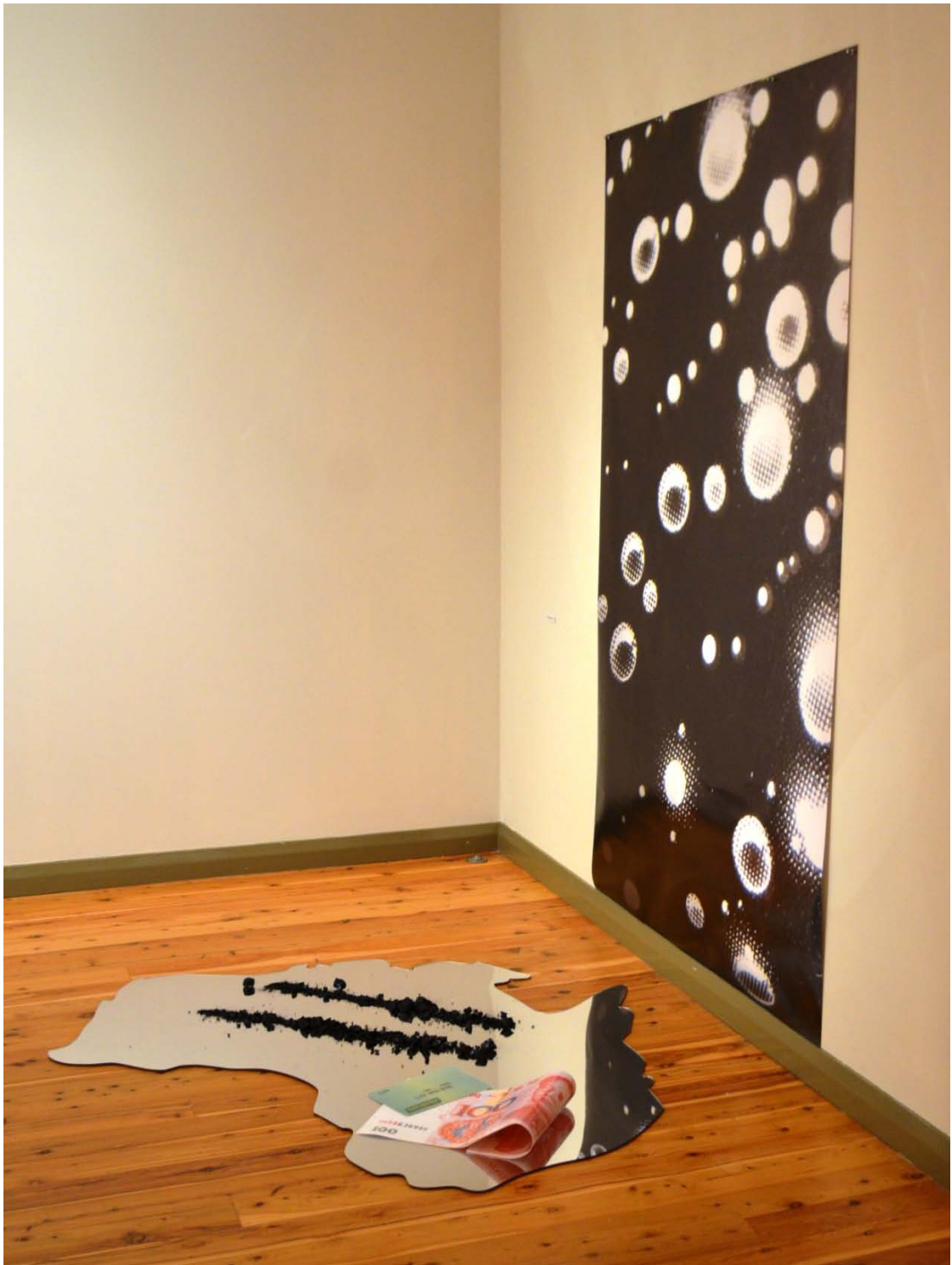
420 x 290mm, Waste, digital print

The process of collecting our household recyclables and trying to reduce waste led me to the inevitable and obvious conclusion that to be alive is to produce waste, and to be human is to be a consumer and a producer of waste.

I saw this represented graphically by a shoe box full of discarded food and drink containers that had been left on the side of the road in McEvoy Street Alexandria, Sydney. The brand on the box of waste is *Human*, a brand stocked by the nearby *FSW Show Warehouse*. A reasonable supposition would be that a family group of customers has consumed the beverages and then discarded the packaging. Here, after the passage of time, were the remains of the polished packages that had enticed these consumers to buy. This waste-that-need-not-be-waste is evidence of the way we humans soil our own nest. The image tells us that humans can be dirty, gluttonous consumers. Our 'brand' is filthy and the container is collapsing.

I considered sending the image to *Human Footwear* in Taren Point, Sydney, but then I thought that perhaps if there is no such thing as bad advertising manufacturers may indeed like the visibility of the discarded packaging of their products.

The challenge is what to do with the packaging that embeds so much energy and is associated with so much carbon emission. How can we re-use or refuse packaging in the first place so that it doesn't become refuse?



***Carbon Fix***



### ***Carbon Fix***

2 x 2 x 2.4m, Coal, acrylic, plastic, paper.

This piece was inspired by newspaper articles reporting China's dependence on Australian coal to fuel its expanding infrastructure, (Denning, 2007) and Australia's dependence on coal exports to sustain the economy (Commonwealth of Australia Department of Resources, Energy and Tourism, 2012). . A mirror was laser-cut to have the outline of Australia, and coal from the Wallerawang Power Station was crushed to a powder and formed into lines to represent black cocaine – a pun on two substances signified by the word 'coke'. A Chinese Renminbi banknote was photographed and enlarged, and rolled into a tube to represent improvised drug paraphernalia and to simultaneously refer to China's dependence on coal and the value to Australia's trade balance.

Coke users are sometimes depicted using a credit card to make lines of coke on a mirror. I chose to use a Medicare card to refer to the population health effects of coal extraction and burning. I photographed and digitally altered my Medicare card. Some letters of my name were removed and the remaining letters were rearranged so that BRETTON SMOUT became TONS OUT. The number was altered to represent the almost 320 million tons of coal that were predicted to be exported in 2013 (Commonwealth of Australia Department of Resources, Energy and Tourism, 2012). The piece was displayed so that observers saw themselves reflected in the mirror of Australia, reflecting our participation in the wealth-creation and energy consumption processes. Also reflected was a large print on the wall behind. This print is a much enlarged image of carbon dioxide bubbles from a soda water label, reminding the viewer of the invisible carbon dioxide that is released from burning coal. The black background of this print matches the black coal beneath.



Thin Air

Thin Air

### ***Thin Air***

200 x 200 x 50mm, Glass bottles, air, aluminium, paint, adhesive labels.

These three bottles are from a more extensive collection of glass bottles that had contained carbonated water. They were collected, stripped of their branding, and used to collect air. Air was collected over a period of years, the year of collection was recorded on the neck of each bottle and the 'product' was re-branded as *Thin Air*. An explanation of the manner in which some technical experimentation contributed to the conception of this work is followed by explanation of its further development.

This work originated from two factors that were intrinsically linked to this research, combined with a chance occurrence. First, awareness of deteriorating air quality and increasing CO<sub>2</sub> was part of the motivation for embarking on the research. Second, the technical requirements of producing low-fired clay and glaze involved experimenting with glass as a cheap source of sodium to be used as flux. The idea for the artwork was born from a chance occurrence - the death of a household fly. These matters are explained in detail below, beginning with practical aspects of collecting and preparing glass for crushing.

I wanted to use ground glass in clay bodies and glazes, and thought clear glass bottles from home consumption would be a possible source. I was drinking soda water occasionally, and the bottles it came in were clear, so I began making plans for crushing them into glass cullet. The bottles came with printed paper labels, and aluminium neck rings, and as these would be sources of contamination, I needed to get the labels and neck-rings off.

I soaked soda water bottles in shower water collected in buckets. When the glue on the label had softened, I carefully peeled the labels off and used my fingernails to scrub off the residue of glue. I let the bottles dry, and after they were dry I levered off the aluminium collar that remained around the neck of each bottle after the screw cap had been removed. When I had taken the lids and collars off the bottles, I considered the fact that both were made of aluminium. Aluminium is a high energy use product, so I knew it would be good

to recycle the aluminium. I collected the caps in a large jar, much as some people collect their small change.

I put the uncapped bottles in boxes ready to transport to the crusher, as detailed in the main body of the thesis. It was at this point that chance intervened in the form of a small household fly.

I found this particular fly dead in one of the uncapped bottles. My assumption was that having flown into one of the bottles this unfortunate insect had been unable to discern the difference between the clear walls of the bottle and the clear air above, and had exhausted its strength attempting to escape. I put the tops back on the bottles to prevent insects flying or climbing into them.

It was then that I noticed that I had bottles full of air. I wondered how long I would be doing this for. Would I have bottles of air from successive years sitting in my house? If so, I would have an air collection. I began to wonder about the value of the air. No doubt the air collected in 2010 would be better than air in future because we are stuck on a course of increasing CO<sub>2</sub>.

I decided to re-label the bottles according to their new content, and to include labelling features that would increase the perceived value of air in our atmosphere. Transparent adhesive labels were chosen in order to draw attention to the contents of the bottles.

The bottles shown contain air bottled in 2010. Placing the year of bottling on the label refers to the practice of displaying the year of vintage on fine wine. The implication is that air from previous years may be better. The air is also unavailable as it is trapped within the bottle. This both increases its value and reinforces its difference from the air outside the bottle. I chose the 'brand name' *Thin Air* to emphasise the fact that air from previous years is of higher quality, because with each successive year, the air is thickening with carbon emissions. It also refers to irretrievable loss, as in the expression 'it vanished into thin air'.

A wispy font was chosen to bear a similarity to cloud, and *Thin Air* became *Thin Air*. On the reverse of the bottle, *Comic Sans MS* was chosen for the font in which smaller text repeats the brand name and the vintage, and a tag line reads 'Breathe easy!' This simultaneously refers to the laissez-faire attitude of those who suggest there is no need to worry about climate change, and to the opposing concern that in future breathing the air will be a health hazard that parallels health hazards of drinking contaminated ground water. Hence the need for bottled clean air. Although much of my work is unsigned, a signature was added because this is a device often used to differentiate a product and add value.

The bottles needed to be displayed as if for sale, and to have the labels visible, so I decided a tiered rack would be best. As transparency was important, I decided to make the display rack out of clear acrylic. The steep graph of increasing CO<sub>2</sub> levels recorded at Cape Grim in Tasmania was used to define the slope of the sides of the stand, and the graph itself was etched onto the side of the display.

The labelling of the bottles full of air and presenting them in a format for sale was an act of giving value to something which is generally regarded as free – the air we breathe. The re-use of the glass bottles also emphasised their value. I also considered how an advertising campaign for *Thin Air* might be created, and how I might involve others in the campaign. I arranged to film the bottling of the air in an obviously clean location – at a beach on the NSW South coast. A number of bottling scenarios were undertaken, two of which are documented here.

In the first scenario I spun around on the spot with the bottle held horizontally in front of me.



*Plate 1. Brett Smout Thin Air Bottling. 2010. South Coast, NSW, Australia. (Rigg, W.)*

In the second scenario the air was scooped with a ladle and poured into a teapot before being poured into a funnel resting in the neck of the bottle. A number of beachgoers were curious about what we were doing and this resulted in some explanations that prompted amusement and interest.



*Plate 2. Brett Smout Thin Air Bottling (2). 2010. South Coast, NSW, Australia.*

A series of stills from these films were integrated into a flip-book exhibited in 2012 alongside the display stand of *Thin Air*.

Another common advertising technique involves the use of models being photographed enthusiastically holding or consuming a product, so I convinced family, friends and surfing buddies from Maroubra to be photographed holding the 'product'. This involved explaining the value of 2010 air to them. There were no refusals, and a range of views about the veracity of anthropogenic climate change emerged.





*Plate 3. Thin Air 'marketing shots'*



**Plate 4. Thin Air 'marketing shots' 2**



**Crack**

## **Crack**

400 x 290mm, Digital print

This work had its origins in the technical component of this research - preparation of sugar cane ash and corn cob ash.

Corn cobs were received as wet cobs with kernels removed by the cannery. They needed to be dried and burnt to produce powdered ash. Sugar cane ash, as received, was a damp black powder, indicating it had not been burned at a high enough temperature to remove carbonaceous material. In order to be useful for consistent glaze preparation, it had to be dried and burned at a temperature high enough to remove most of this material. This was achieved by placing the raw ash or dried cobs in separate containers, firing to a range of temperatures, and observing the results. Although the usual choice of container for this process would be a relatively thick-walled clay crucible or saggar, the containers I chose to use were emptied *Milo* containers, as the lightness of their construction meant that they would require little energy to heat. I had collected several of these, holding them back from our kerbside recycling.

The decision to use these metal containers had unexpected benefits. When the kiln was opened, the metal surface of the cans had oxidised, producing flaked and cracked surfaces with dramatic colour variations. Had I been able to stabilise the surface, I would have exhibited these re-used cans. Instead, I photographed the surfaces, and printed the results to be hung as two dimensional prints, as shown on the preceding page.

Printing the results also enabled me to re-create an approximation of the appearance of the tins as they were when the kiln was opened. I wrapped prints of the surfaces onto empty but unfired *Milo* tins to make *Crack Wrap*.



### ***Crack Wrap***

The re-cycling and re-use of materials in the creation of artwork mirrors the re-cycling and re-use of the materials used as glaze and body constituents in the experiments conducted as part of this research. Recognition of this led to the creation of another artwork that takes recycling a step further by adding the re-cycling of art.



*Bretton's Calcined Corn Ash*

### ***Bretton's Calcined Corn Ash***

400mm (circumference) x 140mm, Tin, paper, digital print.

It is instantly obvious upon viewing this work that the art of Andy Warhol has been appropriated and re-cycled. The can is of course based on Warhol's Campbell's Soup series – itself an appropriation. The colours and fonts chosen are similar to those on the original product, but I have replaced Campbells with Brettons – as in this case I produced the product contained in the can. The can contains the ash of corn cob waste obtained from the cannery at Bathurst.

Warhol's depiction of a commonly available commercial product was in itself a form of re-cycling. Closer inspection of the pictured can or corn ash reveals a range of other elements relating to recycling of waste. The row of fleur-de-lis that decorated the bottom the Campbell's and Warhol labels has been replaced with a row of images of star-shaped portions of tomato plants – the receptacle and sepals that are left on each tomato when truss tomatoes are sold. These were photographed before the stems were discarded in our compost, enabling a form of digital recycling and capturing some value from waste.

The original Campbell's can carried the image of a coin-shaped medal from the Paris International Exposition 1900. This is replaced with an image of a specially minted \$200 Australian coin in reference to the value of waste. Where the original can bore the word *condensed*, the corn ash can bears the word *calcined*. Both words refer to treatment processes, albeit different ones. In the case of the word *calcined* the reference is to the process of calcining, or placing material in a container in a kiln and heating it so that its material properties are changed. It is likely that only those with a background in chemistry or ceramics will understand this reference. Ceramicists are one group to whom this 'product' could be marketed, should it prove useful.



*Certain Doubts*



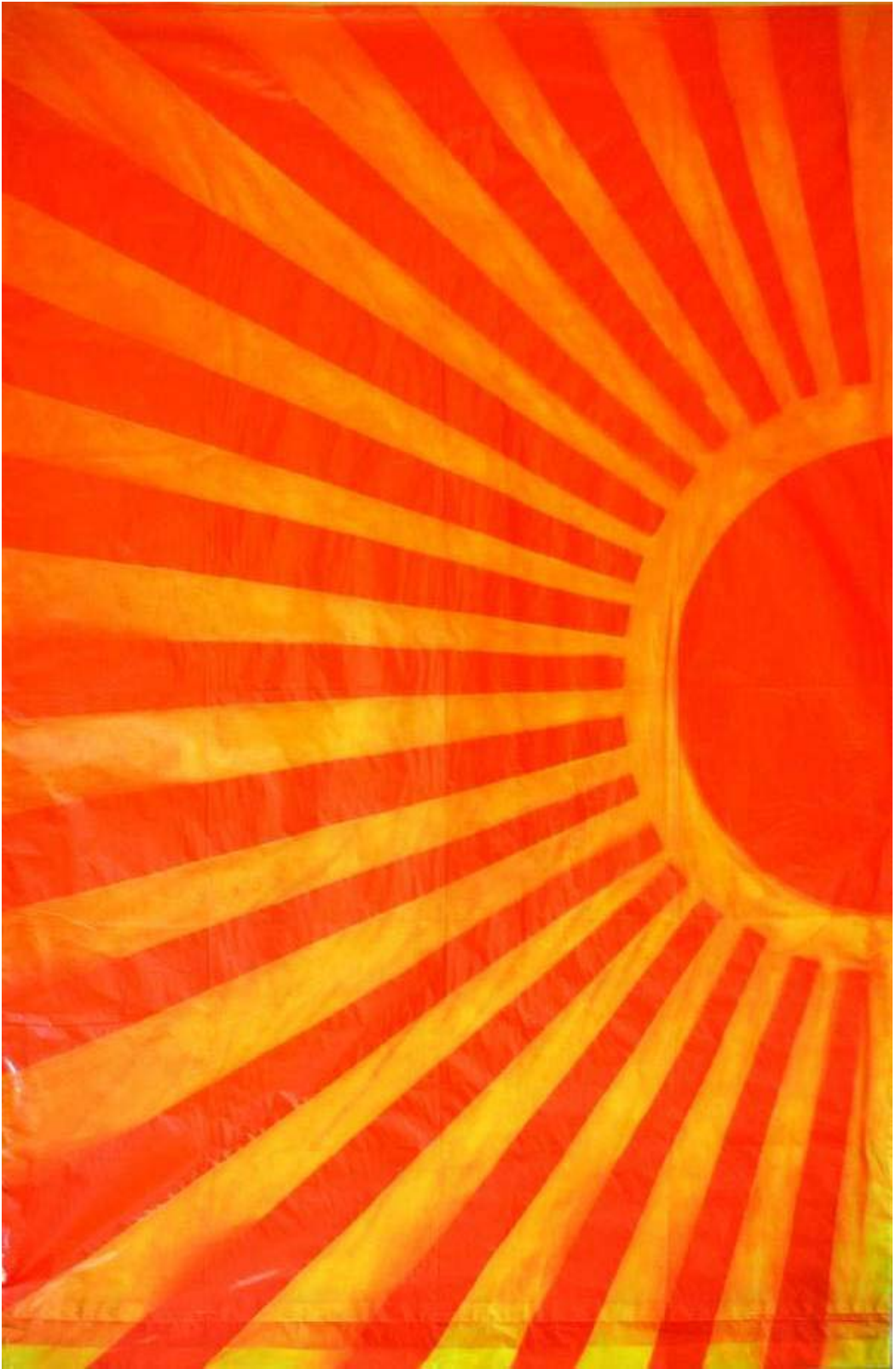
### ***Certain Doubts***

Clay, water, video recording, projector, scientific laboratory coat.

This image, a still from a digital video recording titled *Certain doubts*, captures the moment when a clay tablet bearing the word *certain* collapsed.

This video piece refers to the range of public perceptions of the impact of human activity on climate change, to clay recycling and to the process of transformation. The two words from the title *Certain doubts* are spelt out in relief on separate clay wedges made from recovered waste materials. These wedges are thick at the base and are designed to be self-supporting so the text can be read by being viewed front on. When bone dry, the first wedge - *Certain* – was placed in a fish tank full of water and filmed as it slowly absorbed water and collapsed into a pile of wet clay particles. In this process the word *certain* became blurred and then obliterated. The same process was used for the second wedge – *doubts*. In this word the text of the *b* is in fact an inverted *p*, which looks slightly wrong, and is intended to induce in the viewer a sensation similar to doubt. The decomposition of the second wedge was also filmed. When the videos were edited, they were placed in a loop so that *certain* appears to decompose into a heap which is reconstituted as *doubts*. The loop is continuous and arranged so that the process occurs quickly enough to retain viewer attention.

The looped video is projected onto a scientific lab coat, reflecting the debate about science that has emerged following claims that there was scientific misrepresentation in the IPCC report, and the subsequent attempts to discredit climate science.



**Solar Panel**

## ***Solar Panel***

1200 x 800mm, high density polyethylene, sunlight

The idea for this work occurred as a result of building a kiln to fire with rice husk, in order to capture the energy released when ashing the rice husk. I made a kiln out of a rubbish bin, and as it was to remain outside, I covered it with a garbage bag to preserve it from the elements. After some months I noticed that the orange garbage bag had a tie-dyed appearance because the sunlight had started to decompose and bleach the plastic. I removed and photographed a bag because of its striking appearance. Places where the bag was most exposed to light were most bleached and I realised that this could be exploited by selective exposure.

In these works, common household garbage bags were spread out on the roof of my house. Objects - such as words formed from bisque fired clay alphabet, or material cut to form shapes - were used to mask the sun's rays. After several months, the exposed plastic was judged to be sufficiently bleached by sunlight. The covering text and material were removed and the results were photographed. The words chosen included 'junk', 'garbage', 'waste' 'trash' and 'rubbish'. Each bag had one word. The lines radiating from the text were intended to connote the sunshine which was used to create the artwork, and mimic the radiating sunbursts that are so often used in advertising to add to the perception of excitement and value – in this case referring to the potential value of the discarded materials that garbage bags were manufactured to contain.

In the case of the work pictured, the sun-bleached image is of a stylised sun. Using the medium of sunlight and garbage bags to construct these solar panels can be interpreted as a reference to any missed opportunity of harnessing solar energy.



***Cooling Tower 1***

## ***Cooling Tower 1***

120 x 110mm, Low-fire ceramic.

A number of cooling tower forms were thrown using the low-fire clay developed. The efflorescence that is a quality of the low-fire body is used to introduce variation to the surface on the piece shown, which was fired to 1040°C. The variation obtained is reminiscent of the effects of weathering and particulate accumulation that can be observed on aging cooling towers. Some of the towers were deliberately fired to the point where the low-fire body started to fuse, so that the forms began to slump. This was a replication of the unintended slumping observed during testing of low-fire bodies, and reference to the dangers associated with global warming. It could also be read as a reference to the risk of nuclear meltdown.

The use of the form of the cooling tower was first prompted by an image of environmental messages projected onto cooling towers at the Loy Yang Power Station in the state of Victoria (fig. 3). The assumption promoted by this Greenpeace image was that cooling towers are bad, and the media often uses images of cooling towers when writing negative stories about power stations and environmental degradation. Images of cooling towers can also trigger feelings of dread through associations with nuclear power plants and memories of reports of the meltdown of reactors such as Chernobyl, Three Mile Island, or more recently the Fukushima nuclear reactors in Japan.

Despite the sense of unease and disquiet that cooling towers elicit, the obvious emissions they produce are not particularly harmful to the environment. In fact they emit water vapour as steam, which is particularly evident in cool climates. The search also revealed that the photo sharing site *Flickr* contained multiple images of cooling towers. These cooling towers are situated at decommissioned and fully functioning power stations all over the world, including nuclear, coal-fired and gas-fired power stations.

Viewing these cooling tower images and associated commentary brought new perspectives to the work. First there was the realisation that cooling towers could be considered to be beautiful as well as dreadful. Photographs posted on

the online photo sharing site *Flickr* often attract comments expressing awe and appreciation. This is assumed to be because of many factors including their smooth flowing geometry, their sheer size and capacity to dominate their surroundings, their demonstrations of technological proficiency and power, and the wafting ephemeral plumes of cloud they produce. Add to this the variations in surface resulting from age, lighting or in some cases perforations and even decorations, and it's easy to understand how some people develop affection for them.

The affection with which they are viewed by some has been evident when the continued existence of decommissioned towers has been in question. For example there was much community opposition to the planned destruction of the towers beside the Tinsley Viaduct in Sheffield, England. These towers, built in 1938, were the first power station cooling towers built in the UK, and they were a dominant feature of the landscape. On the 24<sup>th</sup> of August 2008, thousands of people kept a vigil until 3am when the towers were detonated (Plate 6).



**Plate 6. Destruction of Tinsley Cooling Towers [Siandara (2008)]**

Images reproduced from  
<http://www.flickr.com/photos/67611923@N00/sets/72157606918402173>

Video footage and online interviews captured the excitement of the observers, but posted photos of the demolition of towers have commentaries indicating a polarity of views, with some expressing outright disbelief that anyone would care about their destruction, and some expressing grief: 'It's like watching something die'. (Briggs, 2008).



**Pylon**

## ***Pylon***

180 x 280mm, Ceramic

The image above is a small ceramic maquette of a power pylon that will be exhibited as a 2.4 metre high sculpture. An account of a journey I took will help explain the background to conceptualisation and creation of this work.

The images of cooling towers that I had collected and pored over prompted me to visit a working cooling tower, to view the operation first hand. Tours of the Mt Piper Power Station in NSW are provided by Delta Electricity, so a visit was arranged for 19 March 2010, with the purpose of obtaining photographs as well as understanding more about the operation of cooling towers. The tour guide, Wolfgang Kemper, advised that photography was generally not permitted on the tour but was permitted from outside the facility.

I wanted to collect a range of my own images, and to capture the effect of different lighting conditions on the cooling towers I would visit. To achieve this, I left Sydney at 2am, and arrived at Wallerawang at 4.30 am. It was cold and misty, and the air had a faint industrial smell that was no doubt the result of the effluent from the power station.

The first images were obtained in the dark, from public property on the roadside, until dawn brought the attentions of Security, who were politely insistent that photography was not allowed. By that time I had taken the photo below.





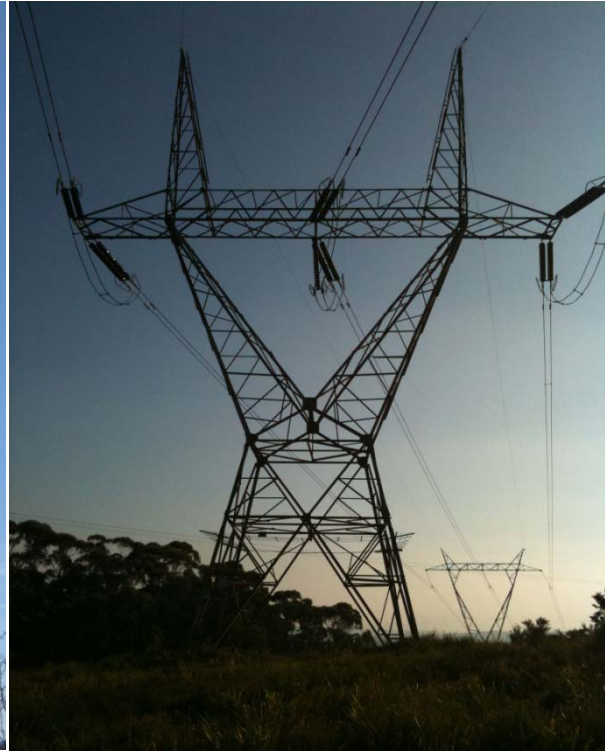
*Plate 7. Wallerawang, NSW cooling tower*

The impressive form of the cooling tower dominates the image, but another feature drew my attention. On either side of the tower there is a power pylon. There was also a pylon in the field near where I was standing. It seemed massive in scale, and in the quiet of the morning it emitted an audible hum. There must be hundreds of thousands of these pylons carrying the electricity produced by coal fired power stations.

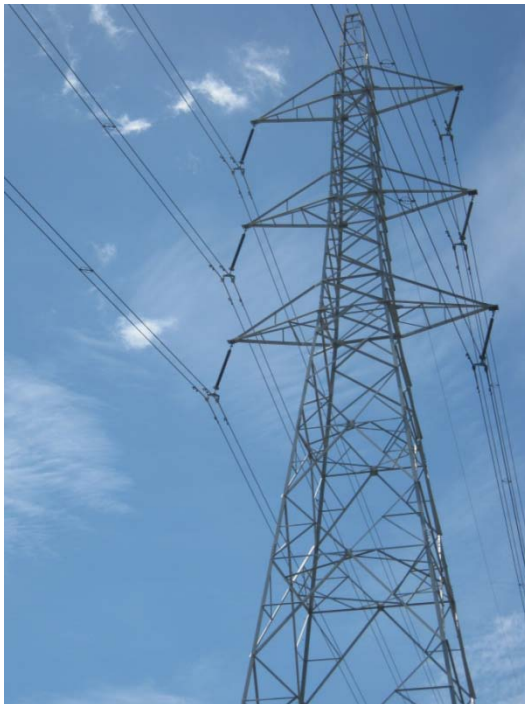
Having previously regarded pylons as ugly constructions and therefore largely ignored their presence, I began to take an interest in their role as an intermediary between production and consumption of electricity. When we switch on the power, it is power that has been carried through wires supported by pylons such as these. I began to observe them more consciously, and began photographing the different types.



*Plate 8. Pylon at Wallerawang, NSW.*



*Plate 9. Pylon at Sherbrook, NSW.*



*Plate 10. Pylon at Auckland, NZ.*



*Plate 11. Pylon at Sherbrook, NSW.*

I stylized the outlines of several and experimented with images that would convey something about them. The image I selected was an image of an energy rating label that came attached to our new refrigerator. This image was distorted using an image manipulation program and printed onto a low

temperature decal, which was applied to the ceramic surface of the maquette. The manner in which the image was distorted conveys a sense of energy being transmitted. The positioning of the centre of the distorted image is such that it approximates where a heart would be if the pylon were humanoid. I wanted it to be clear that these massive pylons are human-made, and thought that this positioning might make it easier for a viewer to make a connection with the sculpture. The black and white centre could also be read as a hole in the heart, introducing the element of danger associated with electricity. These elements all reflect aspects of my experience when standing at the base of a pylon.

The sculpture also needed to be larger than a human scale, and the material from which it was made would need to be able to accept the image. Ceramic was rejected because of the weight that the finished piece would be. Wood with vinyl printed adhesive was also rejected. Although the wood had been alive, a maquette made from wood was somewhat dull and lackluster, and the material was too natural and warm in contrast to the cold engineered quality of real pylons. I decided to print on white acrylic sheet after establishing that at 1200 x 2400mm, sheets were large enough to enable a sculpture larger than human size.

After a test showed that light would show through the printed acrylic, I committed to the idea of having lights mounted within the sculpture. This had three purposes. The lights would enliven the sculpture, it made sense to include electricity among the media used, and light would 'leak' out the sides of the sculpture, much as electricity leaks from the poles and wires of the electricity grid. This waste is one of the weaknesses of centralized electricity distribution from fossil fuel power stations. I used a 2D design program to create a file to control printing and laser cutting, and included holes at various places on the acrylic sheet that functioned as a stabilizer, in order to facilitate mounting of lights within the sculpture.

The sculpture was relatively expensive to create, with the printing and laser-cutting alone costing over \$1400. This could be understood as reflecting the 'gold-plating' of the electricity grid poles and wires that we are told is the primary cause of electricity price increases.



***Shukhov Tower (Recycled) – in progress***

## **Shukhov Tower (Recycled)**

600 x 1000mm (Work in progress) Aluminium cans

When I was using an internet search engine to do an image search for pylons, an image caught my attention.

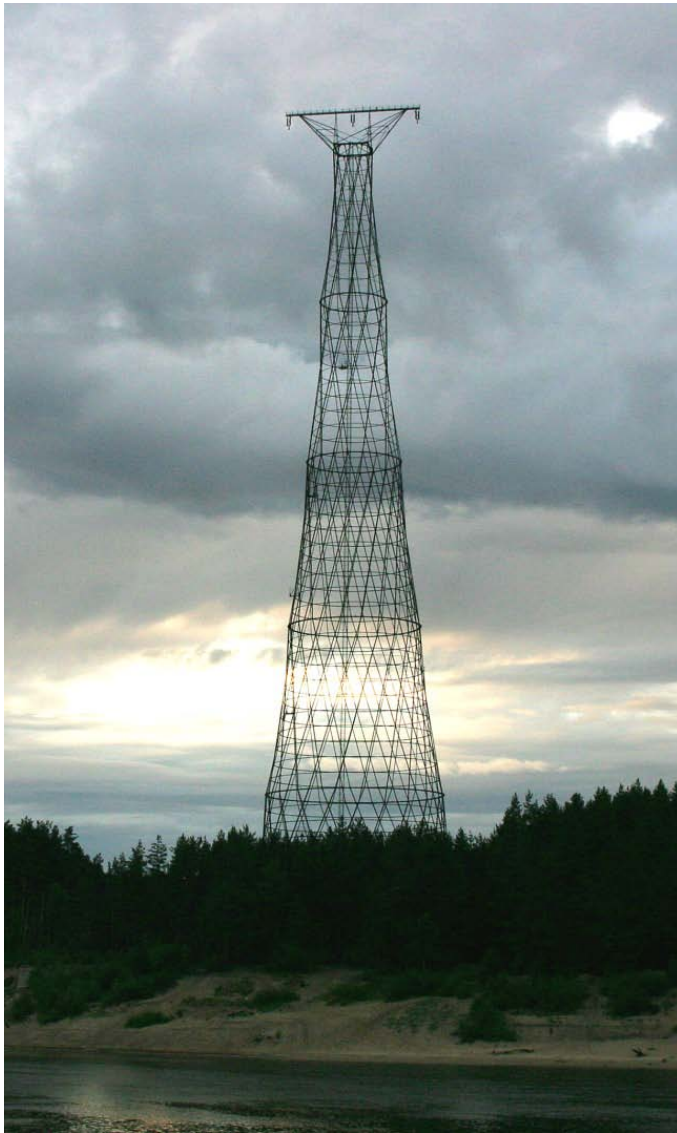


*Plate 12. Shukhov Oka Towers 1988. ( Kazus, I.)*

Image reproduced from:

[http://en.wikipedia.org/wiki/File:Shukhov\\_Oka\\_Towers\\_1988\\_photo\\_by\\_Igor\\_Kazus.jpg](http://en.wikipedia.org/wiki/File:Shukhov_Oka_Towers_1988_photo_by_Igor_Kazus.jpg)

Pictured were two beautiful towering structures that I did not recognize. Visiting the page told me that six of these towers had been constructed on the banks of the Oka River, near Nizhniy Novgorod, Russia, as pylons to carry power lines across the river. These pylons were designed by Vladimir Shukhov, and they are referred to as Shukhov Towers. Today only one remains.



**Plate 13. Shukhov Oka Tower 2006 (Tomilov, V.)**

Image reproduced from  
[http://en.wikipedia.org/wiki/File:Shukhov\\_Tower\\_photo\\_by\\_Vladimir\\_Tomilov.jpg](http://en.wikipedia.org/wiki/File:Shukhov_Tower_photo_by_Vladimir_Tomilov.jpg)

The explanation for this appears in the Wikipedia extract below

The Shukhov Tower was a part of an 110kV power line crossing the Oka River. Between 1927 and 1929, two parallel-running, 110kV, three-phase AC power lines designed by Russian engineer and scientist Vladimir Shukhov were built there. For the Oka River crossing, six hyperbolic pylons (three for each power line) were built, a 20 metre tall anchor pylon, a 68 metre tall crossing pylon on the South shore and a 128 metre tall crossing pylon on the North shore. As the terrain on the

South shore is hilly, the pylons there were lower. In 1989 the power line was rerouted and the 20 and 68 metre pylons were dismantled. The 128 metre pylons were left intact as a monument. Today, only one of the 128 metre pylons stands as the other was illegally demolished to sell its steel in May 2005.

[http://en.wikipedia.org/wiki/Shukhov\\_tower\\_on\\_the\\_Oka\\_River](http://en.wikipedia.org/wiki/Shukhov_tower_on_the_Oka_River)



**Plate 14. Shukhov tower destroyed (Mihadzr, 2005c)**

Reproduced from [http://en.wikipedia.org/wiki/File:Oka\\_Shukhov\\_tower\\_2005\\_destroyed\\_3.jpg](http://en.wikipedia.org/wiki/File:Oka_Shukhov_tower_2005_destroyed_3.jpg)

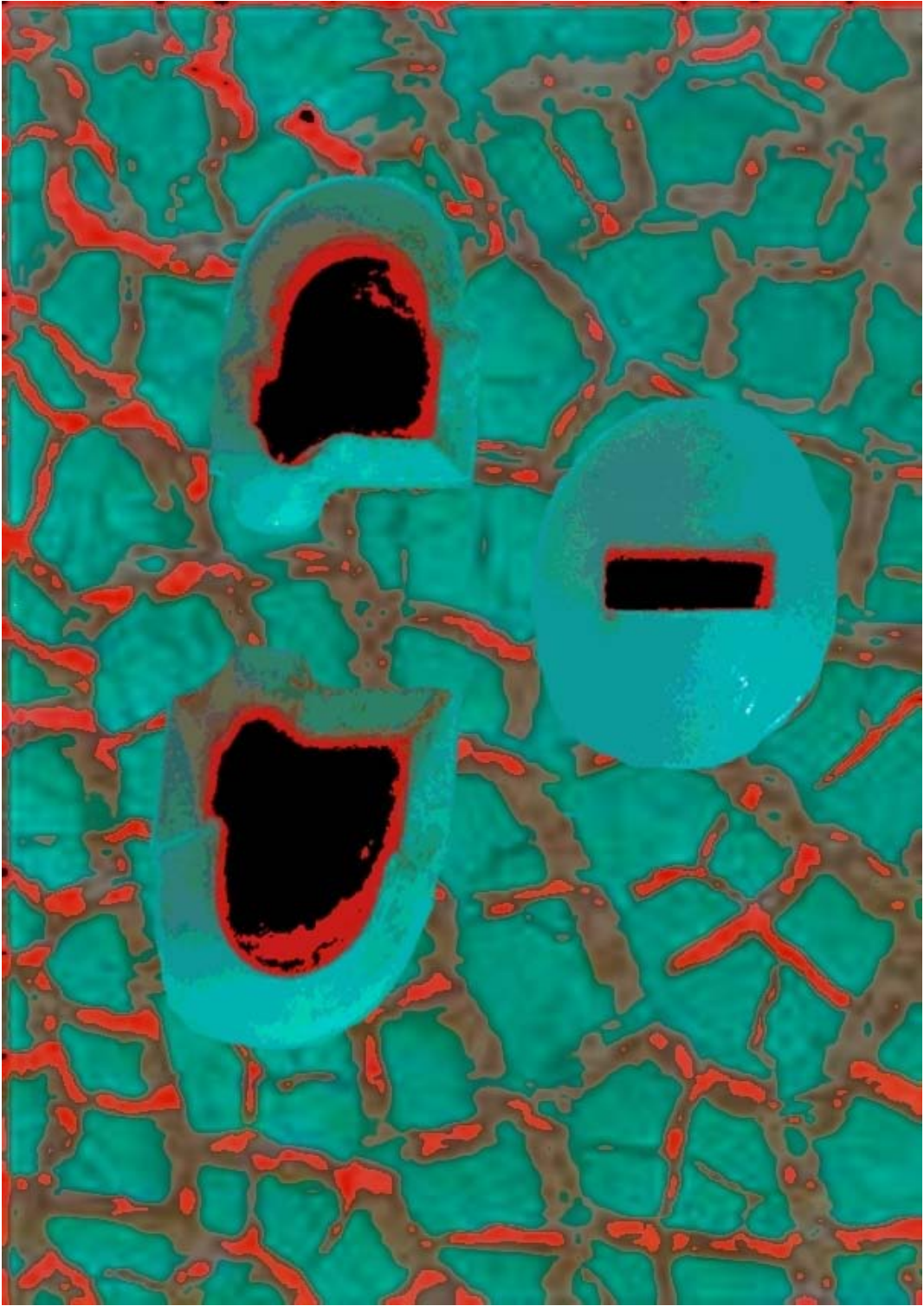
The Shukhov Tower stands as a signpost to a fascinating period of Russian art and architecture that was the subject of Elizabeth Cooper English's (2000) dissertation *"Arkhitektura i mnimosti": The origins of Soviet avant-garde rationalist architecture in the Russian mystical-philosophical and mathematical intellectual tradition*. I was greatly taken with the mystical appearance of the Shukhov Tower, and intrigued by the combination of mathematical precision, beauty, and practicality. There was a formal link with cooling towers, which share the same basis of construction - a hyperboloid of revolution. The fact that one of the towers had been destroyed in order that its steel could be plundered for re-use led me to consider constructing a replica that highlighted the value of embodied energy.

Instead of being made from steel, this replica is being made from re-used aluminium. The aluminium is from energy drink cans held back from our curbside recycling. I used the description of the Shukhov Tower to design a

1:50 replica in 3D, and used the measurements from that to construct the flat bars required. I chose to have the labeling of the energy drink showing to illustrate the energy embodied in the construction.

When finished the sculpture will be just over 2.5 metres tall. Ideally it will be displayed in a space small enough for it to be imposing. It's lightweight construction would also enable it to be elevated and hung in the corner. As well as providing a means of making the piece more imposing and mysterious, this would also be a reference to Russian iconography and to Shukhov's contemporaries Kazimir Malevich and Vladimir Tatlin. These are the two artists who famously fought when, in their Futurist group show Malevich's *Black Square* usurped the corner position for which Tatlin had prepared his *Corner Counter-Reliefs* (Gompertz, 2012).





**Shocked!**

## **Shocked!**

298 x 198mm, ceramic tile.

It was while I was travelling alone on a business trip and still thinking about my thesis and its intention of reducing energy use that I started to notice inanimate faces peering at me. It started with the power sockets. I noticed that they had various expressions, depending what country I was in, so I photographed some of them. When I returned home I noticed that the Australian socket has a somewhat shocked appearance. I saw a conceptual link with electric shock, with the price shocks that are confronting electricity consumers, and potentially with the shocking effect on the environment of electricity generated from burning coal. These concerns, which are present for me when making articles from ceramics, are addressed through the choice of imagery, materials and process.

Italian ceramic wall tiles were obtained from *Reverse Garbage* in Sydney, thereby re-using their embedded energy rather than using energy to produce new tiles. These tiles were morphed into masks by incorporating increasingly distorted images of plastic power sockets. Using low temperature decals these were printed with images of everyday objects – power sockets. The images have been abstracted to form mask-like faces that can be read as expressing shock, horror, doubt and other human emotions.

The image on the tile pictured above is a combination of two manipulated images. One was a photograph of a shaver socket in an Adelaide hotel bathroom. The other was a photograph of dried and cracked quarry tailings on site at Bungendore. The two images were separately coloured and then merged. The merging of the dried cracked clay and the power socket is a reference to the possibility of areas being drought affected as a result of anthropogenic climate changed from burning fossil fuels. The reuse of discarded tiles and the use of low fire decals enabled these ceramic works to be produced in a domestic gas oven at 180°C.



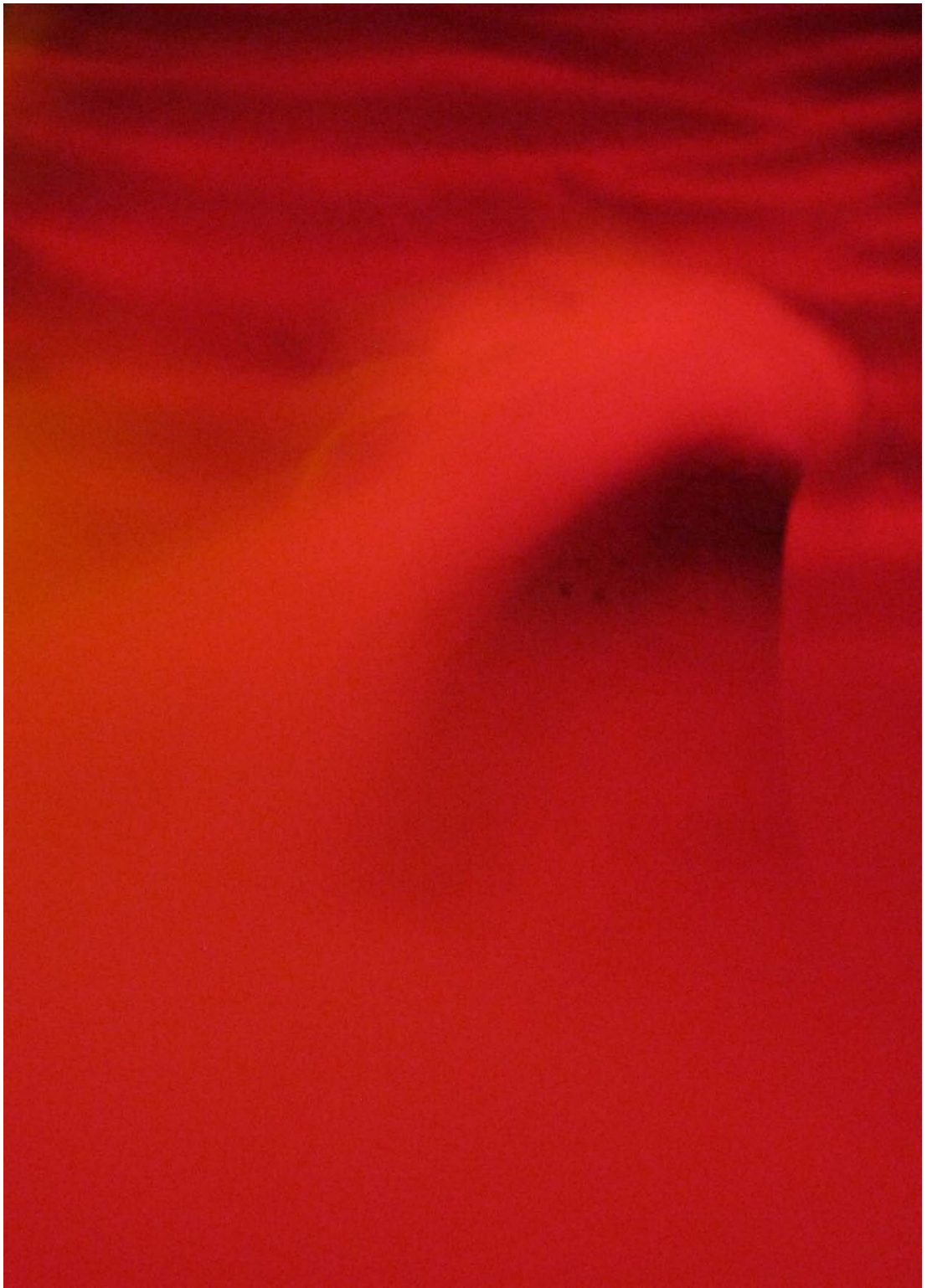
**Cooked**

**Cooked**

300 x 300mm. Low-fire ceramic cookies on high-fire ceramic plate

This work emerged from the process of making test pieces from slabs of experimental clay. I rifled through our cookie cutters in search of a simple rectangle, and came across two that were designed for making gingerbread men and women. I made multiple cookies from BM11.6B and fired them to 1000°C.

Here the low-fire ceramic cookies are presented on a high-fire ceramic plate. The message in the medium is that if we don't change our ways, we may cook.



*Plume*

## ***Plume***

Low-fire ceramic, dry ice, digital print

The paradox involved in making art about wanton generation of CO<sub>2</sub> emissions is that the process of making the art itself generates CO<sub>2</sub>. Is the responsible course of action to simply stop? That course of action would imply that all non-essential action should stop. But is art non-essential? To artists, art-making may seem as essential as breathing – a process that in itself generates CO<sub>2</sub>. So, realistically, we are not going to stop releasing CO<sub>2</sub> into the atmosphere. We don't want to. The contribution of this project has been to develop low-fired ceramics that will enable me, and potentially others, to reduce the amount of CO<sub>2</sub> emissions associated with production of ceramics. It is about accepting the scientific consensus regarding climate change, accepting a degree of personal responsibility, and acting to become part of the solution, as well as part of the problem.

*Plume* expresses the paradox described above by embodying a contribution to the problem and a contribution to the solution in one work.

The image was taken at 4:30 am, in the dark, on my back deck, under a red party light. A vitreous low-fire ceramic cooling tower spews a plume of CO<sub>2</sub> into the night, against a backdrop of rippled sand – an impression of nature taken from a windswept beach. Our party goes on, the world is mysterious and beautiful, and the sand will be there for all time, even if we will not.